Advances in Polymer Science 262

Virgil Percec *Editor*

Hierarchical Macromolecular Structures: 60 Years after the Staudinger Nobel Prize II

Springer

262
Advances in Polymer Science

For further volumes:
http://www.springer.com/series/12

Aims and Scope

The series Advances in Polymer Science presents critical reviews of the present and future trends in polymer and biopolymer science. It covers all areas of research in polymer and biopolymer science including chemistry, physical chemistry, physics, material science.

The thematic volumes are addressed to scientists, whether at universities or in industry, who wish to keep abreast of the important advances in the covered topics.

Advances in Polymer Science enjoys a longstanding tradition and good reputation in its community. Each volume is dedicated to a current topic, and each review critically surveys one aspect of that topic, to place it within the context of the volume. The volumes typically summarize the significant developments of the last 5 to 10 years and discuss them critically, presenting selected examples, explaining and illustrating the important principles, and bringing together many important references of primary literature. On that basis, future research directions in the area can be discussed. Advances in Polymer Science volumes thus are important references for every polymer scientist, as well as for other scientists interested in polymer science - as an introduction to a neighboring field, or as a compilation of detailed information for the specialist.

Review articles for the individual volumes are invited by the volume editors. Single contributions can be specially commissioned.

Readership: Polymer scientists, or scientists in related fields interested in polymer and biopolymer science, at universities or in industry, graduate students.

Special offer:
For all clients with a standing order we offer the electronic form of Advances in Polymer Science free of charge.

Virgil Percec
Editor

Hierarchical Macromolecular Structures: 60 Years after the Staudinger Nobel Prize II

With contributions by

A. Abe · K. Albrecht · A.-K. Appel · S. Bode · D. Crespy · T.J. Deming · R. DeVane · C. Dingels · G. Fiorin · F. Freire · H. Frey · N. Gangloff · J. Groll · D.M. Haddleton · M.D. Hager · K. Hur · Z. Jia · B. Kerscher · M.L. Klein · S. Kobayashi · K. Landfester · R. Luxenhofer · M. Möller · M.J. Monteiro · R. Mülhaupt · K. Müllen · Y. Ohta · E. Quiñoa · R. Riguera · J.G. Rudick · B. Rybtchinski · B. Sandmann · K. Schadt · U.S. Schubert · F. Schüler · J.M. Seco · W. Shinoda · S. Singh · R.H. Staff · F. Topuz · U. Wiesner · T. Yokozawa · Q. Zhang

Springer

Editor
Virgil Percec
Department of Chemistry
University of Pennsylvania
Philadelphia
Pennsylvania
USA

ISSN 0065-3195 ISSN 1436-5030 (electronic)
ISBN 978-3-319-03718-9 ISBN 978-3-319-03719-6 (eBook)
DOI 10.1007/978-3-319-03719-6
Springer Cham Heidelberg New York Dordrecht London

Library of Congress Control Number: 2013957881

Printed on acid-free paper

Springer is part of Springer Science+Business Media (www.springer.com)

Foreword: Memories of Hermann Staudinger by one of his grandchildren

I am delighted to contribute to this special issue of *Advances in Polymer Science* a few memories of my grandfather Hermann Staudinger, whom I knew for almost 20 years until his death in 1965.

With his first wife, Dorothea Staudinger-Förster, he had four children: Eva, born 1907 in Strasbourg; my mother Hilde, born 1910 in Karlsruhe; Hansjürgen, born 1914 in Zürich; and Klara, born 1916 in Zürich. His daughters and his son married and had ten children that I still regularly see.

Because my father, Theodore Rüegg, died soon after my birth in 1946, and since I was his only child, my mother arranged that I would often see her father and her brother Hansjürgen, who became my godfather. I thus had the unique opportunity of often seeing and talking to both of them and of being partly educated by them.

These get-togethers started right after the end of World War II and took place either in Zürich, where we lived, in Basel, or in nearby Freiburg (Germany). During that time, my mother often travelled north loaded with precious food such as butter, bread, sugar, meat, and coffee beans, the essential ingredient for preparing the preferred morning drink of my grandfather. He would also visit us in Zurich several times a year. As a result of the hard times he had endured during the Nazi regime, he had aged considerably and lost weight (Fig. 1).

In the early 1950s, Hermann Staudinger visited his three daughters and their children in the Zürich area at least twice a year, which would often be the occasion for a family reunion. On his 70th birthday, most family members travelled to Freiburg, as can be seen in Fig. 2. The get-togethers with him, his second wife Magda, and her parents Irmgard and Oskar Woit took place in their house in Freiburg. These visits impressed and influenced me greatly. My mother and I were picked up at the Freiburg train station by a chauffeur-driven Borgward car, which brought us to the impressive house at Lugostrasse 14, where the Staudingers welcomed us (Fig. 3).

My grandfather often took me on walks through their large garden surrounding the house to show me the unique collection of plants and flowers. I have been told that he knew all of the more than 250 plants growing there, as well as their Latin names. He checked them daily and took care of them with the help of a gardener.

Fig. 1 Hermann Staudinger with grandson Urs in Zurich in 1948

He originally wanted to become a botanist, but his high school teacher advised him to first study chemistry, the basis of plant and animal life, which we now call the "life sciences." I remember that at Easter time, when the daffodils and tulips surrounding a small pond in the upper part of the garden were in bloom and smelling wonderfully, we strolled around the garden and I listened to my grandfather's stories. These were inspired by Nature, most of them dealing with wild animals of the jungles and savannas: lions, giraffes, elephants, etc. They talked to each other and to the people around them, like in the stories of Doctor Doolittle.

Fig. 2 Family reunion in Freiburg on the 70th birthday of Hermann Staudinger on 23rd March 1951. From left to right: Hilde Rüegg-Staudinger, Dora Lezzi (at the back), Luzia Kaufmann (in front), Hermann Staudinger, Urs Rüegg (between his knees), Peter Kaufmann (at the back), Eva Lezzi-Staudinger, Hansjürgen Staudinger (at the back), Klara Kaufmann-Staudinger, Gabriele Staudinger-Schwarz, statue of Franz Staudinger (father of Hermann). Not in the picture: Magda Staudinger; Max, Jürg and Markus Lezzi; Monika, Reinhard and Peter Staudinger; Gustav and Ulrich Kaufmann (Courtesy of Markus Lezzi)

A follow-up came in the mornings, when I was invited to join my grandfather and Magda: He then told me stories by Wilhelm Hauff, for example the one about "Dwarf Nose," in which a community is described whose only purpose in life is to work, buy and sell, and earn money. Later on, my grandfather's arms and legs became parts of animals, some of them as dangerous as crocodile jaws; there was the frightening roar of lions that made me run away. The breakfasts that followed compensated for all this suffering. It would start with him reciting one of the many poems by Goethe, Schiller, Rilke, and others that he knew by heart. The themes were again mostly linked to Nature, for example the Easter poem in Goethe's

Fig. 3 Magda and Hermann Staudinger in front of their house in 1951

"Faust." The long-awaited fresh bread, sausages, eggs, and cereals turned these mornings into a veritable feast.

We often went on long walks towards Günterstal, a village at the foothills of the Southern part of the Black Forest. A special treat was to eat a slice of the similarly named cake on the hilltop of Schauinsland, which could be reached with a cable car and which would take us high above the dark fir trees to admire the view. In addition to the cake, I enjoyed the walks through the hills in the company of this expert botanist and storyteller. My cousins Luzia and Peter (cf. Fig. 2) occasionally joined us, and hide-and-seek was added to the touristic program.

Two other attractions were just a few hundred meters south of the Freiburg home, one for my grandfather and one for me. He was an enthusiastic supporter of the "Schrebergärten", land lots where families living in cities and not having a garden could plant vegetables, fruits, and flowers. I assume that he considered it important for the spirit to be outdoors, in touch with the elements and watching the plants grow. When a plan was drafted to construct houses on the grounds of these Schrebergärten, he chaired a committee defending their existence; they negotiated with local politicians and other groups involved in the project and, finally, their initiative was crowned with success.

My personal highlight was of a more technical nature: it was possible to observe the passing trains of the "Höllentalbahn" in a large trench. I enjoyed watching the steam engines pulling a few cars behind them coming out of a tunnel and making their way from Freiburg to Titisee and Neustadt in the Black Forest. At the age of about 10, I was put on one of these trains and travelled alone through the "Hell Valley" to the top station. As the personnel had been informed that I was a fan of trains, and since they knew of my grandfather, they invited me to the driver's platform in the locomotive. I could look into the coal fire, feel the heat and the steam, and assist with the maneuvers for switching the engine before going downhill again. This initiation probably led to my intense fascination with trains.

When not behaving well or when important decisions about my future had to be made, my mother used to consult her brother and my grandfather for advice. Towards the end of my high school education, I wanted to become a photographer. However, my grandfather had a long discussion with me about the values of science and higher education. He told me about his life, how much he enjoyed making discoveries, putting them into question and confirming or rejecting them by experiment; he also liked the discussions with his colleagues in the laboratory and the debates with those at other institutions. He was well informed about academic curricula and suggested that I choose one offering a broad perspective of natural science, for example the Swiss Federal Institute of Technology (ETH) in Zurich, where he had worked – as director of the Institute of Chemistry – some 50 years earlier. After several weeks of discussions with friends and relatives, I followed his advice and have never regretted it.

Much is known about Hermann Staudinger's second wife, Magda, but little has been written about his first wife, Dorothea, with whom he bore his four children. Dorothea was very impressed by Herman's father, Franz, who was a high school teacher and an expert on the philosopher Kant, and who had a social mind. Dorothea became involved in community-oriented activities in Zurich and was one of the founders of what is now known as the Coop Supermarkets, which were, at that time, a non-profit organization catering mostly to underprivileged people. She joined the movement of the priest and professor at Zurich University, Leonhard Ragaz, who combined socialism and christianism, was fighting for the underprivileged and minorities. In the early 1920^{s}, Dorothea and Hermann more and more grew away from each other as they followed their own interests: He was excited about research and science and she was more concerned about matters of the society. As a result, they split up and were separated in 1925. Like most people who knew Dorothea,

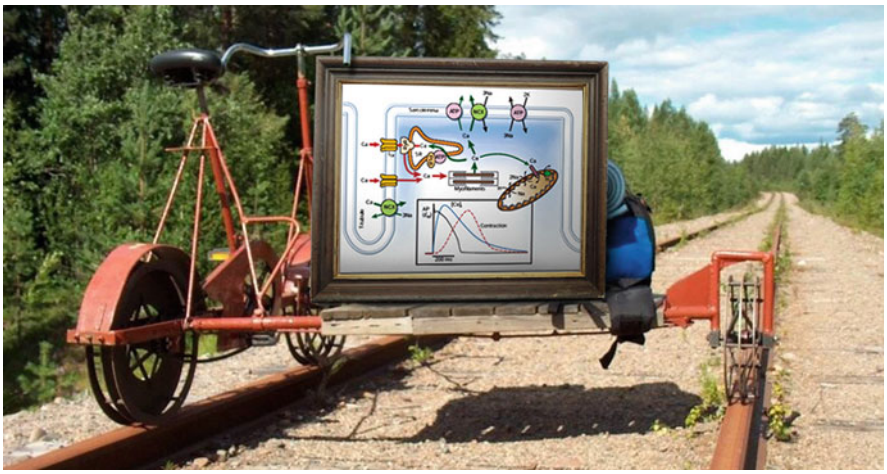

Fig. 4 "Of channels, bicycles and other – mostly public – transporters." Symposium for the author's retirement in July 2012 (Courtesy of one of the author's sons, Martin Ruegg)

I highly respected the thinking and the social ways of my grandmother and I am glad to be able to say a few words about her at this time.

After 20 years as a professor, I retired a year ago. I continue to supervise the research done in my laboratory and continue to teach at the Universities of Geneva and Basel. Also, I keep travelling on trains and bicycles daily – that was the theme of my retirement symposium (Fig. 4).

It is only now, reflecting on the past, that I realize how much I owe my grandfather, his son Hansjürgen, and my mother in coaching me to find my own path in life, both from a professional as well as a personal point of view.

Geneva, Switzerland U.T. Ruegg

Preface

Life and modern society cannot be imagined in the absence of natural and synthetic macromolecules. This volume of *Advances in Polymer Science* is dedicated to the 60th anniversary of the Nobel Prize received in 1953 by Professor Hermann Staudinger (23 March 1881–8 September 1965) "for his discoveries in the field of macromolecular chemistry."

Natural and synthetic macromolecules were known long before Staudinger. However, the status of macromolecular compounds is best reflected by the friendly advice received by Staudinger from Heinrich Otto Wieland, Nobel Prize laureate in 1927. "Dear colleague, abandon your idea of large molecules, organic molecules with molecular weights exceeding 5,000 do not exist. Purify your products such as rubber, they will crystallize and turn out to be low molecular weight compounds." Staudinger also wrote in his memoirs: "Those colleagues who were aware of my early publications in the field of low molecular weight chemistry asked me why I decided to quit these beautiful fields of research and why I devoted myself to such disgusting and ill-defined compounds such as rubber and synthetic polymers which at that time in view of their properties were referred to as grease chemistry ('Schmierenchemie')." The contributions of Hermann Staudinger to the field of macromolecular chemistry, for which he was awarded the Nobel Prize in 1953, are best illustrated by a discussion between the Emperor of Japan and Staudinger, that took place at the Imperial Palace of Japan on 17th of April 1957. His Majesty Emperor Hirohito of Japan asked, "Professor Staudinger, is this a concept that came into your mind to explain various phenomenological behaviors of a group of compounds or did you really prove their existence by rigorous scientific means?" The highly impressed Professor Staudinger answered, "It is this experimental demonstration of the existence of macromolecules which form the essential part of my work in the field of macromolecular science." Therefore, it was Staudinger who demonstrated the covalent rather than colloidal structure of macromolecules.

During the early days of the twentieth century, organic chemists were convinced that natural and synthetic macromolecules were colloidal aggregates of low molecular weight compounds. Staudinger obtained his Ph.D. at the age of 22, with Daniel Vorländer at the University of Halle in 1903. Subsequently, he held faculty

appointments at the University of Strasbourg (1903–1907) where in 1905 at the age of 24 he discovered ketenes. In 1907, he discovered the cycloaddition of ketenes with imines, still the most general and useful method for the synthesis of β-lactams. In the same year, he obtained his Habilitation in the laboratory of Johannes Thiele and moved to the University of Karlsruhe as a junior faculty where, in parallel with his work in the field of organic chemistry, he became interested in polymers. In 1912, at the age of 31, he moved to become full professor at ETH in Zürich and in the same year published his famous book on ketenes. In 1919, he discovered the reaction of azides with phosphines to produce phosphazenes and, subsequently, in the presence of water to yield primary amines. This reaction is known as the "Staudinger reaction" or "Staudinger reduction." In the year 2000, the Staudinger reaction was expanded and elaborated by Carolyn R. Bertozzi into the "Staudinger ligation," which has been labeled by some authors as "a gift to chemical biology." The three Staudinger reactions mentioned here are fundamental in organic chemistry and numerous publications discussing and debating their mechanisms, as well as reviews on them, are being published as I am writing this Preface. No references to them are listed here because most of them are cited in the publications of this special issue. A search of SciFinder will help those interested in finding recent publications on his work and on the very active current research on the Staudinger reactions.

In a publication from 1920, Staudinger coined the name "Makromoleküle" and in 1922 he generated the correct definition of "macromolecules," stating: "For such colloid particles, in which the molecule is identical with the primary particle, and in which the individual atoms of this colloid molecule are linked together by covalent bonds, we propose for better definition the name macromolecule."

In 1926, he moved to the University of Freiburg to replace his "friendly adviser" Heinrich Otto Wieland, who was to be awarded the Nobel Prize in 1927. In Freiburg, Staudinger focused all his research on macromolecules and stayed until he retired from the University in 1951 and as Director of his Institute in 1956. Staudinger received the first Nobel Prize for the field of macromolecular chemistry in 1953, the same year that Watson and Crick published their *Nature* paper on the double helix of the natural macromolecule DNA. In 1940, Staudinger started the Institute of Macromolecular Chemistry at the University of Freiburg, the first in this field in Europe, which received the name "Hermann Staudinger Haus" in 1981. On 19 April 1999, the American Chemical Society together with the German Chemical Society honored the Staudinger Laboratory in Freiburg as an "International Historic Landmark of Chemistry." Wallace H. Carothers, of the Experimental Station of Du Pont, and Hermann F. Mark, to name just two of many, were also influential in establishing the concept of polymers and macromolecules. However, it was the credibility and the reputation of Hermann Staudinger in the field of traditional organic chemistry who helped to set the future of "macromolecular chemistry" as the newest discipline of organic chemistry. If Hermann Staudinger had not started the field of macromolecular chemistry, he most probably would have received a

Nobel Prize for his work in organic chemistry earlier than he received it for macromolecular chemistry, just like his former student from Karlsruhe and Zürich, Leopold Ruzicka, who received it in 1939.

The photo shows on the left from back to front, Virgil Percec (a former postdoctoral student of Hans-Joachim Cantow in the Hermann Staudinger Haus), Helmut Ringsdorf (the last Ph.D. student of Staudinger), Hans-Joachim Cantow (a follower of Staudinger at the Hermann Staudinger Haus), and Hans-Rudolf Dicke (a former Ph.D. student of Walter Heitz). On the right are Martin Möller (a former Ph.D. and Habilitation student of Cantow) and Hubert Bader (a former Ph.D. student of Helmut Ringsdorf). The photo was taken during the IUPAC Symposium on Macromolecules in Amherst, MA, USA (12–16 July 1982). Four of these scientists have contributed to this special issue.

This special issue contains 38 scientific, personal and historic contributions from the fields of organic chemistry, supramolecular chemistry, macromolecular chemistry, bioorganic chemistry, computation science, biotechnology, and nanotechnology. This broad diversity of interests reflects Hermann Staudinger's diversity of scientific interests. From these many outstanding contributors I would like to mention Professor Urs T. Ruegg, one of Staudinger's grandchildren; Professor Helmut Ringsdorf, the last Ph.D. student of Hermann Staudinger; and Professor Jean-Marie Lehn (Nobel Prize in 1987), the inventor of the fields of "supramolecular chemistry" and "supramolecular polymers," the most recent new disciplines of organic chemistry. Many of these contributions provide not only great science but also fascinating stories about the life of Hermann Staudinger, the scientist who paved the way for the birth of macromolecular chemistry and the development of most significant breakthrough technologies of the twentieth century.

16 September 2013 Virgil Percec
Philadelphia, PA, USA

Contents

Adv Polym Sci (2013) 262: 1–38
DOI: 10.1007/12_2013_234

Published online: 20 October 2013

Synthesis and Self-Assembly of Well-Defined Block Copolypeptides via Controlled NCA Polymerization

Timothy J. Deming

Abstract This article summarizes advances in the synthesis of well-defined polypeptides and block copolypeptides. Traditional methods used to polymerize α-amino acid-*N*-carboxyanhydrides (NCAs) are described, and limitations in the utility of these systems for the preparation of polypeptides are discussed. Improved initiators and methods that allow polypeptide synthesis with good control over chain length, chain length distribution, and chain-end functionality are also discussed. Using these methods, block and random copolypeptides of controlled dimensions (including molecular weight, sequence, composition, and molecular weight distribution) can now be prepared. The ability of well-defined block copolypeptides to assemble into supramolecular copolypeptide micelles, copolypeptide vesicles, and copolypeptide hydrogels is described. Many of these assemblies have been found to possess unique properties that are derived from the amino acid building blocks and ordered conformations of the polypeptide segments.

Keywords Block copolypeptide · Living polymerization · *N*-Carboxyanhydride · Polypeptide · Self assembly

Contents

T.J. Deming (✉)
Department of Bioengineering, University of California, 5121 Engineering 5, Los Angeles, CA 90095, USA
e-mail: demingt@seas.ucla.edu

Abbreviations

AM	Activated monomer
ATRP	Atom transfer radical polymerization
Bn-Asp	β-Benzyl-L-aspartate
Bn-Glu	γ-Benzyl-L-glutamate
Bn-Tyr	*O*-Benzyl-L-tyrosine
bpy	2,2′-Bipyridine
CNS	Central nervous system
depe	Bis(diethylphosphino)ethane
DIC	Differential interference contrast
DLS	Dynamic light scattering
DMEM	Dulbecco's modified Eagle's medium
DOPA	*L*-Dihydroxyphenylalanine
GPC	Gel permeation chromatography
HMDS	Hexamethyldisilazane
LSCM	Laser scanning confocal microscopy
MALDI-MS	Matrix-assisted laser desorption ionization–mass spectroscopy
NACE	Non-aqueous capillary electrophoresis
NCA	α-Amino acid *N*-carboxyanhydride
NGF	Nerve growth factor
PA	Poly(L-alanine)
PBLA	Poly(β-benzyl-L-aspartate)
PBLG	Poly(γ-benzyl-L-glutamate)
PBS	Phosphate buffered saline
PDMS	Polydimethylsiloxane
PEG	Polyethylene glycol
PMDG	Poly(γ-methyl-D-glutamate)
PMLG	Poly(γ-methyl-L-glutamate)
PPG	Poly(*racemic*-propargylglycine)
PZLL	Poly(ε-carbobenzyloxy-L-lysine)
ROMP	Ring-opening metathesis polymerization
TEM	Transmission electron microscopy
TFA-Lys	ε-Trifluoroacetyl-L-lysine
TMS	Trimethylsilyl

Z-Lys	ε-Carbobenzyloxy-L-lysine
α-gal-C	α,D-Galactopyranosyl-L-cysteine
α-gal-C^{O2}	α,D-Galactopyranosyl-L-cysteine sulfone

1 Introduction

Biological systems produce proteins that possess the ability to self-assemble into complex, yet highly ordered structures [1]. These remarkable materials are polypeptide copolymers that derive their properties from precisely controlled sequences and compositions of their constituent amino acid monomers. There has been recent interest in developing synthetic routes for preparation of these natural polymers as well as de novo designed polypeptide sequences to make products for applications in medicine (artificial tissue, implants), biomineralization (resilient, lightweight, ordered inorganic composites), and analysis (biosensors, medical diagnostics) [2, 3].

To be successful in these applications, it is important that materials can self-assemble into precisely defined structures. Polypeptides have many advantages over conventional synthetic polymers because they are able to adopt stable ordered conformations [4]. Depending on the amino acid side chain substituents, polypeptides are able to adopt a multitude of conformationally stable regular secondary structures (helices, sheets, turns), tertiary structures (e.g., the β-strand–helix–β-strand unit found in β-barrels), and quaternary assemblies (e.g., collagen microfibrils) [4]. The synthesis of polypeptides that can assemble into non-natural structures is an attractive challenge for polymer chemists.

Synthetic peptide-based polymers are not new materials: homopolymers of polypeptides have been available for many decades; yet, partially due to their heterogeneous nature, they have only seen limited use as structural materials [5, 6]. In recent decades, improved methods in chemical synthesis have made possible the preparation of increasingly complex copolypeptide sequences of controlled molecular weight that display properties far superior to ill-defined homopolypeptides [7]. Furthermore, block copolypeptides, which combine different structural and functional peptide elements, have been prepared and begin to mimic some of the complexities of proteins [8]. These polymers are well suited for applications where polymer assembly and functional domains need to be at length scales ranging from nanometers to microns. These block copolypeptides are macroscopically homogeneous as solids, but dissimilarity between the block segments typically results in phase separation in aqueous media [9]. Synthesis of simple hydrophilic/hydrophobic diblock copolypeptides, when dispersed in water, allows formation of peptide-based micelles, vesicles, and hydrogels that are potentially useful in biomedical applications [10]. The regular secondary structures

obtainable within polypeptide segments provide opportunities for hierarchical self-assembly unobtainable with conventional block copolymers or small-molecule surfactants.

Upon examining the different methods for polypeptide synthesis, the limitations of these techniques for preparation of block copolypeptides become apparent. Conventional solid-phase peptide synthesis is neither economical nor practical for direct preparation of large polypeptides (>100 residues) due to unavoidable deletions and truncations that result from incomplete deprotection and coupling steps. The most economical and expedient process for synthesis of long polypeptide chains is the polymerization of α-amino acid-*N*-carboxyanhydrides (NCAs) Eq. (1) [11, 12]. This method involves the simplest reagents, and high molecular weight polymers can be prepared in both good yield and in large quantity with no detectable racemization at the chiral centers. The considerable variety of NCAs that have been synthesized (>200) allows exceptional diversity in the types of polypeptides that can be prepared [11, 12].

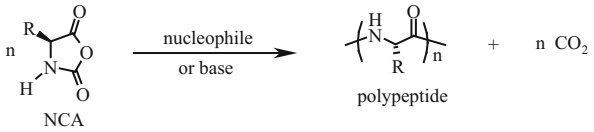

(1)

Since the late 1940s, NCA polymerizations have been the most common technique used for large scale preparation of high molecular weight polypeptides [13]. However, these materials have primarily been homopolymers, random copolymers, or graft copolymers that lack the sequence specificity and monodispersity of natural proteins. The level of control in NCA polymerizations has not been able to rival that attained in other synthetic polymerizations (e.g., vinyl addition polymerizations) where sophisticated polymer architectures have been prepared (e.g., stereospecific polymers and block copolymers) [14]. Attempts to prepare block copolypeptides and hybrid block copolymers using NCAs have traditionally resulted in polymers whose compositions did not match monomer feed compositions and that contained significant homopolymer contaminants [15–17]. Block copolymers could only be obtained in pure form by extensive fractionation steps, which significantly lowered the yield and efficiency of this method. The main factor limiting the potential of NCA polymerizations has been the presence of side reactions (chain termination and chain transfer) that restrict control over molecular weight, give broad molecular weight distributions, and prohibit formation of well-defined block copolymers [18, 19]. Recent progress in elimination of these side reactions has been a major breakthrough for the polypeptide materials field. This review summarizes developments that enable the synthesis of well-defined homo- and block copolypeptides from controlled and living polymerization of NCA monomers. Examples of structures formed by self-assembly of block copolypeptides in solution are also described.

2 Polypeptide Synthesis Using NCAs

2.1 Conventional Methods

NCA polymerizations have been initiated using many different nucleophiles and bases, the most common being primary amines and alkoxide anions [11, 12]. Primary amines, being more nucleophilic than basic, are good general initiators for polymerization of NCA monomers that provide relatively slow polymerization and are well understood. Tertiary amines, alkoxides, and other initiators that are more basic than nucleophilic have found use because they are, in some cases, able to prepare polymers of very high molecular weight where primary amine initiators cannot. Strong base initiators generally promote much faster NCA polymerization compared to primary amine initiators, yet the fine mechanistic details of these systems are poorly understood. Optimal polymerization conditions have often been determined empirically for each NCA and thus there have been no universal initiators or conditions by which to prepare high polymers from any monomer. This is in part due to the different properties (e.g., solubility) of individual NCAs and their polymers but is also strongly related to the side reactions that occur during polymerization.

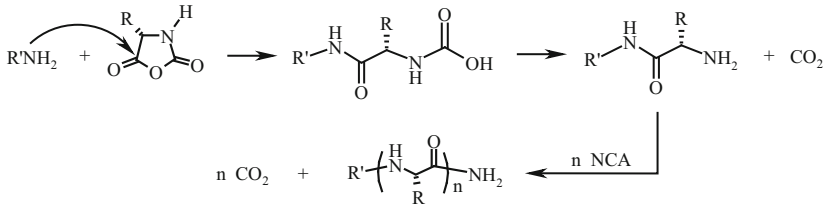

(2)

The most likely pathways of NCA polymerization are the "amine" and "activated monomer" (AM) mechanisms [11, 12]. The amine mechanism is a nucleophilic ring-opening chain growth process where the polymer would grow linearly with monomer conversion if side reactions were absent Eq. (2). On the other hand, the AM mechanism is initiated by deprotonation of an NCA, which then becomes the nucleophile that initiates chain growth Eq. (3). It is important to note that a polymerization can switch back and forth between the amine and AM mechanisms many times: a propagation step for one mechanism is a side reaction for the other, and vice versa. It is because of these side reactions that block copolypeptides and hybrid block copolymers prepared from NCAs using amine initiators under conventional conditions (i.e., 20°C, 1 atm) have structures different than predicted by monomer feed compositions and most probably have considerable homopolymer contamination. These side reactions also prevent control of chain-end functionality, which is desirable for many applications.

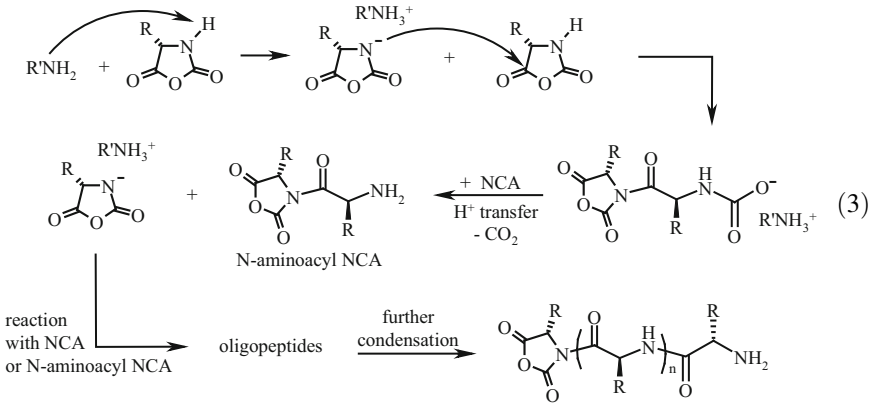

(3)

One inherent problem in conventional NCA polymerizations is that the choice of initiator provides no control over the reactivity of the growing polymer chain end during the course of the polymerization. Once an initiator reacts with a NCA monomer, it is no longer involved in the polymerization and the resulting primary amine, carbamate, or NCA anion endgroup is free to undergo a variety of undesired side reactions. Another problem is one of monomer purity. Although most NCAs are crystalline compounds, they typically contain minute traces of acid, acid chlorides, or isocyanates that can quench propagating chains. The presence of other adventitious impurities, such as water, can cause problems by acting as chain-transfer agents or even as catalysts for side reactions. The high moisture, nucleophile, and base sensitivity of NCAs can make their purification challenging, especially for NCAs that are not easily crystallized. Overall, the abundance of potential side reactions present in reaction media make it difficult to achieve a living polymerization system for NCAs where only chain propagation occurs.

2.2 Initiators for Transition Metal Catalysis

A successful strategy for propagation rate enhancement and elimination of side reactions in NCA polymerizations has been the use of transition metal complexes as catalysts for addition of NCA monomers to polypeptide chain ends. The use of transition metals to control reactivity has been proven in organic and polymer synthesis as a means to increase reaction selectivity, efficiency, and rate [20]. Using this approach, a significant advance in the development of a general method for living NCA polymerization was realized in 1997. Highly effective zerovalent nickel and cobalt initiators [i.e., bpyNi(COD) and $(PMe_3)_4Co$] [21–23] were developed by Deming that allow the living polymerization of many different NCAs into high molecular weight polypeptides via an unprecedented activation of the NCAs to generate covalent metal-containing propagating species. These propagating species were also found to be highly active for NCA addition and increased

polymerization rates more than an order of magnitude compared to amine-initiated polymerizations at 20°C. The metal ions were also found to be conveniently removed from the polymers by simple precipitation or dialysis of the samples after polymerization.

Mechanistic studies on the initiation process showed that both nickel and cobalt complexes react identically with NCA monomers to form metallacyclic complexes by oxidative addition across the anhydride bonds of NCAs [21–23]. These oxidative-addition reactions were followed by addition of a second NCA monomer to yield complexes identified as six-membered amido-alkyl metallacycles Eq. (4). These intermediates were found to further contract to five-membered amido-amidate metallacycles upon reaction with additional NCA monomers. This ring contraction is thought to occur via migration of an amide proton to the metal-bound carbon, which liberates the chain end from the metal Eq. (5) [24]. The resulting amido-amidate complexes were thus proposed as the active polymerization intermediates. Propagation through the amido-amidate metallacycle was envisioned to occur by initial attack of the nucleophilic amido group on the electrophilic C_5 carbonyl of an NCA monomer Eq. (6). This reaction results in a large metallacycle that can contract by elimination of CO_2. Proton transfer from the free amide to the tethered amidate group further contracts the ring to regenerate the amido-amidate propagating species, while in turn liberating the end of the polymer chain.

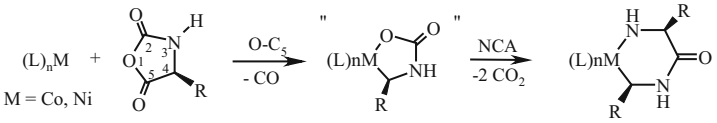

(4)

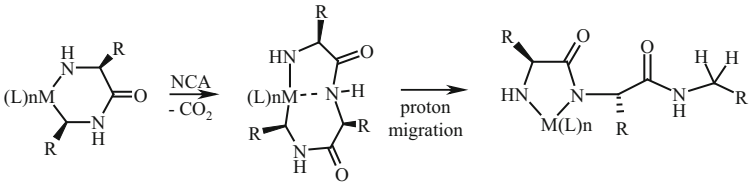

(5)

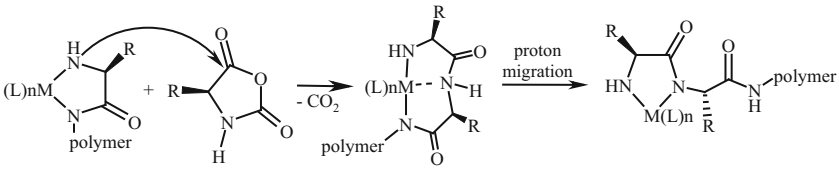

(6)

In this manner, the metal is able to migrate along the growing polymer chain, while being held by a robust chelate at the active end. The formation of these chelating metallacyclic intermediates appears to be a general requirement for obtaining living NCA polymerizations using transition metal initiators. These cobalt and nickel complexes are able to produce polypeptides with narrow chain

length distributions ($M_w/M_n < 1.20$) and controlled molecular weights ($500 < M_n < 500{,}000$) [25]. These polymerizations can be conducted in a variety of solvents (e.g., THF, DMF, EtOAc, dioxane, MeCN, DMAc, nitrobenzene) and over a broad range of temperatures (i.e., 10–100°C) with no loss of polymerization control and with dramatic increases in polymerization rate as temperature is increased. By addition of different NCA monomers, the preparation of block copolypeptides of defined sequence and composition is feasible [7, 26].

This polymerization system is general, and gives controlled polymerization of a wide range of NCA monomers as pure enantiomers (D or L configuration) or as racemic mixtures. In addition to commonly used NCA monomers, such as protected lysine, glutamate, aspartate, and arginine, many hydrophobic amino acid monomers (e.g., leucine, valine, alanine, isoleucine, phenylalanine) as well as other reactive amino acids (e.g., methionine, cysteine, tyrosine, DOPA) have been successfully polymerized in a controlled manner using cobalt and nickel initiators. There is much current interest in functional and reactive polypeptides, and NCAs bearing more complex functionality have also been polymerized using this methodology. The earliest examples were controlled polymerizations of oligoethylene glycol-functionalized lysines [27] and serines [28], which were later followed by polymerization of lysine-based NCAs containing side-chain attached liquid crystal-forming mesogens [29]. Thermoresponsive oligoethylene glycol-modified glutamate NCAs have also been reported by Li and coworkers to polymerize effectively using a nickel initiator [30].

Recently, the Deming laboratory has used cobalt initiators to polymerize sugar-containing NCAs based on lysine [31] and cysteine [32], which yield fully glycosylated, high molecular weight glycopolypeptides that can adopt different chain conformations. Li and coworkers have also used a nickel initiator to polymerize lysine-based NCAs that contain side-chain activated alkyl bromide functionalities, which are useful for growth of vinyl polymers off the polypeptide side chains using atom transfer radical polymerization (ATRP) [33]. It is notable that the active metal centers do not react with the alkyl halide functionalities, which could be problematic if amine initiators were used instead. A key challenge in these recent examples was purification of the highly functional NCAs, which could not be purified by recrystallization. To solve this problem, Kramer and Deming developed an anhydrous flash column chromatography method for NCA purification that enables one to obtain a wide range of difficult-to-crystallize NCAs in suitable purity for controlled polymerization [34], and has made possible the preparation of many new highly functional NCAs [35].

One potential limitation of using zerovalent metal initiators is in the preparation of chain-end functionalized polypeptides because the active propagating species are generated in situ and the C-terminal end of the polypeptide is derived from the first NCA monomer. Consequently, this method does not allow easy incorporation of functionality (e.g., polymer or small molecule) to the carboxyl chain end. For this reason, Deming and coworkers pursued alternative methods for direct synthesis of the amido-amidate metallacycle propagating species and developed allyloxycarbonylaminoamides as universal precursors to amido-amidate

nickelacycles. These simple amino acid derivatives undergo tandem oxidative-additions to nickel(0) to give active NCA polymerization initiators Eq. (7) [36]. These complexes were found to initiate polymerization of NCAs, yielding polypeptides with defined molecular weights, narrow molecular weight distributions, and with quantitative incorporation of the initiating ligand as a C-terminal endgroup. This chemistry provides a facile means to incorporate diverse molecules such as polymers, peptides, oligosaccharides, or other ligands onto the chain ends of polypeptides via a robust amide linkage, and was further elaborated by Menzel's group to grow polypeptides off polystyrene particles [37]. Recently, this methodology was used by Patton and coworkers to attach nickel initiators to silicon oxide substrates and then grow lysine–cysteine and glutamate–cysteine block copolypeptides from the surfaces [38].

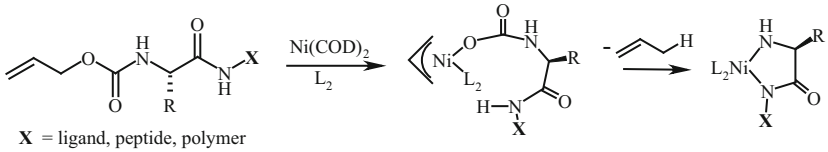

(7)

Allyloxycarbonylaminoamide precursors to NCA polymerization initiators were also recently incorporated into the side chains of lysine-based NCAs by Deming's laboratory [39]. These NCAs underwent controlled polymerization using a cobalt initiator to give the linear polypeptide, with no reaction of the side-chain functionality with the active propagating species or metal initiator precursors. After complete consumption of NCA monomer, and without isolation of the polypeptide, the allyloxycarbonylaminoamide side chains were then activated by addition of stoichiometric zerovalent nickel, which generated active nickelacycle initiators in each polypeptide side chain Eq. (8). Addition of a second batch of NCA monomer led to growth of well-defined cylindrical copolypeptide brushes in a simple, tandem catalysis process that required no intermediate deprotection, polypeptide isolation, or purification steps [39].

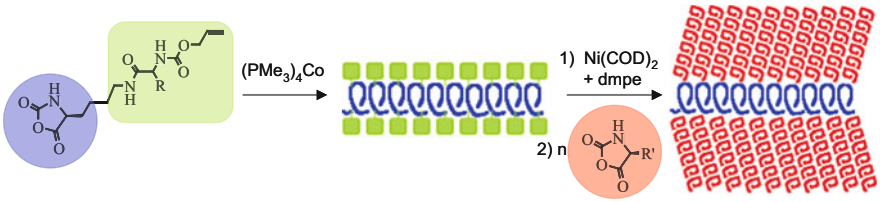

(8)

In related work, Deming's laboratory also developed a means to functionalize the N-terminal ends of living polypeptide chains using electrophilic reagents. When a macromolecular electrophile is used, the resulting product is a polypeptide hybrid block copolymer. It is well known in NCA polymerizations that electrophiles, such as isocyanates, act as chain-terminating agents by reaction with the propagating amine chain ends [11]. Deming and coworkers reported that the reactive living

nickelacycle polypeptide chain ends could be quantitatively capped by reaction with excess isocyanate, isothiocyanate, or acid chloride [40]. Using this chemistry, they prepared isocyanate end-capped poly(ethylene glycol), PEG, and reacted this, in excess, with living poly(γ-benzyl-L-glutamate), PBLG, to obtain PBLG-*b*-PEG diblock copolymers Eq. (9).

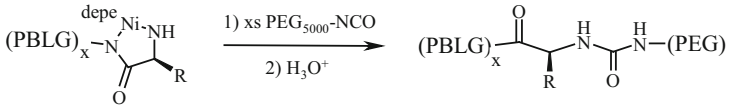

(9)

By knowing the active intermediates in these metal-catalyzed polymerizations, Deming's laboratory was also able to use chiral donor ligands to prepare optically active nickel initiators for the enantioasymmetric polymerization of NCAs [41]. Since polypeptides are chiral polymers, the ability to control stereochemistry during polymerization is potentially important. This is especially true because the self-assembly and properties of polypeptides are critically dependent on the stereochemistry of the amino acid components. Due to constraints imposed by the initial oxidative-addition reactions and the stability of zerovalent cobalt and nickel complexes, only a limited pool of chiral ligands could be used. For example, common chiral aryl-substituted bisphoshines were completely ineffective in promoting oxidative-additions of NCAs with nickel(0). Using optically active 2-pyridinyl oxazoline ligands that were mixed with bis(1,5-cyclooctadiene)nickel in THF, chiral nickel complexes formed that were found to selectively polymerize one enantiomer of an NCA over the other [41]. The highest selectivity was observed with the nickel complex of (*S*)-4-*tert*-butyl-2-pyridinyl oxazoline, which gave a ratio of enantiomer polymerization rate constants (k_D/k_L) of 5.2(0.1) Eq. (10). This initiator also gave an 17% enantiomeric excess of the D-antipode in the copolymer formed at 16 % conversion in the polymerization of racemic NCA. It was found that subtle modification of this ligand by incorporation of additional substituents had a substantial impact on initiator selectivities. These results were a first step towards the ability to readily synthesize optically pure polypeptides from inexpensive racemic monomer pools. The main limitation of this system, however, is the fluxional coordination geometry around nickel(II), which hinders the development of a rigid, chiral environment at the metal center.

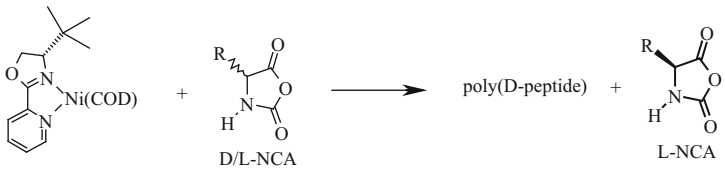

(10)

Subsequently, Deming and coworkers identified other initiating systems based on amido-sulfonamide metallacycles prepared via deprotonation of the corresponding amine complexes. Deming studied a ruthenium(II) amido-sulfonamide complex,

which although not an amido-amidate metallacycle, was recognized to possess all the required features for controlled NCA polymerization Eq. (11) [42]. This complex contains a nucleophilic alkyl amido group, stabilized by a rigid chelate, and a proton-accepting sulfonamide group on the other end of the metallacycle that allows the chain end to migrate off the metal. This ruthenium complex, and the corresponding isoelectronic Cp*iridium(III) (Cp* = C_5Me_5) complex, were found to initiate living polymerizations of NCAs [42], which shows that effective initiators can also be prepared with second and third row transition metals [43]. Furthermore, these initiators were found to give much higher enantiomeric selectivities, as well as polymerization activities, in polymerizations of racemic NCAs compared to the nickel systems studied earlier. This work was elaborated by Peng and Lin, who prepared similar amido-sulfonamide metallacycles using platinum(II) and found that these complexes give controlled polymerization of N_ε-carbobenzyloxy-L-lysine NCA, Z-Lys NCA Eq. (11) [44]. Overall, it can be seen that the use of transition metal-initiated NCA polymerization allows formation of well-defined copolymer architectures that rival those prepared using any polymerization system.

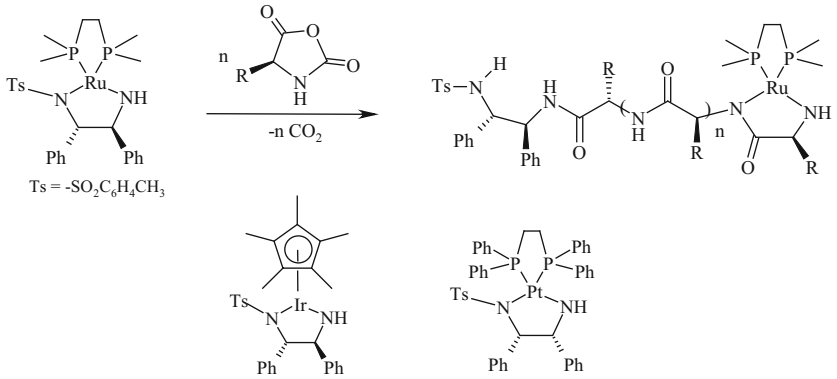

(11)

2.3 Recent Developments Using Amine Initiators

In the past decade, a number of new approaches have been reported to give controlled NCA polymerizations. These approaches share a common theme in that they are all improvements on the use of conventional primary amine polymerization initiators. This approach is attractive because primary amines are readily available and because the initiator does not need to be removed from the reaction after polymerization. In fact, if the polymerization proceeds without any chain-breaking reactions, the amine initiator becomes the C-terminal polypeptide endgroup. In this manner, there is potential to form chain-end functionalized polypeptides or even hybrid block copolymers if the amine is a macroinitiator. The challenge in this approach is to overcome the numerous side reactions of these systems without the luxury of a large number of experimental parameters to adjust.

In 2004, the group of Hadjichristidis reported the primary amine-initiated polymerization of NCAs under high vacuum conditions [45]. The strategy here was to determine if a reduced level of impurities in the reaction mixture would lead to fewer polymerization side reactions. Unlike the vinyl monomers usually polymerized under high vacuum conditions, NCAs cannot be purified by distillation. Consequently, it is unclear if NCAs can be obtained in higher purity by high vacuum recrystallization than by recrystallization under a rigorous inert atmosphere. However, the high vacuum method does allow for better purification of polymerization solvents and the *n*-hexylamine initiator. It was found that polymerizations of γ-benzyl-L-glutamate NCA, Bn-Glu NCA, and Z-Lys NCA under high vacuum in DMF solvent displayed all the characteristics of a living polymerization system [45]. Polypeptides could be prepared with control over chain length; chain length distributions were narrow and block copolypeptides were prepared. This method has been used by Iatrou and coworkers to prepare a number of different block copolypeptides, primarily PBLG segments connected to polymers of lysine, leucine, tryosine, and the imino acid proline, and their microphase-separated morphologies have been studied in the bulk state [46, 47].

For this method, the authors concluded that the side reactions normally observed in amine-initiated NCA polymerizations are simply a consequence of impurities. Because the main side reactions in NCA polymerizations do not involve reaction with adventitious impurities such as water, but instead reactions with monomer, solvent, or polymer (i.e., termination by reaction of the amine-end with an ester side chain, attack of DMF by the amine-end, or chain transfer to monomer) [11], it appears that removal of water or other reaction components is able to inhibit these side reactions. A likely explanation for the polymerization control observed under high vacuum is that CO_2 acts to promote side reactions of growing chains with monomer, polymer, or solvent, and its removal from the reaction medium under vacuum inhibits these reactions and promotes controlled polymerization. A number of early and recent studies support this role of CO_2 as being detrimental to amine-initiated NCA polymerizations, where for some NCAs it is able to decrease chain propagation rate by reversibly forming a carbamate with the amine endgroup and may also catalyze side reactions [48, 49]. Thus, it is reasonable to speculate (vide infra) that removal of CO_2 from NCA polymerizations under high vacuum is the dominant factor in enabling controlled chain growth in these systems. Recently, in polymerizations of *O*-benzyl-L-tyrosine NCA, Bn-Tyr NCA, in DMF, it was determined that although most side reactions are insignificant in the high-vacuum polymerization, some termination of chains by reaction with DMF solvent does occur [50].

Further insights into amine-initiated NCA polymerizations were also reported in 2004 by the group of Giani and coworkers [51]. This group studied the polymerization of ε-trifluoroacetyl-L-lysine NCA, TFA-Lys NCA, in DMF using *n*-hexylamine initiator at different temperatures. In contrast to the high vacuum work, the solvent and initiator were purified using conventional methods and the polymerizations were conducted under a nitrogen atmosphere on a Schlenk line. After complete consumption of NCA monomer, the crude polymerization mixtures were analyzed by GPC and non-aqueous capillary electrophoresis (NACE).

A unique feature of this work was the use of NACE to separate and quantify the amount of polymers with different chain ends, which corresponded to living chains (amine endgroups) and "dead" chains [carboxylate and formyl endgroups from reaction with NCA anions and DMF solvent, respectively, Eqs. (12) and (13)]. Not surprisingly, at 20°C, the polymer products consisted of 78% dead chains and only 22% living chains, which illustrates the abundance of side reactions in these polymerizations under conventional conditions.

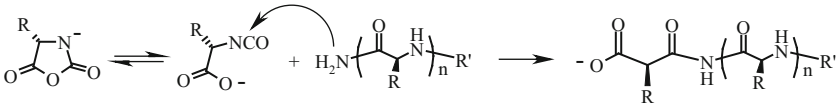

(12)

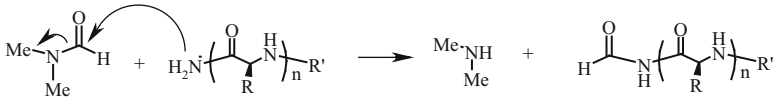

(13)

An intriguing result was found for polymerizations conducted at 0°C, where 99% of the chains had living amine chain ends and only 1% were found to be dead chains. To verify that these were truly living polymerizations, additional NCA monomer was added to these chains at 0°C and resulted in increased molecular weight and no increase in the amount of dead chains. Although TFA-Lys NCA was the only monomer studied, this work showed that controlled NCA polymerizations can be obtained by lowering the temperature. The effect of temperature is not unusual, as similar trends can be found in cationic and anionic vinyl polymerizations [52]. At elevated temperature, the side reactions have activation barriers similar to those for chain propagation. When the temperature is lowered, the activation barrier for chain propagation becomes lower than that of the side reactions and chain propagation dominates kinetically. A key limitation of this method is that these polymerizations are very slow at 0°C, often requiring numerous days to obtain polypeptide chains of modest length. A remarkable feature of this system is that increased impurity/byproduct (i.e., CO_2) levels, as compared to the high vacuum method, did not result in side reactions at low temperature. This result shows that even with CO_2 present, side reactions in amine-initiated NCA polymerzations can be made kinetically insignificant at low temperature.

Since these original studies, a number of groups have used and studied low temperature NCA polymerzations in greater detail. Shao's laboratory reported the synthesis of block copolypeptides of PBLG with segments of alanine, leucine, and phenylalanine at 0°C. Using MALDI-MS analysis, they found that greater than 90% of the PBLG chains were active for the second monomer addition [53]. Schouten and coworkers also reported the controlled polymerization of *tert*-butyl-L-glutamate NCA at 0°C and use of these chains to prepare block copolypeptides with other glutamate ester NCAs [54]. Perhaps the most comprehensive studies of amine-initiated NCA polymerizations at low temperature and/or under vacuum were performed by Heise and coworkers [55]. They examined ten different NCA

monomers and found, using MALDI-MS analysis of endgroups, that most of these, including monomer mixtures for preparation of statistical copolymers, show fewer side reactions at 0°C than at elevated temperatures. In a follow-up study, they combined low temperature polymerizatons with those run under low pressure in order to identify optimal polymerization conditions [49]. Surprisingly, only α-helical-favoring monomers (Bn-Glu, alanine, Z-Lys) showed rate accelerations upon reduction in pressure (and consequent CO_2 removal), whereas non-helicogenic monomers (β-benzyl-L-aspartate, *O*-benzyl-L-serine, *O*-benzyl-L-threonine) were not affected by reaction pressure. Thus, the use of high vacuum or other methods for CO_2 removal to obtain controlled NCA polymerization seems to be highly monomer dependent. Also, the enhancements in polymerization rates seen by removing CO_2 at 20°C were found to be minimal at 0°C, thus indicating that there is no advantage in conducting an NCA polymerization under reduced pressure at 0°C. From this study, it was concluded that helicogenic NCA monomers could be polymerized in a controlled manner at 20°C if CO_2 was removed from the reaction mixture, whereas non-helicogenic monomers should be polymerized at 0°C for optimal control over polymerization [49]. This strategy was validated by preparation of a tetrablock copolypeptide of PBLG-PA-PZLL-PBLA.

A different innovative approach to controlling amine-initiated NCA polymerizations was reported in 2003 by Schlaad and coworkers [56]. Their strategy was to avoid formation of NCA anions, which cause significant chain termination after rearranging to isocyanocarboxylates [11, 12], through use of primary amine hydrochloride salts as initiators. The reactivity of amine hydrochlorides with NCAs was first explored by the group of Knobler, who found that amine hydrochlorides can react with NCAs to give single NCA addition products [57, 58]. Use of the hydrochloride salt takes advantage of its diminished reactivity as a nucleophile compared to the parent amine, which effectively halts the reaction after a single NCA insertion by formation of an inert amine hydrochloride in the product. The reactivity of the hydrochloride presumably arises from formation of a small amount of free amine by reversible dissociation of HCl Eq. (14). This equilibrium, which lies heavily toward the dormant amine hydrochloride species, allows for only a very short lifetime of reactive amine species. Consequently, as soon as a free amine reacts with an NCA, the resulting amine endgroup on the product is immediately protonated and prevented from further reaction. The acidic conditions also assist elimination of CO_2 from the reactive intermediate and, more importantly, suppress formation of unwanted NCA anions.

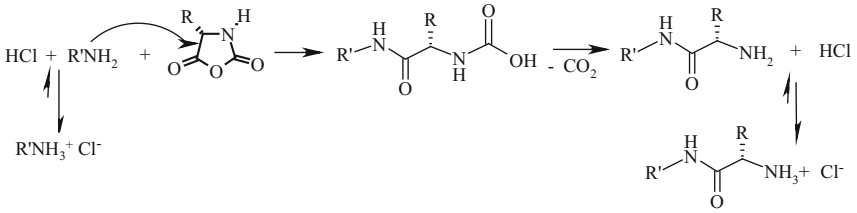

(14)

To obtain controlled polymerization, and not just single NCA addition reactions, Schlaad's group increased the reaction temperature (from 40°C to 80°C), which was known from Knobler's work to increase the equilibrium concentration of free amine, as well as increase the exchange rate between amine and amine hydrochloride [57, 58]. Using primary amine hydrochloride end-capped polystyrene macroinitiators to polymerize Z-Lys NCA in DMF, Schlaad's group obtained polypeptide hybrid copolymers in 70–80% yield after 3 days at elevated temperature. Although these polymerizations are slow compared to amine-initiated polymerizations, the resulting polypeptide segments were well defined with very narrow chain length distributions ($M_w/M_n < 1.03$). These distributions were much narrower than those obtained using the free amine macroinitiator, which argues for diminished side reactions in the polypeptide synthesis. The molecular weights of the resulting polypeptide segments were found to be about 20–30% higher than would be expected from the monomer to initiator ratios. This result was attributed to termination of some fraction of initiator species by traces of impurities in the NCA monomers, although the presence of unreacted polystyrene chains was not reported. Recently, this methodology was extended to the preparation of new hybrid copolymers of poly(Bn-Glu) from poly(2-isopropyl-2-oxazoline) [59] and PEG-amine hydrochloride [60] macroinitiators.

The use of amine hydrochloride salts as initiators for controlled NCA polymerizations shows tremendous promise. The concept of fast, reversible deactivation of a reactive species to obtain controlled polymerization is a proven concept in polymer chemistry, and this system can be compared to the persistent radical effect employed in all controlled radical polymerization strategies [61]. Like those systems, success of this method requires a carefully controlled matching of the polymer chain propagation rate constant, the amine/amine hydrochloride equilibrium constant, and the forward and reverse exchange rate constants between amine and amine hydrochloride salt. This means that it is likely that reaction conditions (e.g., temperature, halide counterion, solvent) will need to be optimized to obtain controlled polymerization for each different NCA monomer, as is the case for most vinyl monomers in controlled radical polymerizations. Within these constraints, it is possible that controlled NCA homopolymerizations utilizing simple amine hydrochloride initiators can be obtained; yet this method may not be advantageous for preparation of block copolypeptides due to the need for monomer-specific optimization.

Another interesting approach to obtaining controlled NCA polymerization using silylated amines was reported in 2007 by Lu and Cheng. Hexamethyldisilazane (HMDS) was used to initiate polymerizations of either Z-Lys NCA or Bn-Glu NCA in DMF at ambient temperature and was found to give well-defined polypeptides of controlled chain length and low polydispersity in high yield [62]. Addition of a second batch of monomer to completed chains afforded block copolymers. Chain growth in this system does not appear to show any of the common side reactions found in amine-initiated NCA polymerization, which is attributed to the unique properties of the *N*-trimethylsilyl (TMS) groups. The HMDS is proposed to transfer a TMS group to the NCA, followed by addition of the silylamine to the resulting

intermediate Eq. (15). This process yields a ring-opened monomer with a TMS-carbamate active endgroup on the growing chain, similar to processes that occur in group transfer polymerization of vinyl monomers [63]. The TMS-carbamate mediates NCA addition in a way that suppresses side reactions. This system has an advantage in that it proceeds at much higher rates (ca. 12–24 h at ambient temperature to obtain DP = 100) compared to low temperature or amine hydrochloride-initiated polymerizations, yet still is slower than transition metal-initiated systems (ca. 30–60 min at ambient temperature).

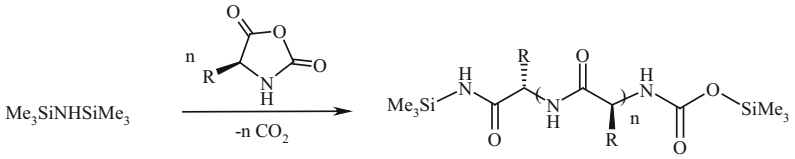

(15)

Cheng and coworkers elaborated this method by showing that a variety of TMS amines can be used as initiators in place of HMDS to give controlled polymerizations by a similar process. These initiators also provide defined C-terminal endgroups on the polypeptides from the TMS amine initiator Eq. (16) [64]. This chain-end functionalization was found to work well for both Z-Lys NCA and Bn-Glu NCA as well as for block copolymers of these monomers. The TMS-carbamate active chain ends are highly moisture sensitive, yet this is not much of an issue because NCAs themselves are moisture sensitive and must be polymerized in an anhydrous environment. This methodology was used to prepare polypeptide-poly(norbornene diimide) brush copolymers via both "grafting from" and "grafting through" approaches [65]. In the grafting from approach, poly (norbornenes) bearing TMS amine functionalities were used as macroinitiators to grow polypeptide brush segments. In the grafting through approach, TMS amine-functionalized norbornene monomers were used to prepare end-functionalized polypeptide segments that were then linked by ROMP of the norbornene endgroups.

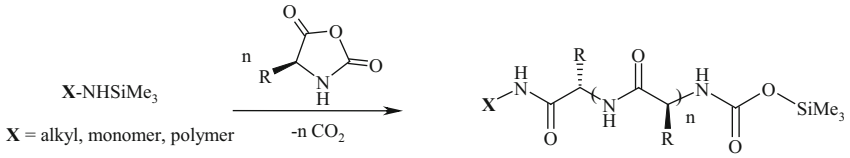

(16)

3 Block Copolypeptide Synthesis and Assembly

For assembly into novel supramolecular structures, block copolypeptides are required that have structural domains (i.e., amino acid sequences) whose size and composition can be precisely adjusted. Such materials have historically proven

elusive using conventional techniques. NCA polymerizations initiated by strong bases are very fast. These polymerizations are poorly understood and well-defined block copolymers cannot be prepared. Primary amine-initiated NCA polymerizations are also not free of side reactions. Even after fractionation of the crude preparations, the resulting polypeptides are relatively ill-defined, which may complicate unequivocal evaluation of their properties and potential applications. Nevertheless, there are many reports on the preparation of block copolypeptides using conventional primary amine initiators [66]. Examples include many hydrophilic–hydrophobic and hydrophilic–hydrophobic–hydrophilic di- and triblock copolypeptides (where hydrophilic residues were glutamate and lysine, and hydrophobic residues were leucine [67, 68], valine [69], isoleucine [16], phenylalanine [15], and alanine [70]) prepared to study conformations of the hydrophobic domain in aqueous solution. More recently, Cameron and coworkers reported the synthesis of novel (α-helix)-*b*-(β-sheet) block copolypeptides using amine initiation [71]. These polymers were reported to have polydispersities ranging from 1.47 to 1.60.

The majority of amine-initiated block copolypeptides were often subjected to only limited characterization (e.g., amino acid compositional analysis) and, as such, their structures and the presence of homopolymer contaminants were not conclusively determined. Some copolymers, which had been subjected to chromatography, showed polymodal molecular weight distributions containing substantial high and low molecular weight fractions [15]. The compositions of these copolymers were found to be different from the initial monomer feed compositions and varied widely for different molecular weight fractions. It appears that most, if not all, block copolypeptides prepared using amine initiators under conventional conditions have structures different to those than predicted by monomer feed compositions and probably have considerable homopolymer contamination due to the side reactions described above.

Block copolypeptides prepared via transition metal-mediated NCA polymerization are well defined, with the sequence and composition of block segments controlled by the order and quantity of monomer added to initiating species, respectively. These block copolypeptides can be prepared with the same level of control found in anionic and controlled radical polymerizations of vinyl monomers, which greatly expands the potential of polypeptide materials. The unique chemistry of NCAs allows these monomers to be polymerized in any order, which is a challenge in most vinyl copolymerizations, and the robust chain ends allow the preparation of copolypeptides with many block domains (e.g., >2). The robust nature of transition metal initiation was shown by the linear, stepwise synthesis of triblock and pentablock copolypeptides Eq. (17) [72, 73]. The N-TMS amine initiators and amine initiators used under high vacuum and/or low temperature conditions have recently also been used to prepare well-defined block copolypeptides [45, 63]. The self-assembly of block copolypeptides has also been under extensive investigation in recent years, typically in aqueous media to mimic biological conditions. In the following sections, the assembly of block copolypeptides into different types of supramolecular assemblies is described.

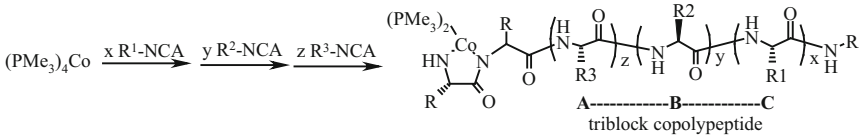

(17)

3.1 Copolypeptide Nanoparticles with Hydrophobic Cores

Micellar nanoparticles and emulsion droplets are widely used to disperse materials for a range of food [74], cosmetic [75], and pharmaceutical [76] applications. These nanoscale assemblies are composed of amphiphilic molecules that self-assemble in water, and include the addition of an oil phase in the case of emulsions [76]. Block copolymers make up a large class of micelle-forming molecules [75, 77, 78] and include some that contain polypeptide segments, which can be enzymatically degraded to natural metabolites and possess ordered conformations not found in conventional polymers. Numerous "rod–coil" micelles have been prepared using α-helical hydrophobic polypeptides conjugated to hydrophilic polyethylene glycol (PEG) segments, such as PEG-*b*-PBLG [79, 80] and PEG-*b*-PBLA [81]. β-Strand polypeptide segments have also been used to facilitate interchain interactions and increase micelle stability [82]. By contrast, micelles prepared solely from polypeptide segments have not been reported until recently. One key reason is the structure inherent in peptides, which typically favors extended conformations and strong interchain interactions that usually prevent formation of a disordered spherical micelle core.

The Deming laboratory was able to prepare block copolypeptide micelles by incorporating disordered racemic hydrophobic segments, which allow packing of the chains into spherical micelles (Fig. 1). They synthesized nonionic, block copolypeptides, poly{N_ε-2-[2-(2-methoxyethoxy)ethoxy]acetyl-L-lysine}-*block*-poly(*racemic*-leucine), or $K^P_x(rac\text{-L})_y$, where x and y are the number of residues in each segment. These copolypeptides have a "reversed" rod–coil structure composed of a hydrophilic, rod-like, α-helical segment attached to a disordered, racemic hydrophobic segment. The self assembly of these block copolypeptides in water was studied, and their compositions were optimized to identify a sample, $K^P_{100}(rac\text{-L})_{10}$, which was able to form well-defined micelles that are very stable against dilution, high temperatures, and various media [83]. Micelle structure was determined using a combination of transmission electron microscopy (TEM) and dynamic light scattering (DLS) measurements, by which the authors observed formation of well-defined, stable spherical copolypeptide micelles approximately 80 nm in diameter (Fig. 1). Furthermore, they were able to encapsulate the anticancer drug camptothecin into the micelles with an efficiency of 76%, showing the potential of these carriers for drug delivery applications.

In a related project, the Deming laboratory also investigated the use of diblock copolypeptides containing racemic hydrophobic segments as surfactants for

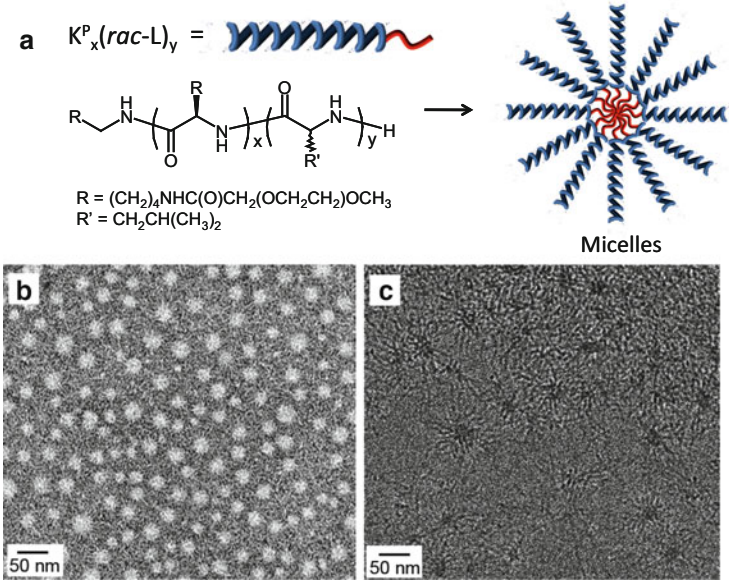

Fig. 1 (**a**) Scheme showing $K^P_x(rac\text{-}L)_y$ block copolypeptides and self-assembly into micelles. (**b**) Negative stain TEM image showing nanostructure of $K^P_{100}(rac\text{-}L)_{10}$ micelles. (**c**) Cryogenic TEM image of a 0.50% (w/v) aqueous suspension of $K^P_{100}(rac\text{-}L)_{10}$. Adapted from [83]

stabilization of nanoemulsion droplets [84]. In these studies, the racemic hydrophobic segment provides better miscibility with the oil phase compared to enantiomerically pure hydrophobic polypeptide segments, and gives much higher surface activity. The resulting emulsions were very stable, and were obtained with nanoscale (10–100 nm) diameters using microfluidic homogenization, making them attractive for delivery of hydrophobic cargos. Remarkably, it was found that the copolypeptide amphiphiles also promote formation of very stable double emulsion droplets that for the first time could be prepared with outer droplet diameters down to 10 nm [84]. The block copolypeptide surfactants designed have the general structure poly(L-lysine · HBr)$_x$-*b*-poly(racemic-leucine)$_y$, $K_x(rac\text{-}L)_y$, where x ranged from 20 to 100, and y ranged from 5 to 30 residues. Diblock copolypeptides were screened for emulsification activity by adding silicone oil (PDMS) to aqueous $K_x(rac\text{-}L)_y$ solutions followed by rotary homogenization and then high-pressure microfluidic homogenization. All $K_x(rac\text{-}L)_y$ samples gave stable nanoemulsions that did not ripen or phase-separate for over 9 months. In addition to PDMS, other immiscible liquids such as dodecane, soybean oil, and methyl oleate gave emulsions using 1 mM $K_{40}(rac\text{-}L)_{20}$ in water. The versatility of this system was shown by formation of stable double emulsions using $R_{40}(rac\text{-}L)_{10}$ or $E_{40}(rac\text{-}L)_{10}$, containing guanidinium or carboxylate functionality of L-arginine (*R*) and L-glutamate (*E*), respectively [84].

To demonstrate their encapsulating ability, both water-soluble and oil-soluble fluorescent markers were loaded into copolypeptide stabilized double emulsions. Water-soluble InGaP/ZnS quantum dots were mixed with fluorescein-labeled

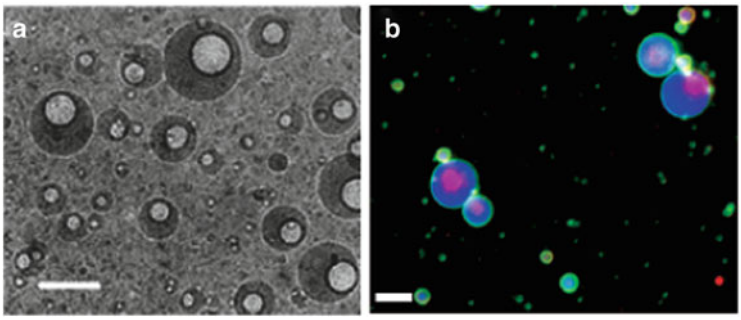

Fig. 2 (**a**) Cryogenic TEM image of size-fractionated K_{40}(*rac*-L)$_{20}$ double emulsions (*scale bar*: 70 nm). (**b**) FITC-labeled K_{40}(*rac*-L)$_{10}$ (*green*) double emulsion loaded with both pyrene (*blue*) and InGaP quantum dots (*red*) (*scale bar*: 5 μm). Adapted from [84]

K_{40}(*rac*-L)$_{10}$ prior to emulsification with silicone oil containing pyrene. Using fluorescence microscopy, both markers and the labeled polypeptide were imaged in the double emulsion droplets (Fig. 2) [84]. Recently, the Deming laboratory attached the ligand biotin to the polypeptide surfactants (i.e., biotin-K_{55}(*rac*-L)$_{20}$) and used these to form stable nanoemulsions capable of specific binding to avidin proteins such as NeutrAvidin [85]. This specific complexation allows preparation of well-defined nanoscale droplets that present a surface coated with NeutrAvidin proteins. They showed that these materials can then be specifically coated with biotinylated ligands, such as polymers or bioactive molecules like antibodies or ligands for cell receptors. These conjugates show promise for targeted drug delivery as well as for presentation of bioactive ligands or immunostimulating molecules in vaccines.

Another type of block copolypeptide nanocarrier was developed using a unimolecular star architecture and was reported by Liu and coworkers [86]. They reacted terminal amine groups on a small polyethyleneimine core successively with a hydrophobic NCA (leucine or phenylalanine) followed by Bn-Glu NCA to yield star polymers with hydrophilic coronas and hydrophobic cores. These materials were found to be able to encapsulate hydrophobic or cationic probe molecules, where the cationic probes were bound as counterions to the anionic polyglutamate segments. In summary, although nanoparticles composed solely of polypeptide components are relatively recent developments, there is substantial interest in this area and it is likely that a wide variety of new materials and structures will be forthcoming.

3.2 Copolypeptide Vesicles

Membranes are important materials for many applications, ranging from separations, to devices such as sensors and fuel cells, to encapsulation of sensitive materials, and to biomedical applications such as drug delivery. Vesicles constructed from polymers

offer many advantages and opportunities over lipid vesicles for all of these applications (e.g., increased stability, tunable functionality, and permeability) [87]. To date, many types of block copolypeptide amphiphiles that form stable vesicular assemblies have been developed. The first of these utilized diethylene glycol-modified lysine residues (i.e., K^P) that impart both non-ionic water solubility as well as ordered α-helical conformations to the hydrophilic polypeptide domains [88]. Most other materials utilize highly charged polyelectrolyte segments to impart both functionality and fluidity to the membranes. More recently, these copolypeptides have included increasingly complex functionality to assist in cargo loading, vesicle targeting, and vesicle disruption.

In 2004, Deming's laboratory studied the roles of chain length and block composition on the assembly of uncharged diblock copolypeptide amphiphiles of the general structure poly(N_ε-2-[2-(2-methoxyethoxy)ethoxy]acetyl-L-lysine)-*block*-poly(L-leucine), or $K^P{}_xL_y$ [88]. These diblock copolypeptide amphiphiles associate very strongly and essentially do not exist as single chains in aqueous solution. This property, in most cases, results primarily in the formation of irregular aggregates if the polymers are simply dispersed in deionized water. A protocol was developed, using organic solvent (THF) and a denaturant (TFA) that allowed annealing of these materials when water is added. Dialysis of the samples allows one to obtain regular assemblies in pure water.

Using this procedure, a number of amphiphilic copolymers were studied in which the hydrophilic domains were varied from 60 to 200 residues in average length and the hydrophobic domains were varied from 10 to 75 residues in average length [88]. All block copolypeptides were expected to adopt rod-like conformations due to the strong α-helix-forming tendencies of both the leucine and ethylene glycol-modified lysine residues [27]. These rod-like conformations provided a flat amphiphile interface upon association in water, thus directly tying polymer conformation to supramolecular structure. Circular dichroism spectroscopy of the copolymers in water confirmed that all samples were α-helical. Using differential interference contrast (DIC) optical microscopy, TEM, laser scanning confocal microscopy (LSCM), and DLS as initial methods for studying the assemblies, some trends were identified [88]. When the hydrophobic poly(leucine) domains were less than 20 residues in length, a significant fraction of oblong or irregular micelles (ca. 100 nm diameter) formed, as observed by DLS and TEM. When the size of the hydrophilic domain was 100 residues, unilamellar vesicles were observed to form with a size range of approximately 2–15 μm diameter (Fig. 3). When the hydrophilic block was increased to 150 residues, the vesicles were much larger in size, approaching 50 μm in diameter. Finally, when the hydrophilic segments were increased to 200 residues long, membrane curvature was hindered such that the major structures formed were flat membrane sheets.

These block copolypeptides, where both hydrophilic and hydrophobic segments were α-helical, gave rise to very stiff membranes, as suggested by the large vesicle diameters and lack of fluidity in the sheets that were formed. Further investigation revealed that these membranes were completely insensitive to osmotic stress, a consequence of their impermeability to water, ions, or other small molecules

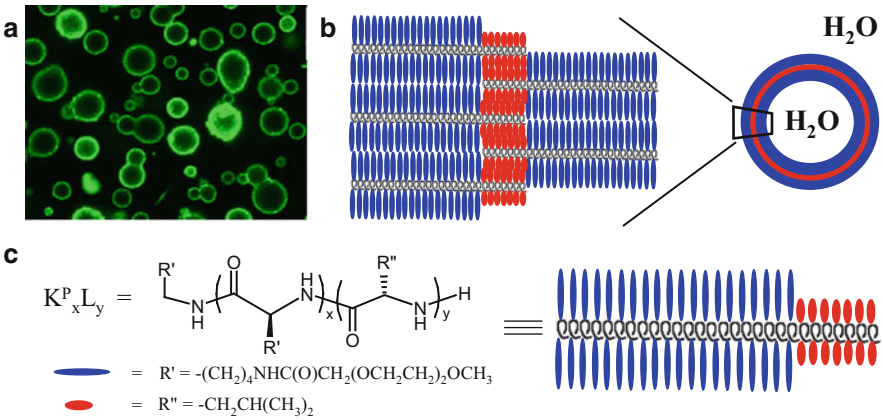

Fig. 3 Non-ionic polypeptide vesicles : (**a**) LSCM image (50 μm wide) of a $K^P{}_{100}L_{20}$ vesicle suspension visualized with fluorescent probes and a *Z*-direction slice thickness of 490 nm. (**b**) Proposed packing of $K^P{}_xL_y$ chains in vesicle walls. (**c**) Structure and cartoon of $K^P{}_xL_y$ chains. Adapted from [88]

[88]. They also could not be reduced in size by liposome-type extrusion techniques, and could only be made smaller by more aggressive sonication methods. The inability of the uncharged vesicles to pass through small pore diameter filters was probably due to membrane rigidity and virtual absence of chain flexibility. One advantage of these materials for many applications is the media-insensitivity of the ethylene glycol coating on the membrane surface. These vesicles were inert towards different ionic media, variations in pH, and the presence of large macromolecules such as proteins in serum. However, the rigidity of these chains created drawbacks in sample processing, namely the need to use denaturants for vesicle formation, which may be problematic for encapsulation of sensitive materials, and difficulty in preparing nanoscale vesicles due to high membrane rigidity.

In 2005, Lecommandoux's group reported on the self-assembly behavior of a short, zwitterionic diblock copolypeptide, poly(L-glutamatic acid)-*b*-poly(L-lysine), $E_{15}K_{15}$ [89]. This polymer has the interesting characteristic that in aqueous solutions near neutral pH ($5 < pH < 9$), both segments are charged and the polypeptide is dispersed as soluble chains. However, if pH is lowered to values below pH 4 or raised above pH 10, one of the segments is neutralized and the chains self-assemble into small vesicles. By adjustment of pH, vesicles with either anionic (high pH) or cationic (low pH) surfaces could be prepared; hence their description as "schizophrenic" vesicles. It is notable that these chains are soluble in water when both segments are highly charged, considering that the formation of water-insoluble polyion complexes between poly(L-lysine) and poly(L-glutamatic acid) is well documented [90]. A key feature of this work is the utilization of short polyelectrolyte segments, which limits such polyion complex formation in dilute solutions.

Deming's group also reported in 2005 on the assembly of charged diblock copolypeptide amphiphiles, utilizing the structure-directing properties of rod-like

α-helical segments only in the hydrophobic domains. Specifically, the aqueous self-assembly of a series of poly(L-lysine)-*b*-poly(L-leucine) block copolypeptides was studied (K_xL_y, where *x* ranged from 20 to 80, and *y* ranged from 10 to 30 residues) as well as the poly(L-glutamatic acid)-*b*-poly(L-leucine) block copolypeptide, $E_{60}L_{20}$ [91]. In other work, it was found that samples with high K to L molar ratios (e.g., $K_{180}L_{20}$) could be dissolved directly in deionized water, yielding transparent hydrogels composed of twisted fibrils (vide infra) [92]. It was reasoned that use of shortened charged segments would relax repulsive polyelectrolyte interactions and allow formation of charged polypeptide membranes. Samples were processed by suspending the polymers in THF/water (1:1) followed by dialysis. Analysis of these assemblies using DIC optical microscopy revealed the presence of large, sheet-like membranes for $K_{20}L_{20}$ and thin fibrils for $K_{40}L_{20}$. The $K_{60}L_{20}$ sample was most promising, as only large vesicular assemblies were observed by DIC [91].

The $K_{60}L_{20}$ polypeptide vesicles obtained directly from dialysis are polydisperse and range in diameter from ca. 5 μm down to 0.8 μm, as determined using DIC and DLS (Fig. 4). For applications such as drug delivery via blood circulation, a vesicle diameter of about 50–100 nm is desired. It was observed that aqueous suspensions of $K_{60}L_{20}$ vesicles could be extruded through nuclear track-etched polycarbonate membranes with little loss of polypeptide material. After two passes through a filter, reductions in vesicle diameter to values in close agreement to filter pore size were observed. These results showed that the charged copolypeptide vesicles are readily extruded, allowing good control over vesicle diameter in the tens to hundreds of nanometers range (Fig. 4). DLS analysis revealed that the extruded vesicles were also less polydisperse than before extrusion and contained no micellar contaminants. The vesicular morphology was also confirmed through TEM imaging of the submicron $K_{60}L_{20}$ suspensions. Thus, it appears that the membranes of the $K_{60}L_{20}$ vesicles are more flexible and compliant than those of purely rod-like uncharged polypeptides. The extruded vesicles were monitored for 6 weeks using DLS and were found to be stable. The vesicles were also found to have high thermal stability. An aqueous suspension of 1 μm vesicles was held at 80°C for 30 min, after which no vesicle disruption could be detected [91]. Only after heating to 100°C for 30 min were the vesicles disrupted, yielding large flat membrane sheets.

Stability of these highly charged polypeptide vesicles in ionic media is important for use in most applications ranging from personal care products to drug delivery. Although the $K_{60}L_{20}$ vesicles are unstable at high salt concentrations (>1 M), they are stable in 100 mM phosphate-buffered saline (PBS) buffer as well as in serum-free Dulbecco's modified Eagle's medium (DMEM) cell culture media [91]. Addition of serum, which contains anionic proteins, resulted in vesicle disruption, most likely due to polyion complexation between the serum proteins and the oppositely charged polylysine chains. Accordingly, it was observed that the negatively charged polypeptide vesicles prepared using $E_{60}L_{20}$ are stable in DMEM containing 10% fetal bovine serum. Based on these results, these charged polypeptide vesicles may have potential as encapsulants for water-soluble therapeutics as an alternative to liposomes. These copolypeptides retain much of the stability of the uncharged polypeptide vesicles described earlier, but allow

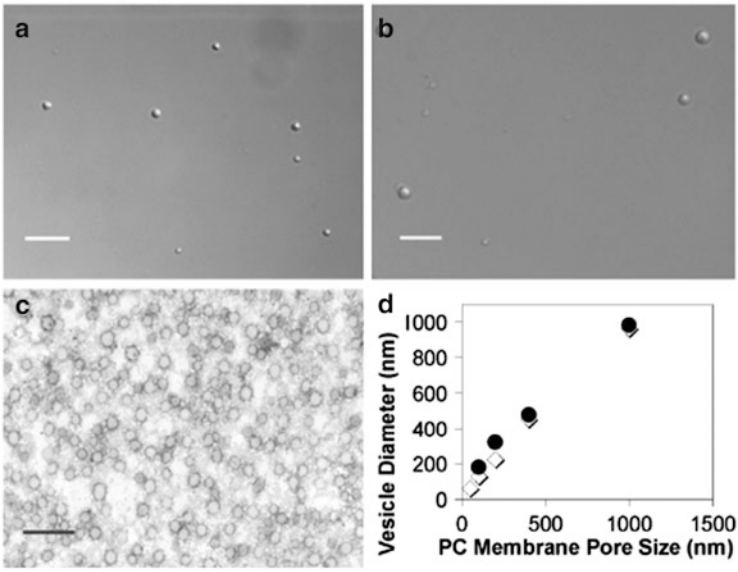

Fig. 4 (**a**, **b**) DIC images of 1% (w/v) polypeptide vesicles extruded through 1.0 μm polycarbonate (PC) filters (*scale bars*: 5 μm): (**a**) $K_{60}L_{20}$ and (**b**) $E_{60}L_{20}$. (**c**) Negative stained TEM image of 0.1% (w/v) $K_{60}L_{20}$ 0.1 μm filtered vesicles (*scale bar*: 350 nm). (**d**) Average diameter (from DLS) of 1% (w/v) $K_{60}L_{20}$ (*circles*) and $E_{60}L_{20}$ (*diamonds*) vesicles versus polycarbonate filter size. Adapted from [91]

straightforward encapsulation and size control due to much simpler processing [91]. Another feature of these charged polypeptide vesicles is the potential for facile functionalization of the hydrophilic polypeptide chains at the vesicle surface either through chemical conjugation to amine or carboxylate residues [93] or through careful choice of charged residues.

Addressing this point, Deming's laboratory reported the preparation of arginine–leucine (i.e., $R_{60}L_{20}$) vesicles that are able to readily enter cells due to the many guanidinium groups of the arginine segments [94]. In this case, the arginine residues play a dual role, being both structure-directing in vesicle formation as well as functional for cell binding and entry. Studies on endocytotsis and intracellular trafficking of these vesicles revealed that they enter HeLa cells primarily via macropinocytosis [95]. They were found to primarily reside in early endosomes, but not in lysosomes, and although some manage to escape into cytoplasm many are trapped within these compartments. Regardless, another study showed that $R_{60}L_{20}$ vesicles were effective at condensing plasmid DNA and transfecting it into a variety of cell lines, showing the vesicles do have potential for intracellular delivery [96]. These DNA carriers are advantageous over many other transfection agents due to their low cytotoxicity.

From the pioneering studies on block copolypeptide vesicles described above, design criteria were established for successful vesicle formation, namely an

α-helical hydrophobic domain connected to a charged hydrophilic domain. Since this original work, many laboratories have prepared different variants of block copolypeptide vesicles based on this scheme. In 2007, Hadjichristidis reported lysine-PBLG-lysine (i.e., $K_xPBLG_yK_x$) triblock copolypeptides, where the helical PBLG core favors vesicle formation [97]. Jing and coworkers prepared vesicle-forming lysine-phenylalanine (K_xF_y) copolypeptides containing α-helical phenylalanine segments [98]. These vesicles were also found to be useful in encapsulating hemoglobin and acting as oxygen carriers. Deming's laboratory also reported the formation of vesicles from dual hydrophilic triblock copolypeptides composed of arginine–glutamate–leucine ($R_xE_yL_z$) or PEGylated lysine–arginine–leucine ($K^P{}_xR_yL_z$) sequences [99]. The use of triblock architectures was intended to retain some homoarginine residues for cell uptake, but have the majority of the hydrophilic segments anionic or uncharged to minimize cytotoxicity, all without disrupting vesicle formation. A number of different compositions were prepared and it was found that, although vesicles exhibiting low cytotoxicity could be formed with a $R_5E_{80}L_{20}$ copolypeptide, the R segments were unable to promote intracellular uptake. With the $K^P{}_xR_yL_z$ samples, the presence of the "PEGylated" outer blocks was able to diminish cytotoxicity while still allowing the center R segments to promote cellular uptake [99].

Using a different approach to vesicle formation, Jan and coworkers prepared lysine–glycine (i.e., K_xG_y) copolypeptides, where the polyglycine segment does not adopt an α-helical conformation and has inherent higher flexibility compared to helical segments [100]. Due to the lack of a rigid hydrophobic segment, and due to the hydrophilicity of glycine compared to leucine or phenylalanine, much longer "hydrophobic" segments were needed to drive self-assembly in water and vesicle formation. A $K_{200}G_{50}$ block copolypeptide was found to form vesicles in water using MeOH/H_2O processing, and was also mineralized with silica for entrapment of molecules [101].

Other recent variants of block copolypeptide vesicles have incorporated functionality within one of the segments. In 2010, Deming's laboratory reported the preparation of lysine–dihydroxyphenylalanine (i.e., $K_{60}DOPA_{20}$)-based vesicles, where the hydrophobic DOPA segments have the added feature of being sensitive to oxidation [102]. DOPA residues are found naturally in mussel byssus and are important components in the ability of byssal threads to adhere underwater and to crosslink into rigid networks [103]. In a biomimetic process, $K_{60}DOPA_{20}$ vesicles were oxidized in aqueous media resulting in crosslinking of the vesicle membranes Eq. (18). The resulting membranes were very robust and stable to organic solvents, freeze drying, and osmotic shock. Similar materials, in the form of glutamate–lysine/DOPA [i.e., $E_x(K_m/DOPA_n)_y$] copolymers were reported in 2012 by Qiao and coworkers [104], where the hydrophobic domains were statistical copolymers of different ratios (*m*:*n*) of lysine and DOPA that could be assembled and oxidized to crosslinked vesicles at high pH.

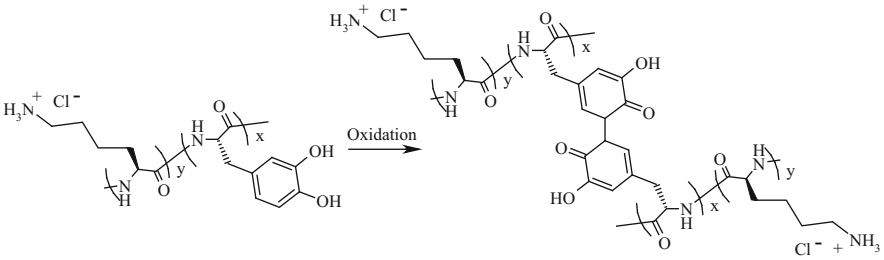

(18)

There is much current interest in synthesis of glycosylated polypeptides, and vesicle-forming amphiphilic copolypeptides that contain sugars in the hydrophilic corona have now also been prepared. In 2012, Lecommandoux, Heise and colleagues reported the preparation of Bn-Glu-propargyl glycine (i.e., $PBLG_{20}PPG_{25}$) diblock copolymers [105]. The propargyl side chains were then modified by copper-catalyzed azide–alkyne cycloaddition with azide-functionalized galactose to give the amphiphilic glycopolypeptide Eq. (19). Because the PPG segment is racemic, it adopts a disordered conformation in glycosylated form. The resulting rod–coil amphiphile was found after DMSO-water processing to assemble into vesicles that were able to bind their complimentary lectin. Deming's laboratory, in 2013, reported a different system prepared from a galactosylated NCA, α,D-galactopyranosyl-L-cysteine (α-gal-C) NCA, and leucine of the composition $(\alpha\text{-gal-C})_{65}L_{20}$, which was able to form vesicles when the side-chain thioether functionalities were oxidized to sulfone groups and after THF-water processing (Fig. 5) [106]. The parent polymer, although water soluble, is α-helical, which prohibits formation of small spherical vesicles. The fully oxidized sulfone derivative $(\alpha\text{-gal-C}^{O2})_{65}L_{20}$ is more polar, increasing its water solubility, and more importantly has a disordered conformation that assists in vesicle membrane formation. In summary, the formation of vesicles has been one of the major applications of block copolypeptides. Early work developed guidelines for formation of these structures, while current work is aimed at increasing the potent functionality and biologically interactive properties of these materials.

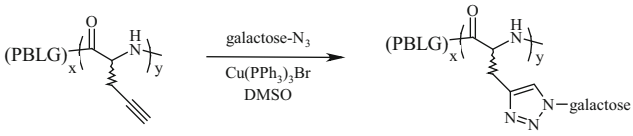

(19)

3.3 Copolypeptide Hydrogels

Hydrogels are a class of materials that have significant promise for use in soft tissue and bone engineering, as well as for localized drug delivery [107]. The key feature of hydrogels that makes them attractive for these applications is their well-hydrated, porous structure that can mimic natural extracellular matrices

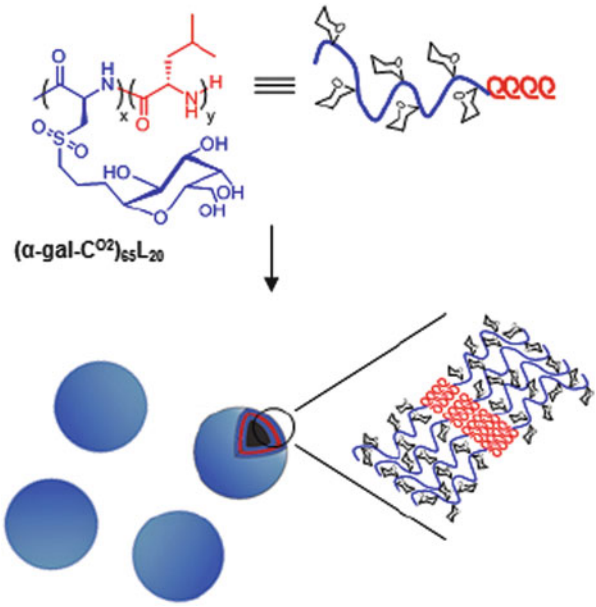

Fig. 5 Structure of amphiphilic glycosylated diblock copolypeptides and their assembly into vesicles. Adapted from [106]

[108]. To replace natural materials, however, many structural and functional features must be built into synthetic hydrogels. Desirable features include biocompatibility; degradability to allow cell in-growth; injectability and fast setting in the wound site; mechanical properties that can be tuned for different uses; control over cell adhesion to the hydrogel matrix; and tunable sustained release of growth factors and biologically active agents [109]. There are many examples where some, or even most, of these features have been incorporated into hydrogels [110]. However, in many cases, hydrogel synthesis and formation becomes very complicated, which limits the practicality of such materials. More importantly, the complexity of these systems, combined with limited means for adjustment of molecular parameters, leads to the inability for independent adjustment of most of the features. For example, it would be advantageous to be able to adjust scaffold rigidity while maintaining a constant hydrogel mesh size. Such a system would allow one to directly measure the effects of scaffold rigidity on cell proliferation. Also, since hydrogel degradation is commonly accomplished using degradable crosslinkers (e.g., in PEG-based hydrogels) [109], it can be difficult to adjust degradation rate without also altering crosslink density and, hence, initial gel mechanical properties [109]. It would be advantageous to have a hydrogel system where many of these desired adjustable features (e.g., gel strength, gel density, adhesive capability, degradation rate, growth factor release rate) could be controlled more or less independently so that meaningful evaluation of their roles in applications could be systematically carried out. Currently, in many systems it is difficult to identify the most important gel characteristics because many features are adjusted simultaneously [110]. Synthetic block copolypeptide hydrogels provide a

platform that allows fine adjustment of many of these parameters as well as incorporation of the essential features required for tissue engineering and drug delivery applications.

The Deming laboratory has developed hydrogels based on amphiphilic block copolypeptides possessing many features that make them attractive as candidates for medical applications [92]. Foremost, through combination of chemical synthesis and structural characterization, a detailed understanding of structure–property relationships in these materials has been established, allowing a high level of control over gel strength, gel porosity, gel functionality, and media stability; many which can be adjusted independent of each other [26]. Second, these physically associated gels are readily injectable through a 30G needle for facile application and filling of wound cavities [92]. Finally, the hydrogels can be prepared to be minimally toxic to cells in culture [111]. Hydrogel formation was first discovered in a series of diblock copolypeptides containing a charged, water solubilizing domain [poly(L-lysine·HBr], K; or poly(L-glutamate Na salt), E] and a α-helical hydrophobic domain [poly(L-leucine), L], i.e., K_xL_y or E_xL_y (Fig. 6) [92]. Hydrogel formation is the result of self-assembly of these polymeric amphiphiles by direct dissolution in water, and the resultant gels possess a network structure composed of nanoscale to microscale porosity and significant material rigidity, despite being composed of >95% water. In order to determine the role played by each copolypeptide domain, a comprehensive study was performed using an array of samples where both overall chain segment length and hydrophilic to hydrophobic composition were systematically varied. It was found that chain length modification of both positively charged polyelectrolyte and hydrophobic segments had significant effects on properties [92]. It is worth noting that analogous samples prepared with negatively charged polyelectrolyte domains, i.e., poly(L-glutamate), were found to behave similarly, which opens the possibility for preparation of both cationic and anionic hydrogels.

Compositional studies with different copolypeptides revealed many trends relating molecular parameters to hydrogel properties. First, as oligoleucine composition was increased, the gel strength was found to increase dramatically. Furthermore, only hydrophobic segments with α-helical conformations were found to form strong gels, as evidenced by the inability of a $K_{160}(rac\text{-}L)_{40}$ sample, where the racemic residues yield a disordered conformation, to form strong hydrogels. It was found that longer polyelectrolyte segments increase interchain repulsions such that the packing of the hydrophobic helices, which prefer formation of flat 2D sheets [88], must distort to minimize the overall energy of the system. The most efficient way to do this, while maintaining favorable helix packing, is to twist the sheets into fibrillar tapes, where tape width is determined by the degree of twist [112]. In this model, the helices are still able to pack perpendicular to the fibril axis, but with a slight twist between planes of parallel packed helices (Fig. 6). TEM imaging of the nanostructure in $K_{180}L_{30}$ does, in fact, reveal a more fibrillar, tape-like nanostructure constituting the hydrogel network (Fig. 6). Overall, copolypeptide gel strength can be adjusted by many molecular parameters such as overall chain length, hydrophilic to hydrophobic composition, and block

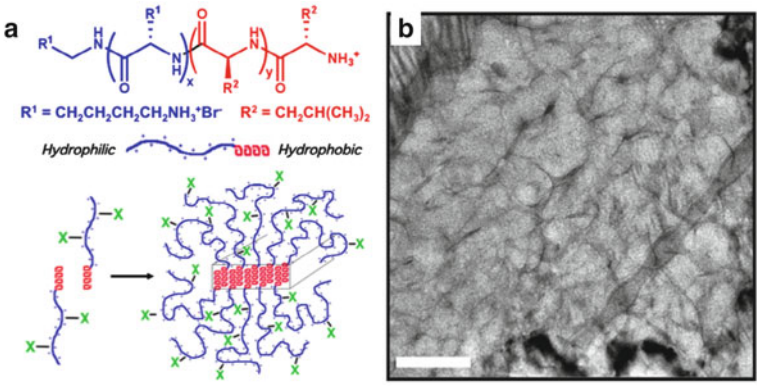

Fig. 6 (**a**) Block copolypeptide hydrogel composition and structure. Block copolypeptides are composed of variable-length chains of hydrophilic and hydrophobic amino acids. In aqueous solution, hydrophobic segments associate into elongated fibrillar assemblies that entangle to form 3D networks with hydrophilic segments exposed. (**b**) Cryogenic TEM image of vitrified $K_{180}L_{30}$ hydrogel (*scale bar*: 200 nm)

architecture, in addition to the conventional method of varying copolymer concentration. By having many means to adjust gel strength, it is possible to optimize or adjust other hydrogel properties (i.e., mesh size, injectability, or surface functionality) while keeping gel strength constant.

To test their suitability for cell culture applications, hydrogel samples were also prepared in DMEM and DMEM containing 5% fetal calf serum and penicillin [113]. Samples of $K_{170}L_{30}$ hydrogels were found to be stable and remained transparent in these media, which was somewhat surprising, since they contain numerous multivalent ions and anionically charged proteins. It is likely that the proteins coat the polylysine segments in the gel since it is known that polylysine homopolymer will complex with many serum proteins in solution [114]. Apparently, the resulting polyelectrolyte complexes retain enough charge or hydrophilicity to solubilize the hydrophobic gel scaffold and prevent precipitation and collapse of the network. The porous microscale morphology was found to persist in the $K_{170}L_{30}$ hydrogels in both the presence of 150 mM NaCl and in DMEM cell culturing medium. Also, cryogenic TEM revealed that the porous nanostructure also persists in the presence of salt. The presence of the porosity and the robustness of the nanostructure even in the presence of significant ionic concentration is a critical self-assembling material characteristic for medical applications. Overall, these copolypeptide hydrogels display remarkable stability in the presence of ionic species. Hydrogels formed from helical or β-sheet-forming proteins and peptides typically show some sensitivity to ions, either requiring them to form gels or disrupting in their presence [115, 116]. Likewise, hydrogels prepared from synthetic polyelectrolytes (e.g., crosslinked polyacrylic acid) are very sensitive to salts, shrinking dramatically as ionic strength is increased [117]. The gelation mechanism for these polypeptides, the association of hydrophobic

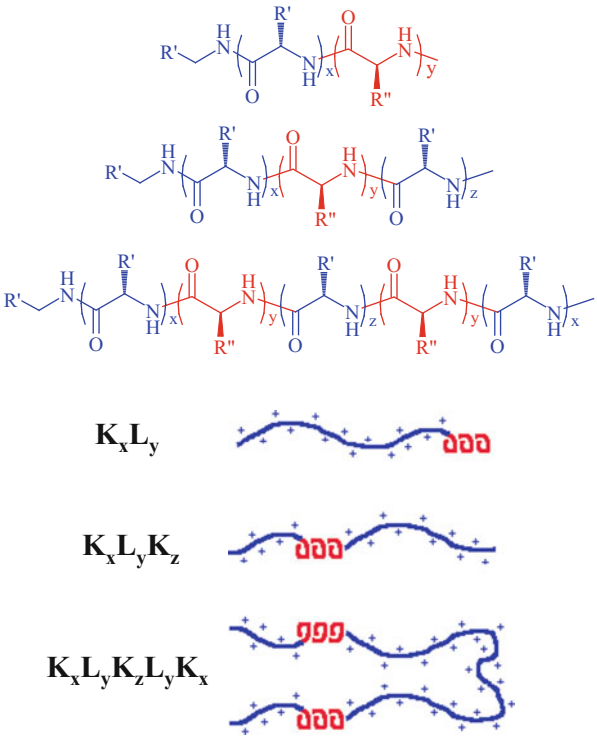

Fig. 7 Structure and scheme of diblock, triblock, and pentablock copolypeptides. $R'-CH_2CH_2CH_2CH_2NH_3^+Br^-$,$R''-CH_2CH(CH_3)_2$. Adapted from [72]

helices, provides a robust structure that is unperturbed under a variety of conditions, including variation of pH, ionic strength, and temperature.

In an effort to further understand hydrogel formation and tuning of mechanical properties, Deming's laboratory investigated $K_xL_yK_z$ triblock architectures, which were found to allow for additional tuning of hydrogel properties (Fig. 7) [72]. In particular, triblocks gave higher gel moduli and improved stability to ionic media compared to diblock copolymers of identical composition. These changes were found to be due to the increased density of K chains at the amphiphile interface, since each hydrophobic segment has a polylysine at both ends compared to only one end for the diblock samples, where this additional steric bulk acts to enhance copolymer assembly into the fibrillar morphology that gives strong networks. Deming's laboratory later studied pentablock copolypeptides of the structure $K_xL_yK_zL_yK_x$ that were expected to possess attributes similar to $K_xL_yK_z$ triblock copolymers, since both have associating L segments capped on each side by K segments (Fig. 7) [72]. Due to the presence of two α-helical L segments per chain, the pentablocks also have the intriguing potential for organized intrachain folding, akin to natural proteins, in addition to intermolecular assembly.

Pentablock copolypeptides of the composition $K_{60}L_{20}K_zL_{20}K_{60}$, where z was varied from 10 to 200, were synthesized by stepwise linear block copolymerization using $(PMe_3)_4Co$ initiator in THF, followed by removal of protecting groups and purification. Deming's laboratory found that $K_{60}L_{20}K_{10}L_{20}K_{60}$ formed clusters of micelle-like aggregates with diameters ranging from 50 to 200 nm, which differed greatly from the fibrillar structures seen with diblock and triblock samples. On the other hand, the $K_{60}L_{20}K_zL_{20}K_{60}$ copolypeptides, when $z > 60$, self-assembled in water to form fibrillar hydrogel assemblies. Furthermore, adjustment of the central K segment length allowed tuning of assembly morphology and hydrogel properties; it was observed that G' increased and minimum gelation concentration decreased as the pentablock central K segments were lengthened. The ability to control intramolecular versus intermolecular assembly of the two hydrophobic L segments in these pentablock sequences gave substantial enhancement of hydrogel properties compared to the corresponding diblock and triblock architectures [72]. The ability to tune intrachain interactions in these materials via molecular design is also a key advance in biomimetic assembly.

Inorganic–organic biocompatible composites have tremendous potential for therapeutic and diagnostic materials applications. Block copolypeptide hydrogels are promising templates for formation of porous composites, where the porous gel scaffold can serve as a template for mineral growth. In 2009, Mallapragada and coworkers reported the use of $K_{170}L_{30}$ hydrogels as templates for assembly of calcium phosphate nanocomposites [118]. The porous nature of the hydrogels, and their ability to form gels at low concentrations, allowed composites to be formed that contained up to 50% inorganic material, approaching the inorganic content of bone. Furthermore, detailed characterization of the composites revealed the mineral phase to be carbonated hydroxyapatite, with elongated plate-like morphology of nanoscale dimensions, similar to natural bone. In a similar study, Li's group studied the ability of a series of K_xL_y hydrogels ($170 < x < 440$; $10 < y < 30$) to direct silica morphology by sol–gel condensation of tetramethylorthosilicate in the presence of the hydrogels [119]. They found that both the polypeptide lengths, as well as nature of anionic counterions used, had significant effects on resulting silica morphology, where either plates or rods of silica could be formed.

Initial quantitative measurements of polypeptide cytotoxicity involved cell culture within three dimensional hydrogel substrates in cell culturing medium [111]. Although polylysine is known to be cytotoxic when free in solution [120], use of higher concentrations of polypeptide above gelation concentrations revealed that both cationic and anionic functionalized gels were promising substrates for short-term cell culture. It is likely that the hydrogel network prevents bulk diffusion of gel-bound lysine chains, thus limiting the amount of polylysine that can interact with the cells. Although the cells remained viable, in neither gel was cell attachment or proliferation observed. The cells, in the presence of either of the hydrogel matrices, retain their spherical shape after 4 h and up to 24 h. Although it appears that cell binding epitopes need to be incorporated into these hydrogels, their peptidic backbone provides many advantages for use of these materials as scaffolds.

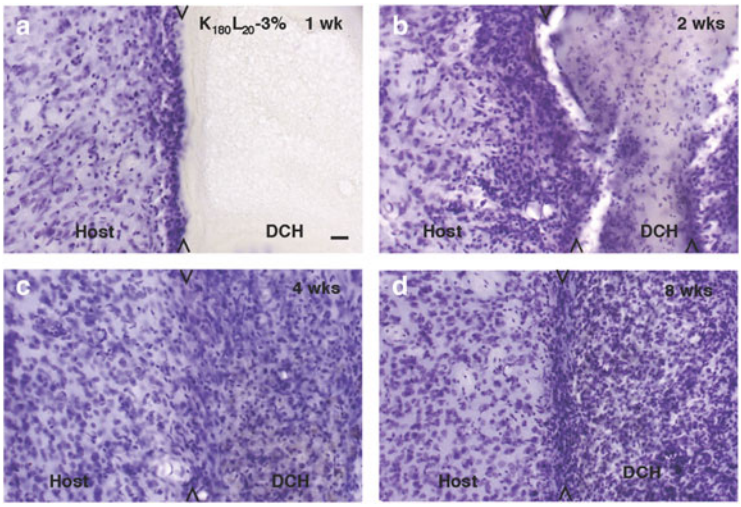

Fig. 8 Time-dependent migration of cells into block copolypeptide hydrogel (*DCH*) deposits in vivo. (**a**–**d**) Light-microscopic images of 3% $K_{180}L_{20}$ at 1 (**a**), 2 (**b**), 4 (**c**) and 8 (**d**) weeks after injection of 2 μL into the striatum in tissue sections stained with cresyl violet. Essentially, no cells are present in the deposits after 1 week in vivo (**a**). After 2 weeks in vivo (**b**), a number of cells have migrated into, and are scattered throughout the deposits. After 4 (**c**) and 8 weeks (**d**), the deposits are densely packed with cells. *Arrowheads* indicate the borders of deposit and host tissue (*scale bars*: 25 mm). Adapted from [121]

These include the straightforward incorporation of chemical functionality by use of functional amino acids, as well as enzymatic degradability.

Following up on this work, Sofroniew, Deming and colleagues studied the biocompatibility of diblock copolypeptide hydrogels in vivo in mouse central nervous system (CNS) tissue [121]. This work was undertaken because biomaterials represent a major opportunity for developing novel CNS treatment strategies based on site-specific delivery of scaffolds that promote the growth and migration of axons or cells derived from host or grafts, or as depots that release diffusible bioactive molecules to act in a locally restricted manner inside the blood–brain barrier. A range of diblock copolypeptide hydrogel formulations with rheological properties similar to brain tissue were injected into mouse forebrain and examined after 1–8 weeks using light microscopy, immunohistochemistry, and electron microscopy. Hydrogel deposits were found to elicit no more gliosis, inflammation, or toxicity to neurons, myelin, or axons than did injections of physiological saline. The size, rigidity, and density of the hydrogel deposits could be varied subtly by altering sample composition and concentration. The $K_{180}L_{20}$ hydrogel was selected for detailed analyses because it formed deposits with desirable physical properties and because lysine is routinely used as a substrate for neural cell cultures. Deposits of unmodified $K_{180}L_{20}$ exhibited time-dependent in-growth of blood vessels and of certain glial cells, and limited in-growth of nerve fibers (Fig. 8). These findings showed that block copolypeptide hydrogels are injectable, re-assemble in vivo to form 3D deposits, exhibit little or no detectable toxicity in the CNS, integrate well

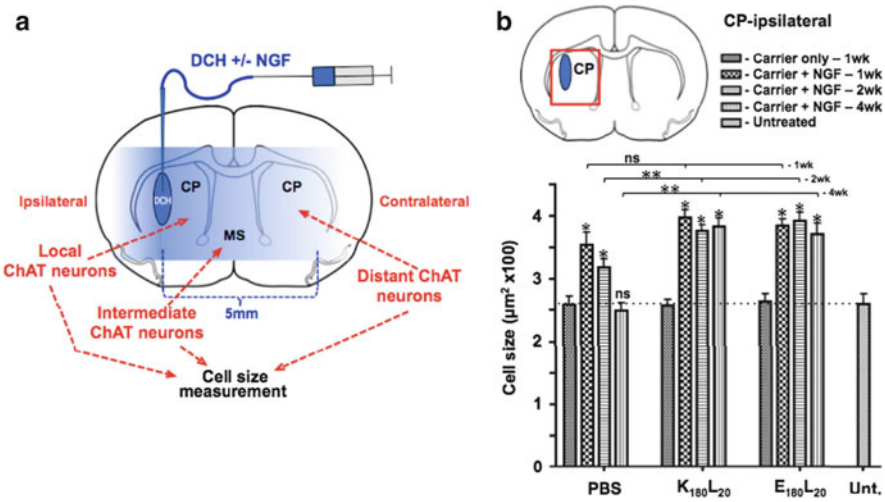

Fig. 9 (**a**) Experimental design to evaluate release of nerve growth factor (*NGF*) from $K_{180}L_{20}$ hydrogel (*DCH*) depots in vivo. NGF is known to induce hypertrophy of basal forebrain cholinergic (*ChAT*) neurons in the caudate putamen (*CP*) and medial septum (*MS*). Depots of DCH with NGF were injected into the CP on one side of the brain. (**b**) Effects of NGF released from DCH depots on local forebrain cholinergic neurons in ipsilateral CP. *Box* outlines the location of cholinergic neurons evaluated in the ipsilateral CP local to the DCH depot. *Graph* shows mean cell area in mm^2 of cholinergic neurons in various treatment groups and at various treatment times, as indicated. $n = 4$ per group, $*P < 0.01$ relative to carrier (*PBS*) only, $**P < 0.01$ for group comparisons as indicated, *ns* non-significant, ANOVA with Newman–Keuls post-hoc pair-wise comparisons. Adapted from [122]

with brain tissue and represent a new class of synthetic biomaterials with potential for applications as depots or scaffolds in the CNS [121].

In a follow up study, Sofroniew, Deming and colleagues examined the loading and release of bioactive hydrophilic molecules from $K_{180}L_{20}$ and $E_{180}L_{20}$ hydrogels in vitro and in vivo [122]. In vitro tests demonstrated sustained release from dialysis cassettes of the representative protein (lysozyme) dissolved in $K_{180}L_{20}$ or $E_{180}L_{20}$ hydrogels. Release times of molecules in vitro varied in relation to hydrogel charge and mechanical properties, and the ionic strength of the media. To evaluate bioactive protein delivery in vivo, they used nerve growth factor (NGF) and measured the size of mouse forebrain cholinergic neurons, which respond to NGF with cellular hypertrophy (Fig. 9). In comparison with NGF injected in buffer, depots of NGF dissolved in either $K_{180}L_{20}$ or $E_{180}L_{20}$ provided significantly longer delivery of NGF bioactivity, maintaining hypertrophy of local forebrain cholinergic neurons for at least 4 weeks and inducing hypertrophy a further distance away (up to 5 mm) from injection sites [122]. These findings show that depots of block copolypeptide hydrogels injected into CNS can provide sustained delivery within the blood–brain barrier of a bioactive protein growth factor that exerts a predicted, quantifiable effect on local cells over a prolonged subacute time.

4 Conclusions

The synthesis of polypeptides by ring-opening polymerization is an area that has been under study for more than five decades. Initially, this field suffered from limitations that necessitated excessive sample purification and fractionation to obtain well-defined polypeptides. Over the last 15 years, vast improvements in NCA polymerizations now allow the synthesis of a variety of block copolypeptides of controlled dimensions (molecular weight, sequence, composition, and molecular weight distribution). Many different block copolypeptides have now been prepared and used to form self-assembled structures with promising properties. The ability to easily adjust chain conformation and functionality in polypeptides, in combination with advanced synthetic methods that enable preparation of complex sequences, has opened up a new, promising field of materials with a wide range of tunable properties.

References

1. Branden C, Tooze J (1991) Introduction to protein structure. Garland, New York
2. Cha JN, Stucky GD, Morse DE, Deming TJ (2000) Nature 403:289
3. van Hest JCM, Tirrell DA (2001) Chem Commun 2001:1897
4. Voet D, Voet JG (1995) Biochemistry, 2nd edn. Wiley, New York, Chap 32
5. Fasman GD (1967) Poly α-amino acids. Dekker, New York
6. Fasman GD (1989) Prediction of protein structure and the principles of protein conformation. Plenum, New York, p 48
7. Deming TJ (2000) J Polym Sci Polym Chem Ed 38:3011
8. Deming TJ (2012) Top Curr Chem 310:1
9. Discher DE, Eisenberg A (2002) Science 297:967
10. Kwon GS, Naito M, Kataoka K, Yokoyama M, Sakurai Y, Okano T (1994) Colloids Surf B Biointerfaces 2:429
11. Kricheldorf HR (1987) α-Aminoacid-N-carboxyanhydrides and related materials. Springer, New York
12. Kricheldorf HR (1990) In: Penczek S (ed) Models of biopolymers by ring-opening polymerization. CRC, Boca Raton
13. Woodward RB, Schramm CH (1947) J Am Chem Soc 69:1551
14. Webster O (1991) Science 251:887
15. Cardinaux F, Howard JC, Taylor GT, Scheraga HA (1977) Biopolymers 16:2005
16. Kubota S, Fasman GD (1975) Biopolymers 14:605
17. Howard JC, Cardinaux F, Scheraga HA (1977) Biopolymers 16:2029
18. Sekiguchi H (1981) Pure Appl Chem 53:1689
19. Sekiguchi H, Froyer G (1975) J Poly Sci Symp 52:157
20. Collman JP, Hegedus LS, Norton JR, Finke RG (1987) Principles and applications of organotransition metal chemistry, 2nd edition. University Science, Mill Valley
21. Deming TJ (1997) Nature 390:386
22. Deming TJ (1998) J Am Chem Soc 120:4240
23. Deming TJ (1999) Macromolecules 32:4500
24. Deming TJ, Curtin SA (2000) J Am Chem Soc 122:5710
25. Deming TJ (2002) Adv Drug Deliv Rev 54:1145

26. Deming TJ (2005) Soft Matter 1:28
27. Yu M, Nowak AP, Pochan DJ, Deming TJ (1999) J Am Chem Soc 121:12210
28. Hwang J, Deming TJ (2001) Biomacromolecules 2:17
29. Schaefer KE, Keller P, Deming TJ (2006) Macromolecules 39:19
30. Chen C, Wang Z, Li Z (2011) Biomacromolecules 12:2859
31. Kramer JR, Deming TJ (2010) J Am Chem Soc 132:15068
32. Kramer JR, Deming TJ (2012) J Am Chem Soc 134:4112
33. Liu Y, Chen P, Li Z (2012) Macromol Rapid Commun 33:287
34. Kramer JR, Deming TJ (2010) Biomacromolecules 11:3668
35. Fu X, Shen Y, Fu W, Li Z (2013) Macromolecules 46:3753
36. Curtin SA, Deming TJ (1999) J Am Chem Soc 121:7427
37. Witte P, Menzel H (2004) Macromol Chem Phys 205:1735
38. Sparks BJ, Ray JG, Savin DA, Stafford CM, Patton DL (2011) Chem Commun 47:6245
39. Rhodes AJ, Deming TJ (2012) J Am Chem Soc 134:19463
40. Brzezinska KR, Curtin SA, Deming TJ (2002) Macromolecules 35:2970
41. Cheng J, Deming TJ (1999) Macromolecules 32:4745
42. Seidel SW, Deming TJ (2003) Macromolecules 36:969
43. Goodwin AA, Bu X, Deming TJ (1999) J Organometallic Chem 589:111
44. Peng Y-L, Lai S-L Lin C-C (2008) Macromolecules 41:3455
45. Aliferis T, Iatrou H, Hadjichristidis N (2004) Biomacromolecules 5:1653
46. Mondeshki M, Spiess HW, Aliferis T, Iatrou H, Hadjichristidis N, Floudas G (2011) Eur Polym J 47:668
47. Graf R, Spiess HW, Floudas G, Butt H-J, Gkikas M, Iatrou H (2012) Macromolecules 45:9326
48. Thunig D, Semen J, Elias H-G (1977) Makromol Chem 178:603
49. Habraken GJM, Peeters M, Dietz CHJT, Koning CE, Heise A (2010) Polym Chem 1:514
50. Pickel DL, Politakos N, Avgeropoulos A, Messman JM (2009) Macromolecules 42:7781
51. Vayaboury W, Giani O, Cottet H, Deratani A, Schué F (2004) Macromol. Rapid Commun 25:1221
52. Odian G (1991) Principles of polymerization, 3rd edn, Wiley, New York
53. Cao H, Yao J, Shao Z (2012) Polym Int 61:774
54. Nguyen L-TT, Vorenkamp EJ, Daumont CJM, ten Brinke G, Schouten AJ (2010) Polymer 51:1042
55. Habraken GJM, Wilsens KHRM, Koning CE, Heise A (2011) Polym Chem 2:1322
56. Dimitrov I, Schlaad H (2003) Chem Commun 2003:2944
57. Knobler Y, Bittner S, Frankel M (1964) J Chem Soc 1964:3941
58. Knobler Y, Bittner S, Virov D, Frankel M (1969) J Chem Soc C 1969(14):1821
59. Meyer M, Schlaad H (2006) Macromolecules 39:3967
60. Lutz J-F, Schütt D, Kubowicz S (2005) Macromol. Rapid Commun 26:23
61. Fischer H (2001) Chem Rev 101:3581
62. Lu H, Cheng J (2007) J Am Chem Soc 129:14114
63. Webster O (2000) J Polym Chem Polym Chem Ed 38:2855
64. Lu H, Cheng J (2008) J Am Chem Soc 130:12562
65. Lu H, Wang J, Lin Y, Cheng J (2009) J Am Chem Soc 131:13582
66. Uralil F, Hayashi T, Anderson JM, Hiltner A (1977) Polym Eng Sci 17:515
67. Auer HE, Doty P (1966) Biochemistry 5:1708
68. Ostroy SE, Lotan N, Ingwall RT, Scheraga HA (1970) Biopolymers 9:749
69. Epand RE, Scheraga HA (1968) Biopolymers 6:1551
70. Ingwall RT, Scheraga HA, Lotan N, Berger A, Katchalski E (1968) Biopolymers 6:331
71. Gibson MI, Cameron NR (2008) Angew Chem Int Ed 47:5160
72. Nowak AP, Sato J, Breedveld V, Deming TJ (2006) Supramol Chem 18:423
73. Li Z, Deming TJ (2010) Soft Matter 6:2546
74. Holt C, Horne DS (1996) Netherlands Milk Dairy J 50:85

75. Alexandridis P, Holzwarth JF, Hatton TA (1994) Macromolecules 27:2414
76. Torchilin VP (2007) Phramaceutical Res 24:1
77. Zhang LF, Eisenberg A (1995) Science 268:1728
78. Wilhelm M, Zhao CL, Wang YC, Xu RL, Winnik MA, Mura JL, Riess G, Croucher MD (1991) Macromolecules 24:1033
79. Jeong YI, Cheon JB, Kim SH, Nah JW, Lee YM, Sung YK, Akaike T, Cho CS (1998) J Control Rel 51:169
80. Nah JW, Jeong YI, Cho CS (1998) Bull Chem Soc Jpn 19:962
81. Kwon G, Naito M, Yokoyama M, Okano T, Sakurai Y, Kataoka K (1993) Langmuir 9:945
82. Kidchob T, Kimura S, Imanishi Y (1998) J Control Rel 51:241
83. Hanson JA, Li Z, Deming TJ (2011) Macromolecules 43:6268
84. Hanson JA, Chang CB, Graves SM, Li Z, Mason TG, Deming TJ (2008) Nature 455:85
85. Hanson JA, Deming TJ (2011) Polym Chem 2:1473
86. Zhuang W, Liao L, Chen H, Wang J, Pan Y, Zhang L, Liu D (2009) Macromol Rapid Commun 30:920
87. Rutjes FPJT, van Hest JCM (2011) Polym Chem 2:1449
88. Bellomo E, Wyrsta MD, Pakstis L, Pochan DJ, Deming TJ (2004) Nat Mater 3:244
89. Rodriguez-Hernandez J, Lecommandoux S (2005) J Am Chem Soc 2127:2026
90. Sela M, Katchalski E (1959) Adv Protein Chem 14:391
91. Holowka EP, Pochan DJ, Deming TJ (2005) J Am Chem Soc 127:12423
92. Nowak AP, Breedveld V, Pakstis L, Ozbas B, Pine DJ, Pochan D, Deming TJ (2002) Nature 417:424
93. Choe U-J, Rodriguez AR, Lee BS, Knowles SM, Wu AM, Deming TJ, Kamei DT (2013) Biomacromolecules 14:1458
94. Holowka EP, Sun VZ, Kamei DT, Deming TJ (2007) Nat Mater 6:52
95. Sun VZ, Li Z, Deming TJ, Kamei DT (2011) Biomacromolecules 12:10
96. Sun VZ, Choe U-J, Rodriguez AR, Dai H, Deming TJ, Kamei DT (2013) Biomacromolecules 13:539
97. Iatrou H, Frielinghaus H, Hanski S, Ferderigos N, Ruokolainen J, Ikkala O, Richter D, Mays J, Hadjichristidis N (2007) Biomacromolecules 8:2173
98. Sun J, Huang Y, Shi Q, Chen X, Jing X (2009) Langmuir 25:13726
99. Rodriguez AR, Choe U-J, Kamei DT, Deming TJ (2012) Macromol Biosci 12:805
100. Gaspard J, Silas JA, Shantz DF, Jan J-S (2010) Supramol Chem 22:178
101. Lai J-K, Chuang T-H, Jan J-S, Wang SS-S (2010) Colloids Surf B Biointerfaces 80:51
102. Holowka EP, Deming TJ (2010) Macromol Biosci 10:496
103. Waite JH (1992) Biol Bull 183:178
104. Sulistio A, Blencowe A, Wang J, Bryant G, Zhang X, Qiao GG (2012) Macromol Biosci 12:1220
105. Huang J, Bonduelle C, Thévenot J, Lecommandoux S, Heise A (2012) J Am Chem Soc 134:119
106. Kramer JR, Rodriguez AR, Choe U-J, Kamei DT, Deming TJ (2013) Soft Matter 9:3389
107. Lee KY, Mooney DJ (2001) Chem Rev 101:1869
108. Peppas NA, Huang Y, Torres-Lugo M, Ward JH, Zhang J (2000) Annu Rev Biomed Eng 2:9
109. Lutolf MP, Hubbell JA (2005) Nat Biotech 23:47
110. Zisch AH, Lutolf MP, Hubbell JA (2003) Cardiovasc Pathol 12:295
111. Pakstis L, Ozbas B, Nowak AP, Deming TJ, Pochan DJ (2004) Biomacromolecules 5:312
112. Aggeli A, Nyrkova IA, Bell M, Harding R, Carrick L, McLeish TCB, Semenov AN, Boden N (2001) Proc Natl Acad Sci USA 98:11857
113. Nowak AP, Breedveld V, Pine DJ, Deming TJ (2003) J Am Chem Soc 125:15666
114. Richert L, Lavalle P, Vautier D, Senger B, Stoltz JF, Schaaf P, Voegel JC, Picart C (2002) Biomacromolecules 3:1170
115. Aggeli A, Bell M, Boden N, Keen JN, Knowles PF, McLeish TCB, Pitkeathly M, Radford SE (1997) Nature 386:259

116. Zhang S, Marini DN, Hwang W, Santoso S (2002) Curr Opn Chem Biol 6:865
117. Tanaka T (1981) Sci Am 244:124
118. Hu Y-Y, Yusufoglu Y, Kanapathipillai M, Yang C-Y, Wu Y, Thiyagarajan P, Deming TJ, Akinc M, Schmidt-Rohr K, Mallapragada S (2009) Soft Matter 5:4311
119. Xia L, Liu Y, Li Z (2010) Macromol Biosci 10:1566
120. Katchalski E, Sela MB (1958) Adv Protein Chem 13:243
121. Yang C-Y, Song B, Ao Y, Nowak AP, Abelowitz RB, Korsak RA, Havton LA, Deming TJ, Sofroniew MV (2009) Biomaterials 30:2881
122. Song B, Song J, Zhang S, Anderson MA, Ao Y, Yang C-Y, Deming TJ, Sofroniew MV (2012) Biomaterials 33:9105

Adv Polym Sci (2013) 262: 39–60
DOI: 10.1007/12_2013_254

Published online: 6 November 2013

Synthetic Glycopolymers: Some Recent Developments

Qiang Zhang and David M. Haddleton

Abstract Glycopolymers are synthetic macromolecules containing sugar moieties. They have shown promise in biorelated applications and the number of synthetic approaches for making these molecules is expanding rapidly. This field benefits from the rapid development of synthetic polymer chemistry, which has seen dramatic progress in the synthesis of functional glycopolymers. Strategies employed in glycopolymer synthesis have been generally carried out as either direct polymerization of glycomonomers or post-glycosylation of pre-formed polymers. This contribution is a short overview of some of the recent developments and will hopefully direct the reader to many papers of interest.

Keywords Glycopolymer · Living radical polymerization · Molecular recognition · Polymerization

Contents

The authors declare the following competing financial interests: D. M. Haddleton is a Director of Warwick Effect Polymers Ltd.

Q. Zhang
Department of Chemistry, University of Warwick, CV4 7AL Coventry, UK

D.M. Haddleton (✉)
Department of Chemistry, University of Warwick, CV4 7AL Coventry, UK

Monash Institute of Pharmaceutical Sciences, 381 Royal Parade, Parkville, Victoria 3052, Australia
e-mail: D.M.Haddleton@warwick.ac.uk

Glycopolymers are generally considered as synthetic macromolecules featuring sugar moieties and have showed promise in some biorelated applications [1]. This field has benefited from the development of elegant synthetic polymer chemistry, and the past two decades have evidenced dramatic progress in the synthesis of functional glycopolymers. Glycopolymer synthesis has been generally carried out by either direct polymerization of glycomonomers or post-glycosylation of pre-formed polymers [2]. As a special case, glycopolymers can also be synthesised via simultaneous copper-catalyzed azide-alkyne cycloaddition (CuAAC) and living radical polymerization (LRP), which is a hybrid of the previous two strategies [3].

By the combination of living polymerization and click chemistry, different strategies have been developed for the efficient synthesis of glycopolymers with defined structure and function. These strategies have already been discussed in detailed reviews separately by Haddleton, Stenzel, Cameron, Maynard and co-authors [1, 2, 4–6]. The applications of glycopolymers such as therapeutic drug delivery, multivalent recognitions with lectins and signal transduction have been summarized in recent reviews by Cameron, Stenzel, Remzi, Kiessling and co-authors [2, 7–9]. Thus, there has been very intensive research on glycopolymer synthesis and application, and most of the research until 2011 has been summarized in previous reviews. However, new strategies have been constantly emerging during 2011–2013 and are described below.

1 Novel Strategies in the Direct Polymerization of Glycomonomers

1.1 Ring-Opening Polymerization

Ring-opening polymerization includes cationic, anionic and enzymatic ring-opening polymerization, which depend on whether the catalyst type or the reactive centre of the propagating chain is a carbocation or carbanion. It has had a long history since the 1950s and has been widely used for polymerization of different functional cyclic monomers [10]. However, its application in the direct polymerization of carbohydrate-containing cyclic monomers has been limited [11, 12]. Recently, the Schubert group synthesized a glucose-substituted 2-oxazoline monomer (Fig. 1) via

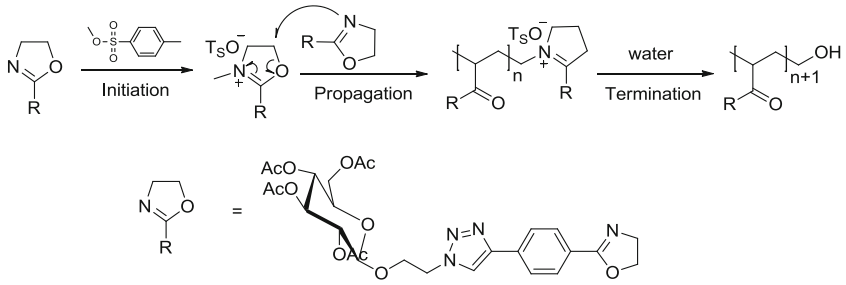

Fig. 1 Synthesis of glyco-poly(2-oxazoline)s by ring-opening polymerization

CuAAC and used this for cationic ring-opening copolymerization (CROP) with 2-oxazoline-based monomers, yielding well-defined glycopolymers bearing functional groups for thiol-ene reactions to tune the properties [13].

Although the polymerization of protected glycomonomers requires high reaction temperatures (~120°C) and long reaction times (overnight) for this CROP, the final glycopolymers show relatively narrow molecular weight distribution (~1.3) and the poly(2-oxazoline) backbones are biocompatible and considered as analogues of poly(amino acids), which may have potential application in drug delivery.

1.2 Copper-Mediated Living Radical Polymerization

Radical species usually have poor chemo- and regioselectivity in organic reactions and tend to undergo bimolecular termination and disproportionation in polymerizations. Thus, in order to have precise control in radical polymerization, a reversible and dynamic equilibrium between active radical growing species and dormant species (Fig. 2) is necessary so that the concentration of active radicals can be kept at a low level. The relatively stable dormant species could avoid side reactions or propagation yet is still able to generate intermediates capable of propagation by dissociation of the leaving groups via chemical catalysis or physical stimuli [14]. Different strategies have been developed to perturb this equilibrium with different leaving groups, including halides, stable radicals and thiolcarbonylthio compounds, via varying dissociation methods such as metal catalysis and addition-fragmentation chain transfer etc. Most of the current methods in living radical polymerizations are based on this concept [15].

Since its discovery in 1994, transition metal-catalyzed LRP has been one of the most popular, versatile and robust polymerization methods for synthesis of various functional polymers with controlled chain length, architecture and molecular weight distribution [16, 17]. The initiators are generally organic halides with potentially active carbon–halogen bonds for radical generation or conventional radical initiators, both of which are either commercially available or can be easily synthesized. The transition metal catalysts generally contain transition metals of groups 8–11, typically including iron, nickel, ruthenium and copper. Copper

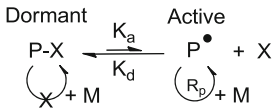

Fig. 2 Reversible and dynamic equilibrium between active radical growing species and dormant species (K_a means rate constant of activation; K_d means rate constant of deactivation; R_p means rate constant of propargation; M means monomer; P-X represents dormant polymer species;P* represents reactive polymer radical species)

catalysts have been the most popular of the transition metal catalysts and are easily handled and highly efficient [15].

Of the copper(I) systems, probably the most well-known is the so-called atom transfer radical polymerization (ATRP), which utilizes the lower oxidation state copper(I) halide and (usually) nitrogen-based ligand complexes as the catalyst. Further research resulted in development of systems such as simultaneous reverse and normal initiation (SR&NI) ATRP, activators generated by electron transfer (AGET) ATRP, activators regenerated by electron transfer (ARGET) ATRP, initiators for continuous activator regeneration (ICAR) ATRP and electrochemically mediated ATRP (eATRP). In these systems, copper (I) generated by reduction of higher oxidation state copper(II) was believed to be always present and act as the predominant activator [18].

For the copper(0) systems, copper(I) is used as a catalyst precursor to generate copper(0), which reacts with organic halides for radical generation. Previous research has suggested that in polar solvents copper(I) halides and nitrogen-based ligand complexes are often unstable to sometimes rapid disproportionation into copper (0) and copper (II) halide and this disproportionation facilitates an fast LRP, in which the radicals are generated from the nascent copper(0) atomic species and the deactivation is mediated by copper(II) halide. Both steps are proposed to proceed via a low activation energy outer-sphere single-electron-transfer mechanism and thus the polymerization was named single electron transfer living radical polymerization (SET-LRP) [19, 20].

The direct polymerization of a protected glycomonomer via ATRP was first reported in 1998 using CuBr/4,4′-di-*n*-heptyl-2, 2′-bipyridine catalyst in veratrole at 80°C [21] (see Table 1). Direct copper-mediated polymerization of unprotected glycomonomers was generally performed in highly polar solvents such as alcohols, dimethylformamide (DMF), dimethyl sulfoxide (DMSO), *N*-methyl-2-pyrrolidone (NMP) or mixtures with water [22]. The main reason for choosing such highly polar solvents is to solubilize the glycomonomer and the obtained glycopolymer, yet in some cases it resulted in low initiation efficiency or polymerization that was out of control [22, 23]. Previous research also revealed that direct aqueous ATRP of unprotected glycomonomers showed poor living character and that high ratios of alcohol as the co-solvent had to be used [24, 25]. The main reason is due to the fast propagation yet inefficient deactivation and the presence of side reactions under aqueous condition, such as hydrolysis of initiator and propagating polymer chain and, more importantly, disproportionation of copper catalyst [26]. Pure water has only been used as the solvent for surface-initiated polymerization, in which cases

Table 1 Specific polymerization conditions for the synthesis of glycopolymers via copper-mediated living radical polymerization

Glycomonomers	Catalysts	Solvents	Reaction temperature (°C)	References
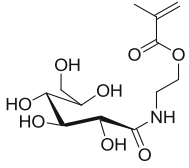	CuBr/ 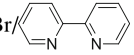	H_2O ×, MeOH, MeOH/H_2O, NMP	20	[24]
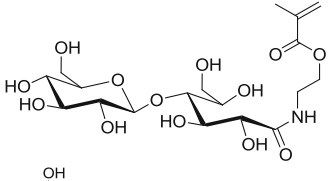				
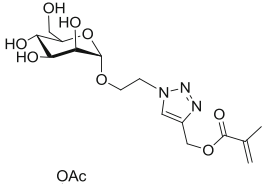	CuBr/ 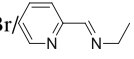	MeOH/H_2O (5:2)	25	[25]
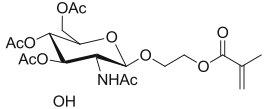	CuBr/ 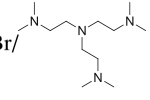	DMSO, MeOH	30	[22]
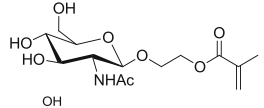				
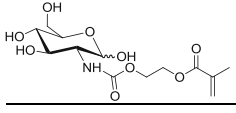	CuBr or CuCl/ 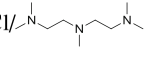	DMSO ×, DMF	40 (CuBr), 90 (CuCl)	[23, 30–32]

(continued)

Table 1 (continued)

Glycomonomers	Catalysts	Solvents	Reaction temperature (°C)	References
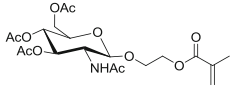	CuCl/ 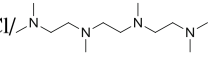	Anisole, DMSO	25 (DMSO), 60 (anisole)	[33, 34]
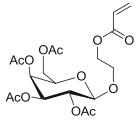	CuBr/ 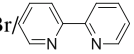	Chlorobenzene	80	[35, 36]
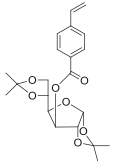	CuBr/ 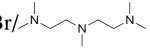	THF	60	[37, 38]
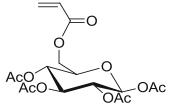	CuBr/ 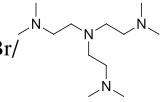	EtOAc	100	[39]
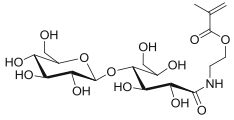	CuBr/$CuBr_2$/ 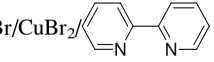	Pyridine/H_2O	25	[40]
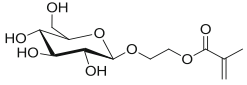	CuBr/ 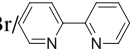	MeOH/H_2O	25	[41]
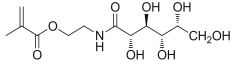	CuCl/$CuCl_2$/ 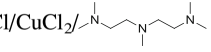	H_2O	30	Surface-initiated polymerization [29]

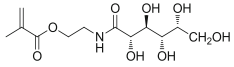	Ascorbic acid/$CuCl_2$ / 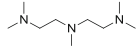	H_2O	30	Surface-initiated polymerization [28]
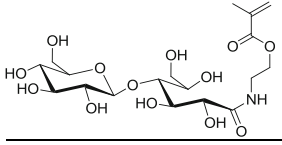	$CuBr/CuBr_2$/ 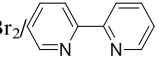	H_2O, NMP	25	Surface-initiated polymerization [27]

the chain end fidelity and molecular weight distribution tend to be difficult to elucidate [27–29]. Thus, more efforts are necessary to develop a proper catalyst system that could efficiently catalyse the polymerization of glycomonomers under different conditions, especially in aqueous media.[1]

1.3 Reversible Addition-Fragmentation Chain Transfer Polymerization

Since the discovery of reversible addition-fragmentation chain transfer (RAFT) in 1998 it has become one of the most popular living polymerization processes because it is tolerant of a wide variety of functional monomers and reaction conditions and also is promising in bio-applications [42, 43]. For the synthesis of glycopolymers, RAFT is probably the most popular LRP route at present (with about twice as many published papers than ATRP/transition metal-mediated strategies for the synthesis of glycopolymers) and different strategies have been developed for polymerization of both protected and unprotected glycomonomers [2, 43]. As an interesting case, direct RAFT polymerization of unprotected glycomonomers in pure water was reported in 2003, at which time direct aqueous ATRP of glycomonomers was still a challenge [24, 44]. Now, most RAFT polymerizations of glycomonomers are conducted in aqueous systems with some ratio of organic solvents (DMF, alcohol, DMSO etc.) with the aim of solubilizing the RAFT agents and radical sources. Most of these polymerizations are carried out at 60–80°C, although use of aqueous RAFT at ambient temperature has already been reported (Table 2) [45].

2 Novel Strategies in the Post-glycosylation of Pre-formed Polymers

2.1 Copper-Catalyzed Azide–Alkyne Cycloaddition Reaction

Copper-catalyzed azide–alkyne cycloaddition (CuAAC) has been widely used in the post-glycosylation of pre-formed polymers, for which the protected alkyne monomers can be first polymerized by various LRP strategies followed by removal of trimethylsilyl (TMS) protection groups using tetrabutylammonium fluoride (TBAF)/acetic acid for click reaction with azido functional sugars (Fig. 3) [59, 60]. This approach avoids the use of hazardous azide-functionalized monomers and utilizes the diversity of well-documented azido functional sugars [59].

[1] X means that in the corresponding literatures H_2O or DMSO were used as the solvent for polymerization, but the polymerization is not successful or out of control under relevant conditions.

Table 2 Specific polymerization conditions for the synthesis of glycopolymers via RAFT

Glycomonomers	RAFT agent	Solvents	Reaction temperature (°C)	References
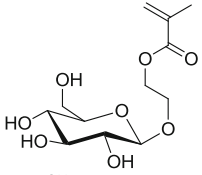	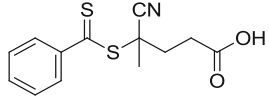	H_2O	70	[44]
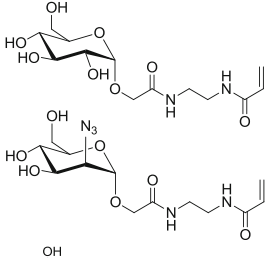	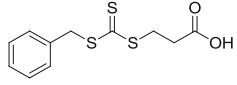	H_2O/DMF (5:1)	70	[46]
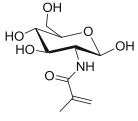	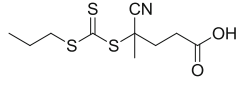	Acetate buffer/ethanol (4:1)	70	[47]
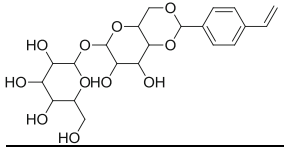	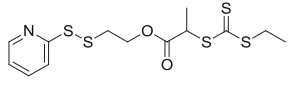	DMF	80	[48]

(continued)

Table 2 (continued)

Glycomonomers	RAFT agent	Solvents	Reaction temperature (°C)	References
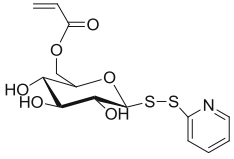	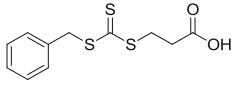	Chlorobenzene	60	[49]
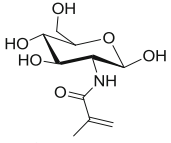	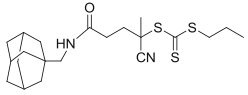	D_2O/DMSO	70	[50]
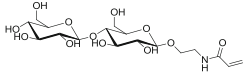	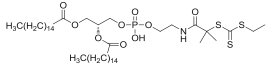	H_2O/DMF (4:1)	70	[51]
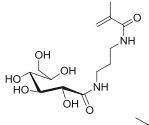	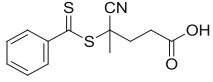	H_2O/DMF (5:1)	70	[52–54]
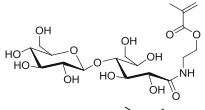				
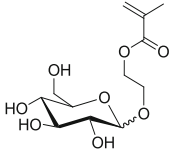	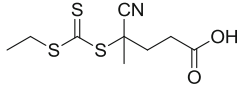	H_2O/EtOH (3:1)	70	[55]

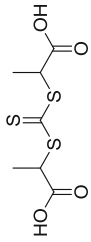	D_2O	60	[56]
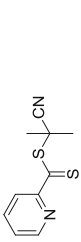	Toluene	75	[57]
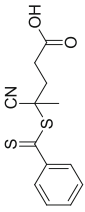	H_2O/DMF (3:7)	75	[58]

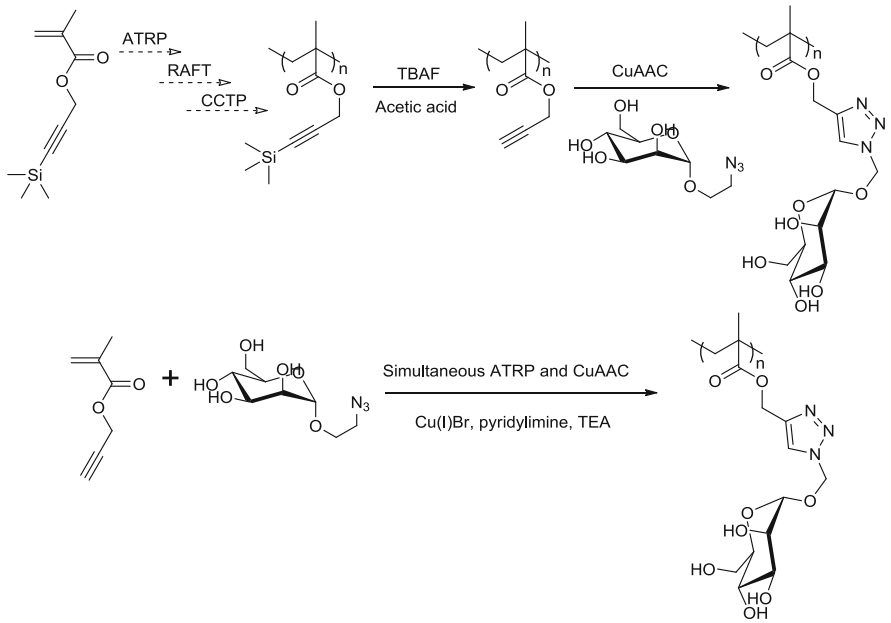

Fig. 3 Synthesis of glycopolymers via CuAAC of azide sugar with alkyne functional polymer or monomer

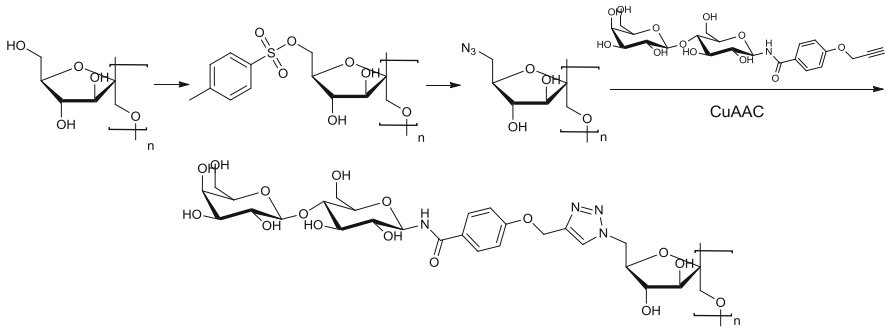

Fig. 4 Synthesis of glycopolymers via CuAAC of alkyne sugar with azido functional insulin

As an inverse approach, an insulin-based glycopolymer was synthesized by sequential chemical modification using tosylation, azidation and subsequent click reaction with alkyne sugars [61]. Due to the low ratio of tosylation, the azido functional insulin tends to be safe and the obtained insulin-based glycopolymers showed enhanced lectin affinity and gelation properties (Fig. 4).

Based on this combination of CuAAC and LRP, one-pot simultaneous ATRP and CuAAC was developed as a new tool for glycopolymer synthesis that utilized unprotected alkyne monomer and azido sugar (Fig. 3) [3]. As an inverse approach, a

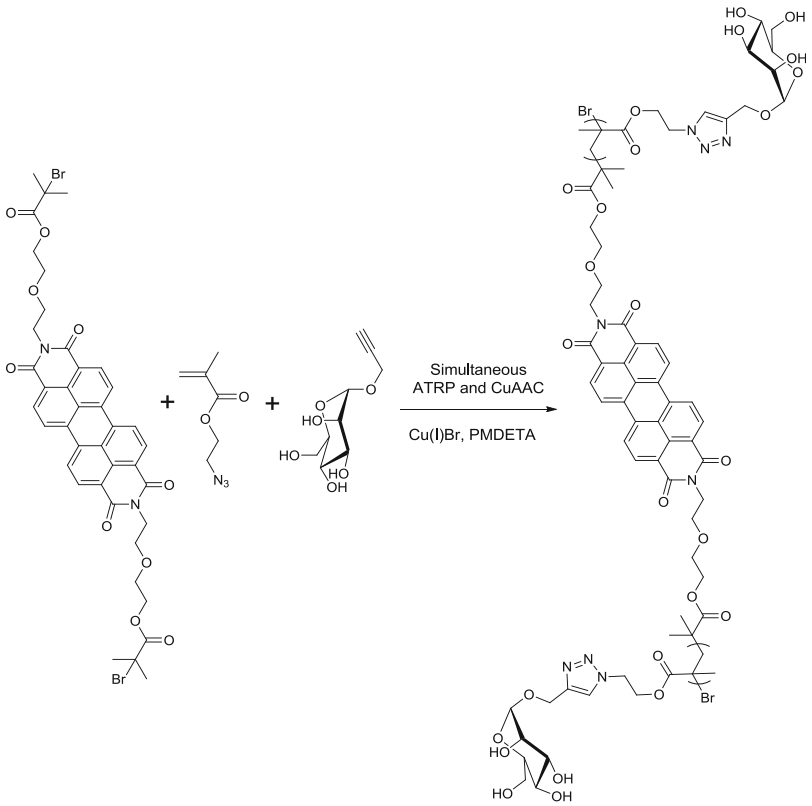

Fig. 5 Synthesis of glycopolymers via simultaneous ATRP and CuAAC using azido monomer and alkyne sugars

fluorescent glycopolymer could be synthesized via similar one-pot ATRP and CuAAC strategy using 2-azidoethyl methacrylate and alkyne mannose (Fig. 5) [62].

2.2 Thiol Click Chemistry

Thiol groups can react with many chemical species with high yields under benign conditions and thus many thiol-related reactions, such as thiol-ene, thiol-yne, thiol-epoxy, thiol-isocyanate and thiol-halogen reactions, are considered to be click-type reactions [63].

The thiol-yne coupling reaction is versatile, robust and can tolerate different functional groups due to its radical nature. It allows facile addition of two thiols to one alkyne group, which is suitable for construction of complex polymer structures such as networks, dendrimers and hyperbranched polymers [63, 64]. Successful glycosylation of linear polymers and dendrimers can be performed via radical-

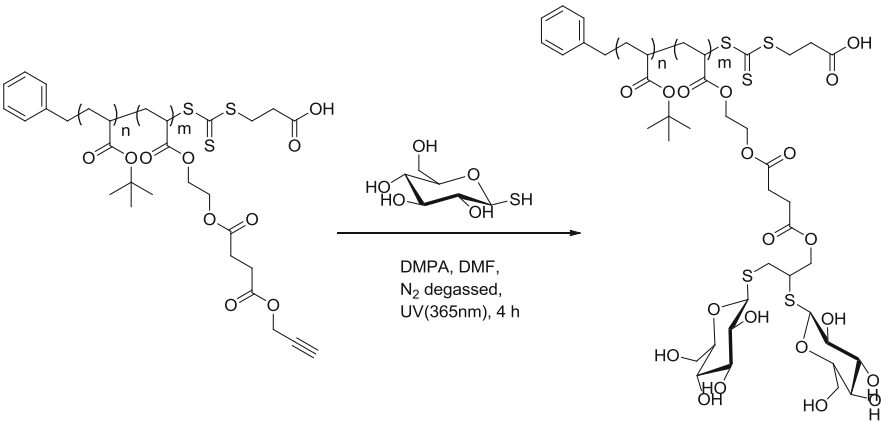

Fig. 6 Synthesis of glycopolymers via thiol-alkyne click reaction

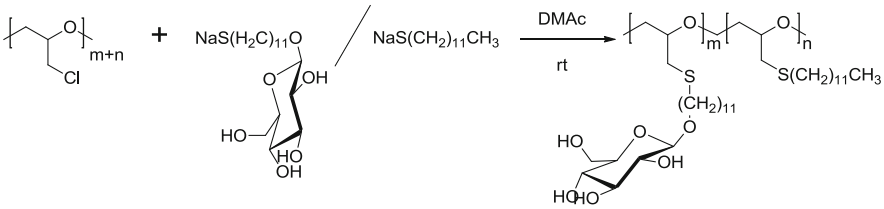

Fig. 7 Synthesis of glycopolymers via thiol-halogen click reaction

mediated thiol-alkyne click reaction, in which the 1-thiol-β-D-glucose reacts with the alkyne group in the presence of photo-initiator and UV light (Fig. 6) [65].

Thiol-halogen reactions, such as nucleophilic substitution reaction of thiocarbohydrate sodium salt with halogen-containing polymers, have been used for direct synthesis of glycopolymers [66]. This is a relatively slow reaction; however, no catalyst is needed and hazardous side products are also avoided. Thus, further research was reported utilizing similar methods (Fig. 7) [67].

2.3 Amine Chemistry

Condensation reactions between ketone groups and aminooxy sugars have become a tool for synthesis of glycopolymers and glycopeptides (Fig. 8) [68–70]. Generally, the reactions can be performed in acetate buffer or organic solvent/water mixtures at ambient temperature or higher temperatures (up to 95°C). The reaction conversion is only partial at ambient temperature but close to full conversion at higher temperature; however, reaction times can be as long as 4–7 days.

In order to eliminate the multistep reactions required for glycopolymer synthesis, free reducing sugars were used directly for the reaction with hydrazide functional polymer (Fig. 9) under acidic conditions in the presence of aniline catalyst [71].

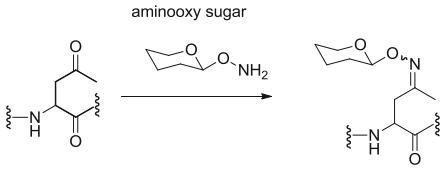

Fig. 8 Synthesis of glycopolymers by the reaction of ketones with aminooxy sugars

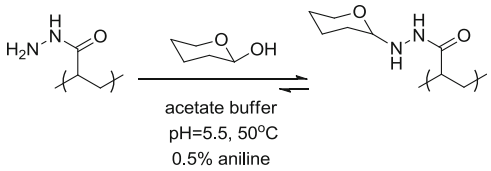

Fig. 9 Synthesis of glycopolymers by reaction of free reducing sugar with hydrazide functional polymer

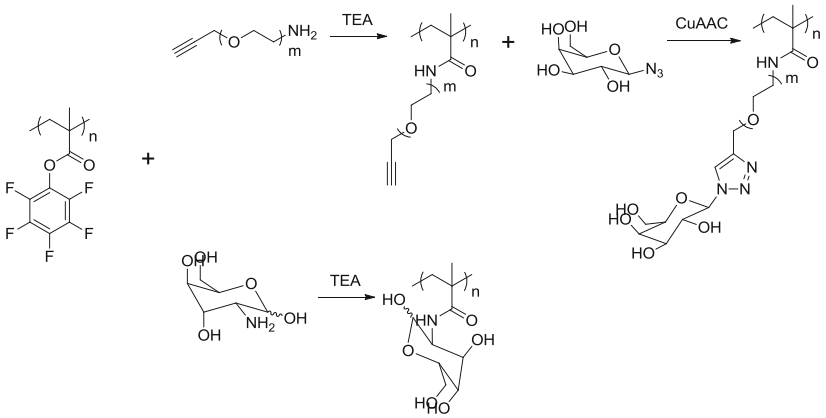

Fig. 10 Synthesis of glycopolymers by reaction of poly(pentafluorophenyl methacrylate) with functional amines

Different sugars, including mannose, fucose, lactose, xylose and panose, were used with this reaction, giving conversions ranging from 34% up to 95%.

Poly(pentafluorophenyl methacrylate) (PPFMA) bearing active ester groups could react with a wide variety of functional amines (Fig. 10). Glycopolymers have been synthesized by direct reaction of PPFMA with glucose amine or first with propargyl amine then with azido sugar via CuAAC, in which case the linker length and density of the glycopolymer could be adjusted by the length of propargyl amines [72, 73].

Other polymers bearing active ester groups, such as highly reactive *p*-nitrophenyl carbonate groups, can also react with amine functional sugars for the synthesis of glycopolymers (Fig. 11) [74, 75]. Utilizing the nucleophilic ring

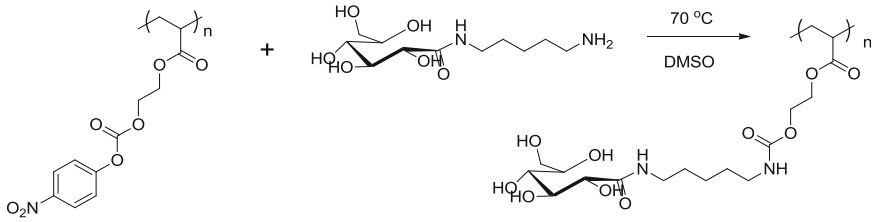

Fig. 11 Synthesis of glycopolymers by reaction of polymers bearing reactive *p*-nitrophenyl carbonate with amine functional sugar

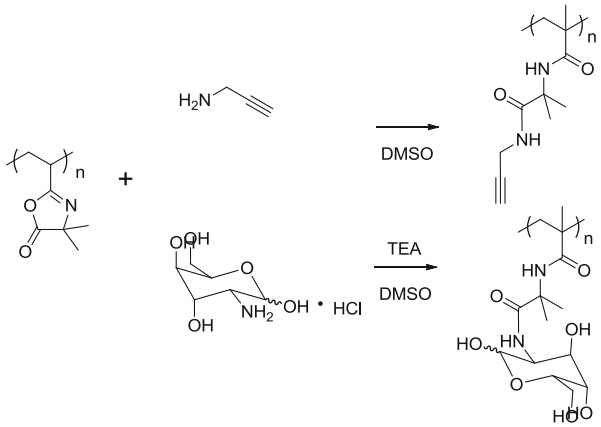

Fig. 12 Synthesis of glycopolymers by reaction of poly(azlactone) with amine functional sugar

opening reaction of azlactone with amine, poly(galactose) glycopolymers with long linker length between carbohydrate and backbone were synthesized by direct post-polymerization modification of poly(azlactone) scaffold and were shown to be very active against cholera toxin (Fig. 12) [76].

3 Novel Applications of Glycopolymers

3.1 Therapeutic Application: Anticancer and Anti-HIV

Carbohydrate-based anticancer agents have been explored with the aim of increasing the efficacy and decreasing the side effects of traditional anticancer Pt-based drugs [77, 78]. Recently, glycopolymer-based dithiocarbamates conjugates modified with gold(I) phosphine (Fig. 13) were synthesized and their cytotoxicity profiles examined. The results suggested that the gold conjugates showed higher accumulation and cytotoxicity to cancer cells due to the existence of glycopolymers and that their effect on normal breast cells was not significant [79].

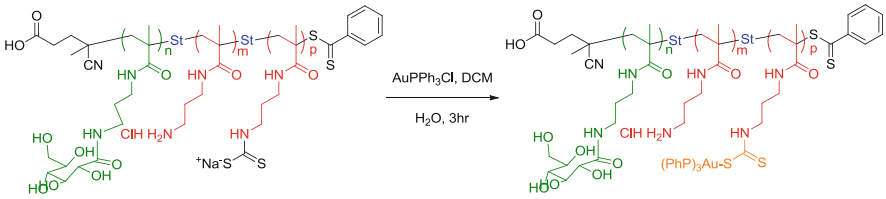

Fig. 13 Synthesis of glycopolymer–dithiocarbamate gold conjugates

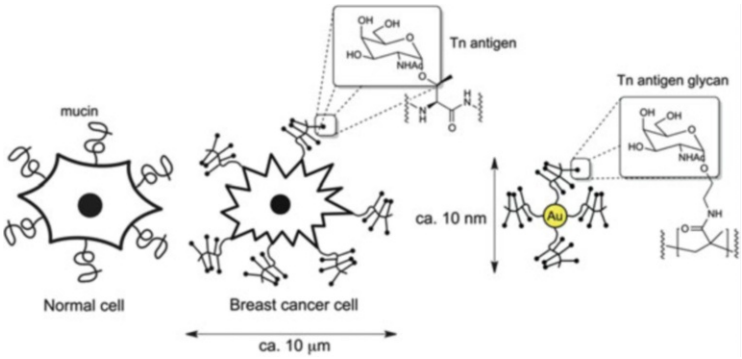

Fig. 14 Multicopy multivalent glycopolymer-stabilized gold nanoparticles as potential synthetic cancer vaccines [58]

Alison et al. synthesized a series of glycopolymers based on *N*-acetyl-D-glucosamine using RAFT and subsequently conjugated these glycopolymers to gold nanoparticles, yielding a type of multicopy multivalent nanoscale glycoconjugate (Fig. 14) [58]. These glycopolymer-stabilized gold nanoparticles could generate strong and long-lasting production of antibodies for selective recognition with Tn-antigen and thus have the potential to be used as a novel anticancer vaccine.

Relatively simple mannose-containing glycopolymers can effectively bind to human dendritic cell-associated lectin (DC-SIGN) and disrupted the interaction of DC-SIGN interactions with HIV envelope glycoprotein gp120, which could be seen as a new therapeutic approach (Fig. 15) [80].

3.2 Biocompatible Materials

Hyperbranched glycopolymers have been synthesized via RAFT (Fig. 16) and tested for blood biocompatibility. The results revealed that glycopolymers are highly haemocompatible and do not induce clot formation, red blood cell aggregation and immune response, suggesting a fine biocompatible material [53].

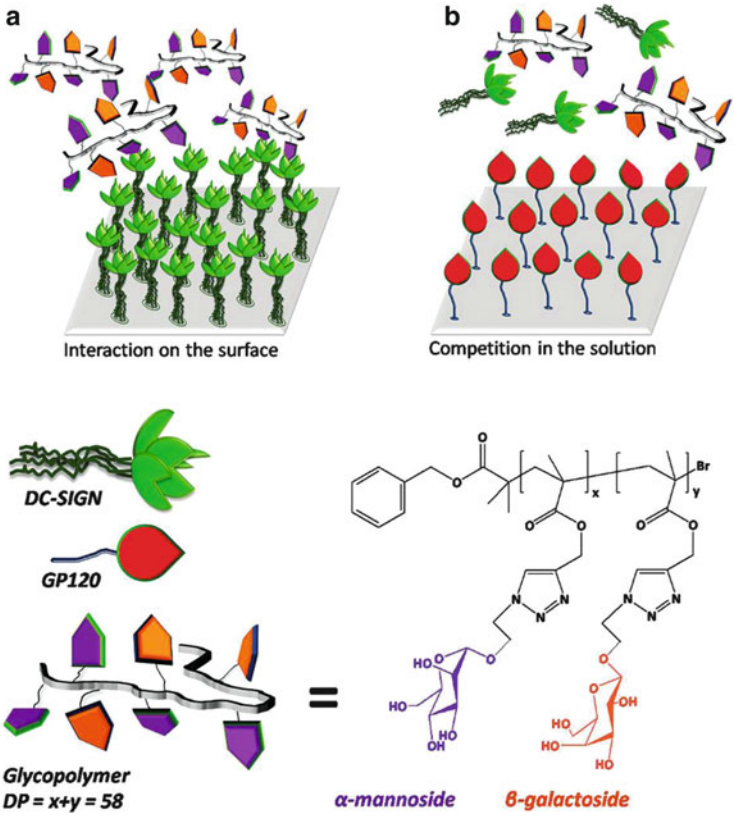

Fig. 15 High-affinity glycopolymer binding to human DC-SIGN and disruption of DC-SIGN interactions with gp120 [80]

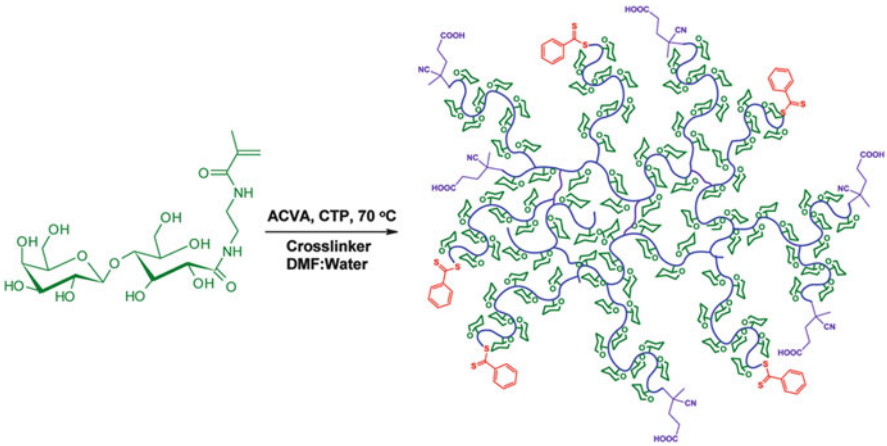

Fig. 16 Synthesis of hyperbranched glycopolymers via RAFT [53]

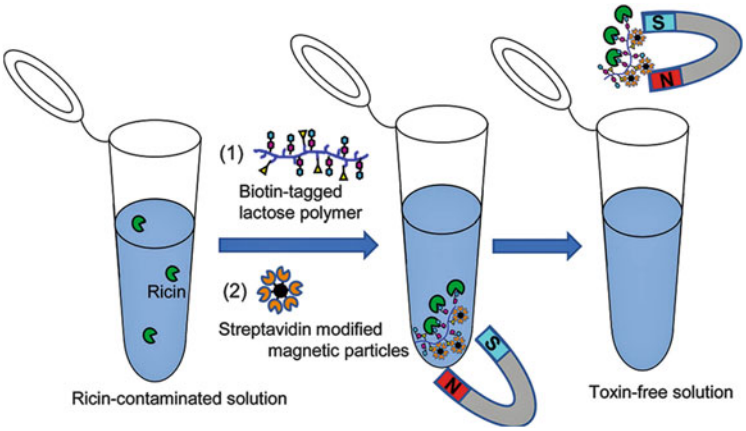

Fig. 17 Ricin decontamination using biotin-tagged lactose polymer [81]

Lactose and biotin-tagged glycopolymer could effectively absorb ricin and the obtained toxin–glycopolymer conjugate could be transferred onto streptavidin-modified magnetic particles for decontamination (Fig. 17) [81].

4 Summary

Glycopolymers represent a challenging and useful target for the synthetic polymer chemist. New polymerization strategies have resulted in a wide range of polymers that show really excellent recognition properties towards lectins. The polymer approach relying on multiple sugar epitopes and a flexible backbone is very different to the traditional organic chemistry approach where complex and elegant synthetic routes are used to put certain sugars in the right spatial orientation for lectin binding. We will see over the next few years if these glycopolymers will find a breakthrough application and, hopefully, this will occur in the near future.

Acknowledgment We appreciate financial support from the University of Warwick and China Scholarship Council (Q.Z.). Equipment used in this research was supported by the Innovative Uses for Advanced Materials in the Modern World (AM2), with support from Advantage West Midlands (AWM), and partially funded by the European Regional Development Fund (ERDF). D.M.H. is a Royal Society/Wolfson Fellow.

References

1. Ladmiral V, Melia E, Haddleton DM (2004) Eur Polym J 40:431
2. Ting SRS, Chen G, Stenzel MH (2010) Polym Chem 1:1392
3. Geng J, Lindqvist J, Mantovani G, Haddleton DM (2008) Angew Chem Int Ed 47:4180

4. Slavin S, Burns J, Haddleton DM, Becer CR (2011) Eur Polym J 47:435
5. Spain SG, Gibson MI, Cameron NR (2007) J Polym Sci A Polym Chem 45:2059
6. Vázquez-Dorbatt V, Lee J, Lin E-W, Maynard HD (2012) Chembiochem 13:2478
7. Spain SG, Cameron NR (2011) Polym Chem 2:60
8. Becer CR (2012) Macromol Rapid Commun 33:742
9. Kiessling LL, Grim JC (2013) Chem Soc Rev 42:4476
10. Kamber NE, Jeong W, Waymouth RM, Pratt RC, Lohmeijer BGG, Hedrick JL (2007) Chem Rev 107:5813
11. Aoi K, Tsutsumiuchi K, Aoki E, Okada M (1996) Macromolecules 29:4456
12. Tsutsumiuchi K, Aoi K, Okada M (1997) Macromolecules 30:4013
13. Kempe K, Weber C, Babiuch K, Gottschaldt M, Hoogenboom R, Schubert US (2011) Biomacromolecules 12:2591
14. Kamigaito M, Ando T, Sawamoto M (2001) Chem Rev 101:3689
15. Ouchi M, Terashima T, Sawamoto M (2009) Chem Rev 109:4963
16. Kato M, Kamigaito M, Sawamoto M, Higashimura T (1995) Macromolecules 28:1721
17. Wang J-S, Matyjaszewski K (1995) J Am Chem Soc 117:5614
18. Matyjaszewski K (2012) Macromolecules 45:4015
19. Percec V, Popov AV, Ramirez-Castillo E, Monteiro M, Barboiu B, Weichold O, Asandei AD, Mitchell CM (2002) J Am Chem Soc 124:4940
20. Percec V, Guliashvili T, Ladislaw JS, Wistrand A, Stjerndahl A, Sienkowska MJ, Monteiro MJ, Sahoo S (2006) J Am Chem Soc 128:14156
21. Ohno K, Tsujii Y, Fukuda T (1998) J Polym Sci A Polym Chem 36:2473
22. Vázquez-Dorbatt V, Maynard HD (2006) Biomacromolecules 7:2297
23. León O, Bordegé V, Muñoz-Bonilla A, Sánchez-Chaves M, Fernández-García M (2010) J Polym Sci A Polym Chem 48:3623
24. Narain R, Armes SP (2003) Biomacromolecules 4:1746
25. Geng J, Mantovani G, Tao L, Nicolas J, Chen G, Wallis R, Mitchell DA, Johnson BRG, Evans SD, Haddleton DM (2007) J Am Chem Soc 129:15156
26. Tsarevsky NV, Matyjaszewski K (2007) Chem Rev 107:2270
27. Yang Q, Ulbricht M (2011) Macromolecules 44:1303
28. Yuan J, Meng J-q, Kang Y-l, Du Q-y, Zhang Y-f (2012) Appl Surf Sci 258:2856
29. Meng J, Yuan J, Kang Y, Zhang Y, Du Q (2012) J Colloid Interface Sci 368:197
30. Muñoz-Bonilla A, León O, Bordegé V, Sánchez-Chaves M, Fernández-García M (2013) J Polym Sci A Polym Chem 51:1337
31. León O, Muñoz-Bonilla A, Bordegé V, Sánchez-Chaves M, Fernández-García M (2011) J Polym Sci A Polym Chem 49:2627
32. Munoz-Bonilla A, Heuts JPA, Fernandez-Garcia M (2011) Soft Matter 7:2493
33. Pfaff A, Shinde VS, Lu Y, Wittemann A, Ballauff M, Müller AHE (2011) Macromol Biosci 11:199
34. Pfaff A, Müller AHE (2011) Macromolecules 44:1266
35. Wang Y, Zhang X, Mu J, Li C (2013) New J Chem 37:796
36. Wang Y, Zhang X, Yu P, Li C (2013) Int J Pharm 441:170
37. Menon S, Ongungal RM, Das S (2013) Polym Chem 4:623
38. Menon S, Das S (2012) Polym Chem 3:2619
39. Lin K, Kasko AM (2012) Biomacromolecules 14:350
40. Chernyy S, Jensen BEB, Shimizu K, Ceccato M, Pedersen SU, Zelikin AN, Daasbjerg K, Iruthayaraj J (2013) J Colloid Interface Sci 404:207
41. Kitano H, Saito D, Kamada T, Gemmei-Ide M (2012) Colloids Surf B Biointerfaces 93:219
42. Chiefari J, Chong YK, Ercole F, Krstina J, Jeffery J, Le TPT, Mayadunne RTA, Meijs GF, Moad CL, Moad G, Rizzardo E, Thang SH (1998) Macromolecules 31:5559
43. Boyer C, Bulmus V, Davis TP, Ladmiral V, Liu J, Perrier S b (2009) Chem Rev 109:5402
44. Lowe AB, Sumerlin BS, McCormick CL (2003) Polymer 44:6761

45. Convertine AJ, Lokitz BS, Vasileva Y, Myrick LJ, Scales CW, Lowe AB, McCormick CL (2006) Macromolecules 39:1724
46. Abdelkader O, Moebs-Sanchez S, Queneau Y, Bernard J, Fleury E (2011) J Polym Sci A Polym Chem 49:1309
47. Smith AE, Sizovs A, Grandinetti G, Xue L, Reineke TM (2011) Biomacromolecules 12:3015
48. Mancini RJ, Lee J, Maynard HD (2012) J Am Chem Soc 134:8474
49. Pearson S, Scarano W, Stenzel MH (2012) Chem Commun 48:4695
50. Buckwalter DJ, Sizovs A, Ingle NP, Reineke TM (2012) ACS Macro Lett 1:609
51. Belardi B, O'Donoghue GP, Smith AW, Groves JT, Bertozzi CR (2012) J Am Chem Soc 134:9549
52. Ahmed M, Narain R (2012) Mol Pharm 9:3160
53. Ahmed M, Lai BFL, Kizhakkedathu JN, Narain R (2012) Bioconjug Chem 23:1050
54. Ahmed M, Narain R (2013) Biomaterials 34:4368
55. Song E-H, Manganiello MJ, Chow Y-H, Ghosn B, Convertine AJ, Stayton PS, Schnapp LM, Ratner DM (2012) Biomaterials 33:6889
56. Albertin L, Wolnik A, Ghadban A, Dubreuil F (2012) Macromol Chem Phys 213:1768
57. Glassner M, Delaittre G, Kaupp M, Blinco JP, Barner-Kowollik C (2012) J Am Chem Soc 134:7274
58. Parry AL, Clemson NA, Ellis J, Bernhard SSR, Davis BG, Cameron NR (2013) J Am Chem Soc 135:9362
59. Ladmiral V, Mantovani G, Clarkson GJ, Cauet S, Irwin JL, Haddleton DM (2006) J Am Chem Soc 128:4823
60. Nurmi L, Lindqvist J, Randev R, Syrett J, Haddleton DM (2009) Chem Commun 2009:2727
61. Izawa K, Akiyama K, Abe H, Togashi Y, Hasegawa T (2013) Bioorg Med Chem 21:2895
62. Xu LQ, Huang C, Wang R, Neoh K-G, Kang E-T, Fu GD (2011) Polymer 52:5764
63. Hoyle CE, Lowe AB, Bowman CN (2010) Chem Soc Rev 39:1355
64. Lowe AB, Hoyle CE, Bowman CN (2010) J Mater Chem 20:4745
65. Kumar J, Bousquet A, Stenzel MH (2011) Macromol Rapid Commun 32:1620
66. Chen Y, Chen G, Stenzel MH (2010) Macromolecules 43:8109
67. Kim JC, Rho Y, Kim G, Kim M, Kim H, Kim IJ, Kim JR, Ree M (2013) Polym Chem 4:2260
68. Marcaurelle LA, Shin Y, Goon S, Bertozzi CR (2001) Org Lett 3:3691
69. Rabuka D, Parthasarathy R, Lee GS, Chen X, Groves JT, Bertozzi CR (2007) J Am Chem Soc 129:5462
70. Godula K, Bertozzi CR (2012) J Am Chem Soc 134:15732
71. Godula K, Bertozzi CR (2010) J Am Chem Soc 132:9963
72. Gibson MI, Fröhlich E, Klok H-A (2009) J Polym Sci A Polym Chem 47:4332
73. Richards S-J, Jones MW, Hunaban M, Haddleton DM, Gibson MI (2012) Angew Chem Int Ed 51:7812
74. Muñoz-Bonilla A, León O, Cerrada ML, Rodríguez-Hernández J, Sánchez-Chaves M, Fernández-García M (2012) J Polym Sci A Polym Chem 50:2565
75. Muñoz-Bonilla A, Bordegé V, León O, Cuervo-Rodríguez R, Sánchez-Chaves M, Fernández-García M (2012) Eur Polym J 48:963
76. Jones MW, Richards S-J, Haddleton DM, Gibson MI (2013) Polym Chem 4:717
77. Huynh VT, Chen G, Souza P (2011) d.; Stenzel, M. H. Biomacromolecules 12:1738
78. Huynh VT, Quek JY, de Souza PL, Stenzel MH (2012) Biomacromolecules 13:1010
79. Ahmed M, Mamba S, Yang X-H, Darkwa J, Kumar P, Narain R (2013) Bioconjug Chem 24:979
80. Becer CR, Gibson MI, Geng J, Ilyas R, Wallis R, Mitchell DA, Haddleton DM (2010) J Am Chem Soc 132:15130
81. Nagatsuka T, Uzawa H, Sato K, Ohsawa I, Seto Y, Nishida Y (2012) ACS Appl Mater Interfaces 4:832

Adv Polym Sci (2013) 262: 61–92
DOI: 10.1007/12_2013_239

Published online: 29 October 2013

Graphene as a Target for Polymer Synthesis

Klaus Müllen

Abstract Graphene has remarkable physical properties, but existing production methods have severe deficiencies that limit its potential use in robust technologies. Opening a reliable and efficient synthetic route to graphene and its functionalized derivatives offers a path to overcome this obstacle for its practical application. Graphene can be regarded as a two-dimensional polymer (2D), and it is here argued that it, along with its derivatives, represents a realistic yet challenging target for polymer synthesis.

In order to demonstrate the possibility of such syntheses, an overview is presented on the evolution of phenylene-based macromolecules. It is shown how classical linear polyphenylenes can be expanded to increasingly more sophisticated structures involving two- and three-dimensional (3D) polyphenylene architectures. A crucial aspect of the meticulous synthetic design of these molecules has been the avoidance of defects within the structures, resulting in the precise control of their physical, especially optoelectronic, properties.

Linear conjugated polymers with defined optical properties have been made by controlling the degree of torsion between the benzene rings. This has included the development of efficient routes to ladder-type polymers and of step-ladder materials. Planar graphene molecules, or nanographenes, in a range of sizes and shapes have been fabricated by the controlled cyclodehydrogenation of 3D polyphenylene dendrimers. By combining knowledge gained from the synthesis of conjugated polymers, polyphenylene dendrimers, and nanographenes, it has proven feasible to make, either by solution or surface-bound methods, graphene nanoribbons with well-defined structures. These functional materials possess properties similar to graphene while displaying improved processability.

Finally, we review less-sophisticated paths towards graphene materials involving processing of graphene oxide, its reduction, and its hybridization with other components. These too have a role to play in acquiring functional graphenes where

K. Müllen (✉)
Max-Planck-Institute for Polymer Research, Ackermannweg 10, 55128 Mainz, Germany
e-mail: muellen@mpip-mainz.mpg.de

a lesser degree of control over the properties is required. This voyage of exploration towards the precise synthesis of conjugated phenylene-based polymers has thus had the dual objectives of fundamental research and practical materials science. En route we have had to meet the sometimes conflicting gauntlets thrown down by these two aims, which has at times involved trade-offs between the theoretically desirable and the reasonably accessible.

Keywords Bottom-up synthesis · Cyclodehydrogenation · Graphene · Nanoribbon · Polyphenylene

Contents

1 Graphene

Graphene, the monolayer subunit of the graphite lattice, has recently attracted great attention in fundamental and applied research. Only the future will tell whether the current excitement is just "hype" or whether there are real hopes for new, significantly improved applications; but, the physical properties of graphene are truly remarkable. What stands out is its unique band structure with a Brioullin zone and very high charge carrier mobility. While this would suggest high-tech applications in electronic devices, graphene and materials derived thereof are also expected to play a key role in energy technologies such as batteries, super-capacitors, and catalysts for fuel cells [1, 2] (see Sect. 8).

What has almost generated as much excitement, especially among non-scientists, is how this wonder-material was first produced. Andre Geim and Konstantin Novoselov [3–5] simply peeled graphene sheets off bulk graphite using cellophane tape! Their breakthrough idea, which has earned them a Nobel Prize, was to deposit this layer on suitable substrates for further physical characterization. This exfoliation technique, although it has produced samples enabling outstanding physical studies, cannot be the basis for robust technologies and, indeed, other preparation methods such as chemical vapor deposition (CVD) have been applied, particularly in attempts at fabricating transparent window electrodes [6–8]. One process

offering the possibility of relatively inexpensive, large scale production is a re-activated old method of graphite exfoliation [9, 10], which involves oxidation of graphite by harsh methods and the thermal or chemical reduction of the resulting graphene oxide sheets after dispersion and processing. We shall return to such "top-down" methods in Sect. 8, but we can anticipate that they will often lack structural perfection, reproducibility, and efficiency. Furthermore, they do not allow precise control over the size or the periphery of the graphene sheets. When considered from the point of view of polymer chemistry, graphene can be regarded as a one-atom thick 2D polymer, and such a structure cries out for chemical "bottom-up" approaches.

Before we introduce the polymer chemistry of graphene materials, however, one additional electronic feature must be introduced: graphene as a 2D π-electron system is a semimetal and thus characterized to have a vanishing band gap. This would not allow on/off behavior in, for example, a field-effect transistor using graphene as the semiconductor [11–15]. Thus, while graphene itself appears of limited use for digital electronics, it has been predicted that a band gap could be opened by geometric confinement such as occurs in graphene nanoribbons (GNRs) [16]. Therefore, a number of further top-down methods have been applied such as "unzipping" of carbon nanotubes [17] or lithography of graphene [18]. Again, from the point of view of polymer synthesis, the resulting nanoribbons still lack structural precision, particularly when looking at the edges of the GNRs. This lack of control is especially important in regards to the widths of GNRs, as it is essential to reach nanometer length scales in order to introduce a band gap.

The present text will focus on concepts towards establishing a reliable polymer chemistry approach for graphenes and graphene nanoribbons, with precise control over their size, edges, and chemical functionalities. Size is critical because electronic transport measurements, for example, require the sheets to form efficient contacts between electrodes. Exfoliated graphene flakes [19] extend well into the micrometer length scale, while graphene monolayers made by CVD cover areas of more than 30 × 30 inches (76 × 76 cm) [7] and, after etching of the substrate, can be processed by roll-to-roll printing [20, 21].

2 Expanding Synthetic Chemistry to Complex Macromolecules

At this point, the reader may ask, is the title just an attempt to follow current fashion, or is graphene a true target for polymer synthesis? This then may provoke the more general question, how does polymer synthesis position itself between classical organic synthesis and other physical methods of material fabrication such as, for example, exfoliation of graphite? Classical organic chemistry takes pride in the complexity of the structures, often natural products, produced. It employs parameters such as reducing the number of synthetic steps (e.g., by using elegant

protocols like cascade reactions) or obtaining high enantiomeric excesses to measure its achievements. When looked upon from this angle, polymer synthesis may appear simple. One could, of course, respond that polymer synthesis, in view of the targeted materials usually being intended to have definite functions, must be practical, high yielding, and, as an additional characteristic, combined with appropriate processing to create a defined macroscopic state of matter. But, even if one accepts that there is a rewarding chemistry beyond the dilute solutions of classical organic chemistry and that a material synthesis is not always concluded by obtaining a satisfactory solution NMR spectrum, some questions remain valid: how complicated can polymer synthesis be, and must it necessarily be restricted to straightforward one-pot methods? Some examples from the current cutting edge of polymer science illustrate these points.

Metallocene-catalyzed polyolefin synthesis [22–26] has been developed to obtain an impressive microstructural precision, and chain-growth polymerization of activated olefins has become more and more controlled [27–30]. These techniques have furnished increasingly demanding polymer topologies such as block copolymers [31–35], star-polymers [36, 37] or core–shell polymer nanoparticles [38–43]. Step-growth polycondensation [44–47] not only differs from other polymerization techniques from the point of view of its kinetics and plots of molecular weight versus conversion, but also requires different experimental techniques. When considering the state-of-the-art here, it is apparent that this field of polymer chemistry has especially profited from the development of new monomeric building blocks, new methods of catalysis, particularly those using transition-metal complexes, and from deeper mechanistic insights [48, 49]. This is nicely illustrated by the case of conjugated polymers with alternating donor (D) and acceptor units (A) [50–65]. Such D–A polymers have acquired enormous importance as the active components in solar cells and field-effect transistors and have defined new benchmarks for high performance organic electronic polymers [66–72]. In the first phase, an ever increasing number of new electron-rich and electron-poor components have been incorporated into the polymers to tune their band gaps and packing behavior [73]. Synthetic methods like Stille or Suzuki coupling have been instrumental for ensuring the strictly alternating inclusion of different building blocks [59, 74]. Obtaining high molecular weights and low polydispersities appears to be crucial for improving device performance [75]. In order to establish the required stoichiometries for optimized polycondensations, pure crystalline stannyl or boronate components are needed, but further aspects such as the acceleration of the reactions by microwave irradiation instead of conventional heating [76, 77], appropriate choice of the catalytic metal–ligand complex [48, 78, 79], end-capping to remove undesirable terminal functional groups [80–85], and rigorous purification of the products could well be added to this list of improvements. Morphological control of conjugated polymers [86, 87], for example, in designing bulk heterojunction solar cells [58–61, 70], has demanded the synthesis of rod–rod and rod–coil block copolymers and, in this context, chain-growth mechanisms involving the living ends of the rod-like segments have become particularly important [81, 88–91].

Conjugated polymers are often poorly soluble in conventional organic solvents. This makes processing from solution and deposition of thin films, as required for electronic devices, difficult [92–100]. Attachment of solubilizing alkyl groups is then indispensable – as long as they do not obstruct the extended π-conjugation. Such substituents may be considered as diluting the electronic effect, but often play an important role in controlling the packing and self-assembly. An alternative way of dealing with intractable polymers is the use of a precursor synthesis. Thereby, a soluble precursor polymer is synthesized, cast into a film, and transformed by heat or irradiation into the supposedly insoluble conjugated target polymer. A well-known case is poly(phenylenevinylene) synthesis [74, 101, 102], where the vinylene unit is established by a 1,2-elimination. A special kind of precursor route will later be introduced for the synthesis of graphene nanoribbons. It is clear, however, that the perfection of the final transformation is decisive for the quality of the material and its performance in a device [103].

Polymer synthesis is thus determined both by the method applied and the envisaged target structure. We now focus on target materials that have played an important role in the development of polymer synthetic methods and that have seen a remarkable renaissance in the service of chemical graphene synthesis.

3 Ribbon (or Ladder) Polymers

Special emphasis is paid to a modular approach in which functionalized benzene moieties serve as building blocks for chain-type (1D), disc-type (2D), and dendrimer-type (3D) graphene derivatives (Fig. 1) [104, 105]. The critical question, when taking on graphene as a challenge for polymer synthesis, is whether any of these polyphenylenes can serve as precursors for graphenes and how the necessary chemical transformation to flat graphene sheets can be accomplished.

It is interesting, indeed, to first present three cases taken from the mid-1990s in which our group focused on the synthesis of so-called ribbon or ladder polymers. These macromolecules have paved the way to graphene nanoribbons, although at that time we did not refer to them as GNRs.

Linear poly(*para*-phenylene)s **1** are prototypical conjugated polymers [106–108]. Electronically, they are characterized by a wide band gap and have played an important role as blue emitters in light-emitting diodes [109–112]. Dieter Schlüter and Gerhard Wegner [79, 113–116] introduced the Suzuki coupling [49, 117] for the synthesis of poly(dialkylphenylene)s, marking a milestone for the synthesis of conjugated polymers (Scheme 1). However, the alkyl substituents required for solubilization cause significant torsion about the inter-ring bonds and thus hamper extended π-conjugation [118, 119].

Therefore, it was our idea to proceed from linear to ladder-type polyphenylene structures by bridging neighboring benzene rings via methylene groups. This would not only enforce a planarization of the whole π-system, but also provide extra carbons to attach solubilizing alkyl chains without compromising the conjugation.

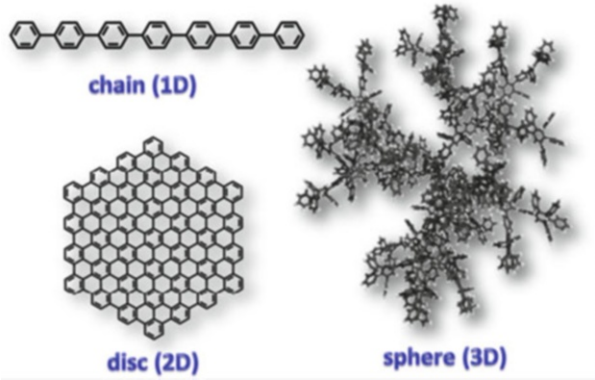

Fig. 1 The benzene ring as modular building block for 1D, 2D, and 3D hydrocarbons

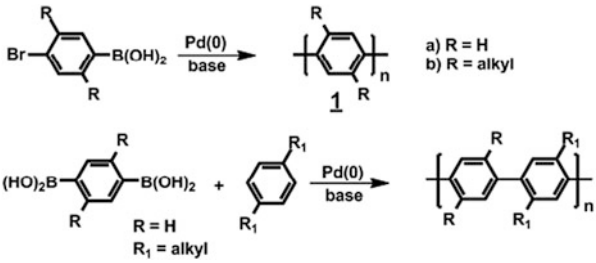

Scheme 1 Synthesis of poly(dialkylphenylene)s by Suzuki coupling using the AB and the AA+BB protocols

The synthesis of these ladder-type polyphenylenes **2** and **3**, as first accomplished in our group by Ullrich Scherf [120, 121], was realized via suitably functionalized polyphenylene precursors **2a** and **3a**, which were then transformed into the target ribbon via a polymer-analogous Friedel–Crafts cyclization [122, 123] (Scheme 2).

The poly(9,9-dialkylfluorene)s **4** use the same principle of alkyl substitution at a methylene bridge [124]. They constitute step-ladder rather than ladder polymers because only every second biphenyl inter-ring bond is free of torsion. Not surprisingly, the blue electroluminescence of the ladder polyphenylene [125, 126] appears bathochromically shifted with respect to that of the polyfluorenes. To better adjust the blue emission to the sensitivity of the human eye, we have made step-ladder polymers in which not two, but rather three, four, or five benzene rings were incorporated in the planarized ladder as in polymers **4a**, **4b** and **4c** (Fig. 2). Andrew Grimsdale and Josemon Jacob in our group developed the fine tuning of physical properties to a high level of sophistication – from light emission [125–127] to single molecule conductance [128].

A polymer-analogous ring closure similar to that of **2** and **3** afforded the ribbon structure **5,** which was composed only of benzenoid rings and, thus, constituted a true graphene nanoribbon [129, 130] (Scheme 3). As in **2** and **3**, a successful two-step protocol was employed. It included the substituted polyphenylene **5a**, which was subjected to multiple formation of six-membered rings by reductively coupling the carbonyl-containing substituents.

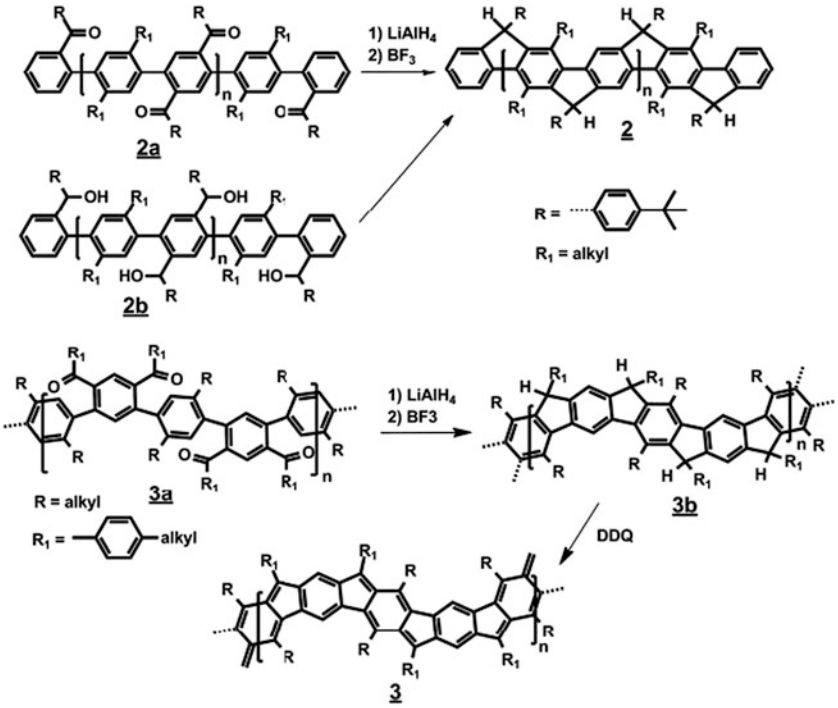

Scheme 2 Synthesis of ladder-type polyphenylenes using *para*- and *meta*-dibenzoyl benzene building blocks, and dehydrogenation of **3b** to polymer **3** with *para*-quinodimethane repeat units. No control over the configuration at the bridging methylene carbons could be achieved

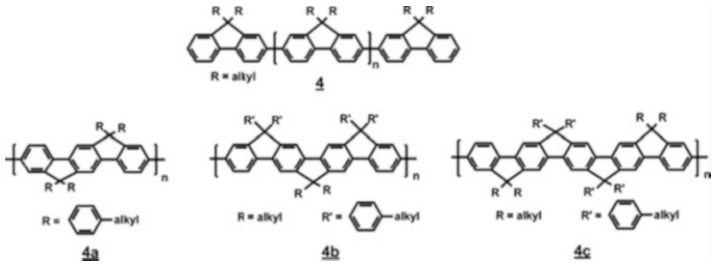

Fig. 2 Polyfluorenes (**4**) and step-ladder polymers (**4a**, **4b**, **4c**)

A closely related case is the synthesis of so-called polyrylenes **6** in which naphthalene repeat units are fused via their four *peri*-positions. Polymer **6** has played an important role in the electronic study of low band gap polymers [131]. We first synthesized the homologous oligomer series **7** and **8** comprising an increasing number of naphthalene units [132–134] (Figure 3).

The synthetic concept foresaw the synthesis of solubilized polyperylene species **9**, which would be subjected to an oxidative fusion including, again, a transition

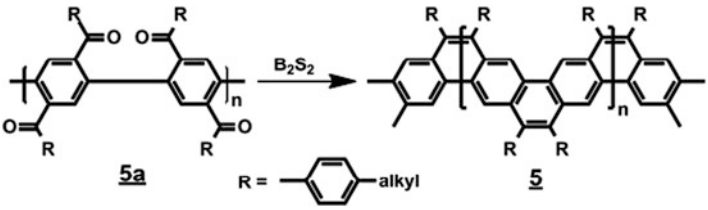

Scheme 3 Ladder-type polyphenylene **5** with vinylene bridges, an early version of graphene nanoribbons

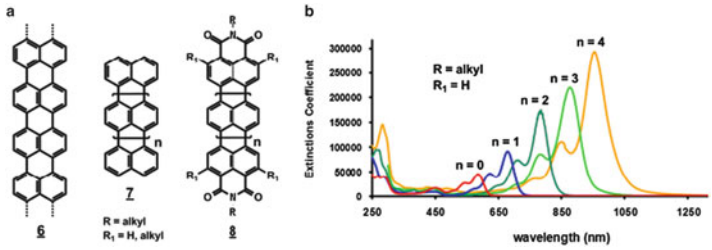

Fig. 3 (**a**) Polyrylene **6** (a graphene nanoribbon) and homologous series of oligomeric rylenes **7** and rylenediimides **8**. (**b**) UV–Vis spectra of **8**

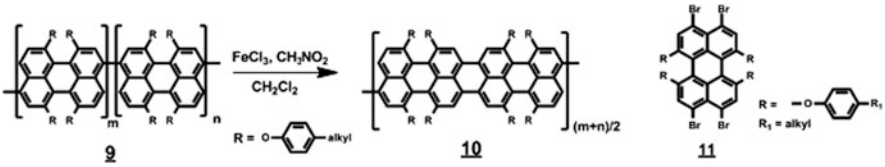

Scheme 4 Oxidative fusion of polyperylenes to polyquaterrylenes

from a linear to a double-stranded target structure **6.** Interestingly enough, this reaction with a kind of C–H-activation allowed us to transform polyperylenes **9** to polyquaterrylenes **10**, but did not lead to more extended ribbon structures (Scheme 4). Only very recently have we been able to provide key intermediates, such as the tetrabromoperylenes **11**, suitable for a straightforward polyrylene ribbon synthesis via parallel aryl–aryl couplings using a Yamamoto-type reaction with Ni(0) [135].

Measurements of thermally stimulated currents in our ladder-type polyphenylenes probe the density of mobile charge carriers after detrapping and reveal extremely low trap densities [136, 137].

Avoidance of structural defects in conjugated polymers is indeed a highly critical issue because such defects not only interrupt the π-conjugation, but also serve as traps for excitons or charges. The perfection of the polymer-analogous-transformations from **2a** or **2b** to **2**, from **3a** to **3**, and from **5a** to **5** is thus a

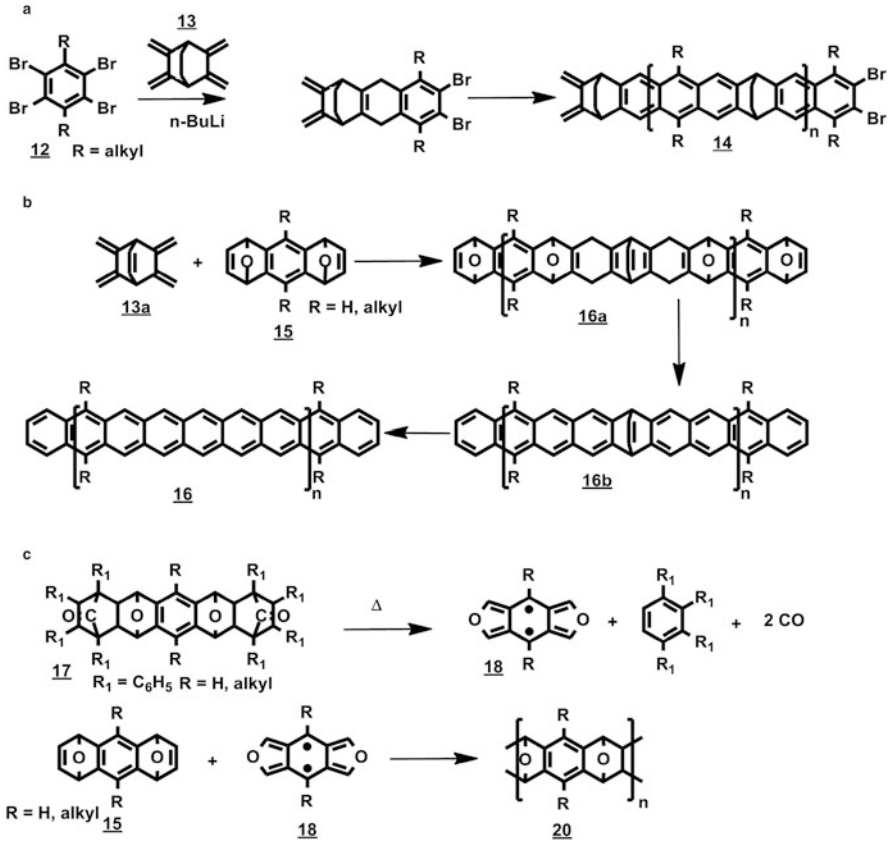

Scheme 5 En route to poly[*n*]acenes

demanding experiment. The polyalcohols **2b** gave better results upon Friedel–Crafts cyclization than the corresponding polyketones **2a**, and the choice of the reagent in the reductive C–C bond formation to produce **5** appeared crucial. Nevertheless, defects did occur and failure to form all bridges in **2** had, for example, severe consequences for the persistence length of the chain [138, 139]. This finding suggests the obvious conclusion that in polymer synthesis it is not only important to avoid defects, but also to detect them. It appeared logical then, and this approach has been pursued since [140, 141] by both our group and that of Schlüter [142], to target poly [*n*]acene structures **20** and to synthesize the required six-membered rings using Diels–Alder cycloadditions [143–145]. A number of diene and dienophile components have been utilized (Scheme 5) and the idea has been to benefit from the perfection of a concerted 4+2 cycloaddition for the precise synthesis of ribbon structures [146].

Reactions of AA+BB type have mainly been considered with double diene systems such as **13** and **13a** or double dienophiles such as **12** and **15**. Even with

reactive dienes and dienophiles there remain troublesome issues such as solubilizing the rigid ribbon structures and, again, of transforming the precursors into the target polymers by dehydrogenation of cyclohexadiene and by deoxygenation of oxa-bridged cyclohexadiene repeat units [147]. Interestingly, graphene oxide (see Sect. 8), a product of graphite oxidation, is nowadays used as an intermediate in graphite exfoliation and believed to incorporate, among many other oxygen-containing functions, epoxy groups. After processing, graphene oxide must be reduced back to graphene, a process that is normally far from complete.

Similarly, neither the deoxygenation nor the dehydrogenation of the ribbon precursor polymers **16a** are believed to proceed quantitatively, and the process is further complicated by the anticipated chemical instability of the target ribbon structure.

4 Polycyclic Aromatic Hydrocarbons as Nanographenes: The Precursor Route

Before dreaming up improved ways to synthesize graphene nanoribbons and their precursors, another synthetic concept must be introduced, and that is cyclodehydrogenation of non-planar oligo- and polyphenylenes towards graphene-like benzenoid polycycles. This reaction has played an important role in our search for graphenes and, like the above transformations, has served as a key tool in fabricating 2D polymers.

In 1995, our attention was attracted to the synthesis of larger and larger polycyclic aromatic hydrocarbons (PAHs). These π-systems, originally pioneered by Erich Clar [148, 149], have long been investigated as test cases for spectroscopy and molecular orbital theory, as carbon-containing constituents of interstellar space [150, 151] and, more recently, as organic semiconductors in electronic devices [103]. It was only a decade after our synthesis of giant PAHs that they became considered as mini-subunits of graphenes and the term "nanographenes" was coined to define graphene structures smaller than 100 nm in size [152]. Our starting point was the high-yield cyclodehydrogenation of the propeller-shaped hexaphenylbenzene **23a** toward hexa-*peri*-hexabenzocoronene **23** upon treatment with oxidants such as iron(III)chloride in dichloromethane at room temperature [153] (Scheme 6).

While appearing conceptually simple, the mechanism of this "graphitization" is quite complex. Two neighboring phenyl groups undergo an electrocyclic ring closure after arenium cation or radical cation formation followed by the elimination of protons [154, 155]. The stepwise flattening of all phenyl units can proceed in different ways, where the radical cation mechanism is less favorable for larger systems [156].

In our hands, the "superbenzene" (C42) **23** was the starting member of a whole new PAH family of varying sizes and symmetries [157, 158] (Fig. 4). A key structural modification relates to the nature of the periphery. Although we have in Fig. 4

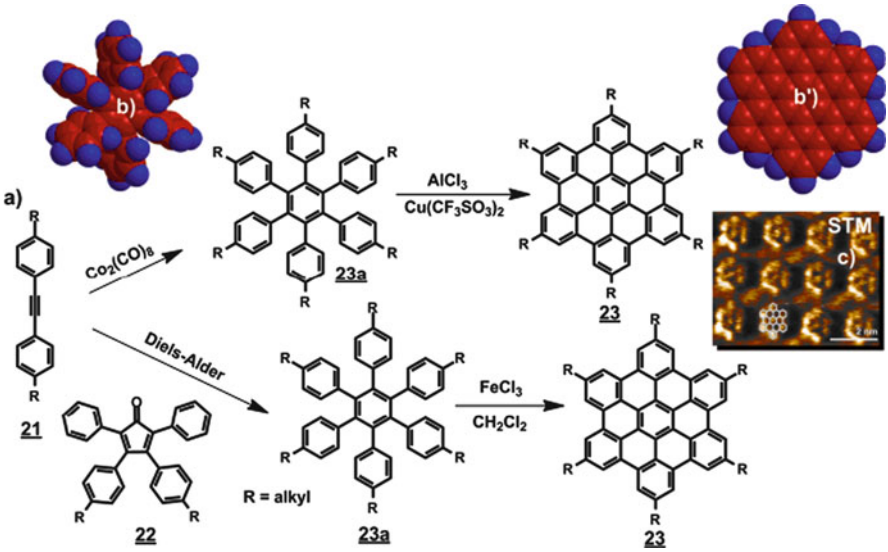

Scheme 6 (**a**) Synthesis of hexa-*peri*-hexabenzocoronenes **23** from hexaphenylbenzenes **23a**. (**b**, **b′**) Representations of **23a** and **23**, respectively. (**c**) STM image of **23** without substituents

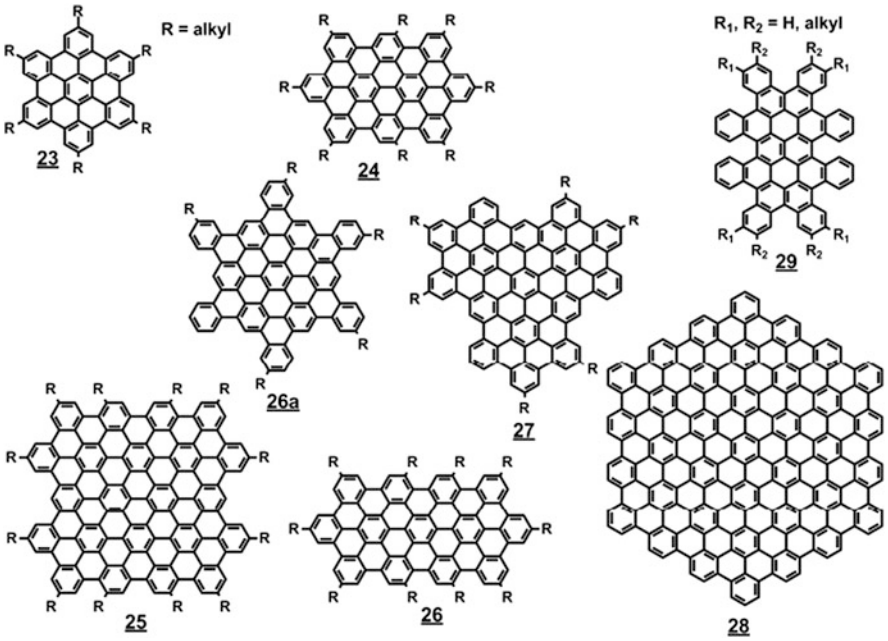

Fig. 4 Large polycyclic aromatic hydrocarbons

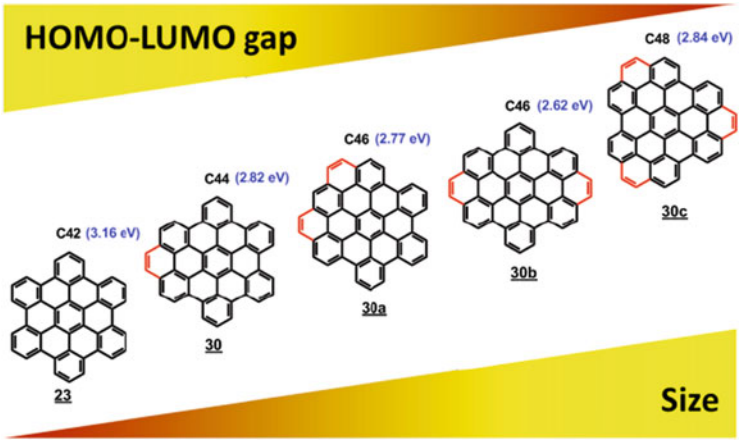

Fig. 5 Polycyclic aromatic hydrocarbons with partial zig-zag peripheries

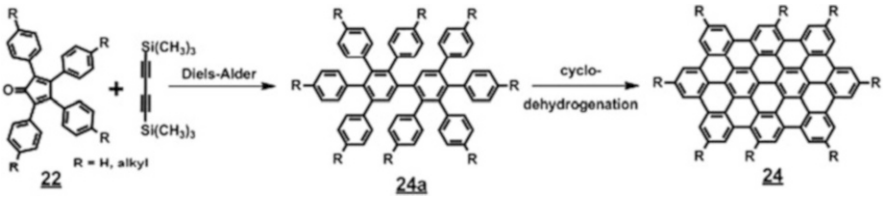

Scheme 7 Two-step synthesis of C60 **24**

focused on armchair and cove-type peripheries, a transition to zig-zag edges has important consequences for the electronic structure [13]. A cove-type edge occurs in the octabenzocircumbiphenyl **29** introduced by Colin Nuckolls and coworkers [159]; even more important for lowering the HOMO–LUMO gap is the presence of zig-zag peripheries, as we have shown for the series **30**–**30c**. Such zig-zag edges (Fig. 5) are particularly important in graphene nanoribbons, as discussed in Sect. 7, since they can give rise to high-spin states.

Our synthesis of these nanographenes always proceeds in a two-step fashion via a non-planar precursor that is finally subjected to planarization. This synthetic protocol has been applied by many other groups and proven its value in different areas of materials chemistry [160–166].

The topology of the twisted precursors must, in a kind of molecular Lego, be made such that all the benzene rings can "fall together" into one plane. The C60 homologue **24** illustrates how to go beyond C42 (Scheme 7). The precursor of the C222 PAH molecule **28a** can be made in different ways using Diels–Alder cycloadditions with tetraphenylcyclopentadienone or cobalt-catalyzed cyclotrimerization of diarylacetylenes [167] (Scheme 8).

It appeared that the perfect flattening, the so-called cyclodehydrogenation, was extremely sensitive to the topologies of the precursors. A relevant model reaction

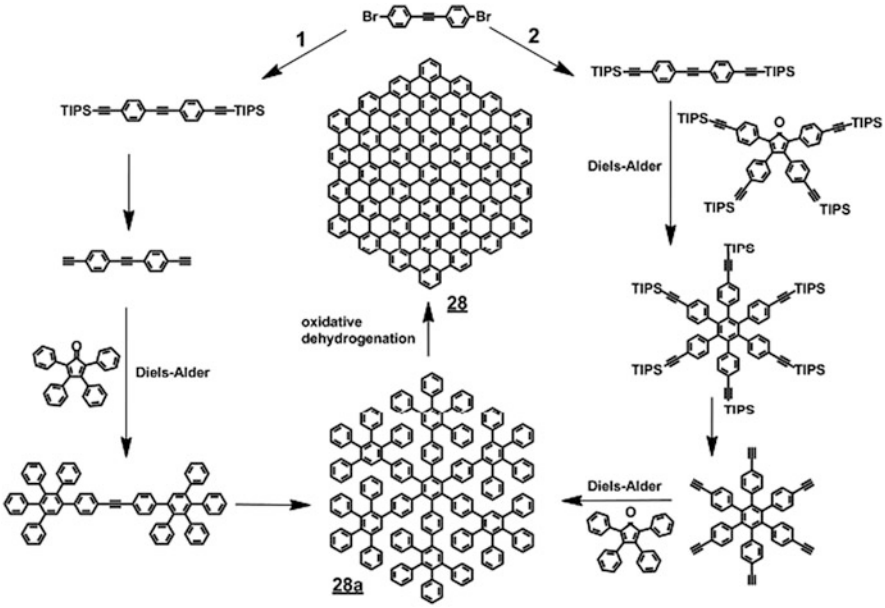

Scheme 8 Synthesis of the giant hexagonal PAH C222 **28**

for GNR polymers (Scheme 9) is the synthesis of supernaphthalene **31**. In this case, a partial pre-planarization of the precursor (i.e. starting from **31a** instead of **32**) enables a higher degree of perfection of the dehydrogenation [168] (Scheme 9).

It is not surprising that the large polycyclic disc structures strongly tend to aggregate and are sparingly soluble in organic solvents. This is why attachment of alkyl chains is mandatory. As convincingly described by Yves Geerts, Mark Watson, Jishan Wu, and Wojtek Pisula in our group, nanophase separation between the hard aromatic core and the soft alkyl mantle leads to the formation of extremely stable discotic mesophases [157, 158], with a high degree of order in the columnar superstructures [169, 170]. Also, solution and melt processing into thin-film devices become possible, which allows control over the packing mode and thus over the charge carrier mobility [14, 171, 172]. The size of these PAHs is a critical issue because it not only enables the straightforward detection of the molecules by scanning tunneling microscopy (STM) with atomic resolution, but also the observation of single-molecule current–potential curves by STM [173–175]. Indeed, diode-like characteristics could be recorded for single PAH molecules and interpreted in terms of a resonant enhancement of the tunneling current [153, 176]. It is thus fair to say that the synthesis and processing of nanosized disc-type PAH molecules have opened new avenues in nanoscience and molecular electronics [170, 173, 177, 178]. The logical question now is: how can we extend the synthesis of giant PAHs to that of polymeric GNRs?

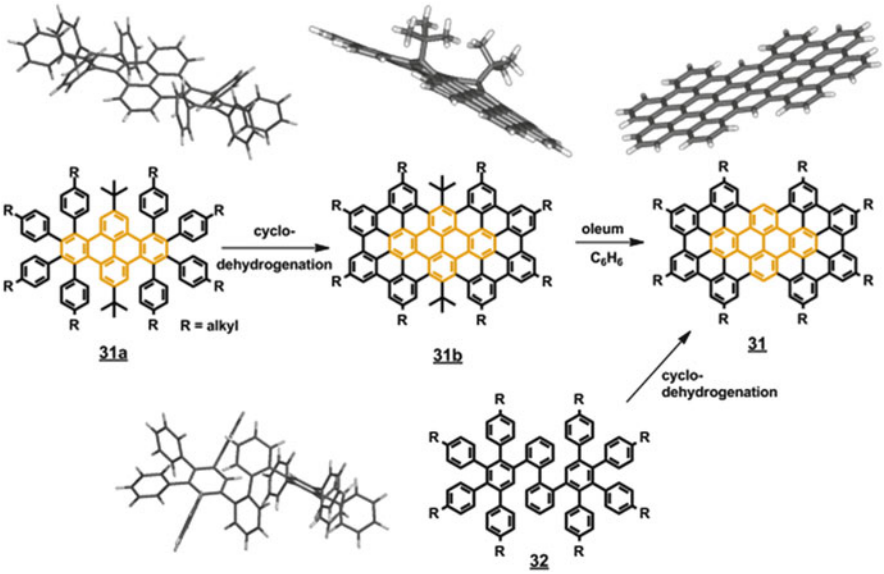

Scheme 9 Synthesis of "supernaphthalene" **31** from **31a** and from **32**

5 Dendritic (3D) Polyphenylenes

At this point, a little detour was rewarding as we discovered that the precursors used for the synthesis of the planarized nanographene molecules turned out to be true dendrimers made from nothing more than twisted, tightly packed, interlocked benzene rings The crystal structure of the C222 precursor **28a** reveals a unique 3D molecule with twisted benzene rings and large voids [167] (Fig. 6).

Upon inspection of this polyphenylene, the reader readily recognizes the central benzene ring (A in Fig. 6) as the core and the C rings as branching points of a general dendrimer structure [179–186]. This realization stimulated us to synthesize larger and larger polyphenylene dendrimers by both convergent and divergent approachs [187–189]. For the divergent approach (e.g., layer-by-layer synthesis), the AB_2-type branching reagent **33** turned out of be crucially important [190]. Indeed, the diene unit of this AB_2 system could react with any multiethynyl core to furnish new pentaphenyl benzene moieties in a Diels–Alder cycloaddition with expulsion of carbon monoxide (Scheme 10).

In this case, the two dienophile functional groups in **33** remained unreacted due to the presence of the bulky triisopropylsilyl (TiPS) protecting groups [191]. Removal of the latter with ammonium fluoride reactivated the ethynyl dienophiles for the next-generation synthesis by another round of addition of the AB_2 systems. The shape and packing density of the dendrimers could be tuned by the choice of the ethynylated core and of the branching reagent (e.g., the AB_4 system **33a**

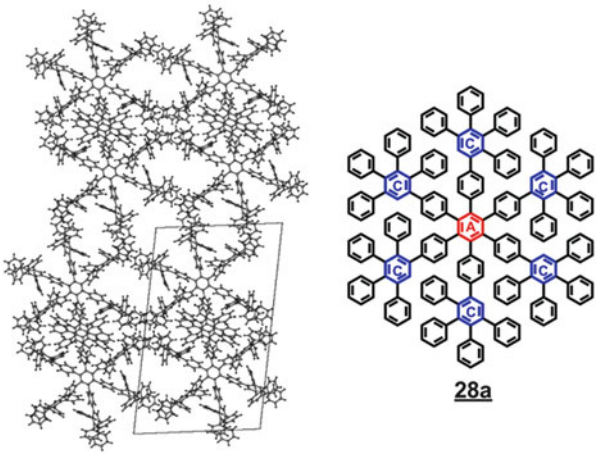

Fig. 6 Crystal structure of the dendritic precursor molecule **28a**: *A* central benzene ring, *C* branching points of central dendrimer structure

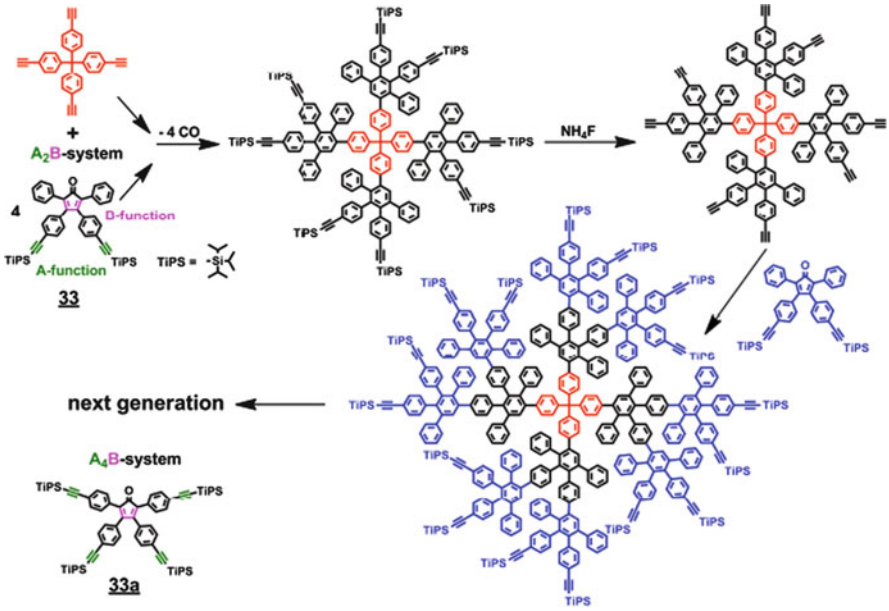

Scheme 10 Synthesis of polyphenylene dendrimers with tetraphenylmethane core by a divergent approach. *TiPS* triisopropylsilyl

instead of **33**). End-capping with a functionalized tetraphenylcyclopentadienones allowed chemical decoration of the surface, including the subsequent synthesis of core–shell particles through grafting reactions.

In a number of papers, our group has proven the high degree of structural perfection of these dendrimers, even for molecular weights in excess of 1 MDa [192–194]. Key roles were played by Martin Baumgarten, Andreas Herrmann, and Tanja Weil. Surprisingly, these giant dendrimers are soluble in organic solvents and, in many cases, the solubility actually increases with molecular weight. Due to their shape-persistence (note that back-bending of the dendron arms is not possible), these dendrimers can serve as molecularly defined, functional nanoparticles [182, 195]. This stands in marked contrast to the situation prevailing in dendrimers made from conformationally flexible repeat units [182, 183]. Indeed, the semirigid character of the PPD scaffolds leads to a perfect nanosite definition of functional groups [190] such as chromophores [196, 197], catalysts [190, 198, 199], or electrolytes [200] at the core, in the scaffold, or on the rim of the dendrimers [201]. Although these aspects are beyond the scope of the present text, it should be mentioned that polyphenylene dendrimers, due to their unique structure and functionalization, have served, for example, as light harvesting complexes [133, 202], receptors for gas sensing [203, 204], and carrier systems for crossing the blood–brain barrier [205, 206].

6 Graphene Nanoribbons: The "Solution" Approach

In turning now to the synthesis of GNRs, the design of the precursor polyphenylene structures is the first and decisive step [207]. In this realm, we have synthesized a series of polyphenylenes, mostly using transition metal-catalyzed aryl–aryl coupling mechanisms (i.e., Suzuki and Yamamoto), with varying aspect ratios, and we have investigated their dehydrogenation [208]. Figure 7 presents only one example. As learned from the oligomeric model cases, the accessibility of the monomeric starting compounds, the ease of their polymerization by aryl–aryl coupling, and the perfection of the final cyclodehydrogenation are the key criteria in judging the chemical pathways to GNRs.

Also, the molecular weights and thus the lengths of the final GNRs are critical parameters in subsequent physical experiments [208, 209]. These include, for example, the attachment of electrodes for charge transport measurements. A key problem concerns solubility and solution processability. Not unexpectedly from our experience with polyphenylene dendrimers, many precursor polymers were soluble in organic solvents, even without additional alkyl substitution, and could be well characterized. However, the oxidative dehydrogenation led to flat, completely insoluble materials and this, of course, also hampered a determination of the structural perfection of the graphenic structure [210]. Three questions had thus to be dealt with: (i) how could we keep the synthesized GNRs soluble, (ii) how could we synthesize non-planar polyphenylene precursors with high molecular weights, and (iii) how could we control the widths to tune the resulting band gaps? [16] A repetitive Diels–Alder cycloaddition between the "double" diene **34b** and the "double" dienophile (AA+BB) afforded high molecular weights of precursor

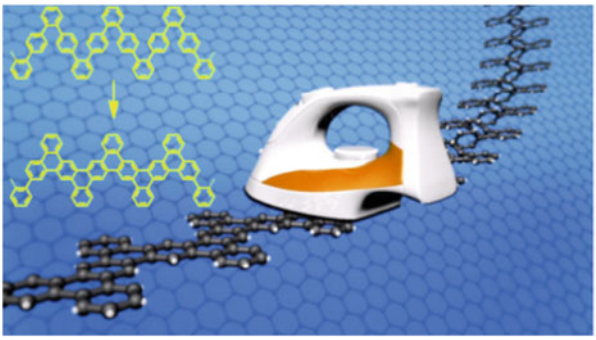

Fig. 7 Synthesis of GNRs using a precursor polyphenylene and its "flattening"

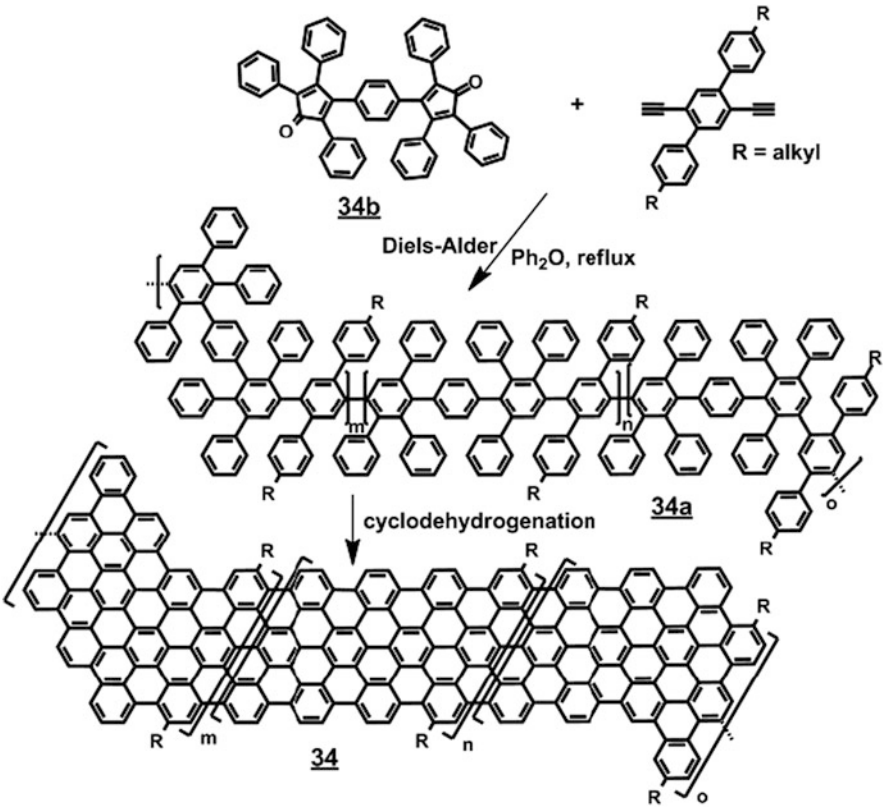

Scheme 11 Synthesis of kinked GNRs by repetitive Diels–Alder cycloaddition (AA+BB route)

polymer **34a**, but the characterization of the dehydrogenation product **34** by electron microscopy pointed toward "graphenic" clusters as a result of strong aggregation [211] (Scheme 11).

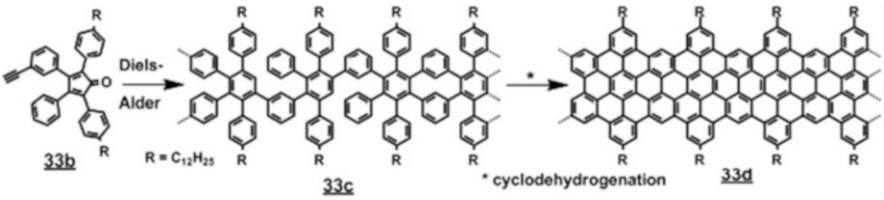

Scheme 12 Synthesis of soluble GNRs by repetitive Diels–Alder cycloaddition (AB route) and dehydrogenation

The following case created a breakthrough. Instead of the above AA+BB combination or the AB_2-type tetrapenylcyclopentadienone **33** for dendrimer synthesis, we made the AB-type species **33b**, which was additionally equipped with long linear or branched alkyl tails. One readily envisages that a polyphenylene **33c** with a rod-like shape is formed in a repetitive Diels–Alder cycloaddition (Scheme 12).

The experience outlined above also suggested that the subsequent dehydrogenation could occur from different conformations and thus afford either straight or kinked graphene nanoribbons.

This ambiguity, however, could largely be avoided by the presence of spatially demanding alkyl chains, which indeed gave rise to straight graphene nanoribbons and also helped to keep the GNRs soluble. This then allowed characterization of the graphene nanoribbons not only by Raman spectroscopy, but also by scanning probe microscopies at the solid–liquid interface after depositing the materials from solution onto substrate surfaces [212]. The GNRs had lengths of up to 200 nm, which was a remarkable case of a demanding polymer synthesis. Xinliang Feng in our group played a key role in developing GNR syntheses. Further, this success laid the groundwork for a bottom-up approach toward graphene species, which allowed much more rigorous structure control than the physical top-down methods; even more so since the widths of the GNRs could be modified by the choice of the monomeric building blocks [209].

What remains to be investigated is, of course, the avoidance of even minor structural defects, the band structure of the GNRs, their processing into thin films and, as mentioned already, their interfacing with electrodes for nanodevice fabrication.

7 Graphene Nanoribbons: The Surface-Bound Approach

The syntheses of graphene nanoribbons and the troublesome problems of keeping the products solution-processable will continue to define challenges for polymer chemistry, but have also suggested another, somewhat unconventional, approach. In a fruitful interaction with the group of Roman Fasel, who are focused on the surface physics and STM detection [213–216] under UHV conditions, we deposited dihalo-substituted, non-planar oligophenylene compounds as precursor

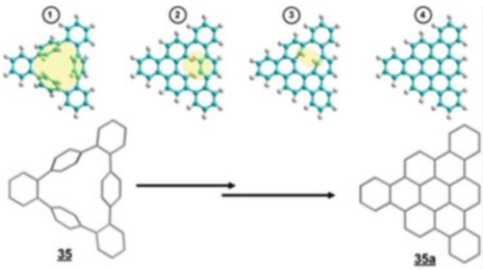

Fig. 8 Surface cyclodehydrogenation of cyclophane **35** via steps *1* to *4*

monomers onto conducting metal surfaces and investigated opportunities of achieving (i) polymerization and (ii) dehydrogenation while monitoring the reaction by STM. Our test case for surface-immobilized chemical transformations of large PAHs was the synthesis and transformation of the cyclophane **35**, where solution photolysis indeed yielded the triangle **35a** via multiple electrocyclic ring closures analogous to the stilbene–phenanthrene interconversion. Interestingly, however, the precursor **35**, when deposited on a Cu(111) surface and subjected to heating, gave the same product [217] (Fig. 8). The stepwise process of planarization (i.e., the sequence of electrocyclic ring closure reactions) could even be followed by STM through the detection of the thickness of a molecule.

At that time we knew from the literature [218, 219] that dibromo derivatives of suitable aromatic molecules, when deposited on metal surfaces and heated, could undergo a C–Br bond cleavage followed by the subsequent polymerization of the resulting diradicals. This prompted us to deposit precursor **36**, which had previously been successfully subjected to conventional polymerization in solution, onto metal surfaces (Scheme 13). We could indeed achieve and visualize the polymerization after carbon–halogen bond cleavage and the subsequent dehydrogenation to give polymer **37** upon further heating [220–222].

This is a remarkable case of surface-bound polymer synthesis with in-situ control by STM. Visualizing the growth of a single polymer chain with atomic precision and in real space is, indeed, an exciting experience for any chemist. It then appeared straightforward, as in the solution chemistry, to modify the dibromo precursor in order to vary the aspect ratios. A promising case, in view of controlling the band structure of the resulting graphene nanoribbons, was the bianthryl compound **38** (Scheme 14). Indeed, this building block could be polymerized again to a non-planar polymer **39**, and then subjected to polymer-analogous dehydrogenation to give the straight nanoribbon **40** by further heating [221, 223]. Elsewhere, we have given a detailed account of the mechanism of the polymerization and dehydrogenation conditions, which is, however, beyond the scope of the present text [224]. A significant aspect of this research was our ability to alter the band gap of the GNRs between ~1.6 and 3.1 eV based on the linear or "chevron"-type architecture, which is crucial for their use in various applications [225].

The crucial issues in the choice of starting compounds are (i) the stabilization of the intermediate diradical upon interaction with the metal; (ii) the diffusion

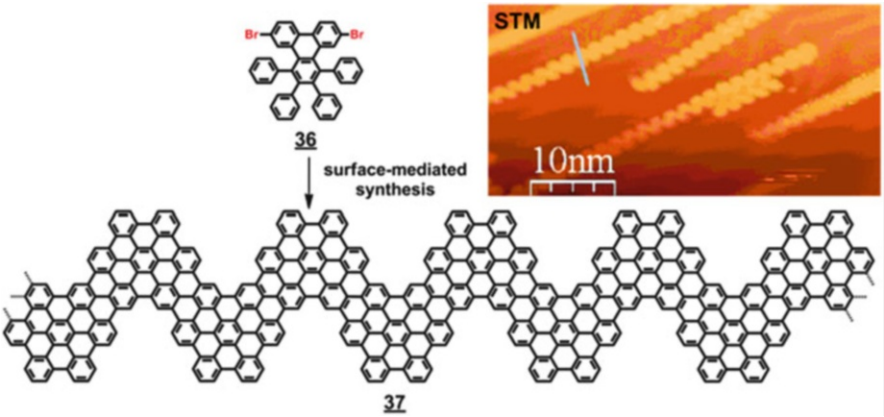

Scheme 13 Surface-mediated synthesis of GNRs based on dibromo precursor **36,** and STM image of **37**

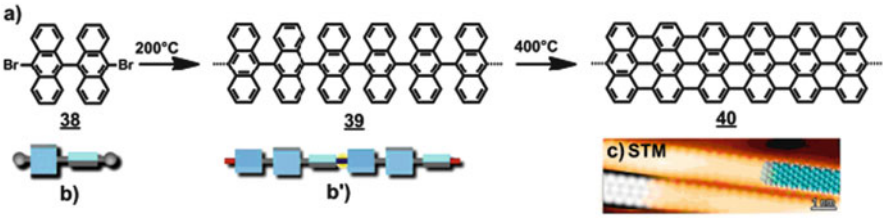

Scheme 14 (**a**) Surface-mediated synthesis of GNRs **40** via the precursor polymer **39** using a dibromo-bianthryl precursor **38**. (**b**, **b′**) Representations of **38** and **39,** respectively. (**c**) STM image of **40** (Reproduced from reference 221 with permission from the Nature publishing group and Macmillan publishers)

of this intermediate on the surface, to find a partner for growth of the chain; and (iii) the non-planarity of the precursor while maintaining minimal steric hindrance between phenyl substituents. Although it is, of course, fascinating to make polymers under in-situ control by STM, there remain many critical issues. One point relates to the occurrence of side reactions such as hydrogen transfer connecting two growing ribbon structures to form complex networks, and the other concerns the mechanistic question of how larger oligomers can diffuse on the surface to find their reaction partner in a step-growth polymerization [224].

The reader might become aware of the fact that this surface-bound polymer chemistry furnishes monolayers, and thus affords only negligible amounts of product. It is therefore logical to ask whether this approach can be scaled up, and the answer is unfortunately, no. In many cases, however, films from a monolayer or from a few layers might give a desired function such as hole injection from an electrode or charge carrier transport in a field-effect transistor. Such syntheses of films made from single or a few layers would represent a highly economic and efficient

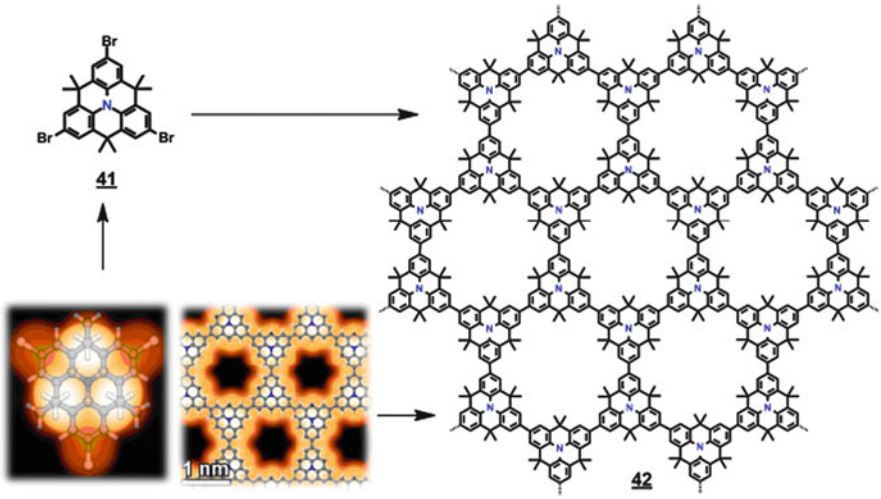

Fig. 9 Surface-supported synthesis of a 2D honeycomb network (**42**) using a tribromo derivative of triangulene (**41**) (Reproduced from reference 227 with permission from the Centre National de la Recherche Scientifique (CNRS) and The Royal Society of Chemistry)

utilization of a material. An illustrative case is the introduction of a tribromo derivative of the triangulene **41** (Fig. 9). Here, one forms a honeycomb network **42** that, due to the design of the monomer, contains atomically precise pores [226–228]. Furthermore, we showed that it was possible to transform hexaiodo-functionalized cyclohexa-*m*-phenylene thin films into "super-honeycombs" and porous graphene structures by heating on a silver substrate. STM of these materials also revealed atomically well-defined pores [229].

Indeed, a simulation predicts that such monolayers, when made perfect over large areas, could serve as unique membranes for the separation of hydrogen and helium. Many possibilities have appeared that also shed light on the corresponding solution processes: (i) diradical intermediates could be stabilized by the surface and thus their polymerization achieved, reactions that would otherwise be suppressed by side reactions such as hydrogen transfer from the solvent; (ii) different monomers such as dihalo- and trihalo precursors could lead to complex topologies such as the Y-shape macromolecule **43** (Fig. 10) to which one could anchor three different contacts; (iii) the use of high Miller-index surfaces could allow for an ordered assembly of monomers at step-edges and lead to polymers in a pre-oriented fashion; (iv) monomers incorporating, for example, nitrogen or boron could lead to a precise placement of the heteroatoms, as doping centers, in the graphene products; and (v) the arm-chair periphery of GNRs can be transformed into a zig-zag structure. The synthesis of GNRs with zig-zag edges will be reported soon.

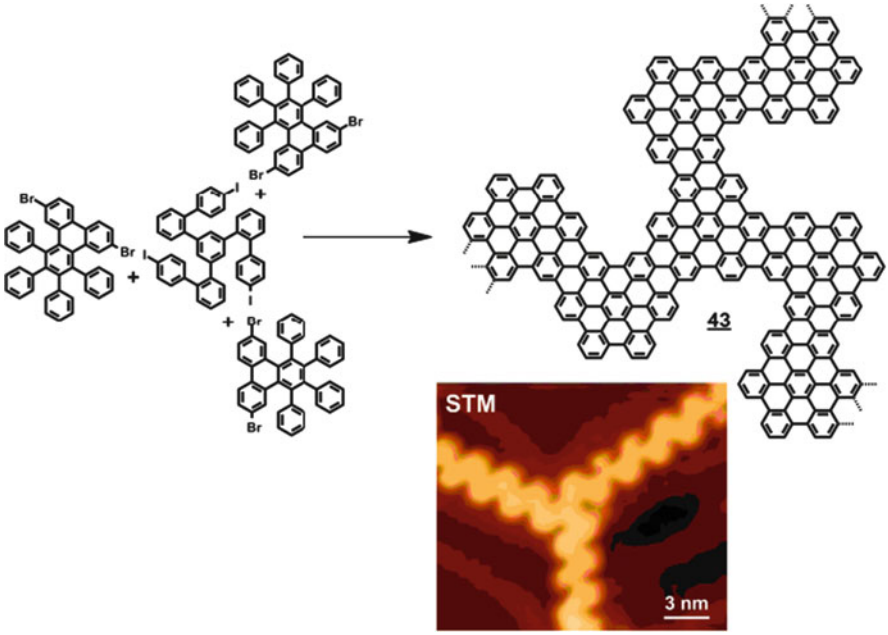

Fig. 10 Synthesis of a Y-shaped GNR and STM image of **43** (Reproduced from reference 221 with permission from the Nature publishing group and Macmillan publishers)

8 From Precision Polymer Synthesis to "Cook-and-Bake"

At this point, the trade-off between the added value of materials synthesis and the complexity of the experimental protocol should again be invoked. When focusing on molecularly defined nanographenes and GNRs, their electronic properties and their use as semiconductors stand in the foreground. Graphenes and related carbon materials, however, can also find applications in other areas such as sensing [230–237], gas separation [238–240], and energy technology [2, 241–244]. The urgent need by society for a safe and sustainable energy supply strongly encourages us to briefly consider their use in energy storage and transformation. Graphite materials have already found extensive use in batteries [245–249] and supercapacitors [250–254]. Increasing energy and power densities are, first, an issue of the electronic structure of the electrodes, whereby inorganic materials are known [255–257] to have distinct advantages over graphite, and, second, of the morphology. The latter must allow efficient ion and electron transport while remaining unobstructed over many cycles. Not surprisingly, graphenes accessible by methods other than molecular synthesis have received attention toward these ends. While CVD deposition of graphene on metal surfaces has already been mentioned for the fabrication of transparent electrodes [7, 8], graphene oxide reduction [258–262] and pyrolysis of carbon-rich precursors [263] come into play as useful and versatile techniques. Graphene oxide, although it must be reduced back to graphene

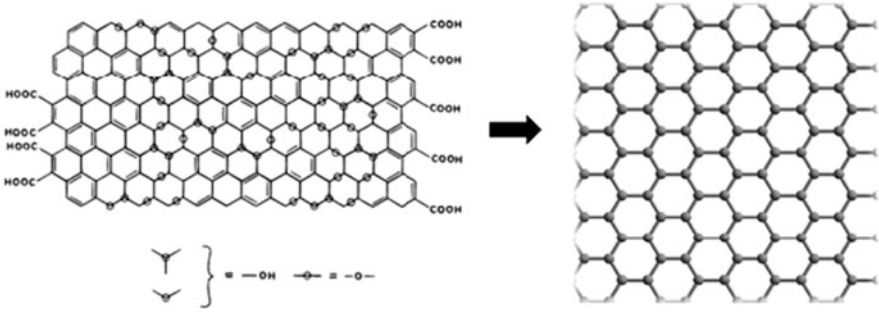

Fig. 11 Reduction of graphene oxide

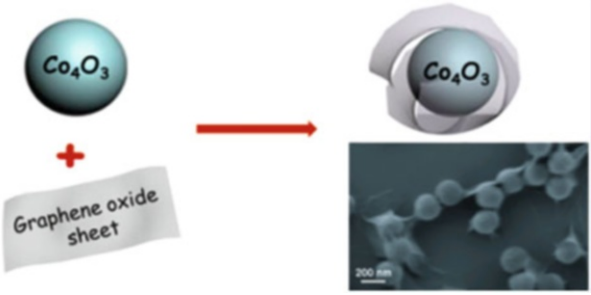

Fig. 12 The best of two worlds: graphene oxide-encapsulated Co_3O_4 nanoparticles (Reproduced from reference 267 with permission from Angew. Chem. Int. Ed. and John Wiley and Sons)

[264–266], offers particular advantages during processing (Fig. 11). In particular, its negative charge allows layer-by-layer-deposition with positively charged polymers.

Also, it can be used to wrap-up positively charged metal oxides and render them morphologically stable during charging and discharging within battery elements [267]. The resulting hybrids thus combine high charge storage capacity with structural stability [268, 269] (Fig. 12).

Regarding energy conversion, the materials needed for fuel cells are proton-conducting polymer membranes and catalysts for oxygen reduction [270, 271]. Platinum catalysts suffer from serious limitations within an envisaged hydrogen technology due to availability and costs [272–274]. There is, however, evidence that graphene sheets possessing nitrogen centers in their periphery possess catalytic activities [275–277] superior to those of platinum. One way of making such materials is by pyrolysis of N-containing hydrocarbons such as the dye-stuff **44** under the conditions of nano-etching [278] (Fig. 13). This is a field that has been significantly advanced by Xinliang Feng and Linjie Zhi [1, 279]. The mechanism of graphene formation is unclear [280], and a synthetic organic chemist might look down at such a "cook-and-bake" method as hopelessly undefined, but it has proven capable of producing large quantities of graphene [279, 281, 282].

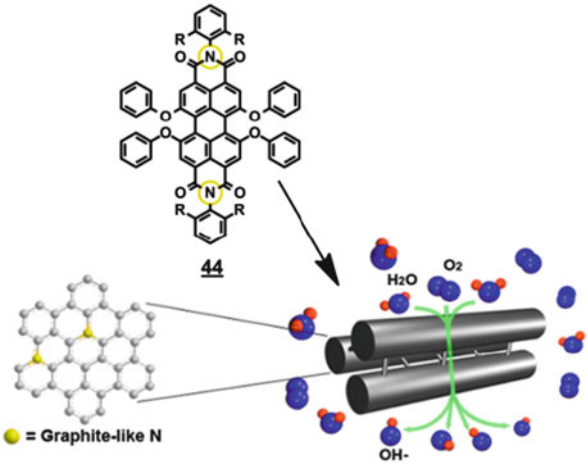

Fig. 13 Nitrogen-doped graphene as metal-free catalyst for oxygen reduction (Reproduced from reference 278 with permission from Angew. Chem. Int. Ed. and John Wiley and Sons)

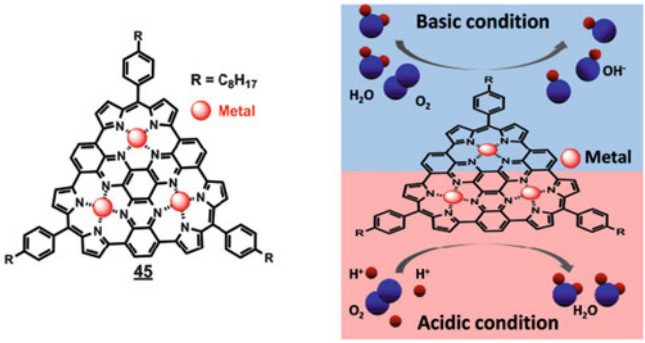

Fig. 14 Trinuclear organometal complex **45** and representation of **45** as catalyst for oxygen reduction

It should be mentioned that we have also synthesized perfectly defined organometal complexes such as **45** as catalysts for oxygen reduction [283]. They function as catalysts in their own right, but also serve as model systems to optimize the desired four-electron transfer in oxygen reduction in pyrolytically formed materials (Fig. 14).

9 Conclusion

What this brief excursion into cruder methods of graphene formation tells us is that the need to obtain a desired material function must be carefully weighed against the synthetic effort required to make the requisite material. This balance is the essence

of material synthesis, but synthetic research should also investigate more sophisticated approaches. There is a profound difference in the level of synthetic complexity required depending upon whether graphene is targeted as a semiconductor, window electrode, catalyst, or anode for a battery. Peeling off graphene from graphite might be considered a "quick and dirty" experiment but it has, in an ingenious way, furnished the material for a whole new physics. Polymer chemistry, by contrast, although offering distinct advantages in terms of structural perfection over a broad length scale and reliable structure–property relations, might have been too complicated to allow such a physical breakthrough. Nevertheless, Scotch-tape manipulation of graphite is not a basis for future robust technologies, and chemical graphene synthesis as outlined above will remain an indispensable tool for graphene-based materials science.

Polymer synthesis equally proves its value when it comes to the functionalization of graphene, such as addition reactions at the edges or in the interior of the sheet. Returning to the role of semiconductors for electronic devices, silicon still adopts a central role and will continue to do so for the foreseeable future. However, graphene nanoribbons appear to be a more serious contender for silicon than the long-studied linear conjugated polymers, but will not be able to attain their potential without us fully utilizing the power and perfection of polymer synthesis.

Acknowledgements Synthetic breakthroughs in the fabrication of small conjugated molecules all the way to complex, functional polyphenylene macromolecules have led to the achievements in the synthesis of graphene and its derivatives. This would not have been possible without the immense efforts of many skilled and creative chemists, both molecular and material, physicists, and engineers that I have had the pleasure of working with. Therefore, I must express my sincerest appreciation for the hard work of my colleagues and students that contributed to this work. I am truly amazed at the successes we have experienced in transforming small molecules into the complex macromolecules discussed herein, and the properties that these structure possess. May we continue this work towards addressing new challenges and breakthroughs in the field of conjugated molecules.

We would like to gratefully acknowledge the generous funding that has contributed to this research by the EU projects DISCEL (G5RD-CT-2000-00321), FP7-Energy-2010-FET Project Molesol (FP7-Energy-2010 256617), EU Project GENIUS (ITN-264694) Superior (ITN-238177) and the Integrated projects RADSAS (NMP3-CT-2004-001561), ONE-P (NMP3-LA-2008-212311), NAIMO (NMP4-CT-2004-500355), MAC-Mes (Grd2-2000-30242), NANOGRAPH (ERC-Adv.-Grant 267160). Additional financial support was provided by Volkswagen Stiftung, MPG (ENERCHEM), BMBF (Projects LiBZ and Graphenoid-Lagen), the German Science Foundation within the frame of the ESF Projects GOSPEL (09-EuroGRAPHENE-FP-001), SONS2-SUPRAMATES and SONS-BIONICS, Korean-German IRTG, DFG Priority Programs SPP 1355, SPP 1459 and the Sonderforschungsbereich SFB 625. Industrial collaborations with BASF AG, Ludwigshafen, Merck KGaA,, SONY, Hoffmann-La Roche AG, DuPont, and Sumitomo Chemical were also essential to the success of this work.

References

1. Wu D, Zhang F, Liang H, Feng XL (2012) Chem Soc Rev 41:6160
2. Yang S, Bachman RE, Feng XL, Müllen K (2013) Acc Chem Res 46:116
3. Geim AK (2009) Science 324:1530

4. Novoselov KS, Geim AK, Morozov SV, Jiang D, Zhang Y, Dubonos SV, Grigorieva IV, Firsov AA (2004) Science 306:666
5. Geim AK, Novoselov KS (2007) Nat Mater 6:183
6. Pang SP, Hernandez Y, Feng XL, Müllen K (2011) Adv Mater 23:2779
7. Bae S, Kim H, Lee Y, Xu X, Park J-S, Zheng Y, Balakrishnan J, Lei T, Ri Kim H, Song YI, Kim Y-J, Kim KS, Ozyilmaz B, Ahn J-H, Hong BH, Iijima S (2010) Nat Nanotechnol 5:574
8. Li X, Magnuson CW, Venugopal A, Tromp RM, Han-non JB, Vogel EM, Colombo L, Ruoff RS (2011) J Am Chem Soc 133:2816
9. Li X, Wang X, Zhang L, Lee S, Dai H (2008) Science 319:1229
10. Stankovich S, Dikin DA, Dommett GHB, Kohlhaas KM, Zimney EJ, Stach EA, Piner RD, Nguyen ST, Ruoff RS (2006) Nature 442:282
11. Chen D, Tang L, Li J (2010) Chem Soc Rev 39:3157
12. Burghard M, Klauk H, Kern K (2009) Adv Mater 21:2586
13. Feng X, Marcon V, Pisula W, Hansen MR, Kirkpatrick J, Grozema F, Andrienko D, Kremer K, Müllen K (2009) Nat Mater 8:421
14. Pisula W, Feng XL, Müllen K (2011) Chem Mater 23:554
15. Diez-Perez I, Li Z, Hihath J, Li J, Zhang C, Yang X, Zang L, Dai Y, Feng XL, Müllen K, Tao NJ (2010) Nat Commun 1:31. doi:10.1038/ncomms1029
16. Osella S, Narita A, Schwab MG, Hernandez Y, Feng XL, Müllen K, Beljonne D (2012) ACS Nano 6:5539
17. Kosynkin DV, Higginbotham AL, Sinitskii A, Lomeda JR, Dimiev A, Price BK, Tour JM (2009) Nature 458:872
18. Tapasztó L, Dobrik G, Lambin P, Biró LP (2008) Nat Nanotechnol 3:397
19. Pang S, Englert JM, Tsao HN, Hernandez Y, Hirsch A, Feng XL, Müllen K (2010) Adv Mater 22:5374
20. Kang J, Hwang S, Kim JH, Kim MH, Ryu J, Seo SJ, Hong BH, Kim MK, Choi JB (2012) ACS Nano 6:5360
21. Kang J, Shin D, Bae S, Hong BH (2012) Nanoscale 4:5527
22. Makio H, Fujita T (2009) Acc Chem Res 42:1532
23. Bochmann M (2004) J Organomet 689:3982
24. Nomura K, Kitiyanan B (2008) Curr Org Syn 5:217
25. Mehdiabadi S, Yiyoung C, Soares JBP (2012) Macromol Symp 313:8
26. Nenov S, Clark CG Jr, Klapper M, Müllen K (2007) Macromol Chem Phys 208:1362
27. Braunecker WA, Matyjaszewski K (2007) Prog Polym Sci 32:93
28. Siegwart DJ, Oh JW, Matyjaszewski K (2012) Prog Polym Sci 37:18
29. Gregory A, Stenzel MH (2012) Prog Polym Sci 37:38–105
30. Grubbs RB (2011) Polym Rev 51:104
31. Torchilin VP (2007) Pharm Res 24:1
32. Read ES, Armes SP (2007) Chem Commun 2007(29):3021
33. Motornov M, Roiter Y, Tokarev I, Minko S (2010) Prog Polym Sci 35:174
34. Darling SB (2007) Prog Polym Sci 32:1152
35. Kim HC, Park SM, Hinsberg DW (2010) Chem Rev 110:146
36. Hadjichristidis N, Iatrou H, Pitsikalis M, Mays J (2006) Prog Polym Sci 31:1068
37. Wilms D, Stiriba SE, Frey H (2010) Acc Chem Res 43:129
38. Otsuka H, Nagasaki Y, Kataoka K (2003) Adv Drug Deliv Rev 55:403
39. Caruso F (2001) Adv Mater 13:11
40. Ballauff M, Lu Y (2007) Polymer 48:1815
41. Matyjaszewski K, Tsarevsky NV (2009) Nat Chem 1:276
42. Klapper M, Nenov S, Haschick R, Müller K, Müllen K (2008) Acc Chem Res 41:1190
43. Diesing T, Rojas G, Klapper M, Fink G, Müllen K (2009) Angew Chem Int Ed 121:6594
44. Yokozawa T (2007) Polycondensation. In: Matyjaszewski K, Gnanou Y, Leibler L (eds) Macromolecular engineering: precise synthesis, materials properties, applications. Wiley-VCH, Weinheim

45. Yagci Y, Tasdelen MA (2006) Prog Polym Sci 31:1133
46. Yokoyama A, Yokozawa T (2007) Macromolecules 40:4093
47. Frauenrath H (2005) Prog Polym Sci 30:325
48. Fürstner A (1996) Active metals: preparation, characterization, applications. VCH, Weinheim
49. Sakamoto J, Rehahn M, Wegner G, Schlüter AD (2009) Macromol Rapid Commun 30:653
50. Boudreault PLT, Najari A, Leclerc M (2011) Chem Mater 23:456
51. Li YF (2012) Acc Chem Res 45:723
52. Kola S, Sinha J, Katz HE (2012) J Polym Sci B Polym Phys 50:1090
53. Wang CL, Dong HL, Hu WP, Liu YQ, Zhu DB (2012) Chem Rev 112:2208
54. Biniek L, Schroeder BC, Nielsen CB, McCulloch I (2012) J Mater Chem 22:14803
55. Facchetti A (2011) Chem Mater 23:733
56. Lin Y, Fan H, Li Y, Zhan X (2012) Adv Mater 24:3087
57. Nielsen CB, Turbiez M, McCulloch I (2013) Adv Mater 25:1859
58. Liang Y, Yu L (2010) Acc Chem Res 43:1227
59. Carsten B, He F, Jung Son H, Xu T, Yu L (2011) Chem Rev 111:1493
60. Sariciftci NS, Smilowitz L, Heeger AJ, Wudl F (1992) Science 258:1474
61. Scherf U, Gutacker A, Koenen N (2008) Acc Chem Res 41:1086
62. Tsao HN, Cho D, Andreasen JW, Rouhanipour A, Breiby DW, Pisula W, Müllen K (2009) Adv Mater 21:209
63. Tsao HN, Cho D, Park I, Hansen MR, Mavrinskiy A, Yoon DY, Graf R, Pisula W, Spiess HW, Müllen K (2011) J Am Chem Soc 133:2605
64. Wang SH, Kappl M, Lieberwirth I, Müller M, Kirchhoff K, Pisula W, Müllen K (2012) Adv Mater 24:417
65. Niedzialek D, Lemaur V, Dudenko D, Shu J, Hansen MR, Andreasen JW, Pisula W, Müllen K, Cornil J, Beljonne D (2013) Adv Mater 25:1939. doi:10.1002/adma.201201058
66. Chen HJ, Guo YL, Yu G, Zhao Y, Zhang J, Gao D, Liu HT, Liu YQ (2012) Adv Mater 24:4618
67. Kanimozhi C, Yaacobi-Gross N, Chou KW, Amassian A, Anthopoulos TD, Patil S (2012) J Am Chem Soc 134:16532
68. He ZC, Zhong CM, Su SJ, Xu M, Wu HB, Cao Y (2012) Nat Photon 6:591
69. Dou LT, Gao J, Richard E, You JB, Chen CC, Cha KC, He YJ, Li G, Yang Y (2012) J Am Chem Soc 134:10071
70. Mishra A, Fischer MKR, Bäuerle P (2009) Angew Chem Int Ed 48:2474
71. Leclerc M (1999) Adv Mater 11:149
72. Henson ZB, Müllen K, Bazan GC (2012) Nat Chem 4:699
73. Boudreault PLT, Najari A, Leclerc M (2011) Chem Mater 23:456
74. Müllen K, Wegne G (eds) (1998) Electronic materials: the oligomer approach. Wiley-VCH, Weinheim
75. Tsao HN, Müllen K (2010) Chem Soc Rev 39:2372
76. Appukkuttan P, Van der Eycken E (2008) Eur J Org Chem 2008:1133
77. Coffin RC, Peet J, Rogers J, Bazan GC (2009) Nat Chem 1:657
78. Yamamoto E, Yamamoto A (1977) Chem Lett 6(4):353
79. Schlüter AD (2001) J Polym Sci A Polym Chem 39:1533
80. Mitschke U, Debaerdemaeker T, Bäuerle P (2000) Eur J Org Chem 3:425
81. Park JK, Jo J, Seo JH, Moon JS, Park YD, Lee K, Heeger AJ, Bazan GC (2011) Adv Mater 23:2430
82. Blouin N, Michaud A, Gendron D, Wakim S, Blair E, Plesu RN, Belletete M, Durocher G, Tao Y, Leclerc M (2008) J Am Chem Soc 130:732
83. Zou Y, Gendron D, Plesu RN, Leclerc M (2009) Macromolecules 42:6361
84. Liang F, Lu J, Ding J, Movileanu R, Tao Y (2009) Macromolecules 42:6107
85. Wu PT, Xin H, Kim FS, Ren G, Jenekhe SA (2009) Macromolecules 42:8817
86. Kim J, Swager TM (2001) Nature 411:1030

87. McQuade DT, Pullen AE, Swager TM (2000) Chem Rev 100:2537
88. Yokoyama A, Suzuki H, Kubota Y, Ohuchi K, Higashimura H, Yokozawa T (2007) J Am Chem Soc 129:7236
89. Lee M, Cho BK, Zin WC (2011) Prog Polym Sci 36:603
90. Myongsoo L, Byoung-Ki C, Wang-Cheol Z (2001) Chem Rev 101:3869
91. Scherf U, Adamczyk S, Gutacker A, Koenen N (2009) Macromol Rapid Commun 30:1059
92. Pisula W, Menon A, Stepputat M, Lieberwirth I, Kolb U, Tracz A, Sirringhaus H, Pakula T, Müllen K (2005) Adv Mater 17:684
93. Pisula W, Tomović Z, Stepputat M, Kolb U, Pakula T, Müllen K (2005) Chem Mater 17:2641
94. Beaujuge PM, Reynolds JR (2010) Chem Rev 110:268
95. Leclère P, Surin M, Jonkheijm P, Henze O, Schenning APHJ, Biscarini F, Grimsdale AC, Feast WJ, Meijer EW, Müllen K, Brédas JL, Lazzaroni R (2004) Eur Polym J 40:885
96. Skotheim TA, Reynolds JR (eds) (2007) Conjugated polymers: theory, synthesis, properties, and characterization. CRC and Taylor & Francis, Boca Raton
97. Skotheim TA, Elsenbaumer RL, Reynolds JR (eds) (1998) Handbook of conducting polymers. Dekker, New York
98. Brédas JL, Silbey R (eds) (1991) Conjugated polymers. Kluwer, Dordrecht
99. Müllen K, Scherf U (eds) (2006) Organic light-emitting devices. Wiley-VCH, Weinheim
100. Kohler A, dos Santos DA, Beljonne D, Shuai Z, Bredas JL, Holmes AB, Kraus A, Müllen K, Friend RH (1998) Nature 392:903
101. Gourley KD, Lillya CD, Reynolds JR, Chien JCW (1984) Macromolecules 17:1025
102. Junkers T, Vandenbergh J, Adriaensens P, Lutsenb L, Vanderzande D (2012) Polym Chem 3:275
103. Schmidt-Mende L, Fechtenkötter A, Müllen K, Moons E, Friend RH, MacKenzie JD (2001) Science 293:1119
104. Schmaltz B, Weil T, Müllen K (2009) Adv Mater 21:1067
105. Sakamoto J, van Heijst J, Lukin O, Schlüter AD (2009) Angew Chem Int Ed 48:1030
106. Gin DL, Conticello VP, Grubbs RH (1992) Polym Mater Sci Eng 67:87
107. Gin DL, Conticello VP, Grubbs RH (1994) J Am Chem Soc 116:10507
108. Gin DL, Conticello VP, Grubbs RH (1994) J Am Chem Soc 116:10934
109. Burroughes JH, Bradley DDC, Brown AR, Marks RN, Mackay K, Friend RH, Burn PL, Kraft A, Holmes AB (1990) Nature 347:539
110. Braun D, Heeger AJ (1991) Appl Phys Lett 58:1982
111. Grem G, Leditzky G, Ullrich B, Leising G (1992) Adv Mater 4:36
112. Trasch S, Niko A, Leising G, Scherf U (1996) Appl Phys Lett 68:1090
113. Rehahn M, Schlüter AD, Wegner G, Feast WJ (1989) Polymer 30:1060
114. Schlüter AD, Wegner G (1993) Acta Polymerica 59:44
115. Rehahn M, Schlüter AD, Wegner G (1990) Macromol Chem 191:1991
116. De Meijere A, Diederich F (eds) (2004) Metal-catalysed crosscoupling reaction. Wiley-VCH, Weinheim
117. Miyaura N, Yamada K, Suzuki A (1979) Tetrahedron Lett 20(36):3437
118. Park KC, Dodd LR, Levon K, Kwei TK (1996) Macromolecules 29:7149
119. Wegner G (2003) Macromol Chem Phys 204:347
120. Scherf U (1999) J Mater Chem 9:1853
121. Leising G, Tasch S, Meghdadi F, Athouel L, Froyer G, Scherf U (1996) Synth Met 81:185
122. Scherf U, Müllen K (1992) Polymer 33:2443
123. Scherf U, Müllen K (1991) Macromol Chem Rapid Comm 12:489
124. Fukuda M, Sawada K, Yoshino K (1993) J. Polym. Sci. Polym Chem 31:2465
125. Jacob J, Sax S, Gaal M, List EJW, Grimsdale AC, Müllen K (2005) Macromolecules 38:9933
126. Jacob J, Sax S, Piok T, List EJW, Grimsdale AC, Müllen K (2004) J Am Chem Soc 126:6987
127. Jacob J, Zhang J, Grimsdale AC, Müllen K (2003) Macromolecules 36:8240
128. Diez-Perez I, Hihath J, Hines T, Wang ZS, Zhou G, Müllen K, Tao NJ (2011) Nat Nanotechnol 6:226

129. Chmil K, Scherf U (1993) Makromol Chem Rapid Comm 14:217
130. Chmil K, Scherf U (1997) Acta Polymerica 48:208
131. Tyutyulkov N, Dietz F, Ivanova A, Müllen K (1999) Dyes Pigments 42:215
132. Quante H, Müllen K (1995) Angew Chem Int Ed 34:1323
133. Weil T, Vosch T, Hofkens J, Peneva K, Müllen K (2010) Angew Chem Int Ed 49:9068
134. Herrmann A, Müllen K (2006) Chem Lett 35:978
135. Yamamoto T (1992) Prog Polym Sci 17:1153
136. Graupner W, Leditzky G, Leising G, Scherf U (1996) Phys Rev B 54:7610
137. List EJW, Kim CH, Shinar J, Pogantsch A, Leising G, Graupner W (2000) App Phys Lett 76:2083
138. Petekidis G, Fytas G, Scherf U, Müllen K, Fleischer G (1999) J Polym Sci B Polym Phys 37(16):2211
139. Somma E, Loppinet B, Fytas G, Setayesh S, Jacob J, Grimsdale AC, Müllen K (2004) Coll Polym Sci 282:867
140. Grimsdale AC, Chan KL, Martin RE, Jokisz PG, Holmes AB (2009) Chem Rev 109:897
141. Grimsdale AC, Müllen K (2006) Adv Polym Sci 199:1
142. Vogel T, Blatter K, Schlüter AD (1989) Makromol Chem Rapid Comm 10:427
143. Wegener S, Müllen K (1991) Chem Ber 124:2101
144. Horn T, Wegener S, Müllen K (1995) Macromol Chem Phys 196:2463
145. Kohnke FH, Mathias JP, Stoddart JF (1989) Angew Chem Int Ed 28:1103
146. Eisenberg D, Shenhar R, Rabinovitz M (2010) Chem Soc Rev 39:2879
147. Wegener S, Müllen K (1993) Macromolecules 26:3037
148. Clar E (1964) Polycyclic hydrocarbons. Academic, London
149. Clar E (1972) The aromatic sextet. Wiley, London
150. Rouillé G, Steglich M, Huisken F, Henning T, Müllen K (2009) J Chem Phys 131:204311
151. Tielens AGGM (2008) Annu Rev Astron Astrophys 46:289
152. Räder HJ, Rouhanipour A, Talarico AM, Palermo V, Samori P, Müllen K (2006) Nat Mater 5:276
153. Stabel A, Herwig P, Müllen K, Rabe J (1995) Angew Chem Int Ed 34:1609
154. Kumar B, Viboh RL, Bonifacio MC, Thompson WB, Buttrick JC, Westlake BC, Kim M-S, Zoellner RW, Varganov SA, Mçrschel P, Teteruk J, Schmidt MU, King BT (2012) Angew Chem Int Ed 51:12795
155. Zhai L, Shukla R, Wadumethrige SH, Rathore R (2010) J Org Chem 75:4748
156. Rempala P, Kroulik J, King BT (2006) J Org Chem 71:5067
157. Watson MD, Fechtenkötter A, Müllen K (2001) Chem Rev 101:1267
158. Feng XL, Pisula W, Müllen K (2009) Pure Appl Chem 81:2203
159. Xiao S, Kang SJ, Wu Y, Ahn S, Kim JB, Loo Y-L, Siegrist T, Steigerwald ML, Li H, Nuckolls C (2013) Chem Sci 4:2018
160. Uribe-Romo FJ, Dichtel WR (2012) Nat Chem 4:244
161. Colson JW, Woll AR, Mukherjee A, Levendorf MP, Spitler EL, Shields VB, Spencer MG, Park J, Dichtel WR (2011) Science 332:228
162. Hill JP, Jin W, Kosaka A, Fukushima T, Ichihara H, Shimomura T, Ito K, Hashizume T, Ishii N, Aida T (2004) Science 304:1481
163. He Y, Yamamoto Y, Jin W, Fukushima T, Saeki A, Seki S, Ishii N, Aida T (2010) Adv Mater 22:829
164. Yan X, Cui X, Li B, Li LS (2010) J Am Chem Soc 132:5944
165. Yamamoto Y, Fukushima T, Suna Y, Ishii N, Saeki A, Seki S, Tagawa S, Taniguchi M, Kawai T, Aida T (2006) Science 314:1761
166. Pradhan A, Dechambenoit P, Bock H, Durola F (2011) Angew Chem Int Ed 50:12582
167. Simpson CD, Brand JD, Berresheim AJ, Przybilla L, Räder HJ, Müllen K (2002) Chem Eur J 6:1424
168. Wasserfallen D, Kastler M, Pisula W, Hofer WA, Fogel Y, Wang ZH, Müllen K (2006) J Am Chem Soc 128:1334

169. Pisula W, Tomović Z, Simpson C, Kastler M, Pakula T, Müllen K (2005) Chem Mater 17:4296
170. Simpson CD, Wu J, Watson MD, Müllen K (2004) J Mater Chem 14:494
171. Pisula W, Kastler M, Wasserfallen D, Mondeshki M, Piris J, Schnell I, Müllen K (2006) Chem Mater 18:3634
172. Pisula W, Zorn M, Chang JY, Müllen K, Zentel R (2009) Macromol Rapid Comm 30:1179
173. Müllen K, Rabe JP (2008) Acc Chem Res 41:511
174. Müller M, Kübel C, Müllen K (1998) Chem Eur J 4:2099
175. Jäckel F, Watson MD, Müllen K, Rabe JP (2004) Phys Rev Lett 92:188303
176. Böhme T, Simpson CD, Müllen K, Rabe JP (2007) Chem Eur J 13:7349
177. Kastler M, Pisula W, Laquai F, Kumar A, Davies RJ, Baluschev S, Garcia-Gutiérrez M-C, Wasserfallen D, Butt H-J, Riekel C, Wegner G, Müllen K (2006) Adv Mater 18:2255
178. Wu J, Pisula W, Müllen K (2007) Chem Rev 107:718
179. Tomalia DA, Naylor AM, Goddard WA (1990) Angew Chem Int Ed 29:138
180. Bosman AW, Janssen HM, Meijer EW (1999) Chem Rev 99:1665
181. Zeng FW, Zimmerman SC (1997) Chem Rev 97:1681
182. Fréchet JMJ, Tomalia DA (eds) (2001) Dendrimers and other dendritic polymers. Wiley, New York
183. Vögtle F, Richardt G, Werner N (eds) (2009) Dendrimer chemistry. Wiley-VCH, Weinheim
184. Astruc D, Boisselier E, Ornelas CT (2010) Chem Rev 110:1857
185. Moore JS (1997) Acc Chem Res 30:402
186. Campagna S, Ceroni P, Puntoriero F (eds) (2012) Designing dendrimers. Wiley, New York
187. Buhleier E, Wehner W, Vögtle F (1978) Synthesis 2:155
188. Bauer RE, Grimsdale AC, Müllen K (2005) Top Curr Chem 245:253
189. Wiesler UM, Weil T, Müllen K (2001) Top Curr Chem 212:1
190. Türp D, Nguyen TTT, Baumgarten M, Müllen K (2012) New J Chem 36(2):282
191. Morgenroth F, Reuther E, Müllen K (1997) Angew Chem Int Ed 36:631
192. Andreitchenko EV, Clark CG, Bauer RE, Lieser G, Müllen K (2005) Angew Chem Int Ed 44:6348
193. Clark CG, Wenzel RJ, Andreitchenko EV, Steffen W, Zenobi R, Müllen K (2007) J Am Chem Soc 129:3292
194. Nguyen TTT, Baumgarten M, Rouhanipour A, Räder HJ, Lieberwirth I, Müllen K (2013) J Am Chem Soc 135:4183
195. Vögtle F (ed) (2001) Dendrimers III: design, dimension, function. Topics in current chemistry, vol 212. Springer, Berlin, Heidelberg
196. Weil T, Reuther E, Müllen K (2002) Angew Chem Int Ed 114:1980
197. Oesterling I, Müllen K (2007) J Am Chem Soc 129:4595
198. Iwasawa T, Tokunaga M, Obora Y, Tsuji Y (2004) J Am Chem Soc 126:6554
199. Tsuji Y, Fujihara T (2007) Inorg Chem 46:1895
200. Yin M, Ding K, Gropeanu RA, Shen J, Berger R, Weil T, Müllen K (2008) Biomacromolecules 9:3231
201. Tomalia DA, Baker H, Dewald J, Hall M, Kallos G, Martin S, Roeck J, Ryder J, Smith P (1985) Polymer 17:117
202. Weil T, Reuther E, Beer C, Müllen K (2004) Chem Eur J 10:1398
203. Lubczyk D, Siering C, Lörgen J, Shifrina ZB, Müllen K, Waldvogel SR (2010) Sens Actuators B 143:561
204. Lubczyk D, Grill M, Baumgarten M, Waldvogel SR, Müllen K (2012) ChemPlusChem 77:102
205. Yin M, Shen J, Gropeanu R, Pflugfelder GO, Weil T, Müllen K (2008) Small 4:894
206. Kuan SL, Stöckle B, Reichenwallner J, Ng DYW, Wu Y, Doroshenko M, Koynov K, Hinderberger D, Müllen K, Weil T (2013) Biomacromolecules 14:367
207. Chen L, Hernandez Y, Feng XL, Müllen K (2012) Angew Chem Int Ed 51:7640
208. Dössel L, Gherghel L, Feng XL, Müllen K (2011) Angew Chem Int Ed 50:2540

209. Schwab MG, Narita A, Hernandez Y, Balandina T, Mali KS, De Feyter S, Feng XL, Müllen K (2012) J Am Chem Soc 134:18169
210. Englert JM, Hirsch A, Feng XL, Müllen K (2011) Angew Chem Int Ed 50:A17
211. Wu JS, Gherghel L, Watson MD, Li J, Wang Z, Simpson CD, Kolb U, Müllen K (2003) Macromolecules 36:7082
212. Yang X, Dou X, Rouhanipour A, Zhi L, Räder H-J, Müllen K (2008) J Am Chem Soc 130:4216
213. Fasel R, Parschau M, Ernst KH (2003) Angew Chem Int Ed 42:5178
214. Rabe J, Bucholz S (1991) Science 253:424
215. Forster JS, Frommer JE (1988) Nature 333:542
216. Frommer J (1992) Angew Chem Int Ed 31:1298
217. Treier M, Pignedoli CA, Laino T, Rieger R, Müllen K, Passerone D, Fasel R (2011) Nat Chem 3:61
218. Lafferentz L, Eberhardt V, Dri C, Africh C, Comelli G, Esch F, Hecht S, Grill L (2012) Nat Chem 4:215
219. Grill L, Dyer M, Lafferentz L, Persson M, Peters MV, Hecht S (2007) Nat Nanotechnol 2:687
220. Kawano S-I, Baumgarten M, Müllen K, Murer P, Schäfer T, Saleh M (2010) Patent no: TW201,008,972
221. Cai JM, Ruffieux P, Jaafar R, Bieri M, Braun T, Blankenburg S, Muoth M, Seitsonen AP, Saleh M, Feng XL, Müllen K, Fasel R (2010) Nature 466:470
222. Saleh M, Baumgarten M, Mavrinskiy A, Schäfer T, Müllen K (2010) Macromolecules 43:137
223. Talirz L, Söde H, Cai J, Ruffieux P, Blankenburg S, Jafaar R, Berger R, Feng XL, Müllen K, Passerone D, Fasel R, Pignedoli CA (2013) J Am Chem Soc 135:2060
224. Ruffieux P, Cai J, Plumb NC, Patthey L, Prezzi D, Ferretti A, Molinari E, Feng XL, Müllen K, Pignedoli CA, Fasel R (2012) ACS Nano 6:6930
225. Linden S, Zhang D, Timmer A, Aghdassi N, Franke JF, Zhang H, Feng X, Müllen K, Fuchs H, Chi L, Zacharias H (2012) Phys Rev Lett 108:216801
226. Schlütter F, Rossel F, Kivala M, Enkelmann V, Gisselbrecht JP, Ruffieux P, Fasel R, Müllen K (2013) J Am Chem Soc 135:4550
227. Bieri M, Blankenburg S, Kivala M, Pignedoli CA, Ruffieux P, Müllen K, Fasel R (2011) Chem Commun 47:10239
228. Wang SH, Kivala M, Lieberwirth I, Kirchhoff K, Feng XL, Pisula W, Müllen K (2011) ChemPhysChem 12:1648
229. Bieri M, Treier M, Cai J, Mansour KA, Ruffieux P, Groning O, Groning P, Kastler M, Rieger R, Feng X, Müllen K, Fasel R (2009) Chem Commun 2009(45):6919
230. He Q, Wu S, Yina Z (2012) Hua Zhang. Chem Sci 3:1764
231. Schedin F, Geim AK, Morozov SV, Hill EW, Blake P, Katsnelson MI, Novoselov KS (2007) Nat Mater 6:652
232. Cao XH, Shi YM, Shi WH, Lu G, Huang X, Yan QY, Zhang QC, Zhang H (2011) Small 7:3163
233. Chen Z, Ren W, Gao L, Liu B, Pei S, Cheng HM (2011) Nat Mater 10:424
234. Zilberman Y, Tisch U, Pisula W, Feng X, Müllen K, Haick H (2009) Langmuir 25:5411
235. Zilberman Y, Ionescu R, Feng XL, Müllen K, Haick H (2011) ACS Nano 5:6743
236. Ionescu R, Broza Y, Shaltieli H, Sadeh D, Zilberman Y, Feng XL, Glass-Marmor L, Lejbkowicz I, Müllen K, Miller A, Haick H (2011) ACS Chem Neurosci 2:687
237. Bachar N, Mintz L, Zilberman Y, Ionescu R, Feng XL, Müllen K, Haick H (2012) ACS Appl Mater Interfaces 4:4960
238. Koening SP, Wang LD, Pellegrino J, Bunch JS (2012) J Scott Nat Nanotechnol 7:728
239. Nair RR, Wu HA, Jayaram PN, Grigorieva IV, Geim AK (2012) Science 335:442
240. Blankenburg S, Bieri M, Fasel R, Müllen K, Pignedoli CA, Passerone D (2010) Small 6:2266
241. Dai LM (2013) Acc Chem Res 46:31
242. Wang HL, Dai HJ (2013) Chem Soc Rev 42:3088
243. Sun YQ, Wu QO, Shi GQ (2011) Energy Environ Sci 4:1113

244. Pumera M (2011) Energy Environ Sci 4:668
245. Yang SB, Feng XL, Zhi LJ, Cao Q, Maier J, Müllen K (2010) Adv Mater 22:838
246. Kaskhedikar NA, Maier J (2009) Adv Mater 21:2664
247. Zhang J, Hu YS, Tessonnier JP, Weinberg G, Maier J, Schlogl R, Su DS (2008) Adv Mater 20:1450
248. Grimsdale AC, Wu JS, Müllen K (2005) Chem Commun 2005(17):2197
249. Yang SB, Cui GL, Pang SP, Cao Q, Kolb U, Feng XL, Maier J, Müllen K (2010) ChemSusChem 3:236
250. Pandolfo AG, Hollenkamp AF (2006) J Power Sources 157:11
251. Frackowiak E, Beguin F (2001) Carbon 39:937
252. Zhang LL, Zhao XS (2009) Chem Soc Rev 38:2520
253. Cui G, Zhou XH, Zhi L, Thomas A, Müllen K (2007) New Carbon Mater 22:302
254. Wu ZS, Winter A, Chen L, Sun Y, Turchanin A, Feng XL, Müllen K (2012) Adv Mater 24:5130
255. Poizot P, Laruelle S, Grugeon S, Dupont L, Tarascon JM (2000) Nature 407:496
256. Chan CK, Peng HL, Liu G, McIlwrath K, Zhang XF, Huggins RA, Cui Y (2008) Nat Nanotechnol 3:31
257. Zhang WM, Hu JS, Guo YG, Zheng SF, Zhong LS, Song WG, Wan LJ (2008) Adv Mater 20:1160
258. Li XL, Zhang GY, Bai XD, Sun XM, Wang XR, Wang E, Dai HJ (2008) Nat Nanotechnol 3:538
259. Eda G, Fanchini G, Chhowalla M (2008) Nat Nanotechnol 3:270
260. Park S, Ruoff RS (2009) Nat Nanotechnol 4:217
261. Dreyer DR, Park S, Bielawski CW, Ruoff RS (2010) Chem Soc Rev 39:228
262. Wang X, Zhi L, Müllen K (2008) Nano Lett 8:323
263. Wang X, Zhi L, Tsao N, Tomović Z, Li J, Müllen K (2008) Angew Chem Int Ed 47:2990
264. Li H, Pang S, Feng XL, Müllen K, Bubeck C (2010) Chem Comm 46:6243
265. Su Q, Pang SP, Alijani V, Li C, Feng XL, Müllen K (2009) Adv Mater 21:3191
266. Liang YY, Frisch J, Zhi LJ, Norouzi-Arasi H, Feng XL, Rabe JP, Koch N, Müllen K (2009) Nanotechnology 20:434007
267. Yang SB, Feng XL, Ivanovici S, Müllen K (2010) Angew Chem Int Ed 49:8408
268. Cui G, Hu Y-S, Zhi L, Wu D, Lieberwirth I, Maier J, Müllen K (2007) Small 3:2066
269. Cui G, Gu L, Zhi L, Kaskhedikar N, van Aken PA, Müllen K, Maier J (2008) Adv Mater 20:3079
270. Yang SB, Feng XL, Wang XC, Müllen K (2011) Angew Chem Int Ed 50:5339
271. Parvez K, Yang SB, Hernandez Y, Winter A, Turchanin A, Feng XL, Müllen K (2012) ACS Nano 6:9541
272. Winter M, Brodd RJ (2004) Chem Rev 104:4245
273. Chen ZW, Waje M, Li WZ, Yan YS (2007) Angew Chem Int Ed 119:4138
274. Lim B, Jiang MJ, Camargo PHC, Cho EC, Tao J, Lu XM, Zhu YM, Xia YN (2009) Science 324:1302
275. Kurak KA, Anderson AB (2009) J Phys Chem C 113:6730
276. Ikeda T, Boero M, Huang SF, Terakura K, Oshima M, Ozaki J (2008) J Phys Chem C 112:14706
277. Panchakarla LS, Subrahmanyam KS, Saha SK, Govindaraj A, Krishnamurthy HR, Waghmare UV, Rao CNR (2009) Adv Mater 21:4726
278. Liu RL, Wu DQ, Feng XL, Müllen K (2010) Angew Chem Int Ed 49:2565
279. Zhi L, Müllen K (2008) J Mater Chem 18:1472
280. Shao YY, Sui JH, Yin GP, Gao YZ (2008) Appl Catal, B 79:89
281. Thomas A (2010) Angew Chem Int Ed 49:8328
282. Paraknowitsch JP, Thomas A (2012) Macromol Chem Phys 213:1132
283. Liu RL, von Malotki C, Arnold L, Koshino N, Higashimura H, Baumgarten M, Müllen K (2011) J Am Chem Soc 133:10372

Adv Polym Sci (2013) 262: 93–108
DOI: 10.1007/12_2013_262

Published online: 16 November 2013

Computer Simulation of Self-Assembling Macromolecules

Giacomo Fiorin, Michael L. Klein, Russell DeVane, and Wataru Shinoda

Abstract Amphiphilic polymers have the ability to self-assemble into supramolecular structures of great complexity and utility. Nowadays, molecular dynamics simulations can be employed to investigate the self-assembly of modestly sized natural and synthetic macromolecules into structures, such as micelles, worms (cylindrical micelles), or vesicles composed of membrane bilayers organized as single or multilamellar structures. This article presents a perspective on the use of large-scale computer simulation studies that have been used to understand the formation of such structures and their interaction with nanoscale solutes. Advances in this domain of research have been possible due to relentless progress in computer power plus the development of so-called coarse-grained intermolecular interaction models that encode the basic architecture of the amphiphilic macromolecules of interest.

Keywords Amphiphilic polymers · Molecular dynamics · Multilamellar micelles · Self-assembly

G. Fiorin and M.L. Klein (✉)
Department of Chemistry and Institute for Computational Molecular Science, Temple University, Philadelphia, PA 19122, USA
e-mail: mlklein@temple.edu

R. DeVane
Modeling and Simulation, Corporate Research and Development, The Procter and Gamble Company, West Chester, OH 45069, USA

W. Shinoda
Health Research Institute, National Institute of Advanced Industrial Science and Technology (AIST), Ikeda, Osaka 563-8577, Japan

Contents

1 Introduction

In the early 1920s, physicists were struggling with the consequences of the birth of quantum mechanics, and quantum chemistry did not exist as a discipline. It is not surprising therefore that, notwithstanding Gilbert N. Lewis [1], there was some confusion among chemists as to the nature of the chemical bond. One of the consequences of this lack of understanding of the fundamentals of molecular structure and bonding was that initially there was little appreciation for the notion that Hermann Staudinger's high molecular weight "macromolecules" really were manifestations of covalent-linked monomeric entities as opposed to simple "aggregates" of monomers [2].

Nowadays we take for granted that both synthetic and natural polymers really are macromolecules. In the decades since Hermann Staudinger's 1953 Nobel Prize [3], driven in part by the immense technological importance of macromolecules in consumer products and advanced materials, a deep understanding has emerged of the phenomenon of macromolecular "aggregation" that underpins the field of supramolecular chemistry, championed by Jean-Marie Lehn [4]. Biology is rife with examples of the latter, which provides inspiration for novel materials development based on either the spontaneous or directed self-assembly of macromolecules.

The year 1953 was important not only because of the Staudinger Nobel Prize, but also because it was the year that the structure of the macromolecule DNA was reported by James Watson and Francis Crick [5], which is the subject of another article in this volume by Ned Seeman [6]. Yet another important milestone was recorded in 1953, namely the first published use of a computer to carry out a simulation of liquid, albeit a liquid composed of argon atoms [7]. This seminal work, which was carried out on the famous MANIAC machine at Los Alamos National Laboratory, by Nick Metropolis and collaborators, was never honored with a Nobel Prize, but nonetheless had an enormous impact across the whole breadth of the physical and life sciences. Indeed, it is inconceivable today that one would attempt a research program dealing with either natural or synthetic macromolecules without the aid of computer simulation as a complement to their design, synthesis, and characterization [8].

The present article deals with the use of large-scale computer simulation techniques to investigate the self-assembly of modest-sized natural and synthetic

macromolecules. Over the 60 years since the invention of this methodology, computers have evolved enormously, along with concomitant algorithm development, such that today computer simulation is capable of being a true partner to experiments.

Amphiphilic polymers have the ability to self-assemble into supramolecular structures of remarkable complexity [8–11]. To understand the formation of such structures, knowing the chemical structure of the macromolecules involved is necessary, but not sufficient. Molecules with similar chemical structure may form strikingly different structures when immersed in the same environment. The reason for this complexity has a relatively simple chemical origin: with the exception of a macromolecule's own chemical bonds, the cohesive forces between its atoms are often outmatched by those between its atoms and those of another macromolecule. As a result, the gap between a simplified "mean field" model and a satisfactory model is so great as to defeat even the most clever reductionist approaches. More often than not, a direct simulation is the only efficient route to modeling the self-assembly of amphiphilic polymers into the plethora of novel structures.

Historically, computational molecular scientists have used many methods to investigate the structures and thermodynamics of polymer assemblies. In recent years, molecular dynamics (MD) simulations with empirical potential energy functions ("potentials") have become, arguably, the preferred approach towards this goal. Aside from defining the thermodynamic coupling between the microscopic model and the macroscopic environment [12–14], and choosing suitable potentials [15–19], MD simulations feature little or no approximation in describing the real motions of polymers during their self-assembly. Therefore, self-assembly into an organized phase, or transformations between different phases, can be predicted with surprising accuracy [11].

2 Coarse-Grained Molecular Dynamics Simulations

One of the primary limitations when using MD is ensuring completeness of the statistical sampling. For model systems of realistic size (up to tens of nanometers of linear dimensions, or a few hundreds or thousands of macromolecules), the longest times accessible to simulation are typically between microseconds and milliseconds. To improve statistical convergence, while retaining the accuracy of the physical model, many approaches have been developed. For example, approaches based upon the addition of external constraints (e.g., thermodynamic integration and umbrella sampling [20, 21]), or the reweighting of high temperature distributions (e.g., parallel tempering [22, 23]) have been used successfully. Unfortunately, these approaches also suffer from limitations specific to the self-assembly phenomenon: namely, the lack of knowledge of the mechanism hampers the definition of the "reaction coordinate" [20, 21]. Moreover, the conditions for performing parallel tempering [22] are difficult to satisfy for increasingly larger systems, when the relative fluctuation of the total energy, $\Delta E/E$, becomes narrower in the thermodynamic limit.

A suitable approach is then to look at the mechanism of self-assembly from a more macroscopic point of view, by choosing a "coarse-grained" (CG) representation of the system [24–27] that combines chemical intuition and rigorous thermodynamics. By this approach, several atoms of the same molecule are combined into a single effective particle. Therefore, the number of terms in the potential energy of the system and the interaction forces decreases dramatically (between 10 and 100 times), typically much beyond what could be achieved even by distributing the calculation across parallel supercomputers. As a second advantage, the potential energy is typically a smoother function of the coordinates of the CG particles than it is of the individual atoms; thus, the finite-differences integration of the equations of motion can greatly benefit from using longer integration steps. Finally, reducing the number of dimensions carries a unique advantage in the study of diffusion-limited processes like phase transitions or self-assembly: when fewer microscopic degrees of freedom are available, collective movements are greatly accelerated.

Many CG models have been developed and used in the past two decades, and not surprisingly, applications have been focusing primarily on the phenomenon of self-assembly and the equilibrium between phases. To some extent, all models that simplify the chemical structure of a macromolecule to focus on its physical properties can be considered as CG models of varied complexity. However, a marked distinction between these models is whether the solvent is modeled implicitly as a continuous medium interacting only with the solute, or explicitly as an ensemble of particles that also interact with each other. For brevity, we discuss only the latter kind of models because the competition between intermolecular forces is crucial to simulate self-assembly. For the purpose of modeling the mechanical properties of membranes and other known structures, implicit solvent models are relatively accurate [28, 29] and are typically lower in computational cost than explicit solvent models.

An early version of a CG model with explicit solvent was developed by Smit et al., to study the dynamical interface between water and oil [26]. A similar strategy was also used by Goetz and Lipowsky [30] to simulate the self-assembly of a model surfactant into micelles and bilayers. Later, Klein and coworkers employed thermodynamic properties derived from atomistic simulations to develop a CG model for surfactants that includes the chemical structure [24, 31]. In this form, the procedure used to obtain the simplified potential functions of the CG model bears some level of similarity to the "force-matching" method used to fit simple potential functions for pairs of atoms against a fully electronic description [32]. Voth and coworkers later essentially followed this latter approach to also define an algorithm based on the force-matching procedure specific for CG–MD [33–35].

As soon as higher computing power became available, it also became possible to calculate thermodynamic and structural properties for model systems of significant size (over 10 nm of linear dimensions), and to improve CG models by direct comparison of these properties with their experimental measurements [25, 36]. Marrink et al. have used a potential energy function with few adjustable parameters to maximize the portability between different computer programs. By this approach, potentials of mean force (PMFs) between groups of atoms were modeled using the

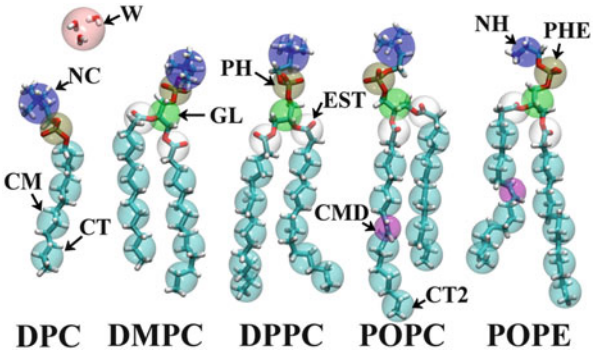

Fig. 1 Coarse-grained (CG) models of selected phospholipid molecules [41]. CG particles (*transparent spheres*) are superimposed onto the atomic structures of the chemical groups that they represent. *NC* choline, *NH* amine, *PH* and *PHE* phosphate, *GL* glycol, *EST* ester, *CM* alkyl group, *CT* and *CT2* terminal alkyl groups, *CMD* monounsaturated alkyl group. The effective water particle (labeled *W*) has the same mass as three water molecules

same functions that are typically used to model interatomic potentials. Later, this model was refined, extended to proteins, and released as the "MARTINI" model [27]. At the same time, Klein and coworkers developed a new CG model (called the SDK model) for surfactants and phospholipids (Fig. 1), using a potential energy function of similar computational cost as the MARTINI model, but with a more detailed energy function, designed to better include the many-body entropic terms [25]. The improved energy function requires a specific reimplementation for computer programs that are specialized in atomistic simulations. However, the SDK CG model is nowadays available on general-purpose simulation programs such as LAMMPS [37], and has been very successful in predicting the self-assembly of macromolecules (Fig. 1) [11, 25, 38–45].

We here highlight several applications of the SDK CG model, such as the self-assembly of biological membranes and more complex supramolecular structures, their transformation by the effect of penetrant macromolecules, and the assembly of membranes into hierarchical structures such as multilamellar vesicles. Finally, we outline the remaining challenges for CG–MD simulations in describing the structural and thermodynamic properties of self-assembling macromolecules.

3 Self-Assembly of Lipids into Biological Membranes

One of the simplest, and yet ubiquitous, structures formed by amphiphilic polymers are biological membranes. In water, phospholipids and cholesterol self-assemble into amphiphilic bilayers, with their hydrophilic groups facing the water phase and the bulk of their hydrophobic groups closely packed. This structure is a typical example of the ability of self-assembled polymers to form a relatively simple structure, whose characteristics cannot be easily predicted on the basis of the chemical nature of

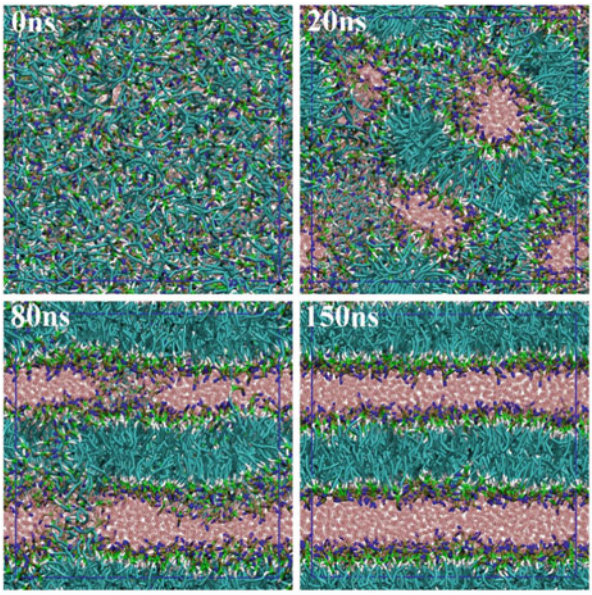

Fig. 2 Formation of a multilamellar stack from a random initial configuration of DMPC (*light blue*) and water (*red*) using the CG model for phospholipids [41], at four snapshots of simulated time. Periodic boundary conditions are applied, as used in most MD simulations to mimic bulk systems: *blue lines* indicate the boundaries of the unit cell. Nucleation of small sections of bilayer is relatively rapid (*top panels*), followed by the fusion of these small sections into two bilayers, separated by two water layers of about 3 nm thickness (*bottom panels*)

its components. As early as the beginning of the twentieth century, the composition of biological membranes had correctly been understood as a mixture of phospholipid and cholesterol by Meyer and Overton, during their studies of the mechanisms of anesthesia [46]. However, it was not until decades later that the bilayer structure could be inferred [47], and not until the mid-twentieth century that this structure could be observed directly by electron microscopy [48, 49].

Only recently have direct MD simulations methods been able to observe the self-assembly of a phospholipid bilayer. An ab initio description of the macromolecules involved that includes its electrons is of course impractical due to its computational cost. However, even approaches where the potential energy function is an empirical force field [15–19] have proven insufficient to observe the self-assembly of a small membrane. For a few hundreds of phospholipid molecules to assemble in a bilayer a few nanometers wide, time scales well beyond the microsecond are required. Although the accessible times by MD simulations have increased dramatically, only in recent years has the microsecond threshold been surpassed effectively.

The availability of CG models for phospholipids has made it possible to observe the self-assembly of Langmuir monolayers of phospholipids [31], bilayers of nonionic surfactants [38], and finally of phospholipids [41], all beginning from initial conditions where lipid or surfactant molecules are completely dissolved in water. Figure 2 shows the self-assembly of a DPMC/water system into a multilamellar stack [41], modeled in periodic boundary conditions by a unit cell of about 20 nm edge. The simulation time required to observe self-assembly (100 ns) is much shorter than that suggested for equivalent simulations at fully atomistic detail. This illustrates the ability of CG models to greatly accelerate many diffusion-limited processes, such as self-assembly.

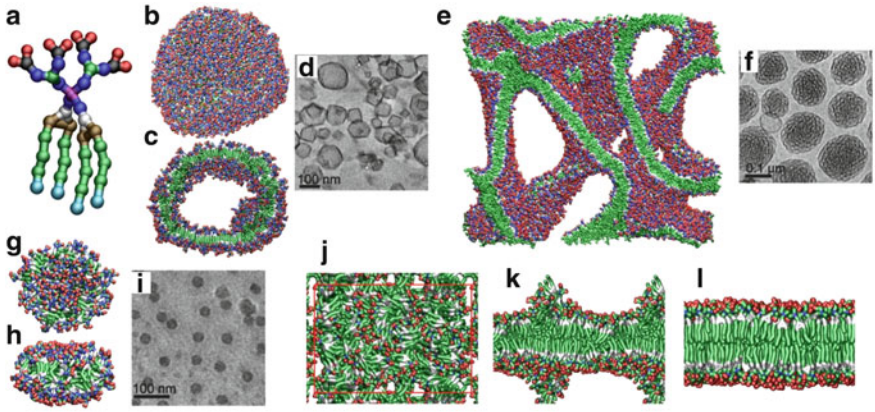

Fig. 3 Self-assembly of amphiphilic Janus dendrimers from CG–MD simulations and cryogenic transmission electron microscopy (cryo-TEM) [8]. (**a**) Macromolecular structure (in CG representation) of one of the synthesized Janus dendrimers. (**b**, **c**) Full view and cross-section view of one vesicle, self-assembled in 80 ns by CG–MD. (**d**) Cryo-TEM image of a sample of vesicles. (**e**) Bicontinuous structures self-assemble in 200 ns at intermediate levels of hydration. (**f**) Cryo-TEM image of a sample of soluble bicontinous particles. (**g**, **h**) Micelles form in 400 ns at high levels of hydration. (**i**) Cryo-TEM image of a sample of micelles. (**j–l**) Sequence of a self-assembly of a small model system at low levels of hydration, starting from a random configuration (**j**), evolving to a lamellar structure in 20 ns (**k**) and into a complete bilayer in 40 ns (**l**): the *rectangle* in (**j**) indicates the periodic boundaries of the simulation cell

4 Self-Assembly of Dendrimers into Complex Architectures

The ability of CG simulations to predict the self-assembly of macromolecules has an immediate application to the synthesis of new macromolecules that recombine the physical and chemical properties of biological molecules to create superstructures of tunable complexity. A particularly interesting group of such macromolecules are dendrimers, multiply branched organic polymers whose internal structure has direct, nontrivial outcomes on the topology of their superstructures. A library of Janus dendrimers (amphiphilic polymers formed by chemically linking two dendritic macromolecules) was recently synthesized, and the structure of their assembly measured by cryo-electron microscopy [8]. The morphologies of the supramolecular assemblies (Fig. 3) range from simpler structures such as vesicles and micelles to more complex, bicontinuous structures, depending on the level of hydration.

The experiments and simulations summarized in Fig. 3 outline a key fact in CG–MD simulations: not only can the "native" supramolecular structure be reproduced by self-assembly in a simulation, but for macromolecules with varied morphologies such as dendrimers, the effects on the supramolecular structure upon changes in the environment can also be reproduced. For example, the effect of the

level of hydration is correctly reproduced from direct observation of the self-assembly of either bicontinuous membranes (Fig. 3e) or micelles (Fig. 3g).

In addition to the obvious dependence on the chemical structure, different preparation techniques at the same level of hydration can lead to different structures. Although the exact sequence of steps cannot be replicated in MD simulations, exploiting the periodic boundary conditions used in the simulations, plus a suitably sized model system, allows one to easily reproduce the correct final outcome. Small model systems (replicated due to periodic boundary conditions) give rise to vesicles or bilayers (Fig. 3b, j), whereas larger model systems allow membranes to form with significant curvature (Fig. 3e) or give rise to micelles (Fig. 3g). Therefore, environmental conditions can be taken into account by CG–MD simulations accurately enough that the correct supramolecular structure is obtained by self-assembly, using no other information other than thermodynamic properties of the building blocks of the macromolecule.

5 Response of Biological Membranes to Addition of Macromolecules

Once a supramolecular structure is formed, the next challenge is set for MD simulations: whether they can predict effectively the response by the supramolecular assembly to the addition of a new component. This is typically a tough challenge for experiments, just as it is for simulations. Due to the large number of molecules involved, it is not unlikely to observe hysteresis when modeling the changes upon insertion of new macromolecules. The model system first reaches one equilibrium phase as it self-assembles, and remains in that phase even after it becomes destabilized after new macromolecules are added. This may be the desired behavior when preparing a supercritical condition in the laboratory; however, for simulations the time gap between the simulated time and the laboratory time may be long enough to generate unwanted hysteresis and prevent an accurate evaluation of the system's response.

The accelerated characteristic times of MD simulations with CG models are invaluable for minimizing this problem and achieving the highest predictive power. As proof of concept, we here review a study of the simulated effect of adding one or more fullerene macromolecules (C540) to a phospholipid bilayer (Fig. 4) and to a multilamellar stack (Fig. 5). In all simulations performed with this model, the insertion of fullerene macromolecules appears to follow unimpeded diffusion into the bilayer structure. Explicit calculation of the potentials of mean force (PMFs) of insertion confirms this fact, both at the atomistic and at the CG level. Following the long time (microsecond) evolution of the fullerene-phospholipid system, large membrane deformations appear that are clearly correlated to increased local concentration of fullerene macromolecules. Coupling between contiguous bilayers in a multilamellar stack (Fig. 5) also suggests that the CG model could be able to produce a multilamellar stack from direct self-assembly.

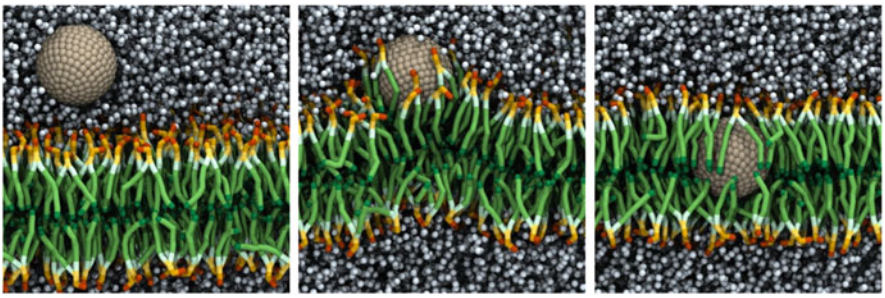

Fig. 4 Self-absorption of one fullerene (C_{540}) macromolecule within a DMPC bilayer. Water particles are shown in *light blue*, the fullerene macromolecule in *beige*, and DMPC molecules with carbons in *green* and head groups in *orange* and *yellow*

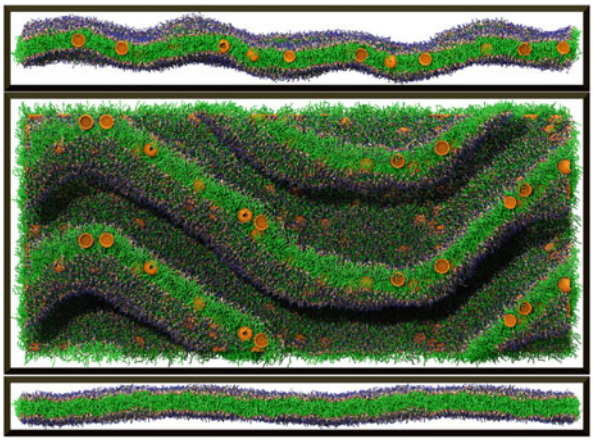

Fig. 5 Structure of a multilamellar stack composed of about 26,000 DOPC lipids and about 1,000,000 CG water particles (not shown for clarity) after the self-absorption of fullerene macromolecules [43]. The *upper panel* shows the system with 320 fullerene macromolecules (C_{540}: DOPC ratio of 1:81) shortly after all of the fullerene monomers have entered the bilayer. The *center panel* shows the fullerene-rich system (replicated once along the vertical) after 100 ns, where large perturbations can be seen in the form of induced curvature on length scales comparable to vesicles sizes. The *lower panel* shows the lipid system after all of the fullerenes have been removed. Within about 20 ns, all of the large undulations dissipate and the bilayer structure has returned to its typical pure lipid planar structure

6 Assembly of Multilamellar Vesicles

Two-dimensional membranes may easily be replicated in three dimensions to produce entirely new morphologies. The simplest example is the multilamellar stack phase, observed at low humidity (less than 50%). After that, a more interesting system is the multilamellar vesicle (MLV), where each unilamellar vesicle (ULV), the containing one and the contained one, has different properties (Fig. 6). The outermost vesicle

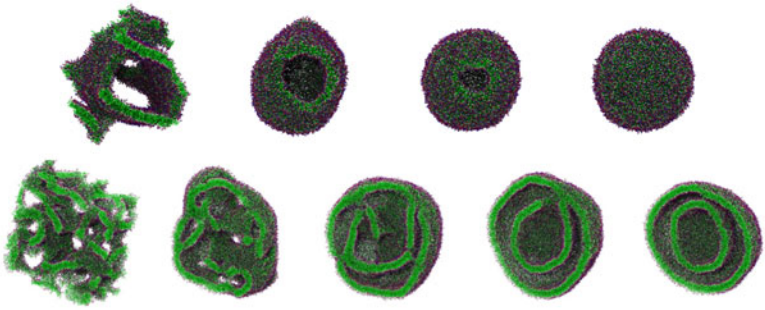

Fig. 6 Liposome formation from a randomly generated DMPC aggregate [45]. *Upper panels*: unilamellar vesicle formation from 5,000 DMPC molecules (shown as the full vesicle). *Lower panels*: the cross-sectional view of the formation of a multilamellar vesicle (MLV) from 20,000 DMPC molecules (shown as cross-section). *Green* indicates aliphatic carbons, *red* and *blue* indicate phospholipid head group particles. Water particles are not shown for clarity

(and to some extent, the innermost vesicle) also experience a strongly anisotropic environment due to the fact that one of the leaflets is within a multilamellar environment and the other faces the bulk water solution. Obviously, one expects that bulk mechanical properties are influenced by such anisotropy. Although a multinanometer thick layer of water separates two adjacent vesicles, such water phase is highly incompressible and has the effect of linking the deformations of the contained vesicle to those of the containing one. However, the multilamellar arrangement can also have an effect on the "microscopic" properties, such as the diffusion times of individual lipid molecules. This hypothesis can be tested easily by CG–MD simulations with explicit solvent.

We prepared ULVs made by 1,512, 2,500, 3,500, and 5,000 DMPC (1,2-dimyristoyl-*sn*-glycero-3-phosphocholine) lipid molecules, respectively. These vesicles were prepared by a series of MD simulations. Briefly, the prepared vesicles are mostly stress-free, because those structures are spontaneously formed from an arbitrary initial aggregate structure during 100–200 ns CG–MD. Timing is supposed to be long enough to see a reasonable partitioning of lipids between inner and outer leaflets of the membrane to relax the stress. We also carried out MD simulation of an MLV, generated by a combination of two ULVs containing 1,512 and 5,000 DMPC lipids, respectively; we simply placed the smaller vesicle inside the larger vesicle. A flat membrane made by 8,194 DMPC lipid molecules was also investigated using three-dimensional periodic boundary conditions, which effectively mimic the multilamellar stack phase.

MD simulations were carried out in the NPT ensemble, with the temperature at 310 K and pressure set at 1 atm. MD simulation of each vesicle system was conducted for 1 μs, although the MD run of the flat membrane was performed for only 300 ns.

We evaluated the lateral diffusion coefficient of each DMPC molecule using the Einstein relation, i.e., based on the computation of the mean square displacement (MSD):

$$\lim_{t\to\infty} \frac{1}{4t} \left\langle (\mathbf{r}(t) - \mathbf{r}(0))^2 \right\rangle$$

The computation of the MSD is straightforward for the flat membrane, though we need particular care for the lipid diffusion in the vesicle membranes. Here we need the definition of lateral motion of DMPC molecules in a vesicle, because the actual motion of lipid involves vesicle diffusion and rotation as well as undulation of membranes. The latter is also ignored in the flat membrane case, where the lipid positions projected on the $x-y$ plane (along the membrane plane) are taken into account for the MSD computation. Removing the lateral motion of the vesicle from the trajectory is straightforward, although the rotational motion is not trivial to remove. We actually did not remove the vesicle rotation from the trajectory, assuming the effect on the MSD to be minor. We ignored the undulation effect in the vesicle system as we did in the flat membrane case, taking a projection of each lipid position on the sphere. Indeed, the vesicles are almost perfect spheres in the present systems. The radius of the sphere to be projected, R, was taken as the average distance of each segment from the center of vesicle. We took the glycerol group of the phospholipid as the representative position of each DMPC molecule and computed its MSD. This was done for convenience although the possible error caused by this choice, instead of the center of mass of the DMPC molecule, is confirmed to be smaller than the statistical error. We computed the lateral MSD of DMPC in inner and outer leaflets separately. Thus, for a vesicle case, we estimated the diffusion on the sphere of radius R using spherical coordinates, as:

$$D = \lim_{t\to\infty} \frac{1}{4t} \left\langle (\mathbf{r}(t) - \mathbf{r}(0))^2 \right\rangle = \lim_{t\to\infty} \frac{1}{4t} \left\langle |R\theta(t)|^2 \right\rangle$$

where:

$$\theta(t) = \cos^{-1}\left(\frac{\mathbf{r}(t)\mathbf{r}(0)}{|\mathbf{r}(t)||\mathbf{r}(0)|} \right)$$

Although this expression is exact in the limit of long time, it can also be used to calculate an "effective" 2D diffusion coefficient (D) of a single lipid molecule in a vesicle membrane; so in this fashion we evaluated D using the slope of the MSD in the time range of 30–50 ns.

Table 1 summarizes the calculated diffusion coefficients, D, from a series of CG MD simulations. As usually found in a CG model, the estimated D is larger than that observed by experiments or all-atom MD simulations by an order of magnitude. We need to rescale the time to quantitatively discuss the dynamical properties, because we took advantage of the enhanced dynamics in the CG system to observe

Table 1 Calculated lateral self-diffusion coefficient (D) of a DMPC molecule in flat and vesicular membranes

		D ($\times 10^{-6}$ cm^2/s)	
Geometry	Number of DMPC molecules	Inner leaflet	Outer leaflet
Flat bilayer	8,142	1.41	
ULV	1,512	0.75	1.53
	2,500	0.92	1.52
	3,500	1.00	1.52
	5,000	1.05	1.55
MLV	1,512	0.72	1.38
	5,000	1.02	1.56

DMPC 1,2-dimyristoyl-*sn*-glycero-3-phosphocholine, *ULV* unilamellar vesicle, *MLV* multilamellar vesicle

the molecular processes occurring beyond the reachable time scale by all-atom simulations. Here, we focus on a comparison of the respective diffusion coefficients of the vesicles simulated.

Interestingly, the lipid diffusion in the outer leaflet of each vesicle is typically enhanced over that in a flat bilayer, but the lipid mobility in the inner leaflet is suppressed. Moreover, the diffusion coefficient of lipid molecules in the outer leaflet is almost constant for any size vesicle, whereas that in the inner leaflet shows a strong size dependency. The outer leaflet of the inner bilayer of the MLV shows slightly lower mobility, due to the effect of the outer bilayer, although a similar effect on the inner leaflet of the opposing bilayer is not evident.

As for the ULV, we should see the convergence of D, as the size of vesicle increases, to the diffusion coefficient of a flat DMPC bilayer. This is not apparently observed in Table 1, suggesting a possible effect on the estimation of D due to the thermal fluctuations or undulation of membranes. The net rotation of the vesicle (each leaflet independently) may also need to be subtracted, although we did not observe a clear motion of this type in the time scale simulated.

7 Perspectives and Challenges

We have briefly reviewed a few applications of our CG model for MD simulations of amphiphilic polymers to predict their self-assembly into supramolecular structures with surprising detail. We speculate that, in the near future, the assembly into complex supramolecular structures will be studied as easily as chemical reactions between small molecules have been modeled successfully in the past few decades by electronic structure methods. However, several potential issues may arise: first and foremost, the accuracy of the CG models used will be put to the test, because higher computing power will allow the study of larger and more complex systems.

Another important challenge to CG–MD simulations of self-assembly will be the ability to properly describe the dynamic equilibrium between chemical species in mixed systems. To remain on the main subject of this brief review, biological

membranes are inhomogeneous mixtures of different lipids. The thermodynamic and mechanical properties of membranes have been modeled by assuming the presence of "lipid rafts," i.e., microdomains with enhanced concentration of certain constituent lipids. Currently, an extensive characterization of lipid rafts by experiment is cumbersome. It is also debatable whether MD simulations possess the required accuracy to predict the formation of such structures. Nevertheless, experimental techniques such as microscopy and computational methods such as CG simulations are now converging to the same scales of length and time. It is highly likely that CG models will become progressively more accurate by complementing measured properties with computational predictions.

Finally, one must consider that many of the supramolecular structures discussed here, and others of similar complexity, are often produced outside thermodynamic equilibrium yet they are effectively treated as the "native" structure of a macromolecular assembly because of the insurmountable time scales required to transition between different phases. On the other hand, this complication is particularly challenging for systems where processing drives them into nonequilibrium states that demonstrate relatively long relaxation time-scales (e.g., days to months). MD simulations of macromolecules in liquid solutions have so far relied on the notion that thermodynamic exchange between all relevant states could always be achieved within the time scale of the laboratory. However, supramolecular structures are formed over a broad range of time scales, sometimes beyond those that allow one to gather a quantitative understanding. A paramount example is that of the crystallization of macromolecules. The study of slow-forming supramolecular structures demands an even higher predictive power from MD simulations, and a continued effort to perfect both CG models as well as the technology required to use them.

References

1. Chemical Heritage Foundation (2010) Chemistry in history: Gilbert Newton Lewis. Chemical Heritage Foundation, Philadelphia. http://www.chemheritage.org/discover/online-resources/chemistry-in-history/themes/molecular-synthesis-structure-and-bonding/lewis.aspx.
2. Deußing G, Weber M (2012) Topic of the month: The life and work of Hermann Staudinger. Guido Deußing, Neuss. http://www.k-online.de/cipp/md_k/custom/pub/content,oid,35205/lang,2/ticket,g_u_e_s_t/~/February_2012_Life_and_work_of_Hermann_Staudinger_part_1.html.
3. Nobelprize.org (2013) The Nobel Prize in Chemistry 1953. Nobel Media AB, Stockholm. http://www.nobelprize.org/nobel_prizes/chemistry/laureates/1953/.
4. Nobelprize.org (2013) Jean-Marie Lehn – biographical. Nobel Media AB, Stockholm. http://www.nobelprize.org/nobel_prizes/chemistry/laureates/1987/lehn-bio.html.
5. Watson JD, Crick FHC (1953) Molecular structure of nucleic acids – a structure for deoxyribose nucleic acid. Nature 171(4356):737–738
6. Seeman NC (2014) Another important 60th anniversary. Covalent and supramolecular macromolecules with complex architecture. Adv Polym Sci. doi:10.1007/12_2013_243
7. Metropolis N et al (1953) Equation of state calculations by fast computing machines. J Chem Phys 21(6):1087–1092
8. Percec V et al (2010) Self-assembly of Janus dendrimers into uniform dendrimersomes and other complex architectures. Science 328(5981):1009–1014

9. Decher G (1997) Fuzzy nanoassemblies: toward layered polymeric multicomposites. Science 277(5330):1232–1237
10. Whitesides GM, Grzybowski B (2002) Self-assembly at all scales. Science 295(5564): 2418–2421
11. Klein ML, Shinoda W (2008) Large-scale molecular dynamics simulations of self-assembling systems. Science 321(5890):798–800
12. Andersen HC (1980) Molecular-dynamics simulations at constant pressure and-or temperature. J Chem Phys 72(4):2384–2393
13. Nosé S, Klein ML (1983) Constant pressure molecular dynamics for molecular systems. Mol Phys 50(5):1055–1076
14. Nosé S (1984) A unified formulation of the constant temperature molecular-dynamics methods. J Chem Phys 81(1):511–519
15. Jorgensen WL et al (1983) Comparison of simple potential functions for simulating liquid water. J Chem Phys 79:926–935
16. MacKerell AD et al (1998) All-atom empirical potential for molecular modeling and dynamics studies of proteins. J Phys Chem B 102(18):3586–3616
17. Cornell WD et al (1995) A 2nd generation force-field for the simulation of proteins, nucleic-acids, and organic-molecules. J Am Chem Soc 117(19):5179–5197
18. Jorgensen WL, Maxwell DS, TiradoRives J (1996) Development and testing of the OPLS all-atom force field on conformational energetics and properties of organic liquids. J Am Chem Soc 118(45):11225–11236
19. Klauda JB et al (2010) Update of the CHARMM all-atom additive force field for lipids: validation on six lipid types. J Phys Chem B 114(23):7830–7843
20. Kirkwood JG (1935) Statistical mechanics of fluid mixtures. J Chem Phys 3(5):300–313
21. Torrie GM, Valleau JP (1977) Monte-Carlo study of a phase-separating liquid-mixture by umbrella sampling. J Chem Phys 66(4):1402–1408
22. Sugita Y, Okamoto Y (1999) Replica-exchange molecular dynamics method for protein folding. Chem Phys Lett 314(1–2):141–151
23. Swendsen RH, Wang JS (1986) Replica Monte-Carlo simulation of spin-glasses. Phys Rev Lett 57(21):2607–2609
24. Shelley JC et al (2001) A coarse grain model for phospholipid simulations. J Phys Chem B 105 (19):4464–4470
25. Shinoda W, Devane R, Klein ML (2007) Multi-property fitting and parameterization of a coarse grained model for aqueous surfactants. Mol Simul 33(1–2):27–36
26. Smit B et al (1990) Computer-simulations of a water oil interface in the presence of micelles. Nature 348(6302):624–625
27. Marrink SJ et al (2007) The MARTINI force field: coarse grained model for biomolecular simulations. J Phys Chem B 111(27):7812–7824
28. Brannigan G, Brown FLH (2004) Solvent-free simulations of fluid membrane bilayers. J Chem Phys 120(2):1059–1071
29. Cooke IR, Kremer K, Deserno M (2005) Tunable generic model for fluid bilayer membranes. Phys Rev E 72(1):011506
30. Goetz R, Lipowsky R (1998) Computer simulations of bilayer membranes: self-assembly and interfacial tension. J Chem Phys 108(17):7397–7409
31. Lopez CF et al (2002) Self-assembly of a phospholipid Langmuir monolayer using coarse-grained molecular dynamics simulations. J Phys-Condens Matter 14(40):9431–9444
32. Ercolessi F, Adams JB (1994) Interatomic potentials from 1st-principles calculations – the force-matching method. Europhys Lett 26(8):583–588
33. Noid WG et al (2008) The multiscale coarse-graining method. II. Numerical implementation for coarse-grained molecular models. J Chem Phys 128(24):244115
34. Noid WG et al (2008) The multiscale coarse-graining method. I. A rigorous bridge between atomistic and coarse-grained models. J Chem Phys 128(24):244114

35. Izvekov S, Voth GA (2005) A multiscale coarse-graining method for biomolecular systems. J Phys Chem B 109(7):2469–2473
36. Marrink SJ, de Vries AH, Mark AE (2004) Coarse grained model for semiquantitative lipid simulations. J Phys Chem B 108(2):750–760
37. Plimpton S (1995) Fast parallel algorithms for short-range molecular-dynamics. J Comput Phys 117(1):1–19
38. Shinoda W, DeVane R, Klein ML (2008) Coarse-grained molecular modeling of non-ionic surfactant self-assembly. Soft Matter 4(12):2454–2462
39. Chiu CC et al (2010) Coarse-grained potential models for phenyl-based molecules: II. Application to fullerenes. J Phys Chem B 114(19):6394–6400
40. DeVane R et al (2010) Coarse-grained potential models for phenyl-based molecules: I. Parametrization using experimental data. J Phys Chem B 114(19):6386–6393
41. Shinoda W, DeVane R, Klein ML (2010) Zwitterionic lipid assemblies: molecular dynamics studies of monolayers, bilayers, and vesicles using a new coarse grain force field. J Phys Chem B 114(20):6836–6849
42. He XB et al (2011) Development of a coarse-grained model for the surfactant family of linear alkylbenzene sulfonates. Biophys J 100(3):147
43. Jusufi A et al (2011) Nanoscale carbon particles and the stability of lipid bilayers. Soft Matter 7 (3):1139–1146
44. Shinoda W, DeVane R, Klein ML (2011) Coarse-grained force field for ionic surfactants. Soft Matter 7(13):6178–6186
45. Shinoda W, DeVane R, Klein ML (2012) Computer simulation studies of self-assembling macromolecules. Curr Opin Struct Biol 22(2):175–186
46. Meyer H (1899) Zur Theorie der Alkoholnarkose. Arch Exp Patholog Pharmakolog 42(2–4): 109–118
47. Danielli JF, Davson H (1935) A contribution to the theory of permeability of thin films. J Cell Comp Physiol 5(4):495–508
48. Robertson JD (1960) The molecular structure and contact relationships of cell membranes. Prog Biophys Mol Biol 10:343–418
49. Sjostrand FS, Anderssoncedergren E, Dewey MM (1958) The ultrastructure of the intercalated discs of frog, mouse and guinea pig cardiac muscle. J Ultrastruct Res 1(3):271–287

Adv Polym Sci (2013) 262: 109–122
DOI: 10.1007/12_2013_269

Published online: 6 November 2013

Nematic Conformation of Chain Molecules Predominating in the Ordered Mesophase

Akihiro Abe

Abstract The physical picture of the nematic conformation has been discussed on the basis of the rotational isomeric state analysis for segmented liquid-crystal (LC)-forming molecules, comprising mesogenic units on both sides of a flexible spacer. The disorientation angles (θ) of the two terminal mesogenic units are calculated for given spatial configurations of the spacer. The observed odd-even character of the thermodynamic quantities at the nematic (N)–isotropic (I) phase transition $T_{NI} = \Delta H_{NI}/\Delta S_{NI}$ has been interpreted in terms of the profiles of the calculated distribution curves $P(\theta) - \theta$. Combined use of rotational isomeric state and ^{2}H NMR techniques has led to an estimate of the conformer fraction in the nematic state. The transition entropies derived on this basis are favorably compared with the constant–volume transition entropies obtained from the pressure–volume–temperature measurement. The observed V–T relation indicates that the expansivity of the nematic LC phase is higher relative to that of the isotropic melt. It has been pointed out that the nematic conformation might possibly gain extra stability from the free volume effect in the LC state. These considerations offer an explanation why amazingly long flexible chain segments can be accommodated in the nematic fluid.

Keywords Conformation of the spacer • Constant-volume transition entropy • Nematic conformation • Odd-even effect • RIS/^{2}H NMR analysis • Segmented LC

Contents

A. Abe (✉)
Tokyo Institute of Technology, 6-27-12 Hiyoshi-Honcho, Kohoku-ku, Yokohama 223-0062, Japan
e-mail: aabe34@xc4.so-net.ne.jp

1 Introduction

Various aspects of segmented liquid crystalline (LC) polymers have been exclusively documented in the literature [1–3]. These molecules often exhibit an enatiotropic nematic (N) LC phase over a certain temperature range between the crystal (C) and isotropic melt (I), and are conventionally called mainchain LCs. Customarily LC-forming molecules comprising a single mesogen, often with a short tail, are called a monomer, and those having two mesogens joined with a flexible spacer are called a dimer, and so forth. In this part of the article, I would like to discuss the sensible way of long flexible spacers adjusting themselves into a partially ordered LC fluid.

As is known from the pioneering work of Vorländer [4], the dimer LC compounds having mesogenic groups on each end of an intervening spacer often exhibit a very profound odd-even trend in their melting behaviors when plotted against the constituent atoms of the spacer. When properly designed, amazingly long flexible segments can be accommodated in an ordered nematic fluid. The effect of the functional group (X) joining the mesogenic unit (Ms) and the spacer in polymers such as $-[\mathrm{Ms}-\mathrm{X}-(\mathrm{CH}_2)_n\mathrm{X}]_x-$ was first pointed out by Roviello and Sirigu [5], who found that the odd-even oscillation of the latent entropy ΔS_{NI} with n (the number of spacer atoms) became substantially weaker when the carbonate group was employed for X in place of ether or ester linkages. The odd-even characteristics of the NI phase transition behaviors $T_{\mathrm{NI}} = \Delta H_{\mathrm{NI}}/\Delta S_{\mathrm{NI}}$ have been extensively studied for dimers, trimers, and polymers, and the results are well-documented in several review articles [6–8]. Various spectroscopic analyses have demonstrated that the orientational correlation among the mesogenic units dispersively located along the backbone is strongly coupled with the geometrical structure and conformational characteristics of intervening spacers. Such a structure-sensitive cooperativity along the flexible chain may be regarded as an example in line with Staudinger's macromolecular concept, brought up in his early days [9].

2 Dependence of Thermodynamic Properties on Degree of Polymerization

Blumstein et al. [10] has reported the molecular weight dependence of the latent entropy ΔS_{NI} for a mainchain LC polyester, poly(4,4′-dioxy-2, 2′-dimethylazoxybenzene dodecanedioyl) (DDA-9). A homologous series of polymer samples (M_n = 700–19,000) , together with the monomer and dimer model compounds were employed in their studies. The value of $\Delta S_{NI,}$ as expressed in terms of a repeating unit, increases very rapidly with the degree of polymerization (DP), reaching an asymptotic value in the oligomeric region. When the unit is converted to the entropy change per spacer, the magnitude of ΔS_{NI} becomes nearly invariant over a wide range of DP from the dimer (9-DDA-9) to polymers: $\Delta S_{NI}/R = \sim 2.1$ (where R designates the gas constant) (Fig. 1). These observations immediately suggest that the conformational contributions arising from the spacer intervening between the two mesogens at both terminals are nearly identical for a given series of LCs beyond the dimer.

It is thus advantageous for conformational studies to work with oligomeric compounds having neat chemical structures. Shortcomings inherent to polymeric LCs, such as polydispersity in DP, structural imperfections due to irregular arrangements such as kink-conformations or hairpins [11], and experimental difficulties associated with the enhancement of NI transition temperatures with DP, can thus be avoided. In the studies mentioned hereafter, detailed analyses were mostly carried out for oligomeric LCs. The knowledge gained through studies on the low DP analogs has been found useful in understanding the spatial arrangements and thermodynamic properties of polymer LCs [12, 13].

3 Influence of Bond Angle Restrictions and Rotational Characteristics on the Odd-Even Effect of Thermodynamic Quantities

For the sake of comparison, thermodynamic properties were examined for a series of dimer model compounds carrying the same chemical constitution except for the linking group X (see Fig. 2). The observed values of $\Delta S_{NI}/R$ are shown for X = carbonate (CBC-*n*), ether (CBA-*n*), and ester linkages (CB-*n*) in Fig. 3 [14]. In accordance with Roviello and Sirigu's finding [5], the carbonate linkage is undoubtedly the origin of the less pronounced oscillation of the dimer [7]. Also included herewith are those obtained for the monomer analog with a carbonate-(*n*OCCB) and ether-type tail (*n*OCB) (see Fig. 2). The odd-even alternation is very weak for both monomer LCs [15–19]. These observations suggest that the chemical structure of the linking group may be an important factor affecting the order–disorder properties of the mainchain LC compounds beyond the dimer.

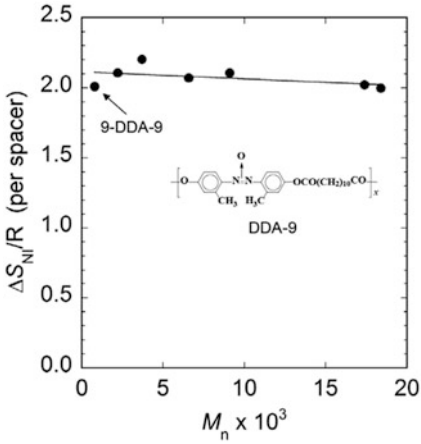

Fig. 1 Plot of the isotropization entropy $\Delta S_{NI}/R$ versus number-average molecular weight M_n for fractionated DDA-9 samples. The dimer model 9-DDA-9 involves two mesogenic units and one intervening spacer. The values of $\Delta S_{NI}/R$ are expressed in terms of the mole of spacers involved. Recalculated from the data reported by Blumstein et al. [10]

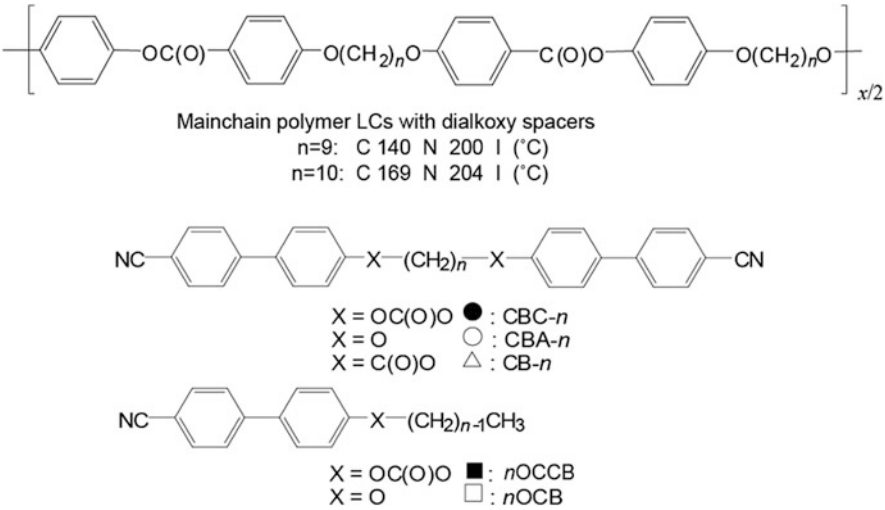

Fig. 2 Illustrative examples of mainchain LCs: polymer, dimer, and monomer. The *symbols* given for the three dimers and two monomers are used in Fig. 3

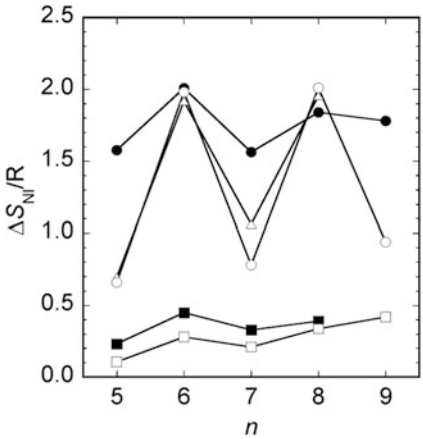

Fig. 3 Effect of the linking group on the odd-even character of the polymethylene-type spacer [14]. The latent entropy, $\Delta S_{NI}/R$, oscillates with the number of methylene units (n) of the spacer. The three *upper curves* represent the dimer, and the two *lower curves* are for the monomer LCs. *Filled symbols* indicate the carbonate-type dimer, α,ω-bis[(4,4′-cyanobiphenyl) oxycarbonyloxy]alkane (CBC-*n*; *filled circles*) and the monomer LC, 4′-*n*-alkoxycarbonyloxy-4-cyanobiphenyl (*n*OCCB; *filled squares*). The *open symbols* indicate the ether-type dimer, α,ω-bis[(4,4′-cyanobiphenyl)oxy] alkane (CBA-*n*; *open circles*), the ester-type dimer, α,ω-bis[(4,4′-cyanobiphenyl)carbonyloxy] alkane (CB-*n*; *open triangles*), and the ether-type monomer LC, 4′-*n*-alkoxy-4-cyanobiphenyl (*n*OCB; *open squares*)

4 Characterization of the Nematic Conformation of the Flexible Spacer

4.1 RIS Analysis of the Orientational Correlation of the Neighboring Mesogens

A theoretical analysis has been put forward on the basis of the conformational distribution estimated within the rotational isomeric state (RIS) approximation [20, 21]. The integrated distribution curves of the disorientation angle θ between the two successive mesogens ($P(\theta) - \theta$) were calculated for spacers comprising odd and even numbers (n) of methylene units in the isotropic conformation [13, 22]. Definition of θ and the bond angles of the linking group (X) adopted in these calculations are shown in Fig. 4. For the ether and ester-type compounds, the profiles of the bimodal distribution are distinctly different for $n =$ odd and even. Whereas the conformers of $n = 9$ are mostly populated in the range $45° < \theta < 100°$ and $145° < \theta < 180°$, the fractional ranges for $n =$ even are $0 < \theta < 30°$ and $85° < \theta < 130°$. The mutual orientation of the mesogenic cores on both terminals of the spacer is antiparallel at $\theta = 0$ and parallel at $\theta = 180°$. In the nematic state, the conformers incompatible with the uniaxial potential field should be suppressed.

Selection of conformers according to this simple rule intuitively suggests that the conformer distribution may yield an odd-even effect with n for the ether and ester series. By the same token, the observed odd-even trend of the order parameter of the

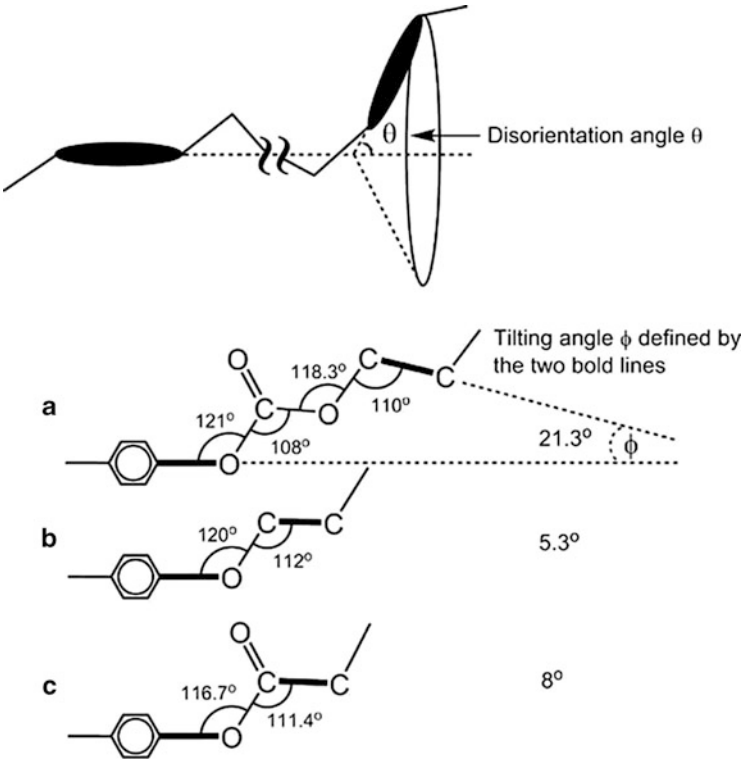

Fig. 4 Definition of the disorientation angle θ and the bond angles of the linking groups (X) used in the RIS analysis: (**a**) carbonate, (**b**) ether, and (**c**) ester. The tilting angles (ϕ) between the first bond of the spacer and the mesogenic core axis (*bold lines*) are estimated to be 21.3°, 5.3°, and 8°, respectively, for the carbonate, ether, and ester group

mesogenic core axis can be easily understood. When the linking group X is replaced by the carbonate group, the bimodal character of the distribution curve is largely lost, and accordingly the distinction between those calculated for $n =$ odd and even becomes obscure. The RIS analysis indicates that the angular distribution is affected by the tilting angle (ϕ) of the first bond of the spacer C_1–C_2 with respect to the mesogenic core axis (shown by the bold lines in Fig. 4). Whereas ϕ is estimated to be 5.3° and 8° respectively for the ether (Fig. 4b) and ester group (Fig. 4c), ϕ amounts to 21.3° with the carbonate linkage (Fig. 4a). The bond angle associated with the carbonate group –O–C(O)–O– is responsible for the depression of the odd-even effect.

4.2 Validity of the Assumption Adopted for Mesogenic Core Axis

As discussed above, the odd-even oscillation should be sensitive to the relative magnitude of the conformer fraction in the nematic state. In a recent work, Centore [23] has investigated the odd-even trend for a series of carbonate dimers containing dimethylbenzalazine mesogens. He suggested that the ΔS_{NI} values of the $n =$ even members may be relatively more suppressed. The odd-even trend may be even reversed by modifying the chemical structure of mesogens. In practice, when the terminal group is replaced by a dibenzoxy terephthalate-type mesogen in the carbonate series (named 3MP-n), the odd members were found to exhibit higher latent entropies than those of $n =$ even [24]. A possible answer to such a delicate variation may be found in the integrated distribution curves of the disorientation angle θ. A larger tilting angle ϕ affects both odd and even distribution curves: While conformers of lower θ values tend to increase in the former curve, those in the range $\theta = 0 - 30°$ are appreciably suppressed in the latter. This suggests that the population of conformers most suited for the nematic order may eventually become comparable. The profiles of the two distribution curves ($P(\theta) - \theta$) are also similar in the intermediate region of θ, indicating that the thermodynamic stabilities of the nematic state are rather close between the $n =$ odd and even in the carbonate series.

Under such conditions, some slight variation in the tilting angle ϕ between the first bond of the spacer and the mesogenic core axis (Fig. 4) might cause a large effect on the odd-even trend in the transition behavior. Experimental observations mentioned above are consistent with what is suggested by the conformational analysis of the carbonate system. In our simplified calculation (see Sect. 5), the biaxiality inherent to the chemical structure is not rigorously taken into account. Admittedly, therefore, the tilting angle ϕ may be affected somewhat by the stereochemical constitution of the mesogenic unit. In effect, the reversed odd-even trend mentioned above (3MP-n) was found to be reproduced by assuming a slightly larger angle for the carbonate linkage in our RIS/^{2}H NMR simulation scheme [24].

4.3 Rotational Characteristics of the Bonds Constituting the Spacer

The distinct odd-even alternation in ΔS_{NI} is a character peculiar to the polymethylene (PM)-type spacers. A comparison between the two different types of spacer, BCBOn (designated as CBA-n in this paper) [25] and MBBE-x with the oxyethylene (OE)-type spacer [26, 27] is shown in Fig. 5, where the latent entropy ΔS_{NI}/R is plotted against the number of constituent atoms (n) of the spacer. For MBBE-x with the OE spacer, irrespective of the parity of n, the ΔS_{NI} versus n plot tends to decrease monotonically with some tiny bumps. The odd-even trend characteristic of the tetrahedrally bonded chain system is rapidly smeared out by the

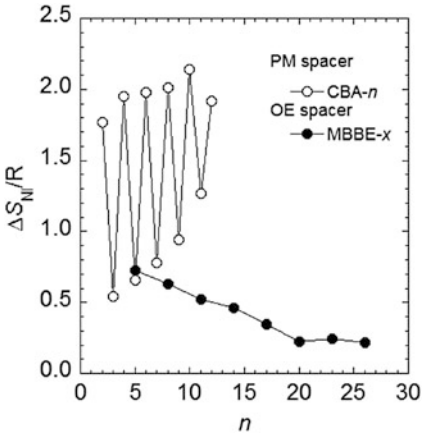

Fig. 5 Variation of the latent entropy $\Delta S_{NI}/R$ with the number of constituent atoms (n) of the spacer: CBA-n (or BCBOn) (*open circles*) [25] and MBBE-x (*filled circles*) [26, 27]. Note that the OE spacers of MBBE-x are expressed by the number of constituent atoms. For consistency, the oxygen atoms of the ether linkage located at both chain terminals are not counted in n

conformational disordering due to the *gauche* preference around the OC–CO bond involved in the OE sequence.

5 Elucidation of the Nematic Conformation and Its Contribution to the NI Transition Entropy

The ^{2}H NMR technique has been shown to be very useful in studying the orientational characteristics of nematic LCs [28–30]. Under an NMR magnetic field, the axis of the nematic domain tends to align along the applied field, and thus the resulting LC phase is taken to be of a monodomain texture. The order parameters $S_{ZZ}{}^{M}$, and $S_{XX}{}^{M} - S_{YY}{}^{M}$ of the mesogenic core comprising a linear array of aromatic nuclei can be accurately determined from the observed dipolar and quadrupolar splittings. The orientational characteristics of the spacer can be similarly estimated by using samples carrying a per-deuterated n-alkane sequence. The nematic conformation of the flexible segment is a quantity defined in the intramolecular coordinate system. With a proper assumption for the molecular axis, approximate values of the bond conformation around the internal C–O and C–C bonds can be elucidated. In fact, a RIS simulation has been performed on the configuration map defined in the intramolecular coordinate system until the observed quadrupolar splittings are properly reproduced [12]. The conformer distribution thus estimated leads to the configurational partition function Z_N for the nematic state. Since the partition function Z_I for the isotropic state is available

from the conventional RIS calculation, the conformational entropy change $S_{NI}{}^{conf}$ at the NI interphase may be obtained as:

$$S_{NI}{}^{conf} = R\ln\left(\widetilde{Z}\right) + RT\mathrm{d}\ln\left(\widetilde{Z}\right)/\mathrm{d}T \quad (1)$$

where $\widetilde{Z} = Z_I/Z_N$. Likewise, the $S_{NI}{}^{conf}$ corresponding to the CN transition may be obtained by setting $\widetilde{Z} = Z_N/Z_C$ in Eq. (1) (note that $Z_C = 1$ for the crystalline state). In fact, the analysis was carried out for representative samples of the carbonate and ether series [13, 14, 31, 32]. The results obtained for CBC-5 and CBC-6, and CBA-9 and CBA-10 (see Fig. 2) are as follows: CBC-5, $S_{NI}{}^{conf}/R = 1.0$ and $S_{CN}{}^{conf}/R = 4.7$; CBC-6, $S_{NI}{}^{conf}/R = 1.5$ and $S_{CN}{}^{conf}/R = 5.1$; CBC-9, $S_{NI}{}^{conf}/R = 1.6$ and $S_{CN}{}^{conf}/R = 7.2$; and CBC-10, $S_{NI}{}^{conf}/R = 1.9$ and $S_{CN}{}^{conf}/R = 7.7$. The odd-even character of the orientational correlation along the chain is reasonably reflected in the conformational transition entropies thus estimated.

The polymer LC illustrated in Fig. 2 contains the ether-type flexible spacer –O$(CH_2)_n$O–, but the axial ratio of the mesogenic core is somewhat larger than the cyanobyphenyl group of CBA-*n*. The ^{2}H NMR analyses were performed by using fully deuterated polymer samples with $n = 9$ and 10, and the results were compared with those of the corresponding dimer CBA-*n* [12]. The order parameter S_{ZZ} tends to be enhanced in the polymeric system, indicating that the orientation of the molecular axis is higher in the nematic LC domain. Conformational analysis of the ^{2}H NMR data collected from the spacers has, however, demonstrated that the spatial configuration of the flexible spacer (i.e., the distribution of conformers in the nematic state) is nearly identical in both dimer and polymer LCs for given values of *n*. These findings were further reinforced by the ^{2}H NMR studies on the trimer model compounds named CBA-T*n* ($n = 9$ and 10) [31]. The results of ^{2}H NMR/RIS analysis are quite consistent with the DP dependence of isotropization entropy (Fig. 1) reported by Blumstein et al. [10].

6 Comparison with the Constant-Volume Transition Entropy

In the above-mentioned RIS/^{2}H NMR analysis, the volume change inevitable to the first-order phase transition is not taken into account. The mainchain LCs normally exhibit stepwise phase transitions with temperature. In most cases, the volume change takes place about 10% at the NI and 90% at the CN transition [32]. In order to confirm the validity of conformational transition entropies, pressure–volume–temperature (*PVT*) measurements were performed for the ether analogs CBA-9 and CBA-10 to determine the NI entropy change at constant volume $(\Delta S_{NI})_V$:

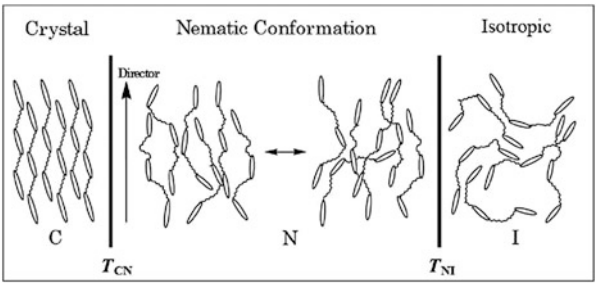

Fig. 6 Representation of the nematic arrangement of mainchain LCs (a trimer model). Although the orientational fluctuation of the entire molecule varies as a function of temperature, the nematic conformation of the spacer remains quite stable over the entire LC region defined by the two phase boundaries (T_{CN} and T_{NI})

$$(\Delta S_{NI})_V = (\Delta S_{NI})_P - \Delta S_V \tag{2}$$

with:

$$\Delta S_V = \gamma \Delta V_{NI} \tag{3}$$

where $(\Delta S_{NI})_P$ is the NI transition entropy under constant pressure, $\gamma = (\partial P/\partial T)_V$ is the thermal-pressure coefficient, and ΔV_{NI} represents the volume change at the NI transition [33–35]. Essentially the same procedure can be applicable for the estimation of the entropy change at constant volume $(\Delta S_{CN})_V$ for the CN transition. The values obtained in this manner are as follows: for CBA-9 $(\Delta S_{NI})_V/R = 0.7 - 1.0$ and $(\Delta S_{CN})_V/R = 7.3 - 9.7$, and for CBA-10 $(\Delta S_{NI})_V/R = 0.8 - 1.8$ and $(\Delta S_{CN})_V/R = 7.8 - 9.2$ [36–38]. In view of the uncertainties involved in the multistage deduction of these values, the correspondence with the conformational entropy changes, $S_{NI}{}^{conf}/R$ and $S_{CN}{}^{conf}/R$, estimated by the RIS/^{2}H NMR technique is reasonable. It should be noted that the order–disorder characteristics inherent to the primary structure of the flexible spacer are precisely controlled in order to develop the LC mesophase. Combined use of spectroscopic and thermodynamic technique has been extended to treat the trimer models CBA-T9 and CBA-T10, and MBBE-6 [26, 38]. As a result, it has been confirmed that 50–60% of the transition entropy $(\Delta S_{tr})_p$ (tr = NI or CN) arises from the variation in the conformational distribution of the spacer at the phase boundary. Although *PVT* data are not available for carbonate LCs, the thermodynamic role of the nematic conformation found between the isotropic and crystalline phases may be similar.

The characteristic features of the nematic ensemble elucidated above are put together in a simple illustration depicted in Fig. 6, which shows nematic arrangements of mainchain LCs in contrast to those of the adjacent isotropic and crystalline phases. In the nematic field, both spacer and mesogenic units at the terminals tend to align along the domain axis. Consequently, the individual mesogenic cores inevitably incline to some extent with respect to the direction of the molecular

extension (Fig. 6), giving rise to a moderate value of the orientational order parameter. As revealed by the studies of magnetic susceptibility [39, 40] as well as optical anisotropy [41], the molecular anisotropy of dimer compounds CBA-*n* ($n = 9, 10$) increases on going from the isotropic to the nematic LC state. Although the flexible spacer takes more extended conformation in the LC state, contribution of the spacer to the orientation-dependent intermolecular (attractive) interactions seems to be small [32]. The nematic conformation of the spacer remains nearly invariant over the entire range of the LC state [42].

The conformational analyses of mainchain LCs have been reported from various laboratories. Although the results seem to vary somewhat depending on the models adopted in the treatment of experimental data, all suggest that flexible spacers prefer to take extended conformations in the nematic state. Efforts to formulate molecular theories to describe the NI transition characteristics of the mainchain LCs in terms of the molecular parameters have also been reported [7, 43, 44]. In an ideal crystalline state, molecules are aligned in a perfect order, often only the most preferred conformation being permitted for the spacer [45]. The structural characteristics of chain molecules in the crystalline, liquid crystalline, and isotropic fluid states must manifest themselves in the conformational entropy of the system upon phase transitions. As the DP of the mainchain LC sample increases, however, the degree of crystallinity tends to be lower, and accordingly the CN transition becomes less sharp [11].

7 Concluding Remarks

In this example, we have attempted to reveal the true nature of nematic conformation characteristic of flexible spacers incorporated in the LC state. The nematic conformation predominates in the individual $–[Ms–X–(CH_2)_n–X]_x–$ units constituting a given polymeric sequence. In an independent work [26], *PVT* studies on the mainchain LCs carrying OE-type spacers have been carried out. It is interesting that the expansivity of the nematic LC phase was found to be larger than that of the isotropic melt. According to the conventional thermodynamic theories of polymeric fluids, the expansivity is closely related to the free volume of the liquid state [46–49].

The order–disorder transition of the mesogenic molecules has been well described by the Maier–Saupe expression in terms of the attractive dispersion interaction [50, 51]. For mesogens of low axial ratios, contribution from the steric repulsion should be relatively minor [52, 53]. In the mainchain LC systems, however, the nematic alignment of the mesogenic cores is largely restricted by the geometrical requirement from the intervening spacers. In compensation, spacers adopt the nematic conformation to cope with the LC formation induced by the anisotropic interactions of mesogenic groups. In this manner, amazingly long flexible chains ($n \sim 14$) can be accommodated, and they seem to enjoy being in the nematic order. Thermodynamic consideration strongly suggests that the loss of

conformational entropy at the I → N transition seems to be compensated to some extent by the increase in the free volume.

The macromolecular concept of Staudinger implies that the physical properties of polymers may be determined not only by the chemical nature of the molecule, but more significantly by the spatial configuration of the entire molecule. As indicated in this work, flexible chain molecules may indeed take isotropic random coil, partially ordered nematic, and the most stable crystalline conformation in response to the thermodynamic requirement of the environment. I should like to dedicate this article to his excellent foresight [54] and pioneering contribution to polymer science [55–57].

Acknowledgment The author thanks Professor Hidemine Furuya for valuable suggestions and help in preparing this manuscript.

References

1. Mingos DMP (ed) (1999) Liquid crystals I, II. Springer, Berlin
2. Demus D, Goodby J, Gray GW, Spiess HW, Vill V (eds) (1998) Handbook of liquid crystals. Wiley-VCH, Weinheim
3. Ciferri A (ed) (1991) Liquid crystallinity in polymers. Wiley-VCH, New York
4. Vorländer D (1927) Z Phys Chem 126:449–472
5. Roviello A, Sirigu A (1982) Makromol Chem 183:895–904
6. Sirigu A (1991) In: Ciferri A (ed) Liquid crystallinity in polymers. Wiley-VCH, New York, Chap. 7
7. Imrie CT, Luckhurst GR (1998) In: Demus D, Goodby J, Grey GW, Spiess HW, Vill V (eds) Handbook of liquid crystals. Wiley-VCH, Weinheim
8. Imrie CT (1999) Liquid crystal dimers. In: Mingos DMP (ed) Liquid crystals II. Springer, Berlin
9. Staudinger H (1961) Arbeitserinnerungen. Hüthig, Heidelberg
10. Blumstein RB, Stickles EM, Gauthier MM, Blumstein A, Volino F (1984) Macromolecules 17:177–183
11. Davidson P (1999) In: Mingos DMP (ed) Liquid crystals II. Springer, Berlin
12. Abe A, Furuya H (1989) Macromolecules 22:2982–2987
13. Abe A, Furuya H, Shimizu RN, Nam SY (1995) Macromolecules 28:96–103
14. Abe A, Furuya H, Nam SY, Okamoto S (1995) Acta Polym 46:437–444
15. Marcelja S (1974) J Chem Phys 60:3599–3604
16. Luckhurst GW (1979) Molecular Field Theories of Nematics In: Luckhurst GW, Gray GW (eds) The Molecular Physics of Liquid Crystals. Academic Press, London
17. Emsley JW, Luckhurst GR, Stockley CP (1982) Proc R Soc Lond A 381:117–138
18. Samulski ET, Dong RY (1982) J Chem Phys 77:5090–5096
19. Abe A, Kimura N, Nakamura M (1992) Makromol Chem Theory Simul 1:401–413
20. Flory PJ (1969) Statistical mechanics of chain molecules. Wiley, New York
21. Mattice WL, Suter UW (1994) Conformational theory of large molecules. Wiley, New York
22. Abe A (1984) Macromolecules 17:2280–2287
23. Centore R (2009) Liq Cryst 36:239–245
24. Abe K, Furuya H, Abe A (1987) Polymer Preprints Jpn 36:916
25. Emsley JW, Luckhurst GR, Shilstone GN, Sage I (1984) Mol Cryst Liq Cryst (Lett) 102:223–233

26. Abe A, Hiejima T, Kobayashi Y, Zhou Z, Nakafuku C (2007) Macromolecules 40:1746–1753
27. Kobayashi N (2004) Master's thesis. Tokyo Polytechnic University, Atsugi
28. Samulski ET, Gauthier MM, Blumstein RB, Blumstein A (1984) Macromolecules 17:479–483
29. Emsley JW (1985) Measurement of orientational ordering by NMR. In: Emsley JW (ed) Nuclear magnetic resonance of liquid crystals. D Reidel, Dordrecht, pp 379–412
30. Yoon DY, Brückner S (1985) Macromolecules 18:651–657
31. Abe A, Takeda T, Heijima T, Furuya H (1999) Polym J 31:728–734
32. Abe A, Furuya H (2010) In: Utracki LA, Jamieson AM (eds) Polymer physics – from suspensions to nanocomposites and beyond. Wiley, New Jersey, Chap. 7
33. Abe A, Furuya H, Zhou Z, Hiejima T, Kobayashi Y (2005) Adv Polym Sci 181:121–152
34. Mandelkern L (1964) Crystallization of polymers. McGraw-Hill, New York, Chap. 5
35. Mandelkern L (2002) Crystallization of polymers, vol 1, 2nd edn. Cambridge University Press, Cambridge, Chap. 6
36. Abe A, Nam SY (1995) Macromolecules 28:90–95
37. Maeda Y, Furuya H, Abe A (1996) Liq Cryst 21:365–371
38. Abe A, Hiejima T, Takeda T, Nakafuku C (2003) Polymer 44:3117–3123
39. Furuya H, Dries T, Fuhrmann K, Abe A, Ballauff M, Fischer EW (1990) Macromolecules 23:4122–4126
40. Furuya H, Abe A, Fuhrmann K, Ballauff M, Fischer EW (1991) Macromolecules 24:2999–3003
41. Furuya H, Okamoto S, Abe A, Petekidis G, Fytas G (1995) J Phys Chem 99:6483–6486
42. Abe A, Shimizu RN, Furuya H (1994) In: Teramoto A, Kobayashi M, Norisuye T (eds) Ordering in macromolecular systems. Springer, Berlin
43. Karahaliou PK, Vanakaras AG, Photinos DJ (2005) Liq Cryst 32:1397–1407
44. Centore R (2007) Liq Cryst 34:729–736
45. Malpezzi L, Brückner S, Galbiati E, Luckhurst GR (1991) Mol Cryst Liq Cryst 195:179–184
46. Flory PJ (1965) J Am Chem Soc 87:1833–1838
47. Abe A, Flory PJ (1965) J Am Chem Soc 87:1838–1846
48. Simha R, Somcynsky T (1969) Macromolecules 2:342–350
49. Beret S, Prausnitz JM (1975) Macromolecules 8:878–882
50. Maier W, Saupe A (1959) Z Naturforsch 14a:882–889
51. Maier W, Saupe A (1960) Z Naturforsch 15a:287–292
52. Flory PJ, Ronca G (1979) Mol Cryst Liq Cryst 54:289–310
53. Flory PJ, Ronca G (1979) Mol Cryst Liq Cryst 54:311–330
54. Staudinger H (1920) Ber Dtsch Chem Ges A/B 53:1073–1085
55. Flory PJ (1953) Principles of polymer chemistry. Cornell University Press, Ithaca, Chap. 1
56. Morawetz H (1985) Polymers – the origins and growth of a science. Wiley, New York
57. Furukawa Y (1998) Inventing polymer science. University of Pennsylvania Press, Philadelphia

Adv Polym Sci (2013) 262: 123–140
DOI: 10.1007/12_2013_260

Published online: 6 November 2013

Helical Polymer–Metal Complexes: The Role of Metal Ions on the Helicity and the Supramolecular Architecture of Poly(phenylacetylene)s

Felix Freire, José Manuel Seco, Emilio Quiñoá, and Ricardo Riguera

Abstract New helical poly(phenylacetylene)s have been successfully designed and synthesised and their properties checked. The new polymers behave as sensors of metal cation valences and/or the polar and donor character of solvents. In the presence of metal salts, poly(phenylacetylene)s form helical polymer–metal complexes (HPMCs) that, in the case of α-methoxyphenylacetic acid (MPA)-containing poly(phenylacetylene), has led to a new family of nanospheres made by complexation between the polymer and divalent metal ions. These HPMC nanostructures present properties such as: (1) their diameter can be tuned to different sizes, (2) the helicity of the polymeric material can be tuned to either of the two helical senses, and (3) they can encapsulate a number of inorganic and organic substances. These polymers also display phenomena such as helical inversion, chiral amplification and axial chirality selection, making them versatile materials.

Keywords Chiral amplification • Helical inversion • Helical polymer-metal complexes • Metal cations • Methoxyphenylacetic acid • Nanospheres • Poly(phenylacetylene)s

Contents

F. Freire, J.M. Seco, E. Quiñoá, and R. Riguera (✉)
Department of Organic Chemistry, Center for Research in Biological Chemistry and Molecular Materials (CIQUS), University of Santiago de Compostela, 15782 Santiago de Compostela, Spain
e-mail: ricardo.riguera@usc.es

1 Introduction

Polyacetylenes (for reviews on polyacetylenes and poly(phenylacetylene)s see [1, 2]) are a versatile family of helical polymers that have attracted the attention of a number of research groups in recent years, mostly due to their capacity to adopt helical structures and, correspondingly, to display axial chirality and due to the properties associated with this structural feature.

Poly(phenylacetylene)s [1, 2] (PPAs) are a class of polyacetylenes in which the monomer repeating units (mru) are derivatives of ethynylbenzene, usually bearing substituents at the *para* position of the phenyl ring. They belong to the so-called dynamic helical polymers, characterised by a low barrier to the inversion between the two helical senses (left-handed and right-handed; *M* and *P*, respectively).

In order to adopt a helical structure, it is necessary for the conjugated double bonds at the polymeric backbone to present a *cis-cisoid* or *cis-transoid* configuration; otherwise, the helix is not formed (*trans-cisoid* or *trans-transoid* configurations) [3]. Nowadays, a number of efficient catalysts, e.g. $[Rh(nbd)Cl]_2$ (where nbd is norbornadiene), are available that provide conjugated double bonds with a high *cis* content in good yields. The *cis* configuration can be easily detected in the polymers by spectroscopic techniques such as NMR or Raman (measuring characteristic vinylic hydrogen chemical shifts and vibrational frequencies from the phenylacetylene backbone, respectively) [3].

Since the pioneering work of researchers such as Percec [4, 5] and others [1, 2], the possibility of achieving helix-sense bias (i.e. helix inversion) on PPAs has stimulated the development of a number of tools for their manipulation; for instance, through specific non-covalent interactions of achiral pendants with chiral molecules [1, 2].

The presence of stereogenic centres in the pendants of PPAs usually leads to the predominance of one helical sense at the helical backbone and thus to an optically active polymer, with a clear CD spectra. These helical polymers can present inversion of their helicity in response to external stimuli such as solvent polarity. This is the case with PPAs containing L- or D-alanine pendants with long alkyl chains, the inversion being ascribed to modifications on the intramolecular hydrogen bonds [6].

Those findings raised the prospect of a rational selection of the pendants, whose conformation could be manipulated by an external stimuli and that change transferred from the pendants to the helical backbone of the PPA. This strategy could be based either on de novo pendant design or by resorting to structures with well-established conformational behaviour under certain stimuli.

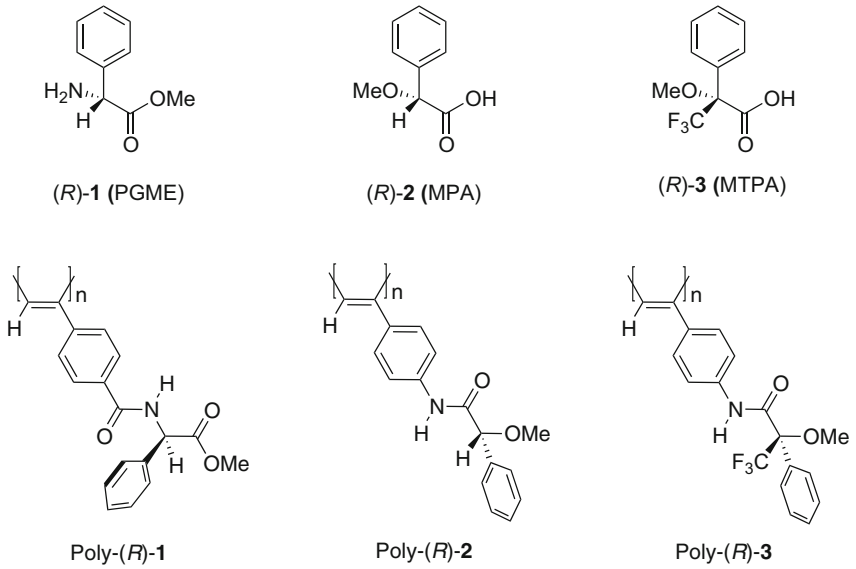

Fig. 1 Structures of CDAs **1**–**3** and corresponding poly(phenylacetylene)s

The latter option seemed very appealing, particularly if we focus on some of the most successful auxiliary reagents for assignment of absolute configurations by NMR [7, 8], known as chiral derivatising agents (CDAs). Their commercial availability, their functionality that allows the easy incorporation into an ethynylbenzene group for polymerisation, their small size and known conformational response to solvent polarity, temperature and complexation are among their potential advantages.

Phenylglycine methyl ester (PGME, **1**), α-methoxyphenylacetic acid (MPA, **2**) and α-methoxy-α-trifluoromethylphenylacetic acid (Mosher's acid, MTPA, **3**) are representative examples of these CDAs (Fig. 1). When they react with chiral substrates (i.e. alcohols, amines, carboxylic acids), the resulting diastereomeric derivatives (esters, amides) present well-defined conformational equilibria among a small set of conformers obtained by rotation around covalent bonds, usually with predominance of a major conformation. This predominant conformer is the main cause of the selective anisotropic effects (i.e. shielding/deshielding) on the chiral substrate that constitutes the basis of NMR methods for configurational assignment in solution.

In a number of cases, the equilibrium between two main conformers has been successfully shifted from one to the other by changing the polarity of the solvent, by varying the temperature or by complexation with metal cations, allowing the development of simpler methods for configurational assignment where only one enantiomer of the CDA is necessary (the preparation of a single derivative from a single CDA enantiomer), instead of the usual two (the preparation of two diastereomeric derivatives from the two CDA enantiomers).

Methods based on the formation of complexes of CDAs with metal cations seem especially interesting for testing using PPAs, due both to the possibility of controlling the conformational equilibria at the pendants that will transmit further effects to the backbone, and to the potential role that metal ions could play in the establishment of supramolecular networks between the polymer chains (interchain bonding), giving birth to new types of nanostructures (i.e. helical polymer–metal complexes, HPMCs).

The results of the work based on the above hypotheses and the incorporation of CDAs **1**–**3** as pendants in PPAs are presented in the next section.

2 Reversible Helical Inversion by Metal Ion Complexation

The previously described PPAs poly-(*R*)-**1** and poly-(*S*)-**1** containing (*R*)- and (*S*)-phenylglycine methyl ester pendants (PGME) [1] were the first polymers chosen to test the potential control of the helicity by complexation with metal cations. Due to the presence of the stereogenic centre, each of these "enantiomeric" polymers had shown by circular dichroism (CD) a defined, but not assigned, backbone helicity, determined by the pendant.

Once synthesised [9], atom force microscopy (AFM) gave important insights into the helicity and morphology of those polymers. In the first place, their helical senses could be assigned. Thus, poly-(*R*)-**1** adopted a right-handed helical conformation (*P*) and poly-(*S*)-**1** a left-handed one (*M*) in $CHCl_3$ (positive and negative Cotton effects, respectively, at 375 nm), thus establishing the correlation between the configuration of the asymmetric carbon at the pendant and the axial chirality of the main chain.

Next, the effect of the complexation with metal cations and the consequent formation of HPMCs were investigated. After the addition of a series of perchlorates of mono- and divalent metal cations (Li^+, Na^+, Ag^+, Mg^{2+} and Ba^{2+}) to the polymers in $CHCl_3$, the CD spectra showed, in all cases, that inversion of the helicity had taken place (opposite CD signs), with Ba^{2+} giving the strongest response; M^{2+} to mru (mol/mol) ratios ranging from ≈6 (THF) to ≈1 ($CHCl_3$) were typically employed. The addition of a scavenger (acetylacetone) reversed the helicity, causing recovery of the original CD spectra (Fig. 2).

These results proved the feasibility of the working hypothesis. Both experimental (AFM, variable-temperature CD, ^{13}C NMR, Fourier transform infrared spectroscopy) and theoretical (discrete Fourier transform, DFT, calculations) evidence point to the mechanistic scenario that follows.

In the absence of metal cations (i.e. Ba^{2+}), the pendants present conformational equilibria in which a certain form (synperiplanar 1, *sp1*) predominates. This conformational preference of the pendants is transmitted to the polyene backbone, which adopts the most stable form [i.e. left-handed in the case of poly-(*S*)-**1**, Fig. 2].

When an appropriate salt [i.e. $Ba(ClO_4)_2$] is added, coordination takes place between the metal cations and the two carbonyl groups (amide/ester) at the

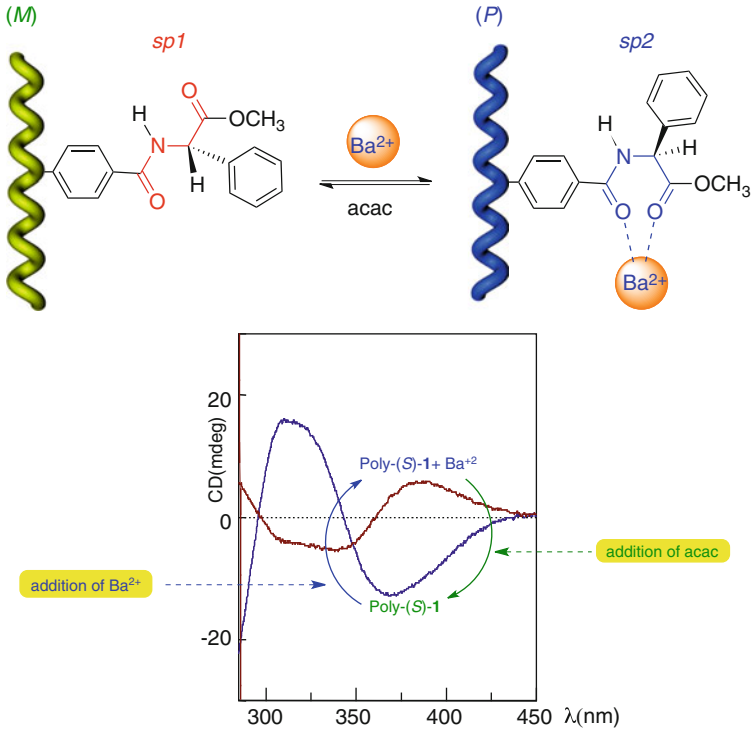

Fig. 2 Reversible helical inversion by metal ion complexation on poly-(*S*)-**1** with Ba^{2+}; *acac* acetylacetone

pendants. For this to happen, rotation around two bonds occurs, and the pendants adopt a new major conformation (*sp2*). The new stable form resulting from the coordination process, places the bulky phenyl group at the other side of the plane that contains the pendant chain bonds and forces the backbone to switch to the opposite helicity [right-handed in the case of poly-(*S*)-**1**, Fig. 2]. Complexation also disrupts the original intramolecular C=O/NH hydrogen-bonding associations that maintain the helical structure prior to the addition of the salt. To sum up, it is the shift in the conformational equilibria of the pendant that causes the change in helicity.

Solvent polarity effects are also highly effective in the control of the pendant conformation and, as a result, in the control of the axial chirality. For instance, the CD bands of poly-(*S*)-**1** moved from negative to positive at 375 nm when going from more polar (i.e. acetone, CH_3CN, DMSO) to less polar (i.e. $CHCl_3$, CH_2Cl_2, 1,4-dioxane, THF) solvents. Right-handed (*P*) and left-handed (*M*) senses predominate in the first and second cases, respectively (Fig. 3).

Theoretical calculations (B3LYP/lanl2dz) showed that the *sp1* conformer of the PGME pendant is less polar than the *sp*2 (2.77 versus 3.47 D). Correspondingly, *sp1* predominates in low and medium polarity solvents and induces a preference for the

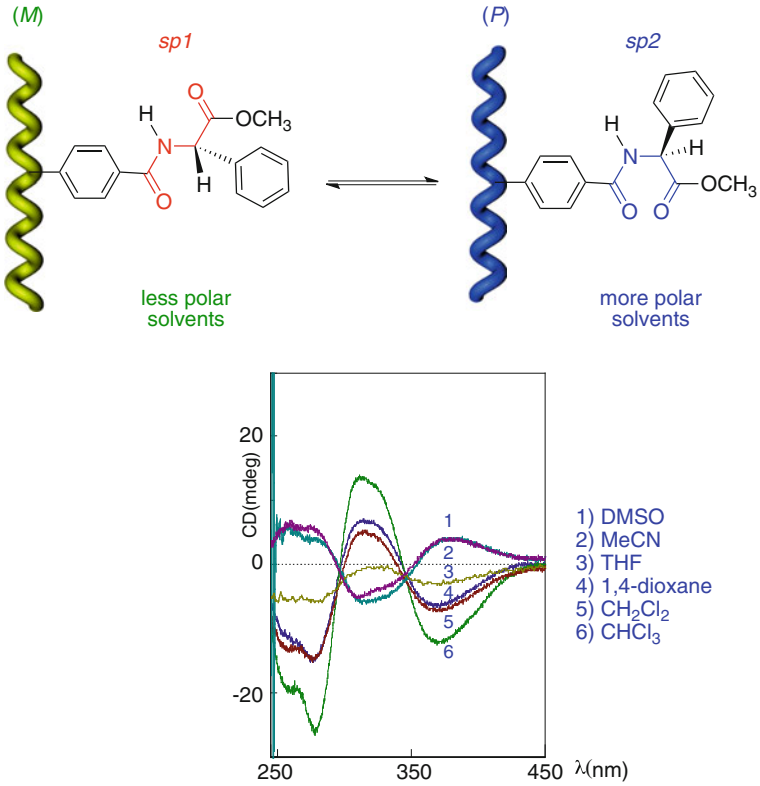

Fig. 3 Helical inversion of poly-(*S*)-**1** by solvent polarity effects

left-handed helicity. On the other hand, the stabilisation of the more polar *sp2* conformer by high polarity solvents switches the preference to the right-handed helicity.

According to the previous results, when divalent cations were added to poly-(*R*)-**1** or poly-(*S*)-**1** in polar solvents such as CH_3CN, helix inversion did not take place because the *sp2* conformer was already the main conformer. On the contrary, an intensification of the CD bands was observed, which was caused by an increase in the original helicity resulting from the growth of the *sp2* population due to the coordination with the cations.

3 Selection of the Helical Sense by Metal Ion Complexation

α-Methoxyphenylacetic acid (MPA, **2**) was another CDA we tested as constituent of the pendants. The fact that MPA amides present in solution a well-defined 1:1 equilibrium between two main conformers, synperiplanar (*sp*) and antiperiplanar

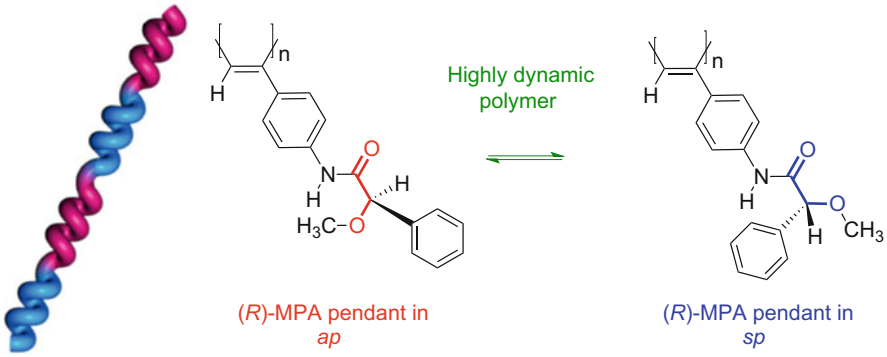

Fig. 4 Main conformers (*ap* and *sp*) at the pendants of poly-(*R*)-**2** leading to a "racemic" helical backbone

(*ap*) [10–13], suggested that although those conformations could present different steric interactions with the surroundings, their ratio could lead to a "racemic" polymer composed of a 1:1 mixture of chains with *M* and *P* helicities (Fig. 4).

Once prepared [14], the two enantiomeric MPA polymers, poly-(*R*)-**2** and poly-(*S*)-**2**, showed null CD spectra in a number of solvents, suggesting the presence of analogous populations of both helical senses. Thus, despite the presence of stereogenic centres at the pendants, the resulting polymer was racemic in its axial chirality. ^{1}H NMR, Raman and differential scanning calorimetry (DSC) [15–18] studies pointed to *cis-cisoid* configurations at their polyene backbones.

Addition of monovalent metal ion salts (i.e. Li^{+}, Na^{+} or Ag^{+} perchlorates) to $CHCl_3$ solutions of poly-(*R*)-**2** originated negative Cotton effects in the vinylic region (380 nm) of the CD spectra.

When divalent metal ion salts were added instead (i.e. Mg^{2+}, Ca^{2+}, Mn^{2+}, Co^{2+}, Ni^{2+}, Zn^{2+}, Ba^{2+}, Hg^{2+}, Pb^{2+} perchlorates), the opposite Cotton effects (positive) were observed (Fig. 5). In both cases, ratios of 0.1 mol M^{+} or M^{2+} to 1.0 mol mru were enough to induce a maximum response from the HPMCs.

These results implied that the MPA polymer responded in two different ways to the valence of the cations tested: negative Cotton effects for monovalent ions and positive effects for divalent ions, thus behaving as a valence sensor for metal cations. No relationship between ionic radii and the observed selectivity bias was found and, as expected, the "enantiomeric" polymer [poly-(*S*)-**2**] gave the opposite results.

In order to distinguish between the behaviour of the two types of cations according to their valence, Fourier transform infrared spectroscopy (FTIR) studies, among others, provided useful information. Coordination with monovalent ions shifted only the carbonyl bands, whereas both carbonyl and methoxy bands underwent noticeable shifts in the case of divalent ions.

Those results point to a plausible scenario whereby monovalent cations coordinate mainly to carbonyl groups and favour the *ap* conformations of the pendants. On the other hand, divalent cations simultaneously coordinate to both carbonyl and methoxy groups, thus favouring the *sp* conformations (Fig. 5). Each conformation

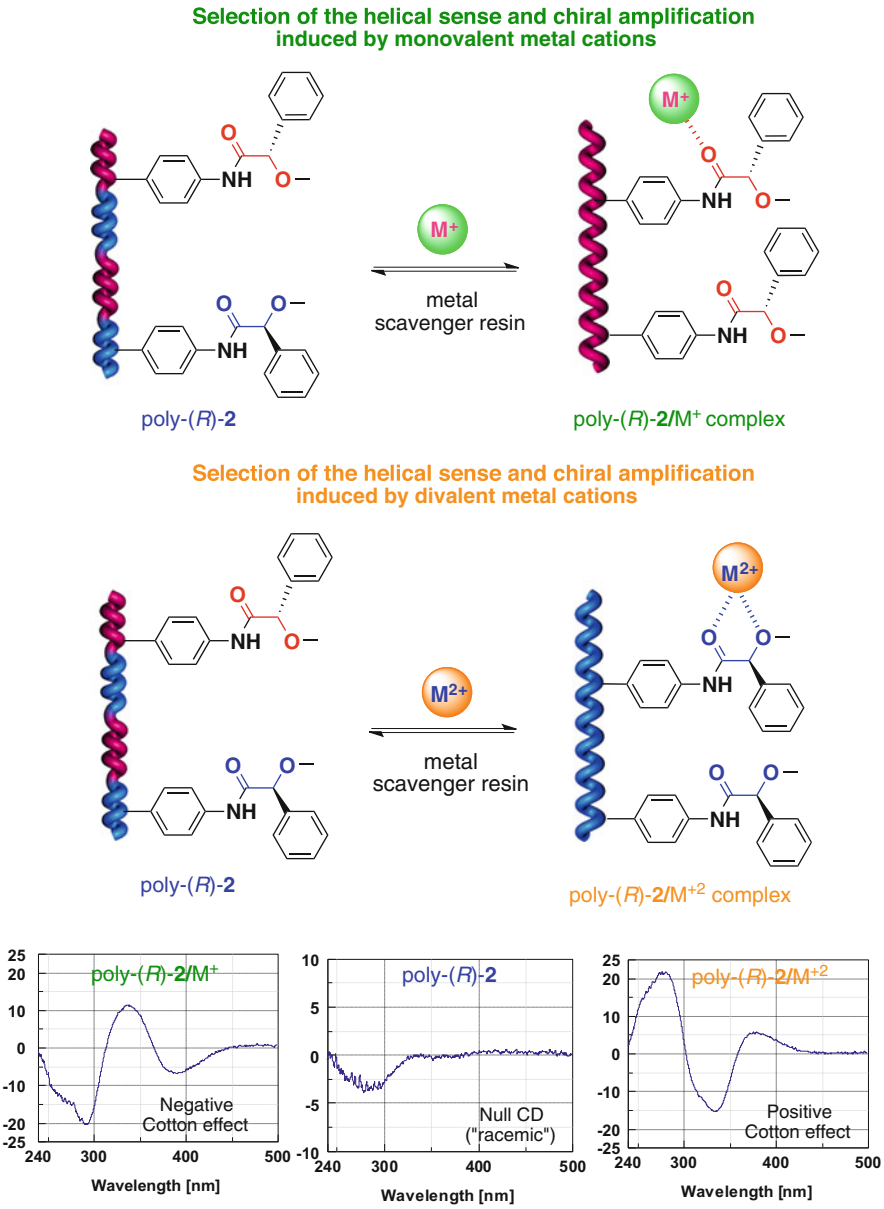

Fig. 5 Selection of the helical sense and chiral amplification by metal ion complexation on poly-(*R*)-**2**. Representative CD spectra are shown

induces a different enantiomeric axial chirality at the polyene backbone and opposite responses in CD. The low energy barrier between the left- and right-handed helical senses makes the dual behaviour of the polymer easy, thus

allowing the evolution from one helical sense to the other according to the valence of the metal ion. The transmission of the changes in the pendants to the skeleton is controlled by the structure and conformation of the complexes and their interactions with the surrounding pendants.

Crucial information on the helical senses and morphologies of the HPMCs was obtained from the AFM images of poly-(*R*)-**2**/Ba^{2+} and poly-(*R*)-**2**/Ag^{+} on highly oriented pyrolytic graphite (HOPG). Results were in full agreement with those previously obtained from CD, confirming the presence of the two enantiomeric axial chiralities.

So, with Ba^{2+}, the single chains were parallel packed, presenting a 3:1 right-handed (clockwise, *P*) pendant disposition, with the periodic oblique stripes forming 60.0° angles and a helical pitch of 3.23 nm (Fig. 6). By contrast, in the case of Ag^{+}, the parallel chains showed a 3:1 left-handed (counterclockwise, *M*) helix with the periodic oblique stripes forming 60.8° angles and a helical pitch of 3.21 nm.

Molecular mechanics (MM) calculations (MMFF94) on the secondary structure of poly-(*R*)-**2** confirmed that a 3/1 right-handed helix was the result when the (*R*)-MPA pendants adopted *sp* conformations (Fig. 6). When the pendants adopted *ap* conformations, the calculations yielded a 3/1 left-handed helix of analogous energy. The angles formed by the oblique stripes and the helical pitches matched the experimental values in both cases.

The values obtained from the external "crests" of the single chains implied internal angles for the polyene backbone close to +75° and −75° for *sp* and *ap* conformations, respectively, and explained the *P* and *M* chirality of the corresponding backbones.

In both cases, poly-(*R*)-**2**/Ba^{2+} and poly-(*R*)-**2**/Ag^{+}, the "external" and "internal" helices (generated by the pendants and by the backbones, respectively) presented the same helical sense, as expected for *cis-cisoid* PPAs.

Knowledge of the secondary structure also allowed correlation of the CD spectra and the type of helicity. For example, in the case of poly-(*R*)-**2**/Ba^{2+}, a positive Cotton effect at the vinylic region corresponds to a clockwise sense at the conjugated double bonds.

4 Chiral Amplification by Metal Ion Complexation

Chiral amplification is an interesting phenomenon in helical polymers [2, 19]. It has been observed in the following three cases:

1. Induction of a predominant helicity in polymers containing achiral repeating units, caused by coordination with adequate chiral substances.
2. In the known "sergeants and soldiers" effect, where a chiral unit "orders" a number of achiral repeating units.
3. In the case of copolymers composed of a mixture of (*R*)- and (*S*)-enantiomeric repeating units with a small enantiomeric excess (*ee*) that originates a predominantly one-handed helical conformation ("majority rule").

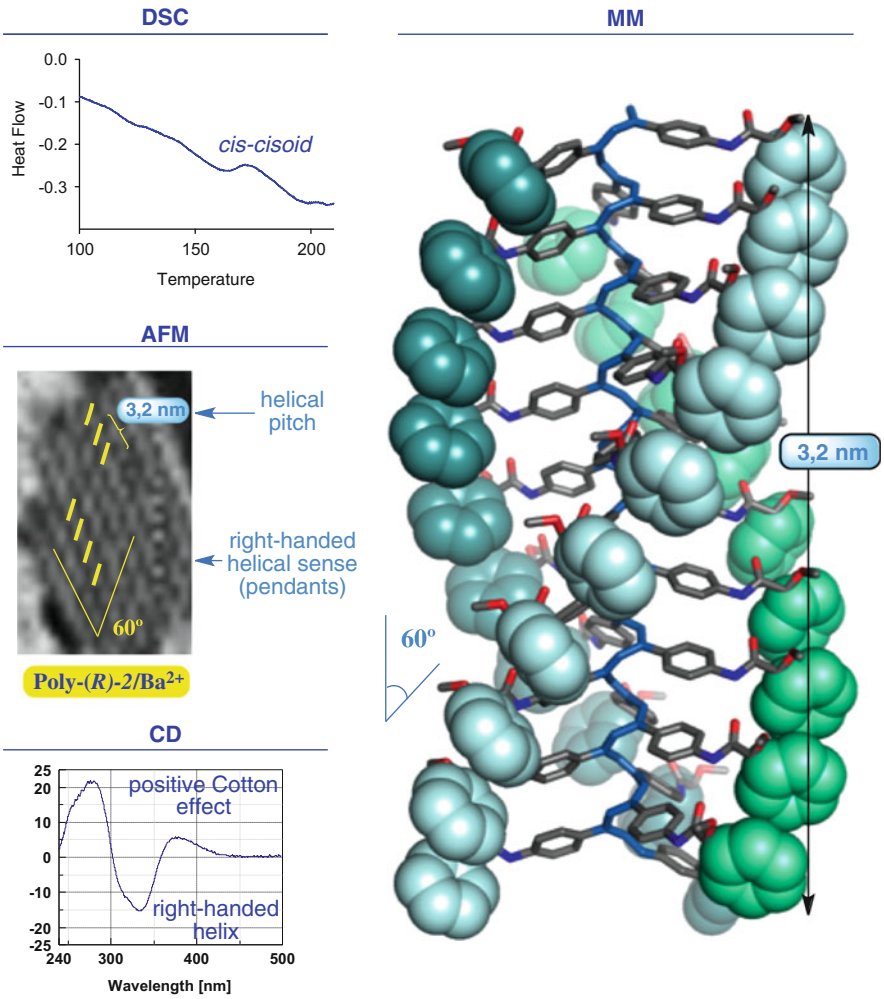

Fig. 6 Structural elucidation of poly-(*R*)-**2**/Ba^{2+} complex by differential scanning calorimetry (*DSC*), atom force microscopy (*AFM*), circular dichroism (*CD*) and molecular mechanics (*MM*) calculations

In the case of the MPA polymers, poly-(*R*)-**2** and poly-(*S*)-**2**, the low metal ion to mru ratios required to achieve maximum CD responses (less than 0.1 in most cases; see Sect. 3) implied that chiral amplification phenomena were operative, with the polymer amplifying the effect of the complexation with the metal ion.

So, it is the selective coordination between mono- or divalent cations and MPA pendants (the different structures and steric requirements of the complexes are transmitted to the polymer backbone) that triggers the amplification phenomenon on the nearby pendants by a domino effect. The predominant right- or left- handed

helicity adopted by the polymer and the associated chiroptical response is determined by the valence of the metal cation. It is should be noted that the external stimulus is achiral in this amplification process.

The versatility of the polymer for helix sense selection and chiral amplification was demonstrated in a number of experiments performed in $CHCl_3$. For instance, once the chiral amplification was obtained with a divalent cation (i.e. cation to mru ratio of 0.1), the helicity could be reversed by addition of a monovalent cation at a higher concentration (i.e. cation to mru ratio of 1.0). The opposite addition sequence (first monovalent, second divalent) acted in a similar way: the axial chirality induced by the cation in excess was predominant. CD spectra analogous to those obtained by step-by-step additions were recorded when mixtures of mono- and divalent cations were added simultaneously.

Cation scavenger resins established the reversibility of the above processes, and the recovered polymers were apt to be reused in the formation of new HPMCs.

5 Nanostructures of Helical Polymer–Metal Complexes

During the studies on HPMCs (see previous sections), the possibility of the metal ions acting as intercalating agents between polymer chains, and thus establishing interchain linkages, was considered. It was observed that HPMCs from the polymers bearing MPA pendants, poly-(*R*)-**2** and poly-(*S*)-**2**, could originate nanostructures such as nanospheres with tuneable size and helicity when perchlorates of divalent metal ions [Mg^{2+}, Ca^{2+}, Mn^{2+}, Co^{2+}, Ni^{2+}, Ba^{2+}, Hg^{2+}, Pb^{2+}] were added in the presence of donor solvents (i.e. THF, acetone) [20].

In general, stable and homogeneous spherical particles with very good polydispersity index (PDI) were formed in solution (in many cases stable for more than one month) in sizes ranging from 60 to 200 nm [i.e. poly-(*R*)-**2** and Ca^{2+} in THF, at a M^{2+} to mru (mol/mol) ratio of 1.0:1.0, generated 100 nm nanospheres; polymer concentration was 0.1 mg/mL]. It was found that larger nanostructures were unstable once generated: progressive aggregation phenomena led to precipitation of the HPMC material.

A very interesting characteristic of the HPMC nanospheres was that their size could be easily modulated. Their dimensions depend on the following three factors:

1. The solvent system: Donor solvents such as THF allowed better control of the particle size because the metal cations were partially coordinated to solvent molecules and thus prevented collapse of the nanostructures. In non-donor solvents (i.e. $CHCl_3$), the cations acted as crosslinking agents that eventually led to HPMC-insoluble materials. This problem could be avoided by adding donor co-solvents (i.e. MeOH, acetone) that stopped both the growth and the collapse of the nanospheres.
2. The element forming the cation: The M^{2+} to mru (mol/mol) ratio needed to form nanospheres of a given size was characteristic for each metal ion. For example,

100 nm diameter nanospheres were formed with Ca^{2+} at a 1.0:1.0 ratio. However, a 3.0:1.0 ratio was required to obtain nanospheres of the same size with Ba^{2+}.

3. The cation to mru ratio: The particles could either "grow" sequentially by adding an extra amount of the cation or "shrink" by adding an extra amount of polymer.

For instance, addition of Ca^{2+} to poly-(*R*)-**2** or poly-(*S*)-**2** (polymer concentration 0.1 mg/mL) at M^{2+} to mru (mol/mol) ratios of 1.0:1.0, 1.2:1.0 and >1.2:1.0 generated nanospheres of 100, 160 and 200 nm, respectively. With Ba^{2+}, ratios of 3.0:1.0, 4.0:1.0 and 5.0:1.0 led to nanospheres of 100, 140 and 170 nm respectively. The usual range of sizes went from 80 to 200 nm (obtained by DLS) for well-defined and stable structures.

On the other hand, a reduction in particle size took place by the sequential addition of extra amounts of polymer to pre-existent nanospheres. For example, nanospheres of 160 nm obtained by addition of Ca^{2+} to poly-(*R*)-**2** [M^{2+} to mru (mol/mol) ratio of 1.2:1.0, PDI 0.18] evolved after addition of an extra amount of poly-(*R*)-**2** (1.0:3.0 ratio) into particles of 112 nm (PDI 0.20) that were further reduced into particles of 90 nm (PDI 0.20) by addition of more poly-(*R*)-**2** (1.0:4.0 ratio).

Most uses of nanoparticles are related to processes on their surface (e.g. use on therapeutic targets) or inside the cavity (e.g. use as nanoreactors), making the chirality of those zones a crucial aspect. In this sense, the ability to tune the helicity of the polymers assembling the nanospheres constitutes an especially relevant property. This ability depends not only on the starting polymer but also on its response to mono- and divalent metal ions that, according to their valence, can play two main roles: as chiral amplification inductors of the helical sense (both mono- and divalent ions) and as crosslinking agents leading to aggregation (divalent ions only).

As a result of the conjunction of these above factors, nanospheres with different helicities and chiroptical responses can be prepared by different strategies. Thus, nanoparticles with right- or left-handed helicity could be obtained by selection of the chirality in the pendant [(*R*)-**2** or (*S*)-**2**]. In addition, it was also found that appropriate use of mono- and divalent cations could cause a single polymer [poly-(*R*)-**2** or poly-(*S*)-**2**] to generate either the right- or left-handed helically oriented nanoparticles. A more detailed explanation of these results follows.

Nanospheres made from poly-(*R*)-**2** presented a predominant helical sense and CD, whereas those made from poly-(*S*)-**2** have the opposite helicity and CD sign. So, in order to get the two axial "enantiomeric" HPMC nanospheres, both polymers are needed. For example, positive CD responses and right-handed helical senses (*P*) predominated in HPMC nanospheres made from poly-(*R*)-**2** and divalent cations (Fig. 7), whereas poly-(*S*)-**2** gave nanoparticles with left-handed helicity (*M*).

When the size of the particles was increased by addition of more metal, they became progressively more "chiral" (increasing CD response) because, as the nanostructures grew, they were composed of chains where one helicity was becoming more and more predominant. Naturally, if 1:1 mixtures of poly-(*R*)-**2** and poly-(*S*)-**2** were used to form the nanoparticles, "racemic" HPMC nanospheres (null CD response at any particle size) composed of polymer chains with equal amounts of both helical senses were obtained.

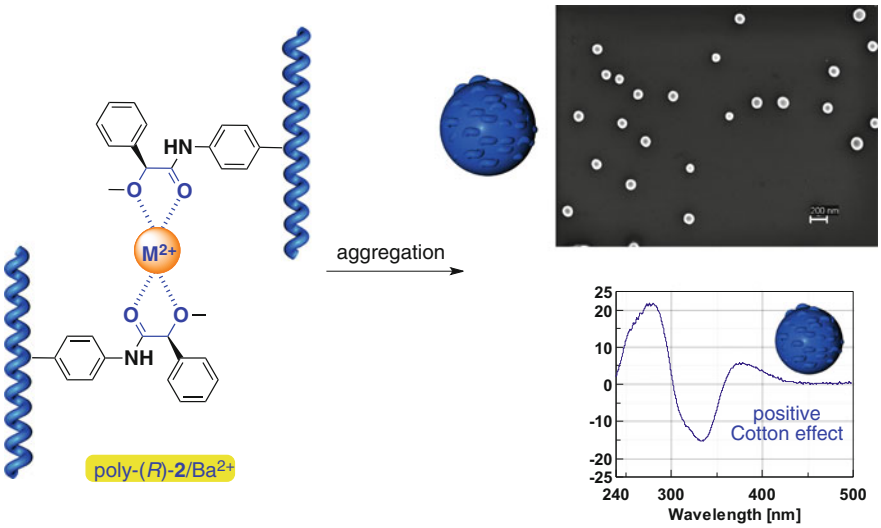

Fig. 7 "Chiral" nanospheres from poly-(*R*)-**2**/Ba^{2+} complex (200 nm scale)

In the second approach, nanospheres with *M* or *P* helical senses could be selectively prepared from a single polymer [i.e. from poly-(*R*)-**2**] as starting material by adequate use of the two roles played by the metal ions, as mentioned above. For instance, divalent cations and poly-(*R*)-**2** led to "right-handed" HPMC nanospheres (as stated above). However, the sequential addition of mono- and divalent cations to that same polymer [poly-(*R*)-**2**] allowed the preparation of the "enantiomeric" nanospheres where "left-handed" helical senses predominated. In both cases, the CD responses at the vinylic region were opposite (positive and negative, respectively, Fig. 8).

The following are examples of standard experiments:

1. Treatment of poly-(*R*)-**2** (null CD) with Ba^{2+} [M^{2+} to mru (mol/mol) ratios ≈0.25; THF/$CHCl_3$ 100 μL/mL] afforded nanospheres with right-handed helical sense (positive CD band at 375 nm; ≈150 nm diameter; *sp* pendants).
2. When the same polymer was treated with Li^+ (M^+ to mru ratio ≈0.40; $CHCl_3$), the expected left-handed helix induction took place without generation of nanostructures (negative CD band at 375 nm; *ap* pendants). Subsequent additions of Ba^{2+} (M^{2+} to mru ratio ≈0.25 and 0.35; THF/$CHCl_3$ 100 μL/mL) to the left-handed soluble HPMC led to the formation of nanospheres of 75 and 130 nm, respectively, that kept the left-handed helicity and the negative CD response originated by Li^+.

In the latter case, monovalent cations simply amplified the left-handed helicities of the poly-(*R*)-**2** chains (monovalent cations do not promote the formation of nanostructures, see Sects. 2 and 3). The subsequent addition of a divalent metal caused the formation of the nanospheres without relevant modifications of the

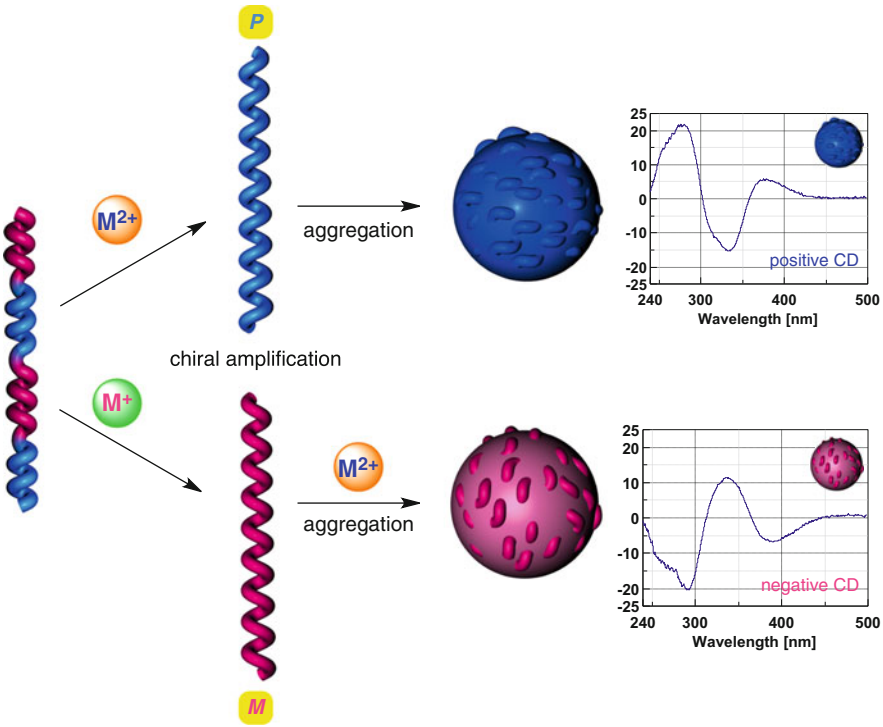

Fig. 8 Nanospheres with *P* or *M* predominant helical senses prepared from a single polymer, poly-(*R*)-**2**

pre-existing left-handed helical sense at the backbone chains. In this case, the divalent cations played a crosslinking role instead of acting as chiral amplification inducers.

6 Potential Uses of HPMC Nanospheres: Encapsulation Studies

The potential of these axially chiral HPMC nanospheres to encapsulate different types of chemical substances was also explored [20] in a set of experiments that proved their capacity to incorporate a number of inorganic and organic compounds.

TEM images clearly showed the presence of 10 nm iron oxide magnetic particles encapsulated inside 200 nm poly-(*R*)-**2**/Ba^{2+} nanospheres (Fig. 9). The encapsulation occurred when the HPMC nanostructures were generated in the presence of a ferromagnetic material and did not modify either the size of the nanospheres or the helicity of the polymer. A visual experiment showed that when a magnet was placed close to a glass vial containing a $CHCl_3$ suspension of the nanospheres with the

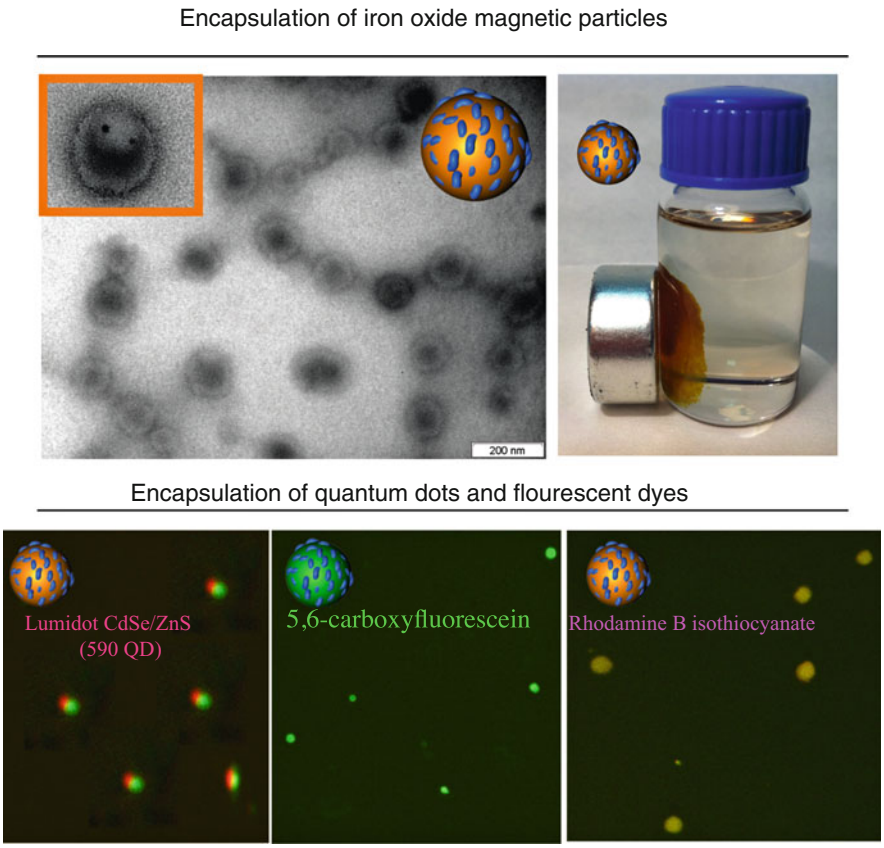

Fig 9 Encapsulation of iron oxide magnetic particles, quantum dots and fluorescent dyes

encapsulated iron oxide particles, all the polymeric material migrated so that it ended up adhered to the vial wall close to the magnet (Fig. 9).

Analogous experiments, monitored by confocal microscopy, performed with quantum dots (Lumidot CdSe/ZnS, 590 nm) and fluorescent dyes (5,6-carboxyfluorescein and rhodamine B isothiocyanate) further confirmed the efficiency of HPMC nanospheres as versatile encapsulating agents (Fig. 9).

7 Helical Sense and Backbone Elongation by Polar and Donor Solvent Effects

MTPA (**3**) is another known CDA that was incorporated as pendant of PPAs. Although the presence of a C_6H_4-NH-C(=O)-C(−OMe) system (as in MPA-PPAs) gave rise to expectations about a similar behaviour of these polymers

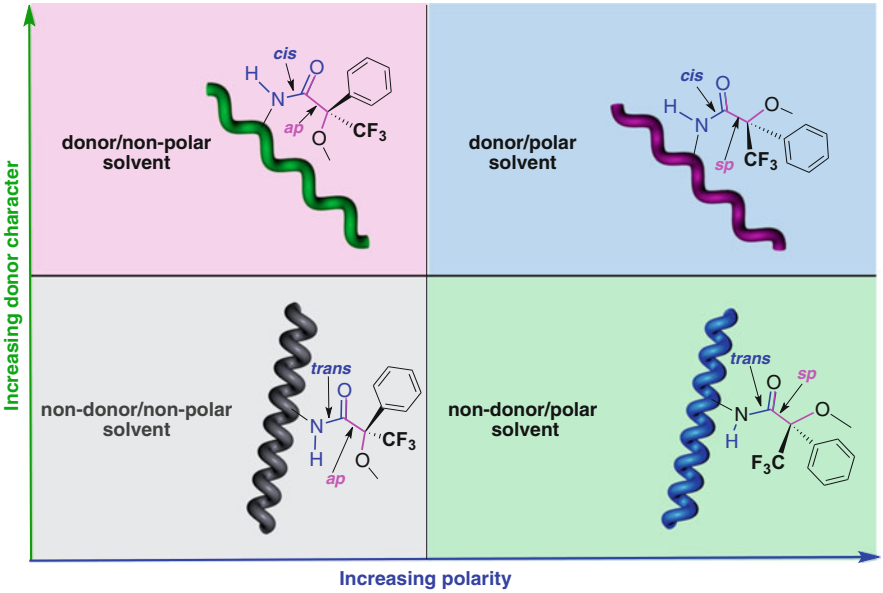

Fig. 10 Correlation between solvent properties and the four different states (helicities and elongations) of poly-(*R*)-**3**

with metal salts, when poly-(*R*)-**3** and poly-(*S*)-**3** [containing (*R*)- and (*S*)-MTPA amide pendants, respectively] were prepared [21] and tested with a selection of mono- and divalent metal cations, no HPMC formation was detected. As the only difference between MTPA and MPA is the presence of the CF_3 group, either steric and/or inductive effects (i.e. on the donor capacity of the oxygen atoms) are probably responsible for this outcome.

However, these polymers showed a very interesting property in solution: both their helical sense and backbone elongation could be selectively tuned. Four responses were obtained according to two different stimuli (the polar or donor character) of the solvent, i.e. *P* or *M* axial chirality and chain lengthening or shortening.

The presence in the MTPA pendants of two bonds whose conformation could be independently tuned by the solvent was responsible for this behaviour. First, an amide group (H−)N−C(=O) sensitive to the donor ability of the solvent can shift the *cis*/*trans* rotamers and, second, a (O=)C−C(−O) bond that responds to the polarity can shift the equilibrium between the *sp* and *ap* conformers. The conformational modification of the pendants was transmitted to the backbone and induced changes in the helicity and/or in the elongation of the polymers (Fig. 10).

AFM and MM studies showed that these polymers in $CHCl_3$ presented identical handedness for the internal (polyene backbone) and the external (pendants) helices (3/1 helix), whereas in THF the internal and external helices (2/1 helix) presented opposite helical senses. DSC traces supported the *cis-cisoidal* and *cis-transoidal* helical structures associated with those structural features.

8 Conclusions

An strategy to obtain new helical polymers based on the incorporation, as pendants of PPAs, of known CDAs with successful past records in other research areas such as configurational assignment by NMR, i.e. PGME (**1**), MPA (**2**), MTPA (**3**), has been tested. The corresponding polymers [poly-(*R*)-**1**, poly-(*S*)-**1**; poly-(*R*)-**2**, poly-(*S*)-**2**; and poly-(*R*)-**3**, poly-(*S*)-**3**] behave as sensors of metal cation valence and/or the polar and donor character of solvents. Phenomena such as helical inversion, chiral amplification and axial chirality selection that are displayed by these polymers make them versatile materials.

Furthermore, the formation of HPMCs has led to a new family of nanospheres made by complexation of divalent metals and MPA-containing PPAs. These HPMC nanospheres present interesting properties such as: (1) their diameter can be tuned to different sizes, i.e. to grow or to shrink, by changing the metal ion or the metal ion to polymer ratio; and (2) the helicity of the polymeric material can be tuned to either of the two helical senses by selection of the starting polymer, or by adequate use of mono- and divalent ions if using a single polymer.

Rational explanations have been given for the helical changes and the process of nanostructure formation, based on the complexation of the pendants, the role of the metal ions, the helicity of the polymer and the character of the solvent.

The fact that these chiral nanoparticles are able to encapsulate different types of inorganic and organic substances opens the door to new supramolecular assemblies with controlled size and tuneable chiral core/surface that can be of great interest in the future as functional matrices for encapsulation and recognition processes.

Although a large number of functional metal–organic particles have been prepared with a wide diversity of metal ions and/or organic ligands, to our knowledge the cases reported here constituted the first examples of HPMCs producing functional nanoparticles.

References

1. Lam JWY, Tang BZ (2005) Acc Chem Res 38:745–754
2. Yashima E, Maeda K, Lida H, Furusho Y, Nagai K (2009) Chem Rev 109:6102–6211
3. Simionescu CI, Percec V, Dumitrescu S (1977) J Polym Sci Polym Chem Ed 15:2497–2509
4. Rudick JG, Percec V (2008) Acc Chem Res 41:1641–1652
5. Rosen BM, Wilson CJ, Wilson DA, Peterca M, Imam MR, Percec V (2009) Chem Rev 109:6275–6540
6. Okoshi K, Sakurai S, Ohsawa JK, Yashima E (2006) Angew Chem Int Ed 45:8173–8176
7. Seco JM, Quiñoá E, Riguera R (2004) Chem Rev 104:17–118
8. Seco JM, Quiñoá E, Riguera R (2012) Chem Rev 112:4603–4641
9. Louzao I, Seco JM, Quiñoá E, Riguera R (2010) Angew Chem Int Ed 49:1430–1433
10. Latypov S, Seco JM, Quiñoá E, Riguera R (1995) J Org Chem 60:1538–1545
11. Seco JM, Latypov S, Quiñoá E, Riguera R (1997) J Org Chem 62:7569–7574
12. López B, Quiñoá E, Riguera R (1999) J Am Chem Soc 121:9724–9725

13. García R, Seco JM, Vázquez S, Quiñoá E, Riguera R (2006) J Org Chem 71:1119–1130
14. Freire F, Seco JM, Quiñoá E, Riguera R (2011) Angew Chem Int Ed 50:11692–11696
15. Percec V, Rudick JG, Peterca M, Wagner M, Obata M, Mitchell CM, Cho W-D, Balagurusamy VSK, Heiney PA (2005) J Am Chem Soc 127:15257–15264
16. Percec V, Aqad E, Peterca M, Rudick JG, Lemon L, Ronda JC, De BB, Heiney PA, Meijer EW (2006) J Am Chem Soc 128:16365–16372
17. Motoshige A, Mawatari Y, Yoshida Y, Seki C, Matsuyama H, Tabata M (2012) J Polym Sci A Polym Chem 50:3008–3015
18. Liu L, Namikoshi T, Zang Y, Aoki T, Hadano S, Abe Y, Wasuzu I, Tsutsuba T, Teraguchi M, Kaneko T (2013) J Am Chem Soc 135:602–605
19. Yashima E, Maeda K, Nishimura T (2004) Chem Eur J 10:42–51
20. Freire F, Seco JM, Quiñoá E, Riguera R (2012) J Am Chem Soc 134:19374–19383
21. Leiras S, Freire F, Seco JM, Quiñoá E, Riguera R (2013) Chem Sci 4:2735–2743

Adv Polym Sci (2013) 262: 141–166
DOI: 10.1007/12_2013_236

Published online: 20 October 2013

Green Polymer Chemistry: Recent Developments

Shiro Kobayashi

Abstract This article briefly reviews research developments on "green polymer chemistry" and focuses on the studies recently performed by our group and related work by some other groups. The green character of polymer synthesis has been viewed from the standpoint of starting materials, polymerization catalyst, reaction solvent, and polymer recycling. Starting materials employ biobased renewable resources such as lactic acid (LA), itaconic anhydride (IAn), succinic anhydride, 1,4-butane diol, etc. Green catalysts include enzymes like lipase and protease. Green solvents are water, supercritical carbon dioxide, and ionic liquids; in particular, water is often used for emulsion systems. From LA and IAn, methacyloyl-polymerizable macromonomers were derived and their copolymerization with a (meth)acryroyl monomer in miniemulsion produced a graft copolymer having LA graft chains. The copolymers are classed as bioplastics from their biomass content ($\geq$25 wt%) and are applicable for coatings. LA chain-containing comb polymers and a star-type polymer were prepared, the latter being currently employed as a coating material. The mechanism of catalysis of the enzymes in the oligomerization of LA alkyl esters was examined to reveal direct evidence that a deacylation step determines the enantioselection. Lipase catalysis was utilized for a polymer recycling system

Keywords Green catalyst · Green polymer chemistry · Green solvent · Green starting materials · Lactic acid

S. Kobayashi (✉)
Center for Fiber and Textile Science, Kyoto Institute of Technology, Matsugasaki, Kyoto 606-8585, Japan
e-mail: kobayash@kit.ac.jp

Contents

1 Introduction

In the last two decades, problems associated with stocks of fossil resources and the methods of energy generation have become extremely important concerns worldwide. These problems are related to the diminishing of resources such as oil, coal, and gas as well as the risks involved in generating atomic energy. The problems are also discussed from the environmental viewpoint, particularly regarding climate change and the need to decrease the amount of carbon dioxide emissions. In the chemistry field, the concept of "green chemistry" was first reported in 1998 [1, 2] and refers to environmentally benign chemistry and chemical technology for a sustainable society. In a similar meaning to green chemistry, "sustainable chemistry" or "green sustainable chemistry" is sometimes used (http://www.gscn.net). Concurrently, the concept of "carbon neutral" was proposed [3], which stresses the importance of employing biobased, renewable starting materials for the synthesis of industrial products to mitigate the carbon dioxide emissions. It is highly required, therefore, that polymeric materials are produced from biomass resources using benign production processes [1, 2, 4], and biobased chemical production from sugar has currently started at the industrial scale [5]. After the proposal of the green chemistry concept, the concept was extended to the field of polymer chemistry as "green polymer chemistry" in 1999, and in fact we have been conducting research based on this concept [6–23].

The concept of green chemistry involves twelve philosophical principles [1]. Among them, the use of renewable resources as starting substrates (starting materials) and green processes (synthetic reactions) are the most important issues for production of a variety of materials. The starting materials recommended are

(1) renewable biobased materials, (2) nontoxic, and (3) environmentally benign. Green synthetic reactions involve (4) efficient catalytic reactions (not a molar reaction), (5) selective reactions to minimize side-products, (6) reactions under mild conditions at a lower temperature to save energy, and (7) reactions in a green solvent like water. From this viewpoint, we have recently conducted green polymer chemistry, e.g., synthesis of polyester-containing polymers by using biobased renewable starting materials and employing nontoxic, environmentally benign lipase enzyme as green catalyst. It should be mentioned that very recently "green polymer chemistry" has become a well-known keyword [20, 24, 25]. In view of the character of this special volume, the present review focuses mainly on our recent results together with the developments of related studies.

2 Green Starting Materials: Biobased Renewable Resources for Polymer Production

There are twelve important platform chemicals listed that are derived from biomass [26]. They include succinic acid, itaconic acid, and glycerol. Some other important biobased renewable chemicals such as lactic acid and 1,4-butanediol are produced via fermentation and/or chemo-enzymatic processes from various biomass sources like corn, sugarcane, wheat, etc. These platform chemicals have been used as starting materials for the production of polymers.

2.1 Lactic Acid-Derived Graft Copolymers Using the Macromonomer Method

Aliphatic polyesters like poly(ε-caprolactone), poly(butylene succinate), and poly (hydroxyalkanoate)s are widely used. An aromatic polyester of poly(ethylene terephthalate) is much more utilized practically. Poly(lactic acid) (PLA) is an aliphatic polyester and has recently attracted major attention. So far, PLA has been a leading polymer produced from biobased resources. High molecular weight PLA is already produced in various ways and used as a green plastic for electronic products, automobile parts, and in biomedical applications [27–40].

PLA has a drawback in its properties, however, which is due to breaking of the PLA chain through ester bond hydrolysis. Until now, various efforts have been made to decrease the bond breaking damage but so far it has been very difficult to suppress the hydrolysis completely. A possible solution to mitigate the damage is not to use PLA as a main chain, but to employ PLA as side chains. Figure 1 illustrates the concept [41].

The macromonomer technique is a practical and convenient method for preparing graft copolymers. So far, PLA has been prepared mainly via two ways: ring-opening polymerization (ROP) of lactide (a six-membered cyclic dimer of

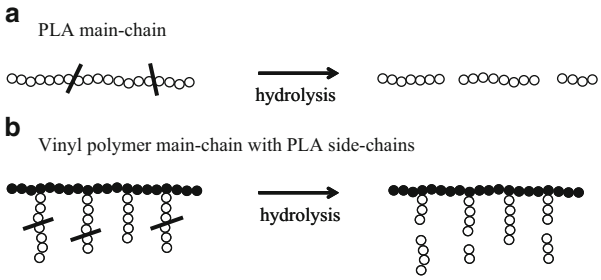

Fig. 1 PLA polymer properties. (**a**) Polymer having PLA as the main chain undergoes a severe loss of properties due to hydrolysis. (**b**) Vinyl polymer main chain having PLA side chains suffers less damage to properties through hydrolysis

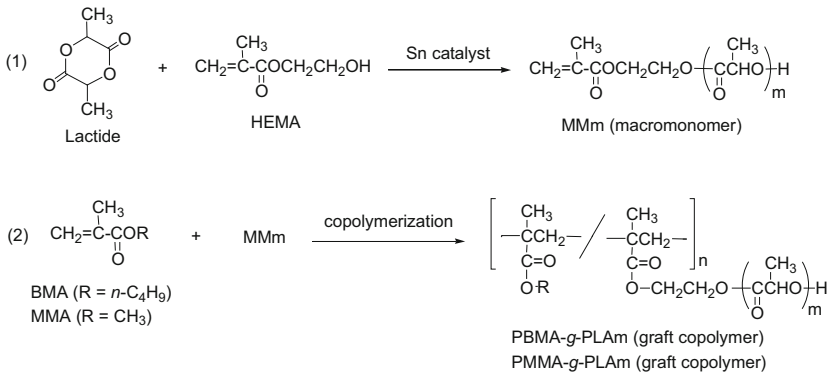

Scheme 1 (*1*) Synthesis of macromonomers (*MMm*) and (*2*) synthesis of graft copolymers. *HEMA* hydroxyethyl methacrylate, *BMA* *n*-butyl methacrylate, *MMA* methyl methacrylate

lactic acid) and direct polycondensation of lactic acid [29, 30]. Thus, we prepared graft copolymers having PLA side chains using the macromonomer technique via ROP. PLA macromonomers (MMm) having a methacryloyl polymerizable group with different PLA chain lengths (average length $m = 4$, 6, 8, 12, 18, and 30) were prepared via ROP of L-lactide using hydroxyethyl methacrylate (HEMA) initiator catalyzed by $Sn(Oct)_2$, as given in reaction (1) in Scheme 1 [41, 42]. It is to be noted that the glass transition temperature (T_g) and melting temperature (T_m) values of MMm were as follows: $m = 4$ (−27°C), 6 (−17°C), 8 (−12°C), 12 (−8°C, 58°C), 18 (30°C, 105°C), and 30 (38°C, 151°C), i.e., when the LA chain length became longer, both values increased to close to those of PLA, ~60°C and ~170°C, respectively.

Radical copolymerization of MMm with a vinyl monomer was examined in an organic solvent or in a miniemulsion. MMm with m value lower than 12 was

Table 1 Radical copolymerization of alkyl methacrylate (BMA or MMA) with MMm to form graft copolymers in an organic solvent[a], and the copolymer properties

Copolymerization in feed B(M)MA/MMm (mol/mol)	Graft copolymer					
	Structure expression	M_n ($\times 10^{-4}$)	B(M)MA/MMm ratio in copolymer (mol/mol)	Biomass content (wt%)	T_g (°C)	Pencil hardness
BMA/MM6 (83/17)	PBMA-*g*-PLA6	2.25	82/18	34	25	<6B
BMA/MM12 (92/8)	PBMA-*g*-PLA12	5.4	92/8	34	31	<6B
BMA/MM18 (94/6)	PBMA-*g*-PLA18	3.69	95/5	34	36	3B
BMA/MM30 (83/17)	PBMA-*g*-PLA30	6.95	84/16	71	50	2B
MMA/MM6 (80/20)	PMMA-*g*-PLA6	4.9	82/18	42	67	H

[a]Toluene as solvent with AIBN initiator at 70°C for 24 h for the upper three reactions and 1,4-dioxane as solvent with AIBN initiator at 60°C for 24 h for the lower two reactions

investigated for a miniemulsion system (see Sect. 2.5). Here, we give the results of solution copolymerization of MMm (having *m* values of 6, 12, 18, and 30) with *n*-butyl methacrylate (BMA) and methyl methacrylate (MMA). Various graft copolymers [PB(M)MA-*g*-PLAm] (reaction 2, Scheme 1) were obtained and their properties are given in Table 1 [41]. The copolymerization produced the copolymers in good to high isolated yields (≥54%), having molecular weight (M_n) between 2.25×10^4 and 6.95×10^4. The copolymer composition was close to the feed monomer ratio, which means that the monomer reactivity ratio of BMA or MMA and MMm was also close, suggesting the formation of a random copolymer structure. In the copolymerization of BMA and MM6, both monomers showed the same copolymerizability, whereas in the case of BMA and MM30, the latter exhibited slightly less copolymerizability. The biomass content of the copolymers was in the range 34–71 wt%. According to the definition of the Japan BioPlastics Association proposed in 2006, "biomass plastic" denotes a plastic containing a biomass content higher than 25 wt%. In this regard, all the graft copolymers can be classed as biomass plastics.

The T_g values of the graft copolymers are also given in Table 1. All the copolymers are amorphous without showing a melting point and are soluble materials. Transparent films were obtained; however, the films were very brittle so the pencil hardness of the copolymer samples was measured. In the four polymer samples having PBMA chains, the higher the T_g value, the greater the hardness. The reason may be mainly due to the higher T_g value with longer PLA chains. A higher T_g value with PMMA chains reflects the higher T_g value of PMMA (105°C), which is a relatively hard material. These graft copolymers will find useful applications as biomass plastics.

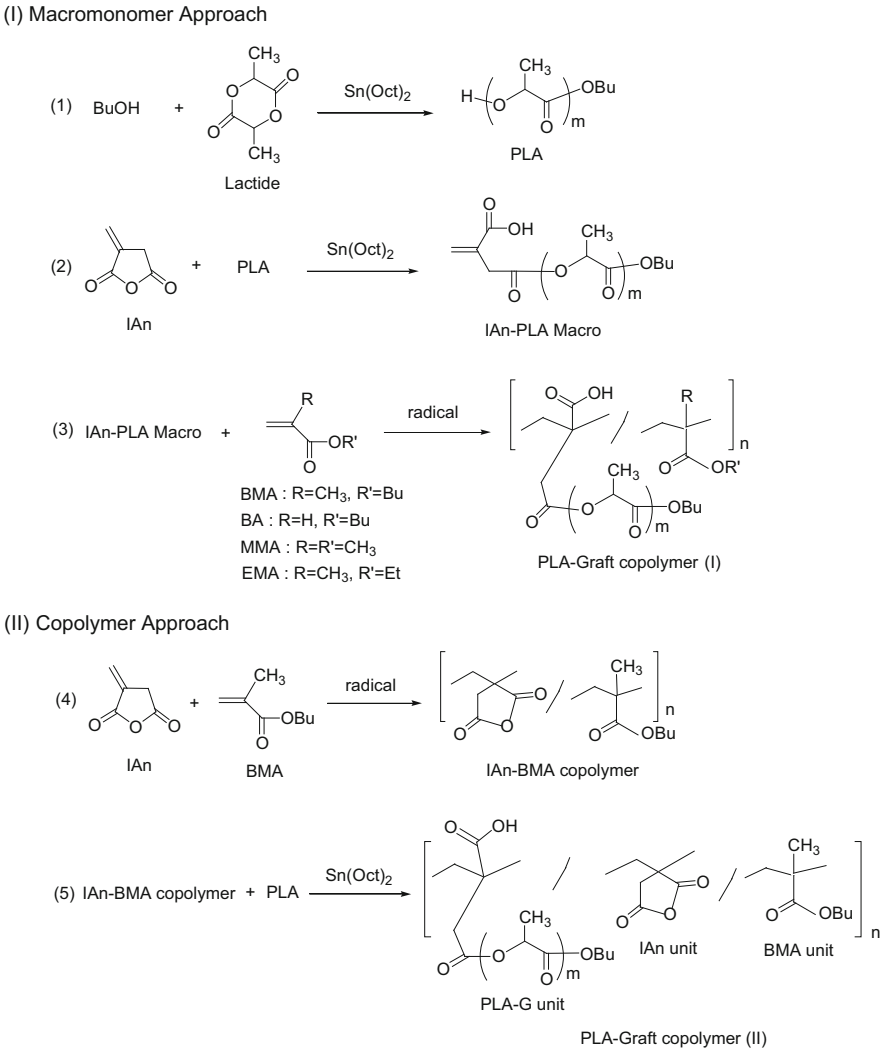

Scheme 2 Synthesis of PLA-graft copolymers via two methods: (*I*) macromonomer approach and (*II*) copolymer approach. See text for description of reactions

2.2 *Graft Copolymers Based on Itaconic Anhydride and Lactic Acid*

Itaconic anhydride (IAn) and lactic acid (LA) were employed as renewable starting materials. PLA-graft copolymers were synthesized via two approaches (as shown in Scheme 2) [43]. First, the macromonomer approach utilized IAn for Sn-catalyzed synthesis of PLA-containing macromonomers (IAn-PLA Macro). The

macromonomer was radically copolymerized with BMA, *n*-butyl acrylate (BA), MMA, and ethyl methacrylate (EMA) to efficiently give graft copolymers [PLA-Graft copolymer (I)] with M_n up to 1.61×10^5 and a biomass content higher than 34 wt%. Second, the copolymer approach employed first IAn as comonomer for radical copolymerization with BMA, giving rise to IAn-BMA copolymer with M_n higher than 5.76×10^4. Then, Sn-catalyzed grafting of PLA onto the IAn moiety of the copolymer produced PLA-Graft copolymer (II) with M_n higher than 5.88×10^4 and a biomass content $\geq$29 wt%.

By using these two approaches employing IAn as a starting reactive material, PLA-graft copolymers were obtained as biomass plastics. The properties of PLA-Graft copolymers (I) were also examined, which revealed possible applications for coatings and plastics. Furthermore, the IAn-containing graft copolymers are a convenient starting biomass polymer, having a reactive IAn moiety in the main chain for further grafting or various functional group-introducing reactions.

2.2.1 Macromonomer Approach

IAn was employed for the first time to prepare an IAn-PLA macromonomer by utilizing the reactive nature of IAn with ring-opening. The macromonomer (IAn-PLA Macro) was prepared via a one-pot two-stage method [reactions (1) and (2) in Scheme 2]. IAn is an unsymmetrical anhydride, and the structure of IAn-PLA Macro given in reaction (2) was the major product, at around 90%. By varying the feed ratio of BuOH and L-lactide, it was possible to tune *m* values ($m = 5$, 6 and 12). The reaction yields were almost quantitative and the functionality of IAn-PLA Macro was realized at ~100% in all cases.

Radical copolymerization of IAn-PLA Macro with a vinyl monomer yielded PLA-Graft copolymer (I) according to reaction (3) in Scheme 2. Copolymerization using BMA as comonomer by AIBN initiator gave PLA-Graft copolymer (I) in high yields in bulk or in toluene, with M_n, up to 1.1×10^5. In 1,4-dioxane, lower copolymer yields with lower molecular weight were obtained. Both IAn-PLA Macro and BMA are of methacryloyl-type structure; the former showed a little less radical copolymerization reactivity toward BMA. The biomass content of PLA-Graft copolymers was in the range of 34–70 wt%, indicating the biomass plastic nature of the graft copolymers.

Likewise, radical copolymerization of IAn-PLA Macro (I) with other three vinyl monomers (BA, MMA, and EMA) produced PLA-Graft copolymers (I) as shown in reaction (3) of Scheme 2. All these product copolymers are biomass plastics (biomass content 46–75 wt%).

Regarding the graft copolymer properties, a PLA-Graft copolymer (I) sample (Macro, $m = 6.0$) derived from BA typically gave a transparent film by casting from a chloroform solution. The sample had a molar ratio Macro:BA = 1.0:2.4, was of high molecular weight ($M_n = 161{,}000$), had a T_g value of 11.2°, and a high biomass content of 59 wt%. It showed a very good elastic property, as shown by the

following data: Young's modulus, 316 kgf/cm^2; tensile strength, 33.7 kgf/cm^2; and elongation at break, 496.1%. These results suggest that the copolymers can be applied for coatings, soft films, etc. [41, 42].

On the other hand, using BMA as comonomer the PLA-Graft copolymer (I) (Macro, $m = 6.0$) having $M_n = 37{,}600$ with biomass content of 53 wt% showed a T_g value of 27.0°C. The copolymer composition was in a molar ratio Macro:BMA = 1.0:2.9. The copolymer sample was very hard and very brittle, as shown by elongation at break of 101.3%. It is understandable from the monomer structure that both the Macro and BMA have an α,α-disubstituted structure of $CH_2{=}CRR'$ and, moreover, that the Macro contains a bulky PLA group of $R{=}CH_2C({=}O)PLA$. Thus, the resulting copolymer should have a main chain with condensed packing, resulting in non-flexible polymeric materials. Therefore, the copolymers from BMA may find applications in hard plastic materials requiring a tough nature, which can probably be accomplished via further crosslinking reactions. Graft copolymers (I) and (II) possess a $-CO_2H$ group in the main chain and, hence, they are derivative polymers of methacrylic acid. Their applications are also conceivable in this direction.

2.2.2 Copolymer Approach

The other way to produce PLA-graft copolymers is shown as reactions (4) and (5) in Scheme 2 [43]. First, IAn-BMA copolymer was prepared via radical copolymerization of IAn and BMA. IAn-BMA copolymers were obtained in good yields, with M_n reaching 1.1×10^5. The next step was grafting the PLA chain onto IAn-BMA copolymer by Sn-catalyzed reaction of PLA to afford PLA-Graft copolymer (II) according to reaction (5) in Scheme 2. In one case, the value of $M_n = 5.76 \times 10^4$ for IAn-BMA copolymer was increased slightly to 5.88×10^4 after the grafting. The grafting reaction is a polymer–polymer reaction, which is generally harder than a polymer–monomer reaction and it is not easy to achieve a high conversion. Therefore, some portions of the anhydride group of the main chain remained unreacted. In this respect, the macromolecular approach seems more effective.

2.3 Comb Polymers via Macromonomer

Comb polymers are those having a graft chain at every repeating unit. Such copolymers can be derived by homopolymerization of a macromonomer (Scheme 3) [41]. Some results of the radical homopolymerization of MMm are given in Table 2 [41]. Normally, the radical polymerization of macromonomers needs a large amount of initiator and, hence, AIBN was employed at 10 mol%. But, regardless of the amount (1 or 5 mol%), polymer yield was relatively high and M_n was between 2.19×10^4 and 9.00×10^4 (M_w was between 2.67×10^4 and 11.0×10^4), showing a high molecular weight of the product comb polymers.

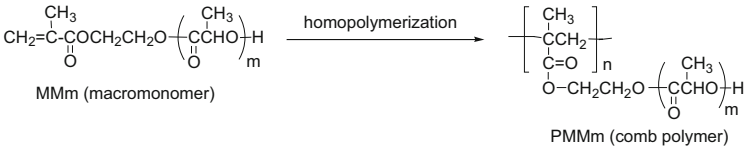

Scheme 3 Synthesis of comb polymer

Table 2 Radical homopolymerization of MMm to comb polymers[a]

AIBN[a] (mol%)	Product comb polymer	Isolated yield (%)	M_n ($\times 10^{-4}$)	Biomass content (%)	T_g (°C)	Pencil hardness
10	PMM4	53	3.84	69		
5	PMM6	57	4.74	77		
1	PMM6	71	9	77	38	2B
10	PMM8	52	4.17	82		
10	PMM12	57	3.67	87	43	B
10	PMM18	53	2.19	91	50	B
10	PMM30	81[b]	3.13 (0.33)[b]	94	58	HB

[a]Radical polymerization of MMm in 1,4-dioxane at 70°C for 24 h except for the third reaction, which was at 60°C for 24 h
[b]The GPC chart shows two peaks. The ratio of the major part to the minor part (given in parenthesis) was 82:18

The biomass content was of course equal to that of the macromonomers MMm. Thus, various comb polymers having high biomass content up to 94 wt% were obtained. To our knowledge, this is the first instance of preparation of comb polymers having PLA as the pendant chain with high biomass content.

These comb polymers are white powders and are soluble materials. They possess T_g values such that when the side chains of PLA became longer, the T_g value became higher. These values reflect well the nature of the PLA chains, as observed with MMm monomers. They formed transparent films via the casting method. Their pencil hardness values (Table 2) were in a narrow range (2B–HB) with a monotonous change along the PLA chain length. For longer side-chain PLA length and, hence, higher T_g, the comb polymer was a little harder. These comb polymers may be applied as soft materials.

2.4 Star-Shaped Lactic Acid Oligomers for Coating Applications

Multifunctional star-shaped oligo(lactic acid)s (oligoLAs) with reactive double bonds were synthesized from the oligoLA polyols. They have application as biobased curable coatings. The outline of the synthesis procedures is shown in Scheme 4, using pentaerythritol as an example of a polyol [44, 45].

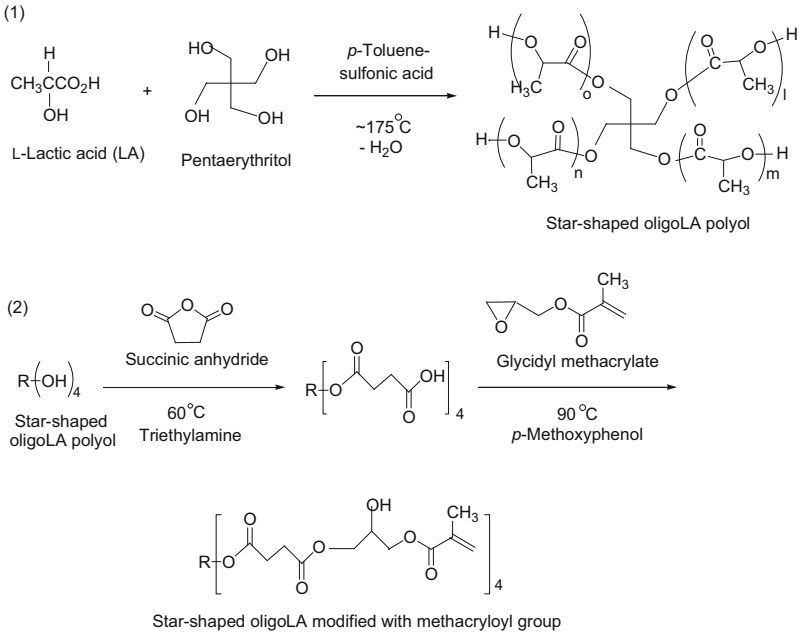

Scheme 4 (*1*) Synthesis of star-shaped oligoLA polyol from LA and pentaerythritol and (*2*) synthesis of star-shaped oligoLA modified with methacryloyl group from the polyol, succinic anhydride, and glycidyl methacrylate

The molecular weight M_n of the star-shaped oligoLA polyol ($l + m + n + o = 14$) obtained by gel permeation chromatography (GPC) was 1,400 with $M_w/M_n = 1.4$. The polyol was shown to be amorphous by differential scanning calorimetry (DSC) and had about 88% biomass content. The polyol was applied as a test coating on the grip part of the Toyota personal mobility vehicle "i-REAL"; the coating was prepared via two-component thermal curing with mixing the polyol and a polyisocyanate hardener (Fig. 2) [44]. The biomass content of the cured coatings was 40 wt%.

The product, a star-shaped oligoLA modified with a methacryloyl group (S-OLAM1) according to reaction (2) in Scheme 4, was of $M_n = 2{,}600$ and $M_w/M_n = 1.3$, with an average of 4.6 methacryloyl groups per molecule and a biomass content of 41 wt% (63 wt% when succinic anhydride was counted as biomass). Instead of pentaerythritol, dipentaerythritol also gave another S-OLAM (S-OLAM2). These S-OLAMs were applied as UV-curable coatings. An example formulation was a mixture of S-OLAM2 (70 wt%), urethane hexaacrylate (30 wt%), and a photo-initiator (5 wt%). The film coating was prepared by air-spraying on polycarbonate and then irradiating using a mercury lamp to form the cured film, whose thickness was 15 μm. Performance data of the UV-cured coating film indicated good initial adhesion, humidity resistance, alkaline

Fig. 2 Coatings on the grip part of TOYOTA personal mobility unit "i-REAL". Reproduced from [44] with permission of the publisher

resistance, and abrasion resistance. The pencil hardness of the cured film was F, and the biomass content of the film was 29 wt% (44 wt% when succinic anhydride taken into account), showing that the film could be classed as a biomass plastic [44, 45].

2.5 Miniemulsion System

From the environmental viewpoint, the solvent used for coating or film-forming materials is important. The macromonomer technique was therefore applied to form a miniemulsion system of PLA-graft copolymers, as a typical example of the use of water as a green solvent. Four MMm macromonomers ($m = 4$, 6, 8, and 12; Scheme 1) were prepared and used as comonomer. In the copolymerization, BMA or BA was employed as the vinyl monomer (reaction 2, Scheme 1) [41]. Sodium dodecyl sulfate (SDS) and sodium dioctyl sulfosuccinate (PEREX), both anionic, were found to be appropriate surfactants. To form a stable emulsion system, ultrasound sonication was applied to the mixture of comonomers and surfactant in water before the copolymerization. Then, radical copolymerization was carried out (Table 3) [41, 42]. Relevant to the use of water as reaction solvent, Sect. 4 describes the use of green solvents in enzyme-catalyzed polymerizations.

With 1.0 or 3.0 wt% of the surfactant, all copolymerizations employing MM4, MM6, or MM8 as comonomer afforded a stable miniemulsion system before and after the reaction. However, the copolymerization system of MM12 gave a miniemulsion before the reaction, whereas after the reaction a small portion (3.9 wt%) of polymer aggregates formed and a stable miniemulsion system was not obtained. Thus, an average chain length longer than 12 was not appropriate for the copolymer emulsification, probably due to the hydrophobic nature of longer PLA chains or SDS not being an effective surfactant, even at 3.0 wt%.

Table 3 Miniemulsion radical copolymerization of alkyl (meth)acrylate (BMA or BA) with MMm to produce graft copolymers, and their properties

Copolymerization reaction[a]		Average particle diameter		Product graft copolymer[b]					
Feed ratio B(M)A/MMm[b] (mol/mol)	Surfactant[c] (wt%)	Before polymerization (nm)	After polymerization (nm)	Structure expression	M_n ($\times 10^{-4}$)	T_g (°C)	Young's modulus (kgf/cm^2)	Tensile strength (kgf/cm^2)	Elongation at break (%)
BMA/MM4 (75/25)	SDS (3.0)	261	175	PBMA-*g*-PLA4	–	35	1,020	25.5	453
BMA/MM6 (83/17)	SDS (1.0)	231	223	PBMA-*g*-PLA6	15.9	30	2,390	92	265
BMA/MM6 (83/17)	SDS (3.0)	265	176	PBMA-*g*-PLA6	13.5	37	1,582	36.7	415
BMA/MM6 (83/ 17)	PEREX (1.0)	220	333	PBMA-*g*-PLA6	16.4	32	1,104	53	95
BMA/MM6 (83/17)	PEREX (3.0)	267	168	PBMA-*g*-PLA6	12.9	–	–	–	–
BMA/MM8 (87/13)	SDS (3.0)	258	105	PBMA-*g*-PLA8	–	40	2,582	58.2	360
BMA/MM12 (92/8)	SDS (3.0)	244	78[d]	PBMA-*g*-PLA12	–	–	–	–	–
BA/MM6 (85/15)	PEREX (1.0)	113	99	PBA-*g*-PLA6	4.95	–	–	–	–

[a]Reaction at 85°C for 0.5 h in H_2O with addition of the surfactant and KPS radical initiator
[b]Biomass content was adjusted in the initial reaction feed to be 34 wt% in all runs
[c]Surfactants used were sodium dodecyl sulfate (SDS) or sodium dioctyl sulfosuccinate (PEREX). The wt% for the total monomers is given in parentheses
[d]Aggregated precipitates were formed in 3.9 wt%

It is to be noted that before and after the reaction, the particle size of the BA/MM6 system (113 and 99 nm, respectively) was much smaller than that of MBA/MM6 system (220 and 333 nm, respectively), both with PEREX 1.0 wt%. BA lacks methyl group and hence is able to form compact particles. The molecular weight of the copolymers was very high, with M_n values ranging from 4.95×10^4 to 1.64×10^5 (M_w values were from 1.01×10^5 to 1.98×10^5).

T_g values of three graft copolymers (PBMA-*g*-PLAm with SDS 3.0 wt%) are 35°C for $m = 4$, 37°C for $m = 6$, and 40°C for $m = 8$. The T_g value of PBMA is 20°C and, hence, these T_g values were much enhanced by the graft chain; for longer graft chains, T_g gradually increased. Physical properties are given in Table 3 for three graft copolymer samples of PBMA-*g*-PLAm (SDS 3.0 wt%, PLA component 34 wt%). The physical strength is higher with the longer graft chain ($m = 8$) than with the shorter graft chain ($m = 4$), whereas the elongation property is higher with the shorter chain than with the longer chain. That is, when the total amount of the PLA component is equal, the longer graft chains (yet with a smaller number of chains) govern the bulk nature of the copolymer rather than the shorter graft chains (even though there is a larger number of chains). This is a good example to demonstrate the property relationship between the graft chain length and the number of graft chains. All of graft copolymers are very elastic, soft materials as can be seen from the elongation data (Table 3) [41, 42].

3 Green Catalysts: Enzyme-Catalyzed Synthesis and Degradation of Polyesters

Enzymes are natural catalysts obtained from living systems. Generally, enzymatic reactions have the following characteristics: (1) high catalytic activity; (2) reaction under mild conditions with respect to temperature, pressure, solvent, pH of medium, etc., bringing about energetic efficiency; and (3) high reaction selectivity of regio-, enantio-, chemo-, and stereoregulation, giving rise to perfectly structure-controlled products. If these in vivo characteristics could be realized for in vitro enzymatic polymer synthesis ("enzymatic polymerization") [13, 20], we may expect the following advantages: (1) perfect control of polymer structures; (2) creation of polymers with a new structure; (3) a clean, selective process without formation of by-products; (4) a low loading process with energy savings; and (5) biodegradable properties of the product polymers in many cases. These are indicative of the "green" nature of enzymatic catalysis for developing new polymeric materials. In fact, many of these expectations have been realized [13, 14, 16–23]. Enzymatic polymerization has been reviewed recently in a special volume [46].

Lipase (triacylglycerol acylhydrolase, EC 3.1.1.3) is an enzyme that catalyzes the hydrolysis of a fatty acid glycerol ester in vivo by bond cleavage; however, it was disclosed that lipase catalyzes a polymerization reaction to give polyesters

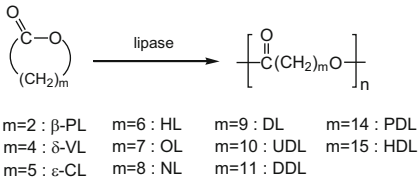

Scheme 5 General scheme for ring-opening polymerization of various lactone monomers: *β-PL* β-propiolactone, *δ-VL* δ-valerolactone, *ε-CL* ε-caprolactone, *HL* 7-heptanolide, *OL* 8-octanolide, *NL* 9-nonanolide, *DL* 10-decanolide, *UDL* 11-undecanolide, *DDL* 12-dodecanolide, *PDL* 15-pentadecanolide, *HDL* 16-hexadecanolide

in vitro with bond forming when the lipase catalyst and substrate monomer are appropriately combined for the reaction. This view seems logical because in vivo enzymatic reactions are virtually reversible. Lipase catalyzes hydrolysis of the ester bond through L-enantioselective cleavage. To conduct green polymer chemistry, we employed lipase as catalyst for synthesis of polymers and oligomers.

3.1 Lipase-Catalyzed Synthesis of Reactive Polyesters

Ring-opening polymerization (ROP) of cyclic esters (lactones) by lipase catalysis to produce polyesters was discovered in 1993 by our group [47, 48] and another [49]. The general method is given in Scheme 5 [19, 20].

Very recently, the ROP was extended to itaconic anhydride (IAn) as a new monomer for lipase-catalyzed ring-opening addition condensation polymerization (ROACP) involving dehydration to produce reactive polyesters [50]. Previously, ROACP reaction of another carboxylic acid anhydride such as succinic anhydride (SAn) or glutaric anhydride (GAn) and a diol using lipase as catalyst was reported to give polyesters in good yields under mild reaction conditions [51]. Attempts to obtain reactive polyesters using a similar reaction (ROACP of IAn and a diol) did not give the expected polyester. However, ROACP reaction of three components (IAn plus SAn or GAn plus a diol) at 25°C in toluene produced reactive polyesters in good to high yields (Scheme 6) [50]. As diols, 1,4-butane, 1,6-hexane, 1,8-octane, and 1,10-decane diols were used. From the SAn reactions, polyesters with M_n values of 650–3,510, and with 1.3–2.6 IAn units per molecule, were obtained. From the GAn reactions, these values were 560–3,690 and 1.2–3.1, respectively. Crosslinking of product polyester indicated a reactive nature, giving a crosslinked hard solid polyester. These polyesters derived from renewable starting materials involve possible applications as macromonomer, telechelics, or crosslinking reagent and the vinylidene group(s) can be used for further modification reactions.

Model reactions using IAn and *n*-octyl alcohol gave useful information on the regioselectivity and substrate selectivity. The regioselectivity at IAn was about the same (~50%) for both α- and β-positions of IAn by lipase catalysis, whereas it was

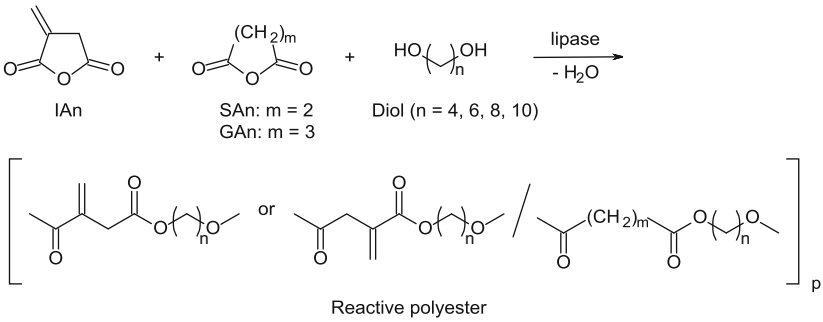

Scheme 6 Lipase-catalyzed ROACP between IAn, SAn or GAn, and a diol

about 90% for β-selectivity with Sn(II) catalyst and without catalyst [43]. The selectivity of lipase catalyst is thought to explain the reactive polyester formation under mild reaction conditions [50].

An interesting ROP of a new cyclic monomer of an *O*-carboxylic anhydride derived from lactic acid with lipase catalysis is to be noted. The polymerization proceeded within a few hours at 80°C with liberation of carbon dioxide and gave PLA in high yields and high M_n of up to 38,400, with low polydispersity $M_w/M_n < 1.4$ [52].

3.2 *Enzyme-Catalyzed Oligomerization of Alkyl Lactates: Enantioselection Mechanism*

New oligomerization reactions of alkyl lactates have been developed recently using enzymatic catalysis, where lipase [53] and protease [54] were employed as enzyme catalysts.

3.2.1 Lipase Catalysis

A recent paper reported that lipase-catalyzed ROP of lactide occurred with enantioselection of D-lactide [55]. Here, a new lipase-catalyzed enantioselective oligomerization of an alkyl lactate (RLa) is described (Scheme 7) [53]; Novozym 435-catalyzed polycondensation of alkyl D-lactates at 50°C gave oligo (D-lactic acid)s (oligoDLAs) at up to 82% yields with $n = 2$–7. Primary alkyl lactates of Et-, Pr-, and Bu-, showed a higher reactivity than longer alkyl lactates like Pe-, Hx-, Hp-, and Oc-. A secondary alkyl lactate of BuDLa showed a decreased reactivity. L-Lactates did not show any reactivity, i.e., enantioselection for D-isomers is very strict.

Scheme 7 Enantioselective oligomerization of D-alkyl lactates

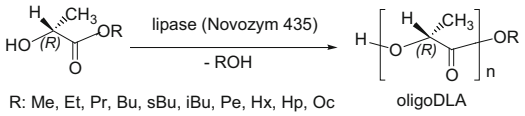

Scheme 8 Lipase-catalyzed hydrolysis of BuDLa and BuLLa

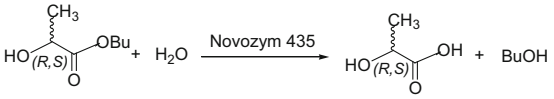

Michaelis–Menten equation (1) and, for simplicity, a pseudo-first order rate Eq. (2) were applied for the reaction analysis:

$$\mathrm{E} + \mathrm{S} \overset{k'}{\rightleftarrows} \mathrm{ES} \overset{k_{\mathrm{cat}}}{\rightarrow} \mathrm{P} + \mathrm{E} \tag{1}$$

$$-\frac{\mathrm{d[S]}}{\mathrm{d}t} = k'[\mathrm{E}]\,[S] = k[\mathrm{S}]\left(k'[\mathrm{E}] = k\right) \tag{2}$$

where E, S, and P denote enzyme, substrate, and product, respectively. Plots of the integrated form of equation (2) gave k values of $3.7 \times 10^4\ \mathrm{s}^{-1}$ for MeDLa; $4.4 \times 10^4\ \mathrm{s}^{-1}$ EtDLa; $3.7 \times 10^4\ \mathrm{s}^{-1}$ PrDLa; and $3.4 \times 10^4\ \mathrm{s}^{-1}$ BuDLa.

In order to elucidate the inhibition function of EtLLa toward the oligomerization of EtDLa, EtLLa was added to the EtDLa reaction. The reaction rate, namely the EtDLa consumption rate (ν_0 mol $\mathrm{L}^{-1}\ \mathrm{s}^{-1}$), was evaluated and the values plotted according to Lineweaver–Burk plots. The plots demonstrated that inhibition of the oligomerization of EtDLa by EtLLa is of a "competitive" nature. From the plots, the Michaelis constant $K_{\mathrm{m}} = 2.35$ mol L^{-1} and the maximum rate $V_{\max} = 1.48 \times 10^{-3}$ mol $\mathrm{L}^{-1}\ \mathrm{s}^{-1}$ were obtained.

Hydrolysis of BuDLa and BuLLa was conducted in THF at 50°C (Scheme 8) [53]. In contrast to the oligomerization, Novozym 435 catalysis induced the hydrolysis of both BuDLa and BuLLa substrates, although BuDLa was consumed faster than BuLLa. Without the enzyme, no hydrolysis reaction took place under similar reaction conditions. The approximate values were $k = 2.1 \times 10^4$ L $\mathrm{mol}^{-1}\ \mathrm{s}^{-1}$ for BuDLa and $k = 0.92 \times 10^4$ L $\mathrm{mol}^{-1}\ \mathrm{s}^{-1}$ for BuLLa; the D-isomer was hydrolyzed about 2.3 times faster than the L-isomer.

These findings led to elucidation of the mechanistic aspects of lipase (Novozym 435) catalysis: enantioselection is operated by the deacylation step as shown in Fig. 3 [53], where only dimer formation is shown for simplicity. It is well accepted that at first the monomer (substrate) is activated by enzyme with formation of an (*R*)-acyl–enzyme intermediate (enzyme-activated monomer, EM) ["acylation of lipase;" step (a) in Fig. 3]. Onto the activated carbonyl carbon of EM, the OH group of the D-lactate nucleophilically attacks to form an ester bond, liberating lipase enzyme and giving rise to D,D-dimer ["deacylation of lipase;" step (b) in Fig. 3].

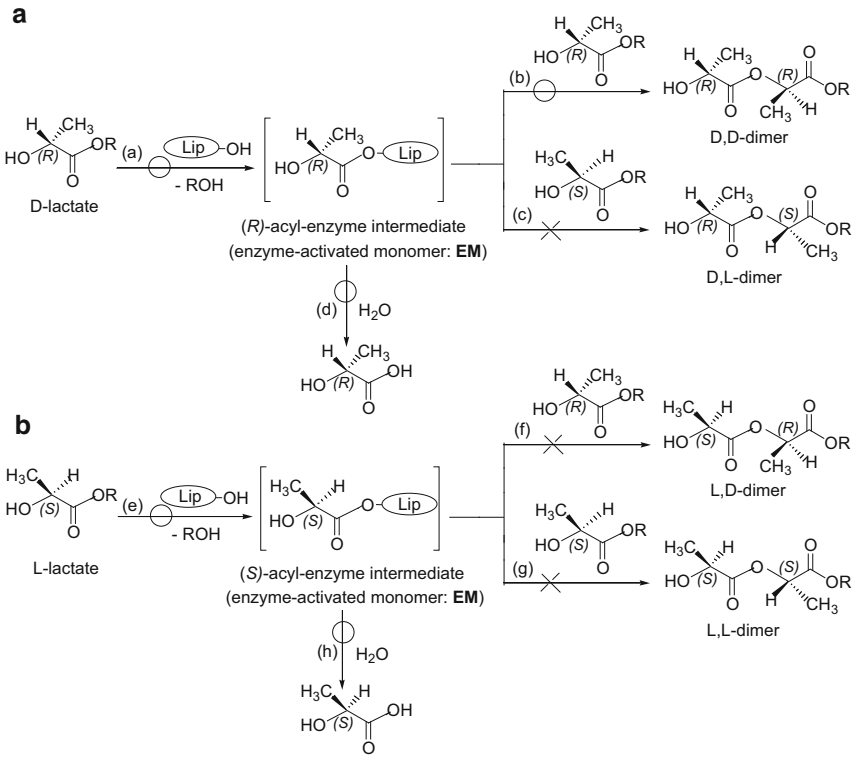

Fig. 3 Lipase-catalyzed reaction pathways of D-lactates (**a**) and L-lactates (**b**): acyl–enzyme intermediate formation steps *a* and *e*, subsequent dimer formation steps *b*, *c*, *f*, and *g*, and hydrolysis steps *d* and *h*. ○ denotes that the step takes place, whereas × denotes that the step does not take place. In steps *b*, *c*, *d*, *f*, *g*, and *h*, the lipase leaving group is omitted

If, in place of the D-lactate monomer, the OH group of the D,D-dimer attacks EM, a D,D,D-trimer will be formed, and the repetition of this type of reaction results in the formation of higher D-oligomers. Since the L-lactate was not consumed, the reaction of EM with the OH group of L-lactate does not occur and the reaction shown in step (c) does not take place. On the other hand, hydrolysis of D-lactate also needs activation to form EM. Then, EM reacts with water to give D-lactic acid, as shown in step (d).

Concerning the reactions of L-lactate monomers, alkyl L-lactates were not consumed at all in the oligomerization. In the hydrolysis, alkyl L-lactates were hydrolyzed to give L-lactic acid [step (h) in Fig. 3]. This is a clear indication that step (e) actually took place to produce *(S)*-acyl–enzyme intermediate EM. However, neither the OH group of D-lactate nor the OH group of L-lactate was allowed to attack EM to give L,D-dimer via step (f) or L,L-dimer via step (g).

Although hydrolysis steps (d) and (h) in Fig. 3 (both deacylations) are not selective due to no chirality in the water molecule, esterification steps (b), (c), (f),

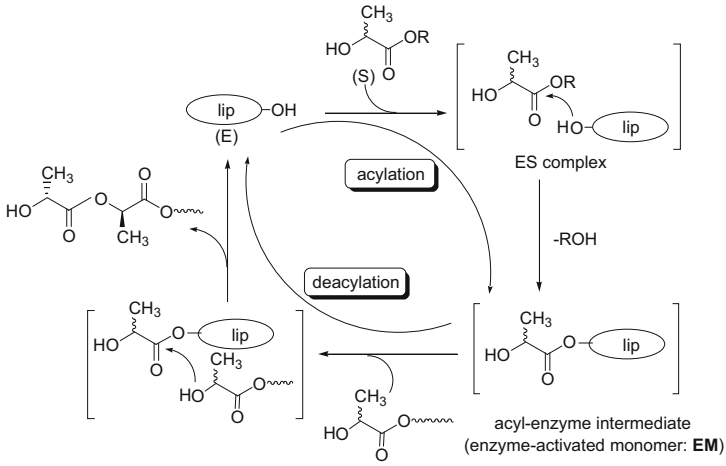

Fig. 4 General mechanism of lipase-catalyzed oligomerization of alkyl lactates

and (g) (all deacylations) are enantioselective. The above results demonstrate that "the enantioselection is governed by the deacylation step". Of the four steps, only step (b) was allowed to give D,D-dimer. The EM formation, via steps (a) and (e), was possible, however, from all alkyl (primary and secondary) D- and L-lactate monomers.

Figure 4 gives a generalized reaction mechanism of lipase (Novozym 435)-catalyzed oligomerization of alkyl lactates (RLa)s [53]. The acylation of RLa takes place regardless of whether it is the D- or L-isomer, as observed by their hydrolysis catalyzed by Novozym 435. In the oligomerization, however, the reaction of (*R*)-acyl–enzyme intermediate (EM) is only possible with the OH group of D-lactate or D-oligoLAs and not with that of L-lactate or L-oligoLAs. The (*S*)-acyl–enzyme intermediate, on the other hand, does not react with the OH group of D- and L-lactates or of D- and L-oligoLAs. Therefore, the deacylation step governs the enantioselection of the oligomerization.

The D-selective reaction of alkyl lactates by lipase catalysis has been applied for the optical resolution of D,L-isomers [56]. Typically, a mixture containing 90.4% BuLLa and 9.6% BuDLa was incubated with an immobilized lipase for 72 h, during which time D-selective oligomerization of BuDLa occurred. After distillation of the reaction mixture, the purity of BuLLa was increased to 98.6%, indicating that lipase catalysis provides a good enantiopurification method.

3.2.2 Protease Catalysis

In nature, proteases are known to hydrolyze proteins to give L-amino acid residues [57]. Proteases were therefore employed as a new catalyst and expected to cause

L-enantioselective oligomerization of alkyl D- and L-lactates (RDLa and RLLa), in contrast to the lipase (Novozym 435)-catalyzed perfect D-enantioselective reaction of Scheme 7. The four proteases examined preferentially gave oligo(L-lactic acid)s (oligoLLAs; dimer ~ pentamer), with moderate to high yields. The enantioselection was L-/D-selective (56/28 to 25/4 in conversion % ratio), showing an opposite direction in enantioselection to that of the lipase [54].

Hydrolysis reaction of ethyl D- and L-lactates (EtLa)s catalyzed by protease were studied; EtLLa was consumed a little faster than EtDLa. The mechanism of the protease-catalyzed oligomerization was similar to that of lipase (as seen in Figs. 3 and 4), but in an L-selective manner; the enantioselection is governed by the deacylation step.

The opposite enantioselection of enzymatic catalysis by protease and lipase has been discussed in the case of PLA depolymerizing hydrolysis [58]. These two classes of enzymes are both serine hydrolases, possessing a catalytic triad of serine, histidine, and aspartic acid; the catalytic active site of the two classes, however, are topological mirror images [59–61]. This difference in the catalytic sites was considered responsible for the opposite selection, where protease was PLLA-preferential and was PDLA-specific [53, 54, 58]. The results of enantioselective oligomerization of alkyl lactates catalyzed by protease and lipase, therefore, may be similarly understood. The enantioselection of Novozym 435 was perfect, and lipases of other origin were not so strong. Proteases were less selective. This selectivity difference is probably because in living systems the substrate of lipase is an ester having an ester linkage like that of RLa, whereas the substrate of protease is a protein having an amide linkage.

3.3 Lipase-Catalyzed Degradation and Polymerization of Polyesters: New Method of Polymer Recycling

Using the characteristics of lipase catalysis, a new method of polymer chemical recycling was proposed [8]. The polyester samples used were poly(ε-caprolactone) (PCL), poly(12-docecanolide) (PDDL), and poly(1,4-butane adipate) (PBA). First, lipase CA-catalyzed degradation of PCL with molecular weight 6.0×10^4 at 60°C was performed in toluene. After 24 h, PCL almost disappeared via hydrolysis to give oligoCL with molecular weight of less than 500. A small amount of water in the reaction mixture is probably involved in the hydrolysis. The solvent was then removed under reduced pressure to give a waxy oligomer mixture containing lipase CA. The mixture was then kept at 60°C for 8 h, yielding a polymer with molecular weight 8×10^3.

The cycle of degradation–polymerization could be performed repeatedly and controlled by the presence or absence of the solvent, using the same catalyst in one pot. This method provided a concept for an environmentally benign process of

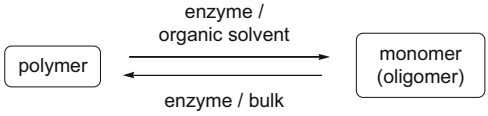

Fig. 5 Concept of polymer recycling using enzyme catalyst

polymer recycling, giving an example of green polymer chemistry. The concept is shown in Fig. 5 [8].

Similarly, chemical recycling of PCL was studied via two routes: the enzymatic conversion of PCL into CL oligomers, and the selective ring-closing depolymerization of PCL into di-CL [62]. Di-CL was readily polymerized by lipase CA catalyst to produce PCL. PBA is a biodegradable synthetic plastic obtained from 1,4-butane diol and adipic acid. PBA with M_w of 2.2×10^4 was degraded into BA oligomers with M_w of 600 by lipase CA catalyst. This cyclic BA was repolymerized into PBA having M_w of 5.2×10^4, an even higher molecular weight than before [63]. PLA could be chemically recycled by lipase via repolymerizable cyclic oligomers having a low molecular weight of a few hundred. PLLA with M_w 1.2×10^5 was transformed into cyclic oligomers by lipase CA catalyst at 100°C [64]. This principle was extended to the continuous degradation system using an immobilized lipase-packed column [65]. A similar recycling system was achieved by lipase catalysis for polyurethanes, poly(ester-urethane)s, and poly(carbonate-urethane)s [66]. Again, the principle of the above recycling systems is that ROP of lactones by lipase catalysis is reversible between polymers and oligomers and can be controlled by changing the reaction conditions.

The effects of the number of molecular branches and the stereochemistry of the PLAs on enzymatic degradation and alkaline hydrolysis have been reported [67]. PLA-containing polymers were prepared by using lipase-catalyzed ROP of lactide (L-lactide, D-lactide, and D,L-lactide). An increased number of PLA branches enhanced the enzymatic degradability and alkaline hydrolyzability when samples of similar M_n were used. The proteinase-catalyzed hydrolysis was preferential for PDLPLA branches; however, alkaline hydrolysis did not show the stereochemical preference.

4 Green Solvents: Water, Supercritical Carbon Dioxide, and Ionic Liquids

In the context of green chemistry, water, supercritical carbon dioxide, and ionic liquids are regarded as typical examples of green solvents. The importance of reaction solvent was described in Sect. 2.5 for radical polymerization, so both enzyme-catalyzed polymerization and degradation have been performed using these solvents.

4.1 Ring-Opening Polymerization in Water and in Miniemulsion

ROP of lactones to various polyesters has been widely studied [19, 68]. Lipase-catalyzed ROP is normally carried out in bulk or in an organic solvent like toluene, 1,4-dioxane, or dibutyl ether [17, 19, 20].

Water was used as solvent for the first time in the lipase-catalyzed ROP of five lactone monomers, ε-CL, OL, UDL, DDL, and PDL (Scheme 5) [69, 70]. Macrolides of UDL, DDL, and PDL are less reactive than lactones of smaller ring size due to lower ring strain when using a usual chemical catalyst [71]. However, they showed higher reactivity in enzyme catalysis and were polymerized by lipase in water to produce the corresponding polyesters; typically, UDL gave polyUDL with M_n 1,300 ($M_w/M_n = 2.1$) in 79% yields at 60°C for 72 h. DDL is hardly soluble in water; however, addition of the lipase gave a white emulsion-like solution, which allowed the ROP. In contrast, a mixture of the lipase and ε-CL or OL did not form an emulsion-like solution, and thus failed to induce the ROP. Therefore, it seems that the enzyme protein behaved like a surfactant [69–71].

A second example of the use of water as medium is the lipase-catalyzed ROP of a lactone in miniemulsions [72]. Typically, a mixture of PDL monomer, water, nonionic surfactant having a PEG chain of molecular weight 2,000, and hexadecane was vigorously stirred for 1 h at 45°C to give a miniemulsion system. To the mixture, a suspension of lipase PS in surfactant solution was added, and the resulting miniemulsion consisting of PDL nanodroplets was subjected to ROP with stirring at 45 or 60°C for up to 24 h to reach a full conversion of PDL. PolyPDL nanoparticles were obtained, which is considered to be a direct synthesis of biodegradable polymer nanoparticles (size < 100 nm). PolyPDL showed a bimodal molecular weight distribution; the majority was of high molecular weight ($>2.0 \times 10^5$). It was possible to introduce a reactive group in the presence of an unsaturated alcohol or acid such as linoleic acid in the reaction system via esterification reactions.

4.2 Lipase-Catalyzed Polyester Synthesis and Degradation in Other Green Solvents

Supercritical carbon dioxide ($scCO_2$) was employed for the first time to prepare polyesters via ROP of lactones. Lipase-catalyzed ROP of ε-CL proceeded to give a polymer (PCL) with molecular weight higher than 10^4. Copolymerization of ε-CL with DDL afforded a random copolyester. The enzymatic polycondensation between divinyl adipate and 1,4-butane diol also took place to produce the corresponding polyester [73]. Later, a similar study on ROP of ε-CL in $scCO_2$ followed [74].

Hydrolytic degradation of PCL by lipase CA catalyst was studied in $scCO_2$ [75]. The addition of acetone (5 vol%) accelerated the degradation of high molecular weight PCL to produce smaller molecular weight (<500) linear and cyclic oligomers, which could be repolymerized by the same catalyst. It is useful that $scCO_2$ is easy to remove after the reaction to recover the catalyst, and the reaction can be recycled.

Ionic liquids are often used as reaction solvent for the synthesis and modification of polymers due to their green character [76]. The first paper on ionic liquids as solvent for enzymatic polymerization appeared in 2002. Lipase-catalyzed ROP of ε-CL and the polycondensation between diethyl adipate or sebacate and 1,4-butane diol were achieved in an ionic liquid such as 1-butyl-3-methyl-imidazolium salts ([bmim][PF_6]). The ROP gave rise to PCL with M_n of 4,200 ($M_w/M_n = 2.7$) in 97% yields at 60°C after 7 days [77]. Lipase CA-catalyzed ROP of ε-CL in three ionic liquids, [bmim][BF_4], [bmim][PF_6], and [bmim][$(CF_3SO_2)_2N$], at 60°C for 24 h produced PCL with a higher M_n of 7,000–9,500 ($M_w/M_n \sim 2.4$) in good yields. In the polycondensation of the above combinations, M_n was up to 5,400 [78]. Since ionic liquids have high boiling points, with tunable nature for hydrophobicity and solubility, the polymerization of polar monomers (which are less soluble in an organic solvent) is suggested as an appropriate way.

A more recent paper reported that by using four kinds of ionic liquid, the ROP of lactide by lipase CA catalyst at room temperature for 24 h produced PLA having molecular weight values reaching 55,000 in 35% yields [79].

5 Conclusions

For conducting "green polymer chemistry", the following aspects are stressed and it is very important that attention is paid to them. Typically, (1) starting materials are biobased renewable resources to mitigate use of fossil-based law materials; (2) synthesis or modification reactions are catalytic, not molar reactions; (3) catalysts are nontoxic and re-usable; (4) reaction solvents are environmentally benign to decrease use of organic solvents; and (5) product polymer structures are subjected to material recycling. The present article is concerned mainly with our recent research results performed in this direction. In particular, results employing lactic acid and itaconic anhydride suggest future materials, as shown in Sect. 2. Also, the characteristics of enzyme catalysis shown in Sect. 3 are to be noted.

It is important to keep paying attention to climate change and global warming, consumption of natural resources, and the method of energy generation and consumption; all of these issues are directly connected with the future environment. As polymer scientists, we are very much required to conduct green polymer chemistry to preserve the environment as well as we can.

References

1. Anastas PT, Warner JC (1998) Green chemistry: theory and practice. Oxford University Press, Oxford
2. Vorvath IT, Anastas PT (2007) Innovations and green chemistry. Chem Rev 107:2169–2173
3. Narayan R (2006) Biobased and biodegradable polymer materials: rationale, drivers, and technology exemplars. In: Khemani KC, Scholz C (eds) Degradable polymers and materials. ACS Symposium Series vol 939. Chap 18, pp 282–306. American Chemical Society, Washington, D.C.
4. Coates GW, Hillmyer MA (2009) A virtual issue of macromolecules: polymers from renewable resources. Macromolecules 42:7987–7989
5. Bomgardner MM (2012) A summer of start-ups for biobased chemicals. Chem Eng News 90(38):10–15
6. Kobayashi S (1999) Enzymatic polymerization – polymer synthesis catalyzed by a natural macromolecule. High Polym Jpn 48:124–127
7. Kobayashi S (1999) Enzymatic polymerization: a new method of polymer synthesis. J Polym Sci A Polym Chem 37:3041–3056
8. Kobayashi S, Uyama H, Takamoto T (2000) Lipase-catalyzed degradation of polyesters in organic solvents. A new methodology of polymer recycling using enzyme as catalyst. Biomacromolecules 1:3–5
9. Sakamoto J, Sugiyama J, Kimura S, Imai T, Itoh T, Watanabe T, Kobayashi S (2000) Artificial chitin spherulites composed of single crystalline ribbons of α-chitin via enzymatic polymerization. Mcromolecules 33:4155–4160
10. Ikeda R, Tanaka H, Uyama H, Kobayashi S (2000) A new crosslinkable polyphenol from renewable resource. Macromol Rapid Commun 21:496–499
11. Higashimura H, Fujisawa K, Moro-oka Y, Namekawa S, Kubota M, Shiga A, Uyama H, Kobayashi S (2000) New crystalline polymers: poly(2,5-dialkyl-1,4-phenylene oxide)s. Macromol Rapid Commun 21:1121–1124
12. Ikeda R, Tanaka H, Oyabu H, Uyama H, Kobayashi S (2001) Preparation of artificial urushi via an environmentally benign process. Bull Chem Soc Jpn 74:1067–1073
13. Kobayashi S, Uyama H, Kimura S (2001) Enzymatic polymerization. Chem Rev 101:3793–3818
14. Kobayashi S, Uyama H, Ohmae M (2001) Enzymatic polymerization for precision polymer synthesis. Bull Chem Soc Jpn 74:613–635
15. Uyama H, Kuwabara M, Tsujimoto T, Nakano M, Usuki A, Kobayashi S (2003) Green nanocomposite from renewable resources: plant oil–clay hybrid materials. Chem Mater 15:2492–2494
16. Kobayashi S, Uyama H (2003) Enzymatic polymerization. In: Kroschwitz JI (ed) Encyclopedia of polymer science and technology, 3rd edn. Wiley, New York, pp 328–364
17. Kobayashi S, Ritter H, Kaplan D (eds) (2006) Enzyme-catalyzed synthesis of polymers. Adv Polym Sci 194
18. Kobayashi S, Ohmae M (2007) Polymer synthesis and modification by enzymatic catalysis. In: Matyjaszewski K, Gnanou Y, Leibler L (eds) Macromolecular engineering: precise synthesis, materials properties, applications, vol 10, Wiley-VCH, Weinheim., pp 400–477
19. Kobayashi S (2009) Recent developments in lipase-catalyzed synthesis of polyesters. Macromol Rapid Commun 30:237–266
20. Kobayashi S, Makino A (2009) Enzymatic polymer synthesis: an opportunity for green polymer chemistry. Chem Rev 109:5288–5353
21. Kobayashi S (2010) Lipase-catalyzed polyester synthesis – a green polymer chemistry. Proc Jpn Acad Ser B 86:338–365
22. Kobayashi S (2011) Green polymer synthesis using enzyme catalysts. In: Misono M, Murahashi S (eds) Green chemistry – chemistry for sustainable society. Kodansha Scientific, Tokyo, pp 192–203

23. Kobayashi S (2012) Enzymatic polymerization. In: Matyjaszewski K, Moeller M (eds) Polymer science: a comprehensive reference, vol 5. Elsevier, Amsterdam, pp 217-237
24. Puskas JE, Sen MY, Seo KS (2009) Green polymer chemistry using nature's catalyst, enzyme. J Polym Sci A Polym Chem 47:2959–2976
25. Cheng HN, Gross RA (eds) (2010) Green polymer chemistry: biocatalysis and biomaterials. ACS Symposium Series, vol 1043. American Chemical Society, Washington, D.C.
26. Werpy T, Petersen G (2004) Top value added chemicals from biomass. The National Renewable Energy Laboratory and DOE National Laboratory, Oak Ridge
27. Tsuji H, Ikada Y (2000) Properties and morphology of poly(L-lactide) 4. Effects of structural parameters on long-term hydrolysis of poly(L-lactide) in phosphate-buffered solution. Polym Deg Stab 67:179–189
28. Moon SI, Lee CW, Miyamoto M, Kimura Y (2000) Melt polycondensation of L-lactic acid with Sn(II) catalysts activated by various proton acids: a direct manufacturing route to high molecular weight poly(L-lactic acid). J Polym Sci A Polym Chem 38:1673–1679
29. Moon S-I, Lee CW, Taniguchi I, Miyamoto M, Kimura Y (2001) Melt/solid polycondensation of L-lactic acid: an alternative route to poly(L-lactic acid) with high molecular weight. Polymer 42:5059–5062
30. Dechy-Cabaret O, Martin-Vaca B, Bourissou D (2004) Controlled ring-opening polymerization of lactide and glycolide. Chem Rev 104:6147–6176
31. Gupta B, Revagade N, Hilborn J (2007) Poly(lactic acid) fiber: an overview. Prog Polym Sci 32:455–482
32. Fukushima K, Chang YH, Kimura Y (2007) Enhanced stereocomplex formation of poly (L-lactic acid) and poly(D-lactic acid) in the presence of stereoblock poly(L-lactic acid). Macromol Biosci 7:829–835
33. Jiang X, Smith MR III, Baker GL (2008) Water-soluble thermoresponsive polylactides. Macromolecules 41:318–324
34. Chuma A, Hom HW, Swope WC, Pratt RC, Zhang L, Lohmeijer BG, Wade CG, Waymouth RM, Hedrick JL, Rice JE (2008) The reaction mechanism for the organocatalytic ring-opening polymerization of L-lactide using a guanidine-based catalyst: hydrogen-bonded or covalently bonded? J Am Chem Soc 130:6749–6759
35. Jing F, Hillmyer MA (2008) A bifunctional monomer derived from lactide for toughening polylactide. J Am Chem Soc 130:13826–13827
36. Pitet LM, Amendt MA, Hillmyer MA (2010) Nanoporous linear polyethylene from a block polymer precursor. J Am Chem Soc 132:8230–8231
37. Nishida H, Andou Y, Watanabe K, Arazoe Y, Ide S, Shirai Y (2011) Poly(tetramethyl glycolide) from renewable carbon, a racemization-free and controlled depolymerizable polyester. Macromolecules 44:12–13
38. Inkinen S, Hakkarainen M, Albertsson A-C, Södergård A (2011) From lactic acid to poly (lactic acid) (PLA): characterization and analysis of PLA and its precursor. Biomacromolecules 12:523–532
39. Stoclet G, Seguela R, Lefebvre JM, Li S, Vert M (2011) Thermal and strain-induced chain ordering in lactic acid stereocopolymers: influence on the composition in stereomers. Macromolecules 44:4961–4969
40. Shin EJ, Jones AE, Waymouth RM (2012) Stereocomplexation in cyclic and linear polylactide blends. Macromolecules 45:595–598
41. Ishimoto K, Arimoto M, Okuda T, Yamaguchi S, Aso Y, Ohara H, Kobayashi S, Ishii M, Morita K, Yamashita H, Yabuuchi N (2012) Biobased polymers: synthesis of graft copolymers and comb polymers using lactic acid macromonomer and properties of the product polymers. Biomacromolecules 13:3757–3768
42. Ishimoto K, Arimoto M, Ohara H, Kobayashi S, Ishii M, Morita K, Yamashita H, Yabuuchi N (2009) Biobased polymer system: miniemulsion of poly(alkyl methacrylate-*graft*-lactic acid)s. Biomacromolecules 10:2719–2723

43. Okuda T, Ishimoto K, Ohara H, Kobayashi S (2012) Renewable biobased polymeric materials: facile synthesis of itaconic anhydride-based copolymers with poly(L-lactic acid) grafts. Macromolecules 45:4166–4174
44. Morita K, Yamashita H, Yabuuchi N, Hayata Y, Ishii M, Ishimoto K, Ohara H, Kobayashi S (2011) Application of star-shaped poly(lactic acid)s to two component and UV-curable coatings. J Network Polym Jpn 32:192–196
45. Morita K, Yamashita H, Yabuuchi N, Hayata Y, Ishii M, Ishimoto K, Ohara H, Kobayashi S (2011) Synthesis of star-shaped oligomeric lactic acids with reactive double bonds and their application to UV curable coatings. In: Proceedings of RadTech Asia 2011. RadTech Japan, Tokyo, pp 126–129
46. Palmans ARA, Heise A (eds) (2011) Enzymatic polymerisation. Adv Polym Sci 237
47. Uyama H, Kobayashi S (1993) Enzymatic ring-opening polymerization of lactones catalyzed by lipase. Chem Lett 1149–1150
48. Uyama H, Takeya K, Kobayashi S (1993) Synthesis of polyesters by enzymatic ring-opening copolymerization using lipase catalyst. Proc Jpn Acad B 69:203–207
49. Knani D, Gutman AL, Kohn DH (1993) Enzymatic polyesterification in organic media – enzyme-catalyzed synthesis of linear polyesters. 1. Condensation polymerization of linear hydroxyesters. 2. Ring-opening polymerization of ε-caprolactone. J Polym Sci A Polym Chem 31:1221–1232
50. Yamaguchi S, Tanha M, Hult A, Okuda T, Ohara H, Kobayashi S (2013) Green polymer chemistry: lipase-catalyzed synthesis of bio-based reactive polyesters employing itaconic anhydride as renewable monomer. Polym J doi:10.1038/pj.2013.62
51. Kobayashi S, Uyama H (1993) Enzymatic polymerization of cyclic acid anhydrides and glycols by a lipase catalyst. Macromol Chem Rapid Commun 14:841–844
52. Bonduelle C, Martin-Vaca B, Bourissou D (2009) Lipase-catalyzed ring-opening polymerization of the *O*-carboxylic anhydride derived from lactic acid. Biomacromolecules 10:3069–3073
53. Ohara H, Onogi A, Yamamoto M, Kobayashi S (2010) Lipase-catalyzed oligomerization and hydrolysis of alkyl lactates: direct evidence in the catalysis mechanism that enantioselection is governed by a deacylation step. Biomacromolecules 11:2008–2015
54. Ohara H, Nishioka E, Yamaguchi S, Kawai F, Kobayashi S (2011) Protease-catalyzed oligomerization and hydrolysis of alkyl lactates involving L-enantioselective deacylation step. Biomacromolecules 12:3833–3837
55. Hans M, Keul H, Moeller M (2009) Ring-opening polymerization of DD-lactide catalyzed by Novozyme 435. Macromol Biosci 9:239–247
56. Ohara H, Yamamoto M, Onogi A, Hirao K, Kobayashi S (2011) Optical resolution of *n*-butyl D- and L-lactates using immobilized lipase catalyst. J Biosci Bioeng 111:19–21
57. Hedstrom L (2002) Serine protease mechanism and specificity. Chem Rev 102:4501–4524
58. Kawai F, Nakadai K, Nishioka E, Nakajima H, Ohara H, Masaki K, Iefuji H (2011) Different enantioselectivity of two types of poly(lactic acid) depolymerases toward poly(L-lactic acid) and poly(D-lactic acid). Polym Deg Stab 96:1342–1348
59. Wilmouth RC, Clifton IJ, Robinson CV, Roach PL, Alpin RT, Westwood NJ, Hajdu J, Schofield CJ (1997) Structure of a specific acyl-enzyme complex formed between β-casomorphin-7 and porcine pancreatic elastase. Nat Struc Biol 4:456–462
60. Ollis DL, Cheah E, Cygler M, Dijkstra B, Frolow F, Franken SM, Harel M, Remington SJ, Silman I, Schrag J, Sussman JL, Vershueren KHG, Goldman A (1992) The α/β hydrolase fold. Protein Eng 5:197–211
61. Borén L, Martín-Matute B, Xu Y, Córdova A, Bäeckvall J-E (2006) *(S)*-selective kinetic resolution and chemoenzymatic dynamic resolution of secondary alcohols. Chem Eur J 12:225–232
62. Ebata H, Toshima K, Matsumura S (2000) Lipase-catalyzed transformation of poly(ε-caprolactone) into cyclic dicaprolactone. Biomacromolecules 1:511–551

63. Okajima S, Kondo R, Toshima K, Matsumura S (2003) Lipase-catalyzed transformation of poly(butylene adipate) and poly(butylene succinate) into polymerizable cyclic oligomers. Biomacromolecules 4:1514–1519
64. Takahashi Y, Okajima S, Toshima K, Matsumura S (2004) Lipase-catalyzed transformation of poly(lactic acid) into cyclic oligomers. Macromol Biosci 4:346–353
65. Osanai Y, Toshima K, Matsumura S (2003) Enzymatic degradation of poly(R, S-3-hydroxybutanonoate) to cyclic oligomers under continuous flow. Green Chem 5:567–570
66. Matsumura S (2007) Enzymatic synthesis of polyesters via ring-opening polymerization. Adv Polym Sci 194:95–132
67. Numata K, Srivastava RK, Finne-Wistrand A, Albertsson A-C, Doi Y, Abe H (2007) Branched poly(lactide) synthesized by enzymatic polymerization: effect of molecular branches and stereochemistry on enzymatic degradation and alkaline hydrolysis. Biomacromolecules 8:3115–3125
68. Lecomte P, Jerome C (2012) Recent developments in ring-opening polymerization of lactones. Adv Polym Sci 245:173–218
69. Namekawa S, Uyama H, Kobayashi S (1998) Lipase-catalyzed ring-opening polymerization of lactones in water. Polym J 30:269–271
70. Kobayashi S, Uyama H, Namekawa S (1998) In vitro biosynthesis of polyesters with isolated enzymes in aqueous systems and organic solvents. Polym Deg Stab 59:195–201
71. Uyama H, Takeya K, Kobayashi S (1995) Enzymatic ring-opening polymerization of lactones to polyesters by lipase catalyst: unusually high reactivity of macrolides. Bull Chem Soc Jpn 68:56–61
72. Taden A, Antonietti M, Landfester K (2003) Enzymatic polymerization toward biodegradable polyester nanoparticles. Macromol Rapid Commun 24:512–516
73. Takamoto T, Uyama H, Kobayashi S (2001) Lipase-catalyzed synthesis of aliphatic polyesters in supercritical carbon dioxide. e-Polymers 4:1–6
74. Loeker FC, Duxbury CJ, Kumar R, Gao W, Gross RA, Howdle SM (2004) Enzyme-catalyzed ring-opening polymerization of ε-caprolactone in supercritical carbon dioxide. Macromolecules 37:2450–2453
75. Takamoto T, Uyama H, Kobayashi S (2001) Lipase-catalyzed degradation of polyester in supercritical carbon dioxide. Macromol Biosci 1:215–218
76. Kubisa P (2005) Ionic liquids in the synthesis and modification of polymers. J Polym Sci A Polym Chem 43:4675–4683
77. Uyama H, Takamoto T, Kobayashi S (2002) Enzymatic synthesis of polyesters in ionic liquids. Polym J 34:94–96
78. Marcilla R, de Jeus M, Mecerreyes D, Duxbury CJ, Koning CE, Heise A (2006) Enzymatic polyester synthesis in ionic liquids. Eur Polym J 42:1215–1221
79. Yoshizawa-Fujita M, Saito C, Takeoka Y, Rikukawa M (2008) Lipase-catalyzed polymerization of L-lactide in ionic liquids. Polym Adv Technol 19:1396–1400

Adv Polym Sci (2013) 262: 167–190
DOI: 10.1007/12_2013_235

Published online: 5 October 2013

From Biocompatible to Biodegradable: Poly(Ethylene Glycol)s with Predetermined Breaking Points

Carsten Dingels and Holger Frey

Abstract Poly(ethylene glycol) (PEG) is the gold standard polymer for biomedical applications. PEG is known for its biocompatibility and antifouling properties and is widely used for bioconjugation. However, like other synthetic polymers in the field, PEG is not biodegradable, limiting its use for parenteral formulations and protein conjugation to a molecular weight range with a specific upper limit (commonly 40–60 kDa) to avoid polyether accumulation in human tissue. For these biomedical applications, but also for other purposes such as cleavable hydrogels and templates for porous membranes, several routes for the insertion of in-chain biocleavable moieties, such as acetals or disulfides, into PEG have been developed. Recently, the synthetic strategies have been extended from step-growth polymerizations of commercially available, telechelic PEGs to more sophisticated routes based on ethylene oxide (co)polymerizations, permitting the incorporation of predetermined breaking points at any position in the PEG chains.

Keywords Acetals · Biodegradation · Drug delivery · PEGylation · Poly(ethylene glycol) · Polyether

Contents

C. Dingels and H. Frey (✉)
Institut für Organische Chemie, Johannes Gutenberg-Universität Mainz, Duesbergweg 10-14, 55099 Mainz, Germany
e-mail: hfrey@uni-mainz.de

Abbreviations

APEG	Amino-pendent polyacetal
AROP	Anionic ring-opening polymerization
DOX	Doxorubicin
EO	Ethylene oxide
EPR	Enhanced permeability and retention
FDA	Food and Drug Administration
GSH	Glutathione
mPEG	Poly(ethylene glycol) monomethyl ether
OLZ	Olsalazin
PDI	Polydispersity index M_w/M_n
PEG	Poly(ethylene glycol)
PEI	Poly(ethylene imine)
PG	Polyglycerol
PU	Polyurethane
TEG	Triethylene glycol

1 Introduction

> [...] In biological processes as well, a slight percentage change in a macromolecule can bring about profound changes in the chemical and physiological behavior of the macromolecular substance.

With these words, Hermann Staudinger referred in his Noble lecture to the degradability of poly-oxymethylene (POM) in contrast to its α,ω-dimethyl ether derivative [1], linking the structure–property relation of an entirely synthetic polyacetal to biological processes. Sixty years later, we realize that his statement is not only true for the natural macromolecules he had in mind, such as DNA or proteins, but also for synthetic polymers designed for in vivo applications.

Besides POM, another polyether was intensively studied by Staudinger – poly (ethylene glycol) (PEG) – as an early example of an "artificial high polymer". Staudinger and coworkers contributed key works both on the investigation of the synthesis of PEG from ethylene oxide as well as on its physicochemical properties (Table 1) [2–5]. Nowadays, this versatile polyether has become the gold standard polymer in drug delivery systems. It exhibits a unique combination of desirable properties rarely found for any other synthetic or natural polymer. PEG is nontoxic,

Table 1 Example table from an early work of Staudinger dealing with PEG

Vergleichende Übersicht der Molekulargewichte, Schmelzpunkte, Viscositäten und Löslichkeiten der verschiedenen Polyäthylenoxyd-Fraktionen.

Mol.-Gew.	Polymerisat.-Grad ca.	Schmp.	Relative Viscosität in Wasser	Relative Viscosität in Benzol	Löslichkeit in Äther
			in 1-molarer Lösung		
4650 4900	110	ca. 59°	1.6312	1.5376	unlöslich
3280 3200	75	„ 56°	1.4587	1.3919	unlöslich
1720 1550	35	„ 50°	1.3425	1.2770	unlöslich
1230 1350	30	„ 35°	1.2518	1.2075	löslich in warmem Äther
440 430	10	flüssig	—	—	löslich in kaltem Äther

The table title reads: "Comparative table of the molecular weights, melting temperatures, viscosities, and solubilities of different poly(ethylene oxide) fractions". The results demonstrate the dependence of the melting point on chain length, a feature that is often used in pharmaceutical applications today. From [2]. Copyright Wiley-VCH. Reproduced with permission

mostly non-immunogenic, and chemically inert [6]. Staudinger was not surprised by its excellent water solubility [2], although this property is not obvious to the common chemist and has been subject to several theoretical studies [7]. PEG is inexpensive and can be produced in a wide range of molecular weights in a well-defined manner with very low polydispersity indices (PDI, M_w/M_n) via oxyanionic polymerization. The polyether is soluble in a variety of organic solvents, which gives access to a vast variety of chemical transformations of its terminal hydroxyl groups. Hence, its functionalities can easily be adjusted to the purpose of its application [8–10]. This versatility in combination with its biocompatibility rendered PEG an important component in everyday products, such as cosmetics, edibles, and some functional textiles, but also in laxatives and drug delivery systems [11].

Several different PEG-based drug delivery systems are subject to current pharmaceutical research, the most prominent being protein PEGylation (the covalent attachment of PEG to a protein) [6, 12–16], stealth liposomes [17], and PEG-based polymeric carriers for low molecular weight drugs [13, 16, 18]. Although all of these methods use PEG, they are based on very different concepts.

Since the late 1970s, when Davis and coworkers covalently attached PEG to bovine proteins [19, 20], PEGylation became one of the most important methods for dealing with the inherent difficulties of protein therapeutics: Proteins undergo fast proteolytic degradation and are often immunogenic, which results in very short body-residence times and a fast decrease below the effective concentration. PEGylation leads to decreased renal elimination, lowered enzymatic degradation

rates, and reduced immunogenicity of the protein/synthetic polymer conjugate compared to the native protein. Together, these effects result in extremely prolonged blood circulation times and thus improved bioavailability of the conjugates. The success of this concept is underlined by the fact that several PEG/protein conjugate drugs have already been approved by the Food and Drug Administration (FDA) [21]. "Stealth liposomes" consist of phospholipid vesicles decorated with PEG chains, anchored to the vesicle's membrane via lipid anchor groups, and are designed as transporters for low molecular weight drugs. Similar to the PEGylation of proteins, the fastening of PEG chains prolongs blood circulation times of the liposomes [17, 22]. Polymeric carriers for low molecular weight drugs rely on Ringsdorf's drug delivery concept [23], which describes the use of a multifunctional, biocompatible synthetic polymer to transport pharmacons along with targeting moieties. These systems became even more important when Maeda and coworkers described the enhanced permeability and retention (EPR) effect for passive tumor targeting with large molecules [24, 25], a central concept in today's anticancer research. PEG has been studied in this context, but suffers from a lack of polyfunctionality, which results in low drug payloads [13, 16, 18, 26]. Therefore, several different strategies have been explored for the synthesis of PEGs with increased numbers of functional groups, such as multi-arm PEGs [27–29], dendrimer-like PEGs [30–35], dendronized PEGs [36, 37], and multifunctional PEGs [38].

The benefits and drawbacks of the use of PEG in drug delivery systems along with those of possible alternative polymeric structures have recently been reviewed [39]. One of the major concerns regarding the application of PEG in the human body is its non-biodegradability. As the blood circulation times rise with increasing molecular weight of PEG [40], the use of high molecular weight polyethers appears to be advantageous. However, the hydrodynamic volume of PEG must not exceed the kidney excretion limit (40–60 kDa) to prevent accumulation of the polymer in the liver [41]. Consequently, degradable high molecular weight PEG derivatives that carry frangible joints in the backbone, but retain all of PEG's valuable properties, are highly desirable. To avoid toxic effects, the degradation products of such systems must not fall below 400 g mol^{-1} [39].

This review focuses on the different synthetic approaches for the incorporation of labile moieties into the PEG chain as predetermined breaking points. The majority of the systems that have been reported to date are based on step-growth polymerization reactions of functional PEG precursors and suitable co-monomers. These strategies suffer from an inherent disadvantage: They yield poorly defined PEG analogues with broadly distributed molecular weights. Very recently, a number of more sophisticated synthetic routes have been investigated that yield degradable PEGs with narrow molecular weight distributions. Although highly interesting, PEGs with cleavable linkers [42] or with cleavable lipids [43–52], which were found to decrease the reduction in bioactivity of PEGylated proteins or increase the bioavailability of pharmacons transported in stealth liposomes, respectively, will not be discussed in this chapter.

Table 2 Cleavable units in degradable PEGs: structures, implementation and degradation conditions

Cleavable unit	Structure	Synthetic approach	Degradation[a]	References
Acetals	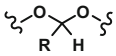	Coupling	pH < 7.4	[53–67]
Acetals	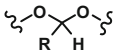	Cleavable inimer[b]	pH < 7.4	[68]
Acetals/ketals	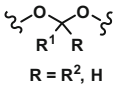	Cleavable initiator	pH < 7.4	[69, 70]
Aconitic acid diamides	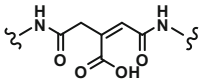	Coupling	pH < 7.4	[71]
Azo groups	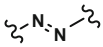	Coupling	Enzymatic	[72, 73]
Carbonates	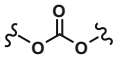	Coupling	Basic hydrolysis	[74–84]
Carboxylates	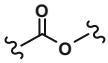	Coupling	Hydrolytic, enzymatic	[30, 72, 73, 85–104]
Disulfides	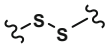	Coupling	Reductive	[89, 105–108]
Hemi-acetals	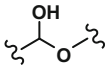	Oxidation	Acidic or basic	[109]
Ortho-esters	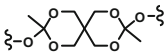	Coupling	pH < 7.4	[110]
Peptides	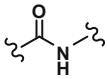	Coupling	Enzymatic	[31, 111–123]
Phospho-esters	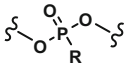	Coupling	Acidic or basic	[124–137]
Urethane	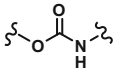	Coupling	(Hydrolytic)	[89, 138–146]
Vinyl ethers	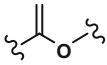	Postpolymerization elimination	pH < 7.4 at 37°C	[147]

[a]Conditions may vary for the same cleavable unit due to different adjacent moieties
[b]Concept results in hyperbranched architectures

2 Synthetic Approaches

The synthetic strategies for the incorporation of cleavable moieties into the backbone of PEG that have been employed to date (Table 2) mirror the inherent challenges related to this task. The most appreciated approach would be direct synthesis via the anionic ring-opening polymerization (AROP) of ethylene oxide (EO), with an oxirane co-monomer providing the additional functionality (analogous to the synthesis of multifunctional PEGs [38]) since copolymers can be

obtained via AROP in a well-defined manner with low polydispersity. In contrast to the multifunctional PEGs, an oxirane co-monomer for the degradable PEGs can hardly, if at all, be synthesized. The degradable moiety would have to resist the harsh basic conditions of the AROP, limiting the choices to acetals, ketals, disulfides, ortho esters, and vinyl ethers. Three-membered cycles including these groups are highly energetic and have not been synthesized or are stable only at very low temperatures, e.g., allene oxide [148] or *cyc*-S_2O [149, 150]. The direct synthesis of polyethers with in-chain acetals by cationic copolymerization of EO and 1,3,5-trioxane is of course known, but the degradation of the resulting polymeric formaldehyde acetals requires low pH conditions, the resulting formaldehyde is toxic, the PDIs are higher than those of anionically synthesized polymers, and the acetal content reported is rather high because the EO units serve as stabilizing fractions to stop the unzipping of terminal oligoacetal blocks [151–153].

2.1 Modification of Commercial PEGs

The majority of all cleavable groups incorporated into the backbone of PEG (summarized in Table 2 along with the corresponding synthetic approaches) can be introduced by coupling of homotelechelic PEGs via addition or condensation reactions. A detailed discussion of the applicable labile units, as well as the synthesis and properties of the obtained materials will be presented in Sect. 3. The main drawbacks common for all of these telechelic-based coupling strategies are the broad molecular weight distributions (M_w/M_n 1.6 to >10) and poor control of the degree of polymerization. These issues are avoided if just two PEG chains are linked to one (multi)functional degradable coupling unit [59, 90, 104, 112, 113, 119, 123], resulting in cleavable PEGs with a single (functional) cleavable joint; however low yields are obtained when none of the termini is blocked as a methyl ether [61]. The PEG coupling approaches are popular because the required dihydroxy PEG telechelics are inexpensive and soluble in many organic solvents, enabling a variety of coupling reactions. In cases where the telechelic PEGs are coupled via a multihetero-functional unit, degradable multifunctional PEGs can be synthesized, as presented by Ulbrich, Říhová and coworkers [89, 107, 113] and the groups of Lee [85, 86] and Brocchini [53, 55], (vide infra, Scheme 5) for example. Furthermore, PEG is, as mentioned before, nontoxic and non-immunogenic and thus easy to handle, whereas all of the strategies that involve the synthesis of the polyether require polymerization of the gaseous EO under anhydrous conditions. A one-step synthetic route to acid-degradable PEGs that relies neither on EO polymerization nor on a PEG coupling reaction was presented by Elisseeff and coworkers [109]. Some of the methylene groups of commercial PEG were oxidized to hemiacetals using Fenton's reagent, thereby introducing acid-labile breaking points. Unfortunately, degradation of the hemiacetals occurred during the synthesis at low degrees of oxidation, which is a drawback that will have to be overcome.

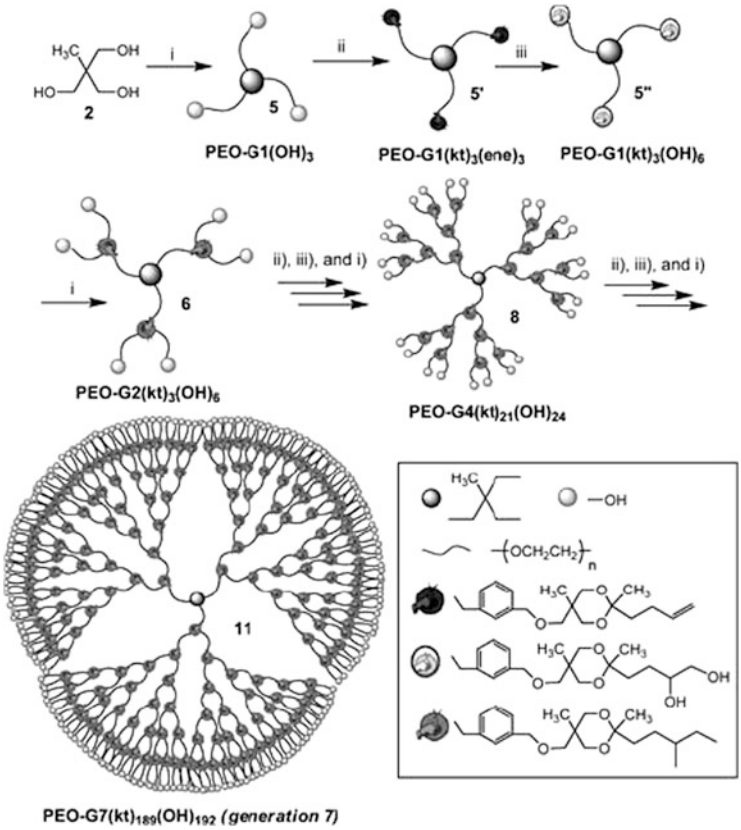

Scheme 1 Synthesis of acid-degradable dendrimer-like PEO. From [69]. Copyright Wiley-VCH. Reproduced with permission

2.2 EO Polymerization Methods

Synthetic approaches to degradable PEGs that do not rely on postpolymerization reactions of commercial PEGs have evolved very recently and rely on initiation from a macroinitiator with a cleavable moiety [69, 70], elimination of HCl from EO/epichlorohydrin copolymers [147] and copolymerization of EO with a cleavable AROP inimer [68]. In 2011, Gnanou, Taton and coworkers presented an elegant synthetic route to acid-degradable dendrimer-like PEOs (poly(ethylene oxide)s, i.e., high molecular weight PEGs) with ketal branching units (Scheme 1) [69]. All of the degradable dendritic PEOs from the second (G2, $M_{n,\ NMR} = 10{,}600$ g mol^{-1}) to the seventh generation (G7, $M_{n,\ NMR} = 446{,}000$ g mol^{-1}) were well-defined, with PDIs below 1.10. Degradation of these materials was proven under different conditions. In extremely acidic media, three samples of different generations (G2, G3, and G7) degraded completely to PEG derivatives with molecular weights of

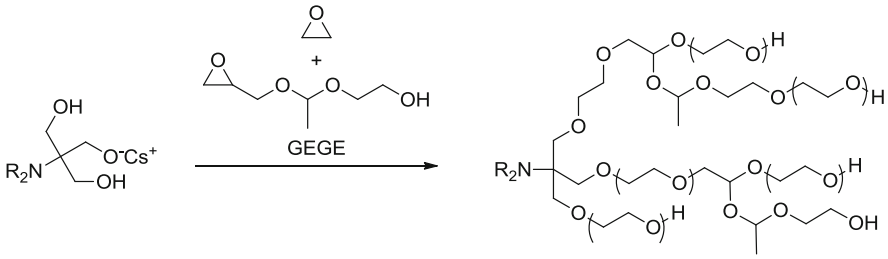

Scheme 2 Single-step synthesis of acid-degradable long-chain branched PEG according to [68], based on an acetal-containing epoxide inimer

around 2,000 g mol^{-1}. At 37°C and pH 5.5, 65% of all ketal groups of G7 were degraded in 80 h, whereas the cleavage of 90% took one week. Of course, the shortcoming of these remarkable and promising structures is their time-consuming synthesis. With the copolymerization of EO and an inimer for the AROP that carried an acetal moiety, 1-(glycidyloxy)ethyl ethylene glycol ether (GEGE), our group presented a one-step synthesis to acid-degradable long-chain branched PEGs (Scheme 2) [68]. Similar to the dendrimer-like PEOs, these structures carry acid-labile moieties at each branching unit and exhibit a large number of hydroxyl groups. The prize paid for the rapid synthesis is the less-defined (i.e., not perfectly branched) architecture, and the fact that the labile moieties do not separate both arms of each branching point from the initiation site, which results in broadly distributed degradation products. Other cleavable AROP inimers were presented in recent work by the group of Kizhakkedathu to generate degradable polyglycerol (PG) [154, 155]. In an elegant approach, they synthesized a series of different ketal inimers and found a much slower degradation for ketals derived from vicinal diols than for ketals of two separated alcohol synthons. These inimers could possibly also be copolymerized with EO to tailor the degradation kinetics of degradable long-chain branched PEGs.

The aforementioned polymerization methods all resulted in branched PEG architectures, but linear degradable PEGs have also been reported. A very promising pathway was reported by Lynd, Hawker and coworkers who copolymerized EO with epichlorohydrin via activated monomer ring-opening polymerization to obtain PEGs functionalized with chloromethyl groups and PDIs below 1.4 [147]. Subsequent elimination of HCl resulted in PEGs with hydrolysis-sensitive vinyl ether units distributed along the backbone (Scheme 3). The degradation of the polyether occurred at pH 7.4 and 37°C to approximately $M_n(t)/M_n(0) = 20\%$ after $t = 72$ h. However, no information on the nature of the terminal functionalities of the degradable polymer, the extent of substitution during the elimination step, and the intended coupling strategy to pharmacons was presented. Poly(ethylene glycol) monomethyl ether (mPEG) with a single acid-labile acetal unit in the backbone can be synthesized by turning the terminal hydroxyl group of mPEG with a low molecular weight into a hydroxyethyl acetal, following a two-step protocol, and subsequent polymerization of EO on this macroinitiator

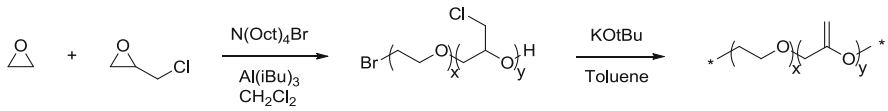

Scheme 3 Linear degradable PEGs according to Lynd, Hawker and colleagues [147]

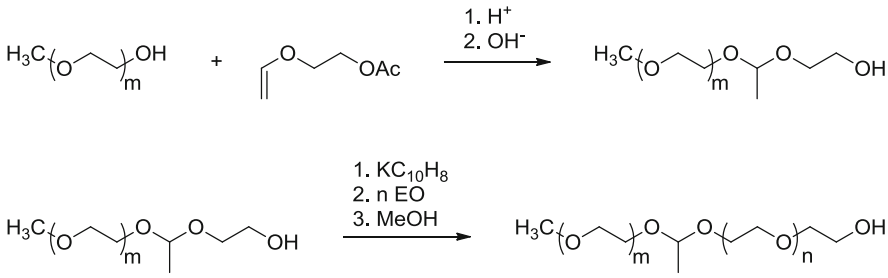

Scheme 4 Synthesis of mPEG with a single cleavable unit at a defined position, according to [70]

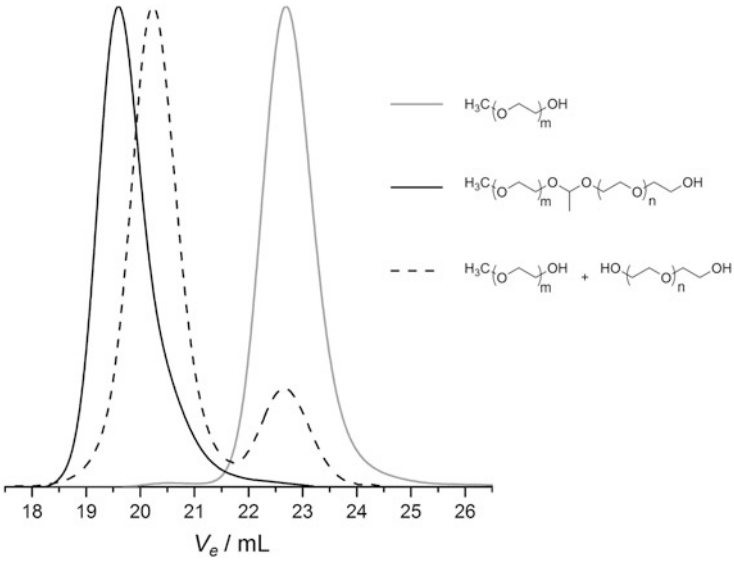

Fig. 1 Size-exclusion chromatograms of degradable mPEG before (*solid black line*) and after (*dashed black line*) degradation and that of the mPEG precursor (*solid grey line*). Adapted with permission from [70]. Copyright 2013 American Chemical Society

(Scheme 4) [70]. The molecular weight of the macroinitiator and the number of added EO units determined the defined position of the acetal in the backbone. Figure 1 shows the size exclusion chromatography (SEC) traces of the degradable mPEG before and after acidic degradation, as well as its precursor. The two well-defined distributions of different molecular weights (dashed line) were attributed to

the used low molecular weight PEG precursor and the added PEG block. These degradable mPEGs might be applicable as substitutes for commercial mPEGs, relying on established protocols for conjugation to proteins or low molecular weight drugs in order to increase the maximum molecular weight of the polyether that can be used in the human body, avoiding the risk of accumulation of PEG in the liver.

3 Different Labile Units for Different Triggers

3.1 Acid-Sensitive PEGs

Most of the labile units listed in Table 2, including most of the PEGs synthesized by previously discussed EO polymerization methods, are cleaved at acidic pH. Acidity is a popular degradation trigger [156], especially for polymeric carriers of anticancer drugs making use of passive targeting of tumors (EPR effect) and the potentially increased acidity of such tissue [157, 158]. Reduced pH is further found in lysosomes (pH 5.5) and endosomes (pH 6.5), extending the possible application of acid-sensitive polymer therapeutics beyond antitumor therapies.

The first attempt to synthesize acid-sensitive PEGs based on a PEG coupling approach capitalized on *cis*-aconitic acid linkers. The obtained polymer was acid-degradable and most likely biocompatible, as shown in a cell viability assay using B16F10 cells as well as a red blood cell lysis assay. However, decarboxylation and crosslinking reactions led to nondegradable linkages [71]. Better results were achieved with the incorporation of acetal moieties in PEGs. Pioneering work by Duncan, Brocchini and coworkers capitalized on the copolymerization of triethylene glycol (TEG) divinyl ether with dihydroxyl PEGs and functional diols, such as protected serinol [53] and diphenols [56, 57]. The former diol allows postpolymerization modification of the resulting amino-pendent polyacetal (APEGs, Scheme 5) with pendant doxorubicin (DOX) moieties [55], whereas among the latter, drugs can be incorporated directly in the main chain [56, 66, 67]. Using telechelic PEG with $M_w = 3{,}400$, degradable PEGs with molecular weights up to 100,000 g mol^{-1} and PDIs of 1.6-2.0 were synthesized. Other synthetic routes to PEG polyacetals involve condensation of PEG diols with the corresponding aldehyde [60, 65] or Williamson ether synthesis from an acetal-containing diol and PEG ditosylate [58, 63, 64]. Although conceptually interesting, these routes do not lead to high molecular weight polyethers, but result in polydisperse (PDI > 2) or, in case of the etherification, ill-defined ($5.8 <$ PDI < 11.6) polymers.

The degradation of acetals in PEG is strongly pH and temperature dependent and, not surprisingly, faster in more acidic media [53, 56, 57, 59, 64–68, 70]. At pH 5.5 and 37°C, total degradation of PEG acetaldehyde acetals requires approximately 3 weeks, but also at pH 7.4 (pH of blood), a significant amount of the labile

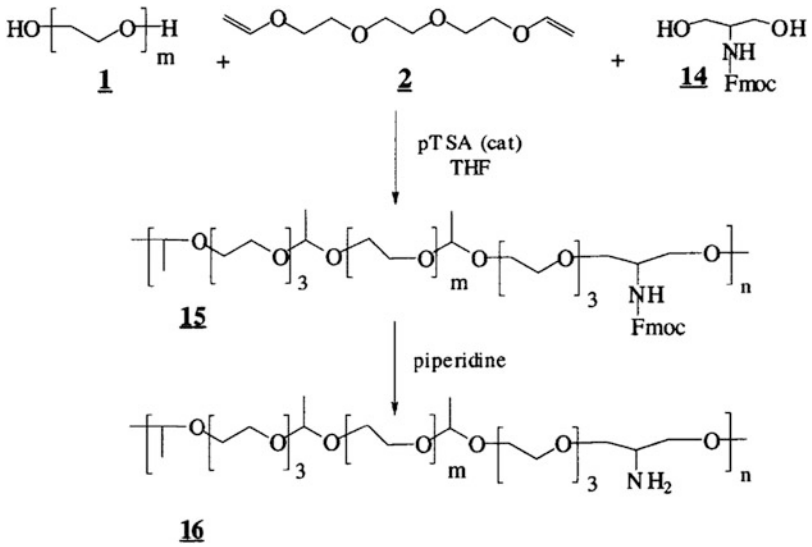

Scheme 5 Synthesis of acid-degradable PEGs with pendent amino groups (APEGs). Reprinted with permission from [53]. Copyright 2002 American Chemical Society

groups are hydrolyzed [53]. Further, the chemical composition of the acetal (i.e., the nature of the aldehyde and alcohol) influences the rate of its hydrolysis: Benzaldehyde acetals degrade faster than aliphatic aldehydes (compare [59] and [65]), and phenolic acetaldehyde acetals are hydrolyzed faster than purely aliphatic ones [56, 57]. Cyclic acetals require harsher conditions than linear ones [58] (also true for PG-based polyketals [154]) and basic moieties, such as amino groups adjacent to the acetal also lead to decreased hydrolysis rates [70]. Biocompatibility and pharmacokinetic tests of acetal-containing PEGs and polymeric prodrugs have been promising so far. APEG (Scheme 5), its derivative without pendant functions, and the degradation products of the latter were non-cytotoxic in an MTT assay after 72 h using B16F10 cells and non-hemolytic within 24 h (Fig. 2) [53]. Furthermore, doxorubicin-loaded high molecular weight APEGs outperformed *N*-(2-hydroxypropyl)methacrylamide copolymer DOX conjugates, showing prolonged blood circulation times, increased passive tumor targeting, and reduced DOX deposition in liver and spleen [55]. Besides their application as degradable polymeric carriers for low molecular weight molecules, acid-labile PEGs are also used for the synthesis of gene delivery vectors [59, 61] and as precursors for degradable hydrogels [58, 62, 63] and triblock copolymers [60, 64, 110]. Wang et al. synthesized a polyacetal from PEG and lilial [3-(4-*tert*-butylphenyl)-2-methylpropanal, used for perfume formulations] to reversibly bind the volatile scent [65].

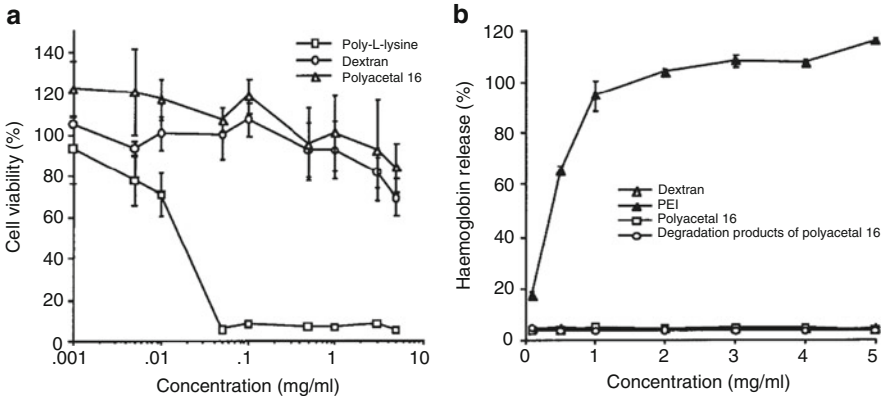

Fig. 2 Biocompatibility assays of polyacetal 16 described in Scheme 5. (**a**) Cytotoxicity assay (B16F10 cells stimulated for 72 h); positive control was poly-L-lysine, negative control was Dextran. (**b**) Red blood cell lysis assay after 24 h; positive control was poly(ethylene imine) (PEI), negative control was Dextran. Adapted with permission from [53]. Copyright 2002 American Chemical Society

3.2 Enzymatically Degradable PEGs

The pool of biodegradable units incorporated in PEG also contains enzymatically cleavable moieties. Most prominent among these are amino acid or oligopeptide linkages, which were applied for the coupling of monofunctional PEG derivatives [31, 112, 113, 119, 123] and as monomers for polycondensation with difunctional PEGs [111, 115–119]. Depending on the inserted amino acid or sequence, the polymers can be cleaved by different proteases such as collagenase, chymotrypsin, or cathepsin B. Of course, PEG-based polypeptides can also be degraded under simple hydrolysis conditions [111, 119]. First studies on such systems exposed the strong dependence of the degradation rate on the length and structure of the peptide linker [111–113]. Whereas chymotrypsin requires a single in-chain phenylalanine residue for the PEG degradation [111], cathepsin B does not cleave PEGs with just a glutamic acid linker [113]. In the latter case, the degradation rate increases by adding a phenylalanine at the C-terminus of the glutamic acid and is even higher by coupling it to the N-terminal site. Further, the corresponding pendant benzylesters undergo proteolysis much faster than the free acid derivatives [113]. The degradable PEGs of this type are also suitable carriers for DOX, which can be bound via enzymatically cleavable oligopeptides [114–117] or an acid-sensitive hydrazone [118]. In contrast to free DOX, these polymer therapeutics exhibited no signs of toxicity in in vivo studies on mice and seemed to inhibit tumor growth [116]. However, no PDI values have been published for most of the PEG copolymers derived from polycondensation, but the available SEC traces indicate broad molecular weight distributions, which is an obstacle for eventual FDA approval [116–118]. PEGs with in-chain amino acid peptide bonds have also

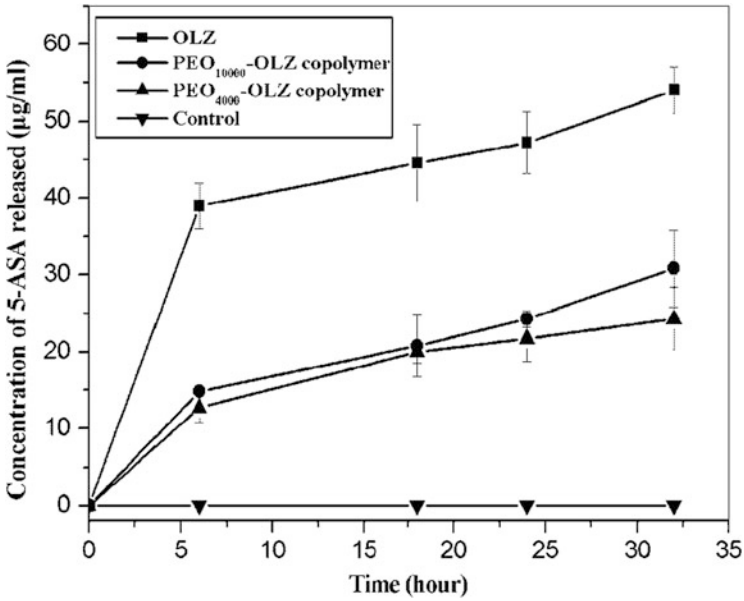

Fig. 3 Release of 5ASA from OLZ and OLZ PEG copolymers in the presence of reductive colon enzymes and benzyl viologen at 37°C. From [72]. Copyright Wiley-VCH. Reproduced with permission

been prepared, mainly to add pending functionalities to the polyether rather than labile joints [120–122] and can be generated in a monodisperse fashion by multistep protection/deprotection protocols [31].

If the required enzyme is solely available at the desired site of drug release, enzymatically degradable PEGs can be applicable for site-specific drug delivery. Azo compounds of *5*-aminosalicylic acid (5ASA), a non-steroidal anti-inflammatory drug, are potent prodrugs for colon-specific delivery of this pharmacon. The free drug would be absorbed in the small intestine, whereas the corresponding azo compounds can reach the colon, where reductive enzymes release 5ASA from its carriers [159]. The copolymerization of PEG diacids of various molecular weights with an Olsalazin (OLZ, 5,5′-azodiscalicylic acid) derivative resulted in PEG-based prodrugs with molecular weights up to 47,000 g mol^{-1} and in-chain carboxylates as well as enzymatically cleavable azo bonds. 5ASA release from the polymeric prodrugs in the presence of reductive enzymes was confirmed (Fig. 3). Comparison of the degradation rates in the presence or absence of rat cecum content indicated that enzymatic azo reduction occurred prior to cleavage of the ester. The ester hydrolysis rates at pH 6.8 (37°C) were dependent on the size of the PEG precursors and were higher for larger polyether segments [72]. Oral administration of the PEG prodrugs to rats confirmed colon-specific drug delivery in vivo [73].

Several different polycondensation routes can be applied for the installation of carboxylates in PEG, e.g., DCC-promoted esterification [72, 73, 87–89], Michael

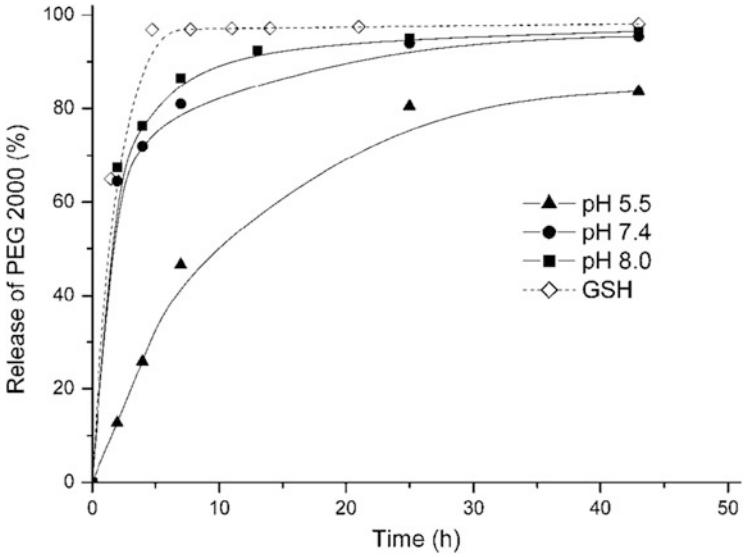

Fig. 4 Degradation of PEG cystine polyester at 37°C: Hydrolytic cleavage of ester moieties at different pH values (*solid symbols*). Reduction of disulfides at pH 5.5 ($c_{GCH} = 5$ mmol) (*diamonds*). From [89]. Copyright Wiley-VCH. Reproduced with permission

addition to acrylates, as well as reactions of PEG with the corresponding acids [97], acid anhydrides [86], acyl chlorides [90–94], and methyl carboxylates [30, 98–102]. Commonly, the polycondensation is conducted during the esterification step, but the thiol oxidation of PEG cysteine diesters [89] and Michael addition of dithiols to PEG di(meth)acrylates [95, 96] were also used to synthesize PEG polyesters. Due to the numerous PEG-based polyesters synthesized for a wide range of applications, we will focus on the works that studied the PEG polyester degradability. Depending on the synthetic pathway and the size of the batched telechelic PEGs, polyesters with molecular weights in the range of 1,000-104,500 g mol^{-1} and typical PDIs of 1.4-2.7 were generated. The ester-containing PEGs can undergo enzymatic degradation, but only a few of them were examined regarding this property [87, 91–93, 104]. Mero et al. observed almost no ester cleavage in a pH 7.4 buffer at 37°C in 24 h, but rapid degradation in mouse plasma within the same time [93]. Typically, the enzymatic degradation at 37°C and neutral pH takes a few days to complete, but comparison of the results is difficult because too many parameters vary (enzymes, linkers, PEG content, size of the PEG segments, observed quantity, type of sample). Carboxylates can further be degraded by simple hydrolysis under both acidic and basic conditions. In theory, degradation rates are expected to be lowest under neutral conditions; however, in the presence of basic moieties, the hydrolysis can be slower in more acidic media (Fig. 4) [86, 89, 104]. Not surprisingly, hydrophilic poly(ether ester)s are hydrolyzed faster than hydrophobic derivatives under the same conditions [72, 88].

3.3 Alternative Labile Groups and Triggers

In analogy to azo units, disulfide linkages have been studied as reductively cleavable joints for the reversible connection of PEG telechelics [89, 105–108]. In contrast to the former, disulfides are reduced by a reduced glutathione (GSH) derivative in the cytosol. The disulfide-containing polyethers can either be synthesized from PEG dithiol precursors under oxidative conditions [89, 105–107] or by a polycondensation of telechelic PEGs and a suitable difunctional disulfide [89]. Depending on the synthetic route, size of the telechelic PEGs, and the reaction conditions, it was possible to obtain poly(ether sulfide)s with molecular weights up to 180,000 g mol^{-1}. In contrast to poly(ether sulfide)s with degrees of polymerization exceeding 12, those prepared from tri-, tetra-, or hexa(ethylene glycol) were almost insoluble in water. Pendant functionalities have been incorporated in these polymers by coupling PEG chains to cystine via urethane or ester bonds. The reductive degradation rate is dependent on the hydrophobicity of the pendant functional groups. Although the disulfides of a polyester from PEG and cystine at cytosolic glutathione concentrations (5 mmol) are reduced even faster than the ester moieties are hydrolyzed at pH 8.0 (Fig. 4), reductive degradation of a corresponding polymer with pendant *p*-nitrophenyl succinates is rather slow under the same conditions (<50% within 2 days) [89]. As poly(ether sulfide)s also undergo reductive degradation when incubated with EL4 T cells [107] and were nontoxic to HepG2 cells [105], these polymers appear to be promising drug carriers.

Besides carboxylates, esters of other biologically relevant acids have been used to synthesize PEG-based polyesters. Physical properties of PEG-derived polycarbonates have been explored since the 1960s [74–78]. More recent studies have focused on the degradability and cell interactions of these materials, but the PEG contents were low (<25%) [80–83]. Water-soluble polymers with higher PEG fractions have been prepared, but no degradation data has been reported for these [160, 161]. PEGs with a single carbonate linker were solely mentioned in patent literature [79, 84].

Poly(*H*-phosphonate)s from PEG diols are generated by the polycondensation of the telechelic polyethers and dialkyl *H*-phosphonates [124–135]. The degradation of PEG polyphosphonates occurs randomly along the polymer chain under slightly basic conditions (pH 8.8, 40% degradation in 12 h) and is more rapid at low pH (pH 1.66, almost complete after 11 h). The degradation rate is further influenced by the polymer concentration because the degradation affords acidic products [134, 137]. These polymers might also undergo enzymatic degradation [137]. Poly(PEG *H*-phosphonate)s carry highly reactive P-H bonds that allow further functionalization, such as the attachment of pharmaceutically active compounds or linker moieties for the conjugation to such molecules [124, 135], as well as oxidation to the corresponding poly(PEG phosphate)s [126–133]. Another synthetic pathway to such polyphosphates is the condensation of PEG diols and alkyl dichlorophosphates [136]. Further information on these interesting materials and their applicability in

drug delivery systems can be found in a substantial monograph on polyphophoesters published recently [137].

Various PEG-based polyurethanes (PUs) have been synthesized, mainly to introduce pendant functionalities along the polymer backbone [138–143], and are usually considered nondegradable under physiological conditions. Biodegradability has been described for numerous polyurethane materials, but seems to occur predominantly at additionally present cleavable units. Therefore, poly(ester urethane)s degrade faster than poly(ether urethane)s [162]. Similar findings were reported for PEG-based PU films using α-chymotrypsin in aqueous, buffered solution. A sample containing an enzymatically cleavable trypsin chain extender eroded much faster than a PU film without such a moiety [144]. The hydrolytic degradation of PEG-based PUs is slow and was investigated on samples synthesized without any chain extender at pH 7.4 (37°C) (15% reduction of M_w within 12 days) [145].

4 Conclusions and Outlook

Based on several speeches at the end of Staudinger's career, in which he emphasized the importance of macromolecular chemistry for the mechanisms of life, it is a safe bet that the combination of synthetic and biological macromolecules would have found his strong approval. It is interesting to note that PEG, as one of the polymers in the focus of his research [2–5], eventually became the gold standard polymer for biomedical applications and bioconjugation and therefore one of the major bridges between these fields. Although PEG has been of scientific interest for several decades, new insights and methods for tuning its properties are of high current interest.

To tackle PEG's most important disadvantage in biomedical applications – its biopersistence – various synthetic pathways have been investigated for inserting into the backbone of PEG a variety of different degradable moieties that can be cleaved under conditions found within organisms. Besides polymer therapeutics, degradable PEGs have also been investigated for the reversible fixation of volatile scents and the synthesis of cleavable hydrogels. The rate of degradation strongly depends on the constitution and chemical environment of the linker as well as the size of the PEG segments. Care has to be taken when comparing the degradation data for different methods. Main parameters that have to be taken into account are the temperature, pH, type of enzyme, concentrations (in case pseudo-first-order kinetics do not apply), and the measured quantity (number of remaining linkers, amount of released telechelic PEG, residual molecular weight). Although many of the presented PEGs gave promising results as biodegradable drug carriers, most of these materials were synthesized in polycondensation reactions and therefore exhibit certain drawbacks, such as broad molecular weight distributions as a direct result of the step-growth kinetics. On the other hand, well-defined degradable PEGs can be obtained by coupling monofunctional PEGs to a (multi)functional labile

unit, but the resulting polymers are limited in their payload, unless synthesized by multistep protection/deprotection protocols. Very recently, a number of strategies have been employed that rely on custom-made PEGs by EO polymerization, either from cleavable initiators or with comonomers that introduce cleavable functionalities (in some cases upon polymer-analogous derivatization). However, to date, none of the EO-based polymers has been tested regarding their biocompatibility, their degradation in vivo, or their suitability as drug carriers. In conclusion, the development of (bio)degradable PEGs has become a fast-evolving field of research that will eventually contribute to a new generation of polymer therapeutics, but will also have an impact on other areas of polymer research and materials science.

References

1. Staudinger H (1953) Die makromolekulare Chemie. Nobel Lecture: Macromolecular chemistry. http://www.nobelprize.org/nobel_prizes/chemistry/laureates/1953/staudinger-lecture.html
2. Staudinger H, Schweitzer O (1929) Über hochpolymere Verbindungen, 20. Mitteil.: Über die Polyäthylenoxyde. Ber Dtsch Chem Ges 62:2395–2405
3. Staudinger H, Lohmann H (1933) Über hochpolymere Verbindungen. 81. Mitteilung. Über eukolloides Polyäthylenoxyd. Justus Liebigs Ann Chem 505:41–51
4. Staudinger H, Lohmann H (1935) Über hochpolymere Verbindungen, 125. Mitteil.: Molekulargewichts-Bestimmungen an hochmolekularen Polyäthylenoxyden. Ber Dtsch Chem Ges 68:2313–2319
5. Staudinger H, Staudinger M, Sauter E (1937) Mikroskopische Untersuchungen an synthetischen hochmolekularen Stoffen. Z Physik Chem B 37:403–420
6. Veronese FM, Pasut G (2005) PEGylation, successful approach to drug delivery. Drug Discov Today 10:1451–1458
7. Kjellander R, Florin E (1981) Water structure and changes in thermal stability of the system poly(ethylene oxide)-water. J Chem Soc Faraday Trans 1 Phys Chem Condensed Phases 77:2053–2077
8. Zalipsky S (1995) Functionalized poly(ethylene glycols) for preparation of biologically relevant conjugates. Bioconjugate Chem 6:150–165
9. Li J, Kao WJ (2003) Synthesis of polyethylene glycol (PEG) derivatives and PEGylated-peptide biopolymer conjugates. Biomacromolecules 4:1055–1067
10. Thompson MS, Vadala TP, Vadala ML, Lin Y, Riffle JS (2008) Synthesis and applications of heterobifunctional poly(ethylene oxide) oligomers. Polymer 49:345–373
11. Dingels C, Schömer M, Frey H (2011) Die vielen Gesichter des Poly(ethylenglykol)s. Chem unserer Zeit 45:338–349
12. Caliceti P, Veronese FM (2003) Pharmacokinetic and biodistribution properties of poly-(ethylene glycol)-protein conjugates. Adv Drug Del Rev 55:1261–1277
13. Greenwald RB, Choe YH, McGuire J, Conover CD (2003) Effective drug delivery by PEGylated drug conjugates: bioconjugates for effective drug targeting. Adv Drug Del Rev 55:217–250
14. Harris JM, Chess RB (2003) Effect of pegylation on pharmaceuticals. Nat Rev Drug Discov 2:214–221
15. Pasut G, Sergi M, Veronese FM (2008) Anti-cancer PEG-enzymes: 30 years old, but still a current approach. Adv Drug Del Rev 60:69–78

16. Pasut G, Veronese FM (2009) PEG conjugates in clinical development or use as anticancer agents: an overview. Adv Drug Del Rev 61:1177–1188
17. Lasic DD, Needham D (1995) The "stealth" liposome: a prototypical biomaterial. Chem Rev 95:2601–2628
18. Greenwald RB (2001) PEG drugs: an overview. J Control Release 74:159–171
19. Abuchowski A, van Es T, Palczuk NC, Davis FF (1977) Alteration of immunological properties of bovine serum albumin by covalent attachment of polyethylene glycol. J Biol Chem 252:3578–3581
20. Abuchowski A, McCoy JR, Palczuk NC, van Es T, Davis FF (1977) Effect of covalent attachment of polyethylene glycol on immunogenicity and circulating life of bovine liver catalase. J Biol Chem 252:3582–3586
21. Alconcel SNS, Baas AS, Maynard HD (2011) FDA-approved poly(ethylene glycol)-protein conjugate drugs. Polym Chem 2:1442–1448
22. Immordino ML, Dosio F, Cattel L (2006) Stealth liposomes: review of the basic science, rationale, and clinical applications, existing and potential. Int J Nanomed 1:297–315
23. Ringsdorf H (1975) Structure and properties of pharmacologically active polymers. J Polym Sci Polym Symp 51:135–153
24. Matsumura Y, Maeda H (1986) A new concept for macromolecular therapeutics in cancer chemotherapy: mechanism of tumoritropic accumulation of proteins and the antitumor agent smancs. Cancer Res 46:6387–6392
25. Seymour LW (1992) Passive tumour-targeting of soluble macromolecules and drug conjugates. Crit Rev Ther Drug Carrier Syst 9:135–342
26. Duncan R (2003) The dawning era of polymer therapeutics. Nat Rev Drug Discov 2:347–360
27. Knischka R, Lutz PJ, Sunder A, Mülhaupt R, Frey H (2000) Functional poly(ethylene oxide) multiarm star polymers: core-first synthesis using hyperbranched polyglycerol initiators. Macromolecules 33:315–320
28. Taton D, Saule M, Logan J, Duran R, Hou S, Chaikof EL, Gnanou Y (2003) Polymerization of ethylene oxide with a calixarene-based precursor: synthesis of eight-arm poly(ethylene oxide) stars by the core-first methodology. J Polym Sci A Polym Chem 41:1669–1676
29. Zhao H, Rubio B, Sapra P, Wu D, Reddy P, Sai P, Martinez A, Gao Y, Lozanguiez Y, Longley C, Greenberger LM, Horak ID (2008) Novel prodrugs of SN38 using multiarm poly (ethylene glycol) linkers. Bioconjugate Chem 19:849–859
30. Hawker CJ, Chu F, Pomery PJ, Hill DJT (1996) Hyperbranched poly(ethylene glycol)s: a new class of ion-conducting materials. Macromolecules 29:3831–3838
31. Berna M, Dalzoppo D, Pasut G, Manunta M, Izzo L, Jones AT, Duncan R, Veronese FM (2006) Novel monodisperse PEG-dendrons as new tools for targeted drug delivery: synthesis, characterization and cellular uptake. Biomacromolecules 7:146–153
32. Feng X-S, Taton D, Chaikof EL, Gnanou Y (2005) Toward an easy access to dendrimer-like poly(ethylene oxide)s. J Am Chem Soc 127:10956–10966
33. Feng X, Taton D, Borsali R, Chaikof EL, Gnanou Y (2006) pH responsiveness of dendrimer-like poly(ethylene oxide)s. J Am Chem Soc 128:11551–11562
34. Feng X, Taton D, Chaikof EL, Gnanou Y (2007) Bouquet-type dendrimerlike poly(ethylene oxide)s with a focal aldehyde and peripheral hydroxyls. Biomacromolecules 8:2374–2378
35. Wilms D, Schömer M, Wurm F, Hermanns MI, Kirkpatrick CJ, Frey H (2010) Hyperbranched PEG by random copolymerization of ethylene oxide and glycidol. Macromol Rapid Commun 31:1811–1815
36. Choe YH, Conover CD, Wu D, Royzen M, Gervacio Y, Borowski V, Mehlig M, Greenwald RB (2002) Anticancer drug delivery systems: multi-loaded N4-acyl poly(ethylene glycol) prodrugs of ara-C.: II. Efficacy in ascites and solid tumors. J Contr Release 79:55–70
37. Pasut G, Scaramuzza S, Schiavon O, Mendichi R, Veronese FM (2005) PEG-epirubicin conjugates with high drug loading. J Bioact Compat Polym 20:213–230
38. Obermeier B, Wurm F, Mangold C, Frey H (2011) Multifunctional poly(ethylene glycol)s. Angew Chem Int Ed 50:7988–7997

39. Knop K, Hoogenboom R, Fischer D, Schubert US (2010) Poly(ethylene glycol) in drug delivery: pros and cons as well as potential alternatives. Angew Chem Int Ed 49:6288–6308
40. Yamaoka T, Tabata Y, Ikada Y (1994) Distribution and tissue uptake of poly(ethylene glycol) with different molecular weights after intravenous administration to mice. J Pharm Sci 83:601–606
41. Pasut G, Veronese FM (2007) Polymer-drug conjugation, recent achievements and general strategies: polymers in Biomedical Applications. Prog Polym Sci 32:933–961
42. Filpula D, Zhao H (2008) Releasable PEGylation of proteins with customized linkers. Adv Drug Del Rev 60:29–49
43. Boomer JA, Thompson DH (1999) Synthesis of acid-labile diplasmenyl lipids for drug and gene delivery applications. Chem Phys Lipids 99:145–153
44. Guo X, Szoka FC (2001) Steric stabilization of fusogenic liposomes by a low-pH sensitive PEG-diortho ester-lipid conjugate. Bioconjugate Chem 12:291–300
45. Boomer JA, Inerowicz HD, Zhang Z-Y, Bergstrand N, Edwards K, Kim J-M, Thompson DH (2003) Acid-triggered release from sterically stabilized fusogenic liposomes via a hydrolytic dPEGylation strategy. Langmuir 19:6408–6415
46. Masson C, Garinot M, Mignet N, Wetzer B, Mailhe P, Scherman D, Bessodes M (2004) pH-sensitive PEG lipids containing orthoester linkers: new potential tools for nonviral gene delivery. J Contr Release 99:423–434
47. Hatakeyama H, Akita H, Kogure K, Oishi M, Nagasaki Y, Kihira Y, Ueno M, Kobayashi H, Kikuchi H, Harashima H (2006) Development of a novel systemic gene delivery system for cancer therapy with a tumor-specific cleavable PEG-lipid. Gene Ther 14:68–77
48. Sawant RM, Hurley JP, Salmaso S, Kale A, Tolcheva E, Levchenko TS, Torchilin VP (2006) "SMART" drug delivery systems: double-targeted pH-responsive pharmaceutical nanocarriers. Bioconjugate Chem 17:943–949
49. Xu H, Deng Y, Chen D, Hong W, Lu Y, Dong X (2008) Esterase-catalyzed dePEGylation of pH-sensitive vesicles modified with cleavable PEG-lipid derivatives. J Contr Release 130:238–245
50. Boomer JA, Qualls MM, Inerowicz HD, Haynes RH, Patri VS, Kim J-M, Thompson DH (2009) Cytoplasmic delivery of liposomal contents mediated by an acid-labile cholesterol-vinyl ether-PEG conjugate. Bioconjugate Chem 20:47–59
51. Kuai R, Yuan W, Qin Y, Chen H, Tang J, Yuan M, Zhang Z, He Q (2010) Efficient delivery of payload into tumor cells in a controlled manner by TAT and thiolytic cleavable PEG co-modified liposomes. Mol Pharm 7:1816–1826
52. Chen D, Jiang X, Huang Y, Zhang C, Ping Q (2010) pH-sensitive mPEG-Hz-cholesterol conjugates as a liposome delivery system. J Bioact Compat Polym 25:527–542
53. Tomlinson R, Klee M, Garrett S, Heller J, Duncan R, Brocchini S (2002) Pendent chain functionalized polyacetals that display pH-dependent degradation: a platform for the development of novel polymer therapeutics. Macromolecules 35:473–480
54. Cheng J, Khin KT, Jensen GS, Liu A, Davis ME (2003) Synthesis of linear, β-cyclodextrin-based polymers and their camptothecin conjugates. Bioconjugate Chem 14:1007–1017
55. Tomlinson R, Heller J, Brocchini S, Duncan R (2003) Polyacetal-doxorubicin conjugates designed for pH-dependent degradation. Bioconjugate Chem 14:1096–1106
56. Vicent MJ, Tomlinson R, Brocchini S, Duncan R (2004) Polyacetal-diethylstilboestrol: a polymeric drug designed for pH-triggered activation. J Drug Target 12:491–501
57. Rickerby J, Prabhakar R, Ali M, Knowles J, Brocchini S (2005) Water-soluble polyacetals derived from diphenols. J Mater Chem 15:1849–1856
58. Kaihara S, Matsumura S, Fisher JP (2007) Synthesis and properties of poly[poly(ethylene glycol)-co-cyclic acetal] based hydrogels. Macromolecules 40:7625–7632
59. Knorr V, Allmendinger L, Walker GF, Paintner FF, Wagner E (2007) An acetal-based PEGylation reagent for pH-sensitive shielding of DNA polyplexes. Bioconjugate Chem 18:1218–1225

60. Cui W, Qi M, Li X, Huang S, Zhou S, Weng J (2008) Electrospun fibers of acid-labile biodegradable polymers with acetal groups as potential drug carriers. Int J Pharm 361:47–55
61. Wong JB, Grosse S, Tabor AB, Hart SL, Hailes HC (2008) Acid cleavable PEG-lipids for applications in a ternary gene delivery vector. Mol BioSyst 4:532–541
62. Betz MW, Caccamese JF, Coletti DP, Sauk JJ, Fisher JP (2009) Tissue response and orbital floor regeneration using cyclic acetal hydrogels. J Biomed Mater Res A 90A:819–829
63. Kaihara S, Matsumura S, Fisher JP (2009) Cellular responses to degradable cyclic acetal modified PEG hydrogels. J Biomed Mater Res A 90A:863–873
64. Kaihara S, Fisher JP, Matsumura S (2009) Chemo-enzymatic synthesis of degradable PTMC-b-PECA-b-PTMC triblock copolymers and their micelle formation for pH-dependent controlled release. Macromol Biosci 9:613–621
65. Wang Y, Morinaga H, Sudo A, Endo T (2011) Synthesis of amphiphilic polyacetal by polycondensation of aldehyde and polyethylene glycol as an acid-labile polymer for controlled release of aldehyde. J Polym Sci A Polym Chem 49:596–602
66. England RM, Masiá E, Giménez V, Lucas R, Vicent MJ (2012) Polyacetal-stilbene conjugates – the first examples of polymer therapeutics for the inhibition of HIF-1 in the treatment of solid tumours. J Contr Release 164:314–322
67. Giménez V, James C, Arminán A, Schweins R, Paul A, Vicent MJ (2012) Demonstrating the importance of polymer-conjugate conformation in solution on its therapeutic output: diethylstilbestrol (DES)-polyacetals as prostate cancer treatment. J Contr Release 159:290–301
68. Tonhauser C, Schüll C, Dingels C, Frey H (2012) Branched acid-degradable, biocompatible polyether copolymers via anionic ring-opening polymerization using an epoxide inimer. ACS Macro Lett 1:1094–1097
69. Feng X, Chaikof EL, Absalon C, Drummond C, Taton D, Gnanou Y (2011) Dendritic carrier based on PEG: design and degradation of acid-sensitive dendrimer-like poly(ethylene oxide)s. Macromol Rapid Commun 32:1722–1728
70. Dingels C, Müller SS, Steinbach T, Tonhauser C, Frey H (2013) Universal concept for the implemantation of a single cleavable unit at tunable position in functional poly(ethylene glycol)s. Biomacromolecules 14:448–459
71. DuBois Clochard M-C, Rankin S, Brocchini S (2000) Synthesis of soluble polymers for medicine that degrade by intramolecular acid catalysis. Macromol Rapid Commun 21:853–859
72. Lai J, Wang L-Q, Tu K, Zhao C, Sun W (2005) Linear azo polymer containing conjugated 5,5′-azodisalicylic acid segments in the main chain: synthesis, characterization, and degradation. Macromol Rapid Commun 26:1572–1577
73. Lai J, Tu K, Wang H, Chen Z, Wang L-Q (2008) Degradability of the linear azo polymer conjugated 5,5′-azodisalicylic acid segment in the main chain for colon-specific drug delivery. J Appl Polym Sci 108:3305–3312
74. Goldberg EP (1963) Elastomeric polycarbonate block copolymers. J Polym Sci C Polym Symp 4:707–730
75. Suzuki T, Kotaka T (1980) Dielectric and mechanical relaxations in randomly coupled multiblock copolymers with varying block lengths: bisphenol-A polycarbonate-poly (oxyethylene) systems. Macromolecules 13:1495–1501
76. Suzuki T, Kotaka T (1983) Morphological and physical properties of randomly coupled multiblock copolymers: bisphenol-A polycarbonate-poply(oxyethylene) systems. Polym J 15:15–23
77. Suzuki T, Chihara H, Kotaka T (1984) Sorption of water by bisphenol-A polycarbonate and polyoxyethylene multiblock copolymers with varying composition and block length. Polym J 16:129–138
78. Tanisugi H, Ohnuma H, Kotaka T (1984) Swelling behavior of bisphenol-A polycarbonate-polyoxyethylene multiblock copolymers in ethanol/water mixtures. Polym J 16:633–640
79. Harris JM, Bentley MD, Zhoa X, Shen X (2002) Patent Application 09/459312, US6,348,558B1

80. Tziampazis E, Kohn J, Moghe PV (2000) PEG-variant biomaterials as selectively adhesive protein templates: model surfaces for controlled cell adhesion and migration. Biomaterials 21:511–520
81. Bourke SL, Kohn J (2003) Polymers derived from the amino acid l-tyrosine: polycarbonates, polyarylates and copolymers with poly(ethylene glycol). Adv Drug Del Rev 55:447–466
82. Sharma RI, Kohn J, Moghe PV (2004) Poly(ethylene glycol) enhances cell motility on protein-based poly(ethylene glycol)-polycarbonate substrates: a mechanism for cell-guided ligand remodeling. J Biomed Mater Res A 69A:114–123
83. Sousa A, Schut J, Kohn J, Libera M (2006) Nanoscale morphological changes during hydrolytic degradation and erosion of a bioresorbable polymer. Macromolecules 39:7306–7312
84. Kozlowski A, McKannan J, McManus SP (2007) Patent Application PCT/US2006/029,929, WO/2007/016560A2
85. Won C-Y, Chu C-C, Lee JD (1998) Novel biodegradable copolymers containing pendant amine functional groups based on aspartic acid and poly(ethylene glycol). Polymer 39:6677–6681
86. Won C-Y, Chu C-C, Lee JD (1998) Synthesis and characterization of biodegradable poly(L-aspartic acid-co-PEG). J Polym Sci A Polym Chem 36:2949–2959
87. Padmaja T, Lele BS, Deshpande MC, Kulkarni MG (2002) Enzymatically degradable prodrugs: a novel methodology for drug linkage. J Appl Polym Sci 85:2108–2118
88. Nagahama K, Hashizume M, Yamamoto H, Ouchi T, Ohya Y (2009) Hydrophobically modified biodegradable poly(ethylene glycol) copolymers that form temperature-responsive nanogels. Langmuir 25:9734–9740
89. Braunová A, Pechar M, Laga R, Ulbrich K (2007) Hydrolytically and reductively degradable high-molecular-weight poly(ethylene glycol)s. Macromol Chem Phys 208:2642–2653
90. Harris JM (2001) Patent Application 08/937846, US06,214,966B1
91. Nagata M, Hizakae S (2003) Synthesis and properties of biodegradable copolymers based on 4,4′-(adipoyldioxy)dicinnamic acid, 1,6-hexanediol, and poly(ethylene glycol)s. J Polym Sci A Polym Chem 41:2930–2938
92. Nagata M, Hizakae S (2003) Synthesis and characterization of photocrosslinkable biodegradable polymers derived from 4-hydroxycinnamic acid. Macromol Biosci 3:412–419
93. Mero A, Schiavon O, Pasut G, Veronese FM, Emilitri E, Ferruti P (2009) A biodegradable polymeric carrier based on PEG for drug delivery. J Bioact Compat Polym 24:220–234
94. Unal S, Lin Q, Mourey TH, Long TE (2005) Tailoring the degree of branching: preparation of poly(ether ester)s via copolymerization of poly(ethylene glycol) oligomers (A2) and 1,3,5-benzenetricarbonyl trichloride (B3). Macromolecules 38:3246–3254
95. Wang N, Dong A, Tang H, Van Kirk EA, Johnson PA, Murdoch WJ, Radosz M, Shen Y (2007) Synthesis of degradable functional poly(ethylene glycol) analogs as versatile drug delivery carriers. Macromol Biosci 7:1187–1198
96. Wang N, Dong A, Radosz M, Shen Y (2008) Thermoresponsive degradable poly(ethylene glycol) analogues. J Biomed Mater Res A 84A:148–157
97. Chen S, Wang Y, Fan Y, Ma J (2009) Synthesis of amphiphilic poly(tetraethylene glycol succinate) and the thermosensitivity of its aggregation in water. J Biomed Mater Res A 88A:769–777
98. Kumar R, Chen M-H, Parmar VS, Samuelson LA, Kumar J, Nicolosi R, Yoganathan S, Watterson AC (2004) Supramolecular assemblies based on copolymers of PEG600 and functionalized aromatic diesters for drug delivery applications. J Am Chem Soc 126:10640–10644
99. Dou S, Zhang S, Klein RJ, Runt J, Colby RH (2006) Synthesis and characterization of poly (ethylene glycol)-based single-ion conductors. Chem Mater 18:4288–4295
100. Wang W, Liu W, Tudryn GJ, Colby RH, Winey KI (2010) Multi-length scale morphology of poly(ethylene oxide)-based sulfonate ionomers with alkali cations at room temperature. Macromolecules 43:4223–4229

101. Bhatia S, Mohr A, Mathur D, Parmar VS, Haag R, Prasad AK (2011) Biocatalytic route to sugar-PEG-based polymers for drug delivery applications. Biomacromolecules 12:3487–3498
102. Wang H-Y, Zhou Y-J, Wang Z, Wang N, Li K, Yu X-Q (2011) Enzyme-catalyzed synthesis of a novel thermosensitive polyester with pendant ketoprofen. Macromol Biosci 11:595–599
103. Wang W, Tudryn GJ, Colby RH, Winey KI (2011) Thermally driven ionic aggregation in poly(ethylene oxide)-based sulfonate ionomers. J Am Chem Soc 133:10826–10831
104. Braunová A, Pechar M, Ulbrich K (2004) Degradation behavior of poly(ethylene glycol) diblock and multiblock polymers with hydrolytically degradable ester linkages. Collect Czech Chem Commun 69:1643–1656
105. Lee Y, Koo H, G-w J, Mo H, Cho MY, Park J-Y, Choi JS, Park JS (2005) Poly(ethylene oxide sulfide): new poly(ethylene glycol) derivatives degradable in reductive conditions. Biomacromolecules 6:24–26
106. Lee J, Joo MK, Kim J, Park JS, Yoon M-Y, Jeong B (2009) Temperature-sensitive biodegradable poly(ethylene glycol). J Biomater Sci Polym Ed 20:957–965
107. Etrych T, Kovár L, Šubr V, Braunová A, Pechar M, Chytil P, Říhová B, Ulbrich K (2010) High-molecular-weight polymers containing biodegradable disulfide bonds: synthesis and in vitro verification of intracellular degradation. J Bioact Compat Polym 25:5–26
108. Hernandez-Mireles T, Rito-Palomares M (2006) New aqueous two-phase systems based on poly(ethylene oxide sulfide) (PEOS) and potassium phosphate for the potential recovery of proteins. J Chem Technol Biotechnol 81:997–1002
109. Reid B, Tzeng S, Warren A, Kozielski K, Elisseeff J (2010) Development of a PEG derivative containing hydrolytically degradable hemiacetals. Macromolecules 43:9588–9590
110. Qi M, Li X, Yang Y, Zhou S (2008) Electrospun fibers of acid-labile biodegradable polymers containing ortho ester groups for controlled release of paracetamol. Eur J Pharm Biopharm 70:445–452
111. Ulbrich K, Strohalm J, Kopeček J (1986) Poly(ethylene glycol)s containing enzymatically degradable bonds. Makromol Chem 187:1131–1144
112. Pechar M, Strohalm J, Ulbrich K (1995) Synthesis of poly(ethylene glycol) block copolymers as potential water-soluble drug carriers. Collect Czech Chem Commun 60:1765–1780
113. Pechar M, Strohalm J, Ulbrich K, Schacht E (1997) Biodegradable drug carriers based on poly(ethylene glycol) block copolymers. Macromol Chem Phys 198:1009–1020
114. Ulbrich K, Pechar M, Strohalm J, Šubr V, Říhová B (1997) Polymeric carriers of drugs for site-specific therapy. Macromol Symp 118:577–585
115. Ulbrich K, Šubr V, Pechar M, Strohalm J, Jelínková M, Říhová B (2000) Hydrophilic polymers for drug delivery. Macromol Symp 152:151–162
116. Pechar M, Ulbrich K, Šubr V, Seymour LW, Schacht EH (2000) Poly(ethylene glycol) multiblock copolymer as a carrier of anti-cancer drug doxorubicin. Bioconjugate Chem 11:131–139
117. Pechar M, Ulbrich K, Jelínková M, Říhová B (2003) Conjugates of antibody-targeted PEG multiblock polymers with doxorubicin in cancer therapy. Macromol Biosci 3:364–372
118. Pechar M, Braunová A, Ulbrich K, Jelínková M, Říhová B (2005) Poly(Ethylene Glycol)-doxorubicin conjugates with pH-controlled activation. J Bioact Compat Polym 20:319–341
119. Pechar M, Braunová A, Ulbrich K (2005) Poly(ethylene glycol)-based polymer carrier of doxorubicin degradable by both enzymatic and chemical hydrolyses. Collect Czech Chem Commun 70:327–338
120. Ramanathan S, Qiu B, Pooyan S, Zhang G, Stein S, Leibowitz MJ, Sinko PJ (2001) Targeted PEG-based bioconjugates enhance the cellular uptake and transport of a HIV-1 TAT nonapeptide. J Contr Release 77:199–212
121. d'Acunzo F, Kohn J (2002) Alternating multiblock amphiphilic copolymers of PEG and tyrosine-derived diphenols. 1. Synthesis and characterization. Macromolecules 35:9360–9365

122. d'Acunzo F, Le T-Q, Kohn J (2002) Alternating multiblock amphiphilic copolymers of PEG and tyrosine-derived diphenols. 2. Self-assembly in aqueous solution and at hydrophobic surfaces. Macromolecules 35:9366–9371
123. Rao Z, Sasaki M, Taguchi T (2013) Development of amphiphilic, enzymatically-degradable PEG-peptide conjugate as cell crosslinker for spheroid formation. Colloids Surf B Biointerfaces 101:223–227
124. Tzevi R, Novakov P, Troev K, Roundhill DM (1997) Synthesis of poly(oxyethylene phosphonate)s bearing oxirane groups in the side chain. J Polym Sci A Polym Chem 35:625–630
125. Pretula J, Penczek S (1990) High-molecular-weight poly(alkylene phosphonate)s by condensation of dialkylphosphonates with diols. Makromol Chem 191:671–680
126. Pretula J, Penczek S (1988) Poly(ethylene glycol) ionomers with phosphate diester linkages. Makromol Chem Rapid Commun 9:731–737
127. Penczek S, Pretula J (1993) High-molecular-weight poly(alkylene phosphates) and preparation of amphiphilic polymers thereof. Macromolecules 26:2228–2233
128. Tzevi R, Todorova G, Kossev K, Troev K, Georgiev EM, Roundhill DM (1993) Immobilization of bioactive substances on poly(alkylene phosphate)s, 1. Immobilization of 2-phenylethylamine. Makromol Chem 194:3261–3269
129. Pretula J, Kaluzynski K, Szymanski R, Penczek S (1997) Preparation of poly(alkylene H-phosphonate)s and their derivatives by polycondensation of diphenyl H-phosphonate with diols and subsequent transformations. Macromolecules 30:8172–8176
130. Wang J, Zhuo R (1999) Synthesis and characterization of phosphoester linkage-containing hydrogels. Eur Polym J 35:491–497
131. Georgieva R, Tsevi R, Kossev K, Kusheva R, Balgjiska M, Petrova R, Tenchova V, Gitsov I, Troev K (2002) Immobilization of aminothiols on poly(oxyalkylene phosphates). Formation of poly(oxyethylene phosphates)/cysteamine complexes and their radioprotective efficiency. J Med Chem 45:5797–5801
132. Troev K, Tsatcheva I, Koseva N, Georgieva R, Gitsov I (2007) Immobilization of aminothiols on poly(oxyethylene H-phosphonate)s and poly(oxyethylene phosphate)s—an approach to polymeric protective agents for radiotherapy of cancer. J Polym Sci A Polym Chem 45:1349–1363
133. Stanimirov S, Vasilev A, Haupt E, Petkov I, Deligeorgiev T (2009) Synthesis and spectral properties of novel fluorescent poly(oxyethylene phosphate) tris(β-diketonate) europium (III) complexes. J Fluoresc 19:85–95
134. Gitsov I, Johnson FE (2008) Synthesis and hydrolytic stability of poly(oxyethylene-H-phosphonate)s. J Polym Sci A Polym Chem 46:4130–4139
135. Kraicheva I, Bogomilova A, Tsacheva I, Momekov G, Momekova D, Troev K (2010) Synthesis, NMR characterization and in vitro cytotoxicity evaluation of new poly (oxyethylene aminophosphonate)s. Eur J Med Chem 45:6039–6044
136. D-A W, Williams CG, Li Q, Sharma B, Elisseeff JH (2003) Synthesis and characterization of a novel degradable phosphate-containing hydrogel. Biomaterials 24:3969–3980
137. Troev KD (2012) Polyphosphoesters. Elsevier, Oxford
138. Nathan A, Bolikal D, Vyavahare N, Zalipsky S, Kohn J (1992) Hydrogels based on water-soluble poly(ether urethanes) derived from L-lysine and poly(ethylene glycol). Macromolecules 25:4476–4484
139. Nathan A, Zalipsky S, Ertel SI, Agathos SN, Yarmush ML, Kohn J (1993) Copolymers of lysine and polyethylene glycol: a new family of functionalized drug carriers. Bioconjugate Chem 4:54–62
140. Nathan A, Zalipsky S, Kohn J (1994) Strategies for covalent attachment of doxorubicin to poly(PEG-Lys), a new water-soluble poly(ether urethane). J Bioact Compat Polym 9:239–251
141. Huang S-Y, Pooyan S, Wang J, Choudhury I, Leibowitz MJ, Stein S (1998) A polyethylene glycol copolymer for carrying and releasing multiple copies of Cysteine-containing peptides. Bioconjugate Chem 9:612–617

142. Liu X-M, Thakur A, Wang D (2007) Efficient synthesis of linear multifunctional poly (ethylene glycol) by copper(I)-catalyzed huisgen 1,3-dipolar cycloaddition. Biomacromolecules 8:2653–2658
143. Liu X-M, L-d Q, Tian J, Laquer FC, Ciborowski P, Wang D (2010) Syntheses of click PEG-dexamethasone conjugates for the treatment of rheumatoid arthritis. Biomacromolecules 11:2621–2628
144. Sarkar D, Lopina ST (2007) Oxidative and enzymatic degradations of l-tyrosine based polyurethanes. Polym Degrad Stab 92:1994–2004
145. Fu H, Gao H, Wu G, Wang Y, Fan Y, Ma J (2011) Preparation and tunable temperature sensitivity of biodegradable polyurethane nanoassemblies from diisocyanate and poly(ethylene glycol). Soft Matter 7:3546–3552
146. Sun X, Gao H, Wu G, Wang Y, Fan Y, Ma J (2011) Biodegradable and temperature-responsive polyurethanes for adriamycin delivery. Int J Pharm 412:52–58
147. Lundberg P, Lee BF, van den Berg SA, Pressly ED, Lee A, Hawker CJ, Lynd NA (2012) Poly [(ethylene oxide)-co-(methylene ethylene oxide)]: a hydrolytically degradable poly(ethylene oxide) platform. ACS Macro Lett 1:1240–1243
148. Chan TH, Ong BS (1978) Chemistry of allene oxides. J Org Chem 43:2994–3001
149. Lo W-J, Wu Y-J, Lee Y-P (2002) Isomers of S_2O: Infrared absorption spectra of cyclic S_2O in solid Ar. J Chem Phys 117:6655–6661
150. Lo W-J, Wu Y-J, Lee Y-P (2003) Ultraviolet absorption spectrum of cyclic S_2O in solid Ar. J Phys Chem A 107:6944–6947
151. Nagahara H, Kagawa K, Iwaisako T, Masamoto J (1995) Initiation mechanism of the copolymerization of 1,3,5-trioxane and ethylene oxide. Ind Eng Chem Res 34:2515–2519
152. Nagahara H, Kagawa K, Hamanaka K, Yoshida K, Iwaisako T, Masamoto J (2000) Acetal copolymer from the copolymerization of trioxane and ethylene oxide. Ind Eng Chem Res 39:2275–2280
153. Yamasaki N, Kanaori K, Masamoto J (2001) Analysis of ethylene oxide sequences of the acetal copolymer from trioxane and ethylene oxide. J Polym Sci A Polym Chem 39:3239–3245
154. Shenoi RA, Narayanannair JK, Hamilton JL, Lai BFL, Horte S, Kainthan RK, Varghese JP, Rajeev KG, Manoharan M, Kizhakkedathu JN (2012) Branched multifunctional polyether polyketals: variation of ketal group structure enables unprecedented control over polymer degradation in solution and within cells. J Am Chem Soc 134:14945–14957
155. Shenoi RA, Lai BFL, Imran ul-haq M, Brooks DE, Kizhakkedathu JN (2013) Biodegradable polyglycerols with randomly distributed ketal groups as multi-functional drug delivery systems. Biomaterials 34:6068–6081
156. Binauld S, Stenzel MH (2013) Acid-degradable polymers for drug delivery: a decade of innovation. Chem Commun 49:2082–2102
157. Wike-Hooley JL, Haveman J, Reinhold HS (1984) The relevance of tumour pH to the treatment of malignant disease. Radiother Oncol 2:343–366
158. Tannock IF, Rotin D (1989) Acid pH in tumors and its potential for therapeutic exploitation. Cancer Res 49:4373–4384
159. Roldo M, Barbu E, Brown JF, Laight DW, Smart JD, Tsibouklis J (2007) Azo compounds in colon-specific drug delivery. Expert Opin Drug Deliv 4:547–560
160. Yu C, Kohn J (1999) Tyrosine-PEG-derived poly(ether carbonate)s as new biomaterials: Part I: synthesis and evaluation. Biomaterials 20:253–264
161. Yu C, Mielewczyk SS, Breslauer KJ, Kohn J (1999) Tyrosine-PEG-derived poly(ether carbonate)s as new biomaterials: Part II: study of inverse temperature transitions. Biomaterials 20:265–272
162. Lendlein A, Sisson A (eds) (2011) Handbook of biodegradable polymers: synthesis, characterization and applications. Wiley-VCH, Weinheim

Adv Polym Sci (2013) 262: 191–238
DOI: 10.1007/12_2013_248

Published online: 6 November 2013

Chain-Growth Condensation Polymerization for Controlled Synthesis of Polymers

Yoshihiro Ohta and Tsutomu Yokozawa

Abstract Typical condensation polymerization is classified as a step-growth polymerization, in which the molecular weight of polymer obtained is difficult to control and the molecular weight distribution theoretically approaches 2 at high conversion. However, the mechanism of condensation polymerization of some monomers has been converted from step-growth to chain-growth by means of activation of the polymer end group by changing substituent effects between the monomer and the polymer, and activation of the polymer end group by intramolecular transfer to it of the catalyst. In this review, we describe the development of chain-growth condensation polymerization (CGCP) through the substituent effect and by catalyst transfer. Furthermore, construction of well-defined polymer architectures, such as block copolymers, star polymers, and graft copolymers by utilizing CGCP is also presented.

Keywords Catalyst-transfer · Chain-growth condensation polymerization · Living polymerization · Polycondensation · π-Conjugated polymers

Contents

Y. Ohta and T. Yokozawa (✉)
Department of Material and Life Chemistry, Kanagawa University, Rokkakubashi, Kanagawa-ku, Yokohama 221-8686, Japan
e-mail: yokozt01@kanagawa-u.ac.jp

Abbreviations

acac	Acetylacetonate
AIBN	2,2'-Azobis(isobutyronitrile)
ATRC	Atom transfer radical coupling
ATRP	Atom transfer radical polymerization
Boc	*tert*-Butoxycarbonyl
CGCP	Chain-growth condensation polymerization
cod	1,5-Cyclooctadiene
DBU	1,8-Diazabicyclo[5.4.0]undec-7-ene
DFT	Density functional theory
DMSO	Dimethyl sulfoxide
dppb	1,4-Bis(diphenylphosphino)butane
dppe	1,2-Bis(diphenylphosphino)ethane
dppf	1,1′-Bis(diphenylphosphino)ferrocene
dppp	1,3-Bis(diphenylphosphino)propane
DSC	Differential scanning calorimetry
GPC	Gel-permeation chromatography
HBPA	Hyperbranched polyamide
HPLC	High-performance liquid chromatography
HT	Head-to-tail
I effect	Inductive effect
LCST	Lower critical solution temperature
LiHMDS	Lithium 1,1,1,3.3.3-hexamethyldisilazide
MALDI-TOF	Matrix-assisted laser desorption ionization time-of-flight
MALLS	Multi-angle laser light scattering
MBAA	*N*,*N*'-Methylenebisacrylamide
MM	Macromonomer
NMP	Nitroxide-mediated polymerization
OOB	4-Octyloxybezyl
P3HT	Poly(3-hexylthiophene)

PEG	Poly(ethylene glycol)
R effect	Resonance effect
RAFT	Reversible addition-fragmentation chain transfer
SEM	Scanning electron microscopy
TEG	Tri(ethylene glycol)
TEM	Transmission electron microscopy
TFA	Trifluoroacetic acid
THF	Tetrahydrofuran
XPS	X-ray photoelectron spectroscopy
XRD	Powder X-ray diffraction

1 Introduction

Condensation polymerization is an important method of polymerization that yields not only engineering plastics such as polyamides, polyesters, and polyimides but also π-conjugated polymers, which have recently received considerable attention with the development of the information technology industry. Generally, polycondensation proceeds in a step-growth polymerization manner, in which condensation reactions between molecules of all degrees of polymerization occur. In the absence of side reactions or cyclization, the average degree of polymerization can be estimated according to the theory established by Carothers [1] and Flory [2], and the molecular weight distribution (M_w/M_n) approaches a value of 2. It has been difficult to synthesize condensation polymers having controlled molecular weight with a narrow molecular weight distribution via step-growth polymerization. To synthesize a polymer with controlled molecular weight and low polydispersity, the polymerization should start from an initiator unit and proceed via chain-growth polymerization without disproportionation or termination. This is the case for so-called living polymerization. Since the discovery of anion living polymerization by Szwarc in 1956 [3], many kinds of living polymerizations have been developed and used to synthesize well-defined polymers with controlled molecular weight and a narrow molecular weight distribution. These polymerization methods have also afforded polymer architectures, such as block and graft copolymers, as well as star polymers, which could construct self-assembled supramolecular architectures with defined shapes and properties. In general, however, living polymerization had been applicable only to addition polymerization of vinyl monomers and exothermic ring-opening polymerization of cyclic monomers, not to polycondensation and polyaddition. If the mechanism of condensation polymerization could be converted from step-growth to chain-growth, living condensation polymerization would be possible.

In condensation polymerization of AB monomers, the chain-growth mechanism could be involved in the following two cases: (1) A change in the effect of the substituent ("change of the substituent effect") induced by bond formation of monomers with initiator and polymer chain end drives the reactivity of the polymer

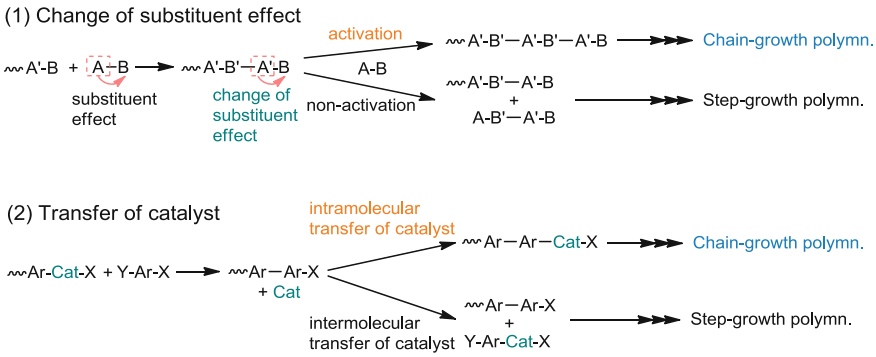

Scheme 1 General scheme of chain-growth condensation polymerization via (*1*) change of substituent effect and (*2*) transfer of catalyst; *Ar* aryl group, *X* halide, *Y* metal

end group to become higher than that of the monomer (Scheme 1(1)). (2) In condensation polymerization based on a coupling reaction with a transition metal catalyst, the catalyst is intramolecularly transferred to and activates the elongated polymer end group after the coupling reaction of the monomer with the polymer (Scheme 1(2)). In this review, we describe chain-growth condensation polymerization (CGCP) by these two approaches and its application to polymer architectures.

2 Early Work

One way to achieve selective reaction of a monomer with the polymer end group is the enhancement of reactivity of the polymer end group by the change of the substituent effect induced by bond formation of the monomer. Aromatic monomers having a nucleophilic site and an electrophilic site at the *para* position are susceptible to the change of the substituent effect through the resonance effect. There are some reports of such selective, though not predominant, reactions of monomers with polymer end groups. For example, Lenz investigated the condensation polymerization of a series of metal *p*-halothiophenoxides and found the amount of unreacted monomer to be higher than predicted from reaction conversion based on Flory's statistical treatment, in which all functional groups of monomer and polymer are of equal reactivity (Scheme 2) [4]. This indicates that the substitution of the halogen atoms on the polymer end groups occurs faster than the substitution of the halogen atoms on the monomers. The enhancement of the reactivity of the polymer end group was attributed to the weaker electron-donating ability of the sulfide linkage in the polymer, as compared to the strong electron-donating ability of the thiophenoxide anion in the monomer. Lenz termed this effect preferential polymer formation. However, the molecular weight and polydispersity of the polymers were not measured, probably because the poly(phenylene sulfide) obtained was insoluble in familiar organic solvents.

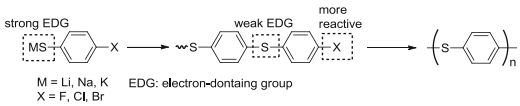

Scheme 2 Polymerization of metal *p*-halothiophenoxides

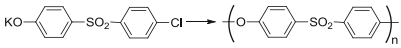

Scheme 3 Polymerization of chlorophenylsulfonyl phenoxide

Scheme 4 Polymerization of potassium salt of 4-fluoro-4′-hydroxybenzophenone

In the condensation polymerization of chlorophenylsulfonyl phenoxide, increased reactivity of the polymer end group was demonstrated by the relation between conversion and reaction time (Scheme 3). Furthermore, comparison of the rate constants for the displacement of chlorine atoms with hydroxide showed that a model of the polymer end group reacted 20 times faster than the monomer. Thus, the electronic effects of a substituent in one ring were transmitted to the other via the sulfone linkage [5].

The rate constant of the polymerization of a potassium salt of 4-fluoro-4′-hydroxybenzophenone was calculated by using linear free energy relationships based on the rate constants of the reaction of substituted 4-halogenobenzophenones with the potassium salts of substituted 4-hydroxybenzophenones (Scheme 4) [6, 7]

According to this calculation, the rate constant of the reaction of the monomer with the polymer was estimated to be tenfold greater than that of the reaction of the monomers with each other. The difference was thought to arise from the deactivating effect of the phenoxide anion in the monomer on nucleophilic substitution in the adjacent ring. In the computer simulation of the variation of the concentration of each molecular species with reaction time, the concentration of the dimer and higher oligomers was always very low in comparison with the slowly decaying monomer concentration. The characteristic aspect of this polymerization is that the first stage of the reaction is very much slower than all later stages. Hence, as soon as the dimer is formed, the other polymeric species are formed rapidly from it. This means that the n-mer is formed mainly by the reaction of the $(n - 1)$-mer with the monomer, that is, by chain-growth polymerization. However, the actual polymerization of this monomer was not reported.

Robello clearly showed that sodium 4-halobenzenesulfinate (**1**) can undergo CGCP and polymerized it in the presence of 4-fluorophenyl sulfone (**2**) as an initiator for a chain-growth polymerization (Scheme 5) [8].

A small amount of **2** served to greatly increase the yield of polymer; in its absence, lower and inconsistent yields of polymer were obtained. This observation

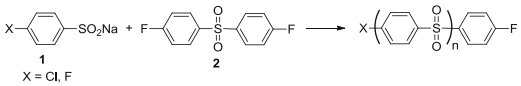

Scheme 5 Polymerization of 4-halobenzenesulfinate (**1**) in the presence of 4,4′-difluorophenyl sulfone (**2**)

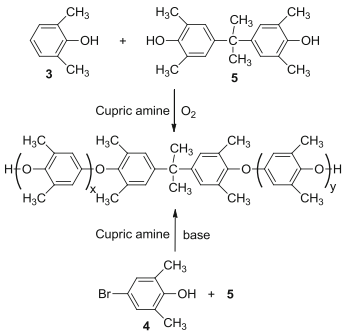

Scheme 6 Oxidative polymerization of 2,6-dimethylphenol (**3**) or 4-bromo-2,6-dimethylphenol (**4**) in the presence of bisphenol **5**

showed that the reaction of two molecules of **1** was very slow, and the reaction of **1** with **2** or with the polymer end group was much faster. However, the polymer that precipitated during the course of the reaction was not soluble; and its molecular weight, as estimated by elemental analysis, was rather low, in contrast to the supposition that the polymerization proceeded by chain polymerization from **2**. The actual polymerization mechanism appeared to be more complicated: step-growth polymerization could occur together with chain-growth polymerization, and chain transfer to the polymer backbone could also occur, both effects resulting in a decreased molecular weight.

Oxidative polymerization of 2,6-dimethylphenol (**3**) or 4-bromo-2,6-dimethylphenol (**4**) has the character of chain-growth polymerization. In the oxidative polymerization of **3** catalyzed by cupric amine complexes, Heitz found that the degree of polymerization of poly(2,6-dimethyl-1,4-phenylene oxide) obtained at low conversion was much higher than expected from the conversion according to Flory's theory [9, 10]. The mole fraction of the oligomers was much lower than that of monomer **3**, indicating that the reactivity of dimer, trimer, and the higher homologues was greater than that of the monomer. This polymerization behavior was attributed to a lower redox potential of the oligomers, compared to that of **3**. This kind of polymerization has been called "reactive intermediate polycondensation". The polymerization of **3** in the presence of diphenol **5**, a bifunctional initiator, was also carried out (Scheme 6). The bifunctional polymer containing the **5** unit and the monofunctional polymer derived from self-polycondensation of **3** were produced in short reaction times. With increasing reaction time, the monofunctional polymer was converted to the bifunctional polymer.

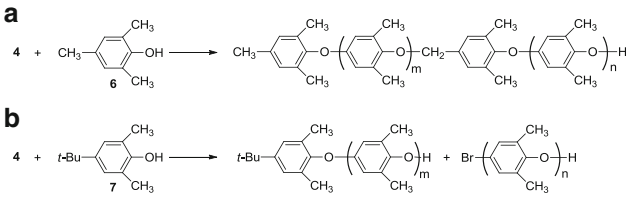

Scheme 7 Phase-transfer catalyzed polymerization of 4-bromo-2,6-dimethylphenol (**4**) in the presence of (**a**) 2,4,6-trimethylphenol (**6**) and (**b**) 4-*tert*-butyl-2,6-dimethylphenol (**7**)

When **4** was used as a monomer, the polymerization proceeded with a base such as potassium *tert*-butoxide to yield a high molecular weight polymer (Scheme 6). Contrary to the oxidative polymerization of **3**, no oxygen was needed for polymer formation, but the bivalent state of copper was necessary. Polymerizations of **4** were also carried out by varying the mole ratio of **5** to yield polymers, the molecular weights of which were in good agreement with the values calculated on the basis of the mole ratio of **4** to **5** ($M_n = 880$–$3{,}900$). The polydispersities were not noted. The low molecular weight fraction characterized by gas chromatography contained monofunctional dimer and trimer formed by **4** itself, without the **5** unit.

Percec also synthesized poly(2,6-dimethyl-1,4-phenylene oxide) by phase-transfer catalyzed polymerization of **4** in the presence of 2,4,6-trimethylphenol **6** as a chain initiator (Scheme 7a) [11].

The polymerization was followed as a function of reaction time. The yields of polymer increased with increasing reaction time and, in contrast to classical step polymerization, the molecular weight of polymer increased rapidly at the beginning of polymerization. The molecular weight and polydispersity of the resulting polymer increased with increasing **4**:**6** mole ratio. With **4**:**6** ratios of 1–5, the M_w/M_n values were 1.14–1.26 for polymer precipitated in methanol. About 18–45% of the structural units derived from **6** were incorporated into the polymer chain as benzyl ether units. These units were formed by α-hydrogen abstraction at the 4-methyl group of 2,4,6-trimethylphenolate. The polymers synthesized with **4**:**6** ratios of 30 and 40 displayed bimodal molecular weight distributions. To suppress the side reaction involving **6**, 4-*tert*-butyl-2,6-dimethylphenol **7** was used instead of **6** (Scheme 7b). The molecular weights of the polymers were controlled from 4,600 to 9,200 by the **4**:**7** ratio, and M_w/M_n was almost constant (1.30–1.42) irrespective of the **4**:**7** ratio. The polymers obtained by using **7** contained structural units derived from **7** only at the chain ends and displayed a monomodal molecular weight distribution, but polymer containing no **7** unit was also produced in a low amount. Other chain initiators were studied for this polymerization, but the molecular weights of the resulting polymers were much higher than calculated values based on a mole ratio of **4**:**6** or **4**:**7** in the feed [12–14].

We realized that monomer **8**, the polymerization of which had been reported by Kricheldorf [15], could undergo an interesting change in the substituent effect during polymerization. Thus, the acyl chloride moiety of **8** would be deactivated by the trimethylsiloxy group of **8** as a strong electron-donating group, whereas the

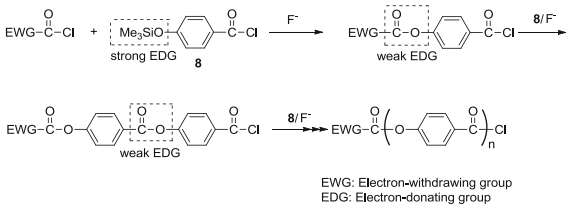

Scheme 8 Proposal of chain-growth condensation polymerization of monomer **8** in the presence of initiator with an electron-withdrawing group

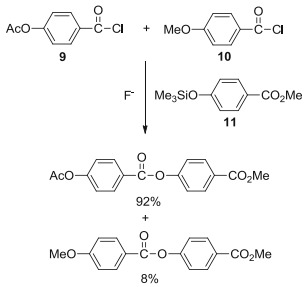

Scheme 9 Model reaction of **11** with 1:1 mixture of **9** and **10**

acyl chloride moiety of the polymer might become more reactive than that of **8** because the ester linkage of the polymer is a weaker electron-donating group than that of the trimethylsiloxy group (Scheme 8). This means that the polymer end group would always be more reactive than the monomer and, thus, would satisfy the requirement for CGCP.

Before attempting polymerization, we performed a model reaction to confirm the difference in the above substituent effects between a monomer and a polymer [16]. We chose **9** as a model of the propagating end, **10** as a model of the acyl group of monomer **8**, and **11** as a model of the nucleophilic site of **8**. When the reaction of **11** with equimolar amounts of **9** and **10** was performed in the presence of fluoride ion at room temperature, **11** reacted selectively with **9** (Scheme 9). The observed selectivity indicated that monomer **8** could undergo CGCP. However, the polymerization of **8** proceeded with concomitant precipitation of polymer, and it was not determined whether CGCP had actually occurred.

A modified monomer in which an octyl group was introduced was prepared to increase the solubility of the polymer, but it was difficult to purify the monomer. Then, the Pd-catalyzed polymerization of 4-bromo-2-octylphenol **12** and carbon monoxide was investigated because this polymerization would afford the same soluble polyester and because insertion of Pd(0) into 4-substituted bromobenzenes had been reported to have similar substituent effects: electron-withdrawing groups enhancing the insertion, and electron-donating groups making the reaction sluggish [17, 18]. The polymerization of **12** and carbon monoxide was carried out in the

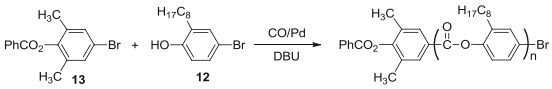

Scheme 10 Polymerization of **12** and carbon monoxide in the presence of initiator **13**, Pd catalyst, and DBU

presence of a Pd catalyst, 1,8-diazabicyclo[5.4.0]undec-7-ene (DBU) as a base, and 4-bromo-2,6-dimethylphenyl benzoate **13** as a chain initiator at 115°C (Scheme 10) [19]. The molecular weight of the polymer obtained increased in proportion to time in the initial stage, and the polymer contained the initiator unit **13**, indicating that CGCP proceeded from **13**. However, the molecular weight gradually decreased in the middle and later stages because the phenoxide of **12** reacted not only with the polymer end group but also with the ester linkage of the polymer backbone (transesterification).

3 CGCP Through the Substituent Effect

3.1 CGCP Through the Resonance Effect

Complete controlled of condensation polymerization by substituent effect-assisted CGCP was first demonstrated in the synthesis of *N*-alkylated poly(*p*-benzamide)s by polymerization of 4-(alkylamino)benzoic acid phenyl esters **14** [20]. Polymerization of phenyl 4-(octylamino)benzoate (**14a**) was carried out in the presence of a base and the initiator **15a**, yielding poly(*p*-benzamide) with a low polydispersity and controlled molecular weight based on the feed ration of **14** to **15a** ($[\mathbf{14}]_0/[\mathbf{15a}]_0$) (Scheme 11).

This polymerization mechanism was explained as follows. Deprotonation of the monomer **14** affords the amide anion **14′**. As shown in the resonance structure of **14′** and **14″**, the strongly electron-donating ability of the amide anion decreases the electrophilicity of the ester carbonyl group at the *para* position. This deactivation suppresses the reaction between the monomers to prevent from step-growth polymerization of **14′**. In the presence of an initiator **15a**, having a reactive ester carbonyl group due to the presence of an electron-withdrawing substituent at the *para* position, **14′** reacts with **15a** to give **16**. Because the amide linkage of **16** is a weakly electron-donating group and does not strongly deactivate the phenyl ester moiety at the *para* position, the ester carbonyl group of **16** has sufficient electrophilicity to react with another **14′**. The polymer propagating group is activated in this manner, and the monomer **14′** reacts selectively with the polymer end to result in chain-growth polymerization.

This polymerization provides not only *N*-alkylated poly(*p*-benzamide)s, but also *N*-unsubstituted ones when the monomer has a removable *N*-alkyl group as a protecting group. Because *N*-unsubstituted poly(*p*-benzamide)s are soluble only

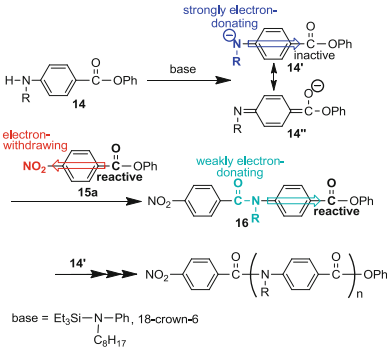

Scheme 11 Proposed polymerization mechanism of chain-growth condensation polymerization of **14**

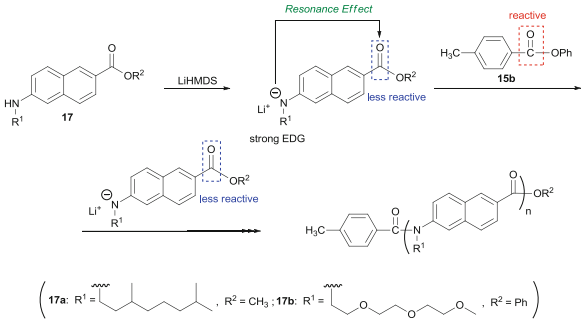

Scheme 12 Synthesis of poly(naphthalenecarboxamide) by chain-growth condensation polymerization of naphthalene monomer **17**

in strong acid and are essentially insoluble in common organic solvents, complete deprotection should be carried out under homogeneous conditions in strongly acidic media. A suitable protecting group is the octyloxybezyl (OOB) group, not only because it can be easily removed by treatment with trifluoroacetic acid (TFA), but also because the octyloxy group enhances the solubility of the protected polymer. If the solubility of the protected polymer is insufficient, control of the condensation polymerization is difficult due to precipitation of the polymer, as in the case of the polymerization of *N*-methoxybenzyl monomer. Polymerization of *N*-OOB monomer gave polyamide with controlled molecular weight and narrow molecular weight distribution. Treatment of the polyamide with TFA resulted in complete removal of the *N*-OOB group from the polyamide [21].

Since resonance effects can work between functional groups not only at the *para* position of benzene, but also at the 1,5- or 2,6-posiotion of naphthalene, we extended the range of monomers, leading to well-defined aromatic polyamides, from benzene monomer to naphthalene monomer (Scheme 12).

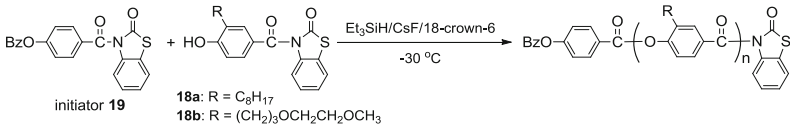

Scheme 13 Synthesis of polyester by chain-growth condensation polymerization of monomer **18**

The polymerization of the methyl ester monomer **17a** bearing a 3,7-dimethyloctyl side chain in the presence of an initiator **15b** and lithium 1,1,1,3,3,3-hexamethyldisilazide (LiHMDS) as a base gave well-defined poly(naphthalenecarboxamide), together with a very small amount of a cyclic trimer, formed by self-condensation of **17a** in the early stage of the polymerization [22]. On the other hand, polymerization of phenyl ester monomer **17b** with the tri(ethylene glycol) (TEG) monomethyl ether side chain yielded poly(naphthalenecarboxamide) with controlled molecular weight in the case of $[\mathbf{17b}]_0/[\text{initiator}]_0 = 10$. Polymerization at higher feed ratio was accompanied by self-condensation to afford polyamides via chain-growth and step-growth polymerization, so that the M_n value of the polymer did not reach the theoretical value. The undesirable self-condensation is accounted for by insufficient deactivation of the electrophilic ester moiety by the electron-donating resonance effect of the amide anion, due to the greater distance between the 2 and 6 positions of the naphthalene ring, in comparison with the corresponding *para*-substituted benzene monomer, which proceeds in CGCP without self-condensation until the feed ratio reaches 100.

To extend the range of application of CGCP of *para*-substituted monomer, the nucleophilic site of the monomer was changed from an amino group to a hydroxyl group. One might think that it would be easy to synthesize well-defined aromatic polyesters, such as poly(4-hydroxybenzoate)s, by CGCP of 4-hydroxybenzoic acid derivatives in a similar manner to that of 4-(alkylamino)benzoic acid derivatives. But, synthesis of well-defined aromatic polyester is more difficult than that of polyamide because polyester easily undergoes transesterification. The monomer can attack the polymer ester linkage to generate a cleaved chain with the phenoxide moiety at one end and the acyl group at the other end, leading to conventional step-growth polycondensation. Actually, transesterification occurred in the condensation polymerization of monomer **18** having an active amide moiety as a good leaving group, even with a weak base such as tertiary amine at room temperature [23]. However, when the polymerization of **18** with initiator **19** was carried out at −30°C with Et_3SiH, CsF, and 18-crown-6 as a base system, transesterification was almost completely suppressed and the molecular weight was controlled up to 7,300 with low polydispersity ($M_w/M_n \leq 1.3$) (Scheme 13) [24].

Substituent effect-assisted CGCP of *para*-substituted monomers are applicable to polymerization of monomer without a carbonyl group. The condensation polymerization of potassium 4-fluorophenolate **20**, which proceeds via aromatic nucleophilic substitution between phenoxide and aryl fluoride, was controlled (Scheme 14).

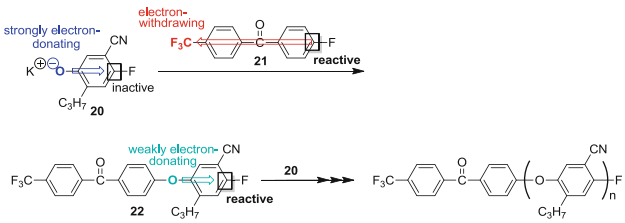

Scheme 14 Synthesis of polyether by chain-growth condensation polymerization of potassium 4-fluorophenolate **20**

The strongly electron-donating ability of the phenoxide of **20** presumably reduces the electrophilicity of the aromatic carbon at the *para*-position. Indeed, **20a** did not polymerize at all in sulfolane at 150°C. When the reaction was carried out in the presence of an initiator **21**, bearing an electron-withdrawing group, **20** reacted with **21** to yield an ether **22**. Because the electron-donating ability of the ether linkage is much weaker than that of phenoxide, the fluorine-connected aromatic carbon of **22** is more reactive than that of **20**, resulting in reaction of **22** with the next monomer. The activation of the aromatic carbon was supported by the lower-field shift of the fluorine signal of **22** in the ^{19}F NMR spectra. The molecular weight of the obtained polyether was controlled by the feed ratio of **20** to **21** up to $M_n = 3{,}600$, with a M_w/M_n ratio of less than 1.1, indicating that polymerization of **20** with **21** proceeds in a chain-growth polymerization manner [25]. Polyether of higher molecular weight was not soluble in the polymerization solvent, and could not be synthesized in a controlled manner. It is interesting that the polyether with low polydispersity from CGCP was more crystalline than the product with broad molecular weight distribution from conventional step-growth condensation polymerization. The powder X-ray diffraction (XRD) pattern of the former was more intense, and the differential scanning calorimetry (DSC) profile showed an exothermic peak at 172°C (cold crystallization) on heating from the glassy state. This implies that the crystallinity of condensation polymers may be controlled by polydispersity [26].

Kim and coworkers conducted CGCP of monomers **23a** and **23b**, in which the trifluoromethyl group works as an electron-withdrawing group and increases solubility of polymer (Scheme 15) [27, 28]. Polymerization of **23a** afforded polyether with $M_n \approx 4{,}000$ and $M_w/M_n < 1.2$. When 4-nitro-3-(trifluoromethyl)benzonitrile was used as an initiator, the polymerization did not proceed in a controlled manner. The cyano group at the *para*-position of the nitro group as a leaving group is so strong as an electron-withdrawing group that transetherification at the ether linkage was likely to occur. The polymerization of **23b** was carried out in the presence of 2-(trifluoromethyl)-4-nitrobenzonitrile as an initiator bearing two electron-with drawing groups at 70°C to yield poly(arylene ether azobenzene) with $M_n = 2{,}000$ and $M_w/M_n = 1.09$. Attempts to increase the molecular weight to more than 5,000 were similarly difficult due to transetherification. The reactivity of initiators with one electron-withdrawing group was too low to initiate the polymerization even at 80°C, at which self-initiated condensation polymerization of **23b** occurred.

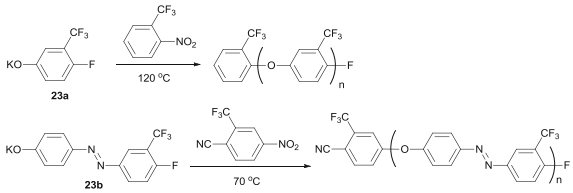

Scheme 15 Synthesis of polyether by chain-growth condensation polymerization of **23a** and **23b**

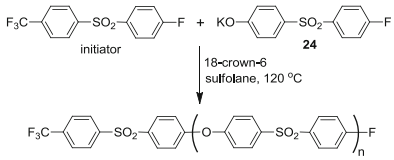

Scheme 16 Synthesis of poly(ether sulfone) by chain-growth condensation polymerization of **24**

Polyether synthesis was applied to prepare a well-defined poly(ether sulfone) by polymerization of **24** (Scheme 16), although the kinetics of polymerization of the chloro-counterpart had been studied earlier. In the polymerization of **24** in the presence of an initiator and 18-crown-6 in sulfolane at 120°C, the molecular weight was controlled up to 5,700, and the molecular weight distribution was less than 1.5 [29]. When the polymerization was carried out at higher feed ratio of monomer to initiator, both chain-growth and step-growth polymerization occurred. The undesirable step-growth polymerization was caused by transetherification of the backbone ether linkage with the monomer and/or fluoride, an effect that is common in the poly(ether sulfone) polycondensation at high temperature. Similar CGCP in the case of poly(ether ketone) has been reported [30].

3.2 CGCP Through the Inductive Effect

In the CGCP of *para*-substituted monomers, the anionic nucleophilic site deactivates the electrophilic site on the *para*-position through the resonance effect (+*R* effect), resulting in suppression of self-condensation of the monomer but selective reaction with an initiator and the propagating end, leading to chain-growth polymerization. If this polymerization method can be applied to the condensation polymerization of *meta*-substituted monomers, well-defined aromatic polymers with higher solubility compared to that of *para*-substituted aromatic polymers are formed. However, one might think that it would be difficult, because the anionic nucleophilic site of the monomer never deactivates the electrophilic site on the *meta*-position through the +*R* effect, and there is little possibility of deactivation through the inductive effect (+*I* effect). However, the acidity of benzoic acid

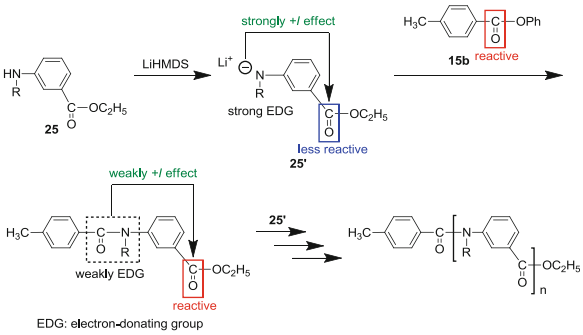

Scheme 17 Proposed polymerization mechanism of chain-growth condensation polymerization of **25**

derivatives shows that the –*I* effect of the *m*-nitro group, a strong electron-withdrawing substituent, is as strong as the –*R* effect of the *p*-nitro group: pK_a of *m*-nitrobenzoic acid is 3.45, and that of *p*-nitrobenzoic acid is 3.44 [31]. Therefore, the strong electron-donating nucleophilic site is expected to show a +*I* effect on the reactivity of the electrophilic site at the *meta*-position as strong as the *R* effect, resulting in suppression of self-condensation of the monomer in a similar manner to the CGCP of *para*-substituted monomers. Indeed, polymerization of ethyl 3-(alkylamino)benzoate **25** was conducted in the presence of LiHMDS as the base and phenyl 4-methylbenzoate **15b** as the initiator in THF at 0°C to obtain *N*-alkylated poly(*m*-benzamide)s with well-defined molecular weight and low polydispersities ($M_w/M_n \leq 1.1$) (Scheme 17) [32].

In this polymerization, the aminyl anion of **25′** deactivates the acyl group at the *meta*-position through the strong +*I* effect, resulting in suppression of the self-polycondensation of **25′**. The aminyl anion of **25′** then selectively reacts with initiator and the polymer chain end, the acyl group of which is more reactive than that of **25′**, and growth continues in a chain-growth polymerization manner. To support this mechanism, density functional theory (DFT) calculations were performed. The activation energies for the propagation and self-condensation were 21.6 and 27.0 kcal/mol, respectively. On the basis of the geometries, energies, and vibrational frequencies obtained, the theoretical rate constants were then evaluated at 298.15 K and 1 atm. The reaction rate constant (1.1×10^{-3} s^{-1}) for the propagation is 8.6×10^{-3}-fold greater than that for the self-condensation (1.3×10^{-7} s^{-1}) and, hence, is consistent with the experimental finding that propagation was observed exclusively over self-condensation; that is, CGCP of *meta*-substituted aminobenzoic ester monomers proceeded.

Poly(*m*-benzamide)s with a variety of *N*-substituents were synthesized [33, 34]. They showed higher solubility than the corresponding *para*-substituted counterparts. Poly(*m*-benzamide)s having an *N*-oligo(ethylene glycol) chain are soluble in water, and the aqueous solution showed reversible clouding on heating. For poly (*m*-benzamide)s with an *N*-TEG chain, a phase separation occurred at around 55°C, where the solubility of the polymers sharply altered. In contrast, the phase

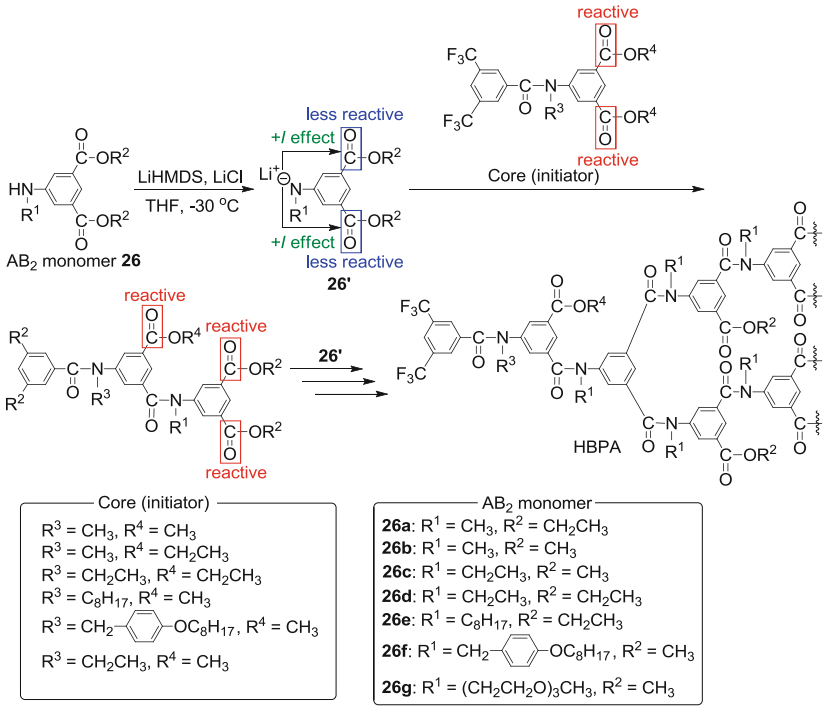

Scheme 18 Proposed polymerization mechanism of chain-growth condensation polymerization of AB_2 monomer **26**

separation of poly(*m*-benzamide)s with a *N*-tetra(ethylene glycol) chain gradually occurred between 58 and 72°C, i.e., a higher temperature than that of poly(*m*-benzamide)s with the *N*-TEG chain. The temperature-dependent phase separation process of each polymer was actually reversible, but a hysteresis on temperature ($\Delta T > 1.5$°C) was observed during heating and cooling cycles (± 0.5°C min^{-1}) [34].

On the basis of the above successful CGCP of *meta*-substituted monomer, the aminyl anion of 5-(methylamino)isophthalic acid ethyl ester **26a** as an AB_2 monomer would also deactivate both the ester moieties through the inductive effect to suppress self-polymerization of the anion of **26′**, leading to chain-growth polymerization of AB_2 monomer (Scheme 18).

Thus, the monomer **26a** was polymerized with LiHMDS as a base in the presence of a core initiator and LiCl at −30°C to yield hyperbranched polyamide (HBPA) with narrow molecular weight distribution ($M_w/M_n \leq 1.14$) and a degree of branching of about 0.5. The matrix-assisted laser desorption ionization time-of-flight (MALDI-TOF) mass spectra showed that all HBPAs with different molecular weights contained the initiator unit. The M_n value of HBPA increased linearly in proportion to the ratio of $[\mathbf{26a}]_0/[\text{initiator}]_0$ up to 40,000, while the M_w/M_n ratio remained at 1.14 or less. Therefore, the polymerization of **26a** proceeds through a chain-growth polymerization mechanism from the initiator without side reaction

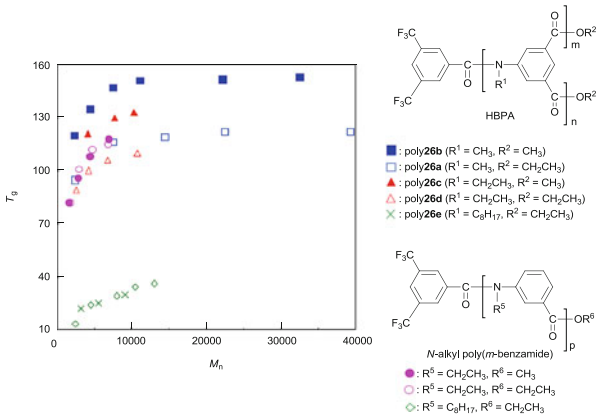

Fig. 1 T_g of hyperbranched polyamides (plane) and linear *N*-alkyl poly(*m*-benzamide)s as a function of M_n

[35]. The CGCP of other AB_2 monomers with *N*-ethyl, octyl, OOB, and TEG groups afforded the corresponding well-defined HBPAs [36, 37]. HBPA with the *N*-OOB group was converted to unsubstituted *N*-H HBPA with low polydispersity by treatment with TFA. Since all HBPAs possess well-controlled molecular weight and low polydispersity, we can evaluate precisely the molecular weight dependency of the glass transition temperature, T_g (Fig. 1).

The T_g values of HBPAs increased with increasing molecular weight up to 10,000, and the T_g values of *N*-methyl HBPAs (poly**26b** and poly**26a**) leveled off when the M_n value was higher than about 20,000. When we compared the T_g values of *N*-methyl HBPA and *N*-ethyl HBPA with similar M_n and the same terminal ester alkyl groups (methyl ester HBPAs: poly**26b** versus poly**26c**; ethyl ester HBPAs: poly**26a** versus poly**26d**), the T_g value of *N*-methyl HBPAs was about 15°C higher than that of *N*-ethyl HBPAs. The T_g value of *N*-octyl HBPA was as low as 30°C or less, being about 80°C lower than that of *N*-ethyl HBPA (poly**26e** vs. poly**26d**). On the other hand, when we compared the T_g values of the methyl ester and ethyl ester HBPAs with similar M_n and the same *N*-alkyl groups (*N*-methyl HBPAs: poly**26b** versus poly**26a**; *N*-ethyl HBPAs: poly**26c** versus poly**26d**), the T_g value of the methyl ester HBPAs is about 25°C higher than that of the ethyl ester HBPAs. These results suggest that the T_g of HBPA is more influenced by the terminal ester alkyl group than by the *N*-alkyl group. We also compared the T_g of *N*-ethyl and octyl HBPAs with those of the corresponding linear *N*-alkyl poly(*m*-benzamide)s. The T_g values of *N*-ethyl poly(*m*-benzamide)s are intermediate between the T_g values of *N*-ethyl HBPA with the methyl ester terminal groups and the ethyl ester counterpart. Meanwhile, the T_g values of *N*-octyl HBPA and *N*-octyl poly(*m*-benzamide) are identical, implying that the T_g values of aromatic polyamides with long *N*-alkyl groups are not affected by the polymer topology [36].

Surface segregation of a variety of *N*-substituted HBPAs in a linear polystyrene matrix after annealing of the blend films was also studied by means of X-ray photoelectron spectroscopy (XPS) [38]. When two polymers with a similar degree

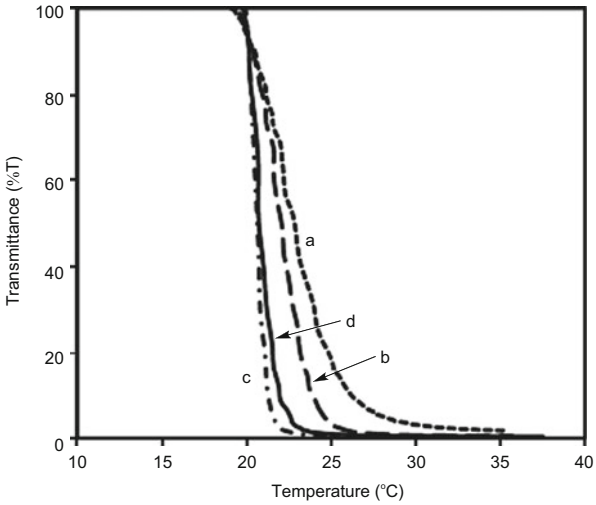

Fig. 2 Transmittance versus temperature curves (500 nm, 0.5°C/min) obtained for 0.25 wt% aqueous solutions of HBPA bearing a TEG chain (*curve a* $M_n = 3{,}810$, $M_w/M_n = 1.15$; *curve b* $M_n = 6{,}760$, $M_w/M_n = 1.15$; *curve c* $M_n = 12{,}900$, $M_w/M_n = 1.11$; *curve d* $M_n = 18{,}600$, $M_w/M_n = 1.19$)

of polymerization are mixed, a lower surface energy component is enriched at the surface. The molecular weight disparity between the components also causes the surface segregation of a smaller component. The latter can be explained in terms of less conformational or translational entropic penalty for the shorter chain at the surface, in addition to the surface localization of chain end groups. If chain ends have a smaller surface energy than the repeating unit, they act as buoys. Thus, when hyperbranched polymer is mixed into a liner polymer, hyperbranched polymer is partitioned to the surface because of the buoys. In addition, the chain dimension of hyperbranched polymer is smaller than that of a liner polymer with comparable molecular weight. This also leads to the surface segregation of hyperbranched polymer in a matrix polymer. When *N*-octyl, ethyl, and methyl HBPAs were compared, the extent of segregation was in this order. This is probably because HBPA with a shorter alkyl side chain can form aggregates, leading to an increase in apparent molecular weight. It is entropically unfavorable for such aggregates to be segregated at the surface.

HBPA bearing a *N*-TEG chain was soluble in water, and a 0.25 wt% aqueous solution of the HBPA exhibited a lower critical solution temperature (LCST) [37]. Phase separation of the HBPA with low molecular weight ($M_n = 3{,}810$, $M_w/M_n = 1.15$) gradually occurred between 19 and 35°C, whereas the solubility of the HBPA with higher molecular weight ($M_n = 12{,}900$, $M_w/M_n = 1.11$; $M_n = 18{,}600$, $M_w/M_n = 1.19$) sharply altered between 20 and 25°C. This result indicated that the thermotransition of the HBPA in aqueous solution becomes sharper with increasing molecular weight until the molecular weight exceeds a certain value. The cloud point was 21–23°C, which was about 30°C lower than that of the corresponding poly(*m*-benzamide) with the *N*-TEG unit (Fig. 2).

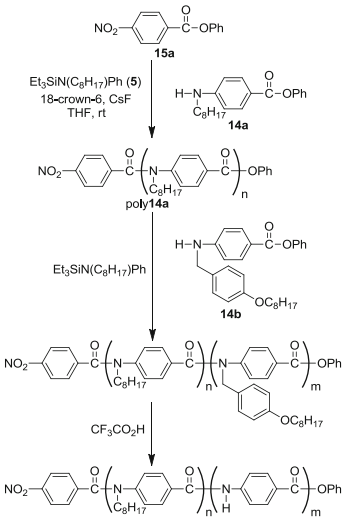

Scheme 19 Synthesis of block copolymer of *N*-alkyl and *N*-H poly(*p*-benzamide)s

4 Polymer Architecture Using CGCP Through the Substituent Effects

4.1 Block Copolymer

Development of condensation polymerization with the character of living polymerization enables condensation polymer architectures to be produced in a similar way to those attained by living polymerization of vinyl and cyclic monomers.

Block copolymers of aromatic polyamides have been synthesized by CGCP of 4-(alkylamino)benzoic acid esters **14**. An example is the block copolymer of *N*-alkyl and *N*-H polyamides shown Scheme 19.

First, *N*-octyl monomer **14a** was polymerized, and then monomer **14b**, with a protecting group on the amino group, and a base were added to the reaction mixture. The added **14b** polymerized smoothly from the ends of the poly**14a** chains to yield the block copolymer of poly**14a** and poly**14b**. The protecting group was quantitatively removed with TFA to afford the desired block copolymer of *N*-alkyl and *N*-H polyamides with narrow molecular weight distribution [21]. The reason **14b** was used for this block copolymerization was that a monomer with a primary amino group did not polymerize under the polymerization conditions [39]. The block copolymer self-assembled in THF by virtue of intermolecular hydrogen bonding of the *N*-H polyamide unit. Scanning electron microscopy (SEM) images showed micrometer-sized bundles and aggregates of flake-like structures. Block copolymers of *N*-octyl- and *N*-fluoroalkyl polyamides with low polydispersity were also synthesized and their self-assembly was studied [40, 41]. Block copolymers consisting of aromatic

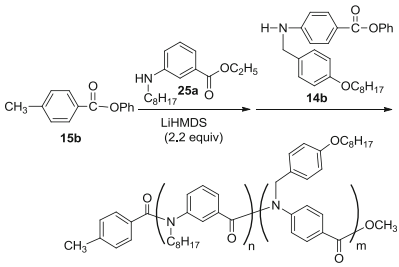

Scheme 20 Synthesis of block copolymer of poly(*m*-benzamide) and poly(*p*-benzamide)

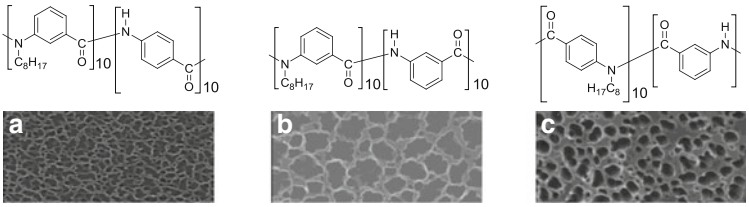

Fig 3 SEM images of (**a**) dried CH_2Cl_2 gel at 5 wt% of diblock copolymer and (**b**, **c**) structures after drying 5 wt% solution of diblock copolymer in CH_2Cl_2

polyamides with different substitution positions were also synthesized by means of sequential CGCP of *N*-alkyl and *N*-OOB monomer (Scheme 20) [42].

In the synthesis of block copolymers of *meta*- and *para*-substituted aromatic polyamides, the *meta*-substituted monomer was first polymerized in the presence of an initiator and LiHMDS, and then postpolymerization of the *para*-substituted monomer was carried out. The OOB group on the amide nitrogen in the obtained block copolymers was removed with TFA to yield block copolymers containing the *N*-H polyamide segment. The obtained block copolymers showed gelating properties at low concentration in various solvents. The SEM analysis of the dried CH_2Cl_2 gel revealed that the block copolymers self-assembled to form a three-dimensional network structure (Fig. 3). The gelating properties are dependent on the substitution position (*meta*- or *para*-) and the composition ratio of the *N*-H poly(benzamide) segment in these block copolymers. The block copolymer containing *N*-H poly(*p*-benzamide) showed extensive gelating properties in solvents ranging from aromatic to aprotic polar solvents.

Well-defined linear-hyperbranched diblock copolymers were also synthesized by CGCP of methyl 3-(4-octyloxybenzylamino)benzoate **25b** and ethyl 5-(methylamino)isophthalate **26a** (Scheme 21) [35].

There are several reports on the synthesis of block copolymers composed exclusively of rigid or semirigid condensation oligomer or polymer [43–53], and these block copolymers appear to have unique and intriguing characteristics due to strong intermolecular interaction. In general, however, such block copolymers are

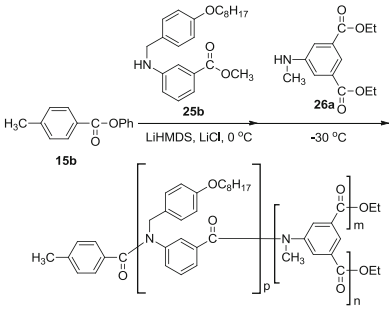

Scheme 21 Synthesis of linear-hyperbranched diblock polyamides

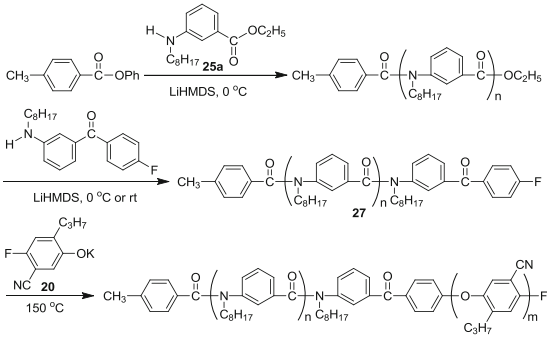

Scheme 22 Synthesis of diblock copolymer of *N*-octyl poly(*m*-benzamide) and aromatic polyether

composed of polymers with a broad molecular weight distribution or oligomers synthesized in a stepwise manner. Synthesis of well-defined diblock condensation copolymer with controlled molecular weight and low polydispersity remains a challenging topic. Diblock copolymers composed poly(*m*-benzamide) and aromatic polyether were synthesized by means of successive CGCP [54]. When an orthogonal initiator for the synthesis of the polyamide and aromatic polyether segments was used, side reactions occurred at the 4-fluorobenzophenone unit of the initiator or the macroinitiator. On the other hand, polymerization of polyamide monomer **25a** with a monofunctional initiator afforded well-defined polyamide, which was subsequently converted to a macroinitiator **27** bearing the terminal 4-fluorobenzophenone unit. Polymerization of polyether monomer **20** in the presence of **27** proceeded in a chain-growth condensation manner from the initiation site of **27** to yield the diblock copolymers of aromatic polyamide and polyether with controlled molecular weight and narrow molecular weight distribution (Scheme 22).

Advantages of polymers obtained by CGCP are not only production of polymer with controlled molecular weight and molecular weight distribution, but also

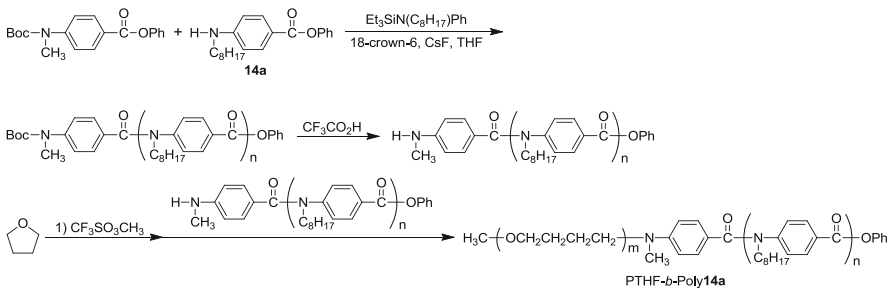

Scheme 23 Synthesis of diblock copolymer of poly(THF) and *N*-octyl poly(*p*-benzamide)

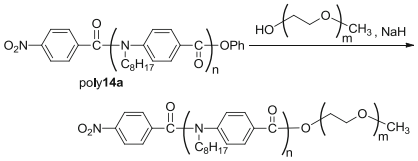

Scheme 24 Synthesis of diblock copolymer of *N*-octyl poly(*p*-benzamide) and PEG

possession of definite end group structures. The end groups of polymers obtained by CGCP are available as the initiation moiety of living anion, cation, and radical polymerization and as the coupling site of radical reactions and condensation reactions. For example, synthesis of block copolymer of polyTHF and polyamide was conducted as shown in Scheme 23). Polyamide with a terminal amino group was prepared by the polymerization of **14a** with an initiator bearing the *tert*-butoxycarbonyl (Boc) group on the amino group, followed by treatment with TFA to remove the Boc group. The terminal amino group of the polymer reacted with living poly(THF) to yield a block copolymer of polyamide and poly(THF). When difunctional living poly(THF) initiated by trifluoromethanesulfonic anhydride was reacted with the above polyamide, polyamide-poly(THF)-polyamide triblock copolymer was produced [55].

Diblock copolymer consisting of poly(ethylene glycol) (PEG) monomethyl ether and polyamide was prepared by the reaction of PEG monomethyl ether with the polyamide, prepared by CGCP of **14a**, in the presence of NaH (Scheme 24). An excess of PEG was used in this polymer reaction, but unreacted PEG could be washed out with water to isolate the block copolymer [39]. Similar reaction of PEG with a polyamide obtained by the CGCP of **14a** with phenyl terephthalate as a bifunctional initiator gave a triblock copolymer PEG-aromatic polyamide-PEG [56].

Diblock copolymer of polystyrene and polyamide was synthesized by the macroinitiator method (Scheme 25). First, polystyrene with a terminal carboxyl group was prepared by anionic living polymerization of styrene, followed by quenching with dry ice, and then the carboxyl group was converted to the phenyl ester by using phenol and a condensation agent. From this terminus, CGCP of **14a**

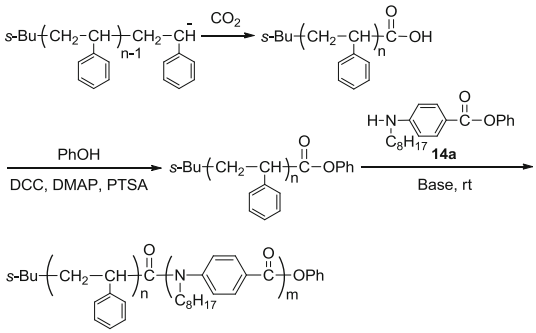

Scheme 25 Synthesis of diblock copolymer of polystyrene and *N*-octyl poly(*p*-benzamide) by chain-growth condensation polymerization of **14a** with polystyrene macroinitiator

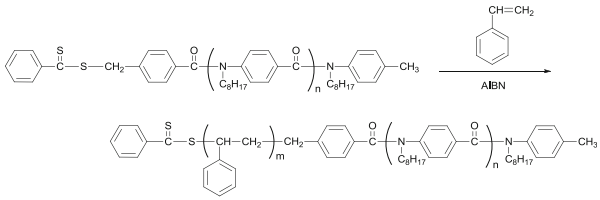

Scheme 26 Synthesis of diblock copolymer of polystyrene and *N*-octyl poly(*p*-benzamide) by RAFT polymerization of styrene with polyamide macro chain transfer agent

was carried out to give the desired block copolymer. When low molecular weight macroinitiators were used, the block copolymers with low polydispersity were obtained in good yields. When high molecular weight macroinitiators were used, the block copolymer was contaminated with the homopolymer of the polyamide. This is probably because the polymer effect of polystyrene decreased the efficiency of initiation from the macroinitiator to induce self-polycondensation of **14a** [57].

Accordingly, the polymer end group of the polyamide was converted to the dithiobenzoate moiety, and reversible addition-fragmentation chain transfer (RAFT) polymerization of styrene was carried out in the presence of this polyamide as a macro-chain transfer agent to yield well-defined diblock copolymer consisting of aromatic polyamide and polystyrene with high molecular weight (Scheme 26) [58].

A macroinitiator of aromatic polyamide for atom transfer radical polymerization (ATRP), which is more easily synthesized than the chain transfer agent for the RAFT polymerization, was also effective for the synthesis of block copolymer of aromatic polyamide and polystyrene with high molecular weight (Scheme 27) [59].

Diblock copolymer of polystyrene and aromatic polyether was also synthesized by CGCP of ether monomer **20** with orthogonal initiator, which was composed by both the initiation site of CGCP and that of ATRP, followed by ATRP of styrene [60]. During study of ATRP of styrene from polyamide macroinitiator, we discovered styrene-assisted atom transfer radical coupling (ATRC) from methacrylic

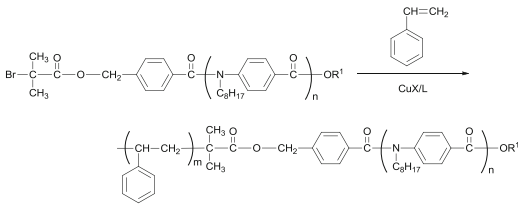

Scheme 27 Synthesis of diblock copolymer of polystyrene and *N*-octyl poly(*p*-benzamide) by ATRP of styrene with polyamide macroinitiator

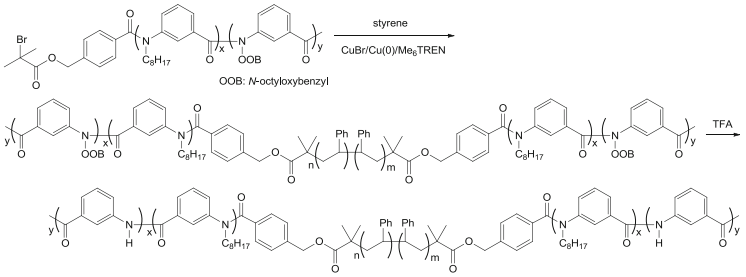

Scheme 28 Synthesis of ABA-type triblock polybenzamide by ATRC

macroradicals at low temperature, and applied this chemistry to synthesis of ABA-type triblock polybenzamides [61]. Thus, couplings of high molecular weight AB-type diblock polybenzamide, 2-bromoisobutyryl-terminated poly(*N*-OOB-*m*-benzamide)-*b*-poly(*N*-octyl-*m*-benzamide), were conducted to yield ABA-type triblock polybenzamides with high coupling efficiency (>94%). The molecular weight was doubled and a narrow molecular weight distribution ($M_w/M_n < 1.18$) was maintained. Selective removal of the OOB groups was achieved, resulting in a poly(*N*-H-*m*-benzamide) segment (i.e., A block) (Scheme 28). Thermal transitions of the diblock and triblock polybenzamides were examined by DSC. In the case of triblock polybenzamides, the T_g value shifted from 45 to 62°C after removal of the OOB groups; this might be ascribed to a confinement effect of the segments at the extremities via strong intermolecular hydrogen-bonding interaction.

Synthesis of well-defined, amphiphilic linear-hyperbranched block copolymer composed of PEG and HBPA was carried out by the condensation reaction [62]. HBPA with a hydroxyl group (HO-HBPA) at the focal point was synthesized by means of CGCP and then condensed with PEG having a COOH group at one end (PEG-COOH) in the presence of a condensation agent (Scheme 29). The desired PEG-*b*-HBPAs with defined molecular weight and low polydispersity were obtained after re-precipitation to remove excess HBPA. The ^{1}H NMR spectrum of PEG-*b*-HBPA in $CDCl_3$ showed both PEG and HBPA signals. However, the spectrum in D_2O did not show signals of the HBPA segment, implying that PEG-*b*-HBPA formed micelles in water, with PEG in the corona and HBPA in the core.

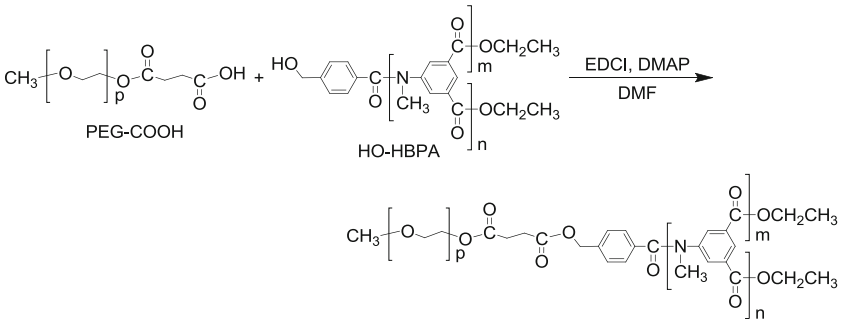

Scheme 29 Synthesis of amphiphilic linear-hyperbranched block copolymer of PEG and HBPA

4.2 Star Polymer

Star-shaped condensation polymers have been prepared by copolycondensation of an A*n* monomer with an AB-type monomer or with A_2 and B_2 monomers [63–66], in which the arm lengths of the polymers obtained are not controlled. Well-defined star-shaped condensation oligomers have been synthesized by the coupling reaction between an A*n* monomer and linear oligomers with monodispersity, which were prepared by a sequential condensation procedure [67–69]. We synthesized star-shaped aromatic polyamides with low polydispersity by a core-first method, which was the CGCP of **14a** from 1,3,5-tris(4-phenyloxycarbonylbenzyloxy)benzene (**28**) having the benzyloxy spacers (Scheme 30) [70]. The benzyloxy linkages of the core of the star polymer were cleaved by hydrogenolysis to yield a polymer with low polydispersity. The M_n of this polymer was one-third of that of the star polymer, indicating that the star polymer possesses exactly three arm chains of a uniform and controlled length. However, the polymerization at higher feed ratios of $[\mathbf{14a}]_0/[\mathbf{28}]_0$ afforded not only the three-armed polymer but also a linear polymer formed by self-polycondensation of **14a**. In the polymerization of **14a** with a monofunctional initiator, no self-polycondensation of **14a** takes place as long as the feed ratio of $[\mathbf{14a}]_0/[\text{initiator}]_0$ is 100 or less [20]. In the polymerization with trifunctional initiator **28**, however, the self-polycondensation occurred even at the feed ratio of ($[\mathbf{14a}]_0$/[initiator site of $\mathbf{28}]_0$) 33, which is much less than 100. Easy occurrence of the self-polycondensation in the polymerization of **14a** with multifunctional initiator **28** is presumably ascribed to the low local concentration of the initiator site in the whole solution except for the area around **28**. Thus, monofunctional initiators homogeneously exist in the solution, whereas multifunctional initiators occur in both the area of high local concentration of the initiator units and the area of low local concentration where self-polycondensation would be liable to occur.

Accordingly, we optimized polymerization conditions for the synthesis of star polyamides by CGCP with LiHMDS by using the porphyrin-cored tetrafunctional initiator **29** (Scheme 31) [71]. Since the target star polymer has an absorption at 430 nm due to the porphyrin ring, whereas the linear polymer formed as a

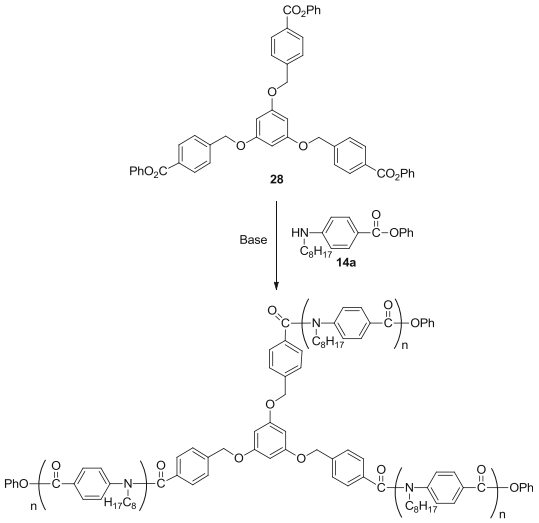

Scheme 30 Synthesis of star-shaped aromatic polyamide by chain-growth condensation polymerization of **14a** with 1,3,5-tris(4-phenyloxycarbonylbenzyloxy)benzene (**28**)

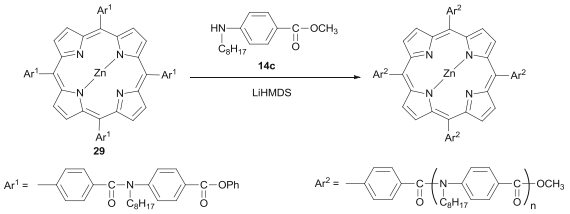

Scheme 31 Synthesis of star-shaped aromatic polyamide by chain-growth condensation polymerization of **14c** with porphyrin-cored tetrafunctional initiator **29**

byproduct does not have this absorption, it was easy to differentiate the star polymer from the linear polymer by GPC with UV detection and to optimize conditions for the selective synthesis of the star polymer. It turned out that the polymerization of the methyl ester monomer **14c** at 10°C, which was higher than the optimized temperature (−10°C) for the synthesis of linear poly**14c** with LiHMDS from a monofunctional initiator, yielded the star polyamide with controlled molecular weight and narrow molecular weight distribution up to the feed ratio of $[\mathbf{14c}]_0/[\mathbf{29}]_0$ of 120. Under the optimized conditions, a variety of well-defined tetra-armed star-shaped poly(*N*-substituted *p*-benzamide)s, including block poly(*p*-benzamide)s with different *N*-substituents, and poly(*N*-substituted *m*-benzamide)s, were synthesized by using tetrafunctional initiator **29** [72].

Star polyethers have been synthesized by a core-first method. AB_2- and A_2B-type mikto-arm star copolymers consisting of aromatic polyether arms as the A segment and polystyrene arms as the B segment were synthesized by using orthogonal trifunctional initiators (Scheme 32) [73].

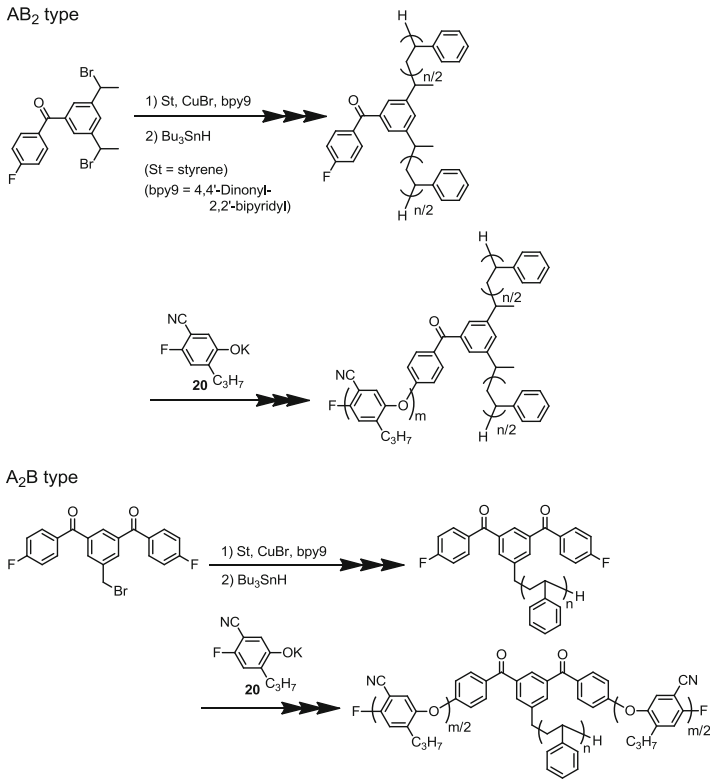

Scheme 32 Synthesis of AB_2- and A_2B-type mikto-arm star copolymers of polystyrene and polyether

Furthermore, $(AB)_3$-type star block copolymer was also prepared using ATRP, CGCP, and a click reaction (Scheme 33) [74]. ATRP of styrene was carried out in the presence of 2,4,6-tris(bromomethyl)mesitylene as a trifunctional initiator, and then the terminal bromines of the polymer were transformed to azide groups with NaN_3. The azide-terminated polystyrene was then used for click reaction with alkyne-terminated aromatic polyether, obtained by CGCP with an initiator bearing an acetylene unit. Excess alkyne-terminated aromatic polyether was removed from the crude product by means of preparative high-performance liquid chromatography (HPLC) to yield the $(AB)_3$-type star block copolymer.

The morphologies of star copolymers AB_2, A_2B, and $(AB)_3$ and linear block copolymer AB, which were annealed under vacuum at 150°C for 2 days, were observed by means of transmission electron microscopy (TEM) (Fig. 4). In the case of a sample of AB-type diblock copolymer, lamellar morphology consisting of alternating dark polystyrene and bright aromatic polyether regions was observed (Fig. 4a). On the other hand, samples of AB_2, A_2B, and $(AB)_3$ star copolymers showed spherical or plate-like morphology (Fig. 4b–d). Such unexpected and novel

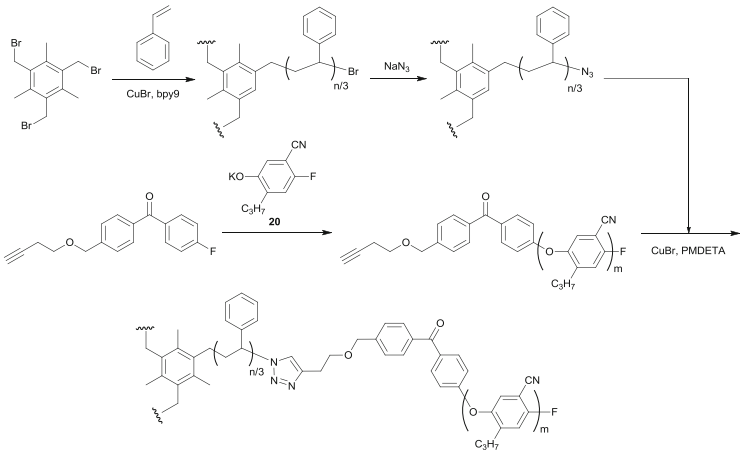

Scheme 33 Synthesis of $(AB)_3$-type star block copolymer of polystyrene and polyether

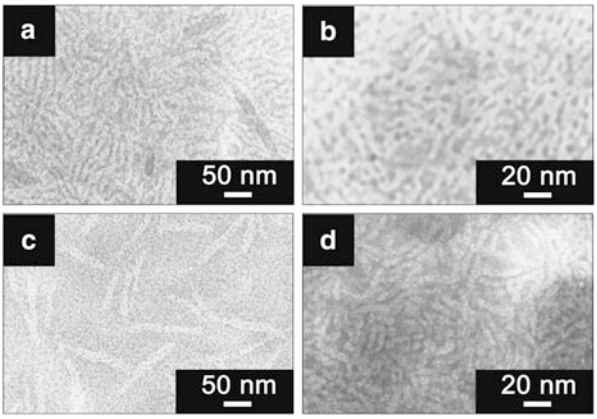

Fig. 4 TEM images of $CHCl_3$ cast of (**a**) AB-type diblock copolymer, (**b**) AB_2-type mikto-arm star copolymer, (**c**) A_2B-type mikto-arm star copolymer, and (**d**) $(AB)_3$-type star block copolymer. The samples were stained with RuO_4 prior to TEM measurement

behavior might arise from the different solubility and crystallinity of the aromatic polyether segments in star copolymers, compared to those of the corresponding linear diblock copolymer.

As an arm-first method, macromonomers (MM) with the styryl terminal moiety were synthesized by CGCP of 3-(alkylamino)benzoic acid esters **25** in the presence of phenyl 4-vinylbenzoate as an initiator, and copolymerization with *N*,*N*'-methylenebisacrylamide (MBAA) as a divinyl monomer in the presence of 2,2'-azobis(isobutyronitrile) (AIBN) at 60°C yielded the corresponding star polymers (Scheme 34) [75].

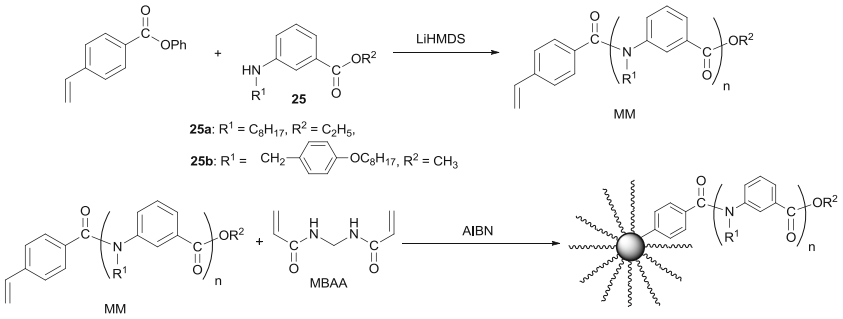

Scheme 34 Synthesis of star-shaped aromatic polyamides by copolymerization of polyamide macromonomer (plane) with MBAA in the presence of AIBN

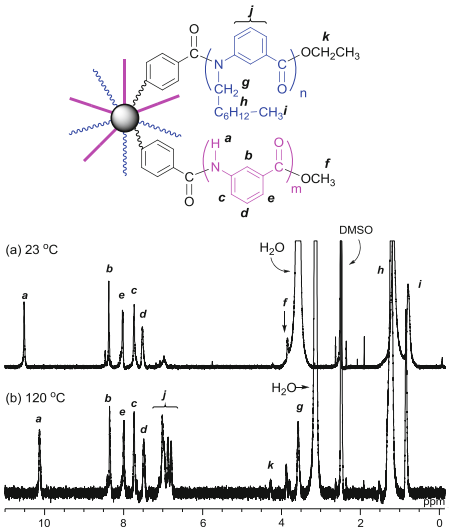

Fig. 5 ^{1}H NMR spectra of mikto-arm star polymer in DMSO-d_6 at (**a**) 23°C and (**b**) 120°C

The number of arms per molecule, determined by multi-angle laser light scattering (MALLS), varied in the range of 36–100 depending on the *N*-alkyl group of **25** and the molecular weight of macromonomer. Block-arm and mikto-arm star polymers consisting of poly(*N*-octyl-*m*-benzamide) and poly(*N*–H-*m*-benzamide) were also synthesized by this method. It should be noted that the ^{1}H NMR spectra of the mikto-arm star polymer in DMSO at 23°C showed a weak signal of the poly (*N*-octyl-*m*-benzamide) moiety, but its intensity increased to the expected level on heating (Fig. 5). This observation indicates that the poly(*N*-octyl-*m*-benzamide) moiety, which is insoluble in DMSO, is packed in the star polymers at 23°C and extended at higher temperatures. It seems intriguing that semirigid aromatic polyamide arms in star polymers can dynamically change their molecular geometry in response to thermal stimulation, as in the case of star polymers composed of flexible coil polymers.

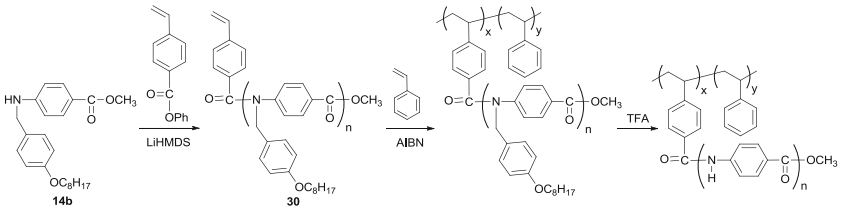

Scheme 35 Synthesis of polystyrene grafted with poly(*p*-benzamide)

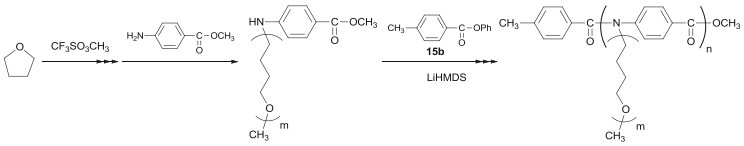

Scheme 36 Synthesis of polyamide grafted with poly(THF)

4.3 Graft Copolymer

Conventional graft copolymers containing condensation polymers were produced by polycondensation of AA and BB monomers, one of which carried a side-chain polymer such as a vinyl polymer or polysiloxane [76–79]. Since those reports, CGCP of phosphoranimine was used to synthesize polymers grafted with well-defined polyphosphazene [80–83]. We recently prepared polystyrene grafted with well-defined poly(*p*-benzamide) and examined its thermal properties [84]. Styryl macromonomer **30** containing poly(*N*-OOB-*p*-benzamide) was first synthesized by CGCP of methyl 4-(OOB-amino)benzoate **14b** with phenyl 4-vinylbenzoate as an initiator. Free radical copolymerization of **30** and styrene in the presence of AIBN at 60°C gave polystyrene-*g*-poly(*N*-OOB-*p*-benzamide), from which the OOB groups on amide nitrogen were removed with TFA (Scheme 35). The T_g value of polystyrene-*g*-poly(*N*-H-*p*-benzamide) was dramatically increased from that of polystyrene (109°C) to 172°C in the case of the graft copolymer containing 4.4 mol% of the grafted poly(*p*-benzamide) chains.

A well-defined aromatic polyamide backbone grafted with conventional polymer was also synthesized. Methyl 4-aminobenzoate bearing polyTHF, which was obtained by quenching the living cationic propagating group of poly(THF) with methyl 4-aminobenzoate, underwent CGCP with LiHMDS to yield a graft copolymer with well-defined polyamide main chain and poly(THF) side chain (Scheme 36) [85].

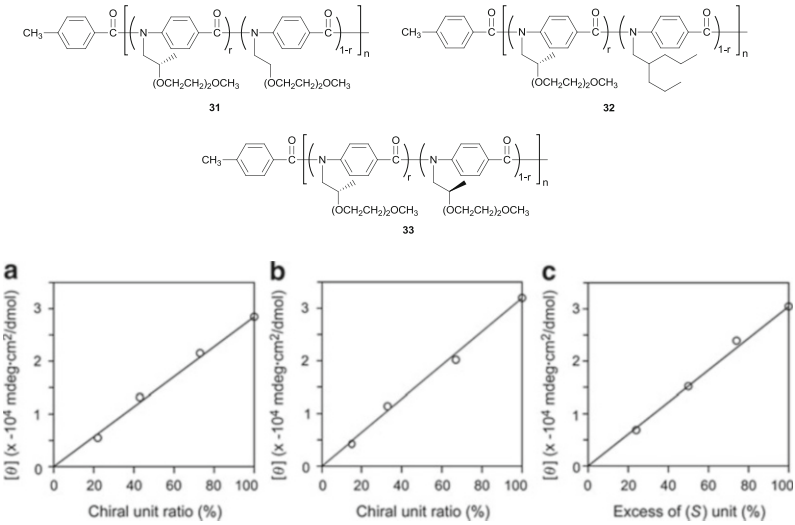

Fig. 6 Plots of CD intensity (261 nm) of (**a**) **31** and (**b**) **32** versus chiral unit ratio, and of (**c**) **33** versus excess of (*S*)-unit. The CD spectra of the copolymers were measured in $CHCl_3$ at 24°C

4.4 Helical Polymer

In the course of our study of CGCP, we found that poly(*p*-benzamide)s bearing a chiral tri(ethylene glycol) side chain as an *N*-substituent adopt a helical conformation with three monomer units per turn in solution [86]. Variable-temperature circular dichroism (CD) studies showed that the CD intensity decreased with increase of temperature, indicating the thermodynamically controlled helical character of this polyamide. The helical structure arises from the *cis* preference of *N*-substituted aromatic amide linkages [87] and the *syn* arrangement of the three consecutive benzene units connected by two amide linkages [88, 89]. In order to elucidate the helical folding, we studied the cooperativity of the monomer units according to the "sergeants and soldiers" [90] and "majority rules" [91] effects by using chiral/achiral random copolymers of poly(*p*-benzamide)s **31** and **32** and (*R*)/(*S*) random copolymer **33** [92]. The CD spectra of the random copolymers **31–33** were similar in shape, and the intensities changed linearly in proportion to the chiral unit ratio of **31** and **32** and the excess of the (*S*) unit in **33**, indicating the absence of cooperativity between the monomer units along these copolymers (Fig. 6).

Polynaphthalenecarboxamide poly**17c** bearing a chiral tri(ethylene glycol) side chain as an *N*-substituent also adopts a helical conformation. In contrast to *N*-substituted poly(*p*-benzamide), the folding of poly**17c** was enhanced by a solvophobic effect and seemed to be completed at 0–15°C in 70% water/methanol (7/3 v/v) [93]. The hydrophobicity of the naphthalene ring of poly**17** is enough to cause intramolecular self-association of the main chain in aqueous solvents. Furthermore, random copolymers of poly(naphthalenecarboxamide) **34** with chiral

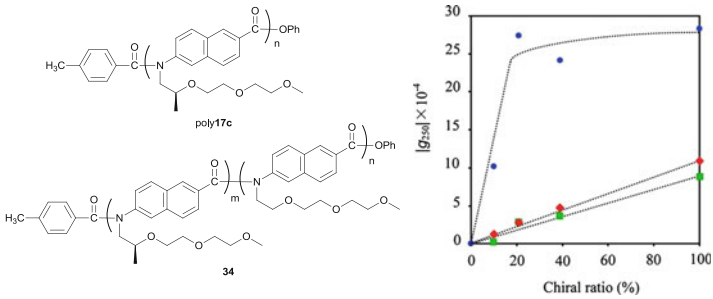

Fig. 7 Plots of Kuhn dissymmetry factor ($g = \Delta\varepsilon/\varepsilon$) at 250 nm of poly**17c** and **34** in chloroform (*diamonds*), methanol (*squares*), and water/methanol at 7/3 (v/v) (*circles*) against chiral unit ratio. The *dotted lines* are simply to guide the eye

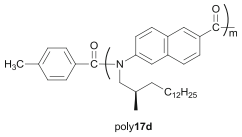

Fig. 8 Helical poly(naphthalenecarboxamide) poly**17d** with a chiral aliphatic side chain

and achiral tri(ethylene glycol) side chains showed chiral amplification based on the sergeants and soldiers effect in aqueous solvent. It should be noted that the chiral amplification was not observed in chloroform and methanol, in which the cooperativity between the monomer units is weak (Fig. 7) [94]. Furthermore, we have found that poly(naphthalenecarboxamide) poly**17d** with a chiral aliphatic side chain adopts a helical structure specifically in cyclohexane by virtue of the solvophobic effect, and observed the sergeants and soldiers effect using the random copolymers (Fig. 8) [95]. These results indicated that the introduction of a naphthalene ring into an aromatic polyamide with a chiral aliphatic side chain enables recognition of the small difference between backbone and side chain in the polymer even in hydrophobic, aliphatic media such as cyclohexane.

5 Catalyst-Transfer Condensation Polymerization

5.1 Kumada–Tamao Coupling Polymerization for the Synthesis of P3HT

Condensation polymerization with a catalyst can involve another mechanism for CGCP, i.e., a catalyst-transfer mechanism in which the catalyst activates the polymer end group, followed by reaction with the monomer and transfer of the catalyst to the

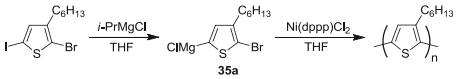

Scheme 37 Synthesis of poly(3-hexylthiophene) by polymerization of **35a** with Ni(dppp)Cl_2

elongated polymer end group, in a similar manner to biological condensation polymerization. In 1992, McCullough and Lowe [96] and Rieke and Chen [97] independently reported the synthesis of regioregulated head-to-tail poly(3-hexylthiophene) (HT-P3HT) by metal-catalyzed condensation polymerization of 5-metalated-2-bromo-3-hexylthiophene with Ni(dppp)Cl_2 or Ni(dppe)Cl_2 [where dppp is 1,3-bis(diphenylphosphino)propane and dppe is 1,2-bis(diphenylphosphino)-ethane] as a catalyst. But, the molecular weight and polydispersity of the products were not well controlled: poly(3-alkylthiophene)s with narrow molecular weight distributions were obtained only after fractionation with Soxhlet extraction [98]. However, we found that the M_n values of polymers increased in proportion to monomer conversion, with low polydispersities bring retained, and were controlled by the amount of the Ni catalyst. The M_n values were proportional to the feed ratio of $[\mathbf{35a}]_0$/[Ni catalyst]$_0$ when the polymerization was carried out at room temperature, with care to use the exact amount of isopropylmagnesium chloride for generation of monomer **35a** from the corresponding bromoiodothiophene (Scheme 37) [99]. Furthermore, the M_w/M_n ratios were around 1.1 up to M_n of 28,700, when the polymerization of **35a** was quenched with hydrochloric acid [100]. McCullough and coworkers also reported that a similar zinc monomer [101] and **35a** from the corresponding dibromothiophene showed the same polymerization behavior [102].

After a detailed study of the polymerization of **35a**, four important points were clarified: (1) the polymer end groups are uniform among molecules; one end group is Br and the other is H; (2) the propagating end group is a polymer-Ni-Br complex; (3) one Ni molecule forms one polymer chain; and (4) the chain initiator is a dimer of **35a** formed in situ. On the basis of these results, we have proposed a catalyst-transfer condensation polymerization mechanism (Scheme 38) [103].

Thus, Ni(dppp)Cl_2 reacts with 2 equivalents of **35a**, and the coupling reaction occurs with concomitant generation of a zero-valent Ni complex. The Ni(0) complex does not diffuse into the reaction mixture but is inserted into the intramolecular C–Br bond. Another **35a** reacts with this Ni, followed by the coupling reaction and transfer of the Ni catalyst to the next C–Br bond. Growth continues in such a way that the Ni catalyst moves to the polymer end group [103]. Several other reactions involving similar intramolecular transfer of metal catalysts have been reported [104–112]. Van der Boom and coworkers demonstrated that the reaction of Ni(PEt_3)$_4$ with a brominated vinylarene results in selective η^2-C=C coordination, followed by intramolecular "ring-walking" of the metal center and aryl-bromide oxidative addition, even in the presence of substrates containing aryl-I (Scheme 39) [111]. Nakamura and coworkers studied the Ni-catalyzed cross-coupling reaction by analysis of kinetic isotope effects and theoretical calculations, and indicated that the first irreversible step of the reaction is the π-complexation of

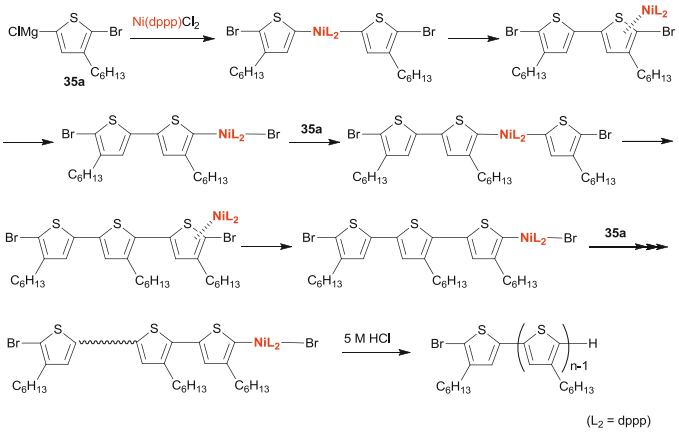

Scheme 38 Proposed polymerization mechanism of catalyst-transfer condensation polymerization of **35a**

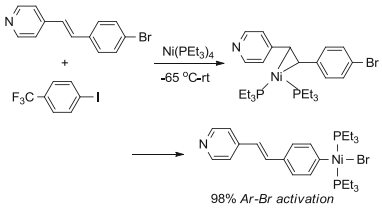

Scheme 39 Intramolecular transfer of Ni catalyst

the Ni catalyst on the π-face of haloarene. In other words, once a Ni/haloarene π-complex forms through ligand exchange, it does not dissociate and proceeds quickly to the oxidative addition step in an intramolecular manner [112].

The influence of the phosphine ligand of the Ni catalyst on the catalyst-transfer condensation polymerization was investigated [113, 114]. The M_n value and the M_w/M_n ratio of polymer were strongly affected by the ligands of the Ni catalyst: Ni(dppe)Cl_2, and Ni$(PPh_3)_4$ gave a polymer with a slightly lower M_n and a slightly broad molecular weight distribution, whereas Ni$(PPh_3)_2Cl_2$, Ni(dppb)Cl_2, and Ni(dppf)Cl_2 [where dppb is 1,4-bis(diphenylphosphino) and dppf is 1,1′-bis-(diphenylphosphino)ferrocene] gave polymers of low M_n and broad molecular weight distribution. After all, Ni(dppp)Cl_2 resulted in the M_n value close to the theoretical value based on the feed ratio of monomer to the catalyst and the narrowest M_w/M_n ratio.

In the chain-growth polymerization of **35a** with Ni(dppp)Cl_2, the chain initiator is a dimer of **35a** formed in situ as mentioned above. Kiriy and coworkers conducted polymerization of **35a** with an externally added initiator, PhNi$(PPh_3)_2$Br, to obtain phenyl-terminated poly(3-hexylthiophene), although the polymerization was less controlled than the polymerization of **35a** with Ni(dppp)

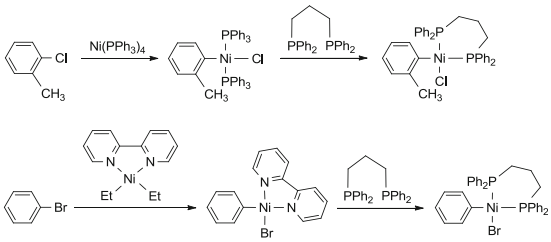

Scheme 40 Synthesis of Ni-initiators for catalyst-transfer condensation polymerization

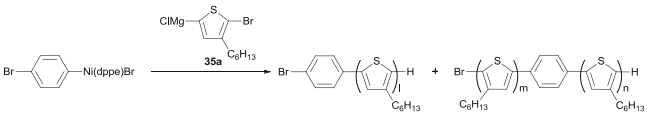

Scheme 41 Bidirectional growth of catalyst-transfer condensation polymerization of **35a** with Br-C_6H_4-Ni(dppe)-Br

Cl_2 [115, 116]. Bronstein and Luscombe [117] and Senkovskyy et al. [118] have independently reported the synthesis of more effective initiator, ArNi(dppp)X (where X=Cl, Br), which yields poly(3-hexylthiophene) with narrow molecular weight distribution. Both methods used the ligand exchange reaction of the primary ArNi(II)X complex with dppp, although Bronstein and Luscombe and Senkovskyy et al. generated the primary Ni(II) complex by using $Ni(PPh_3)_4$ and Et_2Ni (2,2′-bipyridine), respectively (Scheme 40). A protected functional group was introduced to the aryl group of the above initiator according to the Luscombe method [119].

Kiriy and coworkers demonstrated that the catalyst is able to walk along the P3HT backbone up to the opposite end and can initiate polymerization by means of the polymerization of **35a** using Br-C_6H_4-Ni(dppe)-Br as an initiator [120]. In this polymerization, not only P3HT with a bromophenyl end group but also P3HT bearing the phenylene group inside the backbone were obtained (Scheme 41). The content of the product with the internal phenyl ring increased with the increase in polymerization degree. Furthermore, study of the crystallinity and NMR analysis of P3HT obtained with Ni(dppp)Cl_2 showed that one single tail-to-tail defect was distributed over the whole chain [121].

5.2 Generality of Catalyst-Transfer Condensation Polymerization

The chain-growth polymerization of other substituted thiophene monomers instead of **35a** with the hexyl group was investigated (Scheme 42).

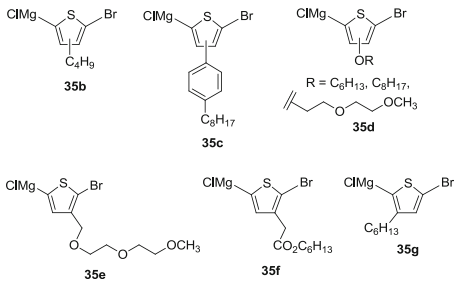

Scheme 42 Thiophene monomers for Kumada–Tamao coupling polymerization with a Ni catalyst

The polymerization of butylthiophene monomer **35b** with Ni(dppp)Cl_2 afforded polymer with low polydispersity (M_w/M_n = 1.33–1.43), although the M_n value was less than 5,500 due to the low solubility of poly**35b** [122]. Aryl-substituted monomer **35c**, the polymer of which may have a stabilized π-conjugated main chain system by virtue of the pendant aromatic group, gave a polymer with the M_w/M_n ratio of 2.15, probably due to the low solubility of the conjugated poly**35c** in the reaction solvent [123]. The polymers from alkoxy-substituted monomers **35d** possessed the M_w/M_n ratio of 1.5–1.7 [124, 125]. The polymerization of alkoxymethyl-substituted monomer **35e** with Ni(dppp)Cl_2 gave a polymer with the M_w/M_n ratio of 1.42, whereas the polymerization with Ni(dppe)Cl_2 resulted in a decrease in the M_w/M_n ratio to 1.15 [126]. The polymerization of a thiophene monomer **35f** containing an ester moiety also showed chain-growth polymerization behavior to yield polymers with the M_w/M_n ratio of 1.25–1.5 [127]. Luscombe and coworkers [128] showed that **35g**, a regioisomer of **35a**, was not polymerized with Ni(dppp)Cl_2 nor ArNi(dppp)Cl. This is ascribed to steric hindrance of the hexyl group of **35g** occurring upon the second transmetalation on the Ni catalyst. This fact is responsible for formation of a highly regioregular P3HT, even under conditions where different regioisomers of the monomer (**35a** and **35g**) exist from 2,5-dibromo-3-hexylthiophene with alkyl Grignard reagent [129]. Geng [130] and Catala [131] independently reported that LiCl promoted the polymerization of **35g** with Ni(dppp)Cl_2 (Scheme 43). The polymerization exhibited living characteristics, but initiation was much slower than propagation, resulting in large polydispersity and higher M_n than the theoretical value based on feed ratio of **35g** to the catalyst. Catala conducted kinetic studies of the polymerization of both **35a** and **35g** with Ni (dppp)Cl_2 in the presence of LiCl. The polymerization rate constant for **35a** in the presence of 4 equivalents of LiCl to monomer achieved a constant value 20 times higher than that obtained without LiCl. For the reverse monomer **35g**, a similar propagation rate was observed when 4 equivalents of LiCl were added. The addition of LiCl enhances the reactivity of the Grignard species, probably by de-aggregation and formation of new complex but it also modifies the Nickel center through a halogen exchange reaction.

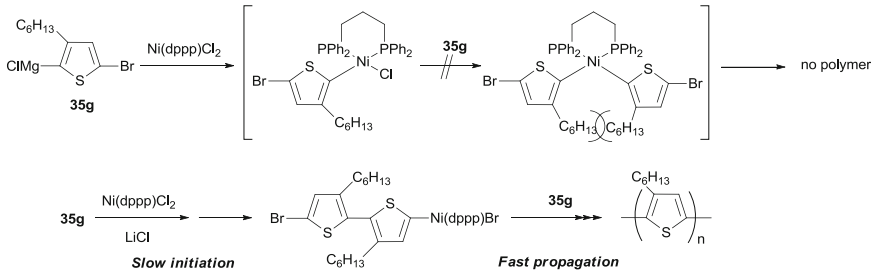

Scheme 43 Catalyst-transfer condensation polymerization of **35g** with Ni(dppp)Cl_2 and LiCl

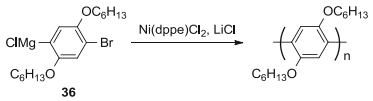

Scheme 44 Synthesis of poly(*p*-phenylene) by catalyst-transfer condensation polymerization of **36** with Ni(dppe)Cl_2 and LiCl

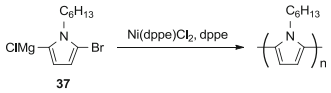

Scheme 45 Synthesis of polypyrrole by catalyst-transfer condensation polymerization of **37** with Ni(dppe)Cl_2 and dppe

It is important to clarify whether catalyst-transfer condensation polymerization is specific to polythiophene or whether it is generally applicable to the synthesis of well-defined π-conjugated polymers. We investigated the synthesis of poly (*p*-phenylene), to see whether a monomer **36** containing no heteroatom in the aromatic ring would undergo catalyst-transfer polymerization. However, all polymers obtained in the polymerization with Ni(dppp)Cl_2, Ni(dppe)Cl_2, or Ni (dppf)Cl_2 possessed low molecular weights and broad molecular weight distribution. Nevertheless, we found that LiCl was necessary for optimizing the CGCP, leading to poly(*p*-phenylene) with low polydispersity, and that the molecular weight was controlled by the feed ratio of **36** to the Ni catalyst (Scheme 44) [132].

We also investigated the condensation polymerization of Grignard-type *N*-hexylpyrrole monomer **37** with a Ni catalyst (Scheme 45). When Ni(dppp)Cl_2 was used as catalyst in a similar manner as for polymerization of hexylthiophene monomer **35a**, a polymer with the M_w/M_n of 1.26 was obtained, accompanied by low molecular weight oligomers. On the other hand, polymerization with Ni(dppe) Cl_2 afforded the polymer with a narrower molecular weight distribution ($M_w/M_n = 1.19$), although oligomeric byproducts were still formed. To suppress the formation of the oligomeric byproduct, we examined the effect of several additives

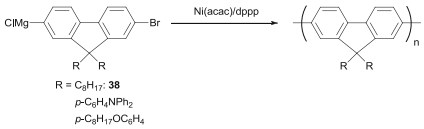

Scheme 46 Synthesis of polyfluorene by catalyst-transfer condensation polymerization of **38** with Ni(acac)$_2$/dppp

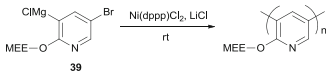

Scheme 47 Synthesis of poly{2-[2-(2-methoxyethoxy)ethoxy]pyridine-3,5-diyl} by catalyst-transfer condensation polymerization of **39** with Ni(dppp)Cl$_2$ and LiCl

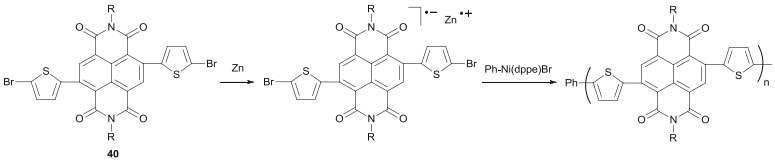

Scheme 48 Chain-growth condensation polymerization of symmetrical dibromo monomer **40**

and found that polymerization of **37** with Ni(dppe)Cl$_2$ in the presence of additional dppe equimolar to the catalyst at 0°C gave a polypyrrole with a low polydispersity ($M_w/M_n = 1.11$) without formation of byproduct. The conversion-M_n and feed ratio-M_n relationships indicated that this polymerization proceeded in a catalyst-transfer polymerization manner [133].

Geng and coworkers reported synthesis of polyfluorene by Kumada catalyst-transfer condensation polymerization of fluorine monomer **38** (Scheme 46). Polymerization of **38** was carried out in the presence of nickel acetylacetonate/1,3-bis(diphenylphosphino)propane [Ni(acac)$_2$/dppp] at 0°C, yielding polyfluorene with controlled molecular weight and low polydispersity [134].

Polypyridine, which is an n-type π-conjugated polymer, was also prepared by catalyst-transfer CGCP (Scheme 47). 5-Bromo-3-chloromagnesio-2-(2-(2-methoxyethoxy)ethoxy)pyridine **39** was polymerized with Ni(dppp)Cl$_2$ in the presence of 2.0 equivalents of LiCl in THF at room temperature to yield poly{2-[2-(2-methoxyethoxy)ethoxy]pyridine-3,5-diyl} with narrow molecular weight distribution and controlled molecular weight based on feed ratio of **39** to Ni(dppp)Cl$_2$ ([**39**]$_0$/[Ni(dppp)Cl$_2$]$_0$) [135].

Polymerization of symmetrical dibromo monomer **40**, consisting of thiophene, naphthalenediimide, and thiophene, also proceeds in chain-growth polymerization manner (Scheme 48) [136]. The first attempt to form a Grignard monomer from **40** for Kumada–Tamao coupling polymerization failed. Activated Zn was next reacted with **40** for generation of an organozinc monomer. Remarkably, however, acidic

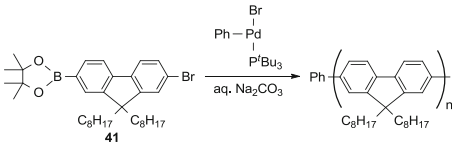

Scheme 49 Catalyst-transfer Suzuki–Miyaura coupling polymerization of **41**

work-up of the prepared **40**/Zn complex resulted in recovery of **40**, but not the hydrized monobromo compound. Electron paramagnetic resonance measurements revealed that the **40**/Zn complex was a radical anion; single electron transfer from Zn to the electron-deficient **40** occurred. This radical anion was polymerized with Ni(dppe)Br_2 or PhNi(dppe)Br at room temperature. The polymerization behavior showed a chain-growth polymerization mechanism: the molecular weight increased with increasing feed ratio of monomer to the Ni catalyst, with retention of low polydispersity (M_n = 25,000–104,000, M_w/M_n = 1.3–1.7), and the phenyl group was introduced into the polymer end group when PhNi(dppe)Br was used.

Suzuki–Miyaura coupling polymerization also proceeds in the catalyst-transfer mechanism. In this polymerization, stable arylpalladium(II) halide complex was used as an externally added initiator, and the aryl group of the complex served as an initiator unit of the polymer. The polymerization of a fluorene monomer **41** was carried out in the presence of ^{t}Bu$_3$PPd(Ph)Br as a catalyst to yield polyfluorene with a narrow polydispersity (Scheme 49). The molecular weight of the obtained polymer increased linearly in proportion to the conversion of monomer with low polydispersity throughout the polymerization, and it also increased linearly in proportion to the feed ratio of **41** to the initiator, up to 17,700 with low polydispersity, indicating that this Suzuki–Miyaura coupling condensation polymerization proceeded through a chain-growth polymerization mechanism [137], as shown in the model reactions [106–108]. The MALDI-TOF mass spectrum of the obtained polyfluorene showed that all the polymers bore the phenyl group at one end. This observation strongly supported the view that ^{t}Bu$_3$PPd(Ph)Br served as an initiator. Poly(*p*-phenylene), P3HT, and poly(9,9′-dioctylfluorene-*co*-benzothiadiazole) were also synthesized by means of chain-growth Suzuki–Miyaura polymerization [138–140].

6 Polymer Architecture Using Catalyst-Transfer Condensation Polymerization

6.1 Block Copolymers of Polythiophene and Other Polymers

Block copolymers composed of polythiophene and conventional polymer have been synthesized. McCullough and coworkers synthesized block copolymers of P3HT and polystyrene or poly(methyl acrylate) by ATRP of the vinyl monomer from a polythiophene macroinitiator, which was prepared in several steps

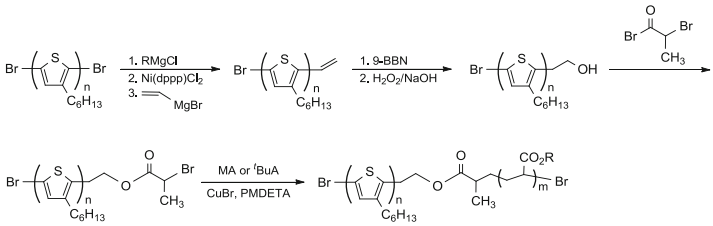

Scheme 50 Synthesis of block copolymer of P3HT and poly(alkyl acrylate) by ATRP from polythiophene macroinitiator

[141]. After the development of catalyst-transfer condensation polymerization of polythiophene, the block copolymer of polythiophene and poly(alkyl acrylate) was prepared more easily. Vinyl-terminated polythiophene was first prepared. The vinyl group was converted to the 2-hydroxyethyl group by hydroboration, followed by esterification with 2-bromopropionyl bromide to give a macroinitiator for ATRP (Scheme 50) [142]. The allyl-terminated polythiophene was also converted to a macroinitiator for ATRP, which led to block copolymers of polythiophene and poly (alkyl methacrylate) [143] or poly(acrylic acid) [144]. This allyl-terminated polythiophene has a bromine atom at the other end, which has an adverse effect on the purity of block copolymers prepared by ATRP. Hawker, Kim, and coworkers reported that replacement of the bromine with a phenyl group, followed by functionalization of the allyl group for the ATRP initiator unit, allowed access to narrower molecular weight distribution diblock copolymers of polythiophene and ATRP-derived vinyl block [145].

RAFT polymerization or nitroxide-mediated polymerization (NMP) was used instead of ATRP for the synthesis of the block copolymer of polythiophene and polyisoprene or polystyrene, because ATRP generates materials containing traces of metals from the catalyst [146]. A block copolymer of P3HT and poly (perylene bisimide acrylate) was also synthesized by NMP from a polythiophene macroinitiator (Scheme 51) [147, 148]. This block copolymer is a crystalline–crystalline donor–acceptor block copolymer and shows microphase separation, implying efficient photovoltaic applications. A similar polythiophene macroinitiator for NMP was used for the synthesis of fullerene-grafted rod–coil block copolymers [149].

Frisbie and Hillmyer used the hydroxyethyl-terminated polythiophene in Scheme 50 as a macroinitiator for the ring-opening polymerization of D,L-lactide (Scheme 52) [150]. The hydroxy-terminated polythiophene was converted to the corresponding aluminum alkoxide macroinitiator with triethylaluminum, followed by ring-opening polymerization of the lactide to yield a block copolymer of polythiophene and polylactide. In thin films of the block copolymers, microphase-separated domains were formed. Upon chemical etching of the polylactide block, nanopitted film, where the crystallinity of the polythiophene phase remained, was observed.

Dai, Su, and coworkers synthesized block copolymers of polythiophene and poly (vinylpyridine) by means of living anionic polymerization of 4-vinylpyridine from

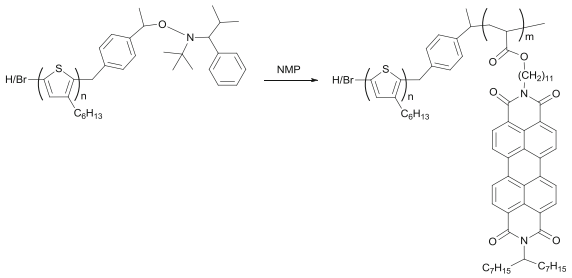

Scheme 51 Synthesis of block copolymer of P3HT and poly(perylene bisimide acrylate) by nitroxide-mediated polymerization from polythiophene macroinitiator

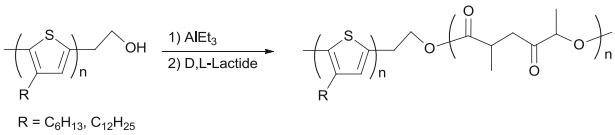

Scheme 52 Synthesis of block copolymer of polythiophene and polylactide by ring-opening polymerization of lactide with polythiophene macroinitiator

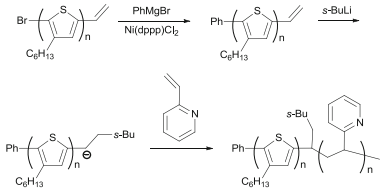

Scheme 53 Synthesis of block copolymers of P3HT and poly(vinylpyridine) by living anionic polymerization of 2-vinylpyridine from polythiophene macroinitiator

the vinyl-terminated polythiophene macroinitiator (Scheme 53) [151]. These block copolymers were able to undergo microphase separation and self-assembly into nanostructures of sphere, cylinder, lamellae, and nanofiber structure with increasing polythiophene segment ratios.

Meijer and coworkers used the allyl-terminated polythiophene to synthesize a block copolymer of P3HT and polyethylene as a crystalline–crystalline block copolymer: the ring-opening metathesis polymerization of cyclooctene in the presence of the allyl-terminated polythiophene was followed by hydrogenation (Scheme 54) [152].

Fréchet and coworkers reported the synthesis of a dendron-modified polythiophene, in which one terminus of P3HT was linked to the focal point of a polyester-type dendron (Scheme 55) [153]. Introduction of the benzylamine moiety to the end group of polythiophene was carried out by the Suzuki–Miyaura coupling reaction of the polythiophene with the H/Br end groups and the corresponding boronic acid hydrochloride. The amino-functionalized polythiophene was then

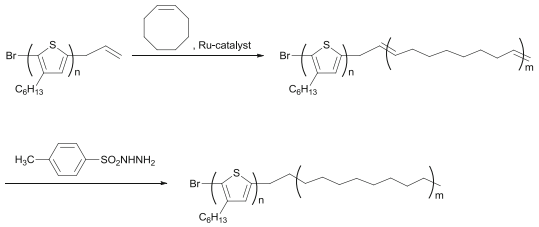

Scheme 54 Synthesis of block copolymer of P3HT and polyethylene by ring-opening metathesis polymerization of cyclooctene with allyl-terminated polythiophene, followed by hydrogenation

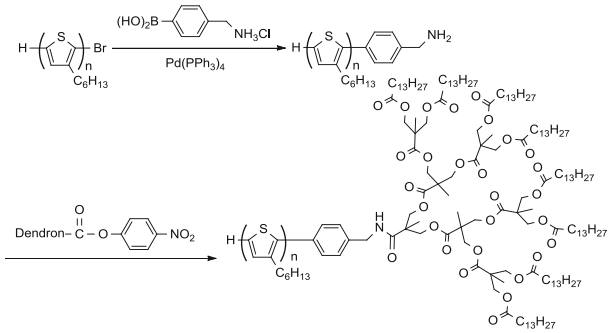

Scheme 55 Synthesis of dendron-modified polythiophene

treated with dendron active ester in the presence of base. Despite the insulating nature of the polyester dendron, a device made with this dendron-modified polythiophene functioned as a transistor, and showed moderate field effect mobilities.

6.2 Block Polythiophenes

Because several substituted thiophene monomers undergo chain-growth polymerization in a living polymerization fashion, a lot of block copolythiophenes **42** [102, 154–162] have been synthesized by successive polymerization in one pot (Scheme 56).

Of these block copolymers, **42a** was first synthesized by McCullough and coworkers [102]. We synthesized block copolymer **42b** having both hydrophobic and hydrophilic side chains in each segment [155]. The thin films of **42c** [157], **42e** [158], and **42i** [161] showed nanofiber structures after annealing, probably because of microphase separation of the crystalline P3HT segment and the other amorphous segment. The block copolymer **42d** is a crystalline–crystalline diblock copolymer, self-assembled into crystalline nanowires in solution. In melt-phase assembly, a microphase-separated lamellar structure with two crystalline domains characteristic

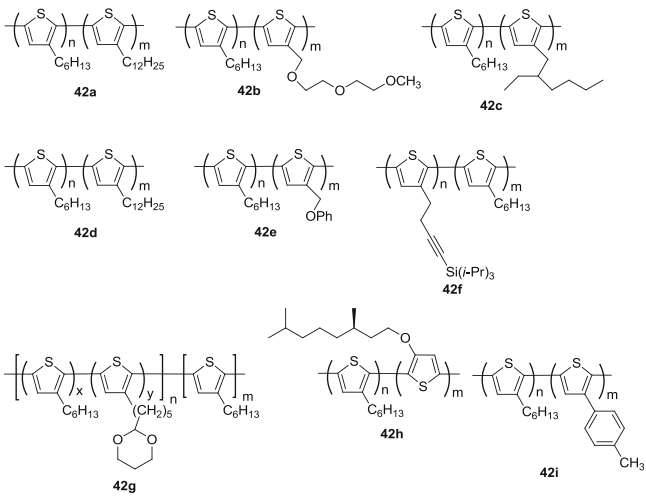

Scheme 56 Block copolythiophenes

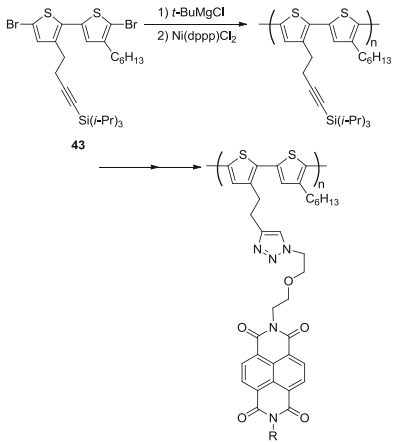

Scheme 57 Synthesis of polythiophene having naphthalene diimide moiety

of the two different side chains was observed [162]. The side chain of block copolymer **42f** [154] was converted to the naphthalimide moiety, as shown in Scheme 57. The diblock copolymer **42g** [159] consists of a block made from a random copolymerization of hexylthiophene monomer and (1,3-dioxa-2-octyl) thiophene monomer and the pure P3HT block. The 1,3-dioxone moiety was converted to the formyl group, followed by introduction of fullerene C60 with the aid of *N*-methylglycine. In the block copolymer **42h**, the chiral segment influences the supramolecular organization of the P3HT segment [160].

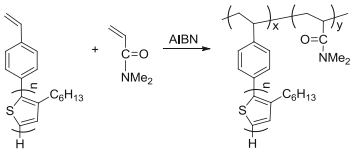

Scheme 58 Synthesis of poly(*N*,*N*-dimethylacrylamide) grafted with P3HT

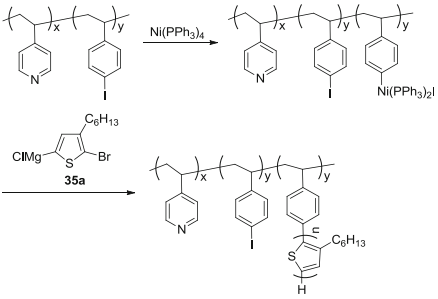

Scheme 59 Synthesis of poly(4-vinylpyridine)-*b*-poly(4-iodostyrene) grafted with P3HT by catalyst-transfer condensation polymerization of **35a** with Ni macroinitiator

6.3 Graft Copolymers of Polythiophene

Chochos and coworkers synthesized a thiophene-grafted copolymer by using polythiophene with Br/H end groups. Thus, Suzuki–Miyaura coupling was performed between the bromo-terminated polythiophene and 4-vinylphenylboronic acid, followed by radical copolymerization with *N*,*N*-dimethylacrylamide to afford the graft copolymer (Scheme 58) [83]. They studied the interaction of the polythiophene chains on the copolymer in water and several organic solvents. It was demonstrated that the polythiophene chains adopt a coil conformation in solvents such as THF and chloroform. However, the polythiophene chains were organized in a single-chain packing form (intrachain interactions) in polar solvents such as ethanol and methanol. When water was used as solvent, the polythiophene chains self-assembled into a stack-like structure due to the increased interchain interactions.

Kiriy and coworkers conducted grafting of P3HT from poly(4-vinylpyridine)-*b*-poly(4-iodostyrene) immobilized on silica particles. This block copolymer adheres strongly to a variety of polar substrates including silicon wafers, glasses, or a metal oxide surface by a polar poly(4-vinylpyridine) block, forming polymer brushes of poly(4-iodostyrene) chains, which react with $Ni(PPh_3)_4$ to generate the Ni initiator for the catalyst-transfer polymerization of **35a**. Unfortunately, the polythiophene grafts of the products are relatively short (~10 nm) (Scheme 59) [163].

7 Conclusion

We have described chain-growth condensation polymerization and the obtained polymers. Chain-growth condensation polymerization was achieved in two ways: (1) activation of the polymer end group by differing substituent effects between the monomer and the polymer, and (2) activation of the polymer end group by transfer of the catalyst. The former method enables us to produce architectures containing well-defined condensation polymers, such as block copolymers, star polymers, graft copolymers, etc, which show interesting properties. We hope to utilize these polymer architectures as new high-performance materials. The latter method affords well-defined π-conjugated polymers, which are expected to have applications as organic electrical materials for photovoltaics, field effect transistors, light-emitting diodes, and so on. Architectures containing π-conjugated polymers were also synthesized by using catalyst-transfer condensation polymerization. Basic research on the phenomena of catalyst transfer on π-conjugated polymers, and applied research for synthesis of well-defined donor–acceptor low band gap polymers for photovoltaics will progress in near feature.

References

1. Carothers WH (1936) Trans Faraday Soc 32:39
2. Flory PJ (1946) Chem Rev 39:137
3. Szwarc M, Levy M, Milkovich R (1956) J Am Chem Soc 78:2656
4. Lenz RW, Handlovits CE, Smith HA (1962) J Polym Sci 58:351
5. Newton AB, Rose JB (1972) Polymer 13:465
6. Lovering JR, Ridd JH, Parker DG, Rose JB (1988) J Chem Soc. Perkin Trans 2:1735
7. Hibbert DB, Sandall JPB, Lovering JR, Ridd JH, Yousaf TI (1988) J Chem Soc Perkin Trans 2:1739
8. Robello DR, Ulman A, Urankar EJ (1993) Macromolecules 26:6718
9. Risse W, Heitz W, Freitag D, Bottenbruch L (1985) Makromol Chem 186:1835
10. Koch W, Risse W, Heitz W (1985) Makromol Chem Suppl 12:105
11. Percec V, Wang JH (1991) J Polym Sci A Polym Chem 29:63
12. Percec V, Shaffer TD (1986) J Polym Sci C Polym Lett 24:439
13. Percec V, Wang JH (1990) Polym Bull 24:493
14. Wang JH, Percec V (1991) Polym Bull 25:33
15. Kricheldorf HR, Schwarz G (1983) Makromol Chem 184:475
16. Yokozawa T, Horio S (1996) Polym J 28:633
17. Schoenberg A, Bartoletti I, Heck RF (1974) J Org Chem 39:3318
18. Schoenberg A, Heck RF (1974) J Org Chem 39:3327
19. Yokozawa T, Shimura H (1999) J Polym Sci A Polym Chem 37:2607
20. Yokozawa T, Asai T, Sugi R, Ishigooka S, Hiraoka S (2000) J Am Chem Soc 122:8313
21. Yokozawa T, Ogawa M, Sekino A, Sugi R, Yokoyama A (2002) J Am Chem Soc 124:15158
22. Mikami K, Daikuhara H, Kasama J, Yokoyama A, Yokozawa T (2011) J Polym Sci A Polym Chem 49:3020
23. Yokoyama A, Iwashita K-i, Hirabayashi K, Aiyama K, Yokozawa T (2003) Macromolecules 36:4328
24. Iwashita K, Yokoyama A, Yokozawa T (2005) J Polym Sci A Polym Chem 43:4109

25. Yokozawa T, Suzuki Y, Hiraoka S (2001) J Am Chem Soc 123:9902
26. Suzuki Y, Hiraoka S, Yokoyama A, Yokozawa T (2003) Macromolecules 36:4756
27. Kim YJ, Seo M, Kim SY (2010) J Polym Sci A Polym Chem 48:1049
28. Heo J, Kim YJ, Seo M, Shin S, Kim SY (2012) Chem Commun 48:3351
29. Yokozawa T, Taniguchi T, Suzuki Y, Yokoyama A (2002) J Polym Sci A Polym Chem 40:3460
30. Shibasaki Y, Araki T, Nagahata R, Ueda M (2005) Eur Polym J 41:2428
31. Hine J (1975) Structural effects on equilibrium in organic chemistry. Wiley, New York
32. Sugi R, Yokoyama A, Furuyama T, Uchiyama M, Yokozawa T (2005) J Am Chem Soc 127:10172
33. Ohishi T, Sugi R, Yokoyama A, Yokozawa T (2006) J Polym Sci A Polym Chem 44:4990
34. Sugi R, Ohishi T, Yokoyama A, Yokozawa T (2006) Macromol Rapid Commun 27:716
35. Ohta Y, Fujii S, Yokoyama A, Furuyama T, Uchiyama M, Yokozawa T (2009) Angew Chem Int Ed 48:5942
36. Ohta Y, Kamijyo Y, Fujii S, Yokoyama A, Yokozawa T (2011) Macromolecules 44:5112
37. Ohta Y, Kamijyo Y, Yokoyama A, Yokozawa T (2012) Polymers 4:1170
38. Hirai T, Huan L, Ohta Y, Yokozawa T, Tanaka K (2011) Chem Lett 40:366
39. Yokozawa T, Ogawa M, Sekino A, Sugi R, Yokoyama A (2003) Macromol Symp 199:187
40. Ohshimizu K, Shibasaki Y, Komura M, Nakajima K, Ueda M (2007) Chem Lett 36:742
41. Ohshimizu K, Shibasaki Y, Ueda M (2007) Polym J 39:777
42. Ohishi T, Sugi R, Yokoyama A, Yokozawa T (2008) Macromolecules 41:9683
43. Chen XL, Jenekhe SA (1996) Macromolecules 29:6189
44. Schmitt C, Nothofer H-G, Falcou A, Scherf U (2001) Macromol Rapid Commun 22:624
45. Tu G, Li H, Forster M, Heiderhoff R, Balk LJ, Scherf U (2006) Macromolecules 39:4327
46. Tu G, Li H, Forster M, Heiderhoff R, Balk LJ, Sigel R, Scherf U (2007) Small 3:1001
47. Park JY, Koenen N, Forster M, Ponnapati R, Scherf U, Advincula R (2008) Macromolecules 41:6169
48. Bloom PD, Sheares VV (2001) J Polym Sci A Polym Chem 39:3505
49. Wang H, Ng M-K, Wang L, Yu L, Lin B, Meron M, Xiao Y (2002) Chem Eur J 8:3246
50. Kros A, Jesse W, Metselaar GA, Cornelissen JJLM (2005) Angew Chem Int Ed 44:4349
51. Hayakawa T, Goseki R, Kakimoto M-a, Tokita M, Watanabe J, Liao Y, Horiuchi S (2006) Org Lett 8:5453
52. Xiao X, Fu Y, Sun M, Li L, Bo Z (2007) J Polym Sci A Polym Chem 45:2410
53. Baek J-B, Tan L-S (2008) Macromolecules 41:1196
54. Yokoyama A, Masukawa T, Yamazaki Y, Yokozawa T (2009) Macromol Rapid Commun 30:24
55. Sugi R, Yokoyama A, Yokozawa T (2003) Macromol Rapid Commun 24:1085
56. Sugi R, Hitaka Y, Sekino A, Yokoyama A, Yokozawa T (2003) J Polym Sci A Polym Chem 41:1341
57. Kim S, Kakuda Y, Yokoyama A, Yokozawa T (2007) J Polym Sci A Polym Chem 45:3129
58. Masukawa T, Yokoyama A, Yokozawa T (2009) Macromol Rapid Commun 30:1413
59. Huang C-F, Yokoyama A, Yokozawa T (2010) J Polym Sci A Polym Chem 48:2948
60. Ajioka N, Suzuki Y, Yokoyama A, Yokozawa T (2007) Macromolecules 40:5294
61. Huang C-F, Ohta Y, Yokoyama A, Yokozawa T (2011) Macromolecules 44:4140
62. Ohta Y, Kanou T, Yokoyama A, Yokozawa T (2013) J Polym Sci A Polym Chem 51:3762
63. Kricheldorf HR, Adebahr T (1993) Makromol Chem 194:2103
64. Kricheldorf HR, Stukenbrock T (1997) Polymer 38:3373
65. Kricheldorf HR, Stukenbrock T, Friedrich C (1998) J Polym Sci A Polym Chem 36:1387
66. Honda K, Maruyama T, Yamamoto T (1997) Synth Met 90:153
67. Aujard I, Baltaze J-P, Baudin J-B, Cogné E, Ferrage F, Jullien L, Perez É, Prévost V, Qian LM, Ruel O (2001) J Am Chem Soc 123:8177
68. Li B, Li J, Fu Y, Bo Z (2004) J Am Chem Soc 126:3430
69. Nicolas Y, Blanchard P, Levillain E, Allain M, Mercier N, Roncali J (2003) Org Lett 6:273

70. Sugi R, Hitaka Y, Yokoyama A, Yokozawa T (2005) Macromolecules 38:5526
71. Yoshino K, Yokoyama A, Yokozawa T (2009) J Polym Sci A Polym Chem 47:6328
72. Yoshino K, Yokoyama A, Yokozawa T (2011) J Polym Sci A Polym Chem 49:986
73. Yamazaki Y, Ajioka N, Yokoyama A, Yokozawa T (2009) Macromolecules 42:606
74. Yamazaki Y, Yokoyama A, Yokozawa T (2012) J Polym Sci A Polym Chem 50:3648
75. Ohishi T, Masukawa T, Fujii S, Yokoyama A, Yokozawa T (2010) Macromolecules 43:3206
76. Yamashita Y, Chujo Y, Kobayashi H, Kawakami Y (1981) Polym Bull 5:361
77. Nagase Y, Mori S, Egawa M, Matsui K (1990) Makromol Chem 191:2413
78. Sato M, Yanahara M, Kobayashi T, Mukaida K-I (1992) Makromol Chem 193:991
79. Sato M, Mangyo T, Mukaida K-I (1995) Macromol Chem Phys 196:1791
80. Prange R, Reeves SD, Allcock HR (2000) Macromolecules 33:5763
81. Allcock HR, de Denus CR, Prange R, Laredo WR (2001) Macromolecules 34:2757
82. Allcock HR, Powell ES, Maher AE, Berda EB (2004) Macromolecules 37:5824
83. Stefopoulos AA, Chochos CL, Bokias G, Kallitsis JK (2008) Langmuir 24:11103
84. Ohta Y, Shirakura T, Yokoyama A, Yokozawa T (2013) J Polym Sci A Polym Chem 51:1887
85. Sugi R, Tate D, Yokozawa T (2013) J Polym Sci A Polym Chem 51:2725
86. Tanatani A, Yokoyama A, Azumaya I, Takakura Y, Mitsui C, Shiro M, Uchiyama M, Muranaka A, Kobayashi N, Yokozawa T (2005) J Am Chem Soc 127:8553
87. Itai A, Toriumi Y, Tomioka N, Kagechika H, Azumaya I, Shudo K (1989) Tetrahedron Lett 30:6177
88. Yamaguchi K, Matsumura G, Kagechika H, Azumaya I, Ito Y, Itai A, Shudo K (1991) J Am Chem Soc 113:5474
89. Azumaya I, Kagechika H, Yamaguchi K, Shudo K (1995) Tetrahedron 51:5277
90. Green MM, Reidy MP, Johnson RD, Darling G, O'Leary DJ, Willson G (1989) J Am Chem Soc 111:6452
91. Green MM, Garetz BA, Munoz B, Chang H, Hoke S, Cooks RG (1995) J Am Chem Soc 117:4181
92. Yokoyama A, Inagaki Y, Ono T, Yokozawa T (2011) J Polym Sci A Polym Chem 49:1387
93. Mikami K, Tanatani A, Yokoyama A, Yokozawa T (2009) Macromolecules 42:3849
94. Mikami K, Daikuhara H, Inagaki Y, Yokoyama A, Yokozawa T (2011) Macromolecules 44:3185
95. Mikami K, Yokozawa T (2013) J Polym Sci A Polym Chem 51:739
96. McCullough RD, Lowe RD (1992) J Chem Soc Chem Commun 1992(1):70
97. Chen TA, Rieke RD (1992) J Am Chem Soc 114:10087
98. Trznadel M, Pron A, Zagorska M, Chrzaszcz R, Pielichowski J (1998) Macromolecules 31:5051
99. Yokoyama A, Miyakoshi R, Yokozawa T (2004) Macromolecules 37:1169
100. Miyakoshi R, Yokoyama A, Yokozawa T (2004) Macromol Rapid Commun 25:1663
101. Sheina EE, Liu J, Iovu MC, Laird DW, McCullough RD (2004) Macromolecules 37:3526
102. Iovu MC, Sheina EE, Gil RR, McCullough RD (2005) Macromolecules 38:8649
103. Miyakoshi R, Yokoyama A, Yokozawa T (2005) J Am Chem Soc 127:17542
104. Nomura N, Tsurugi K, Okada M (2001) Angew Chem Int Ed 40:1932
105. Nomura N, Tsurugi K, RajanBabu TV, Kondo T (2004) J Am Chem Soc 126:5354
106. Sinclair DJ, Sherburn MS (2005) J Org Chem 70:3730
107. Dong C-G, Hu Q-S (2005) J Am Chem Soc 127:10006
108. Weber SK, Galbrecht F, Scherf U (2006) Org Lett 8:4039
109. Strawser D, Karton A, Zenkina EV, Iron MA, Shimon LJW, Martin JML, van der Boom ME (2005) J Am Chem Soc 127:9322
110. Zenkina O, Altman M, Leitus G, Shimon LJW, Cohen R, van der Boom ME (2007) Organometallics 26:4528
111. Zenkina OV, Karton A, Freeman D, Shimon LJW, Martin JML, van der Boom ME (2008) Inorg Chem 47:5114
112. Yoshikai N, Matsuda H, Nakamura E (2008) J Am Chem Soc 130:15258

113. Miyakoshi R, Yokoyama A, Yokozawa T (2008) J Polym Sci A Polym Chem 46:753
114. Mao YX, Wang Y, Lucht BL (2004) J Polym Sci A Polym Chem 42:5538
115. Senkovskyy V, Khanduyeva N, Komber H, Oertel U, Stamm M, Kuckling D, Kiriy A (2007) J Am Chem Soc 129:6626
116. Khanduyeva N, Senkovskyy V, Beryozkina T, Bocharova V, Simon F, Nitschke M, Stamm M, Grotzschel R, Kiriy A (2008) Macromolecules 41:7383
117. Bronstein HA, Luscombe CK (2009) J Am Chem Soc 131:12894
118. Senkovskyy V, Tkachov R, Beryozkina T, Komber H, Oertel U, Horecha M, Bocharova V, Stamm M, Gevorgyan SA, Krebs FC, Kiriy A (2009) J Am Chem Soc 131:16445
119. Smeets A, Van den Bergh K, De Winter J, Gerbaux P, Verbiest T, Koeckelberghs G (2009) Macromolecules 42:7638
120. Tkachov R, Senkovskyy V, Komber H, Sommer J-U, Kiriy A (2010) J Am Chem Soc 132:7803
121. Kohn P, Huettner S, Komber H, Senkovskyy V, Tkachov R, Kiriy A, Friend RH, Steiner U, Huck WTS, Sommer J-U, Sommer M (2012) J Am Chem Soc 134:4790
122. Hiorns RC, Khoukh A, Gourdet B, Dagron-Lartigau C (2006) Polym Int 55:608
123. Ouhib F, Hiorns RC, Bailly S, de Bettignies R, Khoukh A, Preud'homme H, Desbrieres J, Dagron-Lartigau C (2007) Eur Phys J Appl Phys 37:343
124. Sheina EE, Khersonsky SM, Jones EG, McCullough RD (2005) Chem Mater 17:3317
125. Koeckelberghs G, Vangheluwe M, Van Doorsselaere K, Robijns E, Persoons A, Verbiest T (2006) Macromol Rapid Commun 27:1920
126. Adachi I, Miyakoshi R, Yokoyama A, Yokozawa T (2006) Macromolecules 39:7793
127. Vallat P, Lamps JP, Schosseler F, Rawiso M, Catala JM (2007) Macromolecules 40:2600
128. Boyd SD, Jen AKY, Luscombe CK (2009) Macromolecules 42:9387
129. McCullough RD, Lowe RD, Jayaraman M, Anderson DL (1993) J Org Chem 58:904
130. Wu S, Huang L, Tian H, Geng Y, Wang F (2011) Macromolecules 44:7558
131. Lamps JP, Catala JM (2011) Macromolecules 44:7962
132. Miyakoshi R, Shimono K, Yokoyama A, Yokozawa T (2006) J Am Chem Soc 128:16012
133. Yokoyama A, Kato A, Miyakoshi R, Yokozawa T (2008) Macromolecules 41:7271
134. Sui A, Shi X, Wu S, Tian H, Geng Y, Wang F (2012) Macromolecules 45:5436
135. Nanashima Y, Yokoyama A, Yokozawa T (2012) Macromolecules 45:2609
136. Senkovskyy V, Tkachov R, Komber H, Sommer M, Heuken M, Voit B, Huck WTS, Kataev V, Petr A, Kiriy A (2011) J Am Chem Soc 133:19966
137. Yokoyama A, Suzuki H, Kubota Y, Ohuchi K, Higashimura H, Yokozawa T (2007) J Am Chem Soc 129:7236
138. Yokozawa T, Kohno H, Ohta Y, Yokoyama A (2010) Macromolecules 43:7095
139. Yokozawa T, Suzuki R, Nojima M, Ohta Y, Yokoyama A (2011) Macromol Rapid Commun 32:801
140. Elmalem E, Kiriy A, Huck WTS (2011) Macromolecules 44:9057
141. Liu J, Sheina E, Kowalewski T, McCullough RD (2002) Angew Chem Int Ed 41:329
142. Iovu MC, Jeffries-El M, Sheina EE, Cooper JR, McCullough RD (2005) Polymer 46:8582
143. Iovu MC, Zhang R, Cooper JR, Smilgies DM, Javier AE, Sheina EE, Kowalewski T, McCullough RD (2007) Macromol Rapid Commun 28:1816
144. Craley CR, Zhang R, Kowalewski T, McCullough RD, Stefan MC (2009) Macromol Rapid Commun 30:11
145. Lee Y, Fukukawa K-I, Bang J, Hawker CJ, Kim JK (2008) J Polym Sci A Polym Chem 46:8200
146. Iovu MC, Craley CR, Jeffries-El M, Krankowski AB, Zhang R, Kowalewski T, McCullough RD (2007) Macromolecules 40:4733
147. Sommer M, Lang AS, Thelakkat M (2008) Angew Chem Int Ed 47:7901
148. Zhang QL, Cirpan A, Russell TP, Emrick T (2009) Macromolecules 42:1079
149. Richard F, Brochon C, Leclerc N, Eckhardt D, Heiser T, Hadziioannou G (2008) Macromol Rapid Commun 29:885

150. Boudouris BW, Frisbie CD, Hillmyer MA (2008) Macromolecules 41:67
151. Dai C-A, Yen W-C, Lee Y-H, Ho C-C, Su W-F (2007) J Am Chem Soc 129:11036
152. Radano CP, Scherman OA, Stingelin-Stutzmann N, Mueller C, Breiby DW, Smith P, Janssen RAJ, Meijer EW (2005) J Am Chem Soc 127:12502
153. Watanabe N, Mauldin C, Fréchet JMJ (2007) Macromolecules 40:6793
154. Benanti TL, Kalaydjian A, Venkataraman D (2008) Macromolecules 41:8312
155. Yokozawa T, Adachi I, Miyakoshi R, Yokoyama A (2007) High Perform Polym 19:684
156. Yokozawa T, Yokoyama A (2009) Chem Rev 109:5595
157. Zhang Y, Tajima K, Hirota K, Hashimoto K (2008) J Am Chem Soc 130:7812
158. Ohshimizu K, Ueda M (2008) Macromolecules 41:5289
159. Ouhib F, Khoukh A, Ledeuil JB, Martinez H, Desbrieres J, Dagron-Lartigau C (2008) Macromolecules 41:9736
160. Van den Ber K, Huybrechts J, Verbiest T, Koeckelberghs G (2008) Chem Eur J 14:9122
161. Ouhib F, Hiorns RC, de Bettignies R, Bailly S, Desbrieres J, Dagron-Lartigau C (2008) Thin Solid Films 516:7199
162. Wu PT, Ren GQ, Li CX, Mezzenga R, Jenekhe SA (2009) Macromolecules 42:2317
163. Khanduyeva N, Senkovskyy V, Beryozkina T, Horecha M, Stamm M, Uhrich C, Riede M, Leo K, Kiriy A (2009) J Am Chem Soc 131:153

Adv Polym Sci (2013) 262: 239–258
DOI: 10.1007/12_2013_242

Published online: 6 November 2013

Metallopolymers as an Emerging Class of Self-Healing Materials

Benedict Sandmann, Stefan Bode, Martin D. Hager, and Ulrich S. Schubert

Abstract Metallopolymers are highly interesting materials with properties combining typical polymeric features with the properties of metal–ligand complexes. Thereby, the incorporation of different metal complexes into the polymeric material enables the tuning of the resulting material's properties. In particular, ionic interactions between charged metal complexes and the corresponding counterions as well as reversible (switchable) metal–ligand interactions make these materials potentially interesting as self-healing materials. Compared to other self-healing polymers, the research on these materials is still in its infancy. This review summarizes the latest trends in the research regarding this class of materials.

Keywords Ionomers · Metallopolymers · Self-healing materials · Self-healing polymers · Supramolecular polymers

---

This review represents an extension, refocusing, and update of the chapter "Metal-complex based self-healing polymers" in the book "*Self-healing polymers: From principles to applications*" (Wiley-VCH 2013, edited by Wolfgang Binder). Copyright Wiley-VCH Verlag GmbH & Co. KGaA. Reproduced with permission. The book chapter was tailor-made for the special issue of *Advances in Polymer Science*: *Hierarchical polymer structures: 60 years after the Staudinger Nobel Prize*.

B. Sandmann, S. Bode, and M.D. Hager
Laboratory of Organic and Macromolecular Chemistry (IOMC), Friedrich Schiller University, Humboldtstraße 10, 07743 Jena, Germany

Jena Center for Soft Matter (JCSM), Friedrich Schiller University Jena, Philosophenweg 7, 07743 Jena, Germany
e-mail: martin.hager@uni-jena.de

U.S. Schubert (✉)
Laboratory of Organic and Macromolecular Chemistry (IOMC), Friedrich Schiller University, Humboldtstraße 10, 07743 Jena, Germany

Jena Center for Soft Matter (JCSM), Friedrich Schiller University Jena, Philosophenweg 7, 07743 Jena, Germany

Dutch Polymer Institute (DPI), P.O. Box 902, 5600 AX Eindhoven, The Netherlands
e-mail: ulrich.schubert@uni-jena.de

Contents

1 Introduction

The ground-breaking work of Lehn, Pedersen, and Cram has been honored with the Nobel Prize in chemistry "for their development and use of molecules with structure-specific interactions of high selectivity", namely, for their investigations in the field of crown ethers and host–guest interactions [1]. It was the beginning of supramolecular chemistry as a new important research field in chemistry. Lehn defined supramolecular chemistry as the chemistry "beyond the molecule" [2]. Structures of higher complexity are constructed and hold together by a wide range of interactions, like hydrogen-bonding [3], hydrophobic interactions [4], π–π stacking interactions [5], and metal–ligand interactions [6–8]. Thereby, Nature acts as a role model by providing many inspiring examples of supramolecular structures like the DNA structure (double helix), metallo-proteins, etc. [9]. This field of research on noncovalent systems expands the world of covalent high molar mass materials (i.e., synthetic macromolecules or polymers) discovered by Staudinger, who was honored with the Noble Prize in 1953.

In recent years, an area of special interest has been identified that combines both worlds, i.e., covalent and noncovalent macromolecules, in particular the field of metallo(supramolecular) polymers. These materials combine many polymeric with metal complexes and metallic properties, enabling the design of new materials with outstanding properties, e.g., with self-X properties such as self-repair, self-organization, self-assembly, and self-healing. For instance, metallo-polymers have also been utilized for the fabrication of stimuli-responsive structures, resulting in reversible polymeric materials [10]. Due to this fact, metallopolymers have also been discussed in the context of self-healing materials. Their structural elements can feature reversible interactions similar to those known from hydrogen bonding polymers [11–14] or reversible covalently linked polymers [9, 15–19].

The above-mentioned properties, i.e., reversibility and stimuli-responsiveness, are directly linked to the metal–ligand binding strength. By changing the ligand(s) and the corresponding metal ion, respectively, the intrinsic properties of the final material can be tuned.

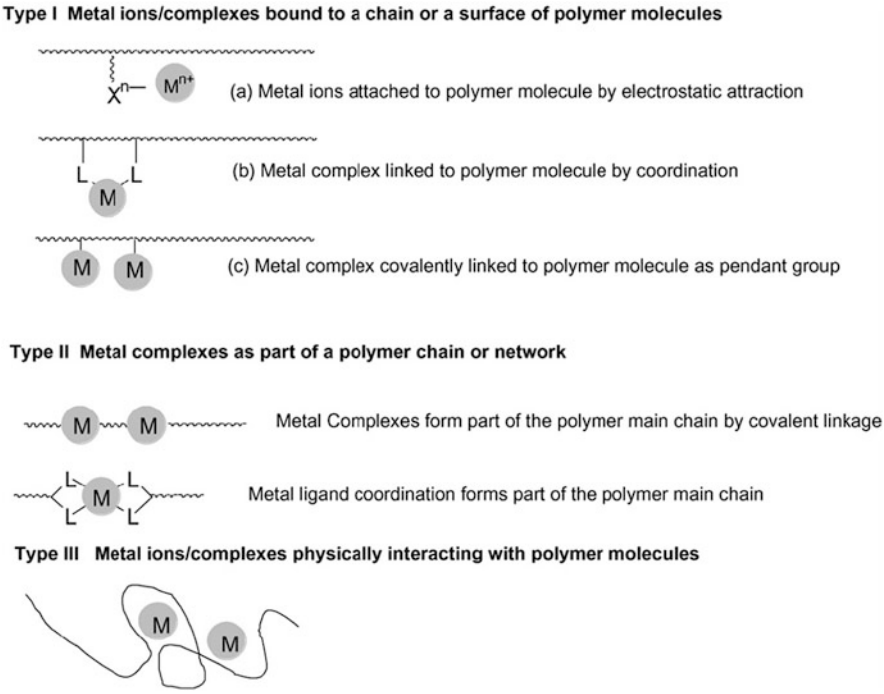

Fig. 1 Various approaches for preparation of metal-containing polymers (the counterions are omitted for clarity) (Copyright 2013 Elsevier) [25]

Ciardelli classified the architecture of metallopolymers into three different types (Fig. 1) [20]. In type I, the metal–ligand pairs are attached to the polymer side chain or as an end group of the backbone by electrostatic interactions, covalent bonds, or metal–ligand coordination (type Ia–Ic, Fig. 1). In type II, the metal ions or complexes are embedded into the main chain by coordinative or covalent associations [21–24]. In type III, the assembly of metal ions into the polymeric arrangement (i.e., the matrix) takes place through physical interactions [25]. In particular, polymers of type I and II are interesting candidates for self-healing polymers. Although conjugated metallopolymers feature very interesting optical properties, non-conjugated polymers have been used nearly exclusively in research on stimuli-responsiveness and self-healing behavior.

The application of metallopolymers as redox-active materials has gained significant importance for creating highly efficient redox conductivity for chemo- and biosensors [26–29], both catalytic and electroluminescent [30–33], magnetic applications [34–37], photovoltaics, and nonlinear optical applications [38–42].

For metal–ligand interactions, the conjunction of both a high binding constant as well as sufficient reversibility represents a challenging task. The stability of a certain complex, a thermodynamic property, is represented by the individual binding constant K. In the case of a very high binding constant between the

ligand(s) and the corresponding metal ion, thermodynamical stable polymers are formed. The physics and properties of these polymers are comparable to classical covalent polymers (Staudinger-like polymers). For a low binding constant, polymeric assemblies only form in the solid state, not in solution (classical inorganic coordination polymers). In contrast, medium binding constants also enable the formation of macromolecular assemblies in solution. The binding constant K depends on several external parameters like pH value, temperature, and solvent polarity as well as on the ligand design and the corresponding metal ion. K can be increased by multiple interacting binding sites, like chelating ligands or multivalent metal ions. Accordingly, for every metal–ligand pair, a detailed investigation of the thermodynamic and kinetic properties is required when a suitable metal–ligand combination is chosen [43].

Kinetically labile metal–ligand interactions open a field for materials with remarkable properties by assembling, disassembling, and reconstructing in a dynamic way. These weak interactions are particularly utilized in materials that have the ability to self-repair [44], self-anneal, and self-correct under certain conditions [45]. Most metallopolymers contain ionic metal complexes. The combination of these positively charged moieties and the corresponding counterions can lead to interesting properties. The melt morphology of diblock copolymers with central metal complexes as linking unit strongly depends on the type and size of the counterions. The groups of Schubert and Gohy investigated the self-assembly of systems having ruthenium ions as the metal, complexed with terpyridine ligands attached to polystyrene (PS) and poly(ethylene oxide) (PEO) [46]. In bulk, the electrostatic interactions between the metal–ligand complex ions and their counterions drive them to form aggregates [47]. This leads to morphologies that are different to their covalent counterpart. Al-Hussein et al. reported highly ordered lamellar structures in the melt of a PS_{20}-[Ru]-PEO_{70} diblock copolymer when bulky counterions were used. Thereby, the metal–ligand complex acting as ionomer is responsible for triggering the microphase separation. This observation can be used to tune the morphology of the metallo(supramolecular) copolymers [48]. The electrostatic interaction between the metal–ligand ions and their associated counterions drives them to form aggregates.

2 Ionomers

The described morphological features for metallopolymers show some parallels with the situation in common ionomers, in which the presence of ionic clusters contributes strongly to the healing process. This has also to be considered for self-healing metallopolymers featuring (ionic) clusters, comparably to ionomers. These latter materials were defined by Tant and Wilkes as a class of ion-containing copolymers. Thereby, the maximum ion group content is about 15 mol% [49]. To distinguish these systems from polyelectrolytes, Eisenberg and Rinaudo further developed the definition, so that ionomer bulk properties are organized by ionic

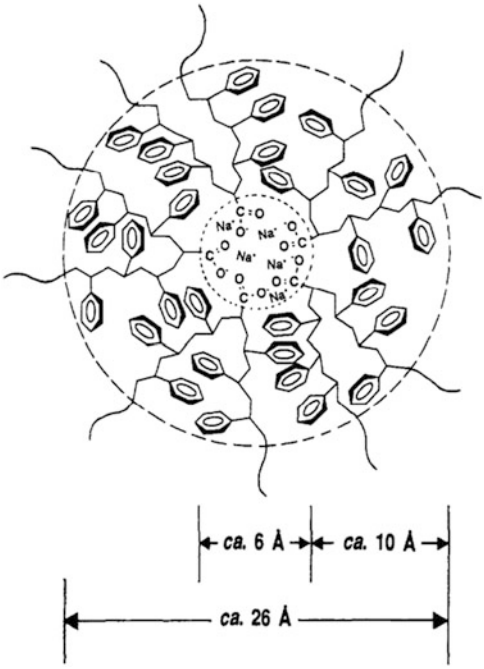

Fig. 2 Region of restricted mobility surrounding a multiplet in a poly(styrene-*co*-sodium methacrylate) ionomer (Reproduced with permission from [52], Copyright 2013 The American Chemical Society)

interactions with respective areas of the polymer structure [50]. Ionomers are generated by a neutralization process. The ionic component (pendant acid groups) is attached to the polymer backbone. After neutralization the ionic groups are part of the polymer structure of the resulting ionomer (or ionic copolymer). The ionic pairs assemble into discrete regions known as multiplets. Eisenberg described in detail the design and constitution of such ionic multiplets (Fig. 2) [51, 52]. In the case of low ionic group contents, the multiplets are isolated. Higher proportions result in an overlapping of the regions with restricted mobility and cluster development (Fig. 3). An increase in the ionic content tremendously influences the mechanical properties of the material [53–56]. Ionic interactions also allow self-healing processes. The reason lies in the reversibility of the cluster formation, so multiple local healing events are possible, e.g., using heat as trigger.

In 2001, Fall investigated the self-healing response by using bullet puncture tests on the commercial poly(ethylene-*co*-methacrylic acid) EMAA materials React-a-Seal®, Surlyn® 8920, and Surlyn® 8940 with varying ionic content [57]. Projectile testing of EMAA copolymers with ionic segments was conducted by Kalista et al. [58–60] and further investigated by Varley [61–65] and van der Zwaag [62, 66]. During the bullet puncture test very high temperatures are generated locally. Due to that, the ionomer was heated above the order–disorder transition and a healing was obtained [58–68]. Furthermore, the heating could also result in melting of the polymer. After the polymer was cooled to room temperature, the aggregates

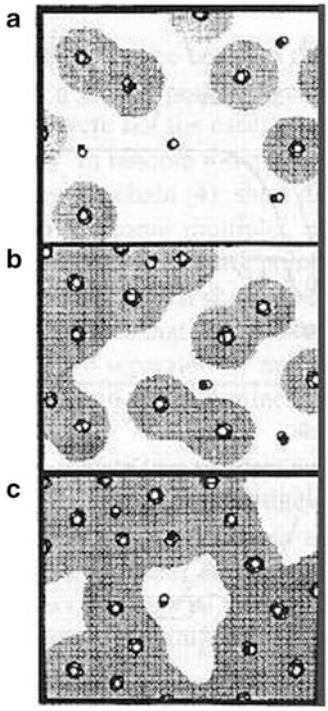

Fig. 3 Morphologies of various ionomers at different ion contents: (**a**) low ion content; (**b**) intermediate ion content; and (**c**) high ion content (Reproduced with permission from [52], Copyright 2013 The American Chemical Society)

(clusters) reformed and the original mechanical properties were recovered. Furthermore, Kalista et al. investigated the self-healing behavior of EMAA materials at temperatures between −50 and 140 °C [60]. The authors could demonstrate that self-healing is possible below the order–disorder temperature due to the reversible formation of hydrogen bonds from the carboxylic acids. Furthermore, they showed that the self-healing efficiency at different temperatures strongly depends on the ionic content. Thus, high ionic contents are better for healing at high temperatures (above the order–disorder transition) and low amounts of cluster are required for healing at low temperatures. Metallopolymers could also feature comparable ionic clusters due to their charged complexes. These could also contribute to the self-healing process.

3 Stimuli-Responsive Metallopolymers

The introduction of metal complexes into polymeric materials can lead to interesting properties and, particularly, the structural properties of these complexes are of importance in self-healing materials [9]. It can be important for the self-healing process that special properties can be changed upon application

of an external stimulus such as light, heat, or change in pH. These stimuli-responsive metallopolymers could be affected in many different ways. As a consequence, the stimuli-responsive metallopolymers are not only interesting candidates for self-healing polymers but also for several other application fields such as sensors [69].

In addition to stimulation by redox processes, the properties of a metallopolymer can also be influenced by other stimuli. An interesting change in metallopolymers was shown by Peng et al. [70]. The authors used the external stimulus light in order to influence the properties of an iron metallopolymer; a redox process from iron(III) to iron(II) could be induced by illumination and this process changed the consistency of the polymer. In this case, a metallopolymer gel, which contains iron(III) ions, was converted into a liquid polymer by simply reducing the iron ions. The subsequent re-oxidation by air led to the original "solid state" system.

Furthermore, the supply of thermal energy could also be used to influence the properties of a metallopolymer and to yield the desired effects. For this purpose, Zhou and coworkers utilized phase-separated ruthenium-containing polymers with two glass transition temperatures [71]. The transitions induced the a kind of mobility that is required for the self-healing process [72].

Beside the mentioned external stimuli, there are also several other possibilities that can influence the polymer properties and structures, leading to changes on the molecular scale and thus, to other changes in the properties of the metallopolymer. For example, Beck and Rowan showed that mechanical energy is adequate (e.g., simple shaking) for generating a change in the properties of the polymer [73]. The authors used an oligo(ethylene gylcol), which was functionalized with two 2,6-*bis*(1'-methylbenzimidazolyl)pyridine units at the termini. In a second step, a metallopolymer was formed by the addition of a lanthanide (lanthanum or europium) and a transition metal ion (cobalt or zinc). In further studies it could be shown that these metallopolymers could also be influenced by other external stimuli [74, 75], e.g., by changes in pH, light, and temperature.

This all-embracing example shows that many different stimuli can affect a metallopolymer to result in the desired properties. In particular, the reversibility of the metal–ligand interaction and the mobility of a metallopolymer are key factors for the implementation of self-healing properties [76, 77]. Additionally, the addressability by other stimuli allows the possibility of triggering healing processes in metallopolymers.

4 Self-Healing Metallopolymers

The above-mentioned properties of metallopolymers are the basic requirements for the generation of self-healing behavior. As a consequence, it is possible to generate a reversible system and to introduce self-healing mechanisms, which is the principle of intrinsic self-healing systems [78–81].

4.1 Biological Archetypes

The self-healing possibilities based on metal–ligand interactions can also be observed in nature. In 2001, Vaccaro and Waite described the ability of mussel byssus threads to heal after an inflicted damage [82]. In the following decade, more detailed insights into the mechanism and the parameters that influence this natural system were collected. Meanwhile, it could be shown that the self-healing behavior is based on an interaction between iron(III) ions and 3,4-dihydroxyphenylalanine (dopa) [83]. The iron center can bind one, two, or three catcheol-based ligands, which are connected with a polymer backbone. The number of bonded ligands depends on the pH value [84–86]. At low pH (below 5), the mono-dopa iron(III) complex is formed, which does not lead to a crosslinking of the polymer chains. The result is an extensible material. By contrast, increasing pH values lead to a more crosslinked polymer network, which provides an increased hardness [83, 87–90]. This principle, which can be found in nature, could also be mimicked by synthetic polymers. For this purpose, poly(ethylene glycol) (PEG) was functionalized with catechol units and Holten-Andersen et al. were able to show the reversibility of the metal–ligand interaction [84, 85].

Beside the iron–dopa interaction, it could be proven that the zinc-histidine system also leads to self-healing behavior of mussel byssus threads, which feature a hierarchical structure [91–93]; a fiber containing a middle block of collagen, which is flanked by histidine-rich parts, in an environment with a high content of zinc ions leads to a reversible crosslinking [93, 94]. The recovery of the mechanical properties of the mussel byssus thread could be demonstrated (Fig. 4) and, furthermore, it was possible to design a model system based on a PEG star functionalized with histidine moieties [95, 96]. These systems were utilized for the generation of metal-containing hydrogels.

4.2 Synthetic Self-Healing Metallopolymers

Several synthetic metallopolymers have been synthesized to obtain self-healing behavior based on metal–ligand interactions. In 2005, Varghese et al. were able to show that a gel based on acryloyl-6-amino caproic acid (A6ACA) can heal scratches if the polymer is dipped into an aqueous copper(II) chloride solution [97]. However, the study did not answer the question of the influence of hydrogen bonds on the self-healing effect, particularly because a medium was selected in which hydrogen bonds exist. Moreover, the mobility of the gel itself could also affect the self-healing behavior; therefore, the particular influence of the metal–ligand interaction on the self-healing process is still unclear.

In addition to the incorporation of the ligand function in the side chain, it is also possible to install the ligand in the main chain of the polymer. Yuan et al. showed that a self-healing behavior can be generated by polymers that feature ligands

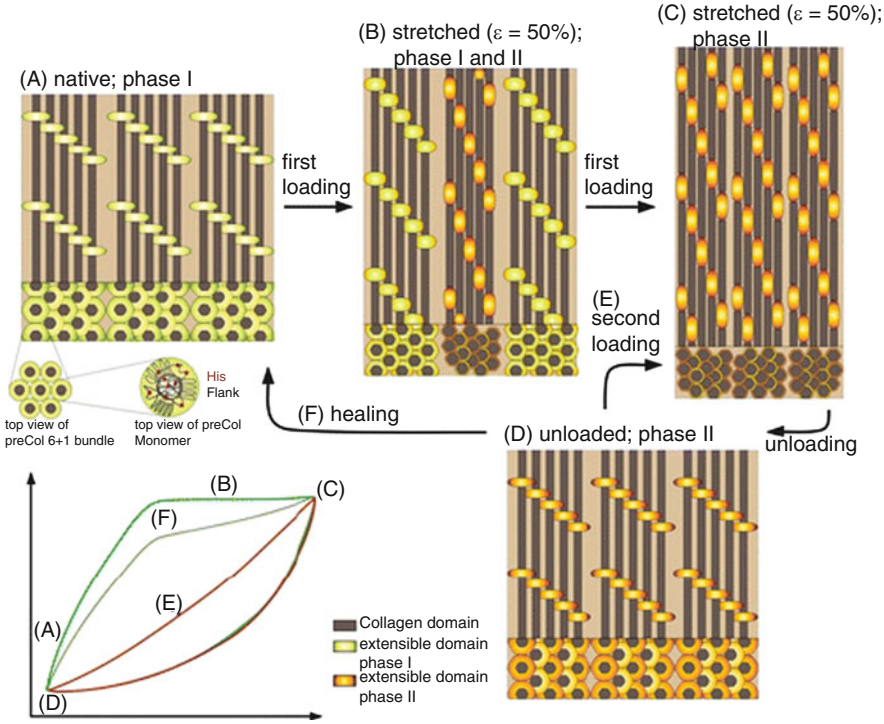

Fig. 4 Molecular model of reversible deformation behavior in mussel byssal threads (Copyright 2013 The American Chemical Society) [95]

within the main chain [98]. The authors used polyurethane analogue polymers as the backbone, in which *bis*(1,2,3-trizol-4-yl) pyridine was incorporated as ligand. Afterwards, these polymers were complexed with zinc(II) and europium(III) ions, respectively, which led to self-healing properties.

In this case, the question also arises as to whether the metal–ligand interaction is the only reason for the self-healing process. There is also the possibility of hydrogen bond formation, which could also contribute to the self-healing properties. In addition, the self-healing efficiency was not quantified.

Furthermore, Terech et al. presented a self-healing metallopolymer gel that was based on the diterpyridyl moiety polymerized by the addition of nickel ions [99]. The resulting linear polymer exhibited very poor mechanical properties and showed a good healing efficiency due to high flexibility of the polymer itself.

In 2011, Rowan and Weder et al. described the self-healing properties of a linear metallopolymer. In order to obtain self-healing behavior, the authors used UV light [44]. For this purpose, poly(ethylene-*co*-butylene) was functionalized with two 2,6-*bis*(1'-methylbenzimidazolyl)pyridine moieties at the termini and the subsequent addition of zinc di[*bis*(trifluoromethylsulfonyl)imide] or lanthanum tri[*bis*(trifluoromethylsulfonyl)imide] led to a linear metallopolymer.

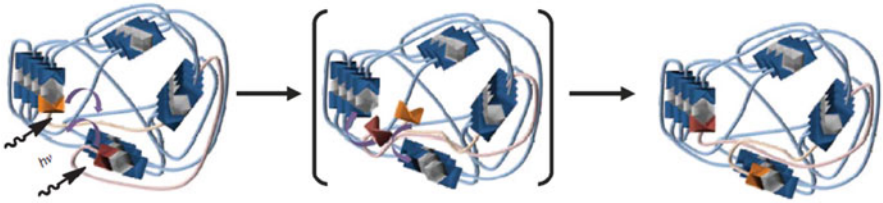

Fig. 5 Proposed self-healing mechanism (Copyright 2013 Nature Publishing Group) [44]

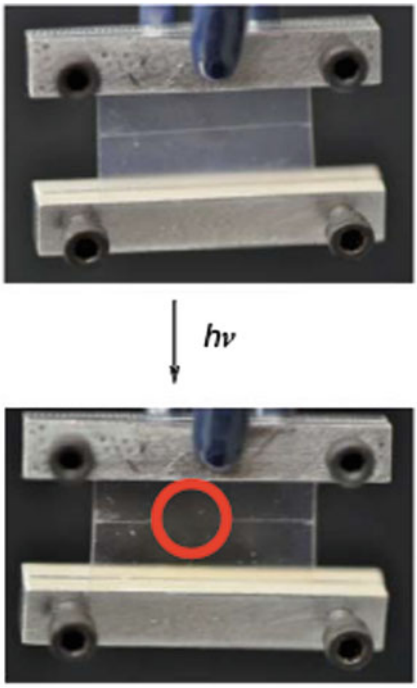

Fig. 6 Demonstration of the self-healing ability of a linear metallopolymer (Copyright 2013 Nature Publishing Group) [44]

This metallopolymer showed self-healing behavior if illuminated by UV light with a wavelength corresponding to the absorption band of the polymer. In this case, energy transfer led to heating of the polymer to 220 °C. The proposed mechanism of the self-healing process is based on the reversibility of the metal–ligand interaction as well as the breakage of metal complex clusters (Fig. 5). The cleavage of the metal complexes increases the mobility of the polymer, which leads to a dynamic motion of the polymers and to the self-healing of inflicted damage. Subsequently, the complexes (and clusters) will be reformed upon cooling,

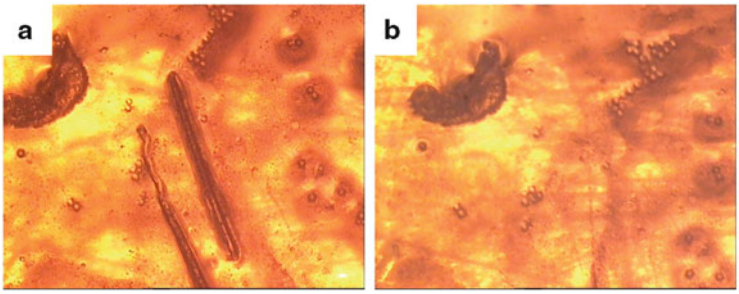

Fig. 7 Self-healing of a metallosupramolecular copolymer network crosslinked by cadmium-terpyridine units: (**a**) scratch and (**b**) healing after 16 h at 80°C (Copyright 2013 The Royal Society of Chemistry) [101]

resulting in an immobilization of the mobile phase and a (complete) healing of the scratch (Fig. 6).

A second example of coatings based on self-healing metallopolymers was recently described by Schubert et al. [100]. A polymer network was synthesized by the crosslinking of terpyridine-functionalized poly(alkyl methacrylates). For this purpose, an iron salt was added, resulting in insoluble and very hard polymer films after drying. Furthermore, it could be shown that decomplexation is not the main process for the self-healing process. In contrast, the ionic interactions between the charged complexes and the counterions (i.e. sulfate) are the basic principle of the self-healing behavior of such crosslinked metallopolymer networks (comparable to ionomers).

Recently, the basic concept of self-healing metallopolymer networks was improved. For this purpose, the Schubert group utilized cadmium(II)-bis-terpyridine complexes [101]. A metallopolymer network based on these complexes was synthesized by the addition of cadmium acetate. The authors could show that these materials behave completely different due to a different coordination of the metal center. Presumably, the acetate moiety also coordinates to the cadmium, but this metal–ligand interaction is much weaker, which results in an improved self-healing behavior (Fig. 7).

4.3 Self-Healing on the Molecular Scale

The above-described examples reveal some basic principles of the self-healing process within metallopolymers. However, a detailed understanding of the process is complicated because different factors play a role (properties of the polymer, binding strength, ionic interactions, etc.). Starting on the macroscopic level, the deformation of the metallopolymer has to be mainly elastic (in particular, when the healing of coatings and thin films is considered). By contrast, plastic deformation will not provide a restoring force. The elastic recovery is important for

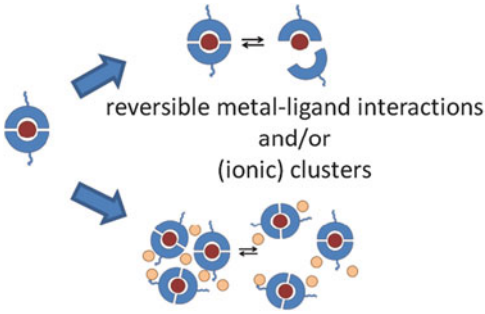

Fig. 8 Metal complexes within the self-healing polymers feature reversibility of the metal–ligand interaction and/or lead to the formation of reversible (ionic) clusters

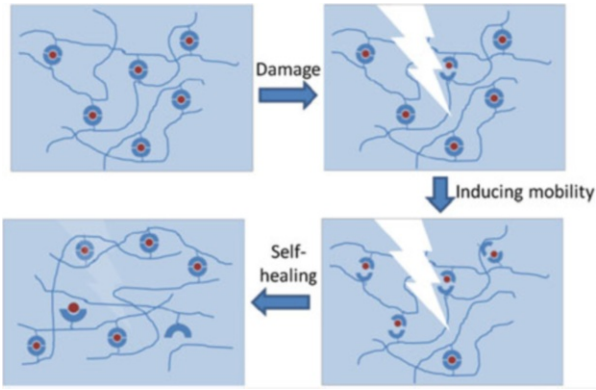

Fig. 9 The self-healing process. The damage can be healed in this case by reversible metal–ligand interactions. The cleavage of these bonds induces mobility, which can lead to closure of the crack. The re-formation of the complexes leads to a new molecular pattern

self-healing because it is the first step of the self-healing process [72]. The healing of bulk materials can also be promoted by bringing the damaged sites into contact.

On the molecular scale (see Fig. 8), the healing of metallopolymers is based on the ionic structure of the complexes and/or on the reversibility of metal complexes, often in combination with an ordered or even hierarchical structure.

Most metal–ligand complexes are positively charged and this could lead to an ionic structure and to a formation of ionic clusters. Comparable to "classic" ionomers, a healing process within metallopolymers could be supported by the ionic interactions of positively charged metal complexes and the corresponding counterions [58, 61]. Moreover, differences in the metal complexes as well as the polymer matrix can also lead to a phase separation, resulting in the formation of clusters [44].

Furthermore, the strength of the metal–ligand bonding can be tuned and, thereby, it is possible to identify a system where the metal–ligand bonding is weak and reversible. As a consequence, the opening and reformation of metal complexes can contribute to the healing process.

After mechanical damage (which will also lead to the cleavage of "normal" covalent bonds) it is possible to induce mobility of the polymer by the cleavage of

metal–ligand interactions and/or the breakage of (ionic) clusters (see Fig. 9). Subsequently, this change leads to healing of the mechanical damage. The original functionality is restored after reformation of complexes and/or clusters (i.e., immobilization). Note that the original structure is not restored, but that a new molecular pattern is created. The phenomena of reversibility and switchability are well known from metal–ligand bonds in solution, but the study of the behavior of the metal–ligand interaction in the solid state is difficult [102–105]. New methods have to be developed in order to investigate these interesting materials in more detail.

5 Conclusion and Outlook

The fascinating material class of metallopolymers combines the world of covalent polymers pioneered by Staudinger with the concepts and systems of supramolecular chemistry and shows interesting properties due to the marriage of polymeric features with the distinct properties of metal complexes. The combination of a wide range of different metal ions with the corresponding ligands allows tuning of the desired properties. In the field of stimuli-responsive polymers, metallopolymers have been frequently applied. Their switchable properties enable the utilization of interesting triggers (e.g., light) for a self-healing process. However, in contrast to other noncovalent interactions (particularly in comparison to the prime example, hydrogen bonds), metal complexes have been applied less frequently in self-healing materials. First examples confirm the great potential of these materials and significant improvements can be expected in the coming years in this field. Nature, which successfully utilizes noncovalent interactions (e.g., in mussel byssus threads), reveals another important issue: the order and spatial arrangement of the metal complexes.

The healing of some synthetic materials has been described on the molecular as well as macroscopic level in recent years.

Metallopolymers, as one of the youngest members of the self-healing polymer family, are a rather new research field. Many possibilities for the design of self-healing polymers are imaginable. Moreover, further intense research is required to clarify the detailed mechanisms of the healing within these materials. A deeper understanding of the behavior of the metal–ligand bonds in the solid state is required. This knowledge can only be gained with the use of new characterization techniques that can reveal the molecular processes within polymeric materials. The utilization of self-healing metallopolymers for potential applications will be the main focus of future research. Due to their fascinating properties (e.g., light absorption or emission), metallopolymers offer the possibility to design new functional coatings [9, 106–109]. For this purpose, the combination of optical and self-healing properties is necessary. This combination could result in a new class of functional coatings. In that context, an improved processability of the self-healing metallopolymer is required and known methods must be applied for these materials [9, 110–112].

Acknowledgements The authors thank the Deutsche Forschungsgemeinschaft (DFG, SPP 1568), the Dutch Polymer Institute (DPI, technolgy area HTE) and the Fonds der chemischen Industrie (FCI) (scholarship for S.B.) for financial support.

References

1. Brunsveld L, Folmer BJB, Meijer EW, Sijbesma RP (2001) Supramolecular polymers. Chem Rev 101:4071–4097
2. Lehn JM (1994) Supramolecular chemistry. Proc Natl Sci Acad USA 106:915–922
3. ten Cate AT, Sijbesma RP (2003) Coils, rods and rings in hydrogen-bonded supramolecular polymers. Macromol Rapid Commun 23:1094–1112
4. Kastner U (2001) The impact of rheological modifiers on water-borne coatings. Coll Surf 183:805–821
5. Lehn JM, Meric R, Vigneron JP, Cesario M, Guilhem J, Pascard C, Asfari Z, Vicens J (1995) Binding of acetylcholine and other quaternary ammonium cations by sulfonated calixarenes. Crystal structure of a [choline-tetrasulfonated calix[4]arene] complex. Supramol Chem 5:97–103
6. Hinderberger D, Schmelz O, Rehahn M, Jeschke G (2004) Electrostatic site attachment of divalent counterions to rodlike ruthenium(II) coordination polymers characterized by EPR spectroscopy. Angew Chem Int Ed 43:4616–4621
7. Schmatloch S, van den Berg AMJ, Alexeev AS, Hofmeier H, Schubert US (2003) Soluble high-molecular-mass poly(ethylene oxide)s via self-organization. Macromolecules 36:9943–9949
8. South CR, Burd C, Weck M (2007) Modular and dynamic functionalization of polymeric scaffolds. Acc Chem Res 40:63–74
9. Whittell GR, Hager MD, Schubert US (2011) Functional soft materials from metallopolymers and metallosupramolecular polymers. Manners I. Nat Mater 10:176–188
10. Weng WG, Beck JB, Jamieson AM, Rowan SJ (2006) Understanding the mechanism of gelation and stimuli-responsive nature of a class of metallo-supramolecular gels. J Am Chem Soc 128:11663–11672
11. Cordier P, Tournilhac F, Soulié-Ziakovic C, Leibler L (2008) Self-healing and thermoreversible rubber from supramolecular assembly. Nature 451:977–980
12. Kitagawa S, Uemura K (2005) Dynamic porous properties of coordination polymers inspired by hydrogen bonds. Chem Soc Rev 34:109–119
13. Montarnal D, Cordier P, Soulié-Ziakovic C, Tournilhac F, Leibler L (2008) Synthesis of self-healing supramolecular rubbers from fatty acid derivates, diethylene triamine, and urea. J Polym Sci A Polym Chem 46:7925–7936
14. Montarnal D, Tournilhac F, Hidalgo M, Couturier J-L, Leibler L (2009) Versatile one-pot synthesis of supramolecular plastics and self-healing rubbers. J Am Chem Soc 131:7966–7967
15. Yuan YC, Yin T, Rong MZ, Zhang MQ (2008) Self healing in polymers and polymer composites. Concepts, realization and outlook: a review. Express Polym Lett 2:238–250
16. Zhang Y, Broekhuis AA, Picchioni F (2009) Thermally self-healing polymeric materials: the next step to recycling thermoset polymers? Macromolecules 42:1906–1912
17. Chen X, Dam MA, Ono K, Mal A, Shen H, Nutt SR, Sheran K, Wudl F (2002) A thermally re-mendable cross-linked polymeric material. Science 295:1698–1702
18. Chen X, Wudl F, Mal AK, Shen H, Nutt SR (2003) New thermally remendable highly cross-linked polymeric materials. Macromolecules 36:1802–1807

19. Kötterizsch J, Stumpf S, Hoeppener S, Vitz J, Hager MD, Schubert US (2013) One-component intrinsic self-healing coatings based on reversible crosslinking by Diels–Alder cycloadditions. Macromol Chem Phys 214:1636–1649
20. Ciardelli F, Tsuchida E, Wöhrle DE (eds) (1996) Macromolecule-metal complexes. Springer, Heidelberg
21. Wong WY, Ho CL (2006) Di-, oligo- and polymetallaynes: syntheses, photophysics, structures and applications. Coord Chem Rev 250:2627–2690
22. Wong WY, Ho CL (2010) Organometallic photovoltaics: a new and versatile approach for harvesting solar energy using conjugated polymetallaynes. Acc Chem Res 43:1246–1256
23. Wong WY, Harvey PD (2010) Recent progress on the photonic properties of conjugated organometallic polymers built upon the *trans-bis*(*para*-ethynylbenzene)*bis*(phosphine)platinum(II) chromophore and related derivatives. Macromol Rapid Commun 31:671–713
24. Ho CL, Wong WY (2011) Metal-containing polymers: facile tuning of photophysical traits and emerging applications in organic electronics and photonics. Coord Chem Rev 255:2469–2502
25. Chan WK (2007) Metal containing polymers with heterocyclic rigid main chains. Coord Chem Rev 251:2104–2118
26. McQuade DT, Pullen AE, Swager TM (2000) Conjugated polymer-based chemical sensors. Chem Rev 100:2537–2574
27. Wild A, Winter A, Hager MD, Schubert US (2012) Fluorometric, water-based sensors for the detection of nerve gas G mimics DMMP, DCP and DCNP. Chem Commun 48:964–966
28. Wild A, Winter A, Hager MD, Schubert US (2012) Fluorometric sensor based on bisterpyridine metallopolymer: detection of cyanide and phosphates in water. Analyst 137:2333–2337
29. Chow C-F (2012) Supramolecular polymeric chemosensor for biomedical applications: design and synthesis of a luminescent zinc metallopolymer as a chemosensor for adenine detection. J Fluorsec 22:1539–1546
30. Holliday BJ, Swager TM (2005) Conducting metallopolymers: the roles of molecular architecture and redox matching. Chem Commun (1):23–36
31. Chen X-Y, Yang X, Holiday BJ (2008) Photoluminescent europium-containing inner-sphere conducting metallopolymer. J Am Chem Soc 130:1546–1547
32. Dennany L, Hogan CF, Keyes TE, Forster RJ (2006) Effect of surface immobilization on the electrochemiluminescence of ruthenium-containing metallopolymer. Anal Chem 78:1412–1417
33. Forster RJ, Hogan CF (2000) Electrochemiluminescent metallopolymer coatings: combined light and current detection in flow injection analysis. Anal Chem 72:5576–5582
34. Batten SR, Neville SM, Turner DR (eds) (2009) Coordination polymers design, analysis and application. Royal Society of Chemistry, Cambridge
35. Manners I (2002) Synthetic metal-containing polymers. 1st edn. Wiley-VCH, Weinheim
36. Werner R, Falk K, Ostrovsky S, Haase W (2001) Metallopolymer with schiff base side chains. Synthesis and characterization of some nickel(II) containing polymers with unexpected cooperative magnetic properties. Macromol Chem Phys 202:2813–2823
37. Djukic B, Dube PA, Razavi F, Seda T, Jenkins HA, Britten JF, Lemaire MT (2009) Preparation and magnetic properties of iron(3+) spin-crossover complexes bearing a thiophene substiuent: toward multifunctional metallopolymers. Inorg Chem 48:699–707
38. Wong WY, Wang XZ, He Z, Chan KK, Djurisic AB, Cheung KY, Yip CT, Ng AMC, Xi YY, Mak CSK, Chan WK (2007) Tuning the absorption, charge transport properties, and solar cell efficiency with the number of thienyl rings in platinum-containing poly(aryleneethynylene)s. J Am Chem Soc 129:14372–14380
39. Wong WY, Wang XZ, He Z, Djurisic AB, Yip CT, Cheung KY, Wang H, Mak CSK, Chan WK (2007) Metallated conjugated polymers as a new avenue towards high-efficiency polymer solar cells. Nat Mater 6:521–527
40. Zhou GJ, Wong WY (2011) Organometallic acetylides of PtII, AuI and HgII as new generation optical power limiting materials. Chem Soc Rev 40:2541–2566

41. Zhou GJ, Wong WY, Lin ZY, Ye C (2006) White metallopolyynes for optical limiting/transparency trade-off optimization. Angew Chem Int Ed 45:6189–6193
42. Wong W-Y, Wang X, Zhang H-L, Cheung K-Y, Fung M-K, Djurisic AB, Chan W-K (2008) Synthesis, characterization and photovoltaic properties of a low-bandgab platinum(II) polyyne functionalized with a 3,4-ethylenedioxythiophene-benzothiadiazole hybrid spacer. J Organmet Chem 693:3603–3612
43. Happ B, Winter A, Hager MD, Schubert US (2012) Photogenerated avenues in macromolecules containing Re(I), Ru(II), Os(II), and Ir(III) metal complexes of pyridine-based ligands. Chem Soc Rev 41:2222–2255
44. Burnworth M, Tang L, Kumpfer JR, Duncan AJ, Beyer FL, Fiore GL, Rowan SJ, Weder C (2011) Optically healable supramolecular polymers. Nature 472:334–337
45. Kurth DG, Higuchi M (2006) Transition metal ions: weak links for strong polymers. Soft Matter 2:915–927
46. Fustin CA, Guillet P, Schubert US, Gohy JF (2007) Metallo-supramolecular block copolymers. Adv Mater 19:1665–1673
47. Al-Hussein M, Lohmeijer BGG, Schubert US, de Jeu WH (2003) Melt morphology of polystyrene-poly(ethylene oxide) metallo-supramolecular diblock copolymer. Macromolecules 36:9281–9284
48. Al-Hussein M, de Jeu WH, Lohmeijer BGG, Schubert US (2005) Phase behavior of the melt of polystyrene–poly(ethylene oxide) metallo-supramolecular diblock copolymer with bulky counterions. Macromolecules 38:2832–2836
49. Tant MR, Wilkes GL (eds) (1987) Viscoelastic behavior of ionomers in bulk and solution, in structure and properties of ionomers. D Reidel, Dordrecht
50. Eisenberg A, Rinaudo M (1990) Polyelectrolytes and ionomers. Polym Bull 24:671
51. Eisenberg A (1970) Clustering of ions in organic polymers. A theoretical approach. Macromolecules 3:147–154
52. Eisenberg A, Hird B, Moore RB (1990) A new multiplet-cluster model for the morphology of random ionomers. Macromolecules 23:4098–4107
53. Bellinger MA, Sauer JA, Hara M (1994) Tensile fracture properties of rigid-rigid blends made of sulfonated polystyrene ionomer and polystyrene. Macromolecules 27:6147–6155
54. Statz RJ (1985) Ethylene copolymer ionomers. In: FB Seymour, T Cheng (eds) History of polyolefins: the world's most widely used polymers. Chemistry and chemists, vol 7. Springer, Heidelberg, pp 177–192
55. Rees R (ed) (1987) Ionomeric thermoplastic elastomers early research – Surlyn and related polymers, in thermoplastic elastomers: a comprehensive review. Carl Hanser Verlag, Munich
56. Hara M, Sauer JA (1994) Mechanical properties of ionomers. J Macromol Sci Polym Rev C34:325–373
57. Fall R (2001) Masters Thesis, Virginia Polytechnic Institute and State University
58. Kalista SJ, Ward TC, Oyetunji Z (2007) Self-healing of poly(ethylene-co-methacrylic acid) copolymers following projectile puncture. Mech Adv Mater Struct 14:391–397
59. Ward TC, Kalista SJ (2007) Thermal characteristics of the self-healing response in poly (ethylene-co-methacrylic acid) copolymers. J R Soc Interface 4:405–411
60. Kalista SJ, Pflug JR, Varley RJ (2013) Effect of ionic content on ballistic self-healing in EMAA copolymers and ionomers. Polym Chem 4:4910–4926
61. Varley RJ, Shen S, van der Zwaag S (2010) The effect of cluster plasticisation on the self healing behaviour of ionomers. Polymer 51:679–686
62. Varley RJ, van der Zwaag S (2008) Towards an understanding of thermally activated self-healing of an ionomer system during ballistic penetration. Acta Mater 56:5737–5750
63. Pingkarawat K, Wang CH, Varley RJ, Mouritz AP (2012) Self-healing of delamination cracks in mendable epoxy matrix laminates using poly[ethylene-*co*-(methacrylic acid)] thermoplastic. Compos A Appl S 43:1301–1307

64. Pingkarawat K, Wang CH, Varley RJ, Mouritz AP (2012) Self-healing of delamination fatigue cracks in carbon fibre-epoxy laminate using mendable thermoplastics. J Mater Sci 47:4449–4456
65. Hughes AE, Cole IS, Muster TH, Varley RJ (2010) Designing green, self-healing coatings for metal protection. Npg Asia Mater 2:143–151
66. Varley RJ, van der Zwaag S (2008) Development of a quasi-static test method to investigate the origin of self-healing in ionomers under ballistic conditions. Polym Test 27:11–19
67. Tadano K, Hirasawa E, Yamamoto H, Yano S (1989) Order-disorder transition of ionic clusters in ionomers. Macromolecules 22:226–233
68. Neppel A, Butler IS, Eisenberg A (1979) Vibrational spectra of polymers. 2. Variable-temperature raman spectroscopy as a probe for ion clustering in ionomers. Macromolecules 12:948–952
69. Stuart MAC, Huck WTS, Genzer J, Muller M, Ober C, Stamm M, Sukhorukov GB, Szleifer I, Tsukruk VV, Urban M, Winnik F, Zauscher S, Luzinov I, Minko S (2010) Emerging applications of stimuli-responsive polymer materials. Nat Mater 9:101–113
70. Peng F, Li GZ, Liu XX, Wu SZ, Tong Z (2008) Redox-responsive gel–sol/sol–gel transition in poly(acrylic acid) aqueous solution containing Fe(III) ions switched by light. J Am Chem Soc 130:16166–16167
71. Zhou GC, Harruna II, Ingram CW (2005) Ruthenium-centered thermosensitive polymers. Polymer 46:10672–10677
72. Wool RP (2008) Self-healing materials: a review. Soft Matter 4:400–418
73. Beck JB, Rowan SJ (2003) Multistimuli, multiresponsive metallo-supramolecular polymers. J Am Chem Soc 125:13922–13923
74. Weng WG, Li Z, Jamieson AM, Rowan SJ (2009) Effect of monomer structure on the gelation of a class of metallo-supramolecular polymers. Soft Matter 5:4647–4657
75. Rowan SJ, Beck JB (2005) Metal–ligand induced supramolecular polymerization: a route to responsive materials. Faraday Discuss 128:43–53
76. Murphy EB, Wudl F (2010) The world of smart healable materials. Prog Polym Sci 35:223–251
77. Wang F, Zhang JQ, Ding X, Dong SY, Liu M, Zheng B, Li SJ, Wu L, Yu YH, Gibson HW, Huang FH (2010) Metal coordination mediated reversible conversion between linear and cross-linked supramolecular polymers. Angew Chem Int Ed 49:1090–1094
78. Hager MD, Greil P, Leyens C, van der Zwaag S, Schubert US (2010) Self-healing materials. Adv Mater 22:5424–5430
79. Herbst F, Döhler D, Michael P, Binder WH (2013) Self-healing polymers via supramolecular forces. Macromol Rapid Commun 34:203–220
80. Billiet S, Hillewaere XKD, Teixeira RFA, Du Prez FE (2013) Chemistry of crosslinking processes for self-healing polymers. Macromol Rapid Commun 34:290–309
81. Brassinne J, Fustin C-A, Gohy JF (2013) Polymer gels constructed through metal–ligand coordination. J Inorg Organomet Polym 23:23–40
82. Vaccaro E, Waite JH (2001) Yield and post-yield behavior of mussel byssal thread: a self-healing biomolecular material. Biomacromolecules 2:906–911
83. Harrington MJ, Masic A, Holten-Andersen N, Waite JH, Fratzl P (2010) Iron-clad fibers: a metal-based biological strategy for hard flexible coatings. Science 328:216–220
84. Holten-Andersen N, Harrington MJ, Birkedal H, Lee BP, Messersmith PB, Lee KYC, Waite JH (2011) pH-induced metal-ligand cross-links inspired by mussel yield self-healing polymer networks with near-covalent elastic moduli. Proc Natl Acad Sci USA 108:2651–2655
85. Barrett DG, Fullenkamp DE, He L, Holten-Andersen N, Lee KYC, Messersmith PB (2013) pH-Based regulation of hydrogel mechanical properties through mussel-inspired chemistry and processing. Adv Funct Mater 23:1111–1119
86. Harrington MJ, Waite JH (2008) pH-Dependent locking of giant mesogens in fibers drawnfrom mussel byssal collagens. Biomacromolecules 9:1480–1486

87. Harrington MJ, Gupta HS, Fratzl P, Waite JH (2009) Collagen insulated from tensile damage by domains that unfold reversibly: in situ X-ray investigation of mechanical yield and damage repair in the mussel byssus. J Struct Biol 167:47–54
88. Harrington MJ, Waite JH (2009) How nature modulates a fiber's mechanical properties: mechanically distinct fibers drawn from natural mesogenic block copolymer variants. Adv Mater 21:440–444
89. Ceylan H, Urel M, Erkal TS, Tekinay AB, Dana A, Guler MO (2013) Mussel inspired dynamic cross-linking of self-healing peptide nanofiber network. Adv Funct Mater 23:2081–2090
90. Krogsgaard M, Behrens MA, Pedersen JS, Birkedal H (2013) Self-healing mussel-inspired multi-pH-responsive hydrogels. Biomacromolecules 14:297–301
91. Waite JH, Qin XX, Coyne KJ (1998) The peculiar collagens of mussel byssus. Matrix Biol 17:93–106
92. Carrington E, Gosline JM (2004) Mechanical design of mussel byssus: load cycle and strain rate dependence. Am Malacol Bull 18:135–142
93. Waite JH, Lichtenegger HC, Stucky GD, Hansma P (2004) Exploring molecular and mechanical gradients in structural bioscaffolds. Biochemistry 43:7653–7662
94. Waite JH, Broomell CC (2012) Changing environments and structure–property relationships in marine biomaterials. J Exp Biol 215:873–883
95. Krauss S, Metzger TH, Fratzl P, Harrington MJ (2013) Self-repair of a biological fiber guided by an ordered elastic framework. Biomacromolecules 14:1520–1528
96. Fullenkamp DE, He L, Barrett DG, Burghardt WR, Messersmith PB (2013) Mussel-inspired histidine-based transient network metal coordination hydrogels. Macromolecules 46:1167–1174
97. Varghese S, Lele A, Mashelkar R (2006) Metal-ion-mediated healing of gels. J Polym Sci A Polym Chem 44:666–670
98. Yuan JC, Fang XL, Zhang LX, Hong GN, Lin YJ, Zheng QF, Xu YZ, Ruan YH, Weng WG, Xia HP, Chen GH (2012) Multi-responsive self-healing metallo-supramolecular gels based on "click" ligand. J Mater Chem 22:11515–11522
99. Terech P, Yan M, Maréchal M, Royal G, Galvez J, Velu SKP (2013) Characterization of strain recovery and "self-healing" in a self-assembled metallo-gel. Phys Chem Chem Phys 15:7338–7344
100. Bode S, Zedler L, Schacher FH, Dietzek B, Schmitt M, Popp J, Hager MD, Schubert US (2013) Self-healing polymer coatings based on crosslinked metallosupramolecular copolymers. Adv Mater 25:1634–1638
101. Bode S, Bose RK, Matthes S, Ehrhardt M, Seifert A, Schacher FH, Paulus RM, Stumpf S, Sandmann B, Vitz J, Winter A, Hoeppener S, Garcia SJ, Spange S, van der Zwaag S, Hager MD, Schubert US (2013) Self-healing metallopolymers based on cadmium *bis*(terpyridine) complex containing polymer networks. Polym Chem 4:4966–4973
102. Lohmeijer BGG, Schubert US (2003) Water-soluble building blocks for terpyridine-containing supramolecular polymers: synthesis, complexation, and pH stability studies of poly(ethylene oxide) moieties. Macromol Chem Phys 204:1072–1078
103. Gohy JF, Lohmeijer BGG, Schubert US (2002) Metallo-supramolecular block copolymer micelles. Macromolecules 35:4560–4563
104. Gohy JF, Lohmeijer BGG, Schubert US (2002) Reversible metallo-supramolecular block copolymer micelles containing a soft core. Macromol Rapid Commun 23:555–560
105. Gohy JF, Lohmeijer BGG, Varshney SK, Decamps B, Leroy E, Boileau S, Schubert US (2002) Stimuli-responsive aqueous micelles from an ABC metallo-supramolecular triblock copolymer. Macromolecules 35:9748–9755
106. Wild A, Winter A, Schlütter F, Schubert US (2011) Advances in the field of π-conjugated 2,2′:6′,2″-Terpyridines. Chem Soc Rev 40:1459–1511
107. Ulbricht C, Beyer B, Friebe C, Winter A, Schubert US (2009) Recent developments in the application of phosphorescent iridium(III) complex systems. Adv Mater 21:4418–4441

108. Wang Q, He Z, Wild A, Wu H, Cao Y, Schubert US, Chui C-H, Wong W-Y (2011) Platinum–acetylide polymers with higher dimensionality for organic solar cells. Chem Asian J 6:1766–1777
109. Schlütter F, Wild A, Winter A, Hager MD, Baumgaertel A, Friebe C, Schubert US (2010) Synthesis and characterization of new self-assembled metallo-polymers containing electron-withdrawing and electron-donating bis(terpyridine) zinc(II) moieties. Macromolecules 43:2759–2771
110. Wild A, Teichler A, von der Ehe C, Winter A, Hager MD, Yao B, Zhang B, Xie Z, Wong W-Y, Schubert US (2013) ZnII bisterpyridine metallopolymers: improved processability by the introduction of polymeric side chains. Macromol Chem Phys 214:1072–1080
111. Wild A, Teichler A, Ho C-L, Wang X-Z, Zhan H, Schlütter F, Winter A, Hager MD, Wong W-Y, Schubert US (2013) Formation of dynamic metallo-copolymers by inkjetprinting: towards white-emitting materials. J Mater Chem C 1:1812–1822
112. Friebe C, Wild A, Perelaer J, Schubert US (2012) Inkjet printing of zinc(II) bis-2,2′:6′,2″-terpyridine metallopolymers: printability and film-forming studies by a combinatorial thin-film library approach. Macromol Rapid Commun 33:503–509

Adv Polym Sci (2013) 262: 259–294
DOI: 10.1007/12_2013_246

Published online: 29 October 2013

Design and Applications of Multiscale Organic–Inorganic Hybrid Materials Derived from Block Copolymer Self-Assembly

Kahyun Hur and Ulrich Wiesner

Abstract Block copolymer (BCP) self-assembly (SA) is a useful tool for designing materials with tunable nanostructure as well as controllable multiscale, hierarchical structure. A combination of BCP SA with inorganic materials results in functional hybrid materials with ordered structures down to the nanoscale, thereby exploiting both the advantageous features of structure tunability from BCP SA and functionality from inorganic materials. Rather than a comprehensive review of the entire field of hybrid materials, this overview summarizes a variety of BCP-derived synthetic approaches developed over the last 10–15 years, with emphasis on work by the Wiesner group at Cornell University on hybrid materials with structural characteristics on multiple length scales. This encompasses hybrids with thermodynamic equilibrium-type BCP nanostructures, controlled nonequilibrium-type structure formation processes leading to structural asymmetries, as well as formation of hierarchical BCP materials with control over nanoscale and macroscale structures. Besides the development of wet-chemical methodologies for their synthesis, this overview also features some promising first applications of such materials. Results suggest that BCP SA directed synthetic approaches may provide routes to cost-effective and large-scale materials fabrication potentially useful for both, new materials discovery and study of fundamental structure – property correlations as well as exploration of the materials in a number of today's most pressing applications including water filtration and energy conversion and storage.

K. Hur
Department of Materials Science and Engineering, Cornell University, Ithaca, NY 14853, USA

Current address: Institute of Multidisciplinary Convergence of Materials, Korea Institute of Science and Technology, Seoul 136-791, South Korea

U. Wiesner (✉)
Department of Materials Science and Engineering, Cornell University, Ithaca, NY 14853, USA
e-mail: ubw1@cornell.edu

Keywords Battery · Block copolymer · Fuel cell · Hybrid · Membrane · Metamaterial · Nanomaterial · Phononics · Photonics · Photovoltaics · Self-assembly · Thermoelectrics

Contents

Abbreviations

1D	One dimensional
2D	Two dimensional
3D	Three dimensional
BCC	Body-centered cubic
BCP	Block copolymer
CASH	Combined assembly by soft and hard
CPS	Close-packed spheres, referring to face-centered or hexagonally close-packed spheres
DIS	Disordered phase
GYR	Gyroid
HEX	Hexagonal cylinder
LAM	Lamellar phases
NIPS	Nonsolvent-induced phase separation

NiSi	Nickel silicide
o-	Oligomeric
PEO	Poly(ethylene oxide)
PI	Poly(isoprene)
PS	Poly(styrene)
SA	Self-assembly
SIM^2PLE	Spinodal-decomposition-induced macro and mesophase separation plus extraction by rinsing
SNIPS	Self-assembly and nonsolvent-induced phase separation
ssDSSC	Solid-state dye-sensitized solar cell
TEM	Transmission electron microscope

1 Introduction

A polymer is a macromolecule composed of many repeated small molecules [1]. Since H. Staudinger received the Nobel Prize 60 years ago for his pioneering work on such macromolecules, polymers have transformed human life and become one of the most important material classes in modern society due to the plethora of applications that have been realized. The importance of polymers and research conducted on them cannot be overemphasized. However, due to its successful history, it has been argued that polymer science today is a maturing scientific field and thus may no longer be exciting enough for the smartest young scientific minds to devote their efforts to [2, 3]. On first sight, it may look like polymers are going to follow the same fate as, for example, metals. Indeed, today over 90% of the polymer market is still dominated by commodity polymers like polyethylene and polypropylene, and despite other projections in the 1980s and 1990s not much has changed about that for decades. So, has the field of polymer science really left its best days behind? We think there are good reasons to believe it has not. In contrast to metals, polymer materials are molecular materials with the whole diversity of chemical structures at their foundation. In the case of commodity polymers, often only a single monomer constitutes the polymer chain. In contrast, the whole diversity of life is based on information encoded into the primary monomer sequence of biological macromolecules. Polymer synthesis therefore continues to constitute a vast territory for innovative research. Furthermore, our understanding of macromolecule-directed biological processes, one might argue, is still in its infancy. For example, the latest science initiative of the US administration on mapping the human brain is based on the fact that a molecular understanding of thought processes in the brain is almost entirely missing, and much of it is based on macromolecules. Most importantly, as biology has demonstrated beautifully, macromolecular materials cannot only provide a plethora of desired functions but, in contrast to the vast majority of polymers used today, they can also be designed for a sustainable economy, an attribute that undoubtedly will become of increasing importance in the future.

Nature provides wonderful inspiration and thus may guide the way in many technological areas, but biological processes at the molecular level are often highly complex and thus cannot provide the answer to all technological challenges, at least not in the foreseeable future. Compared to biological macromolecules, the information content of synthetic macromolecules is often still relatively low. Yet even with only two, three, or four monomers along the synthetic chain, the emerging structural diversity is already quite substantial. Block copolymers (BCP) with two or three (or more) monomers blocked along the chain provide a model polymer architecture for looking at this diversity. While in a very rudimentary way mimicking the complexity of blocked protein primary sequences, BCP self-assembly (SA) can still be understood quantitatively and thus provides a wonderful toolbox for studying the processes of structure formation. Furthermore, as will become apparent from this article, more and more potential applications are emerging in which not only the scalar properties of block copolymers are used, but also in which the block sequence-directed SA structure plays an important direct role. It is to this area of BCP SA that the Wiesner group at Cornell University has devoted much effort to pushing the limits of our understanding of polymer science. In this review, we summarize past achievements of BCP hybrid SA studies, with emphasis on the results of the Wiesner group on such materials, and share our blueprints for the frontiers of polymer research in this particular field of polymer science.

Modern science and technology often seeks "smart" functional materials for today's applications, combining novel functionalities with solution-based processablity, which is usually difficult to obtain from only one type of organic or inorganic material. Much effort has therefore been paid to the synthesis of hybrid materials that combine advantageous features of both organics and inorganics [4]. The Wiesner group has utilized BCP SA to direct the structure of inorganic materials. In order to minimize their free energy, BCPs self-assemble into periodically ordered structures at the nanoscale. Due to the ease of tuning aspects of the chemical structure of BCPs such as chain length and composition, BCPs are of great use in designing such nanostructures from the bottom up. However, BCPs that readily self-assemble into such structures typically lack a variety of desired functionalities, including magnetic or electric properties. Exploiting the power of structural design from BCPs one can use their SA to direct the structure of functional inorganic materials into ordered nanostructures, thereby combining the best of both worlds. Furthermore, BCP SA is a bottom-up type of synthetic approach that is scalable and solution based, and thus relatively cost-effective. It is thus a powerful tool, offering a facile route to synthesis of novel materials that should also be relevant to industrial applications.

This review summarizes more than a decade of research efforts on BCP-derived hybrid materials by the Wiesner group and others. Section 2 provides a brief introduction of BCP SA, serving as background knowledge to unfamiliar readers. The following sections include descriptions of BCP-derived structures (Sect. 3), synthetic methods (Sect. 4), different material classes structure-directed by BCPs (Sect. 5), and potential application areas (Sect. 6). SA structures are important ingredients that BCP scientists can exploit to design novel materials. A variety of the synthetic methods are summarized, encompassing hybrids with thermodynamic

equilibrium-type BCP nanostructures, controlled nonequilibrium-type structure formation processes leading to structural asymmetries, as well as formation of hierarchical BCP materials with control over nanoscale and macroscale structures. Bottom-up BCP SA efforts are described for various materials classes, including ceramics, semiconductors, and metals. Lastly, after introducing the toolbox for fabrication of novel nanomaterials, we describe efforts in several potential application areas that may benefit from BCP-derived nanomaterials. Some of the applications have already been demonstrated, while others are still hypothetical. We hope that this review can thus provide new impetus for future polymer research directions.

2 Block Copolymer Self-Assembly

A block copolymer is a macromolecule composed of two or more chemically distinct polymer blocks that are connected by a covalent bond. The polymer blocks are sometimes thermodynamically incompatible, like oil (hydrophobic) and water (hydrophilic). They can be covalently connected in different ways, resulting in a variety of polymer architectures such as linear, star, and graft block copolymers (see Fig. 1). Due to repulsive interactions between the incompatible polymer blocks, all blocks of the same kind try to mix while staying separated from all other blocks. Such behavior leads to formation of ordered structures, with a periodicity comparable to the size of the BCP chain as measured, e.g., by its end-to-end distance.

In order to better understand the SA behavior, it is instructive to look at entropy and enthalpy changes in the formation of an ordered state. The Helmholtz free energy of an AB diblock copolymer (di-BCP) is approximately given by:

$$F = -\ln Q + \chi_{AB} N f_A f_B$$

where F is the normalized Helmholtz free energy; Q is the single molecule partition function relevant to conformational entropy of the BCP; f_A and f_B are volume fractions of blocks A and B, respectively; χ_{AB} is the Flory–Huggins interaction parameter between A and B monomers; and N is the number of monomers along the chain. The conformational entropy, given by the first term of the equation, leads to mixing of the two blocks, while the enthalpic interactions, given by the second term, usually favor separation of these blocks. The two competing effects result in an ordered periodic structure, for example, if $\chi_{AB}N > 10.5$ with $f_A = f_B$, whereas a disordered (DIS) bulk phase is formed otherwise.

The resulting structure is controllable by varying the block ratio and the degree of polymerization of BCPs, as shown in Fig. 1b. For di-BCPs, the structure changes from close-packed spheres (CPS, referring to face-centered or hexagonally close packed spheres) to body-centered cubic (BCC), hexagonal cylinder (HEX), double gyroid (GYR), and lamellar phases (LAM) (note that the bicontinuous O70

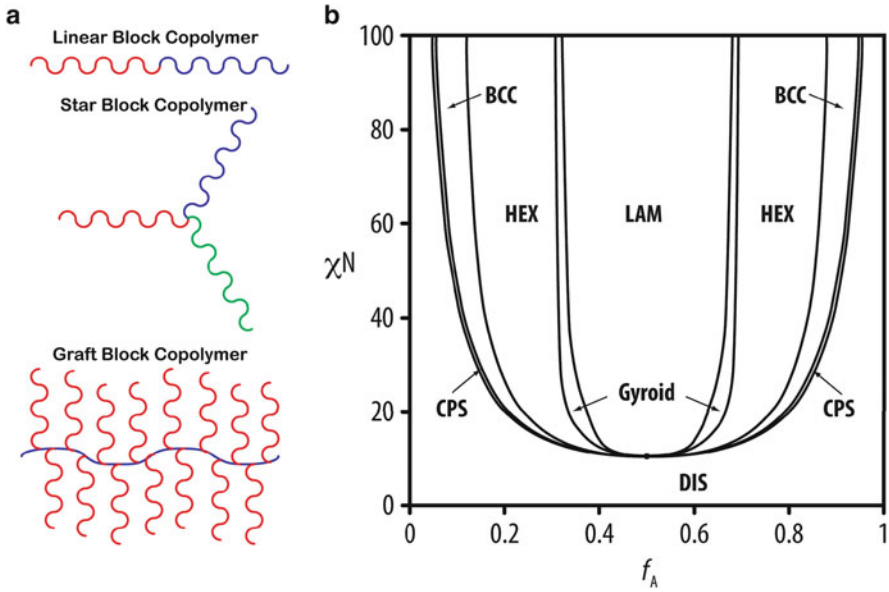

Fig. 1 (**a**) Different block copolymer architectures. (**b**) Phase diagram of a diblock copolymer, where an increasing volume fraction, f_A, at a value of $\chi_{AB}N > 10.5$ leads to different morphologies starting from a disordered phase (DIS) to close-packed spheres (CPS, referring to face-centered or hexagonally close packed spheres), body-centered cubic (BCC), hexagonal cylinder (HEX), double gyroid (GYR), and lamellar phases (LAM)

morphology, not indicated in Fig. 1b, shares boundaries with HEX, GYR, and LAM in very close proximity to the order–disorder transition boundary [5]). The morphology mainly changes in order to minimize interfacial area between energetically repulsive chemical components, e.g., polymer blocks (and inorganic materials in the case of hybrids). However, the conformational entropy of BCPs is non-negligible in BCP SA, particularly in the weak segregation regime of BCPs. Although the entropic free energy is minimal when polymers have the Gaussian chain conformation [6], enthalpic repulsions between incompatible blocks lead to deviations from this conformation thus increasing the conformational entropy contribution to the free energy. These competing interactions enable the formation of a variety of nanostructures.

The lattice dimension of self-assembled structures is further controllable. As a first approximation, it is expected that the periodicity (i.e., lattice dimension) of a BCP-derived structure approximately scales as $N^{1/2}$ since the end-to-end distance of an unperturbed BCP in a theta condition scales as $N^{1/2}$, where N is the degree of polymerization [6]. Therefore, BCP SA is a great tool for designing the nanostructure of materials, offering a means of controlling structure and structural dimensions at the nanoscale.

3 Block Copolymer-Derived Structures

Because many of the physical properties of materials (e.g., photonic, phononic, and mechanical properties) greatly rely on the structural characteristics (i.e., symmetry and structural dimensions), designing the structure of materials is a crucial step for developing novel materials with a targeted physical property. In contrast to top-down approaches, bottom-up approaches have limited freedom in the selection of structures. Among the 230 space groups, only a few tens of space groups have been observed in BCP SA studies. This limitation mainly originates from the simple chemical composition of previously studied BCPs. As discussed earlier, most studies have been conducted on BCPs composed of only a few different chemical blocks, typically ranging from two to five. This is just the tip of the iceberg in a whole variety of combinations that can be achieved with BCP synthesis. However, much effort is needed to synthesize new BCPs with additional blocks due to synthetic challenges such as quantitative terminal group modifications or solvent exchange for additional polymer growth steps. Furthermore, the experimental parameter space associated with different block compositions exponentially expands as the number of blocks increases [7]. A substantial number of BCP-derived structures have already been discovered, some of which are quite intriguing and, due to their useful structural characteristics, may be interesting for future applications. As a first step, it is thus instructive to review the type of structures found to date in BCP condensed phases.

Bottom-up BCP SA provides a facile route to a variety of nanostructures including three-dimensional (3D) and quasicrystalline structures, usually challenging in top-down approaches. This section delineates such BCP-derived 1D, 2D, 3D, and quasicrystalline structures. The dimension of structures, D, is defined by $D = 3 - n$, where n stands for the number of axes that have continuous translational order. For example, the lamellar structure shown in Fig. 2 has an axis of translational order with a nonzero lattice dimension but two axes with continuous translational order. Thus, the dimension of a lamellar structure is $D = 1$ with $n = 2$.

3.1 One- and Two-Dimensional Structures

Lamellar morphology is a 1D structure as shown in Fig. 2, where two or more chemically distinct sheets alternate along one axis. Selective removal of a polymer block leads to the formation of nanosheets [10, 11]. The structure is most frequently observed in BCP SA because it occupies the widest area, e.g., in a diblock copolymer phase diagram as shown in Fig. 1b. Controlling the orientation and spatial arrangement of lamellae on 2D substrate planes via graphoepitaxy [12] has attracted much attention for lithography applications addressing challenging current technical limitations (e.g., low throughput and poor line edge roughness) found in top-down

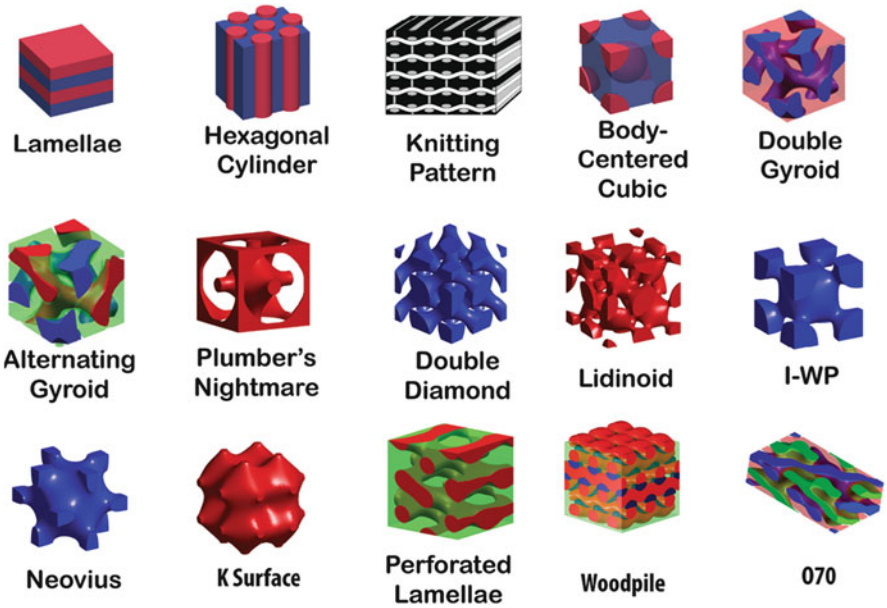

Fig. 2 BCP-derived morphologies (note that Lidinoid, I-WP, K surface, and Neovius structures have not been observed in BCP SA yet). The knitting pattern was reprinted with permission from [8]; Copyright 2001 American Chemical Society. The woodpile structure was reprinted with permission from [9]; Copyright 2008 American Chemical Society

approaches such as extreme ultra-violet (EUV) and e-beam lithography when attempting to attain sub-10 nm line patterns.

Hexagonal cylindrical morphology is a 2D structure as shown in Fig. 2, where cylinders are vertically aligned on a 2D plane in a hexagonal arrangement. A minority polymer block (i.e., shorter polymer block) constitutes the cylinders embedded in a majority (i.e., longer) polymer block. The cylindrical morphology of block copolymers has been employed for high-density storage applications, achieving sub-50 nm structures [13] and potentially providing a low-cost alternative to challenging lithographic techniques.

An interesting layered structure, the so-called knitting pattern, was found in BCP SA [8]. The structure has been observed in "frustrated" ABC triblock terpolymers both experimentally and theoretically, where repulsive interactions between the two terminal blocks are weaker than those between middle block and terminal blocks. The morphology is regarded as a metastable state because the structure formation is driven by the relatively poor solvent miscibility of the middle block [8]. The middle block constitutes cylinders bridging wavy lamellae generated via agglomeration in a poor solvent.

1D and 2D structures are most frequently observed in BCP SA because their phase space is much larger than that of 3D structures. Similar phase behavior is also

observed in BCP-directed inorganic nanostructures [14]. Thus, the importance of these structures cannot be overemphasized. However, alignment of crystallographic axes of 1D and 2D BCP structures is typically required for potential applications that make use of the nanostructures rather than scalar polymer properties.

3.2 Three-Dimensional Cubic Structures

A variety of 3D structures have been observed in BCP SA. The majority of them are cubic and bicontinuous structures, where all polymer blocks are continuous in all three directions. Since cubic structures are isotropic, thus exhibiting isotropic physical properties in any orientation, they can be very useful for applications such as photonics [15, 16], phononics, batteries [17], and membranes. These applications are discussed in Sect. 6.

Discontinuous 3D cubic structures commonly observed in BCP SA are spherical morphologies as shown in Fig. 2. In this case, the minority block of the BCP forms spheres and the spatial arrangement of the spheres varies from body-centered cubic ($Im\overline{3}m$, Q229 space group) to closed packed spheres as the volume fraction of the minority block and/or the product χN decrease [18]. Furthermore, the so-called A15 phase with $Pm\overline{3}n$ symmetry was observed in amphiphilic di-BCPs containing a linear block and a dendron block [17].

A variety of 3D cubic bicontinuous morphologies such as double gyroid, double diamond, and plumber's nightmare have been observed in BCP SA. The gyroid has been observed not only in self-assembled BCPs but also in nature [19, 20], intermetallic materials [21], and surfactants [22]. The gyroid network has chiral helices along various crystallographic directions and thus is characterized by a lack of mirror planes. Gyroid structures usually consist of two minority networks related by an inversion. If these networks are composed of the same material, the structure is a double gyroid with $Ia\overline{3}d$ symmetry and space group Q230. Since inversion symmetry exists, the double gyroid structure is achiral, where respective screw axes with opposite handedness cancel local chirality. The alternating gyroid is composed of two networks from different materials, thus disallowing an inversion center and resulting in a chiral structure. The alternating gyroid, has $I4_132$ symmetry with Q214 space group (see Fig. 2)

A plumber's nightmare structure ($Im\overline{3}m$, Q229 space group) was observed in BCP/oxide hybrid materials [11, 23]. The structure has two intertwining networks, where both networks have the same structure but one of them is shifted along half the diagonal as shown in Fig. 2. Due to structural similarity, a uniaxial contraction of a double gyroid along the axis perpendicular to the [210] plane exhibits similar real (transmission electron microscope, TEM) and reciprocal (small angle X-ray scattering) space images [23].

Recently, the bicontinuous double diamond structure ($Pn\overline{3}m$, Q224 space group) has been experimentally observed in a BCP system [24]. It is believed to be

an unstable phase due to energetically unfavorable chain stretching in the nodes of the minority networks. Local packing of short-range ordered segments, energetically more favorable than random packing, can compensate the free energy penalty from the frustration, resulting in stable bicontinuous double diamond structures.

Although a few 3D isotropic cubic network phases have already been observed, other cubic network phases have stayed elusive in BCP SA, such as the I-WP [25], Neovius [26], K surface [27], and Lidinoid [28] structures (see Fig. 2). Packing frustration of polymer chains in the network nodes of these structures is a primary hurdle for formation of these phases. However, as shown in the cases of the plumber's nightmare and double diamond structures, BCP co-assembly with additive molecules or ordered local packing of monomer units may open new routes to such cubic structures.

3.3 Three-Dimensional Noncubic Structures

A perforated lamellar structure ($P6_3/mmc$, 194 space group) has been frequently observed in BCP SA. The structure is believed to be a metastable phase in di-BCPs since it is energetically less stable than a competing phase, the double gyroid morphology. Thus, the perforated lamellar structure observed experimentally may be a kinetically trapped state that lasts for a reasonably long time period. The structure has layered lamellar sheets that are connected through cylindrical channels. The channels arrange hexagonally and perpendicular to the lamellar planes (see Fig. 2).

A woodpile structure, a similar layered structure with an unidentified space group similar to the O70 space group (*Fddd*), was observed in a BCP/aluminosilicate assembly [9]. In contrast to the perforated lamellar structure, zig-zag cylinders are stacked layer-by-layer (see Fig. 2). Although a zig-zag cylinder is usually energetically less stable than a parallel cylinder due to larger interfacial energy, the relaxed chain conformation of polymer chains, leading to a reduced entropic penalty, may allow the zig-zag cylinder formation.

Most of the noncubic structures are not continuous in all three directions. However, one of the O70 structures (*Fddd*, O70 space group) is bicontinuous, as shown in Fig. 2. Its structural characteristics are quite similar to the gyroid morphologies [29], where triple nodes are connected in all three directions. Non-frustrated ABC triblock terpolymers, where interactions between terminal blocks are most repulsive, generate the bicontinuous structure [29, 30]. Later, it was shown that the structure exists in di-BCP phase space both theoretically and experimentally [5, 31]. Interestingly, it appears in a very narrow regime of di-BCP phase space but occupies quite a wide phase space in non-frustrated triblock terpolymer SA [5, 30].

Despite the nonchiral nature of monomer units, BCPs can generate chiral morphologies such as in the alternating gyroid. Due to the identical free energy

of the two chiral pairs, it is expected that the two structures form with equal probability and that polymer films with alternating gyroid morphology are thus constituted by grain mixtures of the two chiral pairs. In contrast, chiral BCPs can discriminate between two chiral pairs due to differences in free energy between them, leading to the formation of chiral structures. Ho et al. synthesized chiral BCPs and obtained 3D chiral helices [32], where local interactions between chiral components led to a chiral structure at the mesoscale.

Many of these noncubic 3D structures are believed to be metastable because interfacial areas are usually larger than those of 1D lamellar or 2D hexagonal structures, thus leading to higher enthalpic repulsions. Therefore, many of the experimentally observed cases are believed to be long-lived metastable states.

3.4 Quasicrystalline Structures

A quasicrystal is a quasiperiodic structure that is ordered but aperiodic, i.e., it lacks translational order. Its unit cell has defined angles and distances with respect to other unit cells but long-range translational order is missing. In addition to intriguing structural characteristics, the transport properties of quasicrystals are expected to be unique due to the missing translational order. For example, Man et al. showed that photonic quasicrystals are excellent candidates for photonic band gap materials, where the existence of photonic waves is forbidden in photonic band gap ranges [35].

There have been few reports to date on quasicrystalline structure formation from BCPs. Hayashida et al. obtained a 2D quasicrystalline structure, a tiling pattern with 12-fold symmetry, from an ABC star BCP and homopolymer blend (see Fig. 3) [34]. The Bates group at the University of Minnesota generated a 3D dodecagonal quasicrystal from diblock and tetrablock copolymers [33]. These unique structures are mediated by macromolecular packing frustration. However, a substantial number of unanswered questions about the structure formation await further in-depth studies of these interesting morphologies.

BCPs offer a variety of structures including 1D, 2D, 3D, and quasicrystalline structures. BCP SA is a useful approach for generating structures at the mesoscale, ranging from a few to hundreds of nanometers. The structural diversity of BCP SA provides facile access to nanostructures, but flexible polymer blocks used for structure formation usually lack useful chemical and physical properties for applications. The Wiesner group has devoted much effort to combine BCP SA with the properties of functional materials to exploit the power of BCPs as structure-directing agents. The next section summarizes the synthetic strategies used by the Wiesner group for the generation of functional nanomaterials from BCP SA with multiple levels of structural characteristics.

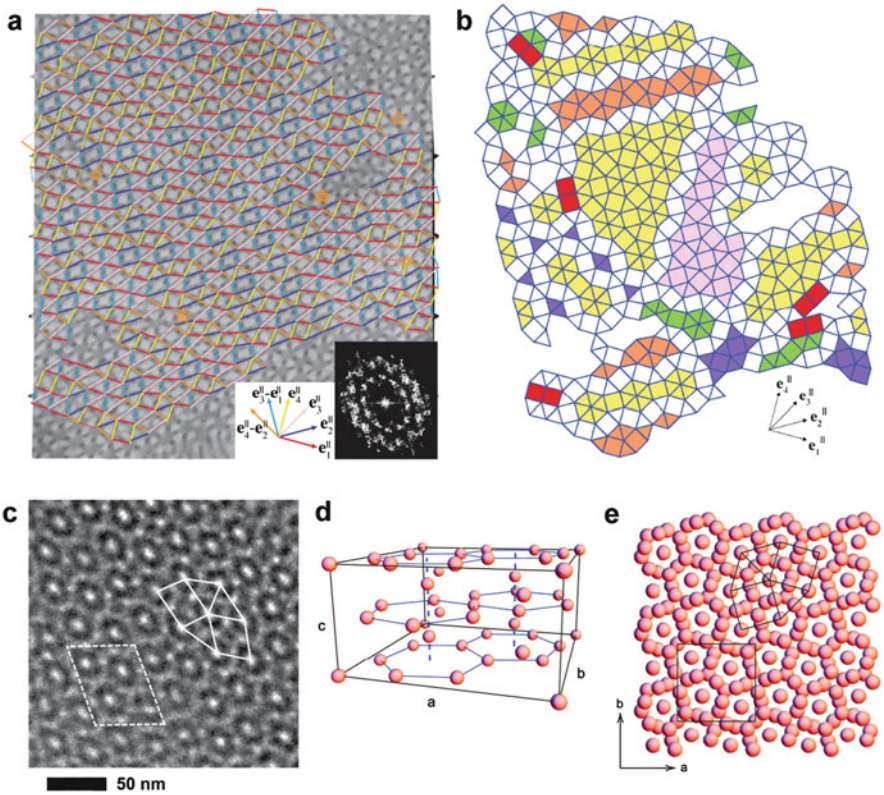

Fig. 3 Quasicrystalline structures observed in BCP SA. (**a**) TEM image of a 2D 12-fold quasicrystal derived from a star block copolymer (the inset shows its FFT pattern). (**b**) Transcribed tiling pattern (reprinted with permission from [34]; Copyright 2010 American Physics Society). (**c**) TEM image and (**d, e**) unit cell of the Frank-Kasper sigma phase obtained from tetra-BCP SA (**c–e** reprinted with permission from [33]; Copyright 2010 AAAS)

4 Synthetic Methods for Controlling Multiple Structural Levels from Block Copolymer Self-Assembly

The Wiesner group utilizes a variety of synthetic strategies for nanomaterial fabrication. This section is divided into three subsections based on different mechanisms of structure formation. Section 4.1 deals with the utilization of BCP-derived equilibrium structures and is most relevant to the structures described in the previous section. In Sect. 4.2, post-processing methods of BCP-derived functional nanomaterials are introduced, leading to polycrystalline and single crystalline nanostructures with, e.g., improved mechanical and electrical properties. Section 4.3 summarizes novel nonequilibrium methods leading to hierarchical structure formation.

4.1 Functional Nanomaterials with an Equilibrium Mesostructure

A widely followed approach for utilizing self-assembled BCP nanostructures for fabrication of functional nanomaterials is to generate ordered porous BCP templates via selective removal of one polymer block. Certain polymers are selectively removable via application of acid, base, heat, or ozone [36]. The resulting porous templates can subsequently be backfilled with functional materials, e.g., via metal oxide solutions or metal deposition. With the Steiner group at Cambridge University in the lead, the Wiesner group helped to fabricate gyroidal titania electrodes for solid-state dye-sensitized solar cells [37] and gyroidal gold nanomaterials for metamaterial applications [38]. Gyroidal minority networks formed by poly(L-lactic acid) were selectively removed by an acid treatment for the former case [37], whereas ozonolysis of polyisoprene was used in the latter [38]. Backfilling of titania into the porous gyroidal template followed by incineration of the template resulted in nanostructured titania electrodes, and electrodeposition of gold on the gyroidal template led to gyroidal gold nanomaterials. This block removal strategy involves two main difficulties. Complete selective etching of thick polymer monoliths can be challenging since an etchant must reach a long-distant template center. Thorough percolation of sacrificial polymer blocks is rare for large bulk samples due to the randomized orientation of crystal axes. Thus, alignment of the crystal axes is usually needed for better etching [39]. The other main difficulty is complete backfilling of a large porous monolith with functional materials. Nanosized pores can easily become clogged during a deposition process if functional materials are deposited, e.g., via chemical vapor or electroless deposition. Furthermore, the use of nanostructured porous BCPs as templates for fabrication of functional nanomaterials requires several steps, including BCP SA, selective etching, and backfilling.

This multistep procedure can be simplified by directly employing BCPs as structure-directing agents for functional inorganic materials in a single SA step. In this approach, additive inorganic materials preferentially localize in one block of the phase-separated nanostructures during BCP SA, usually in the more hydrophilic block, thereby minimizing the enthalpic penalty of mixing with more repulsive blocks. This strategy leads to nanostructured polymer/inorganic hybrid materials in a "one-pot" fashion, without multiple and often tedious post-processing steps. The disadvantage is that, depending on the inorganic additives, long post-SA annealing steps may not be possible thus rendering achievement of long-range order of the nanostructures challenging.

The Wiesner group has synthesized a variety of nanostructured oxide materials via casting solutions of sol–gel-based oxide nanoparticles and a BCP. The sol–gel process generated sol particles of a few nanometers in diameter, and BCPs directed these particles into a single phase-separated block. This process has led to a variety of nanostructures, including lamellar, cylindrical, ABCD woodpile, perforated lamellar, double gyroid, alternating gyroid, and plumber's nightmare structures. Dissolution or disassembly of self-assembled oxide hybrids from majority polymer structures

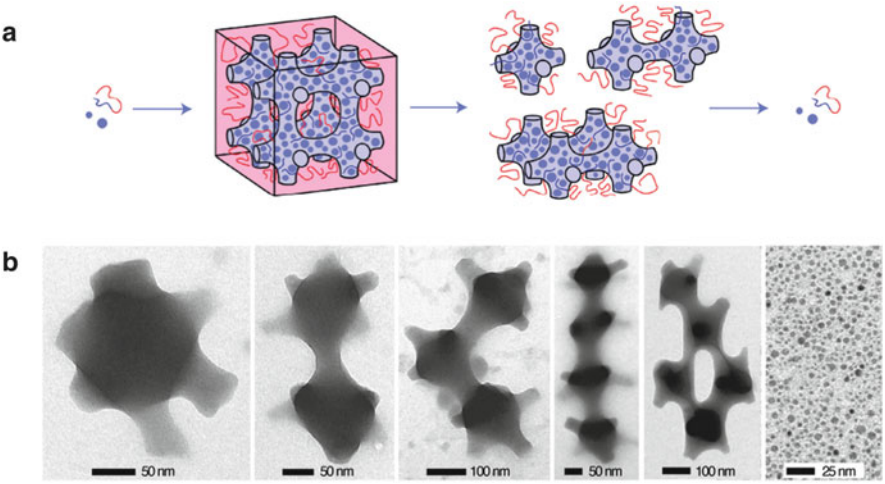

Fig. 4 (**a**) Assembly and disassembly of mesostructured hybrids. (**b**) TEM images of disassembly of mesostructured silica hybrids with plumber's nightmare structure (reprinted with permission from [11]; Copyright 2007 Nature Publishing Group)

resulted in a variety of nanostructured oxide objects such as nanocylinders, hexapods, and other well-defined nano-objects [11, 40] (see Fig. 4). The disassembly was enabled, in part, by the nanoparticle nature of the hybrids.

Such structure direction was successful because sol–gel processes could produce oxide nanoparticles in solution of sizes typically below 5 nm. Larger particles are usually immiscible with moderately sized polymer blocks and segregate from BCPs [11, 41]. The size compatibility between BCPs and oxide particles is crucial for controlled nanostructure formation.

A similar process can be applied to metallic nanoparticles [10, 42]. Nanostructured metals from BCP SA offer high metal content and surface areas compared to other synthetic methods. However, due to the very high surface energy of metals, using BCP SA to direct the structure of metallic materials is usually challenging. In order to prevent particle aggregation and obtain energetically favorable interactions with BCPs, ligands covering the metal nanoparticle surface have to be carefully designed. This BCP/metal nanoparticle SA strategy will be discussed in more detail in the next section.

4.2 Post-processing of BCP-Derived Functional Nanomaterials

Nanostructured materials fabricated by the aforementioned methods are usually amorphous, thus offering relatively poor properties. In order to improve, e.g., electrical properties in the case of semiconducting oxides, thermal crystallization at elevated temperatures has to be implemented, typically resulting in polycrystalline materials.

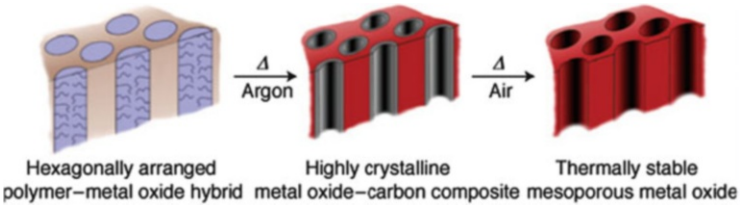

Fig. 5 CASH method for crystallization of metal oxide materials without structural collapse at a high temperature (reprinted with permission from [43]; Copyright 2008 Nature Publishing Group)

However, this process often leads to the loss of ordered mesoporous structures during the crystallization at a high temperature. The Wiesner group developed a novel thermalization process, the "combined assembly by soft and hard (CASH)" chemistries, to retain the mesostructure while crystallizing [43]. CASH is a two-step thermal process (see Fig. 5), which includes thermal treatment of BCP + metal oxide hybrids under an inert gas (e.g., Ar, N_2) to generate a sturdy in-situ carbon scaffold that supports metal oxide nanopores as crystallization occurs. The carbon scaffold can subsequently be oxidized away by letting air into the sample chamber, resulting in the final fully crystallized oxide.

Another type of crystallization process can be induced via laser annealing. Laser annealing with an eximer laser has been widely used in the microelectronics industry for formation of doped crystalline materials, e.g., polycrystalline silicon. The process can be applied to BCP-derived nanostructured semiconducting materials. The Wiesner group utilized the laser annealing technique to generate nanostructured single-crystal silicon and nickel silicide (NiSi), a semiconductor and a metal, respectively (see Fig. 6) [44]. To that end, self-assembled nanoporous oxide thin films (up to 100 nm thick) were prepared by spin-casting of BCP and oxide precursor solutions onto silicon wafers and subsequent polymer removal by heating. Amorphous silicon (or NiSi) was deposited onto the porous template, partially filling the nanopores. Subsequent laser annealing with nanosecond laser pulses resulted in formation of crystalline silicon. Interestingly, this allowed epitaxial single-crystal nanostructured silicon growth on the single-crystal silicon wafer. Furthermore, hetero-epitaxial growth of NiSi in the nanopores could also be demonstrated. In this case, mechanical stresses induced by the lattice mismatch to the substrate were reduced by the nanostructure, thus enabling the hetero-epitaxial growth without delamination.

4.3 Kinetically Controlled Formation of Hierarchical Porous Structures

The aforementioned processes lead to organic–inorganic hybrid materials with ordered structures at the nanoscale. Controlled structural characteristics have been achieved by seeking an equilibrium state of BCP-directed self-assembled nanostructures. The achievable structural diversity can be expanded by kinetic

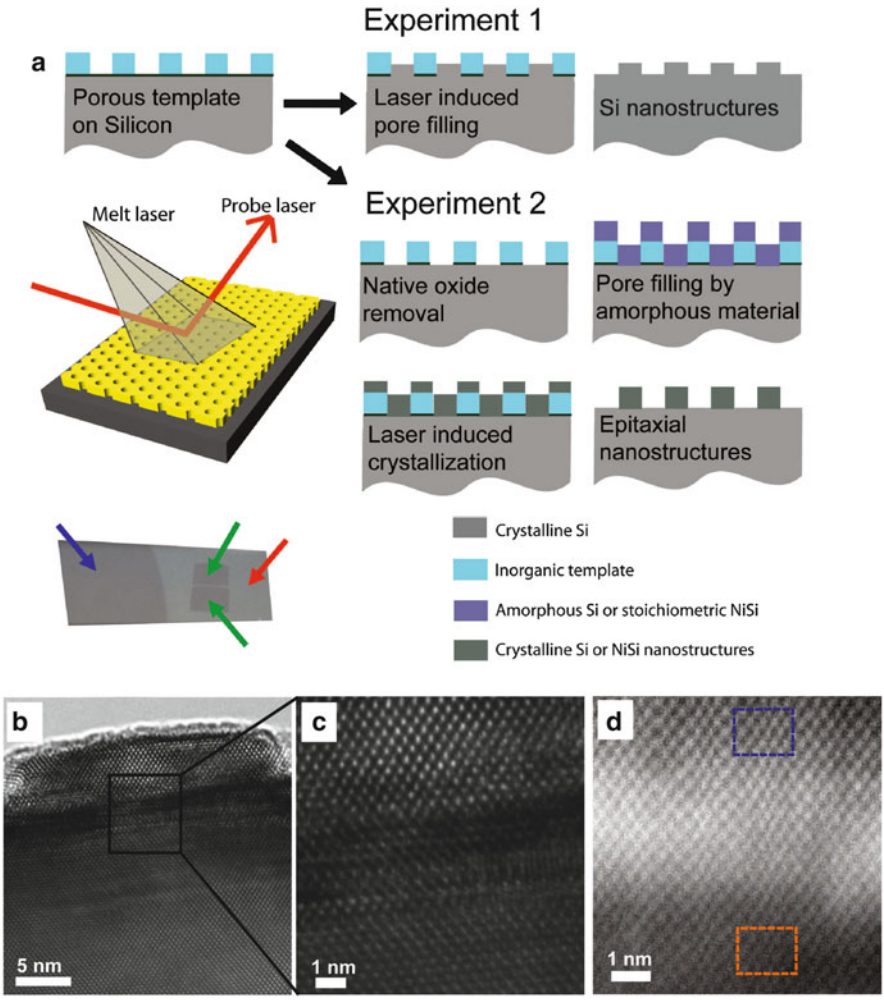

Fig. 6 (**a**) Generation of single-crystal homoepitaxial Si (*experiment 1*) and heteroepitaxial NiSi (*experiment 2*) nanostructures. The left bottom photograph shows Si wafer with bare crystalline Si substrate (blue arrow), with a-Si deposited (red arrow) and spots after laser-induced crystallization (green arrows). Boxes in (d) show regions with (top) and without (bottom) Ni signal in the TEM thus demonstrating the boundaries of the interface. (**b, c**) TEM images of Si nanostructure cross-sections. (**d**) Scanning TEM image of a NiSi pillar cross-section on Si (reprinted with permission from [44]; Copyright 2010 AAAS)

control of the self-assembly process. BCP SA usually occurs below a certain concentration during evaporation of the solvent in BCP solutions. The concentration depends mostly on the solubility of the various blocks of the BCP in the solvent as well as temperature. Despite the existence of a final equilibrium morphology in the condensed state, the resulting structure often varies with experimental parameters because metastable states are frequently observed as a result of the

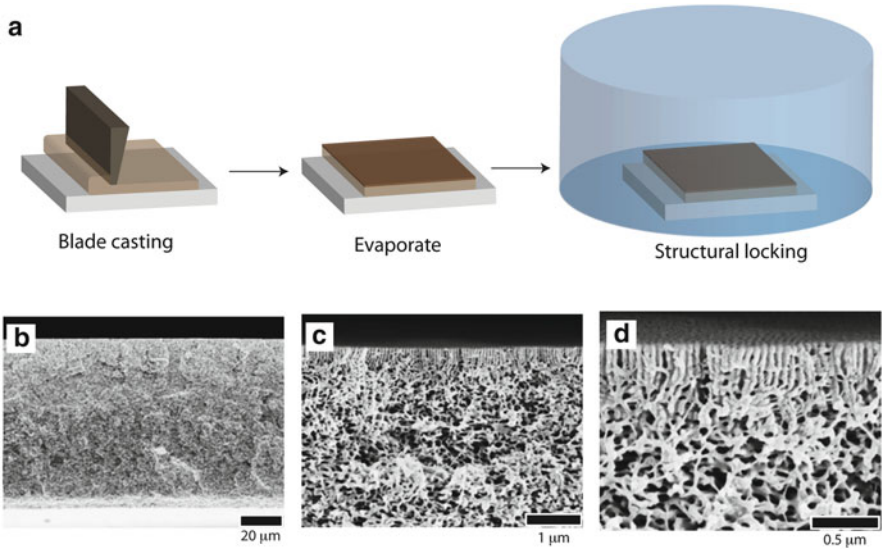

Fig. 7 (**a**) Schematic of SNIPS method. (**b**–**d**) TEM images of an asymmetric hierarchical porous structure produced by the SNIPS method (reprinted with permission from [45]; Copyright 2008 Nature Publishing Group)

long relaxation times characteristic for macromolecular systems. However, kinetic control can offer a route to completely novel structures not achievable from purely equilibrium thermodynamic considerations.

Pinemann et al. for the first time combined BCP SA and nonsolvent-induced phase separation (NIPS), resulting in asymmetric hierarchically structured porous materials, as shown in Fig. 7 [45, 46]. The NIPS process is an industrially well-established method for membrane formation in which asymmetric organic solvent distributions in polymer films upon evaporation are transferred into the solid by plunging the film into a nonsolvent bath (usually water) at intermediate evaporation times. Rapid exchange between organic solvent and water instantaneously precipitates the polymer, thereby translating the gradient film structure into the polymer glass. The NIPS process combined with BCP SA (now referred to as SNIPS) leads to an intriguing hierarchical structure with a macroscale disordered network structure and a mesoscopic ordered nanostructure derived from BCP SA. In particular, in SNIPS, a thin surface layer with dense and vertically aligned BCP-type pores is supported by a macroporous substructure with increasing pore size as one moves away from the surface to the bottom of the film. SNIPS has also been demonstrated for diblock copolymers and triblock terpolymers, the latter enabling membrane formation at intermediate molar masses and leading to small pore sizes without loss of beneficial mechanical properties [47]. The structural characteristics of SNIPS-derived membranes combine high flux with well-defined solute rejection properties, which is very useful for size-selective separation applications.

More recently, another type of hierarchical porous materials has been fabricated via a kinetically controlled two-step process derived from a combination of BCP SA and spinodal decomposition, so-called spinodal-decomposition-induced macro- and mesophase separation plus extraction by rinsing (SIM^2PLE) [48]. A strongly segregating amphiphilic BCP (e.g., polystyrene-*block*-polyethylene oxide, PS-*b*-PEO) and a short oligomer (e.g., o-PEO) were chosen to prepare a blend from solution. Upon solvent evaporation, the BCP/oligomer blend separated into an oligomer-rich phase and a BCP-rich phase. In the BCP-rich phase, the oligomer selectively swelled the PEO block because the oligomer energetically prefers the PEO block to the PI block. Selective removal of the oligomer in the resulting blend by rinsing with a selective solvent retained the structure of the two distinctive phases and resulted in hierarchical pore formation: macropores from the oligomer-rich phase and mesopores from the BCP-rich phase by rising away the oligomer in both phases. Furthermore, varying the quench depth into the miscibility gap by varying the evaporation speed via temperature allowed selection of different BCP mesostructures via different degrees of BCP swelling with the oligomer. There are several experimental requirements for induction of such spinodal decomposition. First, the amphiphilic BCP and the additive should be enthalpically repulsive to generate two phases in the blend. Second, the volume fractions of BCP and additive need to be in a regime where enthalpic repulsive forces dominate the entropic driving force of mixing. Lastly, the resulting structure from the SA is highly dependent on SA kinetics. Thus, the experimental conditions related to the kinetics of SA, such as temperature and solvent choice, need to be carefully controlled. First results suggested, however, that the process, which is dependent on general thermodynamic considerations, may be quite general [48].

This section has summarized fabrication techniques for novel polymeric materials with multiple structural characteristics. These techniques in part offer flexibility in the choice of materials for structure direction, including oxides, semiconductors, and metals. Thus, the techniques provide a useful toolbox for synthesis of various nanostructured materials. The next section outlines in more detail the specific classes of nanostructured materials that have been derived from BCP SA.

5 Classes of Block Copolymer-Derived Hybrid Nanomaterials

A BCP is a good tool for the design of nanostructured materials, as discussed in the previous sections. It offers a flexible platform for a variety of nanomaterials with functionalities and robustness since one can combine BCP SA with a sol–gel process, nanoparticle synthesis, chemical vapor deposition, electrodeposition, or electroless deposition. Thus, in principle, the structural and material diversity obtained from the aforementioned techniques is substantial. This section introduces specific classes of material prepared from BCP-directed SA by the Wiesner group.

5.1 Ceramics

Ceramics are nonmetallic solids, insulators or semiconductors, and include oxides, non-oxides, and composites. Nanostructure formation of ceramics has been studied in the Wiesner group mainly by using BCPs as structure-directing agents for ceramic sol nanoparticles. To that end, ceramic sol nanoparticles prepared by the sol–gel process are mixed with a BCP solution for self-assembly of BCP/ceramic nanoparticles. In this way, a variety of nanostructures are accessible by varying the volumetric ratio of BCP and inorganic sol. The group has extensively studied aluminosilicates and transition metal oxides.

The early work of the Wiesner group on nanostructured aluminosilicates via BCP + ceramic nanoparticle SA was reported in 1997, where solutions of polyisoprene-*block*-polyethylene oxide (PI-*b*-PEO) and aluminosilicate sol were prepared, followed by the evaporation of organic solvents [49]. Morphology changes expected from the phase diagram of di-BCPs were observed on varying the aluminosilicate sol volume fraction in the solutions (see Fig. 8). The selective volumetric increase of the hydrophilic (PEO) block via the addition of the oxide sols led to morphology changes in the hybrids because varying the volume fraction of a block, f, results in morphology changes, as shown in a di-BCP phase diagram (see morphology changes by varying f at a fixed χN). Thus, a variety of BCP-derived nanostructures can be obtained by preparing solutions with different compositions of BCP and inorganic material. The morphology map of PI-*b*-PEO + aluminosilicate SA summarizes a comprehensive series of experiments in which the aluminosilicate volume fraction, f, was varied for a number of different block copolymer compositions [14] (see Fig. 8e).

In particular, several morphologies usually elusive in BCP SA were found in BCP/aluminosilicate hybrids. The plumber's nightmare and woodpile structures were observed in AB di-BCP and ABC triblock terpolymer + aluminosilicate SA, respectively [9, 11, 23]. A theoretical study of di-BCP + homopolymer mixtures showed that the plumber's nightmare structure can be observed in hybrid systems but may be less stable than the formation of two distinct phases in a blend [50]. Thus, the plumber's nightmare structure observed in BCP + aluminosilicate SA may be a long-lived metastable structure. Such long-lived metastable structures could be more pronounced in BCP SA with a sol–gel solution as compared to the SA of a neat BCP due to structural "locking" during BCP SA and simultaneous aluminosilicate condensation. Such structural locking from sol–gel condensation reactions incapacitates subsequent annealing processes in BCP + aluminosilicate SA and thus may limit access to equilibrium structures as well as to better long-range order.

Many oxide semiconductors accessible from sol–gel chemistry such as titania [51, 52] and niobia [53] can be nanostructured by employing the same strategy utilized for aluminosilicate hybrids. In particular, thermal crystallization of such hybrids at a high temperature using CASH chemistries as described in the previous section leads to the formation of polycrystalline oxide semiconductors with interesting electrical properties [43].

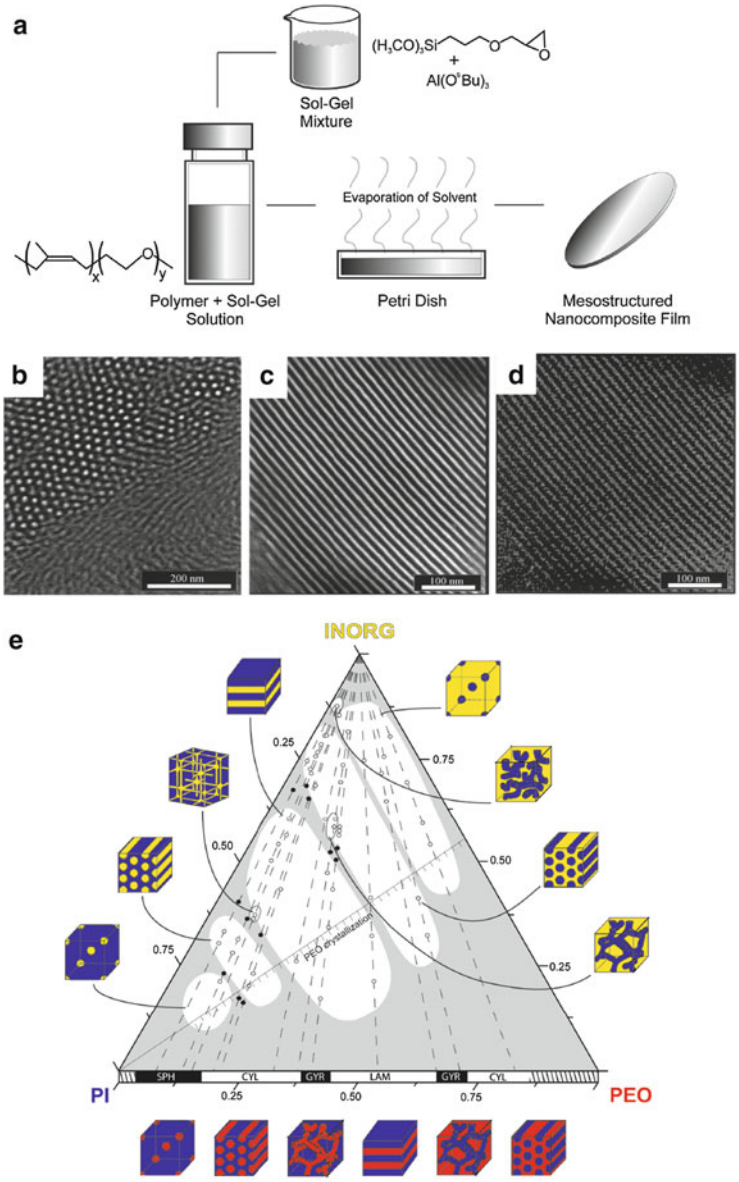

Fig. 8 (**a**) Schematic and (**b**–**d**) TEM images of PI-*b*-PEO BCP + aluminosilicate SA system (reprinted with permission from [49]; Copyright 2010 AAAS). (**e**) Morphology diagram of the same system obtained by adding increasing amounts of aluminosilicate sol to BCPs of different compositions (reprinted with permission from [14]; Copyright 2010 American Chemical Society)

5.2 Silicon

Silicon is one of the most widely used semiconducting materials due to its abundance in nature and its good electrical performance. However, it is not easy to combine BCP SA with silicon deposition due to the decomposition of polymeric materials at high temperatures. The typical processing temperature for chemical vapor deposition of silicon is above 300°C, which is too high for most organic materials to survive. Thus, nanostructured porous templates prepared from BCP SA (i.e., from pure organic materials) are considered inappropriate for silicon deposition. In order to prevent porous template collapse, "hard" porous templates composed of inorganic materials such as oxides have been used that are durable at these temperatures.

Arora et al. prepared nanoporous oxide templates via BCP + oxide sol SA and subsequent thermal removal of polymeric materials [44]. The resulting hard templates maintained their nanostructure during silicon vapor deposition as well as subsequent laser annealing for generating single-crystal silicon. This hard template approach can be generalized, even for other materials that require high temperature vapor deposition processes, thus being a promising route for fabrication of next-generation nanomaterials for electronic and energy-related applications.

5.3 Metals

Recently, nanostructured metals have attracted much attention for a variety of applications such as metamaterials [15], plasmonics [54], and catalysis. The fabrication of nanostructured metals from BCP SA can be very powerful compared with other top-down approaches because 3D large-scale fabrication of materials is possible.

One strategy for formation of nanostructured metals is to utilize BCP + ligand-stabilized metal nanoparticle SA (see Fig. 9) [42]. In this way, superstructures of metal nanoparticles are structure-directed by BCP SA. This approach enables metal nanostructure control in a one-pot fashion and is thus advantageous over other approaches that may require multiple tedious steps. However, the high surface energy of metals renders it very difficult to disperse metal nanoparticles because, without good passivation, they aggregate to minimize their surface area. Thus, in order to avoid metal nanoparticle aggregation, organic ligands have been employed to reduce their surface energy.

Platinum (Pt) nanoparticles were structure-directed by a BCP, resulting in 1D lamellar and 2D hexagonal superstructures [10, 42]. Such superstructured metal nanoparticles can be further processed to generate highly ordered mesoporous metals via pyrolysis. These mesoporous metals are promising for electrocatalysis [42]. This BCP + ligand-stabilized nanoparticle SA can be generalized to other types

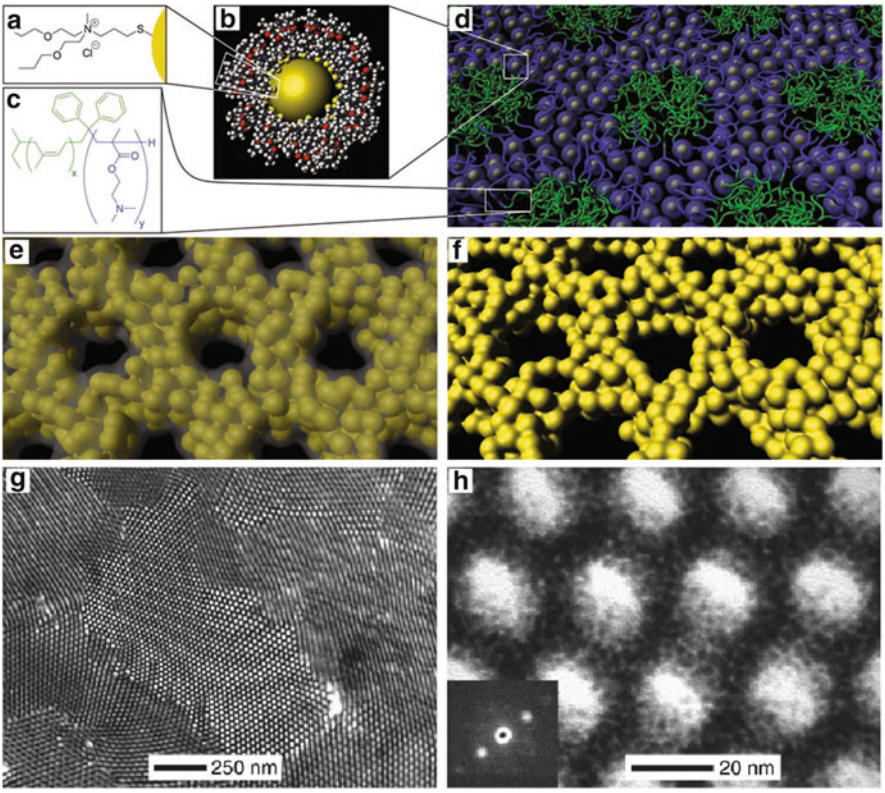

Fig. 9 (**a**–**f**) Materials and steps in BCP-derived mesoporous metal formation. (**a**) Chemical structure of Pt nanoparticle ligand. (**b**) Pt nanoparticle core and a ligand shell (part of the metal surface is artificially exposed for illustrative purposes). (**c**) Chemical structure of the di-BCP. (**d**) Self-assembly of metal nanoparticles with block copolymer, resulting in a regularly ordered structure, such as the inverse hexagonal morphology shown here. (**e**) Pyrolysis of the hybrid under inert atmosphere produces a mesoporous metal composite with thin carbon coating preventing excessive Oswald ripening. (**f**) Plasma treatment of the composite removes the carbon and produces ordered mesoporous Pt. (**g**, **h**) TEM images of an inverse hexagonal hybrid. The *inset* in (**h**) shows the diffraction pattern from a metal nanoparticle (reprinted with permission from [42]; Copyright 2010 AAAS)

of nanoparticles, including semiconducting nanoparticles and quantum dots, thus providing a generalized platform for the generation of periodically ordered mesoporous functional materials [55].

Another strategy is chemical reduction of metal ions on a BCP-derived porous template in a metal salt solution, whereby reduced metals precipitate into the nanopores. The reduction can be achieved by electrodeposition, i.e., by applying an electric potential to a conductive substrate with a nanoporous film in a metal salt solution. As a metamaterial, nanostructured gyroidal gold was fabricated by a combination of BCP SA, ozonolysis, and electrodeposition of gold [38]. To that end, triblock terpolymer PI-*b*-PS-*b*-PEO solution was spun-cast onto a transparent

conductive substrate to form a thin film with alternating gyroid morphology, followed by ozonolysis to remove PI domains, thus resulting in a porous gyroidal polymer template. Applying an electric potential to the transparent conductive substrate led to gold precipitation in the porous template film on the substrate. This approach was quite successful due to metal growth from the bottom of the nanoporous film to the top. The blockage of nanopores from large metal particles is less prominent here than from conformal metal deposition. However, the approach requires an ordered thin porous template on a conductive substrate. Thus, fabrication of thick materials is rather challenging.

Instead of electrodeposition, catalytic reduction of metal ions (i.e., electroless deposition) can be used for metal deposition on nanoporous templates. The Ho group at the National Tsing Hua University in Taiwan successfully deposited nickel on a porous gyroidal template using electroless deposition [56]. The electroless deposition strategy is advantageous in that metals can be deposited on nonconductive substrates. However, since nanopores are very small and easily clogged by large metal particles, complete filling of the nanopores remains challenging.

In this section, we have outlined fabrication of different classes of nanostructured materials via BCP SA. We expect that the scope of these methods will be broadened even further in the future. The resulting nanostructured materials may provide advanced material properties for applications that cannot be attained from conventional materials. In the next section, we summarize several efforts directed towards the application of BCP-directed nanostructured hybrid materials.

6 Application of Block Copolymer Self-Assembly-Directed Materials

Materials research is essential for the improvement of existing technologies as well as the discovery of entirely novel technologies in many areas, including electronics, photonics, energy conversion and storage, and even medicine. Many challenges in modern science and technology could be addressed with better, "smarter" functional materials. The introduction of nanostructured materials in various application areas has seen tremendous emphasis in recent years. For example, in the area of energy conversion and storage nanostructured materials can substantially increase interfacial areas and shorten diffusion pathways over conventional (i.e., micron-scale) analogues, leading to better and faster devices. Furthermore, structural characteristics such as phase symmetry and structural dimensions affect the resulting physical properties, occasionally leading to new physical phenomena such as size-dependent optical properties. This section will discuss selected examples of applications that may benefit from materials with BCP-derived nanostructures. The choices are entirely personal and do not reflect a comprehensive review of activity levels in the field. While some work has already shown promising results, in other cases we will only discuss ideas that are still awaiting experimental realization.

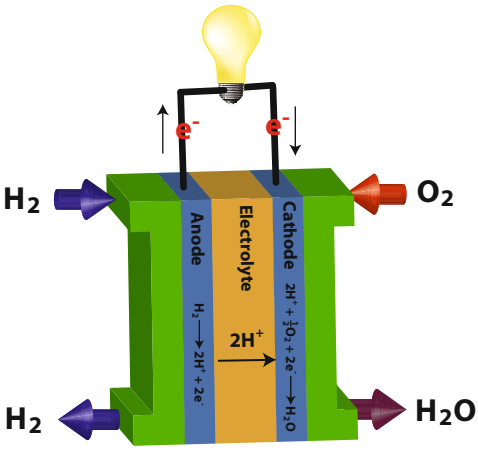

Fig. 10 Schematic of a fuel cell converting chemical energy into electricity

6.1 Fuel Cells

A fuel cell converts the chemical energy of a fuel into electricity. The structurally simplest fuel for a fuel cell is hydrogen, H_2. In a hydrogen fuel cell, hydrogen gas is oxidized at an anode. The resulting protons diffuse through a membrane to the cathode, where they react with oxygen and electrons delivered via an external circuit from the anode to form water (see Fig. 10). The external circuit can be used to drive an electric motor, e.g., in an electric car. Nanoparticles of noble metals such as Pt are widely used as electrode materials. However, such noble metals are usually expensive, thus hampering the practical application of fuel cells. Furthermore, the catalytically active nanoparticles sit on a support, typically made from carbon. Carbon corrodes over time, leading to catalyst nanoparticle aggregation and thus to loss of surface area, ultimately resulting in lowering of fuel cell performance. Catalytic reactions in fuel cell electrodes take place at triple phase boundaries, where the catalytic site has to be in contact with both an electron conductor (e.g., carbon) and an ion conductor (e.g., Nafion). The electrodes also have to be porous enough to let the fuel through to the catalyst particle surface. Designing electrode materials that are cheap and durable, and that fulfill all of the above criteria is a formidable challenge, one where mesoporous nanomaterials are expected to provide major benefits to the application. Nanostructured materials derived from BCP SA may be very useful in this context, at least in the design of electrode supports.

In the previous section we described a BCP SA approach to the synthesis of mesoporous nanostructured Pt metal. This work suggested that catalytic function, mesoporosity, and conductivity can be combined in a single metallic material obtained via a bottom-up approach [42]. The Wiesner group has performed further research into finding an appropriate mesoporous nanostructured conducting oxide to replace the conventional carbon support that lacks durability and to work with intermetallic nanoparticle catalysts rather than the conventional Pt-containing alloys. First results along these lines are promising [57, 58].

Besides electrodes, the low proton conductivity of electrolytes is another challenge to overcome. BCP-derived ordered solid electrolytes may improve the proton conductivities of random polymeric architectures [59]. More in-depth discussion of this issue can be found in the literature [59].

These examples suggest that BCP SA can be a powerful approach for designing better electrodes and electrolytes for fuel cell applications. Although BCP research is not yet regarded as mainstream in fuel cell materials research, its importance for improving fuel cell device performance is most likely going to grow in the future.

6.2 Photonic Crystals and Metamaterials

A photonic crystal is a periodic material that strongly interacts with external electromagnetic fields and exhibits unusual optical phenomena such as a photonic band gap, i.e., a range of frequencies in which the propagation of electromagnetic waves is prohibited [60]. A photonic crystal effect that we utilize in our daily life is the coating of substrates with multilayered thin films (i.e., 1D photonic crystals) that provide anti-reflective or highly reflective properties. The constructive or destructive interference of photons in photonic crystals controls the flow of light. Such interference depends on the wavelength of light and the structural dimensions of the photonic crystals. In a finite range of frequencies, some photonic crystals disallow the existence of any photons and reflect all incoming light irrespective of the incident angle. Such photonic crystals are called complete photonic band gap materials. Complete photonic band gap materials have attracted much attention for their useful applications in such things as lasers and waveguides [60].

A metamaterial is an engineered material that exhibits unusual optical phenomena that may not be found in nature. In this review, we use "metamaterial" as a narrower definition for a periodic metallic material. Metamaterials are attractive in that they enable sub-diffraction-limited photonic applications [61, 62]. The diffraction limit of light originates from the loss of evanescent waves in the far field [63]. Evanescent waves carry the high spatial frequency information that defines small objects. Due to the loss of evanescent waves in the far field, the resolution of objects that can be observed by optical lens systems is limited to the order of the wavelength of light used to image the object.

In theory, a lens system made of a material with a negative refractive index enables unlimited resolution imaging [64]. That is because the loss of evanescent waves in regular materials with positive refractive index is compensated in negative refractive index materials. Thus, evanescent waves can be delivered through such materials. Due to this exciting phenomenon, designing a negative refractive index material, in particular for the frequency range of visible light, has been the subject of significant efforts in metamaterials research for the past decade. A further severe challenge in metamaterials research is the low-cost fabrication of 3D metamaterials at

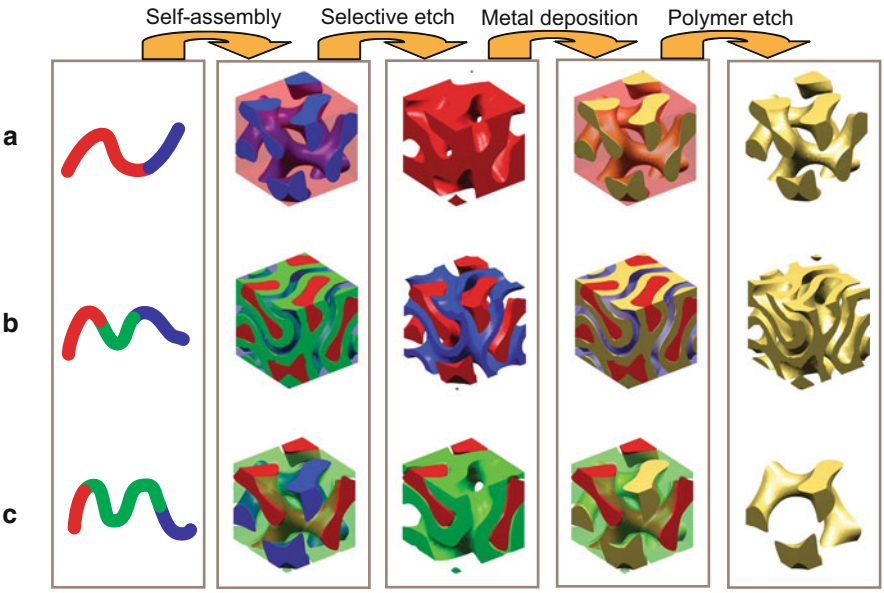

Fig. 11 Routes to three-dimensionally co-continuous metamaterials with (**a**) double gyroid, (**b**) hollow double gyroid, and (**c**) alternating gyroid structures (reprinted with permission from [15]; Copyright 2009 Wiley-VCH)

large scales. Many of the studied metamaterials to date rely on top-down lithographic approaches that require access to cost-intensive nanofabrication facilities, which in turn make large-scale fabrication of 3D metamaterials prohibitive.

For fabricating photonic crystals and metamaterials, bottom-up BCP SA may offer a promising low-cost alternative, in particular for the fabrication of 3D materials (see Fig. 11). As discussed in Sect. 3, a variety of 3D isotropic structures are achievable via SA. However, photonic crystals from BCP SA have a critical limitation for applications. The interference of photons strongly depends on the lattice dimension of the photonic crystal. In order to utilize the unusual diffractive phenomena of photonic crystals, the lattice dimension should be comparable to the wavelength of external light. For example, complete photonic band gap materials reflecting visible light have a lattice dimension of about 250 nm. In contrast, typical materials derived from BCP SA have a lattice dimension of less than 100 nm. Thus, using conventional BCP SA it is not straightforward to extend to photonic crystal applications.

Such limitations do not apply in the field of metamaterials since here plasmons interact with electromagnetic fields. A plasmon is a free-electron oscillation in a metal and exhibits quite distinct photonic behavior from a photon. Generally, for the same frequency, the wavelength of a plasmon is much smaller than that of a photon. For this reason, metamaterials with small lattice dimensions can still

interact with external light of a much longer wavelength. Thus, the BCP SA approach is very promising for fabrication of large-scale and low-cost 3D isotropic metamaterials.

Indeed, the Wiesner group suggested in a computational study that BCP-derived 3D isotropic metamaterials with a double gyroid morphology may have a negative refractive index in the visible regime [15]. This exciting result may motivate the use of other materials derived from bottom-up SA techniques in metamaterials research [65]. Furthermore, in a subsequent collaborative effort with the Steiner and Baumberg groups at Cambridge University, aspects of the proposed properties of the computational studies were seen in alternating BCP gyroid metamaterials backfilled with gold [38, 66].

6.3 Phononics and Thermoelectric Devices

A phonon is a lattice vibration that mediates transport of sound and thermal waves. A phononic crystal is a periodic material engineered to control the propagation of phonon waves. Phononic crystals that manipulate sound waves are sometimes called acoustic metamaterials. As for photonic crystals, BCP SA may be used for fabricating phononic crystals. Also similar to the photonics field, one of the main properties that scientists try to establish in acoustic metamaterials is a phononic band gap, i.e., a frequency range in which phonons cannot exist in the material. Similarly to photonic crystals, phononic crystals can manipulate specific phonons with a wavelength that is comparable to the lattice dimension. For example, a periodic material with a lattice dimension of centimeters manipulates sound waves, whereas a material with a lattice dimension of nanometers strongly interacts with thermal waves. Thus, a phononic crystal derived from BCP SA may be able to control the flow of thermal waves.

The control of thermal waves in such phononic crystals could be applied to generate better thermoelectric materials. The figure of merit for thermoelectric devices, ZT, is proportional to the so-called Seebeck coefficient and to the ratio of electron conductivity to thermal conductivity [67]. Materials with high electron and low thermal conductivities promise high figures of merit, thereby leading to efficient thermoelectric devices. The three parameters are, however, not independent. For example, materials with low thermal conductivity usually have poor electric conductivity. In order to minimize the thermal conductivity of a material without the deterioration of electron conductivity, it is desirable to structure the material with a phononic band gap. The incorporation of phononic band gap structures into thermoelectric materials can reduce their thermal conductivity in that phonons (thermal energy carriers) are missing in the phononic band gap frequency range. Therefore, BCP-derived phononic crystals may in the future become useful for improving the figure of merit for thermoelectric devices.

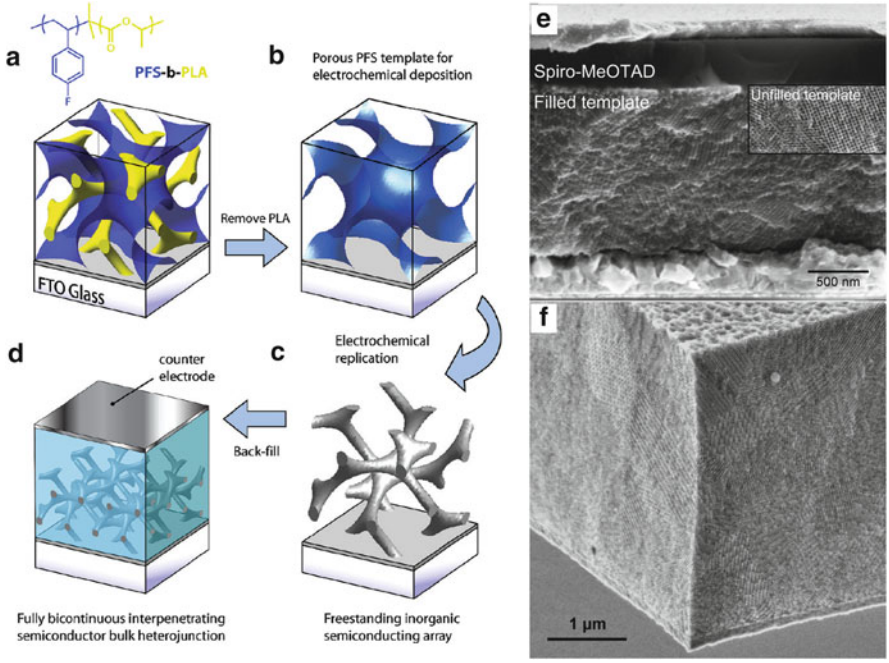

Fig. 12 (**a**–**d**) Gyroid titania network and fabrication of hybrid solar cells. (**e**–**f**) Scanning electron microscope images of the resulting titania electrode (reprinted with permission from [37]; Copyright 2009 American Chemical Society)

6.4 Photovoltaics

Much effort has been devoted to developing photovoltaics with better conversion efficiency from photonic to electric energy. There are many sources of efficiency losses associated with current photovoltaic technologies, such as thermalization, lack of absorption, absorption angle restrictions, and so on [68]. Not all these challenges can be overcome by BCP-derived nanostructures. However, several important issues may benefit from nanostructures derived from BCP SA. We will discuss three strategies based on BCP SA to improve photovoltaic efficiency.

One of the strategies is to minimize the diffusion path of exitons (bound states between an electron and electron hole) generated by photons hitting the active material in a photovoltaic cell. Once separated, holes and electrons should reach anode and cathode electrodes, respectively. During the process, recombination of holes and electrons lead to energy losses via thermal dissipation. In order to reduce such losses, minimizing the diffusion paths of exitons by means of BCP-derived nanostructures may be beneficial. To this end, a thin solid-state dye-sensitized solar cell (ssDSSC) with a 3D gyroidal titania network was fabricated (see Fig. 12) [37]. In contrast to typical disordered nanoparticle networks, the ordered mesoporous

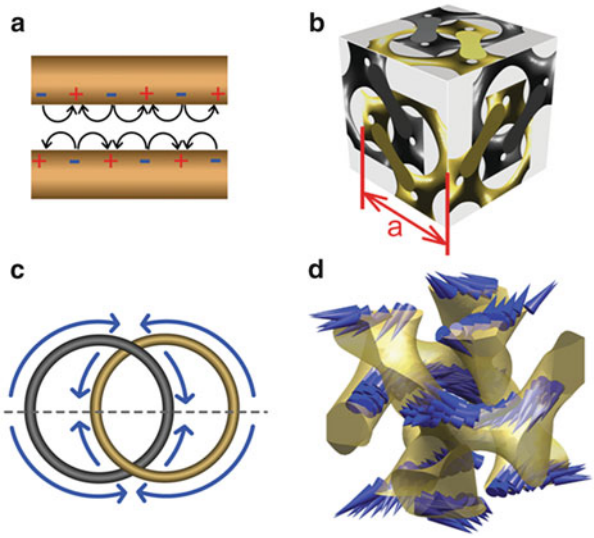

Fig. 13 (**a**) Plasmons oscillate on a 1D metal/insulator/metal waveguide. (**b**) Projected images of a double gyroid metamaterial unit cell, with unit cell length *a*, onto three orthogonal axes (two struts are cut in different planes to show full loops). (**c**) Plasmons oscillate on the closed loops of gyroid networks. (**d**) Calculated coupled plasmon vectors (shown as *arrows*) on a double gyroid metamaterial (reprinted with permission from [15]; Copyright 2009 Wiley-VCH)

gyroidal titania facilitated backfilling with the solid-state hole conductor. Since, in these first experiments, film thickness was limited to below half a micron, the external power conversion efficiency was below 2%. In subsequent experiments, it was shown that ABC triblock terpolymer-directed gyroidal titania electrodes exhibit a high availability of subbandgap states, thus improving photo-induced charge generation [69]. This led to 5% efficiency and ssDSSC devices outperforming, for the first time, back-to-back fabricated titania nanoparticle-based solar cells.

A second strategy for improving photovoltaic efficiency is to integrate photonic crystals into solar cells, thereby controlling the flow of light in the cells [68]. Since photonic crystals and metamaterials can both effectively control the path of light and the near-field profile of electromagnetic waves, their combination with existing solar cell technologies can improve solar cell efficiency, e.g., by extending the path of light in thin-film solar cells. Although BCP SA has been used to generate photonic crystal structures including photonic band gap structures [16], as discussed earlier, typical restrictions of lattice dimensions limit its usefulness for photovoltaics.

In contrast, such limitations are not significant in a metamaterial. Therefore, one could incorporate a BCP SA-directed metamaterial architecture into photovoltaic cells for light management, such as light-trapping inside photovoltaic cells with a metal/insulator/metal waveguide. To that end, we theoretically demonstrated that two independent networks of double gyroid metamaterials form a metal/insulator/metal waveguide (see Fig. 13) [15]. It would be quite interesting to experimentally realize such structures and to explore their impact on photovoltaic cell performance.

Finally, a phononic band gap structure could be incorporated to improve photovoltaic efficiency. Due to zero phonon population within a phononic band gap frequency range, materials with a phononic band gap structure may reduce phonon generation, i.e., thermalization, which is a major energy loss mechanism in

photovoltaic cells. Such phononic band gap structures may be achieved by BCP SA. However, it is not yet obvious to relate the thermalization in photovoltaics with phonon formation. Thus, more in-depth studies have to be performed to assess whether this strategy can be successful.

6.5 Membranes

Membranes can be defined as selective barriers between two phases and have a plethora of applications, including water purification, desalination, drug development, and chemical sensing. BCP SA can be a useful approach for membrane fabrication because tunable structure and narrow size control of membrane pores is possible.

Yang et al. synthesized a thin film with an ordered standing cylinder structure from BCP SA and transferred the film to a porous support to fabricate highly selective membranes with ordered nanochannels for virus filtration [70]. The top thin layer derived from BCP SA provided size-selective pores at the nanoscale.

While very creative, the approach by Yang et al. required several tedious steps for membrane formation, thus making large-scale fabrication challenging. As discussed in Sect. 4, Peinemann et al. proposed an innovative approach (now referred to as SNIPS) that combined NIPS, a well-established process in the membrane industry, with BCP SA to fabricate asymmetric BCP-derived membranes (see Fig. 7) [45]. The membranes exhibit well-ordered, densely packed, and uniform pores in the top surface and a substructure with graded porosity. SNIPS provides a scalable fabrication process of asymmetric BCP membranes with high size selectivity for nanometer-sized solutes.

The Wiesner group applied the SNIPS process to poly(isoprene-*b*-styrene-*b*-4-vinyl pyridine) terpolymer to fabricate scalable membranes with high fluxes and sharp molecular weight cut-offs [47]. Introduction of the third, PI block generated membranes with improved mechanical properties over the diblock copolymer-based materials studied by Peinemann et al. Thus, besides BCP SA as a means to control structure, BCP architectures can further be employed to control the mechanical properties of nanomaterials.

6.6 Lithium Battery

Lithium batteries can benefit from nanostructured electrodes (i.e., anode and cathode) that combine large electric capacity by accommodating as many lithium ions as possible with short diffusion paths. The most widely used anode material is graphite, where lithium ions intercalate between graphite layers. A battery with lithium ions chemically intercalated in an anode composed of a non-lithium material is usually called a lithium ion battery. In order to improve battery capacity, lithium metal has been studied as anode material. A battery with lithium metal anode is called a lithium

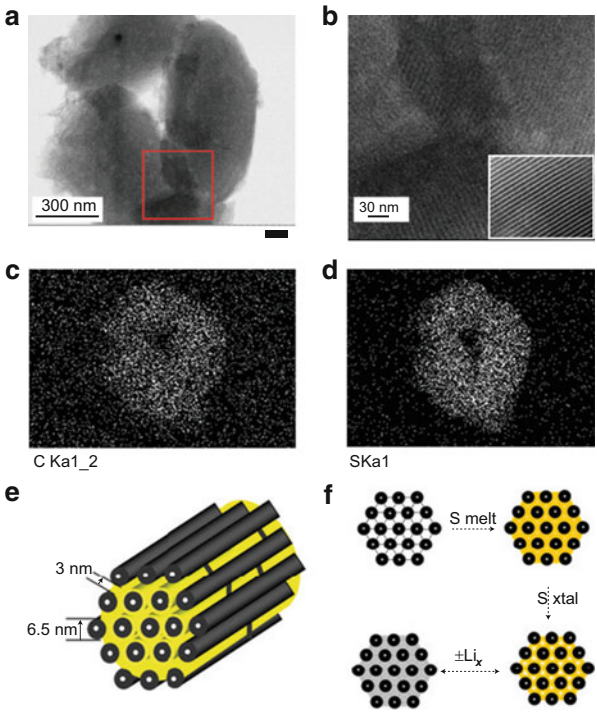

Fig. 14 (**a, b**) TEM images of BCP-derived carbon/sulfur composite particle at different magnifications, where (**b**) is the area outlined by the *square* in (**a**). Corresponding carbon (**c**) and sulfur (**d**) elemental maps showing the homogeneous distribution of sulfur. (**e, f**) Diagrams of the structure and redox processes. Reprinted with permission from [72]; Copyright 2007 Nature Publishing Group

battery or lithium metal battery. Since lithium ions can be oxidized and reduced on the lithium anode surface and lithium metal is the densest lithium ion source without wasted mass on a host material, lithium batteries can have much higher capacity than lithium ion batteries.

Despite such good characteristics, lithium batteries have severe drawbacks. First, there are not many cathode materials that have an appropriate electrochemical potential difference from the lithium anode combined with a large capacity. Second, they are less stable than lithium ion batteries due to dendrite formation on lithium metal surfaces [71]. Dendrites lead to electrical shortage between anode and cathode, which can result in an explosion. These problems may be overcome by utilizing BCP SA.

One of the most promising cathode materials for lithium batteries is sulfur. Sulfur is abundant in nature and an undesirable impurity in petroleum, thus it is very cheap. Lithium batteries with a sulfur cathode, so-called lithium sulfur batteries, have potentially high electric capacity but so far only very poor cyclability. A few charge–discharge cycles induce a significant capacity drop. In order to overcome existing limitations, Ji et al. prepared nanostructured carbon as a sulfur support from BCP SA and showed that this mesoporous carbon holds sulfur inside nanopores (Fig. 14) and led to good cyclability and large cathode capacity [72].

The safety concern owing to dendrite formation can be overcome by introducing a separator between anode and cathode [73] that is mechanically robust and has good lithium conductivity. Cho et al. studied lithium ion transport in nanostructured PEO domains prepared by SA of a linear-dendritic block copolymer containing PEO [17]. They found that lithium conductivity varies strongly as a function of the dimensionality of the nanostructure, with the 3D co-continuous double gyroid structure showing the highest lithium conductivity and the best mechanical properties. Targeting such bicontinuous structures and introducing mechanically robust blocks to a PEO-containing BCP, one may be able to fabricate separators with a high lithium conductivity and good mechanical robustness.

7 Summary and Outlook

In this review, we have summarized fabrication of BCP-derived hybrid nanomaterials and looked at some first promising as well as proposed applications. Bottom-up BCP SA is a promising approach for designing nanomaterials with tunable structures and lattice dimensions. In particular, it allows large-scale and low-cost fabrication of nanomaterials using wet-chemical methodologies. However, due to the lack of material functionality for BCPs with good SA properties (i.e., flexible polymer coil structures), complementary functional materials are often combined with the use of BCP SA to meet the needs of today's applications. To that end, the Wiesner group at Cornell University has made an effort in combining BCP SA with functional inorganic materials, resulting in functional hybrids with ordered structures at the nanoscale. The aims of this review were to highlight the resulting toolbox of BCP-based nanomaterials, to elucidate the emerging design parameters for their controlled formation, and to share our views about where in the future this toolbox may provide innovative solutions for today's application challenges. To that end, we briefly introduced the basics of BCP SA and summarized some of the resulting equilibrium-type nanostructures that one can obtain from it. From there we showed how nanostructure control by SA can be transferred to various other material classes for synthesizing nanostructured hybrid materials. Besides using the principles of equilibrium BCP structure formation, recent results of the Wiesner group and others point more and more to the successful control of BCP structures obtained by using conditions far away from equilibrium. Lastly, we described already-proven and possible future applications that can benefit from BCP SA-directed hybrid nanomaterials. We hope that with this review, on the occasion of the 60th anniversary of Staudinger's Nobel Prize, we are able to demonstrate that polymer science, and in particular the area of BCP SA, is a vibrant research area with a number of emerging and very exciting research directions intimately connected to important and unrealized high-value applications that reach from the design of energy device electrodes to the formation of metamaterials with negative refraction all the way to the fabrication of asymmetric ultrafiltration membranes. We are convinced that this

field of research is going to continue to grow and flourish and hope that some of the most brilliant young minds will join efforts in the future to push the boundaries of our knowledge and understanding and to translate the results into applications that will benefit society.

Acknowledgements This article is based on research over a period of about 15 years in the Wiesner group at the Materials Science and Engineering Department of Cornell University. The work would have been impossible without the help of an enormous number of very motivated, talented and enthusiastic students, postdocs, and collaborators at Cornell and beyond. Equally important, the work was enabled by a continuous stream of financial support, for which we would particularly like to thank the National Science Foundation via the Polymers Program within the Division of Materials Research (current grant DMR-1104773). We thank Joerg Werner for contributing to the lithium battery section.

References

1. Flory PJ (1953) Principles of polymer chemistry. Cornell University Press, Ithaca
2. Antonietti M (2013) Macromol Chem Phys 214:130. doi:10.1002/macp.201200589
3. Wu C (2013) Macromol Chem Phys 214:132. doi:10.1002/macp.201200417
4. Rurack K, Martínez-Máñez R, Wiley InterScience (Online service) (2010) The supramolecular chemistry of organic-inorganic hybrid materials. Wiley, Hoboken
5. Tyler CA, Morse DC (2005) Phys Rev Lett 94:208302
6. Doi M, Edwards SF (1986) The theory of polymer dynamics. Clarendon and Oxford University Press, New York
7. Bates FS, Hillmyer MA, Lodge TP, Bates CM, Delaney KT, Fredrickson GH (2012) Science 336:434. doi:10.1126/science.1215368
8. Ott H, Abetz V, Altstaedt V (2001) Macromolecules 34:2121. doi:10.1021/ma0017079
9. Toombes GES, Mahajan S, Weyland M, Jain A, Du P, Kamperman M, Gruner SM, Muller DA, Wiesner U (2008) Macromolecules 41:852. doi:10.1021/ma071004s
10. Li Z, Sai H, Warren SC, Kamperman M, Arora H, Gruner SM, Wiesner U (2009) Chem Mater 21:5578. doi:10.1021/cm9020673
11. Warren SC, DiSalvo FJ, Wiesner U (2007) Nat Mater 6:156
12. Bita I, Yang JKW, Jung YS, Ross CA, Thomas EL, Berggren KK (2008) Science 321:939. doi:10.1126/science.1159352
13. Park S, Lee DH, Xu J, Kim B, Hong SW, Jeong U, Xu T, Russell TP (2009) Science 323:1030. doi:10.1126/science.1168108
14. Garcia BC, Kamperman M, Ulrich R, Jain A, Gruner SM, Wiesner U (2009) Chem Mater 21:5397. doi:10.1021/cm901885c
15. Hur K, Francescato Y, Giannini V, Maier SA, Hennig RG, Wiesner U (2011) Angew Chem Int Ed 50:11985. doi:10.1002/anie.201104888
16. Maldovan M, Urbas AM, Yufa N, Carter WC, Thomas EL (2002) Phys Rev B 65:165123
17. Cho BK, Jain A, Gruner SM, Wiesner U (2004) Science 305:1598. doi:10.1126/science.1100872
18. Cochran EW, Garcia-Cervera CJ, Fredrickson GH (2006) Macromolecules 39:2449. doi:10.1021/ma0527707
19. Saranathan V, Osuji CO, Mochrie SGJ, Noh H, Narayanan S, Sandy A, Dufresne ER, Prum RO (2010) Proc Natl Acad Sci 107:11676. doi:10.1073/pnas.0909616107
20. Almsherqi Z, Margadant F, Deng Y (2012) Interface Focus 2:539. doi:10.1098/rsfs.2011.0120

21. Grin Y, Wedig U, von Schnering HG (1995) Angew Chem Int Ed Engl 34:1204. doi:10.1002/anie.199512041
22. Sorenson GP, Coppage KL, Mahanthappa MK (2011) J Am Chem Soc 133:14928. doi:10.1021/ja2063555
23. Jain A, Toombes GES, Hall LM, Mahajan S, Garcia CBW, Probst W, Gruner SM, Wiesner U (2005) Angew Chem Int Ed 44:1226. doi:10.1002/anie.200461156
24. Chu C-Y, Lin W-F, Tsai J-C, Lai C-S, Lo S-C, Chen H-L, Hashimoto T (2012) Macromolecules 45:2471. doi:10.1021/ma202057g
25. Wohlgemuth M, Yufa N, Hoffman J, Thomas EL (2001) Macromolecules 34:6083. doi:10.1021/ma0019499
26. Gòždž W, Holyst R (1996) Macromol Theory Simulations 5:321. doi:10.1002/mats.1996.040050212
27. Karcher H (1989) Manuscripta Mathematica 64:291. doi:10.1007/bf01165824
28. Lidin S, Larsson S (1990) J Chem Soc Faraday Trans 86:769. doi:10.1039/ft9908600769
29. Epps TH, Cochran EW, Bailey TS, Waletzko RS, Hardy CM, Bates FS (2004) Macromolecules 37:8325. doi:10.1021/ma048762s
30. Tyler CA, Qin J, Bates FS, Morse DC (2007) Macromolecules 40:4654. doi:10.1021/ma062778w
31. Kim MI, Wakada T, Akasaka S, Nishitsuji S, Saijo K, Hasegawa H, Ito K, Takenaka M (2009) Macromolecules 42:5266. doi:10.1021/ma900205s
32. Ho R-M, Chiang Y-W, Tsai C-C, Lin C-C, Ko B-T, Huang B-H (2004) J Am Chem Soc 126:2704. doi:10.1021/ja039627i
33. Lee S, Bluemle MJ, Bates FS (2010) Science 330:349. doi:10.1126/science.1195552
34. Hayashida K, Dotera T, Takano A, Matsushita Y (2007) Phys Rev Lett 98:195502
35. Man W, Megens M, Steinhardt PJ, Chaikin PM (2005) Nature 436:993
36. Wu D, Xu F, Sun B, Fu R, He H, Matyjaszewski K (2012) Chem Rev 112:3959. doi:10.1021/cr200440z
37. Crossland EJW, Kamperman M, Nedelcu M, Ducati C, Wiesner U, Smilgies DM, Toombes GES, Hillmyer MA, Ludwigs S, Steiner U, Snaith HJ (2009) Nano Lett 9:2807. doi:10.1021/nl803174p
38. Vignolini S, Yufa NA, Cunha PS, Guldin S, Rushkin I, Stefik M, Hur K, Wiesner U, Baumberg JJ, Steiner U (2012) Adv Mater 24:OP23. doi:10.1002/adma.201103610
39. Zalusky AS, Olayo-Valles R, Wolf JH, Hillmyer MA (2002) J Am Chem Soc 124:12761. doi:10.1021/ja0278584
40. Ulrich R, Chesne AD, Templin M, Wiesner U (1999) Adv Mater 11:141. doi:10.1002/(sici)1521-4095(199902)11:2<141::aid-adma141>3.0.co;2-r
41. Thompson RB, Ginzburg VV, Matsen MW, Balazs AC (2001) Science 292:2469. doi:10.1126/science.1060585
42. Warren SC, Messina LC, Slaughter LS, Kamperman M, Zhou Q, Gruner SM, DiSalvo FJ, Wiesner U (2008) Science 320:1748. doi:10.1126/science.1159950
43. Lee J, Christopher Orilall M, Warren SC, Kamperman M, DiSalvo FJ, Wiesner U (2008) Nat Mater 7:222. doi:10.1038/nmat2111
44. Arora H, Du P, Tan KW, Hyun JK, Grazul J, Xin HL, Muller DA, Thompson MO, Wiesner U (2010) Science 330:214. doi:10.1126/science.1193369
45. Peinemann KV, Abetz V, Simon PF (2007) Nat Mater 6:992. doi:10.1038/nmat2038
46. Dorin RM, Marques DS, Sai H, Vainio U, Phillip WA, Peinemann K-V, Nunes SP, Wiesner U (2012) ACS Macro Lett 1:614. doi:10.1021/mz300100b
47. Phillip WA, Mika Dorin R, Werner J, Hoek EMV, Wiesner U, Elimelech M (2011) Nano Lett 11:2892. doi:10.1021/nl2013554
48. Sai H, Tan KW, Hur K, Asenath-Smith E, Hovden R, Jiang Y, Riccio M, Muller D, Elser V, Estroff LA, Gruner SM, Wiesner U (2013) Science 341:530 doi:10.1126/science.1238159
49. Templin M, Franck A, Du Chesne A, Leist H, Zhang Y, Ulrich R, Schädler V, Wiesner U (1997) Science 278:1795. doi:10.1126/science.278.5344.1795

50. Martínez-Veracoechea FJ, Escobedo FA (2009) Macromolecules 42:1775. doi:10.1021/ma802427a
51. Stefik M, Lee J, Wiesner U (2009) Chem Commun 2009(18):2532. doi:10.1039/b818972b
52. Stefik M, Sai H, Sauer K, Gruner SM, DiSalvo FJ, Wiesner U (2009) Macromolecules 42:6682. doi:10.1021/ma900685e
53. Stefik M, Mahajan S, Sai H, Epps TH, Bates FS, Gruner SM, DiSalvo FJ, Wiesner U (2009) Chem Mater 21:5466. doi:10.1021/cm902626z
54. Maier SA (2007) Plasmonics: fundamentals and applications. Springer, New York
55. Rauda IE, Buonsanti R, Saldarriaga-Lopez LC, Benjauthrit K, Schelhas LT, Stefik M, Augustyn V, Ko J, Dunn B, Wiesner U, Milliron DJ, Tolbert SH (2012) ACS Nano 6:6386. doi:10.1021/nn302789r
56. Hsueh H-Y, Huang Y-C, Ho R-M, Lai C-H, Makida T, Hasegawa H (2011) Adv Mater 23:3041. doi:10.1002/adma.201100883
57. Orilall MC, Matsumoto F, Zhou Q, Sai H, Abruña HD, DiSalvo FJ, Wiesner U (2009) J Am Chem Soc 131:9389. doi:10.1021/ja903296r
58. Shim J, Lee J, Ye Y, Hwang J, Kim S-K, Lim T-H, Wiesner U, Lee J (2012) ACS Nano 6:6870. doi:10.1021/nn301692y
59. Elabd YA, Hickner MA (2010) Macromolecules 44:1. doi:10.1021/ma101247c
60. Joannopoulos JD (2008) Photonic crystals: molding the flow of light. Princeton University Press, Princeton
61. Pendry JB, Holden AJ, Robbins DJ, Stewart WJ (1999) IEEE Trans Microwave Theory Tech 47:2075
62. Soukoulis CM, Wegener M (2011) Nat Photon 5:523
63. Novotny L, Hecht B (2006) Principles of nano-optics. Cambridge University Press, Cambridge
64. Pendry JB (2000) Phys Rev Lett 85:3966
65. Ying JY (2012) Nat Chem 4:159
66. Salvatore S, Demetriadou A, Vignolini S, Oh SS, Wuestner S, Yufa NA, Stefik M, Wiesner U, Baumberg JJ, Hess O, Steiner U (2013) Adv Mater 25:2713. doi:10.1002/adma.201300193
67. DiSalvo FJ (1999) Science 285:703. doi:10.1126/science.285.5428.703
68. Polman A, Atwater HA (2012) Nat Mater 11:174
69. Docampo P, Stefik M, Guldin S, Gunning R, Yufa NA, Cai N, Wang P, Steiner U, Wiesner U, Snaith HJ (2012) Adv Energy Mater 2:676. doi:10.1002/aenm.201100699
70. Yang SY, Ryu I, Kim HY, Kim JK, Jang SK, Russell TP (2006) Adv Mater 18:709. doi:10.1002/adma.200501500
71. Orsini F, Du Pasquier A, Beaudoin B, Tarascon JM, Trentin M, Langenhuizen N, De Beer E, Notten P (1998) J Power Sources 76:19. doi:10.1016/S0378-7753(98)00128-1
72. Ji X, Lee KT, Nazar LF (2009) Nat Mater 8:500. doi:10.1038/nmat2460
73. Arora P, Zhang Z (2004) Chem Rev 104:4419. doi:10.1021/cr020738u

Adv Polym Sci (2013) 262: 295–328
DOI: 10.1007/12_2013_238

Published online: 27 September 2013

Synthesis of Cyclic Polymers via Ring Closure

Zhongfan Jia and Michael J. Monteiro

Abstract Cyclic polymers have intrigued scientists for many years and their diffusion process may have important implications for polymer physics. In this contribution, we focus on the ring-closure method for synthesis of linear polymers made by "living" radical polymerization. In the first part, the probability of two chain ends being in a capture volume to undergo ring closure will be described using the well-known Gaussian chain end-to-end distance. The probability for knot or catenane structures will also be discussed. We then describe the thermodynamic Jacobson–Stockmayer theory for monocyclic ring closure, and an empirical equation based on kinetics. Finally, we give examples of ring closure for many different polymer systems, including the formation of many complex cyclic topologies.

Keywords Cyclic polymers · Jacobson–Stockmayer equation · "Living" radical polymerization · Ring-closure

Contents

Z. Jia and M.J. Monteiro (✉)
Australian Institute for Bioengineering and Nanotechnology, The University of Queensland, Brisbane, QLD 4072, Australia
e-mail: m.monteiro@uq.edu.au

Abbreviations

c	Concentration of polymer in g mL^{-1}
K	Constant dependent upon the polymer
K	Equilibrium rate constant
k_{-1}	Rate coefficient for two ends diffusing apart
k_2	Rate coefficient for the chemical reaction between the two chain ends
k_{c1}	Rate coefficient for diffusion of chain ends from different chains within the capture volume
k_{l1}	Rate coefficient for diffusion of two ends of the same chain within the capture volume
l	Length of a covalent bond
M_e	Molecular weight between entanglements
M_w	Weight-average molar mass
N	Total number of polymer molecules in total volume V
N_A	Avogadro's number
P_c	Probability that the two ends of the same chain are within the capture volume
P_L	Probability that chain ends from different chains are within the capture volume
$<r^2>$	Mean square end-to-end distance of the chain
$<r^2>^{1/2}$	Root mean square end-to-end distance
$<S^2>_\theta$	Root mean square radius of gyration in a θ-solvent
T_g^∞	Glass transition temperature at infinite molecular weight
T_g	Glass transition temperature
v_s	Capture volume
$W(r)$	Possibility distribution function
ρ	Density of the polymer

1 Introduction

Cyclic polymers have one of the simplest topologies, yet they have some of the most intriguing properties, many of which remain poorly understood. The physical properties of linear polymers in their melt state can be predicted using the theory of reptation [1, 2]. Linear polymers diffuse within the constraints of adjacent polymer chains, in which the chain ends play a most important role due to their ability to explore a much greater volume than the interior of the chain [1, 3]. Cyclic polymers have no chain ends and, at first sight, one would assume that they diffuse in a very different way and at a much slower rate. Diffusion experiments show the contrary; cyclic polymers have a diffusion rate coefficient approximately twice as fast as linear polymers of the same molecular weight [4]. This is postulated to be due to an amoebae-like motion for the cyclic

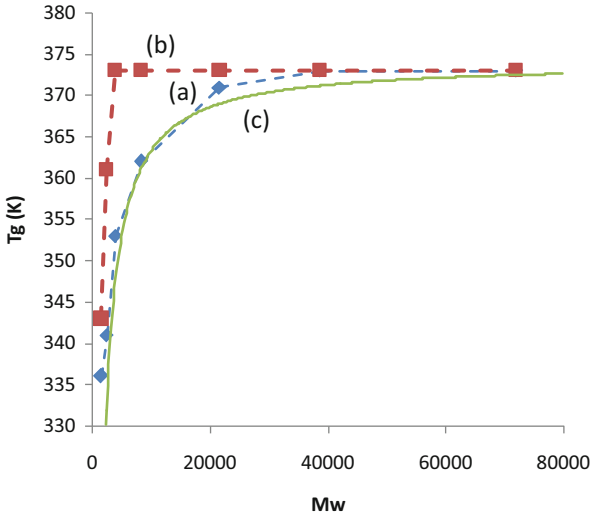

Fig. 1 The effect of molecular weight of polystyrene on T_g for (*a*) linear, (*b*) cyclic and (*c*) the fit of (*a*) with Eq. (1) using $K = 0.78$ and $T_g{}^{\infty} = 374$ K. Data taken from literature [20]

polymers [5]. The compact nature of cyclic polymers, as exemplified by the lower radius of gyration (i.e. $<S^2>_{cyclic}/<S^2>_{linear} = 0.5$ in a theta solvent and 0.526 in a good solvent) [6] are in good agreement with experimental results [7]. The different diffusion and conformational restricted topology of cyclic polymers has resulted in properties quite different to those of their linear counterparts [8]. These include higher density [9], lower intrinsic viscosity [10], lower translational friction coefficients, higher glass transition temperatures [10], higher critical solution temperature [11], increased rate of crystallization [12], and higher refractive index [13].

The glass transition temperature (T_g) is one property that is significantly different for linear and cyclic polymers at low molecular weights (M_w). Linear polymers show an increase in T_g with M_w that can be predicted using the Kanig–Ueberreiter equation [14]:

$$T_g = \left[\frac{1}{T_g{}^{\infty}} + \frac{K}{M_w}\right]^{-1} \tag{1}$$

where $T_g{}^{\infty}$ is the T_g at infinite molecular weight, K is a constant dependent upon the polymer (for polystyrene, $K = 0.78$), and M_w is the molecular weight of the polymer.

In Fig. 1, there is good agreement between experimental (curve a) and Eq. (1)-derived (curve c) T_g values. Cyclic polymers show a different behavior; even at low molecular weights the T_g is high and close to $T_g{}^{\infty}$. Differences in T_g can be explained using free-volume effects [15]. A greater packing of the polymer in the bulk will lead to higher values of T_g. On the other hand, the chain ends of linear polymers increase the free volume and entropy to lower the T_g, a phenomenon that dominates at low molecular weights. At very high molecular weights, the concentration of chain ends for linear polymers becomes insignificant, resulting in the

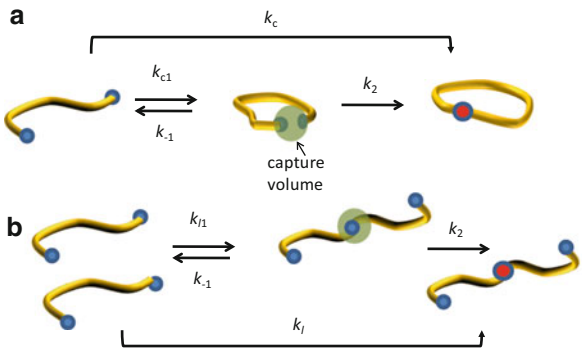

Scheme 1 Encounter pair model for ring closure of (**a**) linear to cyclic polymer chain, and (**b**) multiblock formation

limiting value for T_g (i.e., T_g^{∞}). Dendrimers have many endgroups, which increase with each generational layer. These endgroups result in a decrease in the T_g that is slightly offset by the constraints of the branching points [16]. Significant constraints, as found in crosslinked polymers, can also significantly influence the T_g through the loss of entropy to values much greater than T_g^{∞} [17, 18]. Because cyclic polymers have no chain ends and a compact topology, the lower degree of configurational freedom and the lower free volume results in a higher T_g at lower molecular weights. At very high molecular weights, the configurational constraints become similar to that for linear polymers, resulting in a T_g approaching T_g^{∞} [19].

There has been some debate in the literature over the physical properties of cyclic polymers due to the difficulty in synthesizing pure cyclic polymers without linear contaminants and in producing cyclic polymers in large quantities. This contribution provides an overview of recent techniques used in the synthesis of cyclic polymers, and in particular will focus on the ring-closure method (Scheme 1) in which functional chain ends are covalently coupled to form cyclic polymers. In accord with the theme of this issue, we will highlight the use of "living" radical polymerization to produce polymers with highly functional chain-end functionality to produce compositionally different cyclic polymers. We will discuss the geometry of linear polymers and the probability for the chain ends of the same polymer to be within the capture volume for covalent bond formation. Two models will be discussed to predict the percentage of monocyclic polymer: the first is the well-known equilibrium Jacobson–Stockmeyer equation, and the second is an empirical kinetic relationship developed by Monteiro and coworkers [21]. Finally, we will discuss methods for the synthesis of cyclic polymers by ring closure.

1.1 Chain Conformation for Ring Closure

The shape and motion of a polymer chain play important roles in ring closure. For ring closure to occur, the ends of the polymer chain must first be within the capture radius of a covalent bond, and then undergo a chemical reaction (Scheme 1a).

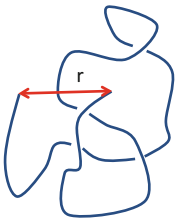

Scheme 2 Representation of a random coil with end-to-end distance of *r*

Because polymer chains are always in dynamic motion, one of the best methods for studying the location (or probability) that two chain ends are within the capture volume is via fluorescence labeling of the chain ends with pyrene [22–25]. The chain ends in Scheme 1a could represent pyrene groups, and when the chain ends are within the capture volume, the two pyrenes produce an excimer. Winnik and coworkers found that k_{c1} was dependent on chain length and close to diffusion rate control, increasing in value with chain length [24]. The reverse process (i.e., k_{-1}) was logically found to be independent of chain length. These researchers also determined the entropy of cyclization, which in turn provided the probability of cyclization to the capture radius. For example, polystyrene with an M_n of 3,900 had a probability of cyclization of 1.61×10^{-5}, while the probability decreased to 5.56×10^{-6} at an M_n of 9,200, demonstrating the sensitivity of cyclization to chain length.

The discussion above highlights the importance of the chain end-to-end distance for ring closure. Conformation of a polymer chain in space can be represented by a "random coil" (Scheme 2). In dilute solutions where the polymer is in a θ-solvent and in the bulk amorphous state, the polymer can be described using the random coil dimensions. The chain end-to-end distance, *r*, fluctuates with time but fits well to a Gaussian distribution.

The time-averaged root mean square end-to-end distance $<r^2>^{1/2}$ can be determined using the simplest freely joined chain of *n* links in which each link has a length *l*. In this model, there are no bond angle or bond rotation restrictions, and it conforms to the well-known random walk. The probability density function $W(x,y,z)$ is a Gaussian distribution function. This function can be easily converted to the distribution function $W(r)$, which now relates the probability of finding one chain end at a distance *r* in any direction from a chain end at the origin, as shown in Eq. (2).

$$W(r) = 4\pi\left(\frac{\beta}{\pi^{\frac{1}{2}}}\right)r^2\exp\left(-\beta^2 r^2\right) \tag{2}$$

where $\beta^2 = 3/(2nl^2)$, *n* is the number of segments, and *l* is the length of a covalent bond.

Figure 2 shows a plot of $W(r)$ versus *r* for polymers at different molecular weights. It can be seen that the probability that the chain ends are within the capture radius (i.e., the distance of a covalent bond) is highly sensitive to molecular weight. The smaller chain length polymer has a greater chance of being in a conformation

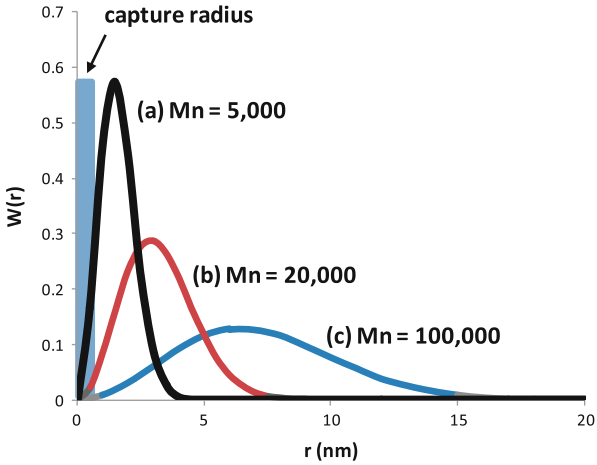

Fig. 2 Probability radical distribution, $W(r)$, as a function of the end-to-end distance (r) of a linear polymer chain for chains of molecular weight (*a*) 5,000, (*b*) 20,000, and (*c*) 100,000. The capture radius is indicated by the *blue box*

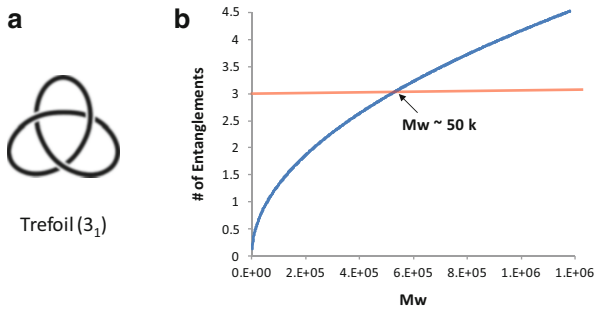

Fig. 3 (**a**) The simplest knot structure (trefoil, 3_1). (**b**) Number of chain entanglements for linear polystyrene using $<S^2>_\theta = 7.9 \times 10^{-18} \times M_w$, where M_w is the molecular weight of the polymer, and $M_e = 18{,}000$ [26]

conducive to ring closure than a polymer with a much higher chain length. This simple analysis is in accord with the kinetic data determined from the pyrene work. In a good solvent for the polymer, the end-to-end distance should be greater than in a θ-solvent. Therefore, carrying out ring closure in a θ-solvent should result in a greater fraction of monocyclics (i.e., where the chain length of the cyclic equals that of the linear starting polymer). However, there is a further complication from the possibility of knot formation upon ring closure. Knots result in the contamination of pure cyclics and can influence the properties. A knot is formed when the starting linear polymer has three or more entanglements arranged as under-over-under or the reverse (see Fig. 3a, which represents the smallest configuration for a knot; denoted as a trefoil, 3_1). Roovers and Toporowski pointed out that the probability of a knot for polystyrene with a molecular weight of 1×10^6 was only 15% in a θ-solvent [26].

The authors use the following equation to calculate the number of chain entanglements in a linear chain.

$$\#\text{of entanglements} = \frac{{M_\mathrm{w}}^2}{N_\mathrm{A} < S^2 >_\theta^{3/2} M_\mathrm{e} \rho} \tag{3}$$

where M_w is the molecular weight of the polymer, N_A is Avogadro's number, M_e is the molecular weight between entanglements, ρ is the density of the polymer, and $<S^2>_\theta$ is the root mean square radius of gyration in a θ-solvent. Using Eq. (3), the number of entanglements increased with molecular weight as shown in Fig. 3b. It can clearly be seen that at molecular weights below ~50,000, the number of entanglements is less than 3. This demonstrates that knots will be absent below this molecular weight. At molecular weights above 50,000, the probability for a knot increases with molecular weight. This probability will be significantly reduced when the polymer is in a good solvent. In the case of ring closure, most cyclizations are carried out using molecular weights below 20,000 and, as such, knots will be highly unfavorable. The potential for catenane formation is also possible but dependent upon the weight fraction of polymer. The polymers must be in close contact and well above the critical overlap concentration, c^*. As will be described in the following Sect. 1.2, higher weight polymer fractions further result in greater multiblock formation. Therefore, the synthetic strategy plays an important role in determining the purity and types of cyclic topologies. For cyclic polymers to find applications, they must have the capability of being made in high amounts and with predicted cyclic structure.

1.2 Model for Ring Closure

In any reaction where the endgroups can react with each other, cyclization is always possible. This was recognized in polycondensation or step-growth polymerizations, in which multiblock and cyclic formation are competing reactions [27–30]. It was further realized that, in principle and assuming 100% chain-end functionality, that the consumption of all endgroups to covalent bonds would produce polymers that are all cyclic (i.e., 100% cyclic), with the distribution skewed to the low molecular weights. Obviously, the time to reach 100% chain-end consumption would be extremely long due to extremely slow diffusion at high conversion. This led researchers to explore the possibility of making monocyclic polymers and to find the conditions to achieve this with minimal multiblock impurities.

To obtain monocyclic polymers, one must overcome the competing step-growth reaction to form multiblocks (Scheme 1b), in which step-growth will dominate the kinetics over cyclization with increasing molecular weight. As discussed above, cyclization depends on the end-to-end distance between the two chain ends [30]. The chain ends have to diffuse within a capture volume (k_{c1}) to allow the chain-end functionalities to undergo a chemically controlled reaction (with rate coefficient k_2) to form a covalent bond (Scheme 1a) [30]. If a chemical reaction does not occur, then the chains can diffuse away from each other with rate

coefficient k_{-1}. This kinetic scheme is similar to that for an "encounter-pair" model, and should $k_{-1} >> k_2$ then cyclization is controlled by its equilibrium kinetics. This allows us to use the well-known thermodynamic Jacobson–Stockmayer (J–S) equation [30] to determine the probability of cyclization at a given polymer molecular weight. The J–S equation is based on statistical mechanics and thus requires large ensembles to produce accurate outcomes. This limits the utility of the J–S equation at low molecular weights, where most ring-closure cyclic reactions are carried out. The kinetic empirical diffusion relationship developed by Monteiro and coworkers provides accurate predictions at such molecular weights [21].

1.2.1 Jacobson–Stockmayer Equation [30]

The relative probabilities from Scheme 1 follow the classic case II type condensation and are given by the following equations:

$$P_c = \left(\frac{3}{2\pi}\right)^{3/2} \frac{v_s}{\langle r^2 \rangle^{3/2}} \tag{4}$$

$$P_L = 2N\frac{v_s}{V} = \frac{2N_A c}{M_w} v_s \tag{5}$$

where v_s is the capture volume, P_c is the probability that the two ends of the same chain are within the capture volume, P_L is the probability that chain ends from different chains are within the capture volume, $<r^2>$ is the mean square end-to-end distance of the chain, N is the total number of polymer molecules in total volume V, N_A is Avogadro's number, M_w is the molecular weight of the polymer, and c is the concentration of polymer (g mL^{-1}). The ratio between monocyclic and other condensed species is given by [31]:

$$\frac{P_c}{P_L} = \left(\frac{3}{2\pi\langle r^2 \rangle}\right)^{3/2} \frac{2,000}{N_A[P]} = \frac{k_c}{k_1[P]} \tag{6}$$

such that:

$$\frac{k_c}{k_1} = \left(\frac{3}{2\pi\langle r^2 \rangle}\right)^{3/2} \frac{2,000}{N_A} \tag{7}$$

and therefore the theoretical percentage of monocyclic is given by:

$$\%\ \text{cyclic} = \frac{P_c}{P_c + P_L} \times 100 \tag{8}$$

where $[P]$ is the concentration (mol L^{-1}) of starting linear polymer in solution.

For polystyrene, Roovers [32] found that in a good solvent $<r^2> = 6.88 \times (1.66 \times 10^{-18} \times M_w^{-1.17})$. The J–S equation was further supported from an empirical relation based on only diffusion coefficients [21].

1.2.2 Empirical Kinetic Relationship [21]

For the kinetic relationship, we calculated the molecular weight dependence empirically from diffusion-controlled rate coefficient data for two ends of the same chain to meet, or ends from different chains to diffuse to each other. As described above, Winnik and coworkers [33, 34] used pyrene fluorescence to determine k_c over a molecular weight range from 3,900 to 27,000, with the relationship $\log k_c = 11.97 - 1.52 \log(M_w)$. The rate coefficient, k_l, is equal to the chain-length dependent termination in free-radical bimolecular termination between two chains of equal length i, represented by the rate coefficient $k_t^{i,i}$, since k_2 for this termination reaction is much greater than k_{-1} (Scheme 1b). We have previously found in dilute solutions (i.e., below c^*) the following empirical relationship [35, 36]:

$$k_t^{i,i} = k_t^0 \cdot i_{SL}^{(\alpha_L - \alpha_S)} \cdot i^{-\alpha_L} \tag{9}$$

where for polystyrene [36], $\log k_t^0 = 8.7$, $\alpha_S = 0.53$, $i_{SL} = 15$, and $\alpha_L = 0.15$. Combining the Winnik relationship for cyclics and our data for termination, we derived the following empirical relationship:

$$\frac{k_l}{k_c} = \frac{k_t^0 \cdot i_{SL}^{(\alpha_L - \alpha_S)} \cdot i^{-\alpha_L}}{10^{(11.97 - 1.52 \log M_w)}} \tag{10}$$

This empirical relationship gave a slightly greater percentage of monocyclic than that predicted from the J–S equations. At the lowest molecular weight, the empirical relationship was in close agreement with experiment, most probably due to the fact that the J–S equations do not hold for chain lengths where Gaussian chain statistics do not apply. This occurs for chain lengths <15 due to short-range interactions and steric effects. Our empirical relationship shows slightly lower k_l/k_c values than those of Jacobson and Stockmayer in the molecular weight range from 3,000 to 22,000.

2 Synthetic Methodologies for Ring-Closure Reactions

Anionic and cationic polymerizations were some of the original techniques used for ring closure due to control over the molecular weight, chain-end functionality, and narrow molecular weight distribution (MWD). However, ionic polymerization requires strict experimental conditions (usually under anhydrous conditions). The

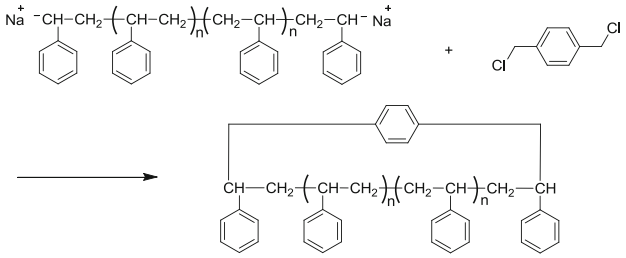

Scheme 3 Synthesis of cyclic PSTY by the combination of living anionic polymerization and bimolecular coupling reaction between polystyryl anions and (1,4-dichloromethyl)benzene

advent of "living" radical polymerization (LRP) provides a far more user-friendly method for making linear polymers with high chain-end functionality and narrow MWDs. Typically, LRP comprises a number of techniques, including copper-catalyzed polymerization (ATRP [37, 38] and SET-LRP [39]) and reversible addition-fragmentation chain transfer (RAFT) polymerization [40, 41]. Combining LRP with many highly efficient organic coupling reactions such as copper-catalyzed alkyne–azide cycloaddition "click" reaction (CuAAC) [42], Diels–Alder addition reaction [43], thiol-ene addition reaction [44], and Glaser coupling [45], polymer chemists can now prepare a range of cyclic polymers with different chemical compositions and topological structures.

In the next section, we will first discuss synthesis of the linear polymer precursors with homodifunctional or heterodifunctional groups, and second, we will discuss the synthesis of cyclic polymers via a ring-closure reaction.

2.1 Ring Closure Through Homodifunctional Linear Polymers

2.1.1 Ring Closure Through Bimolecular Coupling Between Homodifunctional Linear Polymers with Difunctional Small Molecules (A_2 + B_2)

Synthesis of Linear Polymer Precursors by Living Anionic Polymerization

Anionic polymerization first provided an approach for synthesizing polymers with controlled molecular weights and low polydispersity indexes (PDIs) [46]. Geisert and Höcker [47] reported their pioneering work on the preparation of cyclic polystyrene (PSTY) by coupling living dianionic linear PSTY with an electrophile (α, α′-dichloro-*p*-xylene), as shown in Scheme 3. Molecular weights of the cyclic PSTY ranged from 3,000 to 25,000, and the intrinsic viscosity difference between linear and cyclic PSTY was then examined.

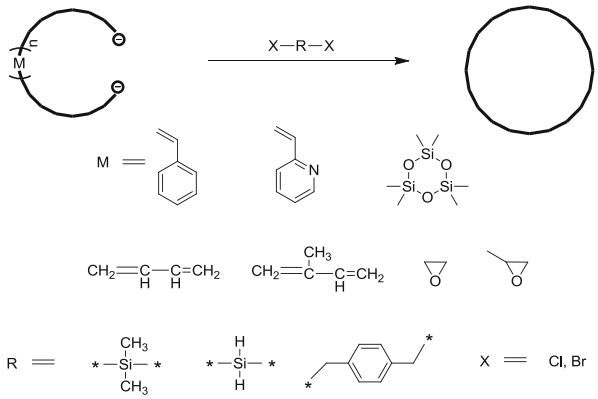

Scheme 4 Other cyclic polymers synthesized by the combination of living anionic polymerization and bimolecular coupling reaction with dihalide

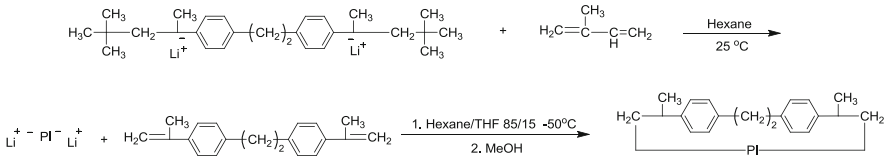

Scheme 5 Synthesis of cyclic PI by the combination of living anionic polymerization and bimolecular coupling reaction with BIPPE

Other attempts made by Rempp et al. [48, 49] and Vollmert et al. [50] used a similar method but changed the solvent conditions using, for example, a mixture of benzene and tetrahydrofuran (THF). This allowed good coupling for the synthesis of cyclic polymers with different building blocks such as poly(2-vinyl pyridine), polybutadiene, poly(dimethylsiloxane), poly(propylene oxide), poly(ethylene oxide), and a variety of other polymers (Scheme 4).

Apart from one-step coupling reactions to cyclize the linear dianionic polymers, a ring-closure reaction through an intermediate chain end transformed from living dianionic polymer was also reported. Cyclic polyisoprene (PI) was synthesized by capping living PI dilithium carbanions with 1,2-bis(4-isopropenylphenyl)ethane (BIPPE) in a binary mixture of hexane and THF at −50°C, as shown in Scheme 5. The resulting cyclic PI dianion was then quenched with methanol to give cyclic PI [51].

Leppoittevin et al. [52] used a similar approach to synthesize cyclic PSTY by capping the living dianionic PSTY with 1,3-bis(1-phenylethylenyl)benzene (MDDPE), followed by deactivation of the dianions with methanol (Scheme 6). The polystyryl dianions were prepared by anionic polymerization of styrene in benzene with a trace of THF to accelerate the initiation step. The polymer was then purified by high performance liquid chromatography (HPLC).

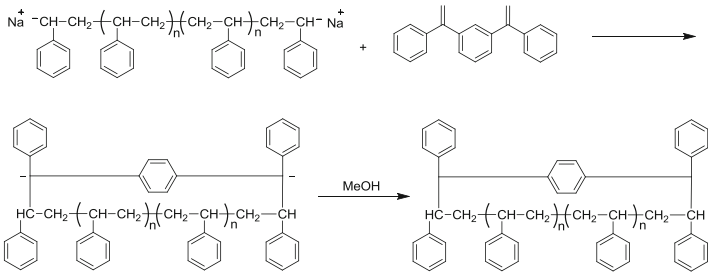

Scheme 6 Synthesis of cyclic polymers by the combination of living anionic polymerization and bimolecular electrophilic coupling reaction between the polystyryl dianions with MDDPE

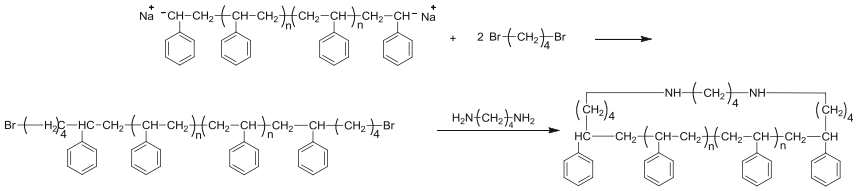

Scheme 7 Synthesis of cyclic PSTY by the reaction between dibromide and diamine

Alternatively, cyclic PSTY was also synthesized through a two-step reaction process reported by Ishizu et al. [53]. First, the living dianionic PSTY was capped with an excess of 1,4-dibromobutane to give an α,ω-dibromo PSTY, and then was reacted with tetrametylenediamine as illustrated in Scheme 7. It is notable that the reaction between bromide PSTY with diamine was carried out in a water/toluene biphase system. The lower concentration of reactants at the interface favored the cyclization reaction, giving a yield of more than 90%.

Synthesis of Linear Polymer Precursor by Living Cationic Polymerization

Although living cationic polymerization is not as widely used as living anionic polymerization, it has been reported for the synthesis of cyclic polymer. Tezuka and coworkers [54] first reported the elegant electrostatic self-assembly and covalent fixation (ESA-CF) process using polymers made by living cationic polymerization. The only monomer they used in cationic polymerization was THF. The linear or nonlinear telechelic poly(THF) with living cyclic ammonium salt cationic groups was terminated by plurifunctional carboxylate counteranions, as shown in Scheme 8. Monocyclic and other unique and complex cyclic architectures were produced (Fig. 4) [55].

Tezuka et al. [56] further extended ESA-CF to other polymer systems. For instance, α,ω-dihydroxyl poly(ethylene oxide) (PEO) was first converted to α,ω-di (*p*-toluenesulfonate)-PEO. The latter was converted to an ammonium with quinuclidine, followed by an ion-exchange reaction with tetra-*n*-butylammonium

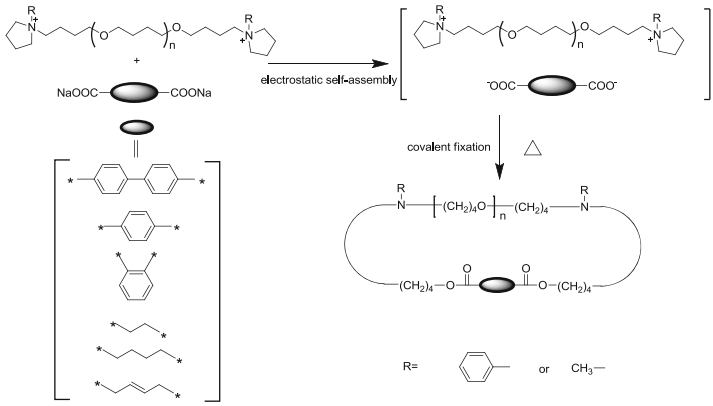

Scheme 8 Synthesis of cyclic poly(THF) by an electrostatic self-assembly and covalent fixation (ESA-CF) process

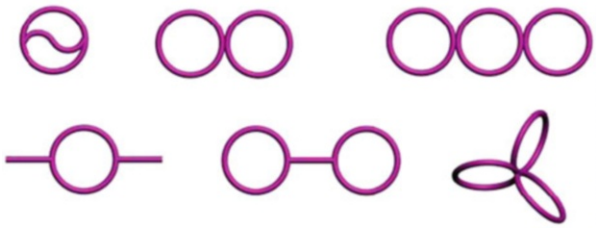

Fig. 4 Various cyclic polymers synthesized by ESA-CF

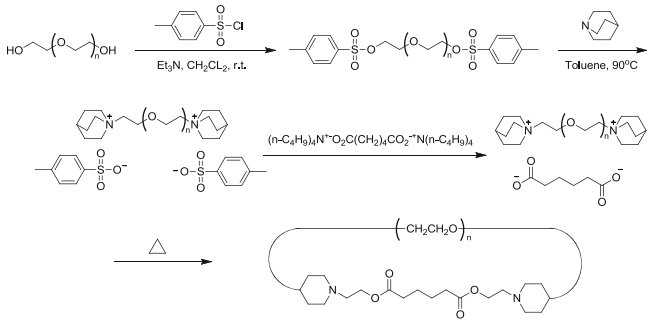

Scheme 9 Synthesis of cyclic poly(ethylene oxide) by ESA-CF

adipate. The yielded PEO with two ion pairs was finally fixed at 130°C to form the stable cyclic PEO, as shown in Scheme 9. The polymer was purified by preparative size-exclusion chromatography (SEC) and confirmed by SEC and MALDI-TOF MS.

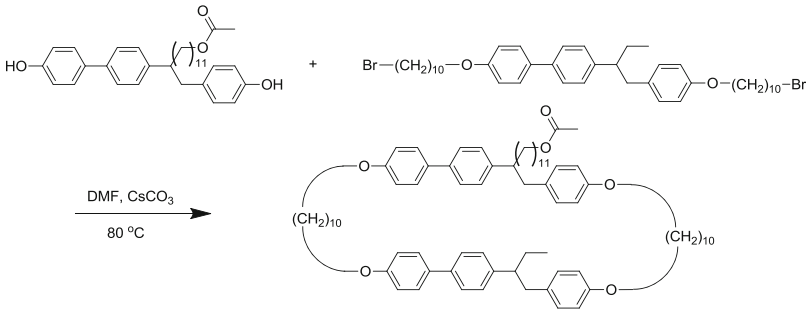

Scheme 10 Synthesis of cyclic oligomer by etherification between bromide and phenol groups

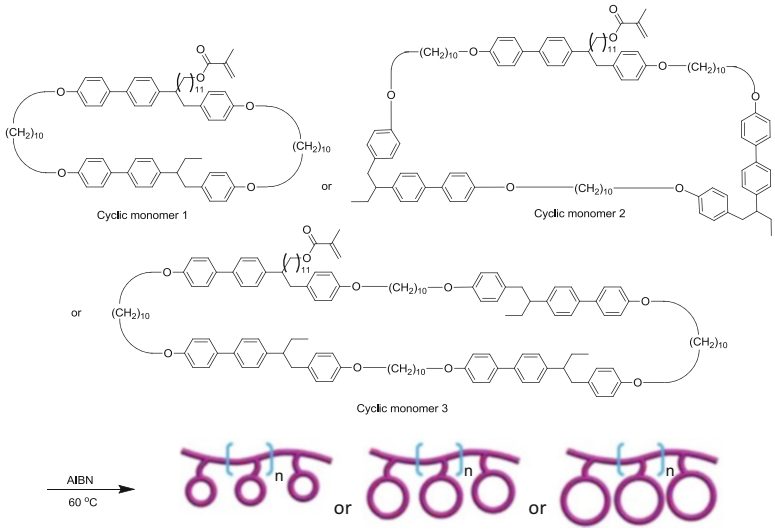

Scheme 11 Synthesis of grafted polymers with cyclic oligomer pendants showing liquid crystalline property

Synthesis of Liquid Crystal Cyclic Oligomer and More Complex Cyclic Architectures

Two decades ago, Percec and coworkers [57–61] synthesized a range of cyclic oligomers with liquid crystal properties. Under dilute conditions and using base catalysis, cyclic oligomers with different units of liquid crystal groups and different length of spacers were obtained through etherification between phenol and bromide (Scheme 10). They further introduced an acrylate to those cyclic oligomers to make cyclic oligomonomers, and then polymerized them to produce grafted polymers with cyclic pendants (Scheme 11). Alternatively, two phenol groups were introduced to the cyclic oligomers, followed by further etherification to produce cyclic spiro-polymer structures (Scheme 12).

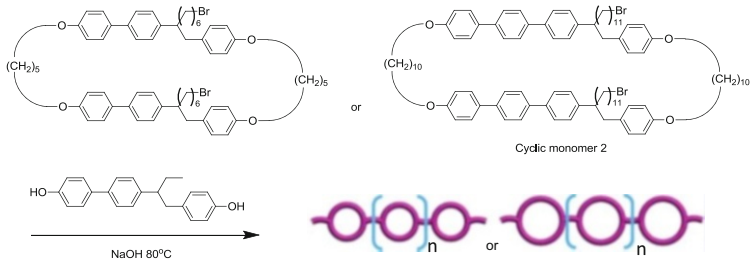

Scheme 12 Synthesis of spiro-polymers from cyclic oligomer blocks showing liquid crystalline property

2.1.2 Ring Closure Through Bimolecular Coupling Between Homodifunctional Linear Polymers with Small Molecules (A_2+B)

In contrast to the difunctional bimolecular coupling reaction $A_2 + B_2$, a linear difunctional polymer precursor (A_2) can also be coupled with a small molecule that does not show obvious difunctional groups (B). However, once one of the telechelic chain ends of the linear polymers reacts with the small molecules, the resulting group can further react with another chain end to form a cyclic polymer. Here we denoted the reaction as $A_2 + B$.

Early work on the synthesis of cyclic polymers through this method was reported by Booth and Price et al. [62]. They synthesized the cyclic polyether from α,ω-dihydroxyl PEO. The dihydroxyl PEO was dissolved in dichloromethane (DCM) into which the powdery KOH was added. One of the hydroxyl groups first reacted with DCM to form the chloromethyl ether. The latter has high reactivity with another hydroxyl group under base conditions. The cyclic PEO was obtained with an acetal linkage, as shown in Scheme 13.

Yu et al. [63] described the same method for preparation of cyclic poly(propylene oxide) (PPO) with an acetal linkage, and achieved 60–75% conversion for a linear PPO of 2,000 molecular weight. Jia et al. [64] used the same method to synthesize cyclic poly(ethylene oxide-*co*-4-glycidyloxy-2,2,6,6-tetramethylpiperydine-1-oxyl) with up to 85% conversion (Scheme 14). The purification of this product was conducted by ultrafiltration using a polymer membrane.

Recently, Tillman and coworkers [65] reported an intramolecular radical trap-assisted atom transfer radical coupling (IRT-ATRC) as shown in Scheme 15. The α,ω-dibromo functional PSTY was first synthesized by ATRP. The bromo chain end was first activated by CuBr/Me_6TREN complex to yield a radical that simultaneously reacted with 2-methyl-2-nitrosopropane to form a nitroxide radical. The another bromo chain end was also activated to a radical and rapidly trapped by nitroxide radical through the well-known ATRC process to form cyclic PSTY. However, in this case, the hydrodynamic volume changes ($\langle G \rangle = M_{pc}/M_{pl}$) from linear to cyclic were mostly greater than 0.85, which is much higher than that of cyclic PSTY made from anionic polymerization (i.e., 0.78). Although the authors ascribed the reason to

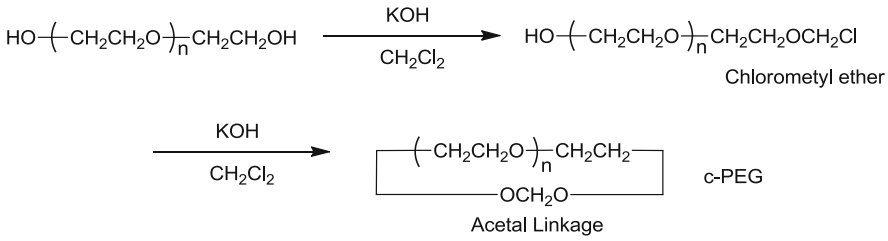

Scheme 13 Synthesis of cyclic PEO through the formation of an acetal linkage with alkaline as catalyst

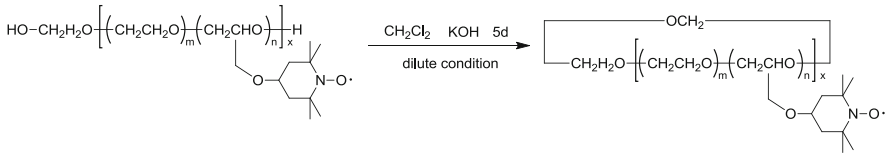

Scheme 14 Synthesis of cyclic poly(ethylene oxide-*co*-4-glycidyloxy-2,2,6,6-tetramethylpiperydine-1-oxyl) through the formation of an acetal linkage with alkaline as catalyst

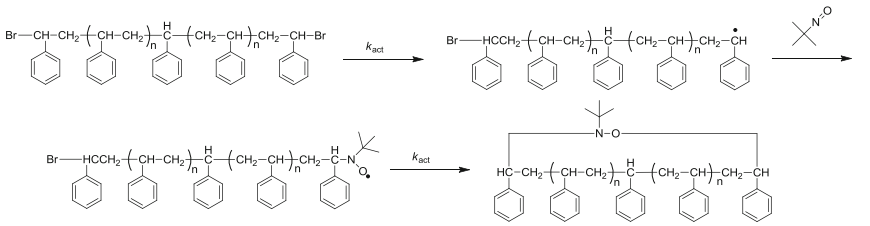

Scheme 15 Synthesis of cyclic PSTY through radical trap-assisted atom transfer radical coupling (RTA-ATRC)

the addition of the *tert*-butyl nitroxide linkage, the purity of the cyclic product was suspicious and might also have contributed to the higher $<G>$ value.

2.1.3 Ring Closure Through Intramolecular Coupling of Homodifunctional Linear Polymers (A_2).

Linear polymers can form cyclic polymers through the coupling reaction between their two homofunctional chain ends using external catalysts. For instance, a dihydroxyl oligo(ethylene glycol) was cyclized to form macrocyclic crown ether through the traditional Williamson etherification reaction. By treating with *p*-toluenesulfonyl chloride (tosyl chloride) in the presence of powdery KOH, one of hydroxyl groups was converted to tosylate. This monotosylate was further reacted with another hydroxyl chain end to form the crown ether. Booth and

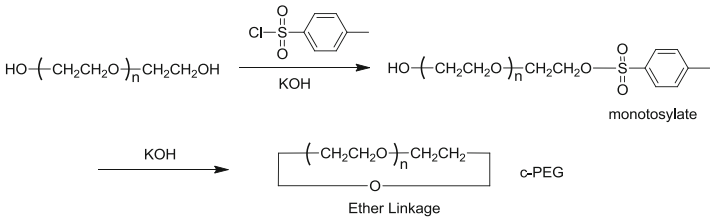

Scheme 16 Synthesis of cyclic PEO through the formation of an ether linkage

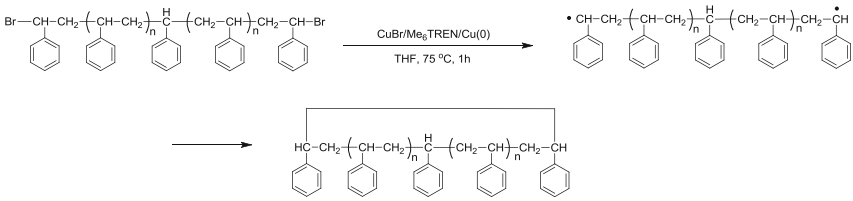

Scheme 17 Synthesis of cyclic PSTY through atom transfer radical coupling (ATRC) reaction

Price et al. [66] developed this method to prepare cyclic PEO as shown in Scheme 16. However, their attempts to prepare high molecular weight cyclic PEO by this method were unsuccessful.

Pang et al. [67] modified the reaction conditions by adding a poor solvent, heptane, for PEG to the reaction solvent THF. They were able to synthesize the cyclic poly(ethylene oxide-*co*-ethoxyethyl glycidyl ether) [poly(EO-*co*-EEGE)] with molecular weights up to 12,000. The addition of heptane improved the ring-closure reaction efficiency by reducing the end-to-end distance. They produced pure cyclic by binding linear unreacted or multiblock polymer chains with α-cyclodextrin.

ATRC usually appears as a side reaction during the ATRP polymerization. For instance, intermolecular ATRC produces high molecular weight multiblock copolymers as side products during the polymerization of styrene using a difunctional initiator by ATRP. However, if the reaction is carried out under dilute conditions, intramolecular radical coupling gives cyclic products. Tillman and coworkers [68] reported a synthetic procedure for making cyclic PSTY using ATRC. Linear dibromo-functional PSTY was activated to a diradical intermediate to form cyclic PSTY through intermolecular radical coupling (ATRC) (Scheme 17).

Cyclization from homodifuctional polymers was also applied for synthesis of cyclic polymers from RAFT-generated polymer precursor. Monteiro and coworkers [69] described the process for making cyclic PSTY from linear PSTY diRAFT. Aminolysis of the two RAFT chain ends produced the active thiol groups that, through a disulfide linkage, produced cyclic PSTY under dilute conditions (Scheme 18). However, if the concentration was relatively high, multiblock linear polymer was obtained as main product. Because the cyclic product was formed

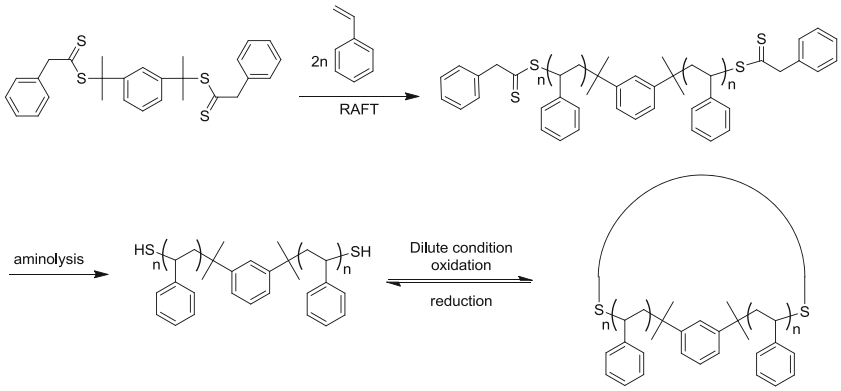

Scheme 18 Synthesis of cyclic PSTY by the combination of reversible addition fragmentation chain transfer (RAFT) polymerization and the formation of a disulfide linkage

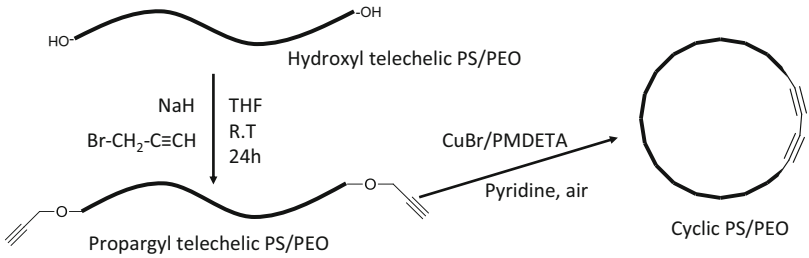

Scheme 19 Synthesis of cyclic PEO and cyclic PSTY by the combination of living anionic polymerization and Glaser coupling

through a disulfide linkage, the cyclic PSTY was easily cleaved by using a reducing agent such as zinc to give back the starting linear product.

Recently, Huang and coworkers reported [70] a Glaser coupling reaction for preparation of the cyclic polymers. The living PEO and PSTY dianion was terminated to form a hydroxyl telechelic PEO and PSTY. Then, the hydroxyl groups were converted to alkyne functional groups by the reaction with propargyl bromide. Under dilute conditions, the alkyne groups were activated by CuBr and PMDETA to form a 1,3-diyne linkage through a Glaser–Hay coupling reaction, thus producing the cyclic PEO and cyclic PSTY (Scheme 19).

Cyclic polymers were also prepared by ring-closure metathesis from α,ω-diallyl linear precursors. Linear polymer precursors can be synthesized by either ring-opening polymerization or living cationic polymerization. Hayashi et al. [71] used ATRP to synthesize α,ω-dibromo poly(methyl acrylate) (PMA) and further functionalized the polymer bromo chain end to diallyl groups. The cyclization was then carried out through the ring-closing metathesis (RCM) reaction in dilute DCM solution using the Grubbs Ru catalyst (Scheme 20).

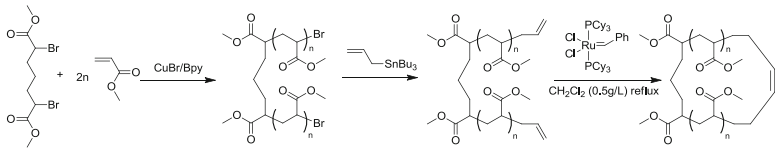

Scheme 20 Synthesis of cyclic poly(MA) by the combination of ATRP and the ring-closing metathesis (RCM) reaction

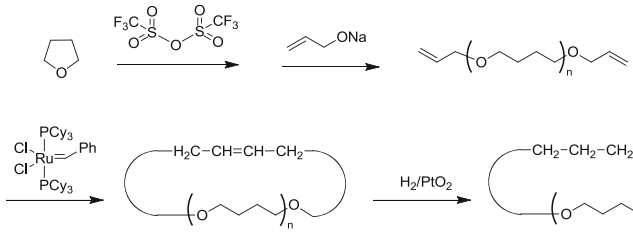

Scheme 21 Synthesis of cyclic poly(THF) by the combination of living cationic polymerization and the ring-closing metathesis (RCM) reaction

Tezuka et al. [72] reported a cyclic poly(THF) by the combination of living cationic polymerization and RCM reaction (Scheme 21). A series of linear poly (THF)s were synthesized with molecular weights ranging from 4,400 to 8,600 and polydispersity indexes of 1.08–1.17. The dianionic poly(THF) was terminated by sodium allyloxide, and the ring-closing metathesis reaction of the allyl-terminated poly(THF)s was then catalyzed using the Grubbs catalyst. The authors further hydrogenated the double bond with the Adam's catalyst (H_2/PtO_2). The crystallization behavior of cyclic poly(THF)s was compared with their linear counterparts, and it was found that the melting temperature (T_m) of the cyclic poly(THF) was about 5°C lower than that of the linear one. This result reflected the different entropic contributions during the crystallizing or melting process.

Living anionic polymerization was also used to make the linear polymer precursors for the preparation of cyclic polymer through RCM. Quirk and coworkers [73] reported the synthesis of cyclic PSTY through the combination of living anionic polymerization and RCM (Scheme 22). The linear PSTY precursors with molecular weights ranging from 2,800 to 38,000 were successfully synthesized using 5-lithio-1-pentene as initiator. The α-(4-pentenyl)poly(styryl)lithium was terminated with *p*-vinylbenzyl chloride. The RCM of linear PSTY was carried out in DCM with Grubbs catalyst as described in the previous example. It was found that for a high molecular weight (i.e., 17,000 Da) of PSTY, the cyclization efficiency was low even in highly dilute solution (i.e., 4.0×10^{-5} mol/L for 17,000 Da versus 1.2×10^{-4} mol/L for 2,000 Da). Further studies showed that the addition of cyclohexane significantly increased the cyclization efficiency and decreased the dimerization. Schulz et al. [74] utilized living anionic polymerization

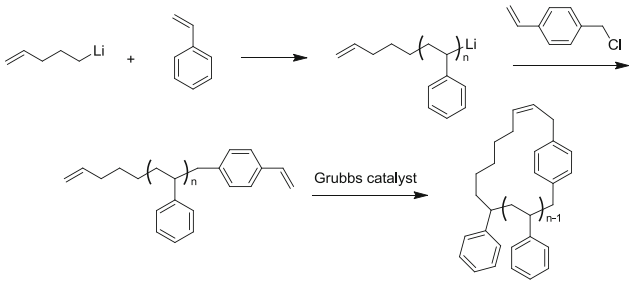

Scheme 22 Synthesis of cyclic PSTY by the combination of living cationic polymerization and the ring-closing metathesis (RCM) reaction

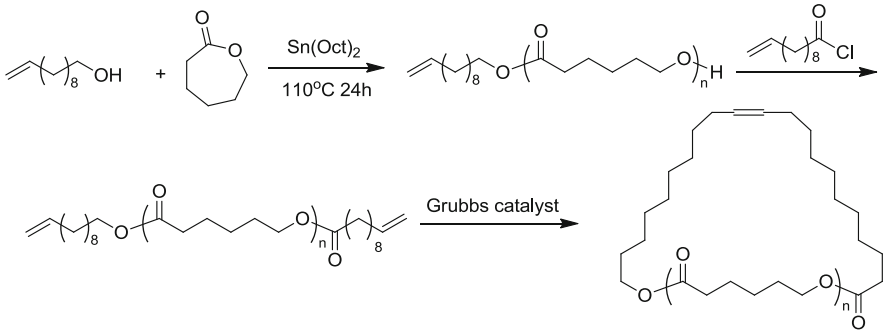

Scheme 23 Synthesis of cyclic poly(ε-CL) by the combination of ring-opening polymerization and the ring-closing metathesis (RCM) reaction

to prepare vinyl functional poly(isobutylene)s and then cyclized them via RCM reaction by using the same Grubbs catalyst.

By using RCM with the Grubbs catalyst, synthesis of cyclic poly(ε-caprolactone) [poly(ε-CL)] was reported by Xie et al. [75]. They used 10-undecen-1-ol as initiator to polymerize the ε-CL with $Sn(Oct)_2$ as catalyst. The hydroxyl chain end of the poly (ε-CL) was further functionalized by the reaction with undecylenic acid chloride to give a divinyl poly(ε-CL). The cyclization was carried out in a one-pot reaction at a polymer concentration of 5.0×10^{-4} mol/L; however, the efficiency of the cyclization was relatively low as their SEC traces showed a large amount of multiblock condensation by-products (Scheme 23).

Synthesis of cyclic polymers through ring-closure reactions of homofunctional linear precursors represents one of the earliest methodologies for the preparation of cyclic polymers through living ionic polymerization. This method not only allowed the preparation of linear polymers with narrow MWDs and accurate control over the molecular weight, but it also favored post-functionalization of the chain ends. However, living ionic polymerization requires stringent experimental conditions that include anhydrous conditions and low temperature and is only suitable for a small range of monomers.

2.2 Ring Closure Through Hetrodifunctional Linear Polymers

Linear polymers with two different functional groups on each end of the polymer chain are usually named α,ω-heterodifunctional polymers. Through the proper combination of the two functional chain ends, cyclic polymers can be made through the intramolecular coupling reaction. This methodology has been widely used to synthesize cyclic polymers with various chemical compositions and chain structures. The advantage of this method compared to the heterodifunctional bimolecular coupling is that there is no issue caused by inaccurate stoichiometries. Moreover, with the complimentary of "living" radical polymerization techniques, by using functional initiators and post-functionalization, these α,ω-heterodifunctional linear polymer precursors can now be made relatively easily. However, intermolecular coupling reactions are unavoidable and therefore highly dilute solution conditions are necessary.

Schappacher and Deffieux [93] first reported the cyclization from heterodifunctional linear polymers. The linear precursor was made from 2-chloroethyl vinyl ether (CEVE) by living cationic polymerization from a styryl vinyl ether with hydroiodic acid and $ZnCl_2$ as catalyst combination. By treating with $SnCl_4$, the iodo endgroup was converted to carbocation and coupled to the styrene chain end to form the cyclic polymer (Scheme 24). With the same strategy, they successfully synthesized a series of cyclic polymer derivatives based on the monomer CEVE.

Further extension of this technique used a similar cyclization reaction from polystyrene by living anionic polymerization [31]. In this case, an acetal functional anionic initiator was used to polymerize the styrene followed by capping with 1,1-diphenylethene and termination with *p*-chloromethylstyrene to introduce a styryl group to another end of the PSTY chain. Then, one of the ethyloxyl groups of the acetal chain end was converted to an iodo group, making the chain end similar to that after polymerization of CEVE using the iodo/$ZnCl_2$ combination. The cyclization reaction was then catalyzed by $SnCl_4$ as shown in Scheme 25.

Kubo and coworkers [76] reported synthesis of cyclic PSTY through living anionic polymerization followed by amidation reaction between the carboxylic acid and amine chain ends. In their work, ortho-ester initiator was applied to polymerize STY by living anionic polymerization. The living chain end was then terminated by 2,2,5,5-tetramethyl-1-(3-bromopropyl)-1-aza-2,5-disilacyclopentane, a protected amine bromo compound, to give a linear PSTY precursor with protected carboxylic acid and protected amine on each end. After deprotection by acid and base, the carboxylic acid and amine group were then released. This linear precursor was then cyclized via an amidation reaction catalyzed by 1-methyl-2-chloropyridinium iodide (Scheme 26). Through modification of initiator structures, the authors then successively reported the synthesis of cyclic poly(methyl methacrylate) (PMMA) and cyclic poly(*tert*-butyl acrylate) (P^tBA). The latter was further converted to cyclic poly(acrylic acid) and cyclic poly(potassium acrylate) [77].

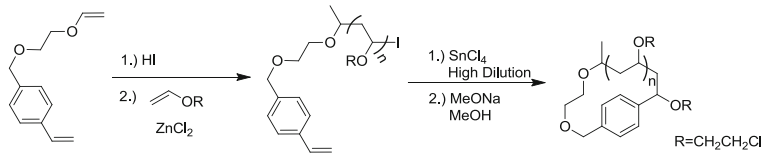

Scheme 24 Synthesis of cyclic poly(2-chloroethyl vinyl ether) through the coupling between iodo- and styryl- groups

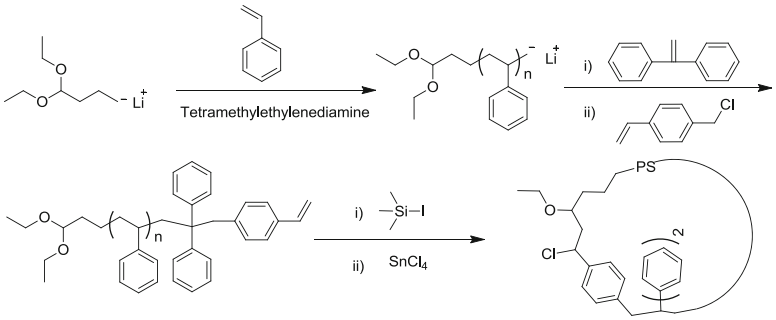

Scheme 25 Synthesis of cyclic PSTY through the coupling between iodo- and styryl- groups

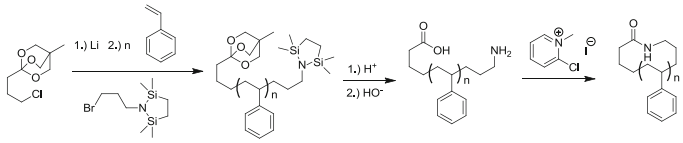

Scheme 26 Synthesis of cyclic PSTY through the amidation between carboxylic acid and amine groups

With the great development of "living" radical polymerization (LRP), one can now easily prepare linear polymers with different monomers and functional chain ends. The past decade has seen a boost in new synthetic strategies for cyclic polymers. Lepoittevin et al. [78] pioneered a new synthetic method for cyclization of PSTY by combining NMRP and esterification. 4-Hydroxyl-2,2,6,6-tetramethyl-pyperidine-1-oxy (HTEMPO) and 4,4′-azobis(4-cyanovaleric acid) were used in a combination, yielding linear PSTY with both hydroxyl and carboxylic acid chain ends. Subsequently, the cyclization reaction was catalyzed by 1-methyl-2-chloropyridinium iodide and triethylamine (Scheme 27). Because the esterification reaction is not highly efficient, especially when used in polymer systems, this method was only successful with low molecular weight PSTY (<4 kDa).

A fast and highly efficient chemical reaction could significantly advance the synthesis of cyclic polymers. One of the most prevalent, highly efficient and

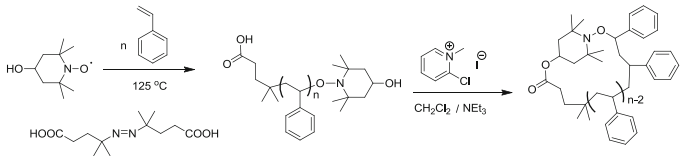

Scheme 27 Synthesis of cyclic PSTY through the esterification between carboxylic acid and hydroxyl groups

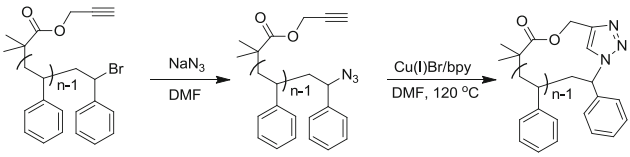

Scheme 28 Synthesis of cyclic PSTY through the combination of ATRP and CuAAC reactions in DMF

versatile techniques is the CuAAC "click" reaction. Combining this with LRP gives a new strategy for the preparation of cyclic polymers. The pioneer work was first reported by Laurent and Grayson in 2006 [79]. They utilized an alkyne functional bromo initiator to polymerize STY monomer by ATRP, followed by a simple azidation to convert the bromide chain end to an azide group. This α-alkyne-ω-azide heterofunctional linear PSTY was then cyclized in DMF with Cu(I)Br and 1,1-bipyridine as catalyst. Because the azidation reaction from bromide to azide is almost quantitative under mild conditions (i.e., in DMF at room temperature overnight), this report showed the great potential of the ATRP/CuAAC reaction combination in cyclization (Scheme 28).

Soon after this report, Liu and coworkers [80] reported the successful synthesis of cyclic poly(*N*-isopropylacrylamide) (PNIPAM) by the same procedure. This method was also successful in preparation of cyclic block copolymers.

Although great progress in the preparation of cyclic polymers by this method has been made, as shown in Laurent and Grayson's initial work, it worth pointing out that the cyclization was carried out under highly dilute conditions, severely restricting this technique for scale-up. For example, the reaction was carried out at high temperature (120°C), in a high boiling point polar solvent (DMF, b.p. = 153°C) and for a long reaction time (25 h) [79, 80]. All these could be a hurdle for broad application of this strategy in cyclic polymers. In 2010, Monteiro and coworkers [21] reported a modified method for cyclic PSTY by the ATRP/CuAAC reaction combination. With a similar linear precursor, they carried out the cyclization reaction in toluene at room temperature in a very short feeding time (~9 min) and post-feeding reaction time (~3 h) (Scheme 29).

The authors used the Jacobson–Stockmayer theory to predict the purity of cyclic product. The results showed that the reaction reached >95% purity at the concentration of 1.85×10^{-3} mol/L in less than 9 min at 25°C. After developing this

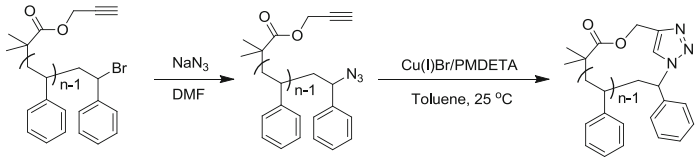

Scheme 29 Synthesis of cyclic PSTY through the combination of ATRP and CuAAC reactions in toluene

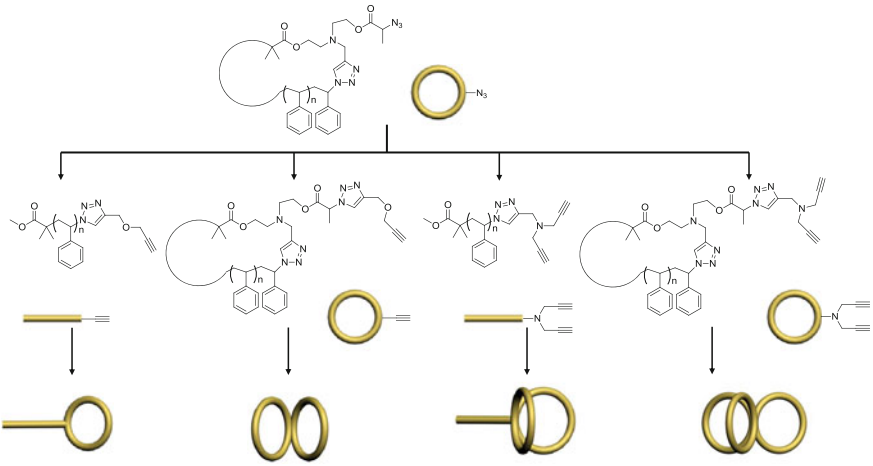

Scheme 30 Synthesis of various cyclic PSTY architectures through the combination of ATRP and CuAAC reactions

cyclization methodology, the same group reported a series of various cyclic architectures by using functional linear and cyclic PSTY as building blocks (Scheme 30).

Monteiro and coworkers also reported the synthesis of cyclic P^{t}BA and PMA by the combination of SET-LRP/CuAAC. A new bromo initiator containing an alkyne and a hydroxyl group was used to control the polymerization of *t*BA and MA via a Cu(0)-catalyzed SET-LRP. The SET process allowed the polymerization completion in less than 2 h at 25°C. It worth noting that there was no coupling reaction between alkyne groups (known as Glaser coupling) observed, which is usually seen in a doubling of the molecular weight. After azidation and cyclization, the hydroxyl group of these monocyclic polymers was readily converted to other functional groups (Scheme 31). The authors also used these monocyclic polymers to build μ-ABC mikto-arm star polymers by the combination of single electron transfer-nitroxide radical coupling and CuAAC (Scheme 32) [81].

As the CuAAC click reaction is fast, highly efficient, orthogonal and highly tolerant to the reaction media, it has also been combined with other living polymerization techniques to produce cyclic polymers of other chemical composition.

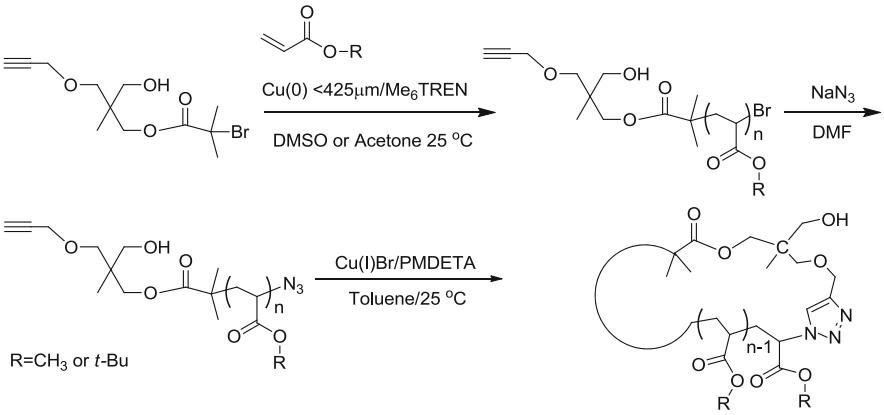

Scheme 31 Synthesis of cyclic P^{t}BA and PMA through the combination of SET-LRP and CuAAC reactions

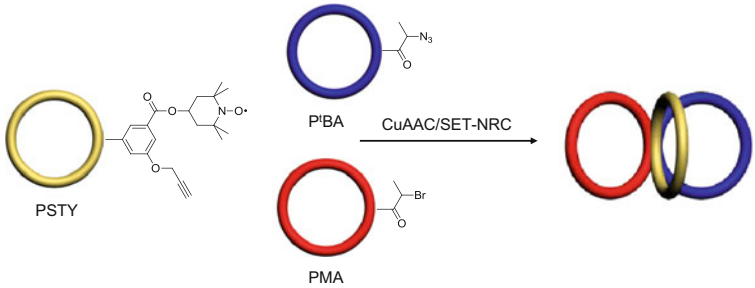

Scheme 32 Synthesis of μ-ABC tricyclic which contained PSTY, P^{t}BA and PMA through the combination of SET-NRC and CuAAC reactions

Winnik and coworkers [11] utilized an azide functional RAFT agent to synthesize azide functional linear PNIPAM followed by a thiol-ene Michael addition reaction with propargyl acrylate, producing α-alkyne-ω-azide PNIPAM. Consequently, the cyclization reaction by CuAAC was achieved in water with $CuSO_4$ and ascorbic acid as the catalyst (Scheme 33). Further, the solution properties showed that the cyclic PNIPAM had higher phase transition temperature due to the endless chain structure of the cyclic compared to the linear counterpart with the same molecular weight.

Monteiro and coworkers [82] reported a RAFT polymerization and CuAAC click reaction combination for the synthesis of functional monocyclic PSTY. An alkyne functional RAFT agent was used to control the polymerization of styrene. The RAFT moiety was converted to an epoxy group by a cascade aminolysis and Michael addition reaction with hexylamine and glycidyl methacrylate, respectively. The epoxy chain end was then converted in one step through the ring-opening reaction with NaN_3 to form an azido and a secondary hydroxyl group. The cyclization was carried out in toluene with CuBr and PMDETA as catalyst at 25°C

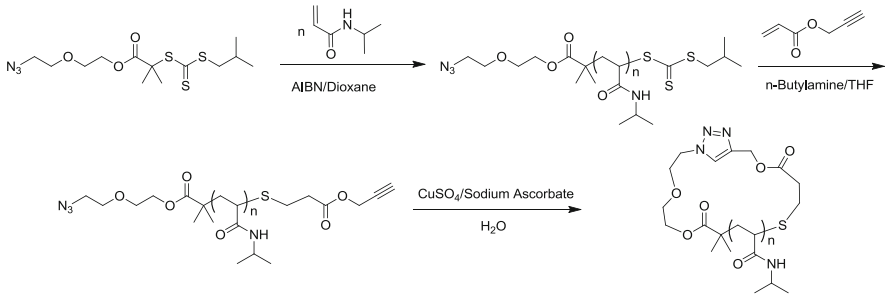

Scheme 33 Synthesis of cyclic PNIPAM through the combination of RAFT and CuAAC reactions

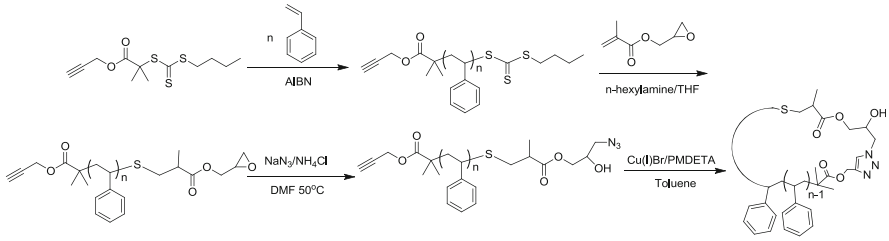

Scheme 34 Synthesis of cyclic PSTY through the combination of RAFT and CuAAC reactions

following the same procedure (Scheme 34). This method allowed the preparation of monocyclic polymer with a hydroxyl group, which could be readily transformed to other functional groups and hence more complex cyclic architectures [82].

Braslau and coworkers [83] synthesized cyclic PSTY through the combination of nitroxide-mediated radical polymerization (NMRP) and CuAAC click reaction. The synthesis procedure was relatively complex compared with other strategies. 1-[4-(Chloromethyl)phenyl]ethyl alkoxyamine was used to mediate the styrene polymerization, followed by successive azidation and oxidative cleavage with ammonium cerium(IV) nitrite in the presence of propargyl alcohol. The azide and alkyne groups were then introduced to each end of the polymer. Finally, the cyclization reaction was carried out in toluene with CuBr and PMDETA as catalyst at 100°C (Scheme 35). The cyclization results showed about 64% click product, as derived from Gaussian curve fitting.

Hadjichristidis and coworkers [84] prepared cyclic diblock copolymer PSTY-*b*-PI by combining living anionic polymerization and CuAAC click chemistry. An α-acetylene-ω-azido-PS-*b*-PI was synthesized by sequential anionic polymerization of styrene and isoprene with 5-triethylsilyl-4-pentynyllithium as initiator, followed by termination reactions with 1,4-dibromobutane and azidation reaction with sodium azide. After deprotection of the acetylene group, the linear α-acetylene-ω-azido-PS-*b*-PI was then cyclized via CuAAC click reaction in the presence of CuBr and PMDETA to afford cyclic block copolymer in dilute solution

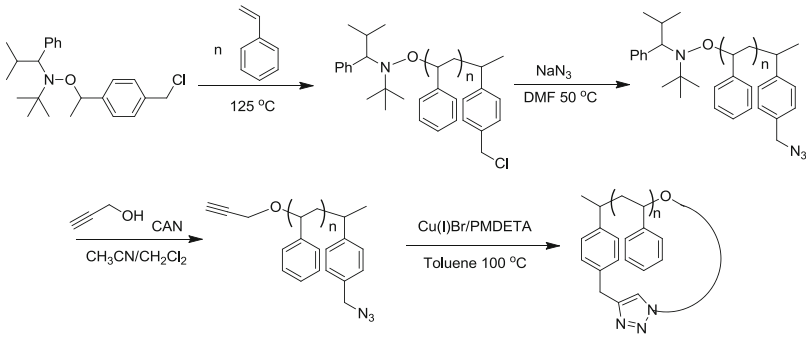

Scheme 35 Synthesis of cyclic PSTY through the combination of NMRP and CuAAC reactions

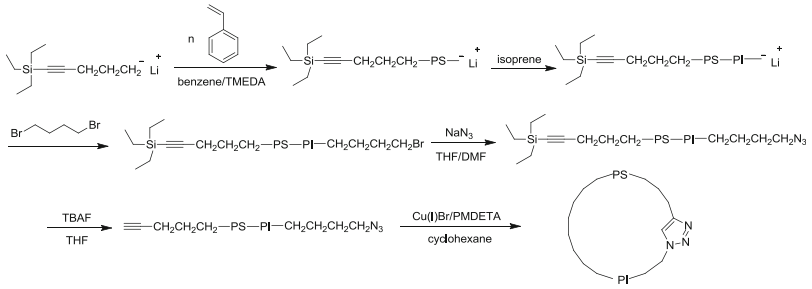

Scheme 36 Synthesis of cyclic PSTY-*b*-PI through the combination of living anionic polymerization and CuAAC reactions

(lower than the equilibrium concentration, $<6 \times 10^{-5}$ g/mL), whereas in concentrated solution (5.3×10^{-2} g/mL) multiblock copolymers were obtained (Scheme 36).

Very recently, Monteiro and Jia [85] reported a thiol-ene reaction for the preparation of cyclic polymer with inherent alkyne functionality from RAFT polymerization. An alkyne-hydroxyl-RAFT agent, through post-polymerization functionalization, was used to introduce an acrylate to the polymer via the reaction of the hydroxyl group with acryloyl chloride. Through the successive aminolysis of the RAFT and thiol-ene reaction between the acrylate group and thiol group, which was generated from aminolysis under hexylamine, alkyne functional monocyclic PSTY, PDMA, PNIPAM, and P^{t}BA were obtained (Scheme 37).

Kakuchi and coworkers [86] reported the synthesis of cyclic poly(δ-valerolactone) (PVL) by combining organocatalytic living ring-opening polymerization and the click reaction. They used 6-azide-1-hexanol as the initiator and 1,8-diazabicyclo-[5.4.0] undec-7-ene (DBU) and 1-[3,5-bis(trifluoromethyl)phenyl]-3-cyclohexylthiourea (BCT) as an organocatalytic combination to produce the azide and hydroxyl groups at each ends. Post-functionalization of the hydroxyl group with 5-hexynoyl chloride afforded the α-alkyne-ω-azide PVL. Click cyclization was carried out in DMF with Cu (I)Br and 2,2'-bipyridine (bpy) as catalyst at 120°C (Scheme 38).

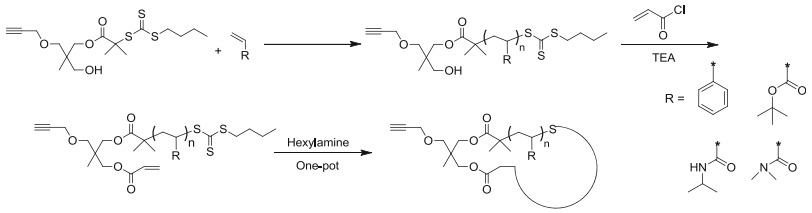

Scheme 37 Synthesis of cyclic PSTY, P^{t}BA, PDMA, and PNIPAM through the combination of RAFT polymerization and thiol-ene click reactions

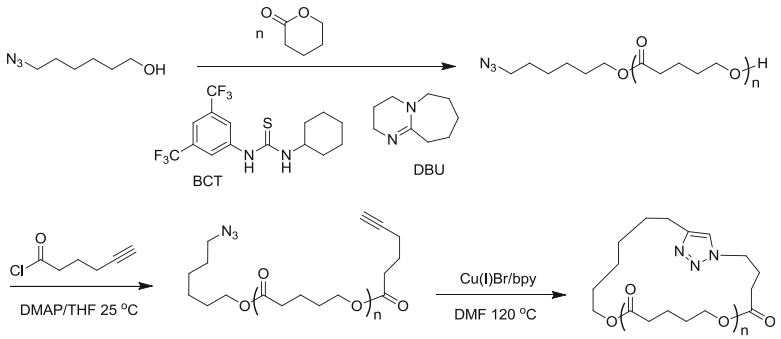

Scheme 38 Synthesis of cyclic poly(δ-valerolactone) through the combination of ring-opening polymerization and CuAAC reaction

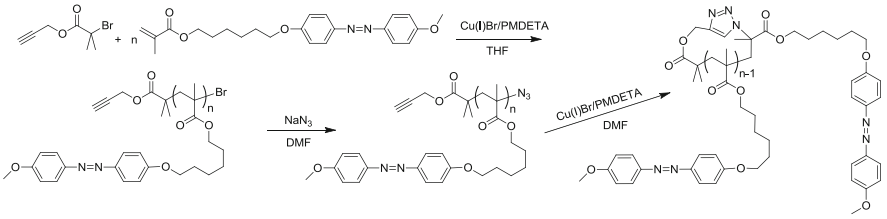

Scheme 39 Synthesis of cyclic azobenzene-containing side-chain liquid crystalline polymer through the combination of ATRP and CuAAC reactions

The above research focused mainly on the common monomers and synthetic methodologies through the combination of ATRP and the CuAAC click reaction. Szoka and Frechet [87] reported the synthesis of cyclic PAA and further grafted poly(ethylene glycol) to the cyclic PAA to give a cyclic grafting copolymer. Further in vivo studies indicated that the cyclic grafting copolymer showed a long circulation time in the blood stream and a high tumor uptake efficiency. Zhao and coworkers [88] reported cyclic azobenzene-containing side-chain liquid crystalline polymers. Monomer 6-[4-(4-methoxyphenylazo)phenoxy]hexyl methacrylate (AzoMA) was polymerized by ATRP with a propargyl functional initiator, followed by azidation. The α-alkyne-ω-azide linear PAzoMA was cyclized via click reaction with CuBr and PMDETA as catalyst in DMF (Scheme 39). Compared

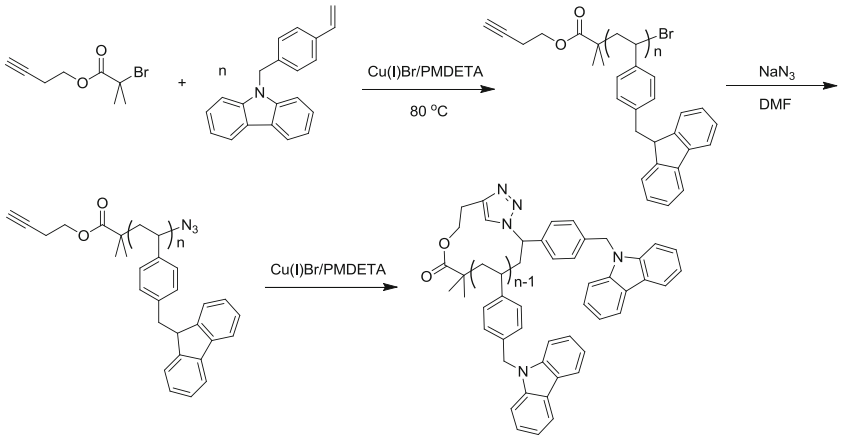

Scheme 40 Synthesis of cyclic polymer containing pendant carbazole units through the combination of ATRP and CuAAC reaction

to their linear precursors, cyclic PAzoMA exhibited a lower T_g, different phase transition temperatures, as well as smaller phase transition enthalpy and entropy. Differences in the liquid crystalline properties were also studied in detail.

Zhu and coworkers [89] reported cyclic polymers with pendant carbazole units. 4-Vinylbenzyl-carbazole (VBCZ) was polymerized by ATRP with an alkyne functional initiator. After azidation, cyclic PVBCZ was efficiently synthesized by CuAAC in DMF (Scheme 40). Cyclic PVBCZ exhibited unique properties in comparison with its linear counterpart: a higher T_g, enhanced fluorescence with a longer fluorescence lifetime, and different redox behavior. These results suggested that the structure—property relationship was strongly affected by the polymer topology.

The Diels–Alder reaction is another heterodifunctional coupling reaction that has been applied for the synthesis of cyclic polymers. The first example was reported by Mizawa et al in 2000 [90]. Linear PMMA was first synthesized by living anionic polymerization with a silane-protected anionic initiator followed by a two-step post-functionalization. The linear α-maleimide-ω-dienyl heterodifunctional PMMA was then cyclized in THF by refluxing for 24 h (Scheme 41).

With the great progress in LRP in the past decade, Durmaz et al. [91] again used the Diels–Alder reaction to synthesize cyclic PSTY and cyclic PSTY-*b*-PCL. They synthesized 9-anthyryl methyl 2-bromo-2-methyl propanoate as an ATRP initiator for the polymerization of styrene to afford linear PSTY with anthyryl chain end. After conversion of the bromo to azido group, the linear PSTY was then "clicked" with a furan-protected maleimide-ω-alkyne heterofunctional linker. Cyclization was achieved by Diels–Alder reaction in toluene with reflux for 48 h. Although their results suggested the successful synthesis of the target cyclic product, the involvement of another step of CuAAC click reaction makes the synthesis procedure more tedious (Scheme 42).

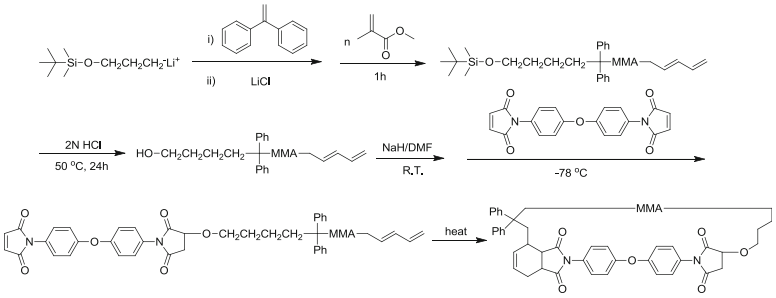

Scheme 41 Synthesis of cyclic PMMA through the combination of living anionic polymerization and Diels–Alder reaction

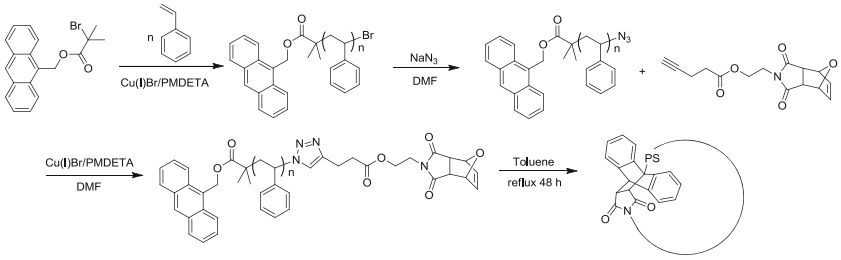

Scheme 42 Synthesis of cyclic PSTY through the combination of ATRP and Diels–Alder reaction

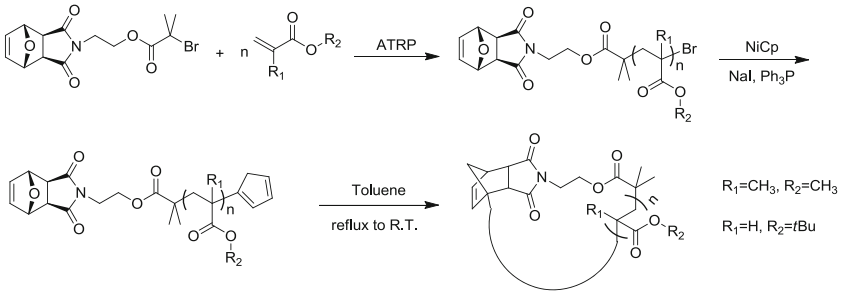

Scheme 43 Synthesis of cyclic PMMA and P^{t}BA through the combination of ATRP and Diels–Alder reaction

Soon after this report, Barner-Kowollic and coworkers [92] modified the synthesis procedure. In this case, furan-protected maleimide functional ATRP initiator was first used to control the polymerization of MMA or *t*BA. The bromo chain end was converted to a cyclopentadienyl group with NiCp2, NaI and triphenyl phosphorus, followed by cyclization in toluene under refluxing. The cyclic product was obtained with nearly quantitative conversion, as shown by ESI-MS characterization (Scheme 43).

3 Conclusion

There has been a resurgence in the synthesis of cyclic polymers through the ring-closure method. This stems from the ability to produce well-defined polymers through "living" radical polymerization with controlled chain length and chain-end functionality. The range of cyclic structures and the many different architectures have driven the field in the past few years. In this contribution, we have provided some fundamental insights into ring closure and the conditions for obtaining high conversions of cyclic polymers. We have also provided many examples of ring-closure reactions, starting with the earliest work through to recent studies.

Acknowledgment M.J.M. acknowledges financial support from the ARC Discovery grant (DP120100973).

References

1. de Gennes P-G (1971) J Chem Phys 55:572
2. Doi M, Edwards SF (1986) The theory of polymer dynamics. Oxford University Press, Oxford
3. Doi M, Edwards SF (1978) J Chem Soc Faraday Trans 2 74:1789
4. Kawaguchi D, Masuoka K, Takano A, Tanaka K, Nagamura T, Torikai N, Dalgliesh RM, Langridge S, Matsushita Y (2006) Macromolecules 39:5180
5. Obhukov SP, Rubinstein M, Duke T (1994) Phys Rev Lett 73:1263
6. Casassa EF (1965) J Polym Sci A Gen Pap 3:605
7. Roovers J (1985) J Polym Sci Polym Phys Ed 23:1117
8. McLeish T (2002) Science 297:2005
9. Orrah DJ, Semlyen JA, Ross-Murphy SB (1988) Polymer 29:1455
10. Clarson SJ, Mark JE, Semlyen JA (1986) Polym Commun 27:244
11. Qiu X-P, Tanaka F, Winnik FM (2007) Macromolecules 40:7069
12. Shin EJ, Jeong W, Brown HA, Koo BJ, Hedrick JL, Waymouth RM (2011) Macromolecules 44:2773
13. Bannister DJ, Semlyen JA (1981) Polymer 22:377
14. Ueberreiter K, Kanig G (1952) J Colloid Sci 7:569
15. Fox TG, Flory PJ (1954) J Polym Sci 14:315
16. Farrington PJ, Hawker CJ, Frechet JMJ, Mackay ME (1998) Macromolecules 31:5043
17. Glans JH, Turner DT (1981) Polymer 22:1540
18. Ueberreiter K, Kanig G (1950) J Chem Phys 18:399
19. Santangelo PG, Roland CM, Chang T, Cho D, Roovers J (2001) Macromolecules 34:9002
20. Gan YD, Dong DH, Hogenesch TE (1995) Macromolecules 28:383
21. Lonsdale DE, Bell CA, Monteiro MJ (2010) Macromolecules 43:3331
22. Char K, Gast AP, Frank CW (1988) Langmuir 4:989
23. Cuniberti C, Perico A (1977) Eur Polym J 13:369
24. Redpath AEC, Winnik MA (1982) J Am Chem Soc 104:5604
25. Winnik MA, Redpath AEC, Svirskaya P, Mar A (1983) Polymer 24:473
26. Roovers J, Toporowski PM (1983) Macromolecules 16:843
27. Stanford JL, Stepto RFT, Waywell DR (1975) J Chem Soc Faraday Trans 1 1(71):1308
28. Gordon M, Temple WB (1972) Makromol Chem 160:263

29. Kricheldorf HR, Schwarz G (2003) Macromol Rapid Commun 24:359
30. Jacobson H, Stockmayer WH (1950) J Chem Phys 18:1600
31. Rique-Lurbet L, Schappacher M, Deffieux A (1994) Macromolecules 27:6318
32. Roovers J (1979) Polymer 20:843
33. Winnik MA, Redpath T, Richards DH (1980) Macromolecules 13:328
34. Winnik MA (1985) Acc Chem Res 18:73
35. Johnston-Hall G, Monteiro MJ (2008) J Polym Sci A Polym Chem 46:3155
36. Johnston-Hall G, Monteiro MJ (2008) Macromolecules 41:727
37. Matyjaszewski K, Tsarevsky NV (2009) Nat Chem 1:276
38. Wang JS, Matyjaszewski K (1995) J Am Chem Soc 117:5614
39. Percec V, Guliashvili T, Ladislaw JS, Wistrand A, Stjerndahl A, Sienkowska MJ, Monteiro MJ, Sahoo S (2006) J Am Chem Soc 128:14156
40. Chiefari J, Chong YK, Ercole F, Krstina J, Jeffery J, Le TPT, Mayadunne RTA, Meijs GF, Moad CL, Moad G, Rizzardo E, Thang SH (1998) Macromolecules 31:5559
41. Moad G, Rizzardo E, Thang SH (2005) Aust J Chem 58:379
42. Kolb HC, Finn MG, Sharpless KB (2001) Angew Chem Int Ed 40:2004
43. Tasdelen MA (2011) Polym Chem 2:2133
44. Lowe AB (2010) Polym Chem 1:17
45. Bedard AC, Collins SK (2011) J Am Chem Soc 133:19976
46. Szwarc M, Levy M, Milkovich R (1956) J Am Chem Soc 78:2656
47. Geiser D, Hoecker H (1980) Macromolecules 13:653
48. Rempp P, Strazielle C, Lutz P (1987) Encycl Polym Sci Eng 9:183
49. Rempp P, Lutz P (1992) Makromol Chem Macromol Symp 62:213
50. Vollmert B, Huang JX (1981) Makromol Chem Rapid Commun 2:467
51. Elmadani A, Favier JC, Hemery P, Sigwalt P (1992) Polym Int 27:353
52. Lepoittevin B, Dourges M-A, Masure M, Hemery P, Baran K, Cramail H (2000) Macromolecules 33:8218
53. Ishizu K, Kanno H (1996) Polymer 37:1487
54. Oike H, Imaizumi H, Mouri T, Yoshioka Y, Uchibori A, Tezuka Y (2000) J Am Chem Soc 122:9592
55. Oike H, Uchibori A, Tsuchitani A, Kim H-K, Tezuka Y (2004) Macromolecules 37:7595
56. Tezuka Y, Mori K, Oike H (2002) Macromolecules 35:5707
57. Percec V, Kawasumi M (1993) Macromolecules 26:3663
58. Percec V, Kawasumi M (1993) Chem Mater 5:826
59. Percec V, Kawasumi M (1993) Macromolecules 26:3917
60. Percec V, Kawasumi M (1993) J Mater Chem 3:725
61. Percec V, Asandei AD, Ungar G (1996) Chem Mater 8:1550
62. Yu G-E, Sinnathamby P, Price C, Booth C (1996) Chem Commun (Cambridge) 1996:31
63. Yu GE, Sinnathamby P, Sun T, Heatley F, Price C, Booth C (1997) Macromol Rapid Commun 18:1085
64. Jia Z, Fu Q, Huang J (2006) Macromolecules 39:5190
65. Voter AF, Tillman ES, Findeis PM, Radzinski SC (2012) ACS Macro Lett 1:1066
66. Sun T, Yu G-E, Price C, Booth C, Cooke J, Ryan AJ (1995) Polymer 36:3775
67. Pang X, Wang G, Jia Z, Liu C, Huang J (2007) J Polym Sci A Polym Chem 45:5824
68. Voter AF, Tillman ES (2010) Macromolecules 43:10304
69. Whittaker MR, Goh Y-K, Gemici H, Legge TM, Perrier S, Monteiro MJ (2006) Macromolecules 39:9028
70. Zhang Y, Wang G, Huang J (2010) Macromolecules 43:10343
71. Hayashi S, Adachi K, Tezuka Y (2007) Chem Lett 36:982
72. Tezuka Y, Ohtsuka T, Adachi K, Komiya R, Ohno N, Okui N (2008) Macromol Rapid Commun 29:1237
73. Quirk RP, Wang SF, Foster MD, Wesdemiotis C, Yol AM (2011) Macromolecules 44:7538
74. Schulz M, Tanner S, Barqawi H, Binder WH (2010) J Polym Sci A Polym Chem 48:671

75. Xie M, Shi J, Ding L, Li J, Han H, Zhang Y (2009) J Polym Sci A Polym Chem 47:3022
76. Kubo M, Hayashi T, Kobayashi H, Tsuboi K, Itoh T (1997) Macromolecules 30:2805
77. Kubo M, Nishigawa T, Uno T, Itoh T, Sato H (2003) Macromolecules 36:9264
78. Lepoittevin B, Perrot X, Masure M, Hemery P (2001) Macromolecules 34:425
79. Laurent BA, Grayson SM (2006) J Am Chem Soc 128:4238
80. Xu J, Ye J, Liu S (2007) Macromolecules 40:9103
81. Jia ZF, Lonsdale DE, Kulis J, Monteiro MJ (2012) ACS Macro Lett 1:780
82. Hossain MD, Valade D, Jia ZF, Monteiro MJ (2012) Polym Chem 3:2986
83. O'Bryan G, Ningnuek N, Braslau R (2008) Polymer 49:5241
84. Touris A, Hadjichristidis N (2011) Macromolecules 44:1969
85. Lu DR, Jia ZF, Monteiro MJ (2013) Polym Chem 4:2080
86. Misaka H, Kakuchi R, Zhang C, Sakai R, Satoh T, Kakuchi T (2009) Macromolecules 42:5091
87. Chen B, Jerger K, Frechet JMJ, Szoka FC (2009) J Control Release 140:203
88. Han D, Tong X, Zhao Y, Galstian T, Zhao Y (2010) Macromolecules 43:3664
89. Zhu X, Zhou N, Zhang Z, Sun B, Yang Y, Zhu J, Zhu X (2011) Angew Chem Int Ed 50:6615
90. Mizawa T, Takenaka K, Shiomi T (2000) J Polym Sci A Polym Chem 38:237
91. Durmaz H, Dag A, Hizal G, Tunca U (2010) J Polym Sci A Polym Chem 48:5083
92. Glassner M, Blinco JP, Barner-Kowollik C (2011) Macromol Rapid Commun 32:724
93. Schappacher M, Deffieux A (1991) Makromol Chem Rapid Commun 12(7):447–53

Adv Polym Sci (2013) 262: 329–344
DOI: 10.1007/12_2013_233

Published online: 29 October 2013

Recent Advances in the Emulsion Solvent Evaporation Technique for the Preparation of Nanoparticles and Nanocapsules

Roland H. Staff, Katharina Landfester, and Daniel Crespy

Abstract The emulsion solvent evaporation technique is a method for preparing nanoparticles and nanocapsules that are particularly adapted for applications requiring materials with high purity and low toxicity, such as for biomedicine or electronics. We discuss here new important advances concerning the elucidation of the mechanism of nanoparticle formation, and the synthesis of nanoparticles with new structures or from new polymers.

Keywords Colloids · Emulsion–solvent evaporation · Miniemulsion · Nanocapsules · Nanoparticles

Contents

Abbreviations

DC-FCCS	Dual-color fluorescence cross-correlation spectroscopy
DLS	Dynamic light scattering
DMF	Dimethyl formamide

R.H. Staff, K. Landfester, and D. Crespy (✉)
Max Planck Institute for Polymer Research, Ackermannweg 10, 55128 Mainz, Germany
e-mail: crespy@mpip-mainz.mpg.de

DMSO	Dimethyl sulfoxide
FRET	Fluorescence resonance energy transfer
HFIP	Hexafluoroisopropanol
NMR	Nuclear magnetic resonance
OCTMS	Octamethylcylotetrasiloxane
PDMS-DE	Polydimethylsiloxane diepoxy terminated
PLLA	Poly(L-lactic acid)
PMMA	Poly(methyl methacrylate)
PPO	Poly(2,6-dimethyl-1,4-phenylene oxide)
PS	Polystyrene
PVAc	Poly(vinyl acetate)
PVCi	Poly(vinyl cinnamate)
PVF	Poly(vinyl formal)
SDS	Sodium dodecyl sulfate

1 Introduction

Imagine that you have synthesized a highly functional and advanced polymer. You want to formulize it as nanoparticles or nanocapsules dispersed in an organic or an aqueous medium. Unfortunately, your synthesis does not allow the use of emulsion [1, 2], miniemulsion [3], or microemulsion polymerization [4, 5] because of demanding reaction conditions. Or, let us imagine that you can perform the aforementioned polymerization in dispersed media but you cannot get rid of some residual monomer and/or initiator/catalyst without destabilizing the nanoparticles. What are the possibilities for preparation of polymer nanoparticles from your polymer?

Burton and O'Farrel addressed these issues for a variety of elastomers and resin latexes by inventing the solvent evaporation process from emulsion droplets, also called the emulsion–solvent evaporation process [6]. In this process, a pre-synthesized polymer or a mixture of different polymers are dissolved in a suitable solvent and mixed with another immiscible liquid containing a surfactant (Fig. 1). Afterwards, the solvent can be evaporated by heating the emulsion or by applying a low vacuum [7]. Two years later, Vanderhoff et al. proposed many possible examples in their patent application [8]. Thereafter, the process was adopted mainly in pharmaceutical science to encapsulate drugs in biodegradable polymers [9, 10], especially in micron-sized capsules and particles [11].

Although most of the reports deal with the preparation of microparticles, nanosized particles and capsules are also accessible, usually by employing ultrasonication to form very small droplets [12] from which the solvent is evaporated. Usually, the continuous phase is an aqueous solution. Inverse systems in which water is the solvent have been reported [13, 14] as well as non-aqueous emulsions [15] such as dimethylformamide-in-paraffin [16], dichoromethane-in-fluorinated solvent for microparticles [17], and formic acid-in-paraffin for

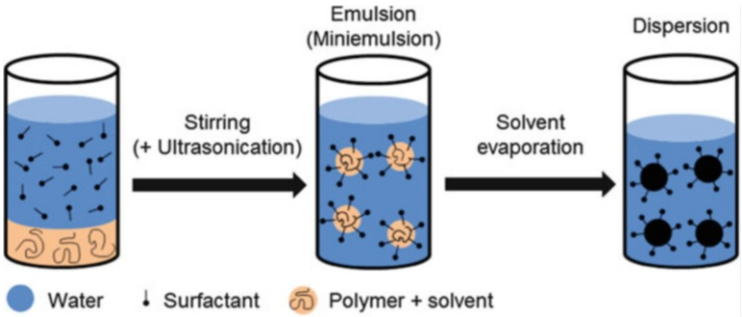

Fig. 1 In the solvent evaporation process from emulsion droplets, the polymer solvent is evaporated from droplets containing the pre-synthesized polymer. The case of a direct emulsion is depicted here, i.e., the continuous phase consists of an aqueous solution

nanocapsules [18]. Nowadays, the process is widely used to generate both micro- and nanosized particles and capsules from a wide variety of different polymers, including but not limited to semiconducting [19], biodegradable [20–22], stimuli-responsive [23] or naturally occurring polymers such as cellulose derivatives [24]. These materials are also used to encapsulate other materials such as magnetic nanoparticles [25, 26], biomaterials [27], perfluorocarbons as contrast agents for ultrasonic imaging [28, 29], dyes for up-conversion [30], or self-healing agents [31, 32] (Fig. 2). It was shown that nanocapsules with hydrophobic liquid core could be successfully fabricated with polymers having completely different thermal and mechanical properties such as poly(L-lactide), poly(methyl methacrylate), poly (phenylene oxide), poly(vinyl formal), poly(vinyl cinnamate), and poly(vinyl acetate) (Fig. 2) [31]. The use of different polymer mixtures or architectures such as polymer blends [19, 33–35], statistical copolymers [32], and block copolymers [23, 36–40] is possible. The latter polymer architecture is especially interesting for introducing an additional spatial segregation in nanoparticles to yield new multicompartment structures, such as nanocapsules or polymer particles with two or more phases, which are discussed in more detail below.

The main advantages of the process as opposed to heterophase polymerizations are its versatility with respect to the polymer that can be used, the simplicity of the method, the fast handling for the preparation of the nanoparticles, and the fact that the produced polymer dispersions do not contain any non-reacted monomers or residual initiator when the pre-synthesized polymer is purified before. The drawbacks lie in the usually broad (20–50%) size distribution of the produced particles and capsules, the usually low solid content of the dispersions, and the presence of residual surfactants. However, the last two issues can be overcome by concentrating the dispersions in vacuo [8] and by dialysis [41], respectively. Both issues were recently simultaneously solved by employing a copolymer with masked amphiphilic and pH-responsive properties. Indeed, the masked groups yielded ionic groups for electrostatic repulsion of the colloids upon reaction with water during the emulsification. The produced carboxylic acid groups were in a sufficient amount

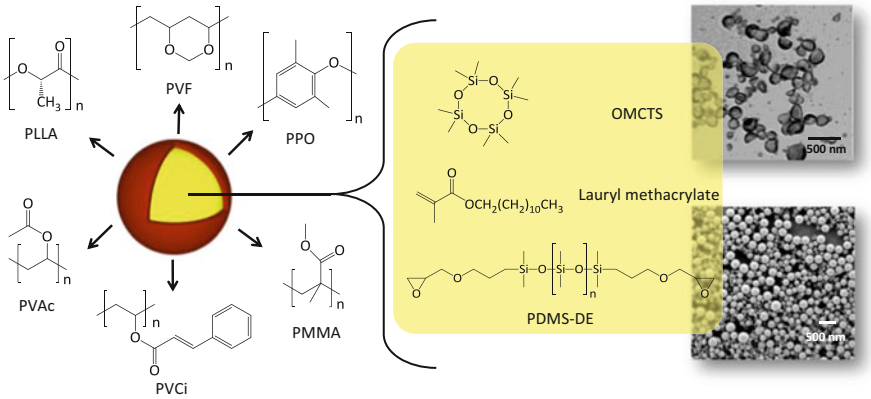

Fig. 2 Scheme showing the versatility of the emulsion–solvent evaporation technique for the preparation of nanocapsules. Polymers with completely different properties could be used to build the shell (*left*) while monomers for self-healing reactions based on various types of polymerization could be encapsulated as liquid core (*right*). *PLLA* poly(L-lactide), *PVF* poly(vinyl formal), *PPO* poly(phenylene oxide), *PMMA* poly(methyl methacrylate), *PVCi* poly(vinyl cinnamate), *PVAc* poly(vinyl acetate), *OMCTS* octamethylcyclotetrasiloxane, *PDMS-DE* polydimethylsiloxane diepoxy terminated [31]

not only to allow a reversible aggregation/re-dispersion upon changes, but also to create emulsions without additional surfactant. The solid content was increased by successive cycle aggregation/re-dispersion in a lower amount of water to concentrate the dispersion of nanocapsules. In miniemulsion polymerization, a possibility for increasing the amount of encapsulated substance without increasing the content of dispersed phase is to dilute the substance and the monomer in a solvent – instead of diluting the substance only in the monomer – and then to evaporate the solvent [42].

2 Solvent Evaporation from Nanodroplets

2.1 Mechanism of the Emulsion–Solvent Evaporation Process

Surprisingly little has been known for many years about the mechanisms governing the emulsion–solvent evaporation process. The main physical processes underlying the process are quite simple: a polymer is dissolved in a good solvent, which is then emulsified in an aqueous medium containing a surfactant. The slow evaporation of the polymer solvent leads to nucleation of the polymer on the water–solvent interface [12]. The mechanism for the removal of the solvent is based on its solubility in the continuous phase, therefore both the temperature and the nature

of the solvent play important roles in the rate of evaporation. The completion of the evaporation can be monitored by gas chromatography [43] or NMR spectroscopy [44] and is usually realized within a few hours [45]. The role of the evaporation on the hardening kinetics of the particles plays an important role, provided that the continuous phase is saturated with the solvent mainly present in the dispersed phase and that the diffusion rate of the solvent of the dispersed phase in the continuous phase is fast compared with the solvent evaporation kinetics. In an experimental study performed with dichloromethane, ethyl acetate, and acetonitrile as solvents, Wang and Schwendeman demonstrated that the rate-limiting step for mass transport of solvent depends on the properties of the solvent [43]. Dichloromethane at room temperature is found to be liquid-side transport limited whereas ethyl acetate and acetonitrile were gas-side transport limited. As expected, the evaporation rate was largely affected by the diameter of the impeller, its rotational speed, and the temperature. The particle's hardening profile could be determined and predicted without needing to measure the concentration of polymer in the solvent in time, but by measuring the concentration of the solvent and by knowing the permeability coefficient of the solvent at the liquid–air interface [43]. After evaporation of the solvent, the dispersions can be dialyzed to remove unwanted or low molecular weight polymer and can be freeze-dried.

One of the most critical properties of nanoparticles is size, hence its control is of outmost importance. Because the particles are formed from droplets, their size is largely dependent on the droplet size. In the case of miniemulsions, the size of the droplets is controlled by the concentration of surfactant [40]. Other parameters such as the nature of the solvent [46], the stirring rate, or ultrasonication time [47] also influence the particle size and particle size distribution. Longer and/or stronger emulsification usually leads to smaller and more narrowly distributed particle size to a certain extent [47]. However, it is difficult to ascribe an observed effect upon changing one parameter to this sole parameter, because most of the parameters are not independent.

Physical processes responsible for the destabilization of emulsions such as Ostwald ripening and coalescence are of crucial importance for the determination of the final particle size and size distribution. It is known that the addition of a small amount of a chemical that is preferentially soluble in the dispersed phase can hinder the Ostwald ripening process [48]. This chemical, sometimes called the osmotic pressure agent because it allows the building of an osmotic pressure upon possible change of chemical composition of the droplets upon Ostwald ripening, is usually a low molecular weight substance that is insoluble in the continuous phase. Thereby, it counteracts the Laplace pressure of the droplets and stabilizes the emulsion droplets. In the solvent evaporation process, no osmotic pressure agent is normally added as the polymer itself can act as osmotic pressure agent because it is insoluble in the continuous phase. However, the concentration of polymer must be above a threshold value to effectively hinder Ostwald ripening [49]. Loxley and Vincent have supposed that the relatively broad size distribution of the obtained particles is caused by coalescence [50]. Dynamic light scattering (DLS) was employed to measure the size of emulsion droplets and the obtained nanoparticles [45]. Based

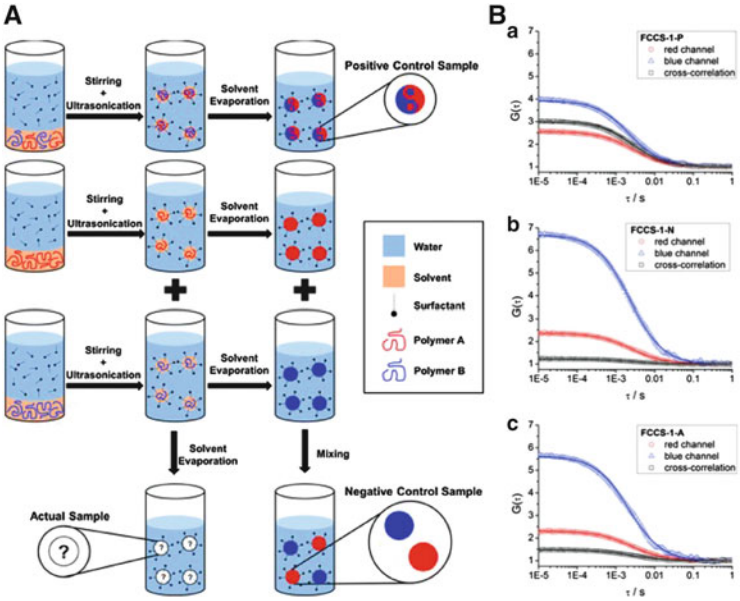

Fig. 3 (**A**) Scheme of the preparation of the samples for both DC-FCCS and FRET investigations. The *colors* represent two different polymers or two differently labeled polymers. (**B**) Correlation curves (*scattered symbols*) and corresponding fits (*lines*) of the DC-FCCS samples: FCCS-1-P positive control sample (*a*), FCCS-1-N negative control sample (*b*), and FCCS-1-A actual sample (*c*) [52]

on these measurements, it was concluded that coalescence plays an important role in particle formation under certain conditions. However, it was shown recently by dual-color fluorescence cross-correlation spectroscopy (DC-FCCS) that coalescence is not significant if the droplets are sufficiently stabilized [51, 52]. Emulsion droplets were separately labeled with two different dyes and mixed (Fig. 3a). The solvent was evaporated to yield nanoparticles and the cross-correlation curves of the temporal evolution of the fluorescence intensity of the labeled nanoparticles were determined by DC-FCCS (Fig. 3b). The amount of double-labeled nanoparticles was measured to be below 10% and therefore significant coalescence did not occur and could not be found responsible for the large size distribution of particles fabricated by the emulsion–solvent evaporation technique as calculated by simulations [52]. Thus, the rather broad particle size distribution probably originates from the emulsification step, pointing out that further development of the process is needed to yield monodisperse nanoparticles. DLS measurements were not conclusive and yield only indirect insight on coalescence. On the contrary, fluorescence resonance energy transfer (FRET) and DC-FCCS measurements allow the direct determination of extent of coalescence either qualitatively or quantitatively, respectively [52].

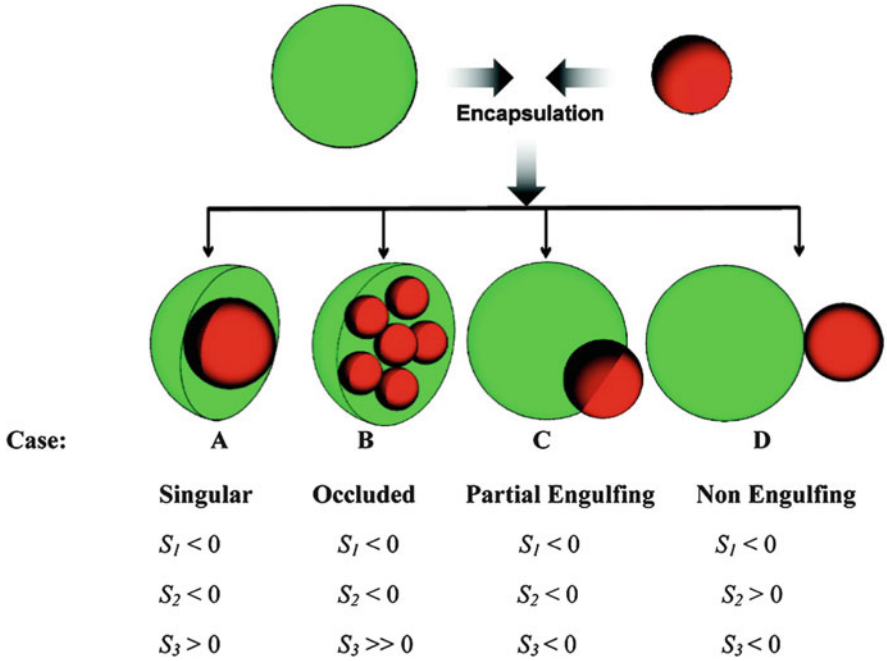

Fig. 4 Morphologies obtained for three immiscible liquids in colloidal systems for cases *A–D* with different combinations of positive and negative spreading coefficients (S_1, S_2, and S_3). Reprinted with permission from [55]. Copyright 2011 American Chemical Society

2.2 Colloidal Structures

Torza and Mason formulated a general theory describing the thermodynamically stable morphologies obtained when three immiscible liquids are mixed, with two of them present in a dispersed phase, using the spreading coefficient S_i that depends on the interfacial tensions of the oil and water phases according to $S_i = \gamma_{jk} - (\gamma_{ij} + \gamma_{ik})$ [53]. This theoretical value can be employed to predict morphologies of micro- or nanoparticles consisting of two immiscible materials. Depending on the sign of the spreading coefficients, one of the substances can be completely (Fig. 4a), partially (Fig. 4c), or not at all (Fig. 4d) engulfed in another material. Occluded structures (i.e., with multicores) are also possible morphologies and can be obtained as a kinetically trapped structure or as a thermodynamically favorable structure when crosslinking is applied in the dispersed phase [54].

In general, the final morphology will be the one with the lowest free Gibbs enthalpy (G_s), which can be calculated by:

$$G_s = \sum_{i,j}^{n} \gamma_{ij} A_{ij} \tag{1}$$

in which γ_{ij} represents the surface tension of the phases i and j, and A_{ij} represents the area of the interface. Therefore, the ratio of the different phases and the amount of

surfactant are of outmost importance for the determination of the final particle morphology. In the case of nanoparticles of a binary blend of a hole-transporting and an electron-transporting polymer, the composition of both phases (i.e., the distribution of one polymer in the other one in the two phases) followed the prediction of the Flory–Huggins theory [56]. The quantum efficiency of devices produced with the nanoparticle blend were found to be improved compared to other methods [57].

However, what happens if G_s cannot be minimized and is stuck in a local minimum on the energy landscape? In this case, the morphology is kinetically but not thermodynamically stable. In addition, other factors such as the crystallization of polymers can also significantly influence the particle morphology [41, 58]. Chen et al. showed that the viscosity of the liquids played a significant role in the morphology of particles composed of polystyrene (PS) and poly(methyl methacrylate) (PMMA) [59]. Indeed, PMMA partially encapsulated PS for high molecular weight polymers whereas the contrary was observed for low molecular weight polymers. Okubo et al. investigated the effect of different stabilizers on the morphology of PS/PMMA particles [33]. Particles stabilized with poly(vinyl alcohol) displayed small dimples whereas for SDS acorn and spherical structures with increasing amount of SDS were observed. Both phenomena were explained by the interplay of solvent evaporation and stabilization by the surfactant. Although high amounts of SDS stabilized both the PS and the PMMA interfaces to water equally well, this was not the case for smaller amounts. Therefore, bowl-like PMMA shells were formed, in which the PS slowly hardened upon further evaporation of the solvent. As the PS contracted because of the ongoing evaporation of solvent, bowl- or dimple-like structures were obtained. These effects were not observed when dichloromethane was used instead of toluene as solvent to be evaporated. This was explained by the fact that toluene is preferentially partitioned in the PS phase, which is not the case for dichloromethane. The molecular weights of the PS and PMMA were also found to play a role on the morphology [34]. Whereas the interfacial tension polymeric droplet against aqueous phase was not dependent on the molecular weight, the interfacial tensions between PS and PMMA in the droplets increased with increasing molecular weight and snowman-like particles could be obtained for high molecular weight polymers.

Besides the well-known core–shell and inverse core–shell [60], or acorn and Janus morphologies obtained with polymers with similar polarities [33], other interesting structures can be formed. Half-spherical structures are accessible by removing the liquid in acorn structures formed with a polymer and a liquid [40, 61]. Onion-like structures are created from block copolymers, for which the phase separation into lamellae causes layered structures that follows the curvature of the particle where they are confined [37, 40, 62]. The diameter of the particle is in this case also very important. Indeed, if the particle size is low enough, core–shell or Janus structures can be obtained [40]. A large variety of different structures were predicted from simulations on diblock copolymer/homopolymer blends [63], star-triblock copolymers in spherical nanopores [64], or on diblock copolymers under different confinements [65–67], among which several have already been prepared

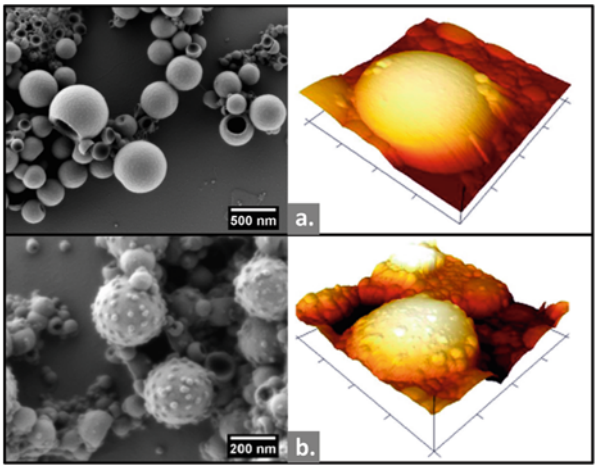

Fig. 5 SEM micrographs (*left*) and 3D perspectives of SFM height images (*right*) of (**a**) patchy nanocapsules of poly(methyl methacrylate-*b*-vinyl ferrocene) and (**b**) the nanocapsules after oxidation with $KMnO_4$. Reprinted with permission from [23]. Copyright 2012 American Chemical Society. The surface of the nanocapsules is relatively smooth before oxidation and presents outgrowths after the selective oxidation of the poly(vinyl ferrocene) patches with $KMnO_4$

by the emulsion–solvent evaporation process. However, these theoretical studies clearly show that many more interesting and highly complex morphologies could be still prepared.

Kinetic morphologies are formed once the free Gibbs energy G_s cannot be minimized to its global minimum, but only to a kinetically stable local minimum. The main reason for a kinetically trapped morphology is a hindered phase separation of the materials inside the particle. This phenomenon can occur when high molecular weight polymers are employed in the process. As diffusion of the chains is necessary for phase separation, one possibility to obtain kinetically trapped morphologies is to increase the viscosity of the polymeric emulsion droplets [68]. One possibility to control the viscosity inside the droplets of polymeric emulsions is to vary the molecular weight of the polymer or the solubility of the polymer in the chosen solvent. Additionally, both the evaporation temperature and the evaporation rate of the solvent are of high importance for the build-up of a thermodynamically stable morphology [36, 37, 69]. However, structures that resemble kinetically trapped morphologies can also be thermodynamically stable when specific ratios of block length in the block copolymers are achieved [23] or if the phase separation occurs in the weak segregation limit [40]. Both cases were used for the generation of patchy nanoparticles and nanocapsules. Functional patchy nanocapsules of poly(methyl methacrylate-*b*-vinyl ferrocene) could be selectively reacted with oxidants to yield different structures (Fig. 5). The concept of multicompartmentation – with many polyvinylferrocene compartments in the form of patches in the nanocapsules shell and one compartment created by the

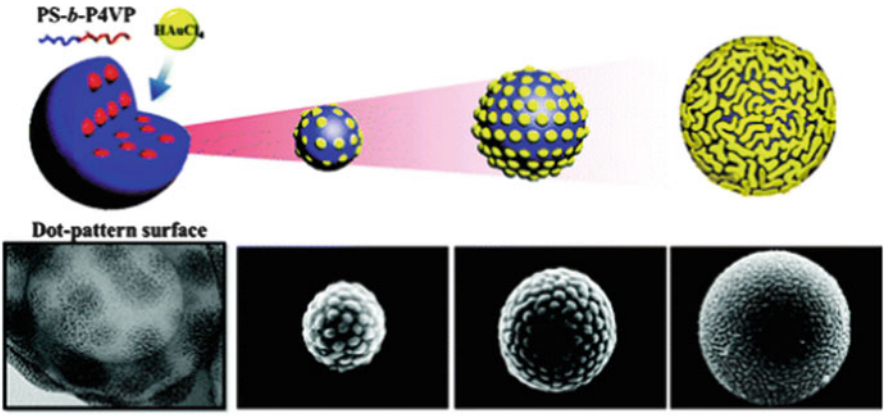

Fig. 6 Scheme (*top*) and SEM micrographs (*below*) showing the morphologies of particles composed of gold nanoparticles (*HAuCl₄*) and poly(styrene-*b*-4-vinylpyridine) (*PS-b-P4VP*) with different diameters. The structures evolved from discontinuous gold domains to quasi-continuous domains when the particle size increased from ~250 to 1,200 nm. Reprinted with permission from [81]. Copyright 2012 American Chemical Society

liquid core and forming a reservoir for the subsequent release of chemicals – was married with the concept of stimuli-responsive materials. Indeed, chemicals could be released from the reservoir compartment by selective oxidation of the responsive patches of poly(vinyl ferrocene) [23].

As previously mentioned, multicompartment morphologies [69] were easily be obtained by using block copolymers [23, 36–40, 62, 71–76]. Such structures can be further compartmentalized by adding inorganic nanoparticles that preferentially migrate to one domain [77, 78].

The obtained structures can be isotropic, i.e. the metal nanoparticles segregate in one type of lamellae in onion-like nanoparticles [78–80], form isotropic surface structures [81, 82] (Fig. 6), or can be anisotropic with regard to the particle geometry. The latter case was based on metal nanoparticles/polymer assemblies [81] or similar assemblies but with a fluorescent dye instead of the metal nanoparticles [83].

Isojima et al. also showed that by varying the ratio of metal nanoparticles to polymer matrix one can obtain both isotropic and anisotropic morphologies [84]. Another way of adding further or changing existing compartments is the removal of one compartment, for example by a selective solvent [85, 86].

In addition, the solvent evaporation from emulsion droplets can also be used on non-polymeric materials [87, 88] such as inorganic nanocrystals of $BaCrO_4$ and others dispersed in an organic solvent. Upon emulsification and evaporation of the organic phase, spherical aggregates of the nanocrystals are formed. This method has also recently been exploited to prepare manganese ferrite/graphene oxide nanocomposites [89] and siRNA-loaded magnetic metal nanoparticles [90].

Among different possible morphologies, capsules (i.e., core–shell particles with one liquid core) are often targeted morphologies for the protection and encapsulation of substances. When nanocapsules are produced from the emulsion–solvent evaporation process, the liquid core material is usually non-functional. However, functional non-solvents can also be used, for example in the form of self-healing agents [31, 32] or of pH-responsive non-solvent [91]. The encapsulation of Grubbs catalysts of monomers for a self-healing reaction based on ring-opening metathesis polymerization by the mild emulsion–solvent evaporation method was found to be advantageous over other methods. Although silica nanocapsules with a hydrophobic liquid core are porous and therefore cannot be used as fillers in a hydrophobic matrix [92], it was not possible to encapsulate Grubbs catalysts in nanocapsules fabricated by free-radical polymerization in miniemulsion polymerization [91]. Furthermore, whereas in interfacial step-growth polymerization the functional units in the monomers needed to form the polymer shell can react with sensitive products such as catalysts [94], the polymer building the nanocapsules shell can be relatively chemically inert. For the pH-responsive core, tertiary amines with long alkyl chains were embedded as liquid core in nanocapsules and could be released to the continuous phase after protonation of the amine [91]. The diffusion of the core out of the nanocapsules allowed for an unprecedented chemical transformation of the liquid core from hydrophobic to aqueous. Finally, swollen PMMA nanocapsules prepared by the emulsion–solvent evaporation technique could be elongated to a core–shell ellipsoidal shape in an electrospinning jet [95].

2.3 Effect of the Nanoconfinement

Because the polymer nanoparticles prepared by the emulsion–solvent evaporation process are highly pure, they are ideal samples for investigating the effect of nanoconfinement on polymer properties such as crystallization. For the crystallization of poly(ethylene oxide) nanoparticles after evaporation of water from inverse miniemulsions, a large supercooling was detected compared to the bulk material [13]. Upon removal of water from the dispersion, the loosely packed poly(ethylene oxide) lamellae slid apart, possibly generating single crystals. Recently, the crystallization of semicrystalline polymers such as syndiotactic and isotactic polystyrene as well as poly(L-lactic acid) (PLLA) was investigated [41]. For all polymers, a decrease in crystallinity with decreasing particle diameter was observed. Both syndiotatic and isotactic polystyrene nanoparticles showed anisotropic structures because the crystallization induced a deformation of the otherwise spherical particles (Fig. 7a, b). For PLLA, it was even possible to control the crystallinity by heating the aqueous dispersion because PLLA cold-crystallizes below 100°C. The extent of cold-crystallization upon heating the PLLA particles was found to be larger for smaller particles than for the larger ones (Fig. 7c).

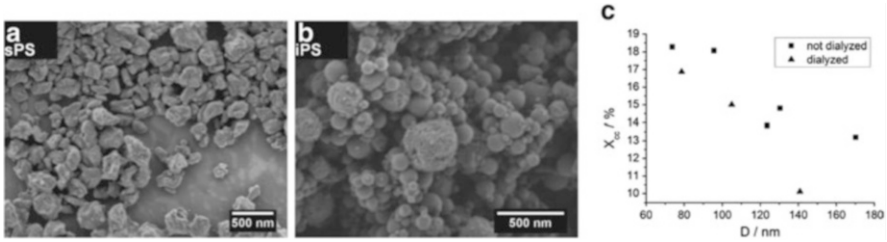

Fig. 7 SEM micrographs of (**a**) syndiotactic polystyrene and (**b**) isotactic polystyrene showing non-spherical strcutures due to the crystallization of the polymers in the dispersed state during the emulsion–solvent evaporation procedure. (**c**) Evolution of the cold-crystallization of PLLA in particles prepared by the emulsion–solvent evaporation process in dependence on the particle diameter [41]

2.4 New Emulsions

Whereas the preparation of particles with solvent evaporation from apolar droplets is widely reported, their preparation from polar droplets is still unusual [13–18]. The challenge is to find a suitable polar solvent with a low boiling point that can solubilizes both the polymer and the substance to be encapsulated. Water as dispersed phase in such cases is not always suitable and has been replaced in non-aqueous emulsions by other polar solvents [15] to allow reactions sensitive to water such as anionic polymerization [96] or reactions requiring high temperature and the absence or removal of water [97]. Dimethyl formamide (DMF), formic acid, formamide, or dimethyl sulfoxide (DMSO) are polar solvents that can be used but that are difficult to remove because of their high boiling points. Recently, hexafluoroisopropanol (HFIP) was proposed as a suitable candidate for the preparation of polymer nanoparticles via the emulsion–solvent evaporation method. It also has the ability to be a good solvent for metallopharmaceuticals that need to be embedded in a carrier material to be delivered in the body [98]. A ruthenium nitrosyl complex designed for phototherapy that is polar but not soluble in water could be successfully encaspulated in polymer nanoparticles after the evaporation of HFIP from HFIP-in-alkane miniemulsions (Fig. 8) [99]. Various polymer matrixes such as gelatin, PLLA, poly(ethylene terephtalate), and poly(vinyl formal) could be used for the physical entrapment of complex. The colloidal stability of the particles was improved by matching the density of the continuous phase to the density of HFIP, and hence *cis*-decalin was found to be more suitable than cyclohexane, hexadecane, and isooctane. The nanoparticles could be re-dispersed in aqeuous solutions after removal of the alkane, and the release of nitric oxide upon irradiation of the aqueous dispersion with a low intensity UV light could be demonstrated in a fluorescence assay.

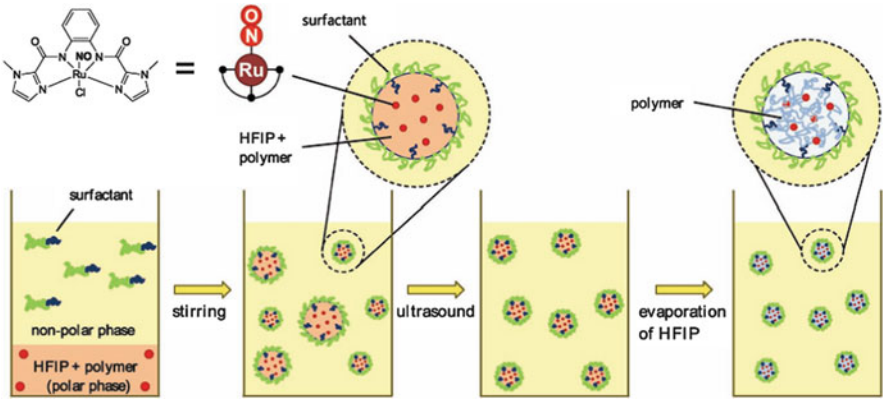

Fig. 8 Encapsulation of a ruthenium nitrosyl complex in polymer nanoparticles in non-aqueous hexafluorisopropanol (*HFIP*)-in-alkane miniemulsion [99]

3 Summary, Conclusions, and Outlook

The main challenges in colloid chemistry nowadays are oriented towards the strategic fields of health and medicine, energy and resource savings, and the design of so-called smart materials allowing the automation of tasks without human intervention. The colloids recently prepared have gained increased complexity either in their shape, chemistry, and/or functions and their design has been largely inspired by the cellular and subcellular systems present in nature. This is the case for the block-copolymer assemblies in nanoparticles and nanocapsules that allows for the coexistence of multicompartmentation and stimuli-responsive exchange of chemicals in the same objects. Because the increase in complexity can be achieved by colloid engineering but also by the subsequent utilization of other processes such as electrospinning of nanoparticles [100], the portfolio of achievable structures is almost unlimited.

A very interesting combination for the preparation of complex nanoparticles is the use of miniemulsions droplets as templates to perform the evaporation of the solvent. Indeed, miniemulsions are particularly stable colloidal systems without significant mass transfer between the droplets, which in turn can be precisely tuned by the concentration of the surfactant. It has been shown that the solvent evaporation process from miniemulsion droplets is uniquely suited to prepare a wide variety of single- and multicompartment nanoparticles and nanoparticles with unprecedented properties. Furthermore, it was shown that the coalescence between miniemulsion droplets does not significantly affect the size distribution of the final nanoparticles obtained by the miniemulsion–solvent evaporation method [52]. Recently, the process of emulsion–solvent evaporation has been significantly improved by the emulsification step being possible without surfactant, and the solid content being increased by successive and reversible aggregation/re-dispersion steps.

Because the emulsion–solvent evaporation is versatile, new nanoparticles structures and nanoparticles from new materials are expected to be reported. Open questions such as how to create very monodisperse nanoparticles via this technique and the influence of the molecular state of the polymer on the nanoparticle and nanocapsule properties such as permeability are expected to be answered in the foreseeable future, helping to create more functional and useful materials.

References

1. Asua JM (2004) J Polym Sci A Polym Chem 42:1025
2. Chern CS (2006) Prog Polym Sci 31:443
3. Crespy D, Landfester K (2010) Beilstein J Org Chem 6:1132
4. Pavel FM (2004) J Disp Sci Technol 25:1
5. Chow PY, Gan LM (2005) Adv Polym Sci 175:257
6. Burton GW, O'Farrel CP (1977) J Elastomers Plastics 9:94
7. Rao JP, Geckeler KE (2011) Prog Polym Sci 36:887
8. Vanderhoff JW, El-Aasser MS, Ugelstad J (1979) US Patent 4,177,177
9. Quintanar-Guerrero D, Allémann E, Fessi H, Doelker E (1998) Drug Dev Ind Pharm 24:1113
10. Freiberg S, Zhu XX (2004) Int J Pharm 282:1
11. O'Donnell PB, McGinity JW (1997) Adv Drug Deliver Rev 28:25
12. Anton N, Benoit JP, Saulnier P (2008) J Contolled Rel 128:185
13. Taden A, Landfester K (2003) Macromolecules 2003(36):4037
14. Atkin R, Davies P, Hardy J, Vincent B (2004) Macromolecules 37:7979
15. Crespy D, Landfester K (2011) Soft Matter 7:11054
16. Fujiyama J, Nakase Y, Osaki K, Sakakura C, Yamagishi H, Hagiwara A (2003) J Controlled Rel 89:397
17. Mana Z, Pellequer Y, Lamprecht A (2007) Int J Pharm 338:231
18. Crespy D, Landfester K (2007) Macromol Chem Phys 208:457
19. Kietzke T, Neher D, Landfester K, Montenegro R, Guntner R, Scherf U (2003) Nat Mater 2003(2):408
20. Nouvel C, Raynaud J, Marie E, Dellacherie E, Six JL, Durand A (2009) J Colloid Interf Sci 330:337
21. Chu CH, Wang YC, Huang HY, Wu LC, Yang CS (2011) Nanotechnology 22:185601
22. Musyanovych A, Schmitz-Wienke J, Mailänder V, Walther P, Landfester K (2008) Macromol Biosci 8:127
23. Staff RH, Gallei M, Mazurowski M, Rehahn M, Berger R, Landfester K, Crespy D (2012) ACS Nano 6:9042
24. Abdel-Mottaleb MMA, Moulari B, Beduneau A, Pellequer Y, Lamprecht A (2012) Eur J Pharm Biopharm 82:151
25. Urban M, Musyanovych A, Landfester K (2009) Macromol Chem Phys 210:961
26. Mistlberger G, Medina-Castillo AL, Borisov SM, Mayr T, Fernández-Gutiérrez A, Fernandez-Sanchez JF, Klimant I (2011) Microchim Acta 172:299
27. Perez C, Sanchez A, Putnam D, Ting D, Langer R, Alonso MJ (2001) J Controlled Rel 75:211
28. Pisani E, Tsapis N, Paris J, Nicolas V, Cattel L, Fattal E (2008) Langmuir 22:4397
29. Pisani E, Tsapis N, Galaz B, Santin M, Berti R, Taulier N, Kurtisovski E, Lucidarme O, Ourevitch M, Doan BT, Beloeil JC, Gillet B, Urbach W, Bridal SL, Fattal E (2008) Adv Funct Mater 18:29633122
30. Wohnhaas C, Friedemann K, Busko D, Landfester K, Baluschev S, Crespy D, Turshatov A (2013) ACS Macro Lett 2:446

31. Zhao Y, Fickert J, Landfester K, Crespy D (2012) Small 8:2954
32. Fickert J, Wohnhaas C, Turshatov A, Landfester K, Crespy D (2013) Macromolecules 46:573
33. Saito N, Kagari Y, Okubo M (2006) Langmuir 22:9397
34. Tanaka T, Nakatsuru R, Kagari Y, Saito N, Okubo M (2008) Langmuir 24:12267
35. Tanaka T, Okayama M, Kitayama Y, Kagawa Y, Okubo M (2010) Langmuir 26:7843
36. Higuchi T, Motoyoshi K, Sugimori H, Jinnai H, Yabu H, Shimomura M (2010) Macromol. Rapid Commun 31:1773
37. Okubo M, Saito N, Takekoh R, Kobayashi H (2005) Polymer 46:1151
38. Tanaka T, Saito N, Okubo M (2009) Macromolecules 42:7423
39. Jeon SJ, Yi GR, Koo CM, Yang SM (2007) Macromolecules 40:8430
40. Staff RH, Rupper P, Lieberwirth I, Landfester K, Crespy D (2011) Soft Matter 7:10219
41. Staff RH, Lieberwirth I, Landfester K, Crespy D (2012) Macromol Chem Phys 213:351
42. Molberg M, Crespy D, Rupper P, Nuesch F, Manson JAE, Lowe C, Opris DM (2010) Adv Funct Mater 20:3280
43. Wang J, Schwendeman SP (1999) J Pharm Sci 88:1090
44. Zhao Y, Berger R, Landfester K, Crespy D (2013) Polym Chem (2014). doi:10.1039/C3PY01096A
45. Desgouilles S, Vauthier C, Bazile D, Vacus JL, Grossiord JL, Veillard M, Couvreur P (2003) Langmuir 19:9504
46. Mainardes RM, Evangelista RC (2005) J Microencapsul 22:13
47. Sansdrap P, Moes AJ (1993) Int J Pharm 98:157
48. Higuchi WI, Misra J (1962) J Pharmaceutical Sci 51:459
49. Miller CM, Blythe PJ, Sudol ED, Silebi CA, El-Aasser MS (1994) J Polym Sci A Polym Chem 32:2365
50. Loxley A, Vincent B (1998) J Colloid Interf Sci 208:49
51. Schaeffel D, Staff RH, Butt HJ, Landfester K, Crespy D, Koynov K (2012) Nano Lett 12:6012
52. Staff RH, Schaeffel D, Turshatov A, Donadio D, Butt HJ, Landfester K, Koynov K, Crespy D (2013) Small doi:10.1002/smll.201300372
53. Torza S, Mason SG (1970) J Colloid Interf Sci 33:67
54. Durant YG, Sundberg DC (1996) Macromolecules 29:8466
55. Trongsatitkul T, Budhlall BM (2011) Langmuir 27:13468
56. Kietzke T, Neher D, Kumke M, Ghazy O, Ziener U, Landfester K (2007) Small 6:1041
57. Kietzke T, Neher D, Kumke M, Montenegro R, Landfester K, Scherf U (2004) Macromolecules 37:4882
58. Romanski FS, Winkler JS, Riccobene RC, Tomassone MS (2012) Langmuir 28:3756
59. Chen YC, Dimonie V, El-Aasser MS (1992) J Appl Polym Sci 46:691
60. Muroi S, Hashimoto H, Hosoi K (1984) J Polym Sci Pol Chem 22:1365
61. Tanaka T, Yamagami T, Nogami T, Minami H, Okubo M (2012) Polym J 44:1112
62. Saito N, Takekoh R, Nakatsuru R, Okubo M (2007) Langmuir 23:5978
63. Yang R, Li B, Shi AC (2011) Langmuir 28:1569
64. Li S, Jiang Y, Chen JZY (2013) Soft Matter 9:4843
65. Yu B, Li B, Jin Q, Ding D, Shi AC (2011) Soft Matter 7:10227
66. Yu B, Li B, Jin Q, Ding D, Shi AC (2007) Macromolecules 40:9133
67. Shi AC, Li B (2013) Soft Matter 9:1398
68. Muscato MR, Sundberg DC (1991) J Polym Sci Pol Phys 29:1021
69. Winzor CL, Sundberg DC (1992) Polymer 33:4269
70. Crespy D, Staff RH, Becker T, Landfester K (2012) Macromol Chem Phys 213:1183
71. Jeon SJ, Yi GR, Yang SM (2008) Adv Mater 20:4103
72. Li L, Matsunaga K, Zhu J, Higuchi T, Yabu H, Shimomura M, Jinnai H, Hayward RC, Russell TP (2010) Macromolecules 43:7807
73. Hales K, Chen Z, Wooley KL, Pochan DJ (2008) Nano Lett 8:2023
74. Wyman I, Njikang G, Liu G (2011) Prog Polym Sci 36:1152

75. Higuchi T, Motoyoshi K, Sugimori H, Jinnai H, Yabu H, Shimomura M (2012) Soft Matter 8:3791
76. Yabu H, Sato S, Higuchi T, Jinnai H, Shimomura M (2012) J Mater Chem 22:7672
77. Jang SG, Audus DJ, Klinger D, Krogstad DV, Kim BJ, Cameron A, Kim SW, Delaney KT, Hur SM, Killops KL, Fredrickson GH, Kramer EJ, Hawker CJ (2013) J Am Chem Soc 135:6649
78. Jeon SJ, Yang SM, Kim BJ, Petrie JD, Jang SG, Kramer EJ, Pine DJ, Yi GR (2009) Chem Mater 21:3739
79. Zhang K, Gao L, Chen Y, Yang Z (2008) Chem Mater 20:23
80. Qiu P, Jensen C, Charity N, Towner R, Mao C (2010) J Am Chem Soc 132:17724
81. Kim MP, Kang DJ, Jung DW, Kannan AG, Kim KH, Ku KH, Jang SG, Chae WS, Yi GR, Kim BJ (2012) ACS Nano 6:2750
82. Hu SH, Gao X (2010) J Am Chem Soc 132:7234
83. Geng J, Li K, Qin W, Ma L, Gurzadyan GG, Tang, Liu B (2013) Small 9:2012
84. Isojima T, Suh SK, Vander Sande JB, Hatton TA (2009) Langmuir 25:8292
85. Deng R, Liu S, Li J, Liao Y, Tao J, Zhu J (1889) Adv Mater 2012:24
86. Deng R, Liang F, Li W, Liu S, Liang R, Cai M, Yang Z, Zhu J (2013) Small. doi:10.1002/smll.201300271
87. Bai F, Wang D, Huo Z, Chen W, Liu L, Liang X, Chen C, Wang X, Peng Q, Li Y (2007) Angew Chem Int Ed 46:6650
88. Lu Z, Yin Y (2012) Chem Soc Rev 41:6874
89. Peng E, Choo ESG, Chandrasekharan P, Yang CT, Ding J, Chuang KH, Xue JM (2012) Small 8:3620
90. Park JW, Bae KH, Kim C, Park TG (2011) Biomacromolecules 12:457
91. Zhao Y, Landfester K, Crespy D (2012) Soft Matter 8:11687
92. Fickert J, Rupper P, Graf R, Landfester K, Crespy D (2012) J Mater Chem 22:2286
93. Fickert J, Makowski M, Kappl M, Landfester K, Crespy D (2012) Macromolecules 45:6324
94. Crespy D, Stark M, Hoffmann-Richter C, Ziener U, Landfester K (2007) Macromolecules 40:3122
95. Herrmann C, Turshatov A, Crespy DA (2012) ACS Macro Lett 1:907
96. Crespy D, Landfester K (2005) Macromolecules 38:6882
97. Schwab MG, Crespy D, Feng XL, Landfester K, Mullen K (2011) Macromol Rapid Commun 32:1798
98. Crespy D, Landfester K, Schubert US, Schiller A (2010) Chem Commun 46:6651
99. Bohlender C, Landfester K, Crespy D, Schiller A (2013) Part Part Syst Char 30:138
100. Crespy D, Friedemann K, Popa AM (2012) Macromol Rapid Commun 33:1978

Adv Polym Sci (2013) 262: 345–362
DOI: 10.1007/12_2013_241

Published online: 20 October 2013

Nanomechanical Function Arising from the Complex Architecture of Dendronized Helical Polymers

Jonathan G. Rudick

Abstract Dendronized polymers that have a cylindrical shape and a helical polymer backbone at the core of the cylinder are able to undergo reversible stretching and contraction of the helix. As the helix expands, the cylindrical macromolecule elongates like a molecular mechanical actuator. When the polymers are self-organized in a columnar lattice, the cylinders can be aligned and the extension of the individual molecules is amplified to macroscopic dimensions and can be employed to perform work. Relationships between the complex architecture of these polymers, their organization in bulk, and emergent function are discussed as an example of the remarkable opportunities that remain to be explored as we commemorate the 60th anniversary of Hermann Staudinger receiving the Nobel Prize for Chemistry.

Keywords Dendronized polymer · Liquid crystal · Self-assembly · Supramolecular chemistry

Contents

J.G. Rudick (✉)
Department of Chemistry, Stony Brook University, Stony Brook, NY 11794-3400, USA
e-mail: jon.rudick@stonybrook.edu

1 Introduction

Commemorating the 60th anniversary of the Nobel Prize being awarded to Hermann Staudinger for his pioneering studies to establish the field of organic polymer chemistry [1, 2] gives us an opportunity to reflect upon the hierarchical structures that are achievable in macromolecules and supramolecular polymers. In 1953, the idea that natural and synthetic sources could be used to prepare organic molecules composed of tens of thousands if not millions of atoms had solidified [2]. At the same time, details of the solid state structures of polypeptides [3–6], poly (nucleic acid)s [7], and polyolefins [8] were only beginning to emerge and reveal perfectly repeating conformations in monomer units that yield helical structures. Molecular design and chemical synthesis strategies to control the handedness of helical polymers have since been established [9–12], opening opportunities for creating materials whose functional properties relate to the organization of helical building blocks [13–15]. Understanding the hierarchy through which information in molecular building blocks is expressed as macroscopic properties and functions is essential if we are to take full advantage of macromolecular materials and supramolecular polymers.

Macromolecules that contain two or more topologically distinct components are complex architectures that can lead to emergent properties or behaviors that are different to those of either of the individual molecular architectures. Dendronized polymers [16–19] are examples of such complex molecular architectures and are composed of a linear polymer backbone and perfectly branched dendritic side chains on each repeat unit (Scheme 1). The molar masses of such polymers emphasize the shift in thinking brought about by Staudinger's concept of macromolecules [1, 2]. Individual dendronized polymers are nanoscopic objects [20–25] whose organization in bulk is determined by hierarchical processes that occur on a different set of length scales compared to conventional polymers [16, 26]. By virtue of the size and shape of dendronized polymers, interest in this complex macromolecular architecture has moved toward how to extract functionality from these nanoscale molecular objects.

Dendronized polymers that have a helical polymer backbone are of special interest for understanding the structure of dendronized polymers as well as the hierarchy of self-assembly and self-organization events that occur upon going from dilute solution to bulk material. Because of the large volume occupied by the dendritic side chains (Scheme 1), the conformational degrees of freedom available to a flexible polymer backbone are reduced [21, 27–34] and it is possible to obtain helical dendronized polymers from a wide range of polymer backbones. Comparison of the structures of dendronized helical polymers with the structures of dendronized polymers with more flexible backbones have confirmed that flexible polymer backbones adopt a helical conformation upon encapsulation within a dendritic sheath [35, 36]. Efforts to program the handedness of helical dendronized polymers [35–42] have helped answer fundamental questions on how homochirality emerged in biological systems [43–45], and these polymers can be

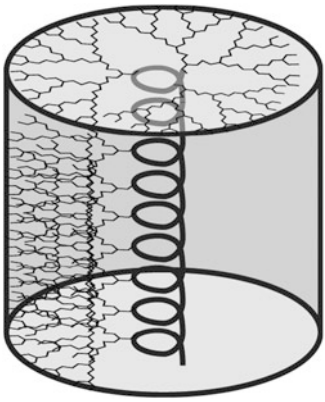

Scheme 1 Dendronized polymers contain dendrons attached to each repeat unit of a polymer that can enforce a helical conformation of the backbone and yield a nanoscale cylindrical object

exploited in technological applications [46–49] .Dendronized helical polymers that are capable of self-organizing into periodical columnar arrays have revealed a unique capacity to function as molecular machines that can amplify nanoscale work to macroscopic dimensions [50–52], and that process is the subject of the remainder of this contribution.

2 Self-Organizable Dendronized Polymer Machines

Self-organizable dendronized polymers include covalent polymers and supramolecular polymers that arrange themselves into periodic or quasiperiodic arrays in bulk or solution [16, 36]. Self-organization in bulk has been observed, almost exclusively [16, 53, 54], from dendrons and dendrimers that contain the amphiphilic units shown in Scheme 2a [22, 55–60]. The amphiphilic building blocks shown in Scheme 2a have a latent propensity to form liquid crystalline mesophases. Percec and coworkers have meticulously investigated the mesophase structures observed in libraries of self-assembling dendrons containing the amphiphilic building blocks in Scheme 2a at their periphery [16, 61–82]. Scheme 2b shows a survey of the diverse lattices and quasiperiodic arrays that this group has identified. The mesomorphism of these building blocks is exceptionally robust, and self-assembling dendrons containing the building blocks in Scheme 2a can impart mesomorphism to a wide range of materials upon dendronization. Polymers [21, 22], electroactive materials [83–86], photoactive materials [87–89], transition metal complexes [90–92], peptides [72–79, 93], dendrimers [94–96], fullerenes [97–102], and inorganic nanoparticles [103, 104] have all been organized in liquid crystalline arrays due to the mesomorphism of amphiphilic dendrons based on the building blocks shown in Scheme 2a.

Polymers dendronized with dendrons containing the amphiphilic building blocks shown in Scheme 2a most frequently self-organize into columnar lattices (e.g., *p*6*mm*) [55, 60, 105], although cubic lattices have also been observed

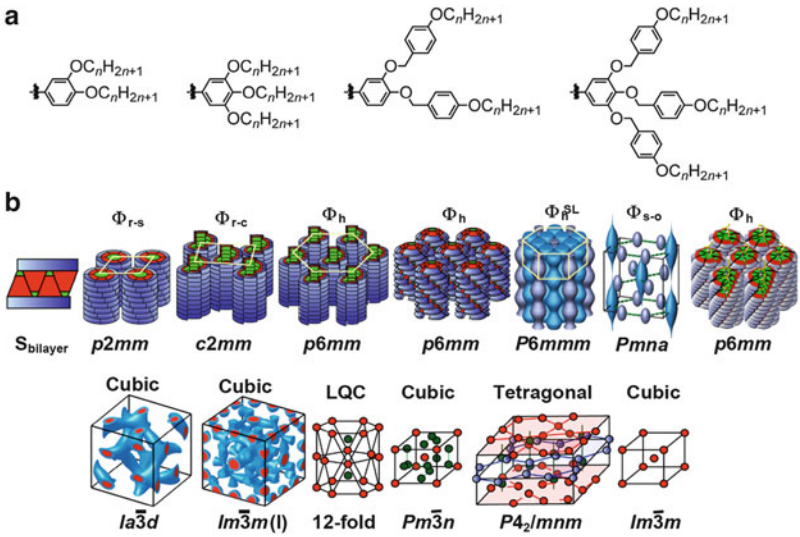

Scheme 2 (**a**) Amphiphilic dendritic building blocks that promote self-organization into (**b**) lattices and quasiperiodic arrays. Part (**b**) adapted with permission from [43]. Copyright 2011 Wiley-VCH Verlag GmbH & Co. KGaA, Weinheim

[21, 106–108]. Because these dendronized polymers self-organize, X-ray diffraction (XRD) studies can provide detailed structural information about the lattice symmetry, diameter of individual dendronized polymer chains, and the internal structure of the polymer. In the columnar lattice, each polymer chain behaves as an individual cylindrical object [109–112]. The polymer backbone is encapsulated in the core of the cylindrical macromolecule, and must adopt a compact conformation that is most likely helical [113, 114]. Drawing or extruding fibers of self-organizable dendronized polymers in the melt induces ordering of the columnar lattice domains so that the cylindrical polymers are aligned along the fiber axis [113–119]. Early XRD studies of oriented fiber samples demonstrated that there is helical order within the individual dendronized polymer chains in a hexagonal columnar (*p6mm*) lattice [113–117]. However, these studies could not definitively show that the polymer backbone adopted a helical conformation, because scattering from the aromatic groups in the dendrons dominates the XRD pattern [113–117]. Self-organization induced by dendrons containing the amphiphilic building blocks in Scheme 2a provides a mechanism to quantitatively characterize the hierarchical process through which dendritic side chains arrange themselves in the cylindrical object through the mesoscale ordering of the nanoscale objects.

Strong corroborating evidence for a helical polymer conformation came from comparative studies of dendronized polymers with either a flexible backbone or rigid helical backbone. Molecular models in which the polymer backbones adopt helical conformations provided the best fit to experimental XRD data for the

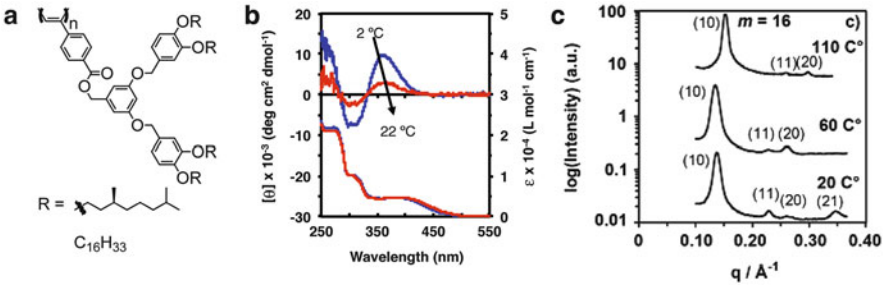

Fig. 1 Selection of helical handedness in self-organizable dendronized polymers. (**a**) Chemical structures of the dendronized poly(phenylacetylene) repeat units. (**b**) Circular dichroism and UV–vis spectra of the polymer with the chiral peripheral groups. (**c**) Plots of the X-ray diffraction data for a representative polymer with achiral peripheral groups, showing that the polymers self-organize in a *p6mm* lattice. Adapted with permission from [122]. Copyright 2005 American Chemical Society

polymer diameter and dendron packing [28]. A proposed helical backbone conformation with frequent helix inversions was also consistent with the apparent contour length of individual dendronized polymers visualized by atomic force microscopy (AFM) [27]. Direct evidence for a helical conformation of the backbone in self-organizable dendronized polymers was obtained through circular dichroism (CD) spectroscopy of dendronized poly(arylacetylene)s in solution [120–125]. *Cis*-Poly(arylacetylene)s adopt helical conformations [126–129], and the handedness of the helix can be determined by chiral side chains [130–135]. Conjugation along the polyene backbone serves as a unique chromophore with which to interrogate conformational order in the dendronized polymers without the interference of the dendrons. Amphiphilic dendrons with chiral alkyl chains at the periphery bias the handedness of the helical backbone, which is observed through the Cotton effect in the long wavelength portion of the CD spectrum (Fig. 1b) [120–123]. Other details of the cylindrical polymer structure (e.g., column diameter and tilt angle of the dendrons) were essentially the same for polymers with achiral or chiral peripheral groups [122], which indicates that all of the dendronized poly (arylacetylene)s contain a helical polymer backbone in the self-organized lattice [120–125, 136]. Furthermore, comparison of the cylindrical polymer dimensions of two large libraries of dendronized polymers (i.e., poly(styrene)s [22] and poly (phenylacetylene)s [136]) suggested that the helical backbone model is general for flexible dendronized polymers that self-organize in columnar lattices [136].

Isomerism along the backbone of *cis*-poly(arylacetylene)s can arise from the different dihedral angles that are possible about the C–C bonds of the main chain. The transoid (*s-trans*) conformation is more extended, whereas the cisoid (*s-cis*) conformation is more compact; and both are helical [126–129]. Degradation of the main chain structure occurs through cyclization reactions of the polyene backbone [126–129, 137–142], which require the polymer to adopt a *cis*-cisoidal conformation. Scheme 3 illustrates the structural transformations that degrade the polymer backbone. 6π-Electrocyclization of triene segments in the backbone occurs under

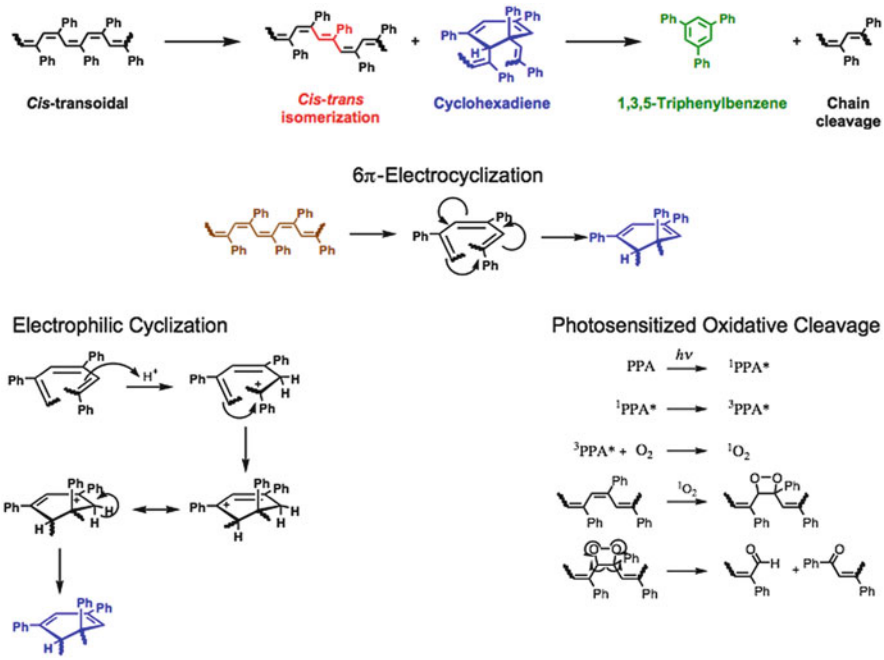

Scheme 3 Mechanistic pathways for structural transformations of *cis*-poly(arylacetylene)s. Adapted with permission from [141]. Copyright 2005 American Chemical Society

all conditions, and cyclization is accelerated in the presence of O_2 or heat [141]. Extrusion of triarylbenzene derivatives with concomitant chain cleavage becomes significant at high temperatures [126–129]. Other oxidation processes also affect the structure of the main chain in solution and in bulk [140, 143]. Self-organizable dendronized poly(arylacetylene)s are less susceptible to 6π-electrocyclization and subsequent chain cleavage by extrusion of triarylbenzene derivatives [122].

Several examples of self-organizable dendronized poly(arylacetylene)s adopt the *cis*-cisoidal conformation in bulk, but most only adopt the *cis*-transoidal conformation. The arrangement of side chains is quite different in the cisoid and transoid conformations, and this difference appears to be a determinant factor of whether or not dendronized poly(arylacetylene)s adopt a cisoidal conformation. Self-organization of the dendronized polymers requires the dendrons to fill space around the polymer backbone to create a nanoscale cylindrical object. If the dendron can adopt a conformation that fills space around the *cis*-cisoidal polymer and achieve the necessary cylindrical shape for self-organization in a columnar lattice, then self-organized arrays of *cis*-cisoidal poly(arylacetylene)s are observed [122, 125]. As the self-organized helical *cis*-cisoidal polymers are heated, the helix begins to unwind or stretch due to cisoid-to-transoid conformational isomerism (Scheme 4) [122, 125]. Thus, at higher temperatures the backbone of the

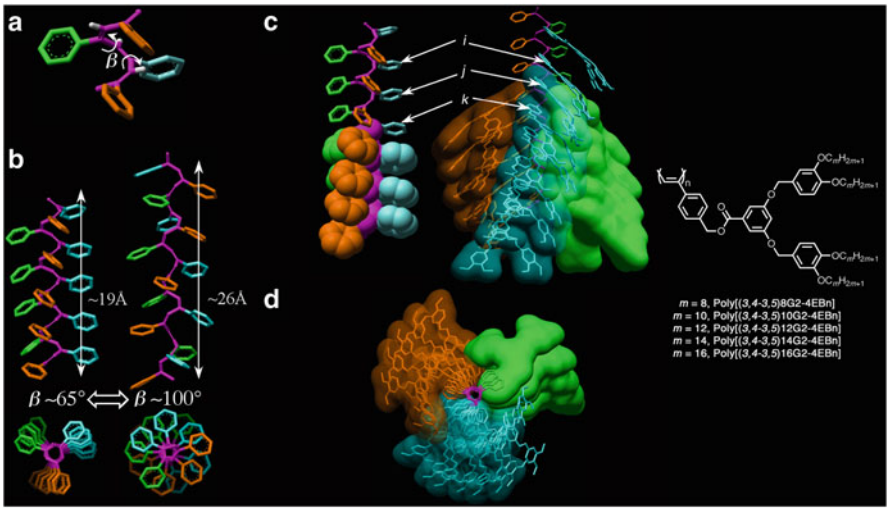

Scheme 4 (**a**–**d**) Models illustrating the thermoreversible cisoid-to-transoid conformational isomerism of dendronized helical poly(arylacetylene)s. Adapted with permission from [122]. Copyright 2005 American Chemical Society

dendronized polymer is more extended. The transition between cisoid and transoid conformations is observed as a first-order transtion in differential scanning calorimetry (DSC) experiments. By avoiding the *cis*-cisoidal conformation, triene sequences in the backbone are less likely to undergo cyclization [122].

Reversible stretching and contraction of the helical polymer backbone encapsulated within a dendritic sheath (Scheme 3) is reminiscent of a mechanical actuator. As the temperature increases, energy is put into the system and converted into motion during the cisoid-to-transoid conformational change. The dendritic sheath restricts the conformational states available to the backbone, and focuses the motion along the length of the cylindrical polymer. Monitoring this motion through XRD studies was possible because the dendronized polymers self-organize in columnar lattices. Oriented fiber samples of the dendronized helical polymers provide structural information about the size of the dendronized polymer as well as the order within the cylindrical object [122–125]. The diameter of the polymer shrinks during the transition from the cisoid conformation to the transoid conformation [122, 125]. At the same time, wide-angle XRD patterns reveal changes in the helical ordering of the dendrons as the conformation of the backbone changes [122]. The arrangement of the dendritic side chains must undergo compensatory conformational changes to accommodate the change in backbone conformation while retaining the cylindrical shape required for packing in a hexagonal (i.e., *p*6*mm*) lattice.

Self-organization of the dendronized polymers contributes a functional element to the behavior of these dendronized helical polymers as materials. In the extruded fiber, the dendronized helical polymers align parallel to the long axis of the fiber

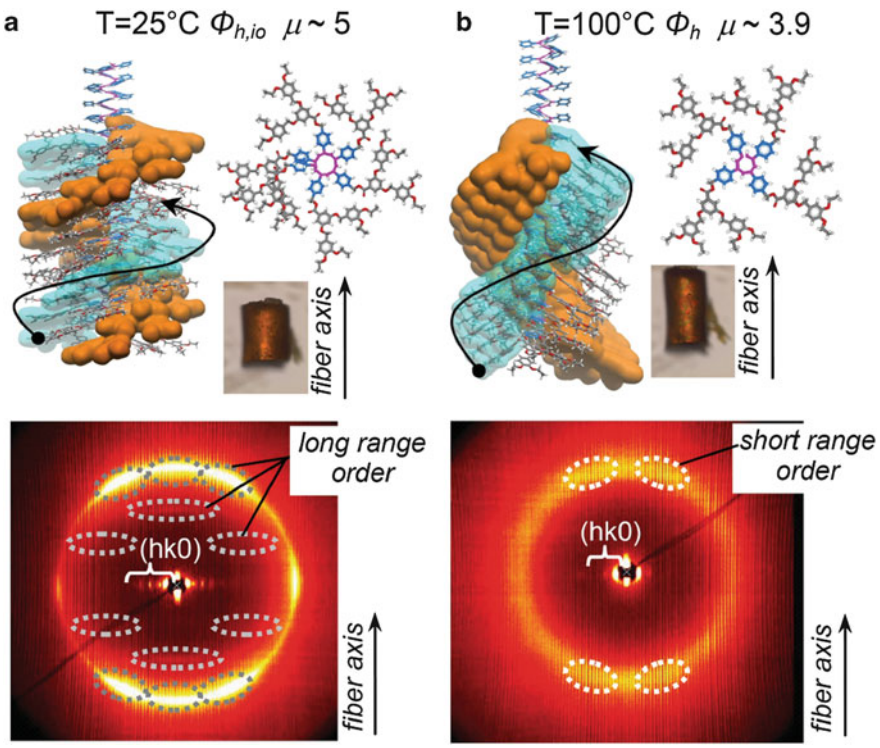

Fig. 2 Molecular models illustrating the structural and conformational changes during the transition from (**a**) cisoid to (**b**) transoid conformation. Optical microscopy images show an extruded fiber sample of the achiral polymer shown in Fig. 1a. Corresponding wide-angle XRD patterns for the cisoid and transoid conformations are shown *below*. Reproduced with permission from [50]. Copyright 2008 American Chemical Society

[122–125]. By orienting the cylindrical polymers along the length of the fiber, the conformational changes and the molecular scale extension/contraction are also expressed in the macroscopic fiber [50]. Anisotropic thermal expansion of the fiber, where the length of the polymer increases proportionally to the extension of the helical backbone, is shown in Fig. 2. The percentage change in the length of the polymer fiber and the percentage change in the molecular length are nearly identical [50]. Anisotropic thermal expansion was also observed from a poly(methacrylate) dendronized with self-assembling dendrons, even before this behavior could be related to the backbone conformation [114], which further validates the helical model for dendronized polymers with flexible backbones.

Macroscopic changes in the extruded fibers of dendronized polymers can be further harnessed to perform work. As the polymer fiber elongates, a force is exerted at the ends of the fiber. That force resulted in the displacement of an object of much greater mass than the dendronized polymer fiber (Fig. 3). This example is one of a few cases where molecular motion in self-organized liquid crystalline

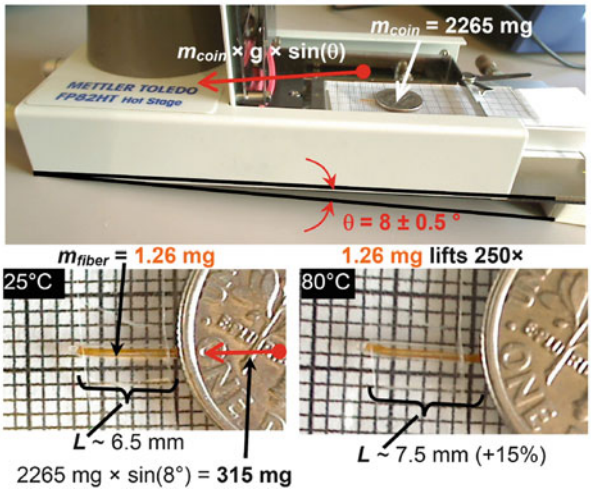

Fig. 3 Experimental setup that demonstrates the macroscopic expansion of the oriented fiber by lifting of a dime on the inclined plane of a Mettler hot stage (*top*). Expanded images collected at 25°C (*bottom left*) and at 80°C (*bottom right*) of the oriented fiber generated from the achiral polymer in Fig. 1a during lifting of 250-times its weight via thermally fueled unwinding of its helix at the cisoid-to-transoid transition. Reproduced with permission from [50]. Copyright 2008 American Chemical Society

materials has been amplified into macroscopic work [50, 144–146]. Unique to the dendronized polymer system [50], though, is the level of detail at which we can understand the nanomechanical function as a series of hierarchical processes.

3 Summary

The complex architecture of polymers substituted on each repeat unit with self-assembling dendrons (i.e., dendronized polymers) has lead to the emergence of nanomechanical function in these materials. Folding of the polymer backbone into a helical conformation is a compromise between the low energy conformations that the backbone will allow and the arrangement of dendrons required to achieve a cylindrical macromolecule, where packing of the dendrons is usually the dominant force. Dendron–backbone combinations that promote the formation of compact helical states can then undergo reversible stretching and contraction of the helical polymer backbone, which is manifest as a molecular-scale mechanical actuator because of the steric volume of the dendrons. Amphiphilic dendrons that promote self-organization of the dendronized polymers into columnar *p6mm* lattices facilitate detailed structural characterization of the molecular-scale events, and provide a mechanism to amplify the motions of individual molecules into macroscopic

events. Cylindrical dendronized polymers orient along the length of a fiber when drawn or extruded, so that stretching and contractions of the helix also occurs along the length of the fiber. Without the high degree of orientation, the anisotropic extension that occurs as the helix unwinds would not be expressed as macroscopic movement and a directional force.

Acknowledgements All of the author's contributions to the work described herein were made as a graduate student at the University of Pennsylvania under the supervision of Prof. Virgil Percec. Financial support from the National Science Foundation to Virgil Percec is gratefully acknowledged.

References

1. Nobelprize.org (1953) The Nobel Prize in Chemistry 1953: Hermann Staudinger. Award ceremony speech. http://www.nobelprize.org/nobel_prizes/chemistry/laureates/1953/press.html
2. Nobelprize.org (1964) Hermann Staudinger – Nobel lecture: macromolecular chemistry. In: Nobel lectures, chemistry 1942–1962. Elsevier, Amsterdam, http://www.nobelprize.org/nobel_prizes/chemistry/laureates/1953/staudinger-lecture.html
3. Pauling L, Corey RB, Branson HR (1951) The structure of proteins: two hydrogen-bonded helical configurations of the polypeptide chain. Proc Natl Acad Sci USA 37(4):205–211. doi:10.1073/pnas.37.4.205
4. Pauling L, Corey RB (1951) The structure of synthetic polypeptides. Proc Natl Acad Sci USA 37(5):241–250. doi:10.1073/pnas.37.5.241
5. Pauling L, Corey RB (1953) Compound helical configurations of polypeptide chains: structure of proteins of the α-keratic type. Nature 171(4341):59–61. doi:10.1038/171059a0
6. Rich A, Crick FHC (1955) The structure of collagen. Nature 176(4489):915–916. doi:10.1038/176915a0
7. Watson JD, Crick FHC (1953) Molecular structure of nucleic acids: a structure for deoxyribose nucleic acid. Nature 171(4356):737–738. doi:10.1038/171737a0
8. Natta G, Pino P, Corradini P, Danusso F, Mantica E, Mazzanti G, Moraglio G (1955) Crystalline high polymers of α-olfeins. J Am Chem Soc 77(6):1708–1710. doi:10.1021/ja01611a109
9. Nakano T, Okamoto Y (2001) Synthetic helical polymers: conformation and function. Chem Rev 101(12):4013–4038. doi:10.1021/cr0000978
10. Hill DJ, Mio MJ, Prince RB, Hughes TS, Moore JS (2001) A field guide to foldamers. Chem Rev 101(12):3893–4012. doi:10.1021/cr990120t
11. Jain V, Cheon K-S, Tang K, Jha S, Green MM (2011) Chiral cooperativity in helical polymers. Isr J Chem 51(10):1067–1074. doi:10.1002/ijch.201100050
12. Kennemur JG, Novak BM (2011) Hierarchical chirality in polycarbodiimides. Isr J Chem 51(10):1041–1051. doi:10.1002/ijch.201100030
13. Aida T, Meijer EW, Stupp SI (2012) Functional supramolecular polymers. Science 335(6070):813–817. doi:10.1126/science.1205962
14. Schwartz E, Le Gac S, Cornelissen JJLM, Notle RJM, Rowan AE (2010) Macromolecular multi-chromophoric scaffolding. Chem Soc Rev 39(5):1576–1599. doi:10.1039/B922160C
15. Yashima E, Maeda K, Iida H, Furusho Y, Nagai K (2009) Helical polymers: synthesis, structures, and functions. Chem Rev 109(11):6102–6211. doi:10.1021/cr900162q
16. Rosen BM, Wilson CJ, Wilson DA, Peterca M, Imam MR, Percec V (2009) Dendron-mediated self-assembly, disassembly, and self-organization of complex systems. Chem Rev 109(11):6275–6540. doi:10.1021/cr900157q

17. Schlüter AD (2005) A covalent chemistry approach to giant macromolecules with cylindrical shape and an engineerable interior and surface. Top Curr Chem 245:151–191. doi:10.1007/b98168
18. Frauenrath H (2005) Dendronized polymers–buiding a new bridge from molecules to nanoscopic objects. Prog Polym Sci 30(3–4):325–384. doi:10.1016/j.progpolymsci.2005.01.011
19. Chen Y, Xiong X (2010) Tailoring dendronized polymers. Chem Commun 46 (28):5049–5060. doi:10.1039/B922777F
20. Kirchhoff PM, Tomalia DA (1987) Rod-shaped dendrimer. US Patent 4,694,064
21. Percec V, Ahn C-H, Ungar G, Yeardley DJP, Möller M, Sheiko SS (1998) Controlling polymer shape through the self-assembly of dendritic side-groups. Nature 391 (6663):161–164. doi:10.1038/34384
22. Percec V, Ahn C-H, Cho W-D, Jamieson AM, Kim J, Leman T, Schmidt M, Gerle M, Möller M, Prokhorova SA, Sheiko SS, Cheng SZD, Zhang A, Ungar G, Yeardley DJP (1998) Visualizable cylindrical macromolecules with controlled stiffness from backbones containing libraries of self-assembling dendritic side groups. J Am Chem Soc 120(34):8619–8631. doi:10.1021/ja981211v
23. Stocker W, Schürmann BL, Rabe JP, Förster S, Lindner P, Neubert I, Schlüter A-D (1998) A dendritic nanocylinder: shape control through implementation of steric strain. Adv Mater 10 (10):793–797. doi:10.1002/(SICI)1521-4095(199807)10:10<793::AID-ADMA793>3.0.CO;2-F
24. Stocker W, Karakaya B, Schürmann BL, Rabe JP, Schlüter AD (1998) Ordered dendritic nanorods with a poly(*p*-phenylene) backbone. J Am Chem Soc 120(37):7691–7695. doi:10.1021/ja980151q
25. Zhuang W, Kasëmi E, Ding Y, Kröger M, Schlüter AD, Rabe JP (2008) Self-folding of charged single dendronized polymers. Adv Mater 20(17):3204–3210. doi:10.1002/adma.200800168
26. Das J, Fréchet JMJ, Chakraborty AK (2009) Self-assembly of dendronized polymers. J Phys Chem B 113(42):13768–13775. doi:10.1021/jp902927p
27. Prokhorova SA, Sheiko SS, Möller M, Ahn C-H, Percec V (1998) Molecular imaging of monodendron jacketed linear polymers by scanning force microscopy. Macromol Rapid Commun 19(7):359–366. doi:10.1002/(SICI)1521-3927(19980701)19:7<359::AID-MARC359>3.0.CO;2-T
28. Percec V, Schlueter D, Ronda JC, Johansson G, Ungar G, Zhou JP (1996) Tubular architectures from polymers with tapered side groups. Assembly of side groups via a rigid helical chain conformation induced via self-assembly of side groups. Macromolecules 29 (5):1464–1472. doi:10.1021/ma951244k
29. Ding Y, Öttinger HC, Schlüter AD, Kröger M (2007) From atomistic simulation to the dynamics, structure and helical network formation of dendronized polymers: The Janus chain model. J Chem Phys 127(9):094904. doi:10.1063/1.2772601
30. Rodríguez-Ropero F, Canales M, Zanuy D, Zhang A, Schlüter D, Alemán C (2009) Helical dendronized polymers with chiral second-generation dendrons: Atomistic view and driving forces for structure formation. J Phys Chem B 113(45):14868–14876. doi:10.1021/jp903782f
31. Ding Y, Kröger M (2010) Rubik cylinder model for dendronized polymers. J Comput Theor Nanosci 7(4):661–674. doi:10.1166/jctn.2010.1410
32. Bertran O, Zhang B, Schlüter AD, Halperin A, Kröger M, Alemán C (2012) Computer simulation of dendronized polymers: Organization and characterization at the atomistic level. RSC Adv 3(1):126–140. doi:10.1039/C2RA22034B
33. Bertran O, Zhang B, Schlüter AD, Kröger M, Alemán C (2013) Computer simulation of fifth generation dendronized polymers: impact of charge on internal organization. J Phys Chem B 117(19):6007–6017. doi:10.1021/jp402695g
34. Browne W, Geissler PL (2010) The susceptibility of α-helical secondary structure to steric strain: coarse-grained simulation of dendronized polypeptides. J Chem Phys 133(14):145102. doi:10.1063/1.3498780

35. Rudick JG, Percec V (2007) Helical chirality in dendronized polyarylacetylenes. New J Chem 31(7):1083–1096. doi:10.1039/B616449H
36. Rudick JG, Percec V (2008) Induced helical backbone conformations of self-organizable dendronized polymers. Acc Chem Res 41(12):1641–1652. doi:10.1021/ar800086w
37. Tian Y, Kamata K, Yoshida H, Iyoda T (2006) Synthesis, liquid-crystalline properties, and supramolecular nanostructures of dendronized poly(isocyanide)s and their precursors. Chem Eur J 12(2):584–591. doi:10.1002/chem.200500868
38. Zhao H, Sanda F, Masuda T (2006) Novel optically acitve polyacetylenes: synthesis and helical conformation of L-lysine-dendronized poly(phenylacetylene). Macromol Chem Phys 207(21):1921–1926. doi:10.1002/macp.200600259
39. Zhang A, Rodríguez-Ropero F, Zanuy D, Alemán C, Meijer EW, Schlüter AD (2008) A rigid, chiral, dendronized polymer with a thermally stable, right-handed helical conformation. Chem Eur J 14(23):6924–6934. doi:10.1002/chem.200800325
40. Zhang A (2008) High-molar-mass, first and second generation L-lysine dendronized polymethacrylates. Macromol Rapid Commun 29(10):839–845. doi:10.1002/marc.200800145
41. Liu K, Zhang X, Tao X, Yan J, Kuang G, Li W, Zhang A (2012) Lysine-based dendronized polymers with preferred chirality. Polym Chem 3(10):2708–2711. doi:10.1039/C2PY20510F
42. Kajitani T, Lin H, Nagai K, Okoshi K, Onouchi H, Yashima E (2009) Helical polyisocyanides with fan-shaped pendants. Macromolecules 42(2):560–567. doi:10.1021/ma802345g
43. Percec V, Leowanawat P (2011) Why are biological systems homochiral. Isr J Chem 51(10):1107–1117. doi:10.1002/ijch.201100152
44. Roche C, Percec V (2013) Complex adaptable systems based on self-assembling dendrimers and dendrons: Toward dynamic materials. Isr J Chem 53(1–2):30–44. doi:10.1002/ijch.201200099
45. Rosen BM, Roche C, Percec V (2013) Self-assembly of dendritic dipeptides as a model of chiral selection in primitive biological systems. Top Curr Chem 333:213–254. doi:10.1007/128_2012_398
46. Gao M, Jia X, Kuang G, Li D, Wei Y (2009) Thermo- and pH-resonsive dendronized copolymers of styrene and maleic anhydride pendant with poly(amidoamine)dendrons as side groups. Macromolecules 42(12):4273–4281. doi:10.1021/ma900085j
47. Laurino P, Kikkeri R, Azzouz N, Seeberger PH (2011) Detection of bacteria using glycodendronized polylysine prepared by continuous flow photopolymerization. Nano Lett 11(1):73–78. doi:10.1021/nl102821f
48. Grotzky A, Nauser T, Erdogan H, Schlüter AD, Walde P (2012) A fluorescently labeled dendronized polymer-enzyme conjugate carrying copies of two different types of active enzymes. J Am Chem Soc 134(28):11392–11395. doi:10.1021/ja304837f
49. Fuhrmann G, Grotzky A, Lukić R, Matoori S, Luciani P, Yu H, Zhang B, Walde P, Schlüter AD, Gauthier MA, Leroux J-C (2013) Sustained gastrointestinal activity of dendronized polymer-enzyme conjugates. Nat Chem 5(7):582–589. doi:10.1038/nchem.1675
50. Percec V, Rudick JG, Peterca M, Heiney PA (2008) Nanomechanical function from self-organizable dendronized helical polyphenylacetylenes. J Am Chem Soc 130(23):7503–7508. doi:10.1021/ja801863e
51. Rudick JG, Percec V (2008) Nanomechanical function made possible by suppressing structural transformations of polyarylacetylenes. Macromol Chem Phys 209(17):1759–1768. doi:10.1002/macp.200800271
52. Feringa BL, Browne WR (2008) Nanomechanics: macromolecules flex their muscles. Nat Nanotechnol 3(7):383–384. doi:10.1038/nnano.2008.194
53. Donnio B, Buathong S, Bury I, Guillon D (2007) Liquid crystalline dendrimers. Chem Soc Rev 36(9):1495–1513. doi:10.1039/b605531c
54. Ponomarenko SA, Boiko NI, Shibaev VP (2001) Liquid-crystalline dendrimers. Polym Sci Ser C 43(1):1–45

55. Percec V, Heck J (1991) Liquid crystalline polymers containing mesogenic units based on half-disc and rod-like moieties. I. Synthesis and characterization of 4-(11-undecan-1-yloxy)-4-[3,4,5-tri(p-n-dodecan-1-yloxybenzyloxy)benzoate]biphenyl side groups. J Polym Sci A Polym Chem 29(4):591–597. doi:10.1002/pola.1991.080290416
56. Malthête J, Collet A, Levelut A-M (1989) Mesogens containing the DOBOB group. Liq Cryst 5(1):123–131. doi:10.1080/02678298908026355
57. Lattermann G (1989) A liquid-crystalline cyclam derivative. Liq Cryst 6(5):619–625. doi:10.1080/02678298908034181
58. Malthête J, Levelut A-M (1991) Mesophase formed by diabolo-like molecules. Adv Mater 3(2):94–96. doi:10.1002/adma.19910030204
59. Lin C, Rigsdorf H, Ebert M, Kleppinger R, Wendorff JH (1989) Structural variations of liquid crystalline polymers with phasmidic-type mesogens. Liq Cryst 5(6):1841–1847. doi:10.1080/02678298908045692
60. Percec V, Heck J (1990) Liquid crystalline polymers containing mesogenic units based on half-disc and rod-like moieties. 2. Synthesis and characterization of poly{2-[3,4,5-tri[*p*-(*n*-dodecan-1-yloxy)benzyloxy]benzoate]-7-[*p*-11-undecan-1-yloxy)benzoate]naphthalene]methyl siloxane}. Polym Bull 24(3):255–262. doi:10.1007/BF00306572
61. Hudson SD, Jung H-T, Percec V, Cho W-D, Johansson G, Ungar G, Balagurusamy VSK (1997) Direct visualization of individual cylindrical and spherical supramolecular dendrimers. Science 278(5337):449–452. doi:10.1126/science.278.5337.449
62. Balagurusamy VSK, Ungar G, Percec V, Johansson G (1997) Rational design of the first spherical supramolecular dendrimers self-organized in a novel thermotropic cubic liquid-crystalline phase and the determination of their shape by X-ray analysis. J Am Chem Soc 119(7):1539–1555. doi:10.1021/ja963295i
63. Percec V, Cho W-D, Mosier PE, Ungar G, Yeardley DJP (1998) Structural analysis of cylindrical and spherical supramolecular dendrimers quantifies the concept of monodendron shape control by generation number. J Am Chem Soc 120(43):11061–11070. doi:10.1021/ja9819007
64. Percec V, Cho W-D, Ungar G (2000) Increasing the diameter of cylindrical and spherical supramolecular dendrimers by decreasing the solid angle of their monodendrons via periphery functionalization. J Am Chem Soc 122(42):10273–10281. doi:10.1021/ja0024643
65. Percec V, Cho W-D, Möller M, Prokhorova SA, Ungar G, Yeardley DJP (2000) Design and structural analysis of the first spherical monodendron self-organizable in a cubic lattice. J Am Chem Soc 122(17):4249–4250. doi:10.1021/ja9943400
66. Percec V, Cho W-D, Ungar G, Yeardley DJP (2000) From molecular flat tapers, discs, and cones to supramolecular cylinders and spheres using Fréchet-type monodendrons modified on their periphery. Angew Chem Int Ed 39(9):1597–1602. doi:10.1002/(SICI)1521-3773(20000502)39:9<1597::AID-ANIE1597>3.0.CO;2-I
67. Percec V, Cho W-D, Ungar G, Yeardley DJP (2001) Synthesis and structural analysis of two constitutional isomeric libraries of AB_2-based monodendrons and supramolecular dendrimers. J Am Chem Soc 123(7):1302–1315. doi:10.1021/ja0037771
68. Ungar G, Liu Y, Zeng X, Percec V, Cho W-D (2003) Giant supramolecular liquid crystal lattice. Science 299(5610):1208–1211. doi:10.1126/science.1078849
69. Percec V, Mitchell CM, Cho W-D, Uchida S, Glodde M, Ungar G, Zeng X, Liu Y, Balagurusamy VSK, Heiney PA (2004) Designing libraries of first generation AB_3 and AB_2 self-assembling dendrons via the primary structure generated from combinations of $(AB)_y$-AB_3 and $(AB)_y$-AB_2 building blocks. J Am Chem Soc 126(19):6078–6094. doi:10.1021/ja049846j
70. Rosen BM, Wilson DA, Wilson CJ, Peterca M, Won BC, Huang C, Lipski LR, Zeng X, Ungar G, Heiney PA, Percec V (2009) Predicting the structure of supramolecular dendrimers via the analysis of libraries of AB_3 and constitutional isomeric AB_2 biphenylpropyl ether self-assembling dendrons. J Am Chem Soc 131(47):17500–17521. doi:10.1021/ja907882n

71. Zeng X, Ungar G, Liu Y, Percec V, Dulcey AE, Hobbs JK (2004) Supramolecular dendritic liquid quasicrystals. Nature 428(6979):157–160. doi:10.1038/nature02368
72. Percec V, Dulcey AE, Balagurusamy VSK, Miura Y, Smidrkal J, Peterca M, Nummelin S, Edlund U, Hudson SD, Heiney PA, Duan H, Magonov SN, Vinogradov SA (2004) Self-assembly of amphiphilic dendritic dipeptides into helical pores. Nature 430(7001):764–768. doi:10.1038/nature02770
73. Percec V, Dulcey AE, Peterca M, Ilies M, Ladislaw J, Rosen BM, Edlund U, Heiney PA (2005) The internal structure of helical pores self-assembled from dendritic dipeptides is stereochemically programmed and allosterically regulated. Angew Chem Int Ed 44 (40):6516–6521. doi:10.1002/anie.200501331
74. Percec V, Dulcey AE, Peterca M, Ilies M, Sienkowska MJ, Heiney PA (2005) Programming the internal structure and stability of helical pores self-assembled from dendritic dipeptides via the protective groups of the peptide. J Am Chem Soc 127(50):17902–17909. doi:10.1021/ja056313h
75. Percec V, Dulcey AE, Peterca M, Ilies M, Nummelin S, Sienkowska MJ, Heiney PA (2006) Principles of self-assembly of helical pores from dendritic dipeptides. Proc Natl Acad Sci USA 103(8):2518–2523. doi:10.1073/pnas.0509676103
76. Peterca M, Percec V, Dulcey AE, Nummelin S, Korey S, Ilies M, Heiney PA (2006) Self-assembly, structural, and retrostructural analysis of dendritic dipeptide pores undergoing reversible circular to elliptical shape change. J Am Chem Soc 128(20):6713–6720. doi:10.1021/ja0611902
77. Percec V, Dulcey AE, Peterca M, Adelman P, Samant R, Balagurusamy VSK, Heiney PA (2007) Helical pores self-assembled from homochiral dendritic dipeptides based on L-Tyr and nonpolar alpha-amino acids. J Am Chem Soc 129(18):5992–6002. doi:10.1021/ja071088k
78. Percec V, Peterca M, Dulcey AE, Imam MR, Hudson SD, Nummelin S, Adelman P, Heiney PA (2008) Hollow spherical supramolecular dendrimers. J Am Chem Soc 130 (39):13079–13094. doi:10.1021/ja8034703
79. Rosen BM, Peterca M, Morimitsu K, Dulcey AE, Leowanawat P, Resmerita A-M, Imam MR, Percec V (2011) Programming the supramolecular helical polymerization of dendritic dipeptides via the stereochemical information of the dipeptide. J Am Chem Soc 133 (13):5135–5151. doi:10.1021/ja200280h
80. Percec V, Peterca M, Sienkowska MJ, Ilies MA, Aqad E, Smidrkal J, Heiney PA (2006) Synthesis and retrostructural analysis of libraries of AB_3 and constitutional isomeric AB_2 phenylpropyl ether-based supramolecular dendrimers. J Am Chem Soc 128(10):3324–3334. doi:10.1021/ja060062a
81. Percec V, Won BC, Peterca M, Heiney PA (2007) Expanding the structural diversity of self-assembling dendrons and supramolecular dendrimers via complex building blocks. J Am Chem Soc 129(36):11265–11278. doi:10.1021/ja073714j
82. Peterca M, Percec V, Imam MR, Leowanawat P, Morimitsu K, Heiney PA (2008) Molecular structure of helical supramolecular dendrimers. J Am Chem Soc 130(44):14840–14852. doi:10.1021/ja806524m
83. Percec V, Glodde M, Bera TK, Miura Y, Shiyanovskaya I, Singer KD, Balagurusamy VSK, Heiney PA, Schnell I, Rapp A, Spiess H-W, Hudson SD, Duan H (2002) Self-organization of supramolecular helical dendrimers into complex electronic materials. Nature 419 (6905):384–387. doi:10.1038/nature01072
84. Shiyanovskaya I, Singer KD, Percec V, Bera TK, Miura Y, Glodde M (2003) Charge transport in hexagonal columnar liquid crystals self-organized from supramolecular cylinders based on acene-functionalized dendrons. Phys Rev B Condens Matter Mater Phys 67 (3):035204. doi:10.1103/PhysRevB.67.035204
85. Percec V, Glodde M, Peterca M, Rapp A, Schnell I, Spiess HW, Bera TK, Miura Y, Balagurusamy VSK, Aqad E, Heiney PA (2006) Self-assembly of semifluorinated dendrons

attached to electron-donor groups mediates their π-stacking via a helical pyramidal column. Chem Eur J 12(24):6298–6314. doi:10.1002/chem.200501195
86. Percec V, Aqad E, Peterca M, Imam MR, Glodde M, Bera TK, Miura Y, Balagurusamy VSK, Ewbank PC, Würthner F, Heiney PA (2007) Self-assembly of semifluorinated minidendrons attached to electron-acceptor groups into pyramidal columns. Chem Eur J 13(12):3330–3345. doi:10.1002/chem.200600901
87. Percec V, Hudson SD, Peterca M, Leowanawat P, Aqad E, Graf R, Spiess HW, Zeng X, Ungar G, Heiney PA (2011) Self-repairing complex helical columns generated via kinetically controlled self-assembly of dendronized perylene bisimides. J Am Chem Soc 133 (45):18479–18494. doi:10.1021/ja208501d
88. Percec V, Peterca M, Tadjiev T, Zeng X, Ungar G, Leowanawat P, Aqad E, Imam MR, Rosen BM, Akbey U, Graf R, Sekharan S, Sebestiani D, Spiess HW, Heiney PA, Hudson SD (2011) Self-assembly of dendronized perylene bisimides into complex helical columns. J Am Chem Soc 133(31):12197–12219. doi:10.1021/ja204366b
89. Percec V, Sun H-J, Leowanawat P, Peterca M, Graf R, Spiess HW, Zeng X, Ungar G, Heiney PA (2013) Transformation from kinetically into thermodynamically controlled self-organization of complex helical columns with 3D periodicity assembled from dendronized perylene bisimides. J Am Chem Soc 135(10):4129–4148. doi:10.1021/ja400639q
90. Lai CK, Serrette AG, Swager TM (1992) Discotic bimetallomesogens: building blocks for the formation of new columnar arrangements of transition metals. J Am Chem Soc 114 (5):1887–1889. doi:10.1021/ja00031a057
91. Serrette AG, Swager TM (1993) Controlling intermolecular associations with molecular superstructure: Polar discotic linear chain phases. J Am Chem Soc 115(19):8879–8880. doi:10.1021/ja00072a067
92. Barberá J, Iglesias R, Serrano JL, Sierra T, de la Fuente MR, Palacios B, Pérez-Jubindo MA, Vázquez JT (1998) Switchable columnar metallomesogens. New helical self-assembling systems. J Am Chem Soc 120(12):2908–2918. doi:10.1021/ja9735012
93. Sato K, Itoh Y, Aida T (2011) Columnarly assembled liquid-crystalline peptidic macrocycles unidirectionally orientable over a large area by an electric field. J Am Chem Soc 133 (35):13767–13769. doi:10.1021/ja203894r
94. Cameron JH, Facher A, Lattermann G, Diele S (1997) Poly(propyleneimine) dendromesogens with hexagonal columnar mesophase. Adv Mater 9(5):398–403. doi:10.1002/adma.19970090507
95. Percec V, Rudick JG, Peterca M, Yurchenko ME, Smidrkal J, Heiney PA (2008) Supramolecular structural diversity among first-generation hybrid dendrimers and twin dendrons. Chem Eur J 14(11):3355–3362. doi:10.1002/chem.200701658
96. Percec V, Imam MR, Peterca M, Cho W-D, Heiney PA (2009) Self-assembling dendronized dendrimers. Isr J Chem 49(1):55–70. doi:10.1560/IJC.49.1.5
97. Maringa N, Lenoble J, Donnio B, Guillon D, Deschenaux R (2008) Liquid-crystalline methanofullerodendrimers which display columnar mesomorphism. J Mater Chem 18 (13):1524–1534. doi:10.1039/B717105F
98. Deschenaux R, Donnio B, Guillon D (2007) Liquid-crystalline fullerodendrimers. New J Chem 31(7):1064–1073. doi:10.1039/B617671M
99. Matsuo Y, Muramatsu A, Kamikawa Y, Kato T, Nakamura E (2006) Synthesis and structural, electrochemical, and stacking properties of conical molecules possessing buckyferrocene on the apex. J Am Chem Soc 128(30):9586–9587. doi:10.1021/ja062757h
100. Kasdorf O, Kitzerow H-S, Lenoble-Zwahlen J, Deschenaux R (2010) Influence of a mesogenic dendrimer on the morphology of polymer-fullerene composites for photovoltaics. Jpn J Appl Phys 49:01AF01. doi:10.1143/JJAP.49.01AF01
101. Lenoble J, Maringa N, Campidelli S, Donnio B, Guillon D, Deschenaux R (2006) Liquid-crystalline fullerodendrimers which display columnar phases. Org Lett 8(9):1851–1854. doi:10.1021/ol0603920

102. Lenoble J, Campidelli S, Maringa N, Donnio B, Guillon D, Yevlampieva N, Deschenaux R (2007) Liquid-crystalline Janus-type fullerodendrimers displaying tunable smectic-columnar mesomorphism. J Am Chem Soc 129(32):9941–9952. doi:10.1021/ja071012o
103. Cordovilla C, Coco S, Espinet P, Donnio B (2010) Liquid-crystalline self-organization of isocyanide-containing dendrimers induced by coordination to gold(I) fragments. J Am Chem Soc 132(4):1424–1431. doi:10.1021/ja909435e
104. Kanie K, Matsubara M, Zeng X, Liu F, Ungar G, Nakamura H, Muramatsu A (2011) Simple cubic packing of gold nanoparticles through rational design of their dendrimeric corona. J Am Chem Soc 134(2):808–811. doi:10.1021/ja2095816
105. Percec V, Lee M, Heck J, Blackwell HE, Ungar G, Alvarez-Castillo A (1992) Re-entrant isotropic phase in a supramolecular disc-like oligomer of 4-[3,4,5-tris(*n*-dodecanyloxy) benzoyloxy]-4-[(2-vinyloxy) ethoxy]biphenyl. J Mater Chem 2(9):931–938. doi:10.1039/JM9920200931
106. Yeardley DJP, Ungar G, Percec V, Holerca MN, Johansson G (2000) Spherical supramolecular minidendrimers self-organized in an inverse micellar-like thermotropic body-centered cubic liquid crystalline phase. J Am Chem Soc 122(8):1684–1689. doi:10.1021/ja993915q
107. Percec V, Holerca MN, Uchida S, Yeardley DJP, Ungar G (2001) Poly(oxazoline)s with tapered minidendritic side groups as models for the design of synthetic macromolecules with tertiary structure. A demonstration of the limitations of living polymerization in the design of 3-D structures based on single polymer chains. Biomacromolecules 2(3):729–740. doi:10.1021/bm015559l
108. Duan H, Hudson SD, Ungar G, Holerca MN, Percec V (2001) Definitive support by transmission electron microscopy, electron diffraction, and electron density maps for the formation of a BCC lattice from poly{*N*-[3,4,5-tris(*n*-dodecan-l-yloxy)benzoyl] ethyleneimine. Chem Eur J 7(19):4134–4141. doi:10.1002/1521-3765(20011001)7:19<4134::AID-CHEM4134>3.0.CO;2-W
109. Percec V, Heck J, Lee M, Ungar G, Alvarez-Castillo A (1992) Poly{2-vinyloxyethyl 3,4,5-tris[4-(*n*-dodecanyloxy) benzyloxy]benzoate}: a self-assembled supramolecular polymer similar to tobacco mosaic virus. J Mater Chem 2(10):1033–1039. doi:10.1039/JM9920201033
110. Percec V, Heck J, Tomazos D, Falkenberg F, Blackwell H, Ungar G (1993) Self-assembly of taper-shaped monoesters of oligo(ethylene oxide) with 3,4,5-tris(*p*-dodecyloxybenzyloxy) benzoic acid and of their polymethacrylates into tubular supramolecular architectures displaying a columnar mesophase. J Chem Soc Perkin Trans 1(22):2799–2811. doi:10.1039/P19930002799
111. Percec V, Heck JA, Tomazos D, Ungar G (1993) The influence of the complexation of sodium and lithium triflate on the self-assembly of tubular-supramolecular architectures displaying a columnar mesophase based on taper-shaped monoesters of oligoethylene oxide with 3,4,5-tris[*p*-(*n*-dodecan-1-yloxy)benzyloxy]benzoic acid and of their polymethacrylates. J Chem Soc Perkin Trans 2(12):2381–2388. doi:10.1039/P29930002381
112. Percec V, Tomazos D, Heck J, Blackwell H, Ungar G (1994) Self-assembly of taper-shaped monoesters of oligo(ethylene oxide) with 3,4,5-tris(*n*-dodecan-1-yloxy)benzoic acid and of their polymethacrylates into tubular supramolecular architectures displaying a columnar hexagonal mesophase. J Chem Soc Perkin Trans 2(1):31–44. doi:10.1039/P29940000031
113. Kwon YK, Chvalun S, Schneider A-I, Blackwell J, Percec V, Heck JA (1994) Supramolecular tubular structures of a polymethacrylate with tapered side groups in aligned hexagonal phases. Macromolecules 27(21):6129–6132. doi:10.1021/ma00099a029
114. Kwon YK, Chvalun S, Blackwell J, Percec V, Heck JA (1995) Effect of temperature on the supramolecular tubular structure in oriented fibers of a poly(methacrylate) with tapered side groups. Macromolecules 28(5):1552–1558. doi:10.1021/ma00109a029
115. Kwon YK, Danko C, Chvalun S, Blackwell J, Heck JA, Percec V (1994) Comparison of the supramolecular structures formed by a polymethacrylate with a highly tapered side chain and its monomeric precursor. Macromol Symp 87(1):103–114. doi:10.1002/masy.19940870113

116. Chvalun SN, Blackwell J, Kwon YK, Percec V (1997) Small angle X-ray analysis of the effect of temperature on the self-assembling columnar structures formed by a polymethacrylate with highly tapered side groups and by one of its low molar mass precursors. Macromol Symp 118(1):663–675. doi:10.1002/masy.19971180186
117. Chvalun SN, Blackwell J, Cho JD, Kwon YK, Percec V, Heck JA (1998) X-ray analysis of the internal rearrangement of the self-assembling columnar structure formed by a highly tapered molecule. Polymer 39(19):4515–4522. doi:10.1016/S0032-3861(97)10131-8
118. Chvalun SN, Blackwell J, Cho JD, Bykova IV, Percec V (1999) A second columnar liquid crystalline phase formed by polymers with highly tapered side chains. Acta Polym 50 (1):51–66. doi:10.1002/(SICI)1521-4044(19990101)50:1<51::AID-APOL51>3.0.CO;2-0
119. Feng S, Xiong X, Zhang G, Xia N, Chen Y, Wang W (2009) Hierarchical structure in oriented fibers of a dendronized polymer. Macromolecules 42(1):281–287. doi:10.1021/ma8015932
120. Schenning APHJ, Fransen M, Meijer EW (2002) Side-chain-functionalized polyacetylenes, 1 liquid crystalline and stereomutational properties. Macromol Rapid Commun 23 (4):265–270. doi:10.1002/1521-3927(20020301)23:4<265::AID-MARC265>3.0.CO;2-5
121. Percec V, Obata M, Rudick JG, De BB, Glodde M, Bera TK, Magonov SN, Balagurusamy VSK, Heiney PA (2002) Synthesis, structural analysis, and visualization of poly(2-ethynyl-9-substituted carbazole)s and poly (3-ethynyl-9-substituted carbazole)s containing chiral and achiral minidendritic substituents. J Polym Sci A Polym Chem 40(20):3509–3533. doi:10.1002/pola.10458
122. Percec V, Rudick JG, Peterca M, Wagner M, Obata M, Mitchell CM, Cho W-D, Balagurusamy VSK, Heiney PA (2005) Thermoreversible cis–cisoidal to cis–transoidal isomerization of helical dendronized polyphenylacetylenes. J Am Chem Soc 127 (43):15257–15264. doi:10.1021/ja055406w
123. Percec V, Aqad E, Peterca M, Rudick JG, Lemon L, Ronda JC, De BB, Heiney PA, Meijer EW (2006) Steric communication of chiral information observed in dendronized polyacetylenes. J Am Chem Soc 128(50):16365–16372. doi:10.1021/ja0665848
124. Percec V, Rudick JG, Peterca M, Aqad E, Imam MR, Heiney PA (2007) Synthesis, structural, and retrostructural analysis of helical dendronized poly(1-naphthylacetylene)s. J Polym Sci A Polym Chem 45(21):4974–4987. doi:10.1002/pola.22265
125. Percec V, Peterca M, Rudick JG, Aqad E, Imam MR, Heiney PA (2007) Self-assembling phenylpropyl ether dendronized helical polyphenylacetylenes. Chem Eur J 13 (34):9572–9581. doi:10.1002/chem.200701008
126. Simionescu CI, Percec V, Dumitrescu S (1977) Polymerization of acetylenic derivatives. XXX. Isomers of polyphenylacetylene. J Polym Sci Polym Chem Ed 15(10):2497–2509. doi:10.1002/pol.1977.170151018
127. Simionescu CI, Percec V (1979) Polypentadeuterophenylacetylene isomers. J Polym Sci Polym Lett Ed 17:421–429. doi:10.1002/pol.1979.130170705
128. Simionescu CI, Percec V (1980) Polyarylacetylenes: structure and properties. J Polym Sci C Polym Symp 67:43–71. doi:10.1002/polc.5070670105
129. Simionescu CI, Percec V (1980) Thermal cis–trans isomerization of cis-transoidal polyphenylacetylene. J Polym Sci Polym Chem Ed 18:147–155. doi:10.1002/pol.1980.170180114
130. Aoki T, Kokai M, K-i S, Oikawa E (1993) Cheiral helical conformation of polyphenylacetylene having optically-active bulky substituent. Chem Lett 22(12):2009–2012. doi:10.1246/cl.1993.2009
131. Yashima E, Maeda K, Okamoto Y (1999) Memory of macromolecular helicity assisted by interaction with achiral small molecules. Nature 399(6735):449–451. doi:10.1038/20900
132. Louzao I, Seco JM, Quiñoá E, Riguera R (2010) Control of the helicity of poly (phenylacetylene)s: from the conformation of the pendant to the chirality of the backbone. Angew Chem Int Ed 49(8):1430–1433. doi:10.1002/anie.200905222

133. Freire F, Seco JM, Quiñoá E, Riguera R (2011) Chiral amplification and helical-sense tuning by mono- and divalent metals on dynamic helical polymers. Angew Chem Int Ed 50 (49):11692–11695. doi:10.1002/anie.201105769
134. Freire F, Seco JM, Quiñoá E, Riguera R (2012) Nanospheres with tunable size and chirality from helical polymer–metal complexes. J Am Chem Soc 134(47):19374–19383. doi:10.1021/ja3061112
135. Leiras S, Freire F, Seco JM, Quiñoá E, Riguera R (2013) Controlled modulation of the helical sense and the elongation of poly(phenylacetylene)s by polar and donor effects. Chem Sci 4 (7):2735–2743. doi:10.1039/C3SC50835H
136. Percec V, Rudick JG, Peterca M, Staley SR, Wagner M, Obata M, Mitchell CM, Cho W-D, Balagurusamy VSK, Lowe JN, Glodde M, Weichold O, Chung KJ, Ghionni N, Magonov SN, Heiney PA (2006) Synthesis, structural analysis, and visualization of a library of dendronized polyphenylacetylenes. Chem Eur J 12(22):5731–5746. doi:10.1002/chem.200600009
137. Percec V, Rinaldi PL (1983) A ^{13}C-NMR study of the microstrucure of polyphenylacetylenes prepared with $MoCl_5$ and WCl_6. Polym Bull 9(10–11):548–555. doi:10.1007/BF00265243
138. Percec V, Rinaldi PL (1983) ^{13}C-NMR studies of thermally isomerized polyphenylacetylenes prepared with $MoCl_5$ and WCl_6 catalysts. Polym Bull 9(12):582–587. doi:10.1007/BF00307882
139. Percec V (1983) Microstructure of polyphenylacetylene obtained by $MoCl_5$ and WCl_6 type catalysts. Polym Bull 10(1–2):1–7. doi:10.1007/BF00263230
140. Percec V, Rudick JG, Nombel P, Buchowicz W (2002) Dramatic decrease of the cis content and molecular weight of *cis*-transoidal polyphenylacetylene at 23°C in solutions prepared in air. J Polym Sci A Polym Chem 40(19):3212–3220. doi:10.1002/pola.10421
141. Percec V, Rudick JG (2005) Independent electrocyclization and oxidative chain cleavage along the backboine of *cis*-poly(phenylacetylene). Macromolecules 38(17):7241–7250. doi:10.1021/ma051060y
142. Percec V, Rudick JG, Aqad E (2005) Diminished helical character in para-substituted cis-transoidal polyphenylacetylenes due to intramolecular cyclization. Macromolecules 38 (17):7205–7206. doi:10.1021/ma051536d
143. Karim SMA, Nomura R, Masuda T (2001) Degradation behavior of stereoregular cis-transoidal poly(phenylacetylene)s. J Polym Sci A Polym Chem 39(18):3130–3136. doi:10.1002/pola.1294
144. Eelkema R, Pollard MM, Vicario J, Katsonis N, Ramon BS, Bastiaansen CWM, Broer DJ, Feringa BL (2006) Molecular machines: nanomotor rotates microscale objects. Nature 440 (7081):163. doi:10.1038/440163a
145. Yang H, Buguin A, Taulemesse J-M, Kaneko K, Méry S, Bergeret A, Keller P (2009) Micron-sized main-chain liquid crystalline elastomer actuators with ultralarge amplitude contractions. J Am Chem Soc 131(41):15000–15004. doi:10.1021/ja905363f
146. Percec V, Imam MR, Peterca M, Leowanawat P (2012) Self-organizable vesicular columns assembled from polymers dendronized with semifluorinated Janus dendrimers act as reverse thermal actuators. J Am Chem Soc 134(9):4408–4420. doi:10.1021/ja2118267

Adv Polym Sci (2013) 262: 363–388
DOI: 10.1007/12_2013_250

Published online: 27 October 2013

Aqueous Supramolecular Polymers Based on Aromatic Amphiphiles: Rational Design, Complexity, and Functional Materials

Boris Rybtchinski

Abstract Self-assembled polymeric nanoscale systems that are robust yet adaptive are of primary importance for fabricating multifunctional stimuli-responsive nanomaterials. Noncovalent interactions in water can be strong, and biological systems exhibit excellent robustness and adaptivity. Synthetic amphiphiles can also result in robust assemblies in water. Can we rationally design water-based noncovalent polymers? Can we program them to perform useful functions that rival covalent materials? We review here advancements related to these questions, focusing on aromatic self-assembly in aqueous media. Regarding functional materials, we present examples from our work on water-based recyclable noncovalent membranes, which can be used for size-selective separations of nanoparticles and biomolecules. These systems introduce the paradigm of noncovalent nanomaterials as a versatile and environmentally friendly alternative to covalent materials. We also address emerging rational design principles for creating 1D, 2D, and 3D functional nanoarrays hierarchically assembled from well-defined molecular units in aqueous media, enabling new synthetic strategies for fabricating complex water-based materials.

Keywords Hydrophobic interactions · Membranes · Noncovalent materials · Perylene diimides · Self-assembly - water

I dedicate this review to the memory of my friend and colleague, Prof. Michael Bendikov, whose untimely passing is a great loss to those who knew and loved him, and to the entire Chemistry Community. Michael was a great man and a great scientist. His passion for chemistry will always be an inspiration.

B. Rybtchinski (✉)
Department of Organic Chemistry, Weizmann Institute of Science, Rehovot 76100, Israel
e-mail: boris.rybtchinski@weizmann.ac.il

Contents

1 Introduction

Research on supramolecular polymers represents a central theme in supramolecular science [1]. From a fundamental standpoint, one-dimensional supramolecular fiber is the simplest supramolecular motif and serves as an analog of covalent polymeric chains. Noncovalent supramolecular polymers have two main advantages in comparison with their covalent counterparts: they are easy to make using self-assembly and they are adaptive, i.e., capable of structural changes and depolymerization by external stimuli [1]. However, these attractive properties present key challenges related to robustness and rational design: noncovalent interactions result in relatively weak bonds, whereas multiple molecular units and interaction modes render synthesis of predesigned structures very difficult.

Noncovalent interactions in water are crucial in biological systems, providing bonding motifs that are robust yet adaptive [2], and mediate unique molecular recognition patterns [3]. Is it possible to utilize the unique properties of water by employing synthetic amphiphiles in order to create supramolecular polymers with high robustness? If so, can we rationally design such water-based noncovalent polymers? Can we program them to perform useful functions?

A number of supramolecular systems in water display ample robustness. For example, noncovalent interactions have been employed to create stable macroscopic sacs [4], a self-healing hydrogel having exceptional mechanical strength [5], and multifunctional stimuli-responsive molecular printboards [6]. Hydrophobic interactions have been recently shown to induce a dramatic change in chemical properties. Thus, pyrophoric white phosphorus (P_4) that ignites in air is rendered air-stable within the hydrophobic cavities of self-assembled cage molecules in water, but is readily oxidized when displaced from a cavity with a more strongly binding guest molecule [7], thus demonstrating its adaptivity. Supramolecular fibers and their three-dimensional (3D) networks in water, as well as supramolecular hydrogels, can be sufficiently robust and biocompatible for biomedical applications [8].

Hydrogel networks, spanning the bulk of the material and entrapping water, are especially advantageous for creating solid-like materials. Can we create noncovalent materials that will represent a viable alternative to conventional covalent systems? It has been suggested that materials consisting mostly of water, having a robust and uniform 3D network (such as hydrogels), based on strong noncovalent interactions, may lead to adaptive, versatile, and environmentally friendly "water-based plastics" that are stimuli-responsive and recyclable, unlike conventional polymer-based plastic materials [5]. The challenge lies in the rational design of supramolecular hydrogels, since it involves at least two levels of hierarchy: the formation of fibers and their further interaction to form a 3D network that entraps water [9].

Robustness and rational design of water-based assemblies are crucial for developing functional noncovalent polymeric materials. An additional important property to consider is the intrinsic complexity of aqueous self-assembly. Whereas the structure of aqueous equilibrating systems can be rationalized using Israelachvili packing parameters, kinetically controlled assemblies do not comply with them [10–13]. Thus, when strong noncovalent interactions are involved, kinetic control allows the formation of multiple products and may dominate the outcome of self-assembly processes [14–17]. Furthermore, specific molecular interactions can result in very complex assemblies, where both kinetic control and multiple interaction modes play a significant role. For example, complex and diverse structures (dendrimerosomes) were shown to self-assemble from relatively simple dendritic amphiphiles [18], allowing access to a new family of complex nonconventional nanostructures in water. Aqueous self-assembly of simple polyalcohol-based amphiphiles such as glycerol monoolein or phytantriol leads to cubosomes, which are bicontinuous nanostructures having cubic morphology created by bilayers with complex periodic structures [11]. Advantageously, aqueous self-assembly promotes unique structural complexity, yet the factors leading to such complexity are presently not well understood. Lack of a mechanistic understanding and the complex nature of the systems present a significant challenge for rational noncovalent synthesis in water.

In this review we focus on two key questions: (1) Can we encode noncovalent structural motifs rationally employing strong hydrophobicity? (2) How can we fabricate noncovalent water-based materials that rival covalent ones? Clearly, both goals are directly linked because if we can control the structure we can control the function. We begin this review with an overview of the properties of aromatic amphiphiles and their assembly aptitudes, followed by examples from our work that address structure encoding and the development of noncovalent water-based materials.

2 Aromatic Amphiphiles

Hydrophobic interactions between extended hydrophobic surfaces can be very strong [19, 20]. For rigid, flat hydrophobic surfaces of 5 nm^2 in size, the "unfavorability" of their exposure to water is more than 30 kcal/mol, as estimated using oil–water

interfacial tension energy (70 cal/Å^2), a good approximation for hydrophobic interactions between rigid surfaces larger than 1 nm^2 [19]. In this respect, aromatic surfaces are especially attractive due to the synthetic availability of molecules having rigid hydrophobic surfaces of several square nanometers. Aromatic molecules that are connected via appropriate linkers allow further extension of the hydrophobic surface area. Stacking (van der Waals) interactions between the aromatics further enhance the bonding [21]. Thus, well-defined molecular amphiphiles having large aromatic cores may serve as an excellent toolbox for creating robust hydrophobic assemblies.

Until recently, studies on the self-assembly of aromatic amphiphiles have been relatively limited, in striking contrast to the vast literature on the assembly of aliphatic amphiphiles. Yet, in the late 1990s, seminal studies by Whitten et al. revealed two important features of aromatic amphiphiles: their assemblies showed enhanced robustness and a high order in comparison with the aliphatic systems. The advantageous ordering was attributed to the specific interactions of aromatic cores [22, 23].

Recent extensive work by Lee et al. utilized well-defined PEGylated aromatic amphiphiles that self-assemble in water into nanoarrays with unusual morphologies, high robustness, and advantageous stimuli-responsiveness. This important work has been recently reviewed [24].

The complexity of aromatic self-assembly in water has been demonstrated by Percec et al. A large library of aromatic amphiphiles has been studied, indicating that a significant number of individual compounds can be assembled into nonconventional structures such as toroids, bicontinuous arrays, etc., and can exhibit high order and/or result in multiple products. These assembly modes cannot be rationalized using simple packing parameters, and the observed morphologies extend far beyond the micelle–fiber–bilayer paradigm of aqueous self-assembly [18]. Specific molecular interactions appear to be responsible for the observed complexity [25].

In view of the complex assembly modes, how can one assemble a supramolecular polymer from an aromatic amphiphile? The simplest approach for assembling 1D polymeric structures would be to use a design based on aromatic stacking. Molecular stacks are intrinsically 1D systems, and one can restrict the assembly to such a stack, taking into account that the aromatic core imposes strong hydrophobic interactions that are further enhanced by van der Waals interactions. Interestingly, such simple molecular fibers in water can be obtained only in a few cases, usually involving complementary noncovalent bonding [26]. This is because aromatic core interactions are not the only hydrophobic interactions operating in the self-assembly of aromatic amphiphiles (see Sect. 3.5).

A valuable strategy for achieving aqueous aromatic 1D systems involves synergetic interactions. Two prominent examples include the use of electrostatics [27] and peptide self-assembly (hydrogen bonding/hydrophobic) as complementary interactions [26]. For example, oligothiophene bolamphilies decorated with two small peptide sequences assemble in water into 1D molecular fibers with strong π–π intermolecular electronic coupling [28]. These supramolecular polymers can further

interact to form hydrogels. Naphthalene diimides decorated with dipeptides have also been shown to assemble into helical molecular fibers [29]. Faul et al. employed a combination of hydrophobic and electrostatic interactions to assemble supramolecular polymers from two oppositely charged dyes: a perylenediimide and a copper phthalocyanine derivative [30]. Photoactive donor (pthalocyanine) and acceptor (perylene diimide) molecules were arranged in a "double cable" motif, addressing the concept of molecular heterojunction systems relevant to solar energy conversion.

The complexity of aromatic self-assembly in aqueous media is exemplified by the formation of tubular structures from relatively simple amphiphiles. The 1D nanotubes are hierarchically ordered supramolecular polymeric structures in which the interaction of aromatic moieties brings about an assembling motif that, in synergy with additional interactions, results in tubular morphology [24]. For example, the nanotubes assembled from benzocoronene derivatives feature interactions between aromatic moieties and alkyl side groups that produce separate domains and result in long, highly ordered nanotubes [31]. Such aromatic/alkyl interplay represents a simple yet powerful tool for controlling the self-assembly aptitudes of aromatic amphiphiles (see Sect. 3.5). Partially oxidized benzocoronene nanotubes exhibit electrical conduction, which is due to long-range intermolecular electronic communication through graphite-like molecular arrays. The latter system illustrates the power of aromatic self-assembly in water, enabling robust functional materials constructed from small molecules.

Self-assembly of aromatic amphiphiles in aqueous media presents both opportunities and challenges: robust ordered systems with interesting functions can be easily assembled, but the rational synthetic approaches needed to achieve such arrays remain to be developed. In addition, an intriguing question arises: does the robust yet adaptive character of the aromatic assemblies make them viable candidates to challenge the performance and stability of conventional covalent materials? In the following sections we will describe our work on encoding structures and functions in the regime of strong hydrophobic interactions (Sect. 3), and address the challenge of creating functional noncovalent materials for real-life applications (Sect. 4).

3 Structure Encoding

3.1 Code: Electrons/O_2. Reversible Structure/Function Switching via Redox Chemistry

We chose perylene diimide (PDI) as a basic aromatic unit in our systems. PDI-based amphiphiles benefit from high stability, diverse synthetic strategies, and advantageous photonic and electronic properties [32].

When we began working with PDI-based amphiphiles we decided to target the simplest supramolecular structure – a 1D stacked polymeric chain that will be robust yet adaptive (capable of reversible depolymerization). In this respect, PDI systems have many advantages, including unique redox behavior in water: they can

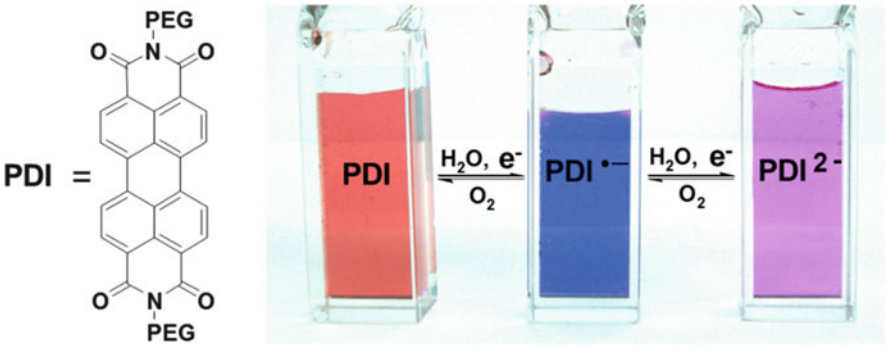

Fig. 1 Reduction of PDI cores brings about a change in the photonic, magnetic, and solvation properties (*PEG* refers to PEG17) [33]

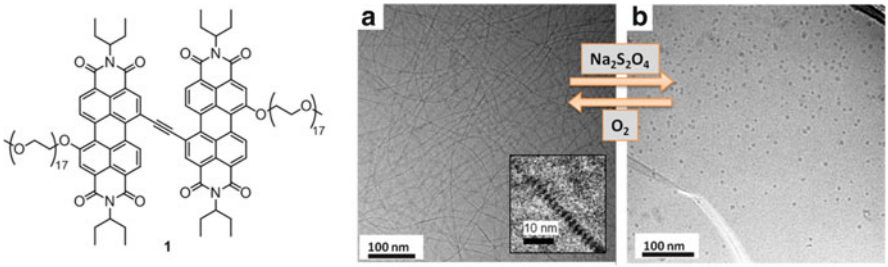

Fig. 2 Structure of bis-PDI amphiphile **1** and cryo-TEM images (**a**, **b**) showing reversible fission of the fibers based on **1** (10^{-4} M, water:THF = 4:1, v/v). (**a**) Nanoribbons having a segmented structure (see *inset*); (**b**) 8-nm spherical assemblies obtained upon reduction [34]

be reduced to radical anions and dianions, which can be converted back to neutral species upon facile reaction with oxygen (simply by exposure to air) (Fig. 1). Charging the PDI system results in a more hydrophilic anion species (and electrostatic repulsion), which can be used to encode adaptivity via injection of electrons into the PDI-based assembly [33]. Importantly, reversible charging should result in turning on and off not only of different structure modes but also the functions typical for these modes, so that reversible depolymerization may also lead to function switching (multifunctionality).

In addressing 1D stack formation, compound **1** was designed to have an extended flat aromatic core constructed from two PDI units, a strongly hydrophobic moiety, and hydrophilic polyethylene glycol (PEG) groups (Fig. 2). Two PDI units connected via ethynyl linker resulted in a large, rigid, and completely flat aromatic core. The bolaamphiphilic structure is supposed to further restrict aromatic interactions, resulting in a molecular stack that should lead to molecular fibers. PEG groups are neutral, and thus the self-assembly is based on hydrophobic/π–π interactions, without the involvement of charged species. Compound **1** was found to

assemble into uniform micron-long, ~3-nm-thick nanofibers in aqueous medium (Fig. 2a).

Upon addition of sodium dithionite, **1** was reduced to $\mathbf{1}^{3-}$ and the fibers underwent fission, leading to the formation of ~8-nm spherical assemblies (Fig. 2b). This drastic change in morphology upon reduction was due to the decreased hydrophobicity (enhanced solvation) of the anionic species and their mutual electrostatic repulsion. Upon exposure to air, the anions were oxidized back to the neutral PDI state and the supramolecular fibers were restored (Fig. 2). The reduction/oxidation sequence can be performed several times, without altering the observed structures. Electrochemical reduction also leads to reversible fission. The sequence represents reversible supramolecular depolymerization–polymerization in situ, which is accompanied by a change in rheological behavior and altered electronic and photonic properties of the assemblies. The latter is manifested by efficient exciton movement in the fibers, which is switched off upon reduction and restored upon oxidation. In general, long nanofibers (nanowires) are often utilized for functional (signal transduction) and physical connectivity, and their reversible disassembly is important for switching on and off such functionality. In polymers based on **1**, simple redox encoding leads to adaptive behavior involving reversible structural and functional transformations in situ.

The system showed predesigned robustness and adaptivity, but we realized that the fiber structure is substantially more complex than that expected from our initial design. Thus, cryo-TEM studies revealed that the fibers are not built from single molecular PDI stacks but instead are ribbons with a complex segmented structure (Fig. 2a), resulting from hierarchical hydrophobic interactions due to the presence of two distinct hydrophobic moieties: the aromatic system and alkyl groups. In our later work, we were able to take advantage of this intrinsic anisotropy of PDIs by using it to encode crystalline-like structures in water (see Sect. 3.5).

3.2 Code: Metal Coordination. Diversity via Coordination Chemistry

A typical strategy for noncovalent synthesis is based on the paradigm "one assembling unit forms a single assembly," whereby the structure of a primary building block elicits the assembly structure. Apparently, this strategy can be significantly expanded if a single generic covalent building block can generate multiple structural and functional motifs.

In order to achieve such diversity-oriented noncovalent synthesis, we focused on designing a primary covalent unit with built-in functionality that can be expediently modified, leading to changes in the overall structure. The reversible supramolecular depolymerization described in the previous section utilizes this concept, yet it is based on a single type of input, the reduction of a PDI unit, implying the use of simple binary on/off switching. To achieve a high degree of diversity (i.e., a system allowing multiple inputs) we aimed at two levels of self-assembly encoded in a

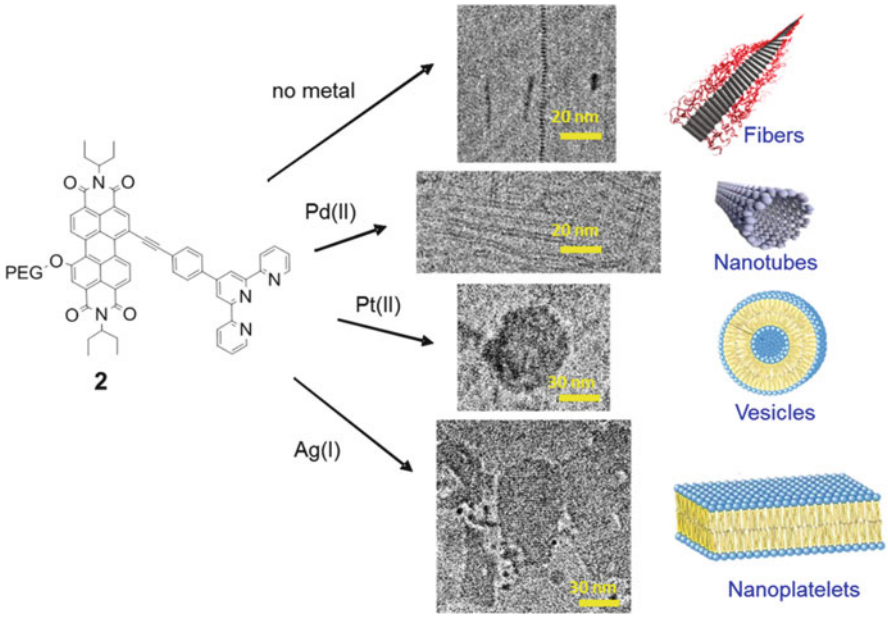

Fig. 3 Diversity via coordination chemistry. Metal coordination results in square planar complexes as revealed by cryo-TEM images (2×10^{-4} M, water:THF = 9:1, v/v) [35]

covalent building block: a permanent self-assembly motif and a tunable motif that allows diverse modifications. Based on this idea, our primary building block, compound **2**, was designed to possess an amphiphilic moiety (PEG-PDI) and a tunable unit (a terpyridine ligand) capable of binding a wide variety of metal centers (Fig. 3).

We decided to prepare square planar metal–terpyridine complexes of **2** in order to compare the systems with ones having similar geometries and different metal centers that were thought to influence the assembly outcome. To this end, Ag, Pd, and Pt complexes of **2**, possessing square planar geometry, were prepared via simple coordination chemistry. Their aqueous self-assembly and that of a free ligand resulted in four completely different morphologies (Fig. 3): segmented fibers (free ligand), nanotubes (Pd complex), vesicles (Pt complex), and crystalline nanoplatelets (Ag complex). This striking diversity has been rationalized based on the influence of metal centers on the noncovalent interactions. The cationic Pd center is a hydrophilic moiety, creating a nonsymmetric amphiphilic motif (having a large PEG-PDI-small Pd) prone to assemble into tubular structures[36]. The Pt-terpyridine complexes exhibit Pt–Pt interactions [37] that enhance hydrophobic binding/stacking. In the case of the Ag complex, the coordinated water molecules appear to rigidify the assembly, due to a chain of hydrogen bonds within the hydrophobic core. The assemblies have advantageous light-harvesting properties such as good spectral coverage and fast exciton hopping (investigated using femto-second transient absorption).

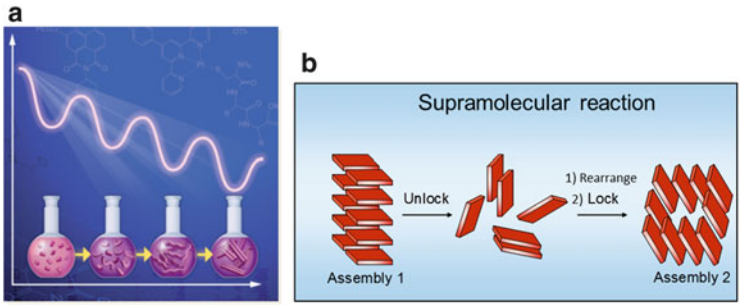

Fig. 4 (**a**) Formation of different kinetic products along the reaction coordinate. (**b**) Transformation involving controlled pathway dependence [38]

3.3 Code: The Self-Assembly Pathway. Complexity via Kinetic Control

Metals can serve as advantageous codes for modifying the covalent units to regulate hydrophobic assembly, but whether it is possible to obtain diverse products from an unmodified primary building block is an intriguing question. In covalent polymerization, identical monomers may result in different polymer structures (e.g., isotactic versus syndiotactic); the same is generally true for many covalent transformations. Can this be achieved for supramolecular polymers? This relates to a fundamental issue in aqueous self-assembly: if strong hydrophobic interactions are involved, one can expect a breakdown of thermodynamic control. Thus, in the regime of strong noncovalent interactions (multiple) stable kinetic products may form from a single primary building block, along the supramolecular reaction path, analogously to covalent reactions (Fig. 4). To address this possibility, we designed amphiphile **3** with an extended aromatic system that is expected to result in strong hydrophobic interactions. In this system, peptide ligands provide structural complexity and enable different interaction modes, leading to diverse structures [38]. Self-assembly was induced by mixing water (aggregating solvent) with a solution of **3** in THF (the disaggregating solvent). The very strong hydrophobic interactions acting on **3** critically raise the energy barrier that must be overcome to equilibrate and thus reassemble the system. Hence, in solutions with high water content (and therefore large kinetic barriers), **3** forms kinetically trapped supramolecular assemblies.

Depending on the pathway of self-assembly (i.e., the order, rate, and timing of solvent mixing), a variety of different supramolecular polymer morphologies can be obtained, ranging from relatively short, strongly curved fibers with ~3 nm diameter and polydisperse length (10–100 nm), to very long (> 200 nm), straight, highly ordered, and tightly packed fibers of ~5 nm in diameter (Fig. 5). The fibers of various morphologies, obtained via different assembly pathways, were kinetically trapped in water/THF (95:5, v/v) and were stable over months and did not undergo transformation, even upon heating. This demonstrates the effect of increased noncovalent robustness: it is possible to achieve structural diversity by the kinetic

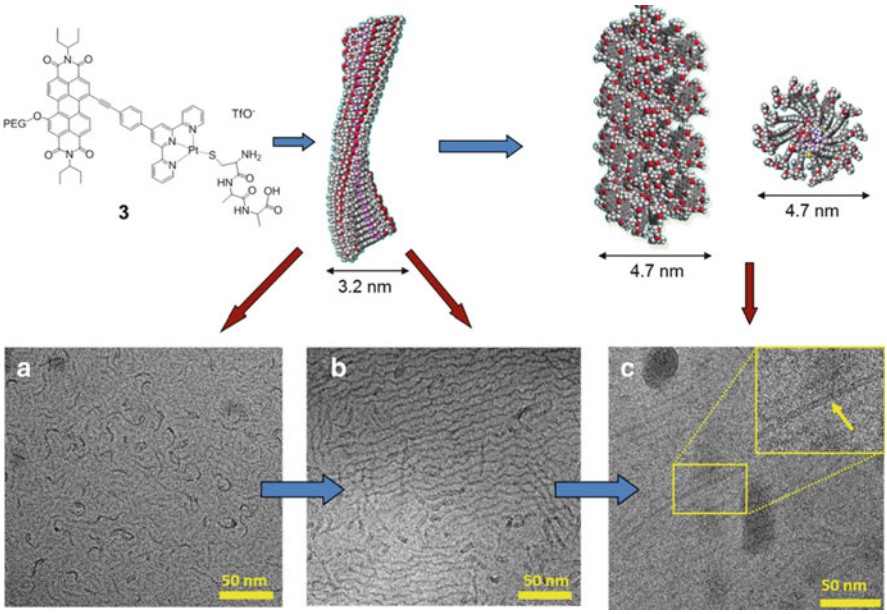

Fig. 5 Evolving self-assembly of compound **3** (10^{-4}M, water:THF = 4:1). Cryo-TEM images of (**a**) short curved fibers; (**b**) longer curved fibers; and (**c**) long thicker tube-like fibers, where the molecular helical 3-nm-thick fibers (**a**, **b**) are converted into straight tubular 4.5-nm fibers. In good agreement with the molecular models (3.2 and 4.7 nm fiber widths). The assembly development can be stopped by the addition of water (water:THF = 95:5, v/v) [38]

trapping of different assemblies based on a single primary building block. Addition of THF to the kinetically trapped systems leads to its evolution towards a more ordered system. However, this process can be stopped by the addition of water, and continued again by the addition of THF. Such a lock/unlock sequence can be viewed as a supramolecular reaction that transforms less ordered assemblies into more ordered ones and it can be triggered and stopped at any point of evolution. Thus, kinetically controlled noncovalent self-assembly in aqueous medium employing well-defined molecular units and driven by strong hydrophobic interactions enables pathway-dependent assembly sequences, in which different supramolecular polymers based on a single molecular building block can be obtained via stepwise evolution. Pathway-dependent assembly of molecular systems in water may significantly augment the current methodology of noncovalent synthesis.

3.4 Code: Directional Pairwise Hydrophobic Interactions

The directionality is important for creating 1D molecular nanofibers (supramolecular polymers). Hydrogen bonding is intrinsically directional, and a variety of noncovalent

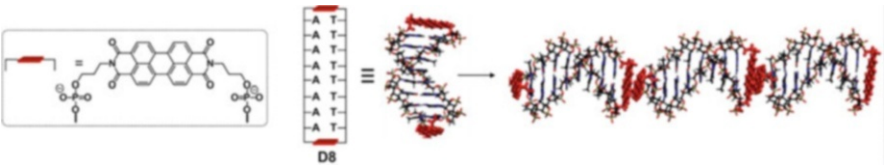

Fig. 6 **D8** supramolecular polymerization, depicting end-to-end association. The structure of the PDI linker is shown on the *left* [48]

dendrimeric [39] and polymeric systems [40–42] based on strong hydrogen bonds in organic solvents or in the solid state have been developed. In contrast, owing to the lack of directionality of hydrophobic interactions [43], the rational design of supramolecular polymers in water is challenging [34, 40, 43–50]. Can we design a hydrophobic analog of a hydrogen bond where a pair of aromatic units will interact along a well-defined direction?

3.4.1 Pairwise Interactions in DNA-PDI Dumbbells

One of the strategies that may lead to pairwise interactions in the case of aromatic systems is to protect one of the two aromatic surfaces, thus compelling the unprotected surface to engage in pairwise interactions. In collaboration with Prof. F. D. Lewis (Northwestern University), DNA dumbbell conjugates possessing PDI termini linking A-tracts of various lengths were synthesized and their self-assembly was investigated (Fig. 6). Cryo-TEM images obtained from dilute solutions of the eight-base-pair dumbbell (**D8**) in aqueous buffer containing 100 mM NaCl show the presence of structures corresponding to linear end-to-end assemblies of 10–30 dumbbell monomers, consistent with analyses of the UV–vis and fluorescence spectra of these structures. Assembly size was dependent upon the concentration of dumbbell and salt as well as the temperature. Kinetic analysis of the assembly process by means of salt jump stopped-flow measurements showed that it occurs by a salt-triggered isodesmic mechanism in which the rate constants for association and dissociation in 100 mM NaCl were 3.2×10^7 M^{-1} s^{-1} and 1.0 s^{-1}, respectively, much faster than the typical rate constants for DNA hybridization. These observations constituted the first example of using hydrophobic association for assembling small DNA duplex conjugates into supramolecular polymers, which is the result of pairwise interactions.

3.4.2 A Directional Pairwise Motif Based on Unprotected Aromatics

The previous work describes pairwise interactions that result from protecting the aromatic surface. Is it possible to achieve pairwise interactions by employing unprotected hydrophobic surfaces? In addressing this goal, our design of pairwise stacking/hydrophobic interactions was based on the idea that a rigid scaffold may

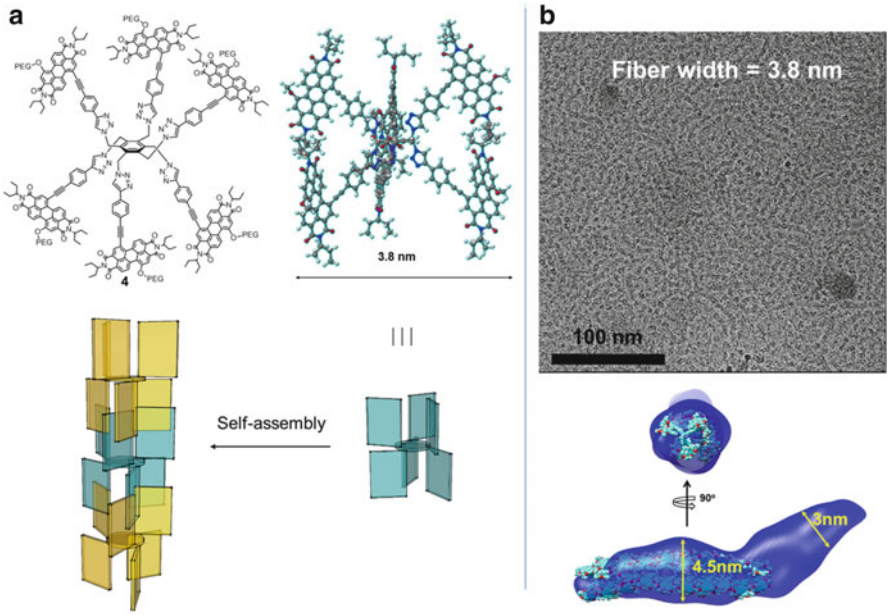

Fig. 7 (**a**) *Top*: Structure (*PEG* refers to PEG17) and molecular model (hydrophobic core, PEGs are omitted for clarity) of **4**. *Bottom*: Self-assembly pattern of **4** (alternate molecular units are given in different colors). (**b**) *Top*: Cryo-TEM image of a solution of **4** (10^{-5} M) in water/THF (7:3 v/v) showing tube-like fibers. *Bottom*: Two views of the overlay of the SAXS molecular envelope (in transparent surface mode; calculated from SAXS data obtained for the same solution of **4**) and the molecular model of **4** [55]

restrict interactions between hydrophobic moieties, provided that their hydrophobic surfaces are approximately parallel to the axis of the scaffold (and the polymer), in contrast to a conventional perpendicular arrangement (as in discotic systems). As a scaffold, we employed hexa-substituted benzenes (HSB), which are bi-facially segregated systems where 1,3,5 substituents are situated above the phenyl plane and the 2,4,6 substituents below it, rendering HSB platforms advantageous for construction of tripodal ligands, receptors, and cages [51, 52]. In order to create a directional self-assembling motif based on π–π stacking and hydrophobic interactions, we designed and synthesized (using click chemistry) 1,3,5-trisubstituted (bearing ethyl groups at 2,4,6 positions) and hexasubstituted molecules, in which aromatic amphiphiles (PDIs bearing PEG) are attached to a HSB scaffold through rigid linkers (Fig. 7 presents hexa-PDI derivative **4**). Our modeling studies revealed a sterically favorable alternate arrangement ("1,3,5 up/2,4,6 down") of substituents in both systems, with the PDI cores approximately parallel to the scaffold axis (especially in sterically crowded **4**, Fig. 7a). The interactions between multiple PDI units (multivalent supramolecular interactions [53, 54]) should further enhance the directionality and bond strength, leading to a 1D assembly motif, which is schematically depicted in Fig. 7.

Both compounds self-assemble into molecular fibers in a water/THF mixture (7:3 v/v), as shown by cryo-TEM, complying with the predesigned pairwise stacking motif. Thus, the fibers assembled from **4** display tubular structures with a diameter of 3.8 ± 0.4 nm. The diameter of the interior lower-contrast part is 2.0 ± 0.2 nm, and the higher-contrast wall thickness is 0.9 ± 0.2 nm. The length of the fibers is 183 ± 96 nm. The identical fibrous structures assembled from **4** were also observed in pure water. The fiber dimensions and fine structure are in excellent agreement with the molecular model based on pairwise stacking, and, as expected, in the case of **4**, all the molecules in the fibril structure interact through the aromatic surfaces of PDI units (Fig. 7a) located on both sides of the benzene core.

The thermodynamics of supramolecular polymerization of **4** was studied using fluorescence spectroscopy, revealing strong association constants (~10^9 M^{-1}). The thermodynamic parameters of the process indicate that it is both enthalpically ($\Delta H = -8.5$ kcal/mol) and entropically driven ($T\Delta S = 3.6$ kcal/mol), with the dominant enthalpic contribution that arises due to the large hydrophobic surfaces involved in polymer formation. Photonic studies using ultrafast spectroscopy reveal that the supramolecular polymers based on aromatic pairwise interactions differ significantly from the continuous stack systems, enabling exciton confinement (trapped excimers) that leads to localized emission, rather than the exciton hopping that is typical of most aromatic stacks. Directional pairwise hydrophobic interactions regulated by scaffold geometry serve as a convenient strategy for rational design of supramolecular polymers in aqueous noncovalent synthesis.

3.5 Code: Anisotropic Hierarchical Hydrophobic Interactions. 2D Crystalline Arrays.

Crystallization is an especially important area of organic self-assembly, enabling ultimate long-range ordering. Understanding of and control over crystallization of organic molecules is a long-standing challenge of fundamental importance for organic materials, pharmaceuticals, and other fields. For example, crystalline aromatic structures constitute the core components of organic electronic devices, whose optimal performance requires a high degree of order [56]. The simplest view of an aromatic organic crystal involves an array where 1D aromatic stacks interact to form an ordered periodic structure. We note that soluble 2D crystalline nanosheets represent a very interesting target because they can mimic the properties of thin films and self-assembled monolayers, covering large areas with ordered nanometer-thick material.

We noted that in several cases (see Sects. 3.1, 3.2, and 4.1) our supramolecular polymers have complex segmented morphologies, where individual segments are aromatic stacks that interact via alkyl "edges." This prompted us to consider a design in which the extended "segments" will interact to form a highly ordered crystalline array (Fig. 8). We chose to make PDI bolaamphiphiles with smaller hydrophilic groups (carboxylic acids, **5** and **6**; Fig. 8) or larger hydrophobic cores

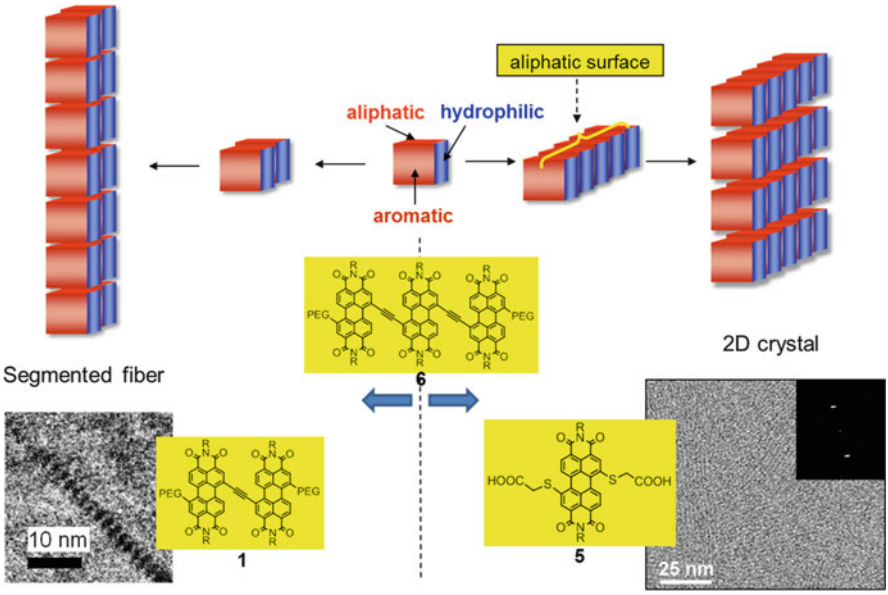

Fig. 8 Self-assembly aptitudes in the case of anisotropic hydrophobic interactions (*R* ethyl propyl, *PEG* refers to PEG17). Compound **1** forms segmented fibers, whereas **5** assembles into 2D crystals (as shown by cryo-TEM). Compound **6** can yield segmented fibers or crystals, depending on the self-assembly conditions. The interplay of interactions between the aromatic core and the alkyl "edges" drives the assembly, which can be further adjusted by adding an organic co-solvent (THF) [57]

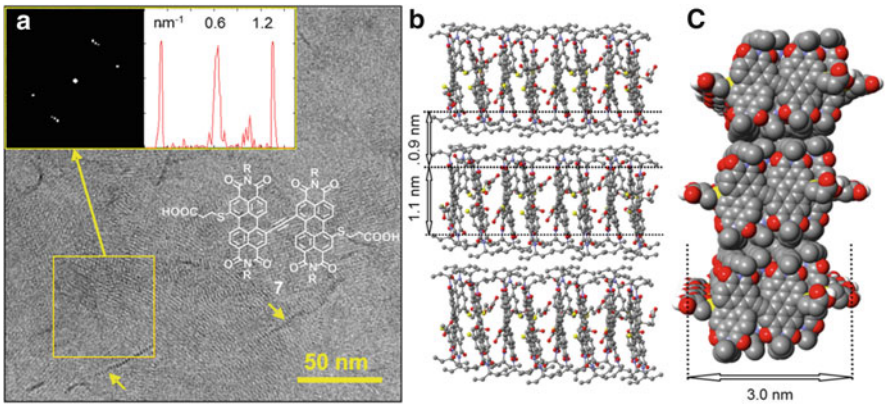

Fig. 9 (**a**) Cryo-TEM image of a 1×10^{-4} M solution of **7** in water (pH 10). *Inset*: Fast Fourier transform (FFT) analysis of the marked area. *Arrows* point to high contrast structures corresponding to the monolayer cross-section. Molecular model of **7** is also shown (hydrogens are omitted for clarity). (**b**) Interacting stacks and dimensions corresponding to the dark and light contrasting stripes in the assemblies. (**c**) Side view (space-filling representation) showing the width of the assembly (monolayer cross-section) [57]

(**7**; Fig. 9) because both are anticipated to promote interaction via aromatic surfaces, leading to the formation of long stacks. This was implemented in the synthesis of compounds **5**–**7** (Figs 8, 9) that have PDI cores functionalized with two alkyl groups (ethyl propyls attached at imide positions), and two hydrophilic groups (PEG or carboxyl, attached to the aromatic core) [57].

Compounds **5**–**7** assemble into crystalline-like 2D arrays, as revealed by cryo-TEM and AFM measurements, and largely preserve their structure upon drying. According to the concept presented in Fig. 8, this assembly motif is generated by a hierarchical mode of two distinct hydrophobic interaction types induced by an aromatic core and alkyl groups, suggesting that a simple design strategy can be used to obtain crystalline organic assemblies in water [57]. Importantly, photonic properties of these assemblies resemble those of solid-state crystals, as manifested by spectral broadening and large red shifts, typical of PDI crystals. The studies on exciton dynamics using femtosecond transient absorption also revealed that **6** and **7** exhibit fast exciton diffusion. Remarkably, compound **7** exhibits exciton diffusion constants that are even slightly higher than those of solid-state crystalline perylene tetracraboxylic acid dianhydride (PTCDA), a benchmark exciton diffusion system.

The light absorption properties, the ordered 2D morphology, and the nanoscale thickness appear to be useful for fabricating light-harvesting systems. Remarkably, relatively simple molecular systems can be designed to undergo self-assembly into extended ordered arrays by simply putting them in aqueous solutions, thus allowing facile, cost-efficient, and environmentally friendly fabrication, and the processing of water-based photonic and electronic materials.

4 Water-Based Noncovalent Polymeric Materials

4.1 Adaptive Hydrogel

The crystalline systems described in the previous section represent an entry into photonic and electronic materials. Hydrogels constitute another interesting class of systems relevant to the area of water-based functional materials. Hydrogels are composed of water and a small amount (usually 0.1–10 wt%) of gelator molecules that create a water-entrapping 3D network over the entire bulk of the material, resulting in solid-like viscoelastic behavior. In the case of water-based supramolecular systems, gelation may occur when supramolecular fibers (polymers) interact, forming a network [58]. Thus, in order to design a supramolecular gel, one needs to introduce an additional level of interaction - the entanglement of fibrous assemblies. This proved to be a difficult task because the rational design of gelator molecules is extremely challenging, and most hydrogels have been discovered serendipitously[58].

In our pursuit of metal-coordinating supramolecular polymers, we prepared compound **8** so that it has a bipyridyl (bipy) linker connecting two PDI moieties. One of the consequences of having bipy is the completely flat geometry of the

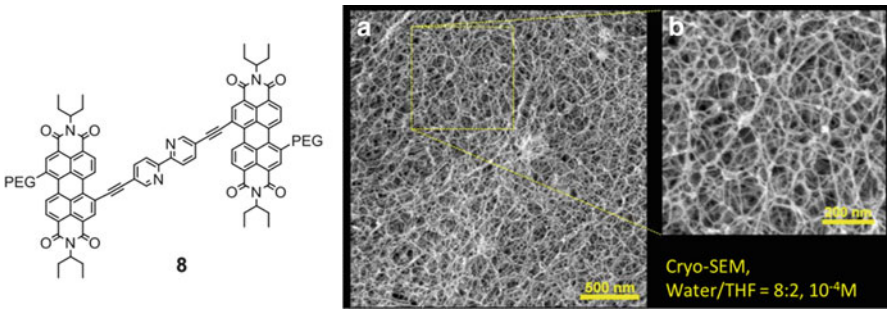

Fig. 10 Structure of **8** and cryo-SEM images (**a**, **b**) showing 3D network formation (constructed from segmented fibers) in fluid solution [59]

aromatic core. Compound **8** assembles into micron-long segmented fibers, analogously to compound **1**, and these fibers further interact to form a 3D network that exists in fluid solution even at relatively low concentrations, as shown by cryo-SEM (Fig. 10)[59]. At concentrations higher than 6×10^{-3}, a gel is formed that exhibits typical viscoelastic properties and a long-range order, giving rise to birefringence. Why does fiber entanglement occur? Although initially not a part of our design, the large hydrophobic core of **8** results in a slightly hydrophobic fiber surface, leading to enhanced interactions. Corroborating this idea, 3D network formation is extremely sensitive to PEG length such that longer (by just 1–2 units) PEGs result in low entanglement, whereas the shorter ones result in precipitation. This underscores the importance of precise tuning of hydrophilic/hydrophobic ratio, to which gelation is very sensitive. Regarding the aromatic core, we screened a large number of bolaamphiphilc PEG-PDI compounds having various linkers between the PDIs, and so far bipy proved to be optimal, resulting in the superior gelation ability of **8**.

The gel based on **8** shows multiple stimuli responsiveness. Redox chemistry employing sodium dithionite and air leads to reversible sol–gel phase transition and birefringence switching (Fig. 11). The robustness of our hydrogel is revealed by its unusual temperature-responsiveness. Typically, supramolecular gels undergo a reversible gel–sol transition when heated to moderate temperatures (e.g., ~60°C) [60] owing to the breakdown of supramolecular fibers, the consequence of weak noncovalent interactions. In contrast, the gel of **8** can be heated in a sealed vial to 100°C without displaying fiber fission. Furthermore, when approaching 100°C the fibers begin to bundle, resulting in temperature-induced contraction, which creates a more dense material with greater stiffness (Fig. 12a). This temperature-responsiveness is reversible because the shrunken gel slowly expands to its original volume when cooled to room temperature. A gel-to-sol transition can be reversibly induced by chemical reduction using sodium dithionite (Fig. 12b), resulting in fiber fission, analogous to compound **1** (see Sect. 3.1).

The 3D supramolecular network of **8** has promising potential as a light-harvesting scaffold, exhibiting excellent solar spectrum coverage and efficient

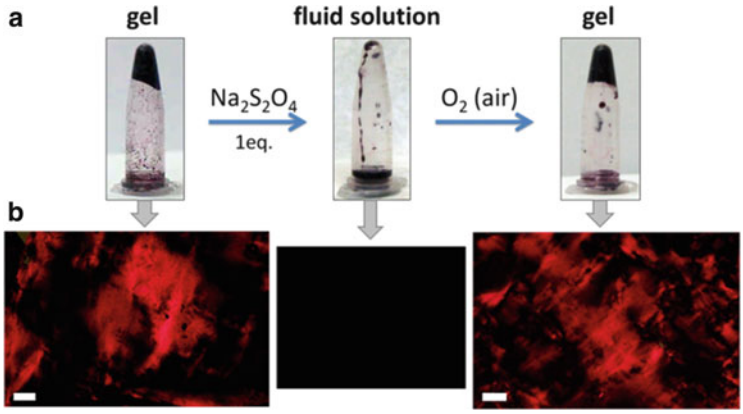

Fig. 11 (**a**) Reversible gel–sol switching using redox chemistry accompanied by (**b**) birefringence switching (*scale bar*: 200 μm) [59]

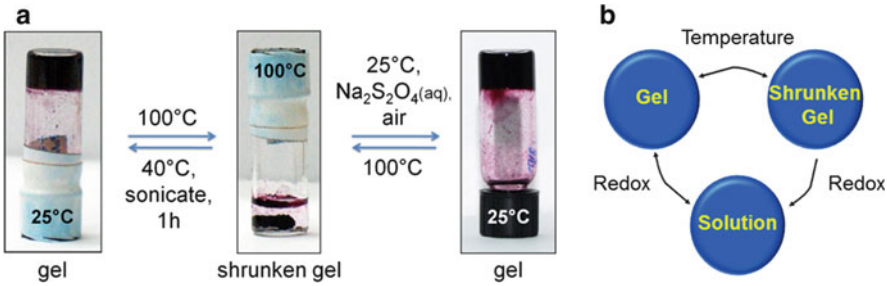

Fig. 12 (**a**) Temperature responsiveness and (**b**) multiple stimuli responsiveness of the gel [59]

exciton-hopping (with site-to-site hopping times of 2 ps), enabling the efficient collection and transport of excitation energy [59].

4.2 Recyclable Noncovalent Membranes

4.2.1 Nanoparticle Separations

Working with the aqueous solutions of **8,** we made an intriguing observation – when we filtered the solutions over standard syringe filters with 400 nm pores, the material was quantitatively retained (deposited) on the filters (Fig. 13a, b), with virtually no observable amount of **8** coming through (even upon applying moderate pressure), in contrast to the majority of assemblies we had been investigating. Despite the fact that the system is composed of relatively small molecules, the hydrophobic interactions appeared to be very strong, prompting us to state that the 3D networks of **8** display unique robustness. This would be an empty claim without

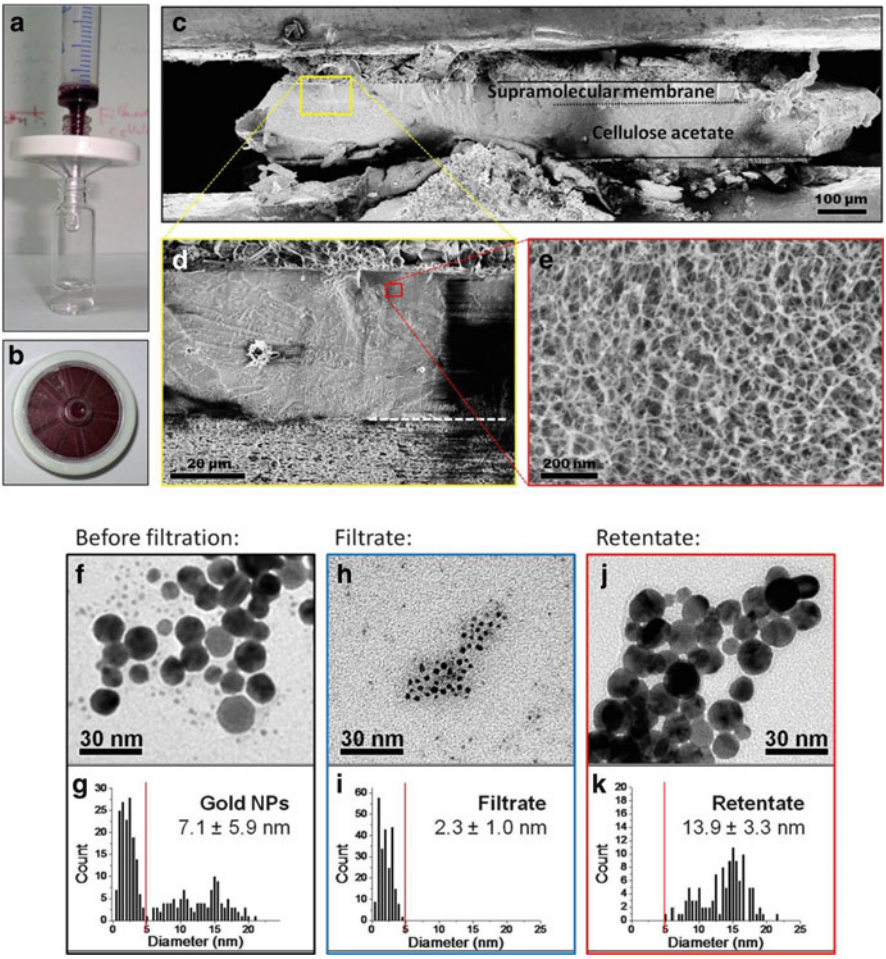

Fig. 13 (**a**) One-step fabrication of a ~45-µm-thick membrane by filtering a solution of **8** over a cellulose acetate syringe filter (0.45 µm pore size). (**b**) The prepared supramolecular membrane. (**c**) Cryo-SEM image of the membrane cross-section. (**d**) Magnified area showing the sharp border between the supramolecular membrane and the support. (**e**) The porous nanostructure of the membrane. (**f–k**) Filtration of gold nanoparticles over a supramolecular membrane: (**f**) Gold nanoparticles before filtering and (**g**) corresponding size histogram. (**h**) Gold nanoparticles in the filtrate and (**i**) size histogram. (**j**) Retained nanoparticles and (**k**) size histogram [61]

answering the following question – what is it good for? How valid is the idea that hydrophobic assembly is robust enough to make a useful functional material, or to compete with polymeric systems in real-life applications?

We investigated the deposited material using cryo-SEM to reveal the formation of a porous gel-like layer with relatively uniform pores (Fig. 13c–e). The structure was strikingly reminiscent of that of filtration membranes, motivating us to investigate the system as a size-selective separation membrane. Assuming that it possesses

sufficient robustness, our supramolecular system, having a fibrous 3D network with nanoscopic pores, should be able to separate particles having nanoscopic sizes. Notably, all commercially available filtration membranes are composed of high molecular weight polymers or ceramics [62–65]. The technological application of membrane-based techniques includes various large-scale industrial processes, including food processing, biomedical applications, and water purification [62, 66], while most separation processes deal with aqueous solutions. Membranes for pressure-driven filtration applications pose a dilemma in material science: on the one hand, high material robustness is required (the membrane must be stable and must retain its nanoscopic structure under the pressure and flux of solvent and solutes); on the other hand, adaptive properties are highly desirable (e.g., membranes with a dynamically controllable pore size, self-healing, and recyclability).

The membranes were fabricated in one step by filtering a solution of **8** in water over a commercial cellulose acetate support, thus forming a layer with a 3D fibrous nanostructure (Fig. 13a–e) [61]. Other commercial supports are suitable as well, and cellulose acetate was selected due to its availability, good wettability, and low costs. The supramolecular membranes were stable under a pressure-driven (up to 0.8 bar of overpressure) flux of water for several hours and could be used immediately after preparation to separate various nanoparticles according to size. The nature of the particles and their capping layers did not influence the membrane's performance. The membrane thickness was readily adjusted by changing the amount of supramolecular solution that was used for its preparation. A thin (~12 μm) membrane was used for filtering various gold nanoparticles, and it consistently showed a 5-nm cutoff size (an example is shown in Fig. 13f–k). The membrane's permeance (pressure normalized flux) of 1.1×10^2 L h^{-1} m^{-2} bar^{-1} is comparable to commercially available membranes with similar rejection properties.[1]

To investigate the mechanism underlying the observed size-selective separation, we performed cryo-SEM imaging of a membrane sample that was prepared following Au nanoparticle deposition, which revealed that the particles permeate through the membrane, with the depth of permeation depending on the nanoparticle size (Fig. 14a) (depth filtration mechanism [62]). Evidently, even a very thin membrane layer exhibited a nice particle distribution, suggesting that size separation of particles smaller than 5 nm in the regime of chromatography should be feasible. This can be important for semiconductor nanoparticles (quantum dots, QD), whose photonic properties strongly depend on the size, with several classes of QDs exhibiting a substantial variation of photonic characteristics in the 1–5 nm range. Addressing this possibility, we used a 45-μm-thick membrane to fractionate a mixture of 2.5 and 4.0-nm CdTe quantum dots. The large particles penetrated the supramolecular network slower than the small ones, resulting in chromatographic separation according to size (Fig. 14b).

[1] See for example technical specifications of Koch Membrane Systems HFM-100/180, HFK-131, or GE Osmonics KN1CP04700.

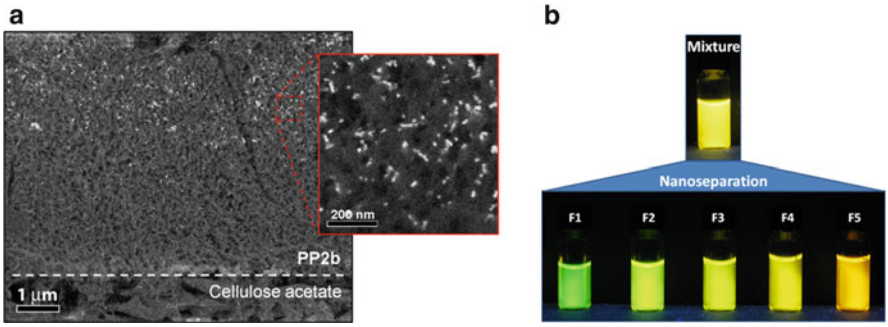

Fig. 14 Size-selective chromatography of nanoparticles: (**a**) Backscattered electron cryo-SEM image of the cross-section of a supramolecular membrane that was used for filtering gold nanoparticles. Retained particles (10–20 nm) appear as *bright spots*, revealing that size-selective capture takes place in the interior of the supramolecular membrane rather than on its surface. (**b**) Chromatographic fractionation of cadmium telluride quantum dots according to size. *Top*: a mixture of small (~2.5 nm) and large (~4.0 nm) particles in UV-light ($\lambda = 365$ nm); *bottom*: successively collected fractions *F1–F5*. Small particles rapidly traverse the membrane, whereas increasing amounts of larger particles are collected in subsequent fractions [61]

Importantly, the membrane's stability critically depends on hydrophobic interactions. Addition of ethanol to the aqueous solution traversing the membrane drastically weakens these interactions, leading to an instantaneous disassembly of the supramolecular membrane [61]. In this way, the membrane material is recycled: it is easily cleaned, reassembled, and deposited again to produce another ultrafiltration membrane, making possible multiple, consecutive recycling sequences with reproducible membrane performance (Fig. 15). Disassembly of the membrane with aqueous ethanol also released retained nanoparticles. It is worthwhile noting that obtaining retained particles is not always feasible with classic filters when using simple "dead-end" filtration setups, Which are the ones most commonly used at the laboratory scale. The simple fabrication of the membrane, as well as its performance, versatility (filtration and chromatographic regimes), and recyclability represent a significant advantage over conventional membranes with similar rejection properties and performances.

4.2.2 Protein Separation

Following our work on nanoparticle separations, we were interested in membrane-based separations of biological systems, such as proteins, DNA, and viruses, which are important in the field of biotechnology, where polymeric ultrafiltration membranes are used on an industrial scale. Bioseparations represent two key challenges for noncovalent materials: (1) stability at physiological pH and salt concentration, and (2) biocompatibility, i.e., maintaining the structure and function of the filtered biomolecules. In particular, the high salt concentrations under physiological conditions may significantly alter the structure of supramolecular assemblies,

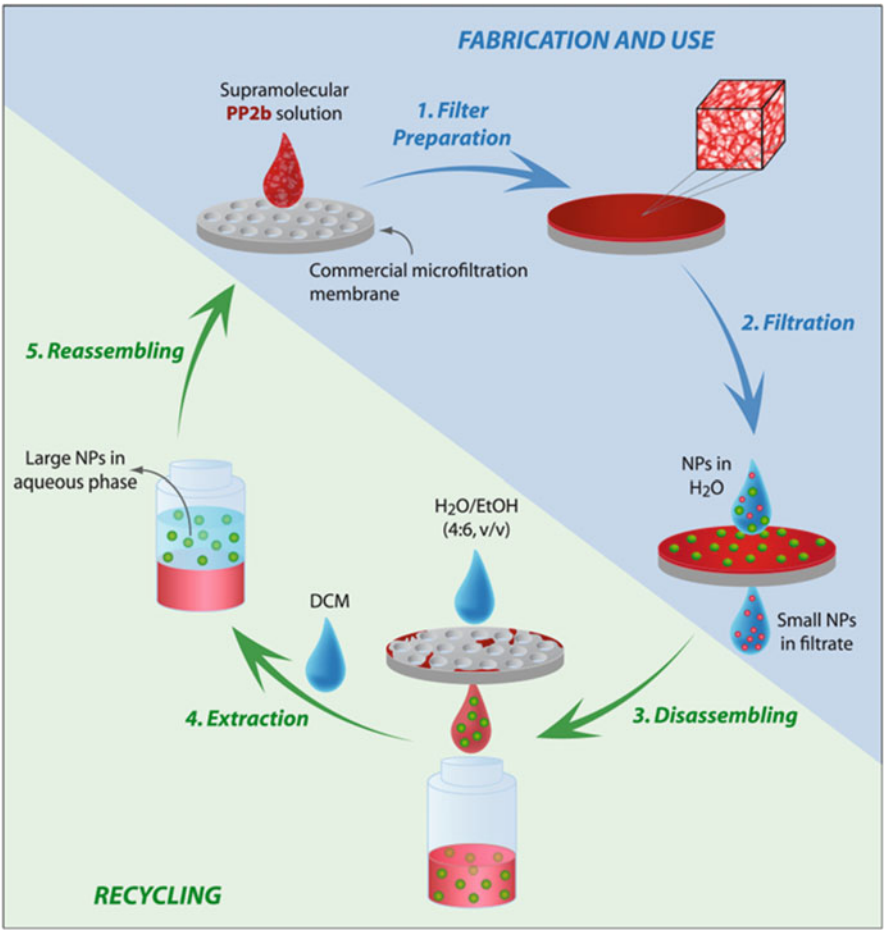

Fig. 15 Fabrication, use, and recycling of a supramolecular membrane based on compound **8** (labeled as *PP2b*) [61]

precluding the applicability of noncovalent arrays for bioseparations. Yet, if strong hydrophobic interactions exist, the assemblies may be essentially nondynamic, with nonpolar groups entirely segregated from the aqueous phase. Therefore, they will not respond to the environment and are analogous to a covalent system. PEG groups that can be partially involved in interfiber interactions may also not be available to interact with ions. To our delight, supramolecular membranes based on **8** proved to be quite stable: they remain robust (no detectable leaching of membrane material) and exhibit stable flow rates under physiological conditions (e.g., 150 mM NaCl or in a buffer containing 20 mM MOPS, 70 mM KCl, and 10 mM $MgCl_2$), indicating that a porous 3D network is preserved [67]. In addition, PEG groups provide a potentially biocompatible hydrophilic environment and minimize the unfavorable electrostatic adsorption of biological macromolecules.

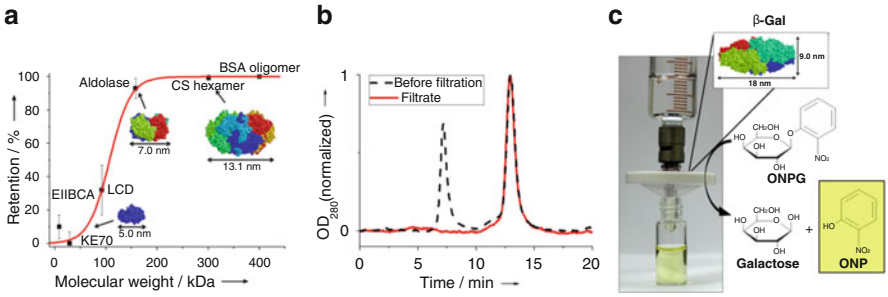

Fig. 16 (**a**) Protein retention against molecular weight (*squares*) and sigmoid fit (*curve*). Protein structures of KE70, aldolase, and CS hexamer are shown. (**b**) Gel filtration chromatogram of a mixture of BSA oligomers and monomers before filtration (*dashed line*), and its filtrate (*solid line*). Filtration quantitatively removes BSA oligomers (retention time (rt) 7 min) from the mixture. Small BSA aggregates (rt 11–12 min) are removed as well. The filtrate contains pure monomeric proteins (rt 13 min). (**c**) Hydrolysis of ONPG into galactose and ONP, catalyzed by membrane-immobilized β-galactosidase [67]

In order to characterize the membrane's performance in protein separation, we carried out filtration experiments using a mixture of six proteins of different sizes: EIIBCA, 8.7 kDa; KE70, 29 kDa; L-carnitine dehydratase (LCD), 92 kDa; aldolase, 158 kDa; citrate synthase (CS) hexamer, 301 kDa; and BSA oligomer, ≥400 kDa. Filtration experiments were carried out using pressure-driven flow ($\Delta p = 0.8$ bar) of a feed solution over a freshly prepared supramolecular membrane on cellulose acetate support. We observed that protein retention is clearly size-dependent (Fig. 16a), exhibiting a 150 kDa molecular weight cutoff, which corresponds to an 8 nm hydrodynamic diameter cutoff. The retention is dominated by size-selective capture (e.g., sieving), rather than specific (e.g., electrostatic) protein adsorption. The cutoff value is in the upper range of commonly used ultrafiltration membranes in biotechnology, allowing the removal of large proteins, nucleic acids, lipids, and other large lysate components. In particular, rapid and quantitative removal of protein aggregates from monomers is a promising application, as was demonstrated by facile separation of a mixture of BSA monomers (67 kDa) and oligomers (≥400 kDa) (Fig. 16b) [67].

The supramolecular membrane material can be cleaned and re-used multiple times; it maintains its separation characteristics after recycling; and the retained proteins can be partially recycled from the membrane by dispersing the used supramolecular membrane in buffer solution, and subsequently removing membrane material via quick centrifugation. Most importantly, the filtration did not affect the enzymatic activity of filtered proteins (both passing and retained), underscoring the biocompatibility of the supramolecular material.

Enhancing its versatility, the supramolecular membrane can also be used to immobilize large enzymes, which enables one to carry out heterogeneous biocatalysis. β-Galactosidase (β-Gal, a large enzyme catalyzing the hydrolysis of glycosidic bonds of β-galactopyranosides) was immobilized (simply by depositing it from buffer

solution) on the membrane, and an activity assay solution containing a substrate (*o*-nitrophenyl-β-galactoside, ONPG) was run through it, resulting in enzyme-catalyzed hydrolysis of ONPG, as manifested by the yellow color of the reaction product (Fig. 16c). The biocatalytic conversion is very stable; it was performed for 6 h under a continuous flow of substrate through the membrane, exhibiting a constant reaction yield of 90% [67]. Overall, our water-based noncovalent membranes are robust, recyclable, and biocompatible, suggesting new avenues for manipulating biological systems.

Addressing the viability and versatility of water-based noncovalent polymeric materials, we have shown that hydrophobic interactions are adequate for creating noncovalent membranes for size-selective separation of nanoparticles and proteins. These membranes exhibit separation properties similar to their covalent counterparts. Unlike conventional membranes, our systems are fully recyclable and more versatile, shaping a paradigm of water-based materials as a viable alternative to covalent systems.

5 Summary

Supramolecular polymers constructed from aromatic amphiphiles in aqueous media can be based on several design concepts. One design is derived from an analogy with hydrogen bonding and relies on pairwise directional interactions. Another design utilizes the intrinsic anisotropy of hydrophobic interactions stemming from aromatic and aliphatic moieties. The outcome of self-assembly in this case can be controlled via tuning of the size and nature of the aromatic, aliphatic, and hydrophilic groups, whose hierarchical assembly modes enable noncovalent synthesis of photofunctional fibers or crystalline arrays. Coordination chemistry has proven to be a convenient tool for promoting diversity-oriented noncovalent synthesis. Furthermore, strong hydrophobic interactions can lead to a breakdown of thermodynamic control; thus, kinetic trapping can be used to regulate self-assembly, enabling diversity and complex supramolecular transformations, where pathway-dependence serves as a powerful synthetic tool. We believe that an important future research direction is mechanistic studies, so that supramolecular transformations will be rationally designed on the basis of retrosynthetic approaches. This requires creating an intellectual framework for noncovalent synthesis, akin to the mechanistically driven methodologies used for covalent synthesis.

Water-based noncovalent polymeric materials such as adaptive membranes or robust self-healing plastic-like hydrogels may generate a paradigm shift in material science, thus introducing the concept of recyclable/self-healing materials that perform as well as the covalent materials, while being more adaptive, versatile, and prone to advantageous fabrication and processing. Similarly to biological systems, these materials largely consist of water, which also make them cost-efficient and environmentally friendly.

Acknowledgments I am grateful to my group members and collaborators who worked on the projects described in this review. This research was supported by the Israel Science Foundation, the Minerva Foundation, the US-Israel Binational Science Foundation, the Gerhardt M. J. Schmidt Minerva Center for Supramolecular Architectures, the Helen and Martin Kimmel Center for Molecular Design, and the Yeda Sela Fund.

References

1. Aida T, Meijer EW, Stupp SI (2012) Science 335:813–8177
2. Krieg E, Rybtchinski B (2011) Chem Eur J 17:9016–9026
3. Oshovsky GV, Reinhoudt DN, Verboom W (2007) Angew Chem Int Ed 46:2366–2393
4. Capito RM, Azevedo HS, Velichko YS et al (2008) Science 319:1812–1816
5. Wang Q, Mynar JL, Yoshida M et al (2010) Nature 463:339–343
6. Ling XY, Reinhoudt DN, Huskens J (2009) Pure Appl Chem 81:2225–2233
7. Mal P, Breiner B, Rissanen K et al (2009) Science 324:1697–1699
8. Cui HG, Webber MJ, Stupp SI (2010) Biopolymers 94:1–18
9. Steed JW (2011) Chem Commun 47:1379–1383
10. Holder SJ, Sommerdijk NAJM (2011) Polym Chem 2:1018–1028
11. Spicer PT (2005) Curr Opin Colloid In 10:274–279
12. Rosen BM, Wilson CJ, Wilson DA et al (2009) Chem Rev 109:6275–6540
13. Rybtchinski B (2011) ACS Nano 5:6791–6818
14. Prins LJ, De Jong F, Timmerman P et al (2000) Nature 408:181–184
15. Prins LJ, Neuteboom EE, Paraschiv V et al (2002) J Org Chem 67:4808–4820
16. Lohr A, Würthner F (2008) Angew Chem Int Ed 47:1232–1236
17. Korevaar PA, George SJ, Markvoort AJ et al (2012) Nature 481:492–496
18. Percec V, Wilson DA, Leowanawat P et al (2010) Science 328:1009–1014
19. Chandler D (2005) Nature 437:640–647
20. Meyer EE, Rosenberg KJ, Israelachvili J (2006) Proc Natl Acad Sci USA 103:15739–15746
21. Grimme S (2008) Angew Chem Int Ed 47:3430–3434
22. Song XD, Geiger C, Farahat M et al (1997) J Am Chem Soc 119:12481–12491
23. Whitten DG, Chen LH, Geiger HC et al (1998) J Phys Chem B 102:10098–10111
24. Kim HJ, Kim T, Lee M (2011) Acc Chem Res 44:72–82
25. Peterca M, Percec V, Leowanawat P et al (2011) J Am Chem Soc 133:20507–20520
26. Wall BD, Tovar JD (2012) Pure Appl Chem 84:1039–1045
27. Faul CFJ, Antonietti M (2003) Adv Mater 15:673–683
28. Diegelmann SR, Gorham JM, Tovar JD (2008) J Am Chem Soc 130:13840–13841
29. Shao H, Nguyen T, Romano NC et al (2009) J Am Chem Soc 131:16374
30. Guan Y, Yu SH, Antonietti M et al (2005) Chem Eur J 11:1305–1311
31. Zhang G, Jin W, Fukushima T et al (2007) J Am Chem Soc 129:719–722
32. Görl D, Zhang X, Würthner F (2012) Angew Chem Int Ed 51:6328–6348
33. Shirman E, Ustinov A, Ben-Shitrit N et al (2008) J Phys Chem B 112:8855–8858
34. Baram J, Shirman E, Ben-Shitrit N et al (2008) J Am Chem Soc 130:14966–14967
35. Golubkov G, Weissman H, Shirman E et al (2009) Angew Chem Int Ed 48:926–930
36. Zhou Y, Shimizu T (2008) Chem Mater 20:625–633
37. Yam VW-W, Wong KM-C, Zhu N (2002) J Am Chem Soc 124:6506–6507
38. Tidhar Y, Weissman H, Wolf SG et al (2011) Chem Eur J 17:6068–6075
39. Zimmerman SC, Zeng F, Reichert DEC et al (1996) Science 271:1095–1098
40. De Greef TFA, Smulders MMJ, Wolffs M et al (2009) Chem Rev 109:5687–5754
41. Brunsveld L, Folmer BJB, Meijer EW et al (2001) Chem Rev 101:4071–4097
42. Castellano RK, Rudkevich DM, Rebek J (1997) Proc Natl Acad Sci USA 94:7132–7137
43. Rehm TH, Schmuck C (2010) Chem Soc Rev 39:3597–3611
44. Chen Z, Lohr A, Saha-Moller CR et al (2009) Chem Soc Rev 38:564–584

45. Harada A (2006) J Polym Sci A Polym Chem 44:5113–5119
46. Zayed JM, Nouvel N, Rauwald U et al (2010) Chem Soc Rev 39:2806–2816
47. Besenius P, Portale G, Bomans PHH et al (2010) Proc Natl Acad Sci USA 107:17888–17893
48. Neelakandan PP, Pan ZZ, Hariharan M et al (2010) J Am Chem Soc 132:15808–15813
49. Arnaud A, Belleney J, Boue F et al (2004) Angew Chem Int Ed 43:1718–1721
50. Obert E, Bellot M, Bouteiller L et al (2007) J Am Chem Soc 129:15601–15605
51. Kilway KV, Siegel JS (2001) Tetrahedron 57:3615–3627
52. Hennrich G, Anslyn EV (2002) Chem Eur J 8:2219–2224
53. Auletta T, Dordi B, Mulder A et al (2004) Angew Chem Int Ed 43:369–373
54. Badjic JD, Nelson A, Cantrill SJ et al (2005) Acc Chem Res 38:723–732
55. Ustinov A, Weissman H, Shirman E et al (2011) J Am Chem Soc 133:16201–16211
56. Pope M, Swenberg CE (1999) Electronic processes in organic crystals and polymers. Oxford University Press, Oxford
57. Shahar C, Baram J, Tidhar Y et al (2013) ACS Nano 7:3547–3556
58. Estroff LA, Hamilton AD (2004) Chem Rev 104:1201–1218
59. Krieg E, Shirman E, Weissman H et al (2009) J Am Chem Soc 131:14365–14373
60. Jong J, Feringa B, Esch J (2006) Responsive molecular gels. Molecular gels. Springer, Dordrecht, pp 895–927
61. Krieg E, Weissman H, Shirman E et al (2011) Nat Nanotechnol 6:141–146
62. Baker R (2004) Membrane technology and applications. Wiley, New York
63. Vandezande P, Gevers LEM, Vankelecom IFJ (2008) Chem Soc Rev 37:365–405
64. Benfer S, Árki P, Tomandl G (2004) Adv Eng Mater 6:495–500
65. Ulbricht M (2006) Polymer 47:2217–2262
66. Shannon MA, Bohn PW, Elimelech M et al (2008) Nature 452:301–310
67. Krieg E, Albeck S, Weissman H et al (2013) PLoS One 8:e63188

Adv Polym Sci (2013) 262: 389–414
DOI: 10.1007/12_2013_237

Published online: 20 October 2013

Peptoids for Biomimetic Hierarchical Structures

Niklas Gangloff and Robert Luxenhofer

Abstract Life as we know it is impossible without formation of hierarchical structures. First and foremost, proteins, that is, sequence-specific polypeptides, are nature′s vanguard in this respect. Peptoids and polypeptoids are structural isomers and analogs to peptides and polypeptides. Here, we review the advancements over the last few years on biomimetic hierarchical structures obtained using polypeptoids. Although the inherently more flexible amide bond in peptoids make the stabilization of secondary structure challenging, it also gives us a tool to direct the conformation of the amide bond by design. As will be seen, this is a particularly important feature of peptoids.

Keywords High-precision polymer · Secondary structure · Self-assembly · Sequence-specific polymer · Synthetic biology · Tertiary structure

Contents

N. Gangloff and R. Luxenhofer (✉)
Functional Polymer Materials, Chair of Chemical Technology of Materials Synthesis, University Würzburg, Röntgenring 11, 97070 Würzburg, Germany
e-mail: robert.luxenhofer@uni-wuerzburg.de

1 Introduction

The 1950s and 1960s were years of great importance in the world of macromolecules, both synthetic and natural. In this issue, we honor the sixtieth anniversary of Hermann Staudinger's Nobel Prize, which he received "for his discoveries in the field of macromolecular chemistry" (http://www.nobelprize.org/nobel_prizes/chemistry/laureates/1953/ Accessed 28 June 2013). Among the many discoveries in chemistry in the twentieth century that tremendously changed human life, synthetic macromolecules such as plastics, resins, and elastomers have probably had, and continue to have, the biggest impact in the daily life of billions of humans.

In the same year as Staudinger received his Nobel Prize, Watson, Crick, Wilkins, and Franklins uncovered the double-helical hierarchical assembly of DNA, for which some of them received the Nobel Prize in physiology and medicine in 1962 (http://www.nobelprize.org/nobel_prizes/medicine/laureates/1962/ Accessed 28 June 2013). Linus Pauling, another Nobel laureate in chemistry, received his Prize in 1954 for "his research into the nature of the chemical bond and its application to the elucidation of the structure of complex substances" (http://www.nobelprize.org/nobel_prizes/chemistry/laureates/1954/). A few years prior -in 1950/1951- Pauling, Corey, and Branson deciphered the nature of helices and sheets in proteins [1, 2]. Perutz and Kendrew used these structural clues to unravel the 3D structure of proteins, namely myoglobin and hemoglobin for the first time in 1958. Another Nobel Prize in chemistry was due (http://www.nobelprize.org/nobel_prizes/chemistry/laureates/1962/ Accessed 28 June 2013). Only 5 years later, Robert Bruce Merrifield made a contribution, which is still the bread and butter of thousands of chemists, biologists, and other researchers in the life sciences [3]. Accordingly, Merrifield received the Nobel Prize in chemistry for developing the most important tool for the non-biological synthesis of sequence-specific (macro)molecules such as peptides, small proteins, and oligonucleotides (http://www.nobelprize.org/nobel_prizes/chemistry/laureates/1984/ Accessed 28 June 2013).

Considering hierarchical structures, proteins are among the most versatile polymers nature has to offer. To describe the complex protein structure, four different levels of hierarchy are used. The primary structure describes the sequence of the building blocks, amino acids. The nature of the peptide bond (in combination

with steric effects of residues) favors the formation of secondary structures, i.e. the local spatial arrangement of the linear chain into turns, helices, sheets, and ribbons. The 3D spatial arrangement of such secondary structures in relation to each other eventually leads us to tertiary structures. If several, duly ordered peptide chains assembly into a well-defined functional superstructure, we use the term quaternary structure. Hemoglobin represents such an assembly, but the term quaternary structure is also used at times for much more complex structures such as virus capsids [4] or chromatin [5].

Very recently, synthetic biologists have been working successfully to rival the structural versatility found in proteins. Using the so-called DNA origami, very intricate patterns were created, albeit often in 2D on surfaces [6]. Although the natural versatility and complexity of RNAs should not go unmentioned, we will concentrate here on peptidomimetic structures for reasons that should become apparent.

The exact control over the hierarchical structure of proteins is of paramount importance for their biological function. Minor errors can have devastating effects. Alzheimer's disease is only one of many severe medical disorders that can be traced to misfolding of proteins [7].

Folding and misfolding of proteins is a complex event that in nature takes place in the complex intracellular environment [8]. The secondary structure formation is driven strongly by the nature of the primary structure, with some amino acids being strong promoters of α-helices and others favoring the formation of β-sheets. Hydrogen bonding is an important factor in these processes and formation of these secondary structures is much faster than the overall assembly (see [9] and references therein). The formation of tertiary structures, however, requires more time and appears to be guided not so much by the secondary structure but more by the topology or contact order, which is the average distance of residues in the primary sequence that are in contact in the folded state. In this case, hydrophobic interactions are an important factor [10, 11].

Here, we review the possibilities for the formation of hierarchical structures using peptoids. Peptoids comprise an oligo- or polyglycine backbone but are, in contrast to peptides, substituted at the amide nitrogen. For the sake of readability, we do not differentiate between oligopeptoids and polypeptoids in this account. It is also noted that we do not differentiate per se between uniform and non-uniform peptoids although we are aware that there are major differences. We would rather differentiate on a case-by-case basis. In general, however, in the vast majority of cases for which hierarchical peptoid structures have been reported, the peptoids were uniform oligopeptoids.

We would like to draw the attention of the interested reader to several previous review articles on polypeptoids, some of them similar in design and scope to our present contribution [12–14]. In particular, we would like to refer to a beautiful contribution by Zuckerman, in which he outlined the "Peptoid Origins" [15]. Similarly, the brief yet comprehensive commentary by Wetzler and Barron describes the "progress in the de novo design of structured peptoid protein mimics" [16].

Here, we aim to give our perspective on the advances, remaining problems, and potential of biomimetic hierarchical structure that can be (potentially) created from polypeptoids. In our opinion, of the different synthetic polymers, polypeptoids form a very interesting platform for the study of complex hierarchical structure.

2 Primary Structure: Synthetic Possibilities

The primary structure of a polypeptide or any other polymer (i.e. the sequence of monomer units) is defined by the synthesis of the polymer. Alternatively, modification after polymer synthesis may alter the identity of certain moieties. This is called polymer analog(ue or ous) modification by polymer chemists, or posttranslational modification [17] in protein biosynthesis. In both cases, this may [18] or may not [19] involve some changes in the sequence of the monomer units; more often, this is not the case.

The dispersity of a macromolecule is a defining factor thereof. The method by which a polymer is synthesized is directly related to its dispersity Đ (Đ $= M_w/M_n$) [20]. Non-controlled polymerizations such as free radical polymerization or step-growth polymerization should yield dispersities of $Đ \approx 2$, in theory. Controlled radical polymerizations will often yield dispersities below 1.2, and many colleagues refer to such products as monodisperse. So-called living polymerizations should ideally lead to polymers that have a molar mass distribution that follows a Poisson distribution (if initiation is considerably faster than propagation), for which the dispersity should depend solely on the degree of polymerization (DP) ($Đ \approx 1 + 1/\mathrm{DP}$). This is the lowest dispersity that can be achieved via polymerization. To obtain even better-defined polymers, we need to use iterative synthesis methods, such as solid phase peptide synthesis (SPPS), which was pioneered by Merrifield. Solid phase organic synthesis is, in general, a widely applicably concept that can be used to create sequence-specific oligomers or small polymers such as oligo(*m*-phenylene ethynylene)s [21]. More regularly, polymers containing amide bonds between the repeat units are prepared [22]. The solid-phase submonomer synthesis (SPSS) of peptoids is very similar to the Merrifield approach. However, some modifications result in synthetic advantages, which will be discussed briefly below.

2.1 Iterative Synthesis

The solid phase-supported synthesis of peptoids was first reported using protected and N-substituted amino acids [23]. A major bottleneck of this approach was the difficult and expensive monomer synthesis. Accordingly, Zuckermann and coworkers developed a different approach in which a monomer unit is formed in two reaction steps. First, a haloacetic acid is coupled to the resin and, second, S_N2 substitution of the halogen with a primary amine takes place (Fig. 1a). The crucial

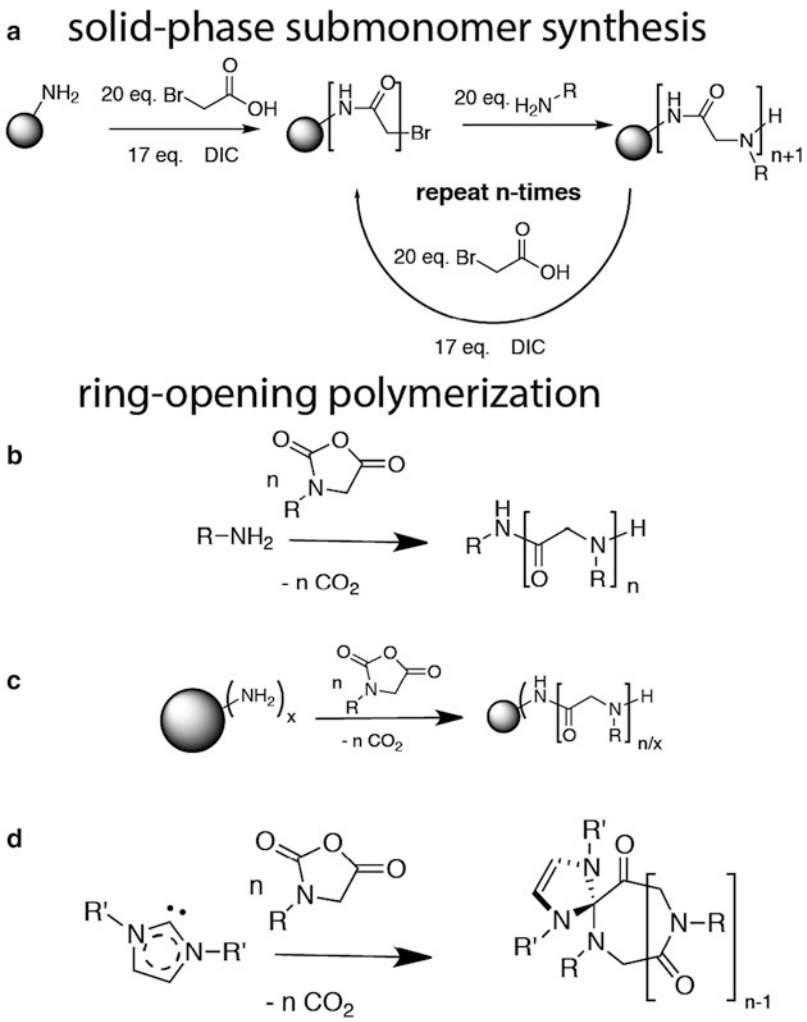

Fig. 1 Synthetic approaches towards peptoids by either (**a**) solid-phase submonomer synthesis or (**b–d**) ring-opening polymerization initiated by nucleophiles such as (**b**) amines in solution, (**c**) amines on solid-phase resins, or (**d**) *N*-heterocyclic carbenes in solution

advantage in this SPSS approach lies in the use of primary amines to introduce the substituent. In contrast to protected amino acids, these are not only readily available in a large variety, but are also often rather inexpensive. Early on, Zuckermann et al. investigated peptoids with side chains that are found at the C_α in amino acids (Fig. 2) but also introduced side chains, which have no counterpart in proteinogenic amino acids (Fig. 3).

Using this method, uniformity with respect to chain length ($Đ = 1,\overline{0}$) and monomer sequence is possible, in theory. In reality, purities ≥95% are regularly

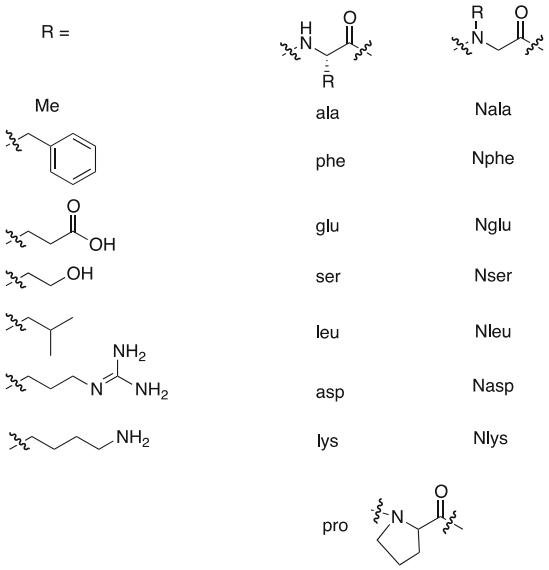

Fig. 2 Comparison of a selection of proteinogenic amino acids and their corresponding N-substituted glycine

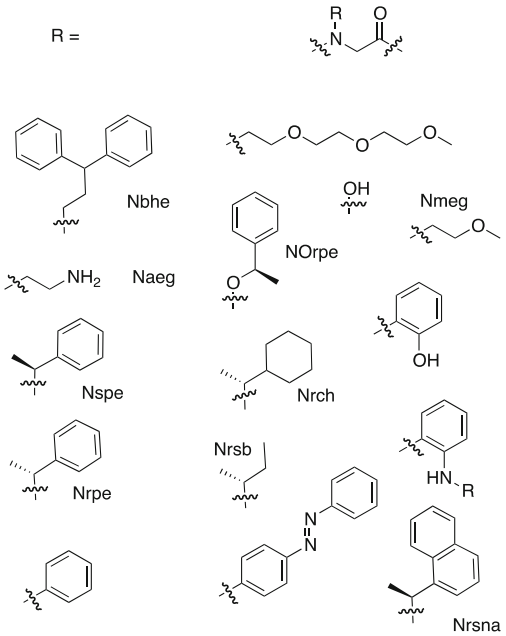

Fig. 3 Small selection of peptoid side chains that have been realized to date. They may be used to direct the adjacent amide bond into either *cis*- or *trans*-conformation, introduce charges along the peptoid backbone, or modify solubility of the peptoid

reported for peptoids with 50 monomer units or less. This is, however, after purification. For one-shot synthesis, a 50-mer is typically regarded as the limit to retain reasonable yields [15]. However, what is considered a reasonable yield often remains unclear.

A large variety of peptoid side chains have been introduced (Fig. 3) [24–27]. Moreover, commercially available automated peptide synthesizers can be used for SPSS. Typically, SPSS is used to prepare sequence-specific peptoids, but Rosales et al. have also demonstrated the successful preparation of highly repetitive sequences that resemble homopolymers, without chain length dispersity [28]. The SPSS is also ideally suited for automation to create large combinatorial libraries via the mix-and-split method [15].

2.2 *Living Polymerization of N-Substituted* N-*Carboxyanhydrides*

The preparation of peptoids by ring-opening polymerization (ROP) of N-substituted *N*-carboxyanhydrides (NNCA, Fig. 1b–d) was first reported as early as 1926 [29]. A few years earlier, the debate over whether macromolecules even existed was still in progress [30], but by this time, Staudinger's concept of polymers [31] was well accepted. Also Sigmund and Wessely recognized the possible formation of polymers in this first report on polysarcosine, without giving any characterization of the substance. That came more than 20 years later, when Waley and Watson studied the kinetics of the polymerization of sarcosine *N*-carboxyanhydride (Sar-NCA) in the laboratories of Courtaulds Ltd. [32]. In this contribution, Waley and Watson provide evidence that the Sar-NCA polymerization was one of the first polymerizations that – in retrospect – was found to exhibit a living character, several years before Szwarc published his famous paper entitled "'Living' polymers" [33].

We find it particularly remarkable that the living anionic and cationic polymerization of unsaturated compounds was a huge success, despite the relatively difficult preparative conditions, while the living character of the Sar-NCA polymerization, which is much easier to handle, went virtually unnoticed by the community (or at least this is our perception 50 years later). Only a handful of research groups studied this class of monomers during the following decades, and mainly to better understand polypeptides [34, 35]. Even less studied was polysarcosine as a material [36–40].

Only a few years ago, Zhang and coworkers discovered a new way to polymerize NNCAs, via catalysis using *N*-heterocyclic carbenes (Fig. 1d) [41]. In passing, they reported on the living polymerization of *N*-butylglycine *N*-carboxyanhydride. This was probably as remarkable as the main finding of the paper because, at that time, only Sar-NCA had been studied in considerable detail. Since then, a few groups have expanded the molecular toolkit of the NNCA polymerization considerably (Fig. 4), but it certainly trails the versatility achievable with SPSS and is not likely to get close in the foreseeable future [14, 42]. Side chain versatility of polymerized peptoids is based on polymer analog modifications [43, 44]. However, polymerization of NNCAs gives access to linear [45, 46] or cyclic [47] hydrophilic,

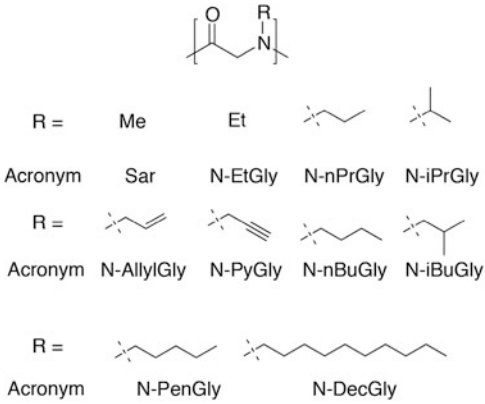

Fig. 4 Molecular toolkit available for the ring-opening polymerization of N-substituted *N*-carboxyanhydrides

hydrophobic, thermoresponsive [48, 49], or amphiphilic peptoids as well as multiblock copolypeptoids [50] with high definition and reproducibility. Also, NNCA polymerization can be performed on surfaces [51] or solid supports [52] without loss of control (Fig. 1c). The possibility to polymerize NNCAs directly on solid supports that are also employed in SPPS or SPSS opens new avenues for the combination of sequence-specific peptoids from step-wise synthesis and narrowly distributed peptoids obtained via polymerization.

3 Secondary Structure Mimetics

Prediction of the secondary structure in proteins has been very successful from the start when Pauling and Corey developed a model for helices in polypeptides. Since then, it has been found that homopolypeptides of natural amino acids have a strong tendency to form secondary structures, either the α-helix or β-sheets [30].

In contrast, it is well known that polysarcosine adopts a random coil formation in aqueous solution. In addition, polysarcosine not only exhibits excellent solubility in water but is also very well soluble in a wide range of organic solvents [45].

Because the backbone of peptoids is inherently flexible and does not favor the *cis*- or *trans*-conformation of the amide moiety sufficiently to induce secondary structure formation, special synthetic strategies are necessary to favor either *cis*- or *trans*-conformation in peptoids.

Peptoids bearing C_α-chiral substituents have been shown to favor the *cis*-conformation (Fig. 5b) [53, 54]. Another way to favor a *cis*-conformation of the amide bond is to implement a favorable interaction between the backbone and the substituent orbital of an adjacent aromatic side chain, which was possible using *N*-α-chiral acetanilide or *N*-1-naphtylethyl substituents ($n \rightarrow \pi^*_{C=O}$ and hydrogen bonding or $n \rightarrow \pi^*_{Ar}$ and steric interactions, respectively) [55]. Interestingly, the *cis*-conformation was only favored in polar solvents, whereas in non-polar solvents

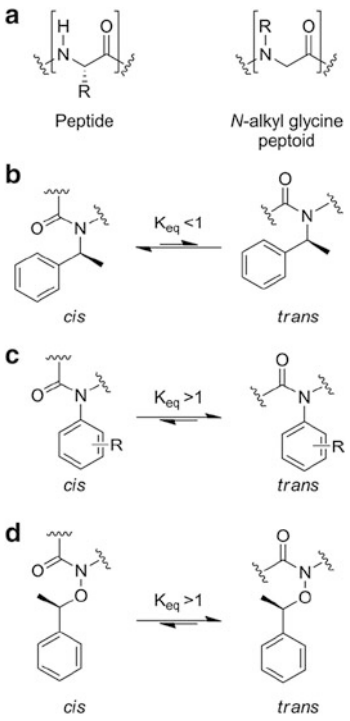

Fig. 5 (**a**) General structure of peptides and *N*-alkyl glycine peptoids. (**b**) Bulky α-chiral substituents induce *cis*-conformation of the amides in peptoids whereas (**c**) *N*-aryl and (**d**) chiral *N*-alkoxy residues direct towards the *trans*-conformation. Reproduced from [57], with permission from Wiley Periodical Inc

the *trans*-conformation was the predominant species. This gives the possibility to design solvent-dependent folding of peptoids.

In contrast, *trans*-amide conformation was strongly favored when aryl substituents were introduced directly at the backbone nitrogen (Fig. 5c) [56]. Similarly, hydroxyl and alkoxyl substituents were demonstrated to direct the amide bond into a *trans*-conformation (Fig. 5d) [57, 58].

3.1 Helices

The first and, to date, most intensively investigated secondary structure motif discovered in proteins were helices [1, 2] Interestingly, the first CD spectra of peptoids with C_α-chiral substituents closely resembled CD spectra of α-helices with a double peak at 203 and 220 nm [59]. Molecular mechanics calculation suggested that these spectra were due to formation of helices that are similar to poly-L-proline type I helices (Fig. 6) [53]. The periodicity of the helix was found to comprise three residues per turn and a pitch of approx. 6 Å. Barron and coworkers investigated the influence of the chain length on the helix stability. It is known that in the case of helicogenic amino acids, oligomers form β-sheets (DP $\lessapprox$ 10) [30, 35]. As chains become longer, they adopt a helical structure. In contrast, in helicogenic peptoids,

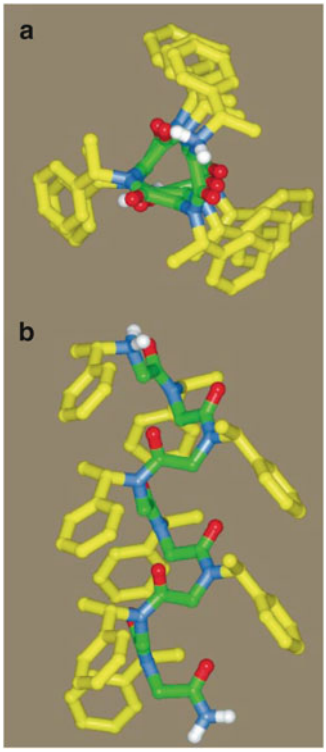

Fig. 6 Predicted structure of $(Nspe)_8$. The atoms along the peptoid backbone are color-coded (*green* carbon; *red* oxygen; *blue* nitrogen; *white* hydrogen); side chain carbon atoms are depicted in *yellow*. The original stereo diagram can be found in [53]. Reproduced from [53], with permission from Current Biology Ltd

helices are observed for oligomers as short as five monomer units and the stability increases up to DP = 15. Interestingly, about 50% of the monomer units must carry α-chiral side chains for helices to form [60–62]. This value in fact fits very well with observations made in 1963 by Fasman and Blout for copolymers of prolin (helicogenic) and sarcosine (non-helicogenic) [63].

Secondary structures such as helices are not restricted to uniform peptoids but have also been described for non-uniform peptoids and structural isomers [47, 64]. Similar to the early reports on helical peptoids, this was achieved by introducing chiral side chains. Interestingly, linear peptoids yielded less intense circular dichroism as compared to cyclic ones, suggesting less stable helices.

Peptoid helices are not stabilized by H-bonding. Regarding the stability of peptoid helices, a mixed impression can be gained from the literature. On the one hand, peptoid helices are very stable against typical denaturants, such as urea and temperature [65]. On the other hand, conformational stability is typically less than that of α-helices. This is evidenced by a rather low persistence length of peptoid helices and low $K_{cis/trans}$ values [60]. Spectroscopic evidence also shows that poly-L-proline helices are less rigid in solution than previously suggested [66, 67]. Similarly, the persistence length of the helices from C_α-chiral peptoids were found to range between 4 and 1 nm, depending on the chain length. Larger persistence

lengths were found for short peptoid sequences as compared to achiral polymers of similar structure. For longer peptoids, the differences were only minor [68]. More bulky substituents can help to sterically stabilize such helices, as has been shown by Blackwell and coworkers [55, 69]. Incorporating the *N*-1-naphtylethyl side chain, peptoid helices showed higher $K_{cis/trans}$ values while retaining the overall helix structure (poly-L-proline type I helix). The authors argued that this would help to increase the water solubility of such helical peptoids because less helix-inducing monomers are necessary. However, it may be argued that the 1-naphtylethyl residues imposed a much more pronounced hydrophobic character as compared to the 1-phenylethyl residues. As has been discussed before, *N*-aryl substituents stabilize the *trans*-conformation in peptoids. Regarding the helix, this translates into poly-L-proline type II helices, as predicted and confirmed by Kirshenbaum and coworkers [56].

Several approaches have been reported for chemical modification of peptoid helices [70–72]. Functionalized helices are interesting for fostering formation of higher-order structures or modifying the solubility. The chemical modification can also be used conveniently to stabilize peptoid helices. For example, Wennemers and colleagues studied helices of 4-azidoproline (Azp) [73]. Although (4*R*)Azp stabilized the poly-L-proline type I helix, its enantiomer (4*S*)Azp destabilized it. Modification of the peptoid was conveniently achieved by click chemistry. Kirshenbaum et al. introduced mutually reactive groups (alkyne and azide) at i and i+3 positions of helicogenic peptoid sequences. By coupling i and i+3 moieties together, very short peptoids were stabilized towards helical structures. Using this approach, the authors claim to be able to reduce the amount of helicogenic building blocks. However, this advantage is partly negated by the need to incorporate at least two residues to stabilize the helix [70].

Zuckermann et al. described a different approach and introduced 1-phenylethyl peptoid side chains with functional groups in the *para*-position of the phenyl ring (Fig. 7). Thus, the functionalities are present at the outer perimeter of the peptoid helices. As such, it allows mimicking of the interaction between α-helices in coiled coils and helix bundles in proteins [74–76].

Bräse, Muhle-Goll and coworkers reported on functional peptoid helices [77]. In order to create cell-penetrating peptoids, butylamine residues were incorporated into peptoids. NMR spectroscopy and molecular modeling revealed an extended pseudo-helical structure with predominant *cis*-conformation in the backbone. The electrostatic repulsion between the side chains leads to maximization of the spacing of the ammonium residues and thus dominates the conformation of the peptoid. With a pitch of 7.7 Å, the charge distribution is somewhat less dense compared to α–helical peptides. Nevertheless, the peptoids were effective transporters, similar to other cell-penetrating peptides.

Kang et al. used a peptoid helix to position porphyrins in different relative orientations. It was found that whether the porphyrins were positioned cofacial, slipped-cofacial, or unstructured had profound effects on the degree of J-aggregation, the resulting color, and excitonic coupling [78]. The authors suggest

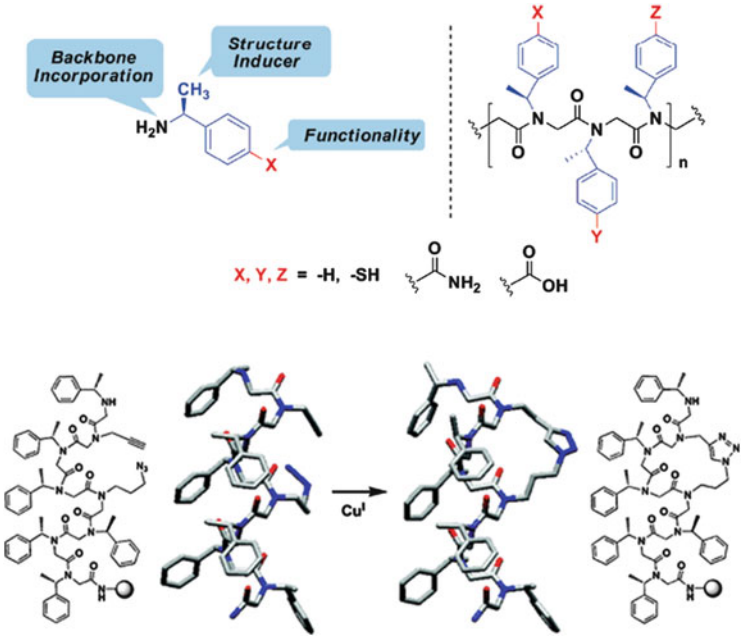

Fig. 7 Representation of the introduction of functional moieties into the perimeter of peptoid helices to modify solubility, helix stability, or formation of higher-order structures. For example, click chemistry has been used to covalently link i and i+3 positions in peptoid sequences, stabilizing the helix structure. Reproduced from [72] and [70], with permission from American Chemical Society

that such structures could be interesting as molecular wires and for the fabrication of artificial photosynthetic complexes.

3.2 Loops, Turns, and Ribbons

Loops and turns are of fundamental importance in many proteins [79–82]. In order to mimic proteins, the successful fabrication of such structures is an important milestone. Barron, Radhakrishnan and coworkers were the first to report on a peptoid nonamer that exhibits a loop-like structure [83]. Interestingly, the nonamer comprised 1-phenylethyl substituents ($Nspe_9$) which, according to reasons discussed earlier, is considered helicogenic. Indeed $Nspe_6$ and $Nspe_{12}$ did give CD spectra that suggest a helical character of the peptoid, whereas the CD spectrum of the nonamer $Nspe_9$ is quite distinct from the other two (Fig. 8). Instead of the expected all-*cis*-conformation, four amide bonds were found to exhibit *trans*-conformation. Formation of the loop is entirely dependent on the formation of H-bonding, which stands in contrast to the peptoid-based secondary structure discussed hitherto. The loop becomes unstable in solvents that can undergo

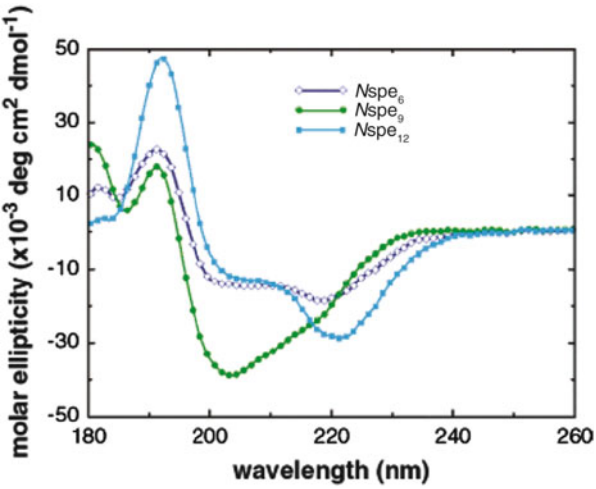

Fig. 8 As evidenced by circular dichroism spectroscopy, the secondary structure of *N*-(1-phenylethyl)glycine oligomers depends strongly on the number of repeat units. Whereas the hexamer *N*spe$_6$ and the dodecamer *N*spe$_{12}$ form helical structures, the nonamer *N*spe$_9$ forms a loop. Reproduced from [83], with permission from American Chemical Society

H-bonding. Therefore, it can be viewed as a starting point for the creation of loops that undertake relevant structural changes upon binding to an external partner (solvent, another peptide, etc.). This is, after all, an important feature of loops in proteins [82].

Shortly after this first study, Gorske and Blackwell were able to show that incorporation of fluorinated aromatics modified the folding behavior. Incorporation of only one unit of 1-pentafluorophenylethyl residue at the N-terminus of a nonamer stabilized the loop. As a result, addition of a protic solvent (methanol) was better tolerated with respect to the conservation of the loop structure [84].

Later, it was shown that other small structural changes within one monomer unit can have a strong influence on the formation of secondary structures. Blackwell et al. prepared peptoid octamers of the helicogenic Nspe that carried a single 1-(nitrophenyl)ethyl residue at the N-terminus. Interestingly, the position of the nitro-moiety (2 or 4 of the phenyl ring) either destabilized or stabilized the threaded loop discussed previously for Nspe$_9$ [85].

Two different approaches were used to induce formation of turns, another important structural motif in proteins. Both approaches have in common that it was necessary to deviate from the peptoid backbone [25, 86]. Apella and coworkers employed a triazole ring to induce a hairpin-like structure (Fig. 9a) [86]. Importantly, this secondary structure was confirmed in aqueous media. In contrast, Blackwell and colleagues introduced a tripeptoid, in which one monomer unit was attached to a peptoid side chain. Moreover, a critical design element was that this substituent was able to undergo H-bonding (Fig. 9b) [25]. Thus, it may be argued that the unique character of peptoid-based secondary structures, which typically are ensured without employment of H-bonding, is lost to some degree.

Very recently, Blackwell and coworkers reported on a peptoid-based ribbon structure. Such ribbons are also found in proteins and may function as cell-membrane-modifying agents and antibiotics [87]. The ribbon structure was

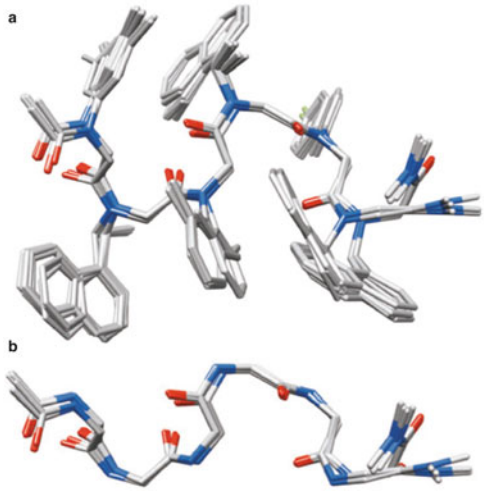

Fig. 9 An ensemble of ten superimposed low-energy structures of a ribbon-forming peptoid hexamer as determined by NMR spectroscopy, depicted with (**a**) and without (**b**) the side chains that induce this secondary structure motif. Reproduced from [87], with permission Wiley-VCH

realized by alternating *cis*- and *trans*-directing substituents in a peptoid hexamer (Fig. 9). This ribbon exhibits, similarly to peptide ribbons, a helical twist with a helical rotation of 36°. Interestingly, $n \rightarrow \pi^*_{C=O}$ interactions, which are important in many helical conformation of peptoids, do not play a major role for this conformation. Circular dichroism studies in acetonitrile/water mixture as well as in methanol showed that the peptoid ribbons were fairly stable in polar and protic solvents. With respect to the backbone, the peptoid ribbon can be described as a series of turns, similar to that observed in peptide ribbons [88].

Overall, research in peptoid-based secondary structures has made tremendous advances in the last few years. Researchers now understand the folding behavior even better and, recently, the first de novo structure prediction was presented [89]. Also, the first tentative studies towards application of peptoid secondary structures can be found in the literature. A peptoid heptamer that includes a side chain with TEMPO (2,2,6,6-tetramethylpiperidine-1-oxyl) showed a strong potential for enantioselective catalytic transformations. Importantly, the enantioselectivity was strongly dependent on the sequence of the peptoid [90]. In enzymes, the tertiary structure is important for their catalytic activity. Therefore, it is only natural that researchers are also attempting to mimic the tertiary structure of proteins with peptoids. In a few cases, these attempts have already proved fruitful.

4 Tertiary Structure Mimetics

The tertiary structure of a protein describes the 3D assembly of atoms in the protein (i.e., one individual polypeptide chain) and is critically determined by the primary and secondary structure. In the words of a polymer scientist, one might call this an

unimolecular assembly (micelle). However, this terminology is not entirely consistent because unimolecular micelles in polymer sciences are typically considered to be composed of dendritic or star-like structures and not linear amphiphiles [91, 92]. In any case, although the previous section discussed issues that may not appear immediately relevant to the traditional polymer chemist, this section briefly reviews recent results that are very interesting with respect to polymer self-assembly.

4.1 Globular Structures

Peptoids have been used as model compounds for many decades to better understand the behavior of peptides. Recently, Zuckermann et al. designed a peptoid 100-mer to study the coil-to-globule transition [93]. It has been established that hydrophobic interactions are an important driving force in the folding of polypeptides in proteins [94–98].

By the reduction to peptoids, Zuckermann and colleagues were able to rule out any effects of H-bonding and secondary structure on the folding and reduce the issue to hydrophobic effects [93]. In this work, two different peptoids were investigated. The first had a regular distribution of the two different repeat units, whereas the second exhibited a more clustered, protein-like distribution with different domains. The sequence of the latter was obtained by molecular dynamics calculations (Fig. 10a). When the coil-to-globule collapse of the two peptoids was experimentally studied by small-angle X-ray scattering and dye incorporation, it became clear that the protein-like sequence collapses to a more compact globule and did so in a more defined manner, that is, the collapse took place in a smaller window of solvent composition (Fig. 10b). This result should help us to improve our understanding of protein folding. However, this also demonstrates the importance of polymer definition and polymer microstructure on the aggregation. We have recently compared the aggregation and endocytosis of random copolymers and block copolymers. Dynamic light scattering provided evidence that the aggregates of the random copolymers were smaller but less defined. When we compared the endocytosis of the copolymers in MCF7-ADR cells, we found a distinct difference [99]. The random copolymer entered the cells much more readily than the block copolymer. Similarly, in an in vitro model of the blood–brain barrier, transport of the dye rhodamine 123 across the barrier was different for block and random copolymers of otherwise similar composition [100]. Although the aggregates in this study were about one order of magnitude larger than the globules studied by Zuckermann, similar effects on the interaction with biological entities may be observed for the peptoids.

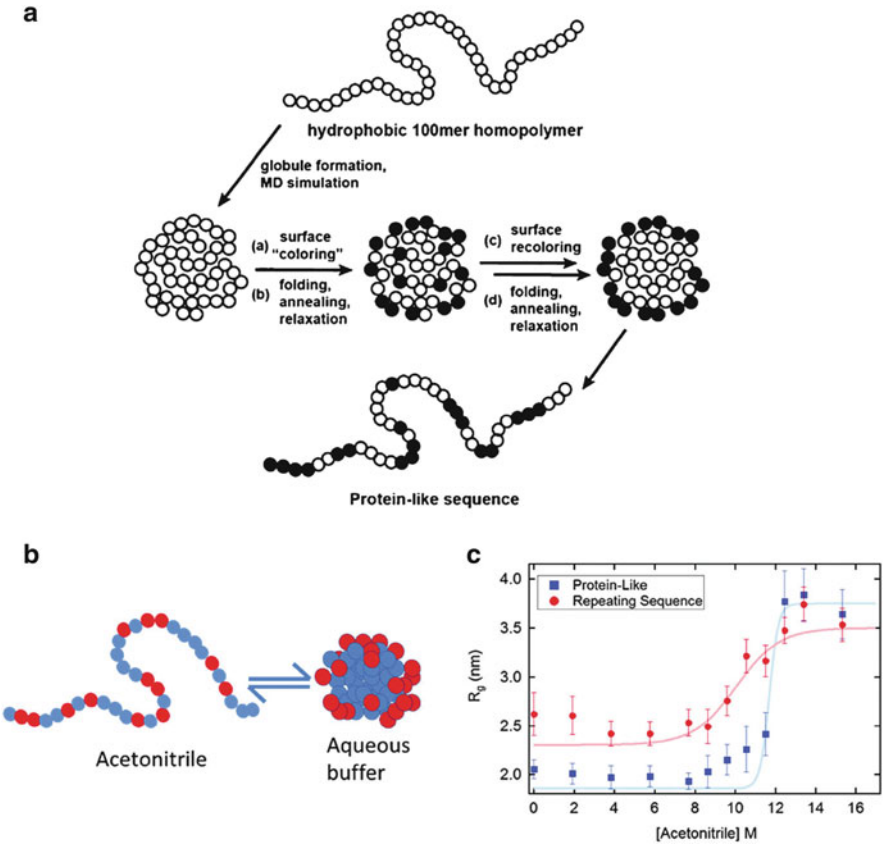

Fig. 10 (**a**) Using molecular dynamics, protein-like peptoid sequences were obtained by iterative process of globule formation and addition/redistribution of polar residues on the globule surface. (**b**) Globule-to-coil transition was induced by titration with acetonitrile, which leads to unfolding of the globules. (**c**) The transition is more pronounced and sharper in the case of the protein-like sequence. Reproduced from [93], with permission from American Chemical Society

4.2 Multihelical Bundles

Bundles of helices are an important feature of tertiary structure in transmembrane proteins and elsewhere. Zuckermann and co-workers used a combinatorial approach to screen 3,400 different 15-mer peptoids for their ability to form aggregates of helices [101]. As a design concept, every third residue unit was chosen from a pool of 12 hydrophobic residues and the remaining monomer units were hydrophilic. Such amphiphilic helices result in structures in which one sector (approximately one third to one half of the outer surface) of the helix is hydrophobic and the rest is hydrophilic (Fig. 11). Hits were identified by fluorescence assay because peptoids that assemble into a structure with a hydrophobic core should

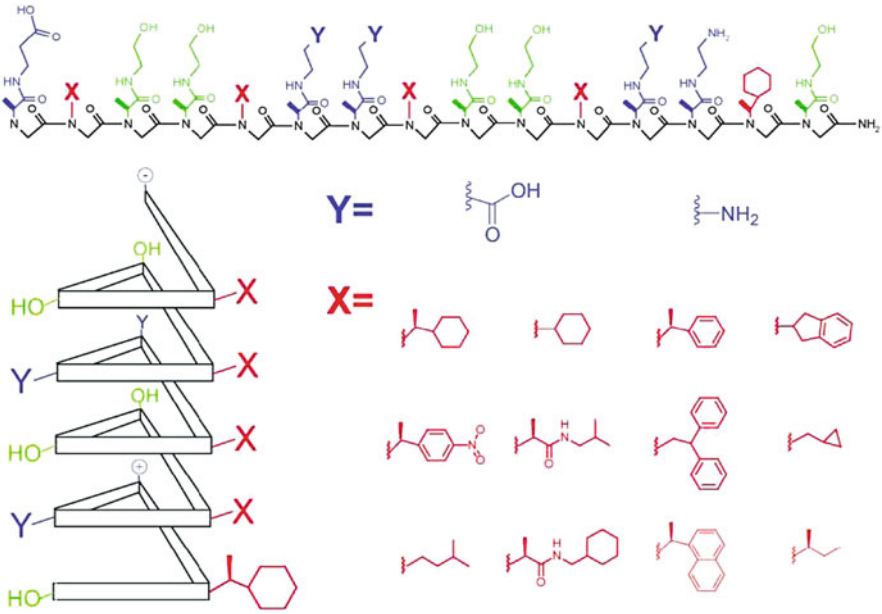

Fig. 11 Library design for 15-mer amphiphilic peptoid sequences with a threefold periodicity: *green* non-ionic hydrophilic residues, *blue* ionic hydrophilic residues, *red* hydrophobic residues. Please note that most substituents are α-chiral to support helix formation. Reproduced from [101], with permission from Elsevier Science Ltd

show an increase in the observed fluorescence intensity. Thus, only about 3% of the prepared peptoids were considered a hit. Size-exclusion chromatography confirmed that these structures formed aggregates with aggregation numbers of 3–4 whereas control peptoids did not.

This concept was later refined when several helices were covalently linked. It was found, using Förster resonance energy transfer (FRET), that these peptoids undergo a cooperative transition into aggregates with a hydrophobic core that was tentatively assigned to a tertiary structure similar to that found in folded proteins (Fig. 11) [102]. In many proteins, the tertiary structure is not (only) stabilized via covalent bonds but also via complex formation with metal ions. Alternatively, metals may act as cofactors for enzyme catalysis, may be stored and distributed using such complexes, or distort enzyme structure and lead to toxicity [103–107]. Zuckermann and coworkers designed a peptoid that should assemble into a two-helix bundle with a zinc-binding site, formed by introduction of a thiol and a imidazole moiety. The position of these chelating moieties was varied and it was found that the positioning had a major effect on the Zn affinity, with apparent k_d values differing by several orders of magnitude. Important to note, zinc had no appreciable effect on the helical structure of the peptoids. Optimized peptoids

exhibited subnanomolar affinities and showed selectivity for Zn over other divalent cations [108].

In summary, a number of crucial tertiary structure motifs have been already realized using peptoids. The final hierarchical level in proteins is the quaternary structure, which will be discussed in the following section.

5 Quaternary Structure Mimetics and Self-Assembly of Peptoids

The previous sections described concepts and structures for realizing secondary and tertiary structure using peptoids. In this, relatively little overlap could be identified with traditional polymer chemistry and self-assembly.

The subject of this section is the self-assembly of different peptoid (macro-) molecules, something which could be also termed the quaternary structure. We are aware that for structural biologists, quaternary structure is a more or less exactly defined supramolecular assembly of multiple folded proteins. We shall not be so strict, if only to leave room for creativity in what might be accomplished with peptoids in the future. In this section, we will discuss briefly supramolecular structures that have been reported using peptoids. Naturally, this is a field much closer to the heart of the polymer chemist.

5.1 Sheets

Sheets, in particular β-sheets, are part of the tertiary structure of proteins. However, to the best of our knowledge, such sheets that comprise only one individual peptoid chain have not been reported to date.

Zuckerman and coworkers have prepared polypeptoids (36-mers), in which anionic or cationic (A) and hydrophobic (B) monomer units alternate in different patterns (AB, ABB, and ABBB). When two such peptoids of the same architecture but opposite charge were mixed, globular aggregates formed. However, within several hours, large but ultrathin sheets of 2.7 nm thickness formed in high yields (Fig. 12) [109]. The peptoid chains were highly extended, as evidenced by aberration-corrected transmission electron microscopy. Extraordinarily large aspect ratios and the exceedingly simple preparation of these sheets by simple mixing of appropriate peptoids are highlights of this approach [110]. Similar sheets are also possible from a single peptoid [111]. The cationic and anionic moieties could be either incorporated in an alternating or block-like manner as long as the hydrophobic and ionic moieties were alternating. Because the aggregation is dependent on electrostatic and hydrophobic interactions, the sheet formation was pH dependent and organic solvents could perturb the hydrophobic interactions, destroying the aggregates.

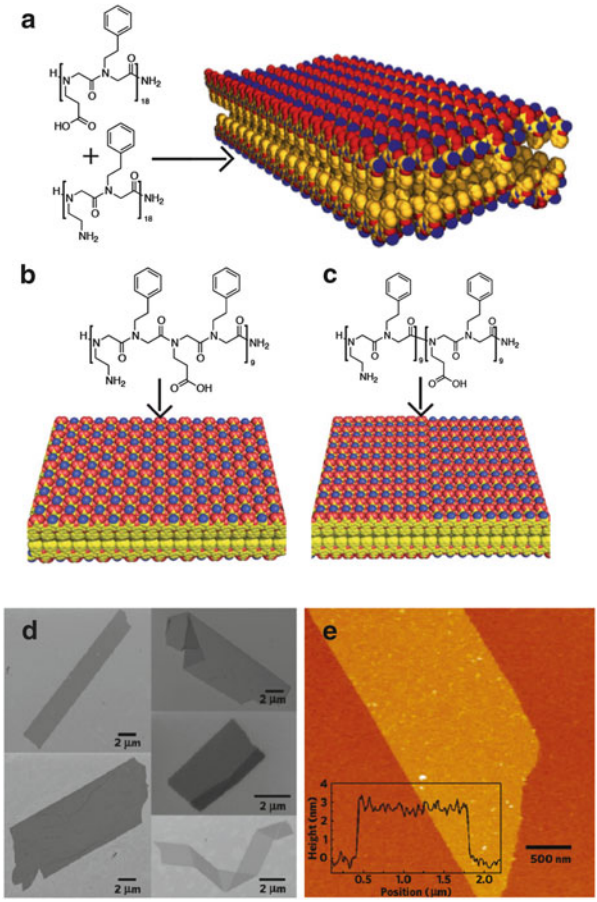

Fig. 12 (**a**–**c**) Molecular models of 2D sheets formed by self-assembly of amphiphilic oligopeptoids. (**d**) Scanning electron microscopy images and (**d**) atomic force microscopy height scans of sheets formed from two different peptoids (**a**) on substrate. Reproduced, with modification, from [109] and [111], with permission from Macmillan Publishers Ltd. and Wiley Periodicals Inc

5.2 Superhelices

Another important structural feature that can be viewed as a quaternary structure according to our definition and that is regularly found in proteins and nucleic acids is the superhelix (e.g. collagen fibrils) or coiled-coils.

Superhelices are also accessible via self-assembly of peptoids. For this, the same peptoids that were described for sheet formation in the previous section were used. Only in this case, peptoids of the same charge were dissolved in water. When anionic and hydrophobic monomer units were strictly alternating, the polymers formed nanosheets upon dissolution in water. After several days, however, superhelical structures appeared that, once formed, were stable for months in solution (Fig. 13). The helices were submicron (624 ± 69 nm) in diameter and were found to be up to 40 µm long. Most interestingly, the observed helices were homochiral, despite the fact that the building blocks are achiral (Fig. 13). Again,

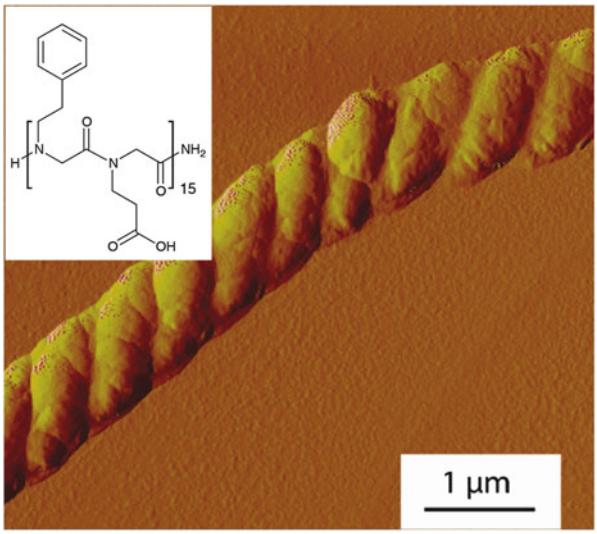

Fig. 13 Atomic force microscopy scan of a superhelix formed from a sequence specific 15-mer with alternating hydrophobic and anionic moieties. Reproduced, with modifications from [112], with permission from the American Chemical Society

ABB and ABBB monomer patterns did not result in defined structures. It is important to note that the superhelices only formed when about 50–70% of the carboxylates were deprotonated, giving an optimal balance between charge repulsion and water solubility [112].

5.3 Nanotubes

In a series of papers, Kimura and coworkers studied the self-assembly of amphiphilic peptoid–peptide hybrid block copolymers [113]. Although the hydrophobic peptide block (six alternating repeats of leucine and 2-aminoisobutyric acid) was uniform, the peptoid part was synthesized via nucleophilic living ring-opening polymerization (NuLROP) of sarcosine-NCA. Two different lengths of the hydrophilic block were investigated, DP = 10 and DP = 27. The polymer with the longer hydrophilic block resulted in very homogenous nanotubes. Upon addition of the polymer with the shorter hydrophilic block, Y-junctions appeared (Fig. 14). Such Y-junctions have also been observed in other systems and represent very interesting building blocks for the assembly into structures of higher hierarchy [114]. Upon addition of polymers of identical composition but different chirality (from the leucine), the tubes merged into spherical assemblies upon heating due to formation of stereocomplexes [115]. The same group provided evidence that the curvature of the formed nanotubes depends on the ratio of the length of the different blocks of different chirality, underlining the importance of tight synthetic control. As mentioned before, the hydrophobic block was prepared by solid-phase synthesis and was therefore uniform [116].

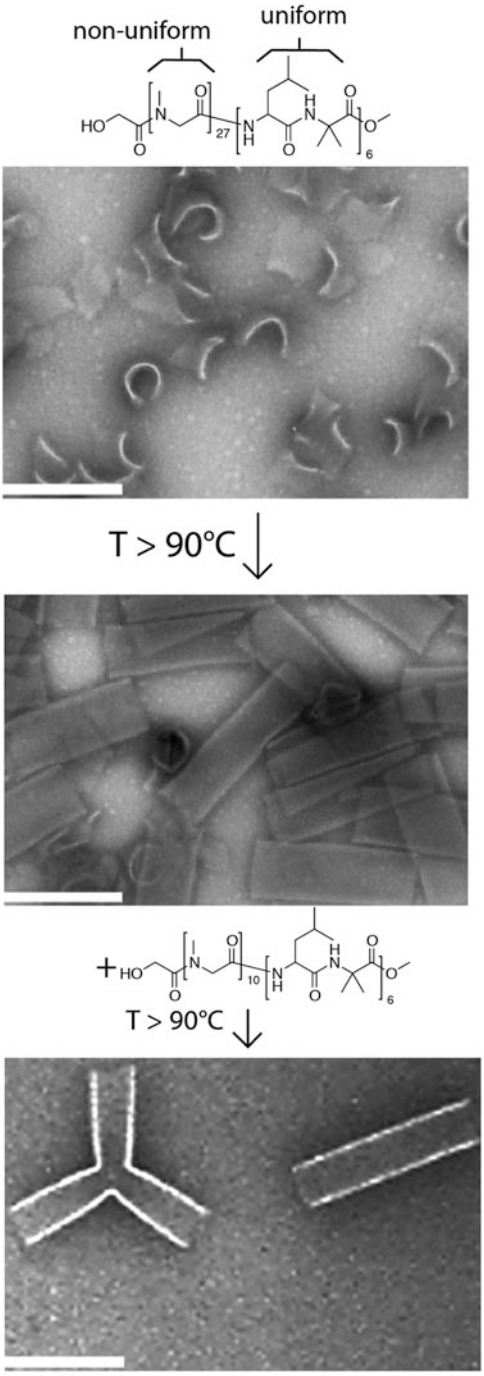

Fig. 14 Block copolymer, comprising a non-uniform polysarcosine block and a uniform dodecapeptide, assembles to curved sheets in water (*top image*). Upon heating, these transform into well-defined tubes (*center image*). Addition of a block copolymer with a shorter water-soluble block leads to the formation of three-way tubular structures (*lower image*). *Scale bars*: 200 nm. Reproduced, with modifications, from [113], with permission from Wiley-VCH

5.4 Worm-like Micelles

Zhang and coworkers studied the differences between self-assembly of cyclic and linear nonionic amphiphilic copolypeptoids of *N*-methyl- and *N*-decylglycine [117]. The differences were minor with respect to the final product but differed in the formation kinetics. Initially, spherical micelles formed in methanolic or aqueous solutions/suspensions. However, within a few days, both materials eventually formed cylindrical (worm-like) micelles. These micelles were only a few nanometers in diameter but several microns in length.

6 Conclusion and Outlook

Peptoids are an extremely versatile materials platform. They can be prepared either in a step-wise synthesis to yield sequence-specific oligomers and small polymers or by ring-opening polymerization. Both synthetic approaches are very interesting for the formation of hierarchical structures. As opposed to solid-phase peptide synthesis, SPSS uses reagents that are typically very inexpensive and readily available in a large variety. Although the sequence-specific uniform peptoids have been studied in great detail and tremendous advances have been made, the non-uniform peptoids that are accessible via ring-opening polymerization have been studied much less. In part, this can be attributed to the fact that it was established only very recently that NuLROP of NNCAs is very versatile and can be used to prepare complex yet well-defined polymers. The future will show whether this synthetic promise can be translated into interesting and complex hierarchical structures via self-assembly. From the perspective of a polymer chemist, it will be particularly interesting to see what contribution non-uniform peptoids make possible. We now have the tools to combine SPSS and ring-opening polymerization, but whether these tools are particularly helpful in creating more complex hierarchical structure more easily remains to be elucidated.

Clearly, the potential that peptoids hold for the preparation of hierarchical structures and self-assemblies has not been fully explored. We think that recent advances in both SPSS and NuLROP extend this potential even further. For the creation of hierarchical structures, peptoids appear to be an ideal platform due to the synthetic flexibility and definition available for peptoids, but much remains to be done.

Many authors have stated that one goal is the preparation of a peptoid-based synthetic enzyme. It appears that all the pieces for this puzzle are now available and we expect the puzzle to be solved in the near future.

Acknowledgement We gratefully acknowledge financial support from the German Plastics Center SKZ and the Universität Würzburg for start-up funding.

References

1. Pauling L, Corey RB (1950) J Am Chem Soc 72:5349
2. Pauling L, Corey RB, Branson HR (1951) Proc Natl Acad Sci USA 37:205
3. Merrifield RB (1963) J Am Chem Soc 85:2149
4. Taylor DJ, Krishna NK, Canady MA, Schneemann A, Johnson JE (2002) J Virol 76:9972
5. Bram S, Butler-Browne G, Baudy P, Ibel K (1975) Proc Natl Acad Sci USA 72:1043
6. Han D, Pal S, Nangreave J, Deng Z, Liu Y, Yan H (2011) Science 332:342
7. Chiti F, Dobson CM (2006) Annu Rev Biochem 75:333
8. Gething M-J, Sambrook J (1992) Nature 355:33
9. Dobson CM (2003) Nature 426:884
10. Plaxco KW, Simons KT, Baker D (1998) J Polym Sci Pol Phys 277:985
11. Makarov E (2003) Protein Sci 12:17
12. Fowler SA, Blackwell HE (2009) Org Biomol Chem 7:1508
13. Sun J, Zuckermann RN (2013) ACS Nano 7(6):4715–4732
14. Luxenhofer R, Fetsch C, Grossmann A (2013) J Polym Sci Polym Chem 51:2731
15. Zuckermann RN (2011) Biopolymers 96:545
16. Wetzler M, Barron AE (2011) Biopolymers 96:556
17. Walsh CT, Garneau-Tsodikova S, Gatto GJ (2005) Angew Chem Int Ed 44:7342
18. Yokoyama M, Inoue S, Kataoka K, Yui N, Sakurai Y (1987) Makromol Chem Rapid 8:431
19. Luxenhofer R, Jordan R (2006) Macromolecules 39:3509
20. Stepto RFT (2010) Polym Int 59:23
21. Mio MJ, Prince RB, Moore JS, Kuebel C, Martin DC (2000) J Am Chem Soc 122:6134
22. Hartmann L, Börner HG (2009) Adv Mater 21:3425
23. Simon RJ, Kania RS, Zuckermann RN, Huebner VD, Jewell DA, Banville S, Ng S, Wang L, Rosenberg S, Marlowe CK, Spellmeyer DC, Tan R, Frankel AD, Santi DV, Cohen FE, Bartlett PA (1992) Proc Natl Acad Sci USA 89:9367
24. Yoo B, Kirshenbaum K (2008) Curr Opin Chem Biol 12:714
25. Stringer JR, Crapster JA, Guzei IA, Blackwell HE (2010) J Org Chem 75:6068
26. Shah NH, Kirshenbaum K (2008) Org Biomol Chem 6:2516
27. Kapoor R, Eimerman PR, Hardy JW, Cirillo JD, Contag CH, Barron AE (2011) Antimicrob Agents Chemother 55:3058
28. Rosales AM, Murnen HK, Zuckermann RN, Segalman RA (2010) Macromolecules 43:5627
29. Sigmund F, Wessely F (1926) H-S Z Physiol Chem 157:91
30. Kricheldorf HR (2006) Angew Chem Int Ed 45:5752
31. Staudinger H (1920) Chem Ber 53:1073
32. Waley SG, Watson J (1949) P Roy Soc Lond A Mat 199:499
33. Szwarc M (1956) Nature 178:1168
34. Sisido M, Imanishi Y, Higashimura T (1977) Makromol Chem 178:3107
35. Kricheldorf HR (1987) α-Aminoacid-N-carboxyanhydrides and related materials. Springer, New York
36. Kidchob T, Kimura S, Imanishi Y (1996) J Contr Release 40:285
37. Kidchob T, Kimura S, Imanishi Y (1997) J Appl Polym Sci 63:453
38. Kidchob T, Kimura S, Imanishi Y (1998) J Contr Release 50:205
39. Aoi K, Hatanaka T, Tsutsumiuchi K, Okada M, Imae T (1999) Macromol Rapid Commun 20:378
40. Aoi K, Nakamura R, Okada M (2000) Macromol Chem Phys 201:1059
41. Guo L, Zhang D (2009) J Am Chem Soc 131:18072
42. Zhang D, Lahasky SH, Guo L, Lee C-U, Lavan M (2012) Macromolecules 45:5833
43. Lahasky SH, Serem WK, Guo L, Garno JC, Zhang D (2011) Macromolecules 44:9063
44. Robinson JW, Schlaad H (2012) Chem Commun 48:7835
45. Fetsch C, Grossmann A, Holz L, Nawroth JF, Luxenhofer R (2011) Macromolecules 44:6746
46. Fetsch C, Luxenhofer R (2013) Polymers 5:112

47. Guo L, Li J, Brown Z, Ghale K, Zhang D (2011) Biopolymers 96:596
48. Lahasky SH, Hu X, Zhang D (2012) ACS Macro Lett 1:580
49. Robinson JW, Secker C, Weidner S, Schlaad H (2013) Macromolecules 46:580
50. Fetsch C, Luxenhofer R (2012) Macromol Rapid Commun 33:1708
51. Schneider M, Fetsch C, Amin I, Jordan R, Luxenhofer R (2013) Langmuir 29:6983
52. Gangloff N, Fetsch C, Luxenhofer R (2013) Macromol Rapid Commun 34:997
53. Armand P, Kirshenbaum K, Falicov A, Dunbrack RL, Dill KA, Zuckermann RN, Cohen FE (1997) Fold Des 2:369
54. Armand P, Kirshenbaum K, Goldsmith RA, Farr-Jones S, Barron AE, Truong KT, Dill KA, Mierke DF, Cohen FE, Zuckermann RN, Bradley EK (1998) Proc Natl Acad Sci USA 95:4309
55. Gorske BC, Stringer JR, Bastian BL, Fowler SA, Blackwell HE (2009) J Am Chem Soc 131:16555
56. Shah NH, Butterfoss GL, Nguyen K, Yoo B, Bonneau R, Rabenstein DL, Kirshenbaum K (2008) J Am Chem Soc 130:16622
57. Jordan PA, Paul B, Butterfoss GL, Renfrew PD, Bonneau R, Kirshenbaum K (2011) Biopolymers 96:617
58. Crapster JA, Stringer JR, Guzei IA, Blackwell HE (2011) Biopolymers 96:604
59. Kirshenbaum K, Barron AE, Goldsmith RA, Armand P, Bradley EK, Truong KT, Dill KA, Cohen FE, Zuckermann RN (1998) Proc Natl Acad Sci USA 95:4303
60. Wu CW, Sanborn TJ, Zuckermann RN, Barron AE (2001) J Am Chem Soc 123:2958
61. Wu CW, Sanborn TJ, Huang K, Zuckermann RN, Barron AE (2001) J Am Chem Soc 123:6778
62. Wu CW, Kirshenbaum K, Sanborn TJ, Patch JA, Huang K, Dill KA, Zuckermann RN, Barron AE (2003) J Am Chem Soc 125:13525
63. Fasman GD, Blout ER (1963) Biopolymers 1:99
64. Luxenhofer R, Huber S, Hytry J, Tong J, Kabanov AV, Jordan R (2013) J Polym Sci Polym Chem 51:732
65. Sanborn TJ, Wu CW, Zuckermann RN, Barron AE (2002) Biopolymers 63:12
66. Doose S, Neuweiler H, Barsch H, Sauer M (2007) Proc Natl Acad Sci USA 104:17400
67. Best RB, Merchant KA, Gopich IV, Schuler B, Bax A, Eaton WA (2007) Proc Natl Acad Sci USA 104:18964
68. Rosales AM, Murnen HK, Kline SR, Zuckermann RN, Segalman RA (2012) Soft Matter 8:3673
69. Stringer JR, Crapster JA, Guzei IA, Blackwell HE (2011) J Am Chem Soc 133:15559
70. Holub JM, Jang H, Kirshenbaum K (2007) Org Lett 9:3275
71. Vaz B, Brunsveld L (2008) Org Biomol Chem 6:2988
72. Seo J, Barron AE, Zuckermann RN (2010) Org Lett 12:492
73. Kümin M, Sonntag L-S, Wennemers H (2006) J Am Chem Soc 129:466
74. Yu YB (2002) Adv Drug Deliv Rev 54:1113
75. Lupas AN, Gruber M (2005) Adv Protein Chem 70:37
76. Xu T, Shu J (2009) Soft Matter 6:212
77. Sternberg U, Birtalan E, Jakovkin I, Luy B, Schepers U, Bräse S, Muhle-Goll C (2013) Org Biomol Chem 11:640
78. Kang B, Chung S, Ahn YD, Lee J, Seo J (2013) Org Lett 15:1670
79. Leszczynski JF, Rose GD (1986) Science 234:849
80. Fiser A, Do RKG, Sali A (2000) Protein Sci 9:1753
81. Shehu A, Kavraki LE (2012) Entropy 14:252
82. Wheatley M, Wootten D, Conner T, Simms J, Kendrick R, Logan T, Poyner R, Barwell J (2012) Br J Pharmacol 165:1688
83. Huang K, Wu CW, Sanborn TJ, Patch JA, Kirshenbaum K, Zuckermann RN, Barron AE, Radhakrishnan I (2006) J Am Chem Soc 128:1733
84. Gorske BC, Blackwell HE (2006) J Am Chem Soc 128:14378

85. Fowler SA, Luechapanichkul R, Blackwell HE (2009) J Org Chem 74:1440
86. Pokorski JK, Miller Jenkins LM, Feng H, Durell SR, Bai Y, Appella DH (2007) Org Lett 9:2381
87. Crapster JA, Guzei IA, Blackwell HE (2013) Angew Chem Int Ed 52:5079
88. Karle IL, Flippen-Anderson J, Sukumar M, Balaram P (1987) Proc Natl Acad Sci USA 84:5087
89. Butterfoss GL, Yoo B, Jaworski JN, Chorny I, Dill KA, Zuckermann RN, Bonneau R, Kirshenbaum K, Voelz VA (2012) Proc Natl Acad Sci USA 109:14320
90. Maayan G, Ward MD, Kirshenbaum K (2009) Proc Natl Acad Sci USA 106:13679
91. Newkome GR, Moorefield CN, Baker GR, Saunders MJ, Grossman SH (1991) Angew Chem Int Ed 30:1178
92. Kurniasih IN, Liang H, Kumar S, Mohr A, Sharma SK, Rabe JP, Haag R (2013) J Mat Chem B 1(29):3569-3577 doi:10.1039/c3tb20366b
93. Murnen HK, Khokhlov AR, Khalatur PG, Segalman RA, Zuckermann RN (2012) Macromolecules 45:5229
94. Wiggins PM (1997) Physica A 238:113
95. Arai M, Kuwajima K (2000) Adv Protein Chem 53:209
96. Hecht MH, Das A, Go A, Bradley LH, Wei Y (2004) Protein Sci 13:1711
97. Zarrine-Afsar A, Wallin S, Neculai AM, Neudecker P, Howell PL, Davidson AR, Chan HS (2008) Proc Natl Acad Sci USA 105:9999
98. Dill KA, Ozkan SB, Shell MS, Weikl TR (2008) Annu Rev Biophys 37:289
99. Barz M, Luxenhofer R, Zentel R, Kabanov AV (2009) Biomaterials 30:5682
100. Hemmelmann M, Metz VV, Koynov K, Blank K, Postina R, Zentel R (2012) J Contr Release 163:170
101. Burkoth TS, Beausoleil E, Kaur S, Tang D, Cohen FE, Zuckermann RN (2002) Chem Biol 9:647
102. Lee B-C, Zuckermann RN, Dill KA (2005) J Am Chem Soc 127:10999
103. Theodore Gillman MH (1958) Brit Med J 2:635
104. Coleman JE (1992) Annu Rev Biochem 61:897
105. McCall KA, Huang C-C, Fierke CA (2000) J Nutr 130:1437S
106. Blasie CA, Berg JM (2002) Biochemistry 41:15068
107. Magyar JS, Weng T-C, Stern CM, Dye DF, Rous BW, Payne JC, Bridgewater BM, Mijovilovich A, Parkin G, Zaleski JM (2005) J Am Chem Soc 127:9495
108. Lee B-C, Chu TK, Dill KA, Zuckermann RN (2008) J Am Chem Soc 130:8847
109. Nam KT, Shelby SA, Choi PH, Marciel AB, Chen R, Tan L, Chu TK, Mesch RA, Lee BC, Connolly MD, Kisielowski C, Zuckermann RN (2010) Nat Mater 9:454
110. Sanii B, Kudirka R, Cho A, Venkateswaran N, Olivier GK, Olson AM, Tran H, Harada RM, Tan L, Zuckermann RN (2011) J Am Chem Soc 133:20808
111. Kudirka R, Tran H, Sanii B, Nam KT, Choi PH, Venkateswaran N, Chen R, Whitelam S, Zuckermann RN (2011) Biopolymers 96:586
112. Murnen HK, Rosales AM, Jaworski JN, Segalman RA, Zuckermann RN (2010) J Am Chem Soc 132:16112
113. Kanzaki T, Horikawa Y, Makino A, Sugiyama J, Kimura S (2008) Macromol Biosci 8:1026
114. Jain S, Bates FS (2003) Science 300:460
115. Ueda M, Makino A, Imai T, Sugiyama J, Kimura S (2011) Chem Commun 47:3204
116. Ueda M, Makino A, Imai T, Sugiyama J, Kimura S (2011) J Pept Sci 17:94
117. Lee CU, Smart TP, Guo L, Epps TH, Zhang D (2011) Macromolecules 44:9574

Adv Polym Sci (2013) 262: 415–430
DOI: 10.1007/12_2013_268

Published online: 16 November 2013

Stimuli-Sensitive Microgels from Native Elastin: An Easy Approach for a Drug Release System

Smriti Singh, Fuat Topuz, Krystyna Albrecht, Jürgen Groll, and Martin Möller

Abstract Thermo- and pH-responsive microgels were prepared from solubilized native elastin by crosslinking of the elastin lysine residues with poly(ethylene glycol) diglycidyl ether (PEG-DGE) and with bis(sulfosuccinimidyl) suberate (BS3). In the first case, a peptide-PEG conetwork was obtained whereas, in the second case, the elastin peptides were interlinked with hydrophobic bridges. The structure of the microgels was controlled by the ratio of crosslinker to elastin and by performing the crosslinking reaction in an inverse minielemulsion, yielding particles with a diameter in the submicron range. Depending on the degree of crosslinking, the hybrid microgels exhibited a volume change transition at 37 and 35.5°C and pH responsivity in the range of 5–7 for microgels crosslinked with PEG-DE and BS3, respectively. This temperature- and pH-responsive behavior can be assigned to the well-investigated coacervation of elastin peptides, demonstrating that the elastin functionality is abolished only by rather dense crosslinking. In spite of the broad distribution in the molecular weight of the elastin molecules, the microgels remained soluble. Light scattering and sedimentation experiments demonstrated that the coacervation occurred predominantly intramolecularly, i.e., by collapse in the core while the corona stabilized the colloidal dispersion against precipitation. Preliminary experiments were conducted to evaluate the suitability of these microgels for use as a drug-release system and demonstrated

S. Singh, F. Topuz, and M. Möller (✉)
DWI-Interactive Materials Research and Institute of Technical and Macromolecular Chemistry, RWTH Aachen University, Forckenbeckstrasse 50, 52056 Aachen, Germany
e-mail: moeller@dwi.rwth-aachen.de

K. Albrecht and J. Groll
DWI-Interactive Materials Research and Institute of Technical and Macromolecular Chemistry, RWTH Aachen University, Forckenbeckstrasse 50, 52056 Aachen, Germany

Department and Chair of Functional Materials in Medicine and Dentistry, University Hospital Würzburg, Pleicherwall 2, 97070 Würzburg, Germany

cytocompatibility, enzymatic degradability by elastase, and entrapping and slow release of a water-soluble biopolymer (Texas Red-labeled dextran with $M_w = 70{,}000$). In summary, we present an easy entry to functional biohybrid microgels, where the responsiveness to temperature and pH can be exploited further for application of the microgel as a drug carrier.

Keywords Inverse miniemulsion · Microgels · Native elastin · pH responsive · Thermoresponsive

Contents

1 Introduction

Covalently crosslinked hydrogel particles of size in the nanometer to micrometer range (i.e., microgels), have found increasing interest for controlled and targeted drug delivery [1–3]. These particles are soft colloids that are swollen by the aqueous medium in which they are dispersed. Typically, they have a gradient in the distribution of their crosslinks, such that the corona contains more dangling ends and the crosslinks are more densely distributed in the core. This gradient not only results in a gradient of the swelling but also in a gradient of the solubility/solubilization, mostly due to endgroup effects [4]. Thus, if the solvent quality is decreased, the hydrogel particles tend to collapse first in the core and maintain a solubilizing corona. In this aspect they can be regarded as a primitive analogue to proteins that can adopt a globular structure with the hydrophilic segments directed towards the outside.

In the medical application of micro- and nanoparticles for the therapeutic delivery of an active ingredient important aspects are:

Premature removal from the circulating blood must be avoided before the target is reached
Active ingredients must not be leached out
The particles must be taken up in the organ to be treated
The particle itself must be degraded afterwards so that the polymer does not remain in the body to exert unwanted long term effects.

Here, hydrophilic micro- and nanogels can provide certain advantages. Protein adsorption or opsonization makes nanoparticles recognizable for phagocytic cells, but is strongly reduced for hydrogels due to their hydrophilic nature and high water content [1, 5]. Active ingredients may be linked covalently or entrapped in the network and released by degradation. Targeting is promoted by the high mobility of the soft gel particles in the smallest capillaries. As for other nanoparticles, targeting can be effected by the EPR effect (enhanced permeability and retention) observed for tumor tissue [6] and by decoration with specific ligands, (e.g., peptides and glucosides). In contrast to solid nanoparticles, hydrophilic nanogels can be designed to respond to changes in temperature and pH by a change in the degree of swelling. Furthermore and due to their open structure, degradability can be designed to be triggered rather specifically and instantaneously by changes in the environment. The latter may be achieved by biohybrid nanogels or nano-conetworks, where the biological constituent ensures a specific responsiveness and degradability. Beyond the scope of this work, modern tools to design biopolymers open further perspectives to introduce specific and predictable bioactive functions, such as the ability to present receptor-binding ligands, cell-triggered proteolytic degradation, and natural remodeling.

Here we report on the synthesis and properties of micro-conetworks from solubilized elastin derivatives using poly(ethylenglycol) (PEG) prepolymers or bis(sulfosuccinimidyl)suberate (BS3) as crosslinker for the elastin. We demonstrate that such micro-conetworks can be prepared in an easy procedure from soluble elastin peptides obtained by partial hydrolysis of native elastin. Because of the biodegradability of the elastin peptide, such hydrogels are fully biodegradable. The molecular weight of the remaining PEG chains is chosen sufficiently low so that these can be removed from the body via the renal system. In addition to the biocompatibility and biodegradability, the elastin component provides thermal and pH-dependent transformation at 35.5 or 37°C and pH 5–7, depending on the crosslinker used, from a swollen hydrogel to a globular state. Potentially, the responsiveness of the elastin component to pH and temperature can be exploited to trigger endosomal uptake in cells and release of drugs bound to the network. Based on these findings, it appeared attractive to us to prepare hydrophilic micro-conetworks of soluble elastin, as prepared by standard methods [7]. We expected that such hydrogel colloids can be prepared even from solubilized elastin samples that undergo coacervation like the well-defined elastin-like peptides (ELPs) [8–11], and that such particles can serve as a carrier for drugs where loading and release as well as internalization by cells can be affected by the volume change phase transition.

Elastin is the primary structural component of elastic tissues, e.g., it accounts for about 50 wt% of the total vascular extracellular matrix [12, 13]. Primarily it is formed from tropoelastin molecules as a precursor that assemble to microfibrils and are covalently interlinked by enzymatic oxidation of four lysine residues to desomosine units. The primary structure comprises hydrophilic segments with the lysine units and repeating hydrophobic polypenta- and polyhexapeptide sequences [14] that act as an entropic spring [15, 16]. Furthermore, temperature- and pH-dependent coacervation has been demonstrated for tropoleastin and ELPs [17, 18]. This coacervation effect is thought to be related to the self-assembly mechanism for the formation of the microfibrils [12, 19]. The controlled coacervation of ELPs has been exploited for novel and intriguing drug delivery concepts, e.g., injectable depots of an ELP fusion protein [10]. Another example is ELP block copolymers fused to a protein, which assemble into thermoresponsive micelles [11]. This concept has been extended to enable specific uptake into tumor cells by temperature-controlled assembly only in the tumor, as is possible in hyperthermia therapy. ELP block copolymers were conjugated to pentaarginine blocks that were presented at the surface of the micelles and triggered cell penetration only when they were assembled by the micelle formation. The experiments indicated that endocytosis plays an important role in internalization [20].

2 Experimental Details

2.1 Materials

Soluble elastin ES12 was purchased from Elastin Company (USA) as a salt-free lyophilized powder. Elastin Company indicates a molecular weight of 60,000 Da, but that the sample contains lower molecular weight peptides and smears on PAGE. Coacervates are formed at pH 5 and 37°C. Samples were dissolved in borate buffer (pH 9). Poly(ethylene glycol) diglycidyl ether (PEG-DGE) ($M_W = 526$ g/mol) and bis(sulfosuccinimidyl) suberate (BS3) ($M_W = 572.43$ g/mol) were purchased from Sigma Aldrich (Germany) and Piercenet Biotechnology Inc (USA) respectively. *N*-Hexane (99%, VWR), Span 80 (Sigma), Tween 80 (Sigma), tetrahydrofuran (99% Sigma Aldrich), Texas Red dextran ($M_W = 70$ KDa, *Leunonostoc* bacteria, Invitrogen) were used as received. Dialysis membranes (molecular weight cut-off 3.5, 25, and 100 kDa) were purchased from Spectrum Laboratories.

2.2 Elastin-PEG DGE and Elastin-BS3 Microgels

Microgels were prepared by the inverse miniemulsion method with molar ratios of elastin to crosslinker of 1:2, 1:1.5, 1:1 1:0.5, and 1:0.25. By agitation for 10 min,

25 mg (4.166×10^{-4} mmol) of elastin was dissolved in 125 μL of 0.04 M PBS buffer (pH 9) and dispersed in 1.25 mL *n*-hexane containing 37.5 mg surfactant (3:1 weight ratio of Span 80 and Tween 80). Subsequently, the dispersion was ultrasonicated under ice cooling for 60 s using a Branson sonifier W450 with a ¼ horn at a duty cycle of 30% and output control of 90%. Crosslinking was effected by addition of PEG-DGE or BS3 followed by a further sonication for another 60 s. The dispersion was further agitated for 45 min at room temperature before the reaction was quenched by addition of 1.5 mL of acidic water (pH 3). Separation of the microgels was achieved by centrifugation at 10,000 rpm for 30 min with subsequent decantation of the supernatant. Microgels present in the aqueous layer were carefully washed with hexane (2 × 1.5 mL) and THF (4 × 2.5 mL) in order to remove the surfactants and unreacted elastin. The remaining organic solvents and acid were removed by dialysis. Purified microgels were stored in Millipore water at 4°C for further use.

2.3 XTT Cytotoxicity Test

Cytocompatibility of the BS3-elastin microgels with molar ratio of 1:0.5 was investigated by XTT-based cell proliferation assay (Roche XTT Cell Proliferation Kit II, catalog no. 1465015) according to the manufacturer's guidelines. The gels were prepared on the bottom of 96-well polystyrene plates. Human umbilical vein endothelial cells (HUVECs) (10,000 per well) and 500 μL of 10% fetal bovine serum medium were added to the wells (1.77 cm^2), and the mixtures were incubated in 5% CO_2 at 37°C for 96 h. To halt the experiment, aliquots of XTT stock solution (5 mg/mL) were added to each experimental well group at a ratio of 50/100 μL/μL of medium. Experimental plates were incubated for 4 h, and samples (100 μL) from each well were transferred to 96-well plates and quantified using a TECAN reader at a λ of 490 nm and a reference λ of 655 nm.

2.4 Sedimentation Analysis

Sedimentation of microgels was investigated with a LUMiFuge 114 separation analyzer (L.U.M. GmbH, Germany). Measurements were performed in glass tubes at acceleration velocities of 500–3,000 rpm at 20°C. The slope of the sedimentation curves was used to calculate the sedimentation velocity, indicating the colloidal stability of the samples.

2.5 Field Emission Scanning Electron Microscopy

Field emission scanning electron microscopy (FESEM) analysis was performed with a HITACHI S-4800 instrument in a cryo-mode with secondary electron image resolution of 1.0–1.4 nm at voltages of 1–15 kV. For all measurements, aqueous solutions of nanogels with a concentration of 5 mg/mL were rapidly vitrified in liquid propane and transferred to the high vacuum Balzers BF freeze-etching chamber. Fracture surfaces were prepared by means of a lever and etched by sublimation of the vitrified water for 5–15 min.

2.6 UV–Visible Spectrophotometer

UV–visible spectra were determined using a Varian Cary 100 Bio-UV-Visible split-beam spectrophotometer running with Cary WinUV scan application with a capacity of measuring six samples at a time. Samples were scanned at 500 nm. A high-intensity Xe flash lamp was used as the source for UV light, which permits taking 80 data per second.

2.7 Zeta Potential Measurements

Measurements were performed at 20°C as a function of pH in the range of 3–10 by addition of 0.01 M HCl or 0.01 M NaOH using a Malvern Zetasizer Nano ZS. Microgel solutions with a concentration of 5 mg/mL were dialyzed in standard 1 mM KCl solution and measured in disposable polystyrene cuvettes. One hundred scans were made for each sample and the zeta potential was calculated using Henry's equation. Expert System software was used for data interpretation.

2.8 Dynamic Light Scattering

Microgel solutions of about 1 mg/mL in double-distilled water were passed through a 5-μm poly(tetrafluoroethylene) membrane filter. The particle sizes were measured by photon correlation spectroscopy performed at an angle $\theta = 90°$with a setup consisting of an ALV-SP8 goniometer, an ALV-SIPC photomultiplier, a multiple τ digital real-time ALV-7004 correlator, and a solid state laser (Koheras) with a wavelength of 473 nm as the light source. Sample cuvettes were immersed in a toluene bath and thermostatted within an error of ±0.1°C. Autocorrelation functions (ACF) of intensity fluctuations g_2 (q, t) in the self-beating mode were measured and expressed by the Siegert relation:

$$g_2(q,t) = A\left(1 + \beta|g_1(q,t)|^2\right) \tag{1}$$

where t is the decay time, A is a measured baseline, β is the coherence factor, and $g_1(q,t)$ is the normalized first-order electric field time correlation function related to the measured relaxation rate Γ according to Eq. (2):

$$g_1(q,t) = \mathrm{e}^{-\Gamma t} = \int G(\Gamma)\,\mathrm{e}^{-\Gamma t}\,\mathrm{d}\Gamma \tag{2}$$

Deconvolution of the measured intensity autocorrelation was achieved by the DTS software. For a pure diffusive relaxation, Γ is related to the translational diffusion coefficient D at $q \to 0$ and $c \to 0$ according to Eq. (3):

$$D = \Gamma/q^2 \tag{3}$$

The hydrodynamic radius R_h is calculated by the Stokes–Einstein equation as $R_h = {}^{k_\mathrm{B}T}\!/_{6\pi\eta D}$ with q, k_B, T and η being the scattering vector, the Boltzmann constant, absolute temperature, and solvent viscosity, respectively. A hydrodynamic radius distribution was calculated from the Laplace inversion of $g_1(t)$ by using the CONTIN procedure. Thermoresponsivity of nanogels was investigated between 10 and 55°C. In order to check the reversibility of the hydrodynamic radius with temperature transition, five heating and subsequent cooling cycles were performed. Influence of pH was investigated at 20°C.

2.9 Circular Dichroism Spectroscopy

Circular dichroism (CD) measurements were carried out with an Olis 17 DSM; a Cary 17 monochromater was used with a spectral output of 184–260 nm. CD spectra were measured at protein concentrations of 0.5 mg/mL using a cell with 0.090 mm light path in the wavelength range of 190–260 nm, with a bandwidth of 2.00 nm and with number of increments of 50 with an integration time of 20 s at 20°C. CD spectra were expressed in terms of mean residue ellipticity (deg cm^2 dmol^{-1}). The depicted data represent an average of five scans.

2.10 Enzymatic Degradation

Degradation of microgels was investigated in 5 mM elastase in PBS buffer at 37°C and followed by measuring the hydrodynamic radius of the microgels by dynamic light scattering (DLS) after every 180 s for a total time of 24 h.

2.11 Model Drug Release

PEG-DGE-1:0.25, PEG-DGE-1:0.5, BS3-1:0.25, and BS3-1:0.5 crosslinked microgels loaded with Texas Red-dextran were prepared by adding the dextran (15 wt% of dextran with respect to elastin) to the aqueous phase in the inverse emulsion in which the microgels were synthesized, under the same conditions as the blank samples. In order to determine the amount of Texas Red-dextran taken up by the micro-conetworks, the extracted Texas Red-dextran in the separated water was quantified by measuring the absorbance at 596 nm and using a standard calibration curve. The difference from the feed was taken as the amount loaded to the microgels. To study the release of loaded dextran at 20 and 40°C, the microgels were taken up in 10 mL PBS buffer at pH 5 by shaking the cuvettes at 100 rpm. After leaving for 0, 1, 5, 10, 15, 25, 36, 48 or 72 h, the microgels were centrifuged. The release was monitored by measuring the extinction of the supernatants. The sedimented microgels were resuspended in fresh buffer solution. All studies were performed in triplicate and the cumulative release was normalized to the original uptake:

$$\text{Encapsulation efficiency\%} = (D_t/D_0) \times 100, \tag{4}$$

where D_t is the actual amount of the dextran in the microgel at time t and D_0 is the initial amount of dextran in the microgel.

3 Results and Discussion

Solubilized native elastin with a molecular weight range of 10–60 kDa was dispersed in an inverse miniemulsion and crosslinked by reaction of PEG-DGE or BS3 with the ε-amino groups of lysines in the sequence of the elastin peptide fragments (Scheme 1).

PEG-DGE crosslinked microgels can be regarded as a conetwork of the hydrophilic PEGs and the thermoresponsive elastin. In contrast, the linking groups of the BS3 crosslinked microgels are hydrophobic and are expected to promote precipitation above the coacervation temperature. The crosslinking density was varied by adding different amounts of the telechelic linkers. In Table 1, the amount of linker is given as a molar ratio of elastin and linker based on the molecular weight of $M_n = 60{,}000$. Ratios of 4–0.5 crosslinker per elastin molecule correspond to relatively low crosslinking degrees because of the lower molecular weight fraction in the elastin sample. It must be noted, however, that the microgels were fractionated by separation of very loosely crosslinked and very small particles during the isolation/sedimentation procedure. Thus, the crosslinker ratios can only be taken as an indication of the relative variation in crosslinking density. Figure 1 depicts the most densely crosslinked microgels (elastin to crosslinker ratio of 0.5) by scanning electron microscopy (SEM) cryo-electron micrographs as quenched from ambient

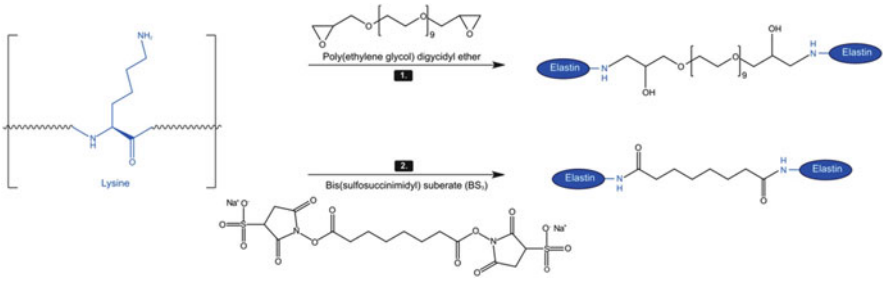

Scheme 1 Elastin chemical crosslinking reactions

Table 1 Hydrodynamic radii (R_h) and swelling ratios as a function of crosslinker concentration at 20°C

	PEG-DGE			BS3		
$\frac{\text{ES 12}}{\text{Linker}}$ (mol/mol)	R_h (PDI) (nm)	$\frac{R_h(50°)}{R_h(20°)} \times 100$ (%)	$\frac{R_h^3(50°)}{R_h^3(20°)} \times 100$ (%)	R_h (PDI) (nm)	$\frac{R_h(50°)}{R_h(20°)} \times 100$ (%)	$\frac{R_h^3(50°)}{R_h^3(20°)} \times 100$ (%)
4	878 (0.5)	53	15	752 (0.5)	63	24
2	735 (0.5)	49	11	431 (0.5)	63	23
1	680 (0.5)	56	17	225 (0.5)	89	70
0.67	370 (0.5)	67	27	215 (0.4)	92	77
0.5	334 (0.5)	63	63	170 (0.5)	96	86

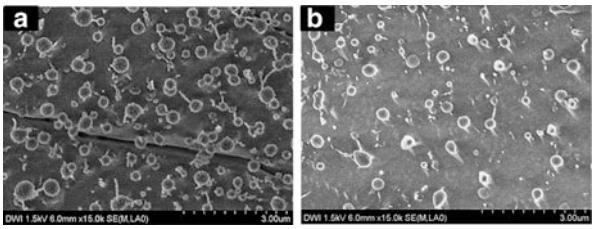

Fig. 1 Cryo-FESEM images showing (**a**) elastin-PEG-DGE and (**b**) elastin-BS3 microgels prepared with 0.5 equivalents of the crosslinker

temperature, i.e., below the coacervation temperature. Irrespective of the type of crosslinker, both samples demonstrate the formation of spheres with diameters in the range of 250 nm $< d <$ 550 nm for PEG-DGE and 200 nm $< d <$ 350 nm for BS3-based crosslinking. These sizes are in good agreement with the hydrodynamic radii determined by light scattering (see Table 1). In many cases, the electron micrographs demonstrate the presence of protrusions, indicating a gradient in density from the core towards the outside, as established for microgels prepared by precipitation polymerization [4].

In order to verify that the microgel samples are in general biocompatible we used a cell proliferation assay. All microgel samples were proven cytocompatible throughout the 6-day cell culture experiment, with no significant effect on cell proliferation. These results demonstrate that ES12 microgels may be used for further in vitro or in vivo experiments.

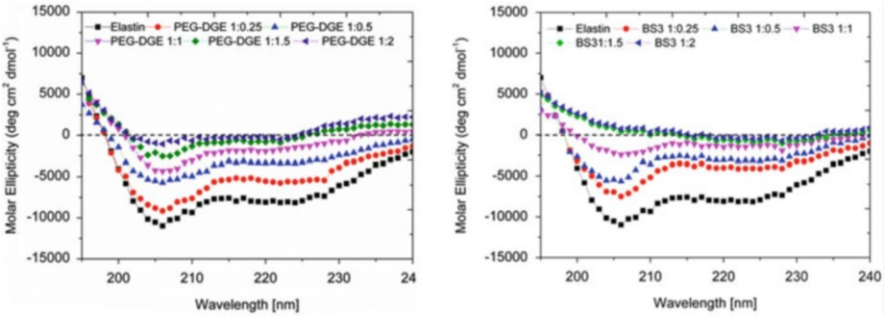

Fig. 2 CD spectra of elastin before and after crosslinking in a PEG-DGE (*left*) and BS3 (*right*) microgel

Circular dichroism spectroscopy allows one to follow conformational changes of the elastin peptides that are caused by the crosslinking. Solubilized elastin exhibits a negative band near 200 nm that is characteristic of unfolded proteins with segments in the PPII conformation [8, 21]. Upon coacervation, the CD spectra indicate a conformational change to an α-helix with two negative bands at 208 and 224 nm and a positive band at 193 nm [8]. Figure 2 displays the CD spectra of ES12 measured at 20°C and of samples crosslinked by different amounts of PEG-DGE and BS3. The negative band at 222 nm indicates the onset of the formation of α-helical conformations. In a first approximation, we calculated a helix content of 22%, and 11% for the samples with least PEG-DGE and BS3 respectively [22–24]. For high degrees of crosslinking, the CD spectra indicated a fully disordered elastin structure. The change in CD spectra suggests that the conformation-controlled coacervation becomes impeded by higher degrees of crosslinking of the microgels.

All microgel samples were characterized by DLS regarding the hydrodynamic radius and the polydispersity at 20°C and at 50°C, the latter temperature being in the regime where the elastin ES12 undergoes coacervation, i.e., above the temperature of 37°. Results are summarized in Table 1. The light scattering data demonstrate a significant shrinkage of the particle size when the temperature was raised from 20 to 50°C. It must be noted that the crosslinking was achieved at room temperature, i.e., under conditions where the elastins were fully soluble.

Remarkably, all particles remained soluble or dispersable as single particles, irrespectively of whether they were compacted by a high degree of crosslinking or by raising the temperature above the volume change transition. This can be regarded as indicating preferential collapse in the core of the particles while hydrophilic segments and endgroups remain oriented towards the outside. Also, sedimentation experiments demonstrated an increase in the rate of sedimentation that corresponds to intramolecular collapse of the dispersed microgel particles, i.e., the rate of sedimentation changes in a rough approximation with $1/R_h$ [25].

Figure 3 depicts the corresponding plots of the temperature versus the hydrodynamic radii. As expected from the CD experiments, the volume change transition became as less pronounced and even vanished with the strength of elastin

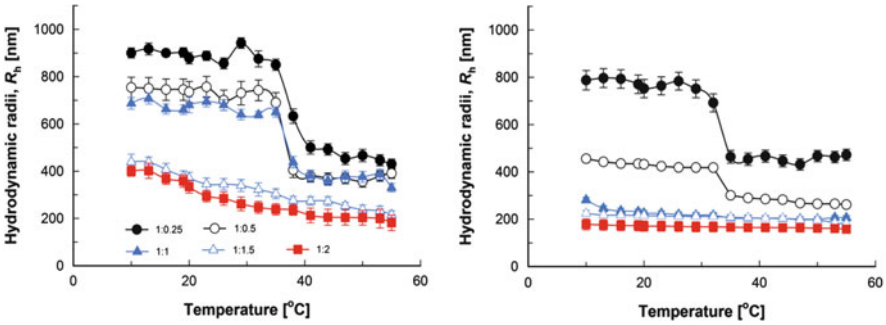

Fig. 3 Hydrodynamic radius (R_h) of PEG-DGE (*left*) and BS3 (*right*) crosslinked microgels as a function of temperature (10–55°C)

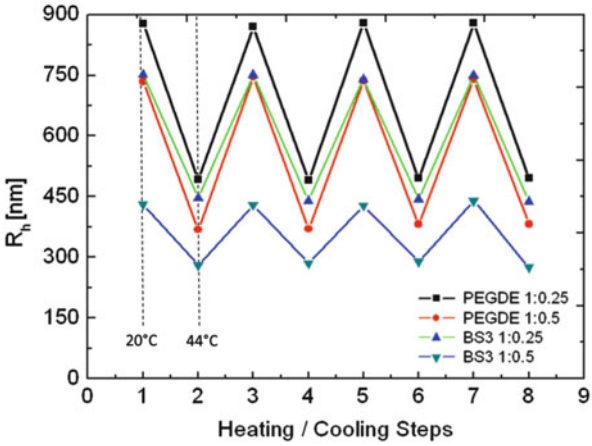

Fig. 4 Hydrodynamic radii (R_h) during changes upon repeated heating and cooling of PEG-DGE (1:0.25), PEG-DGE (1:0.5), BS3 (1:0.2), and BS3 (1:0.5) crosslinked microgels

crosslinking. At low degrees of crosslinking, the volume change transition was well developed, irrespectively of whether the gel particles were crosslinked by the hydrophilic PEG-DGE or the hydrophobic BS3. Correspondingly, the swollen hydrodynamic radii of the BS3-elastin microgels were in general smaller than those of the PEG-DGE-elastin microgels and also the volume change occurred at lower temperature. This is similar to the behavior of polyacrylamide microgels with amide residues that differ in their hydrophilicity.

For the least crosslinked microgels, with ES12 to crosslinker ratio equal to 4, DLS experiments and R_h determinations were repeated within four heating and cooling cycles, alternating the temperature between 20 and 44°C (Fig. 4). The repeated change in R_h was reversible and also the polydispersity index (PDI) of the microgels did not broaden, demonstrating that neither coagulation nor extraction of free chains occurred to a significant extent.

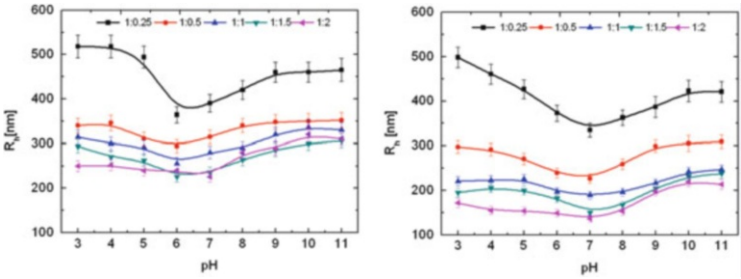

Fig. 5 Change in hydrodynamic radius (R_h) as a function of pH (3–11) for (**a**) PEG-DGE (*left*) and (**b**) BS3 (*right*) crosslinked microgels

Soluble elastin prepared by the method of Partridge [7] has an isoelectric point around pH 5. Correspondingly, we measured isoelectric points between pH 5 and 6 for ES12-PEG-DGE and around 6 for BS3 crosslinked microgels. For the elastin at low ionic strength, it has been reported that the coacervation temperatures exhibit a minimum around pH 5, i.e., coincident with the isoelectric point. Correspondingly, a pH-dependent collapse has been expected for the microgels. This was confirmed by the variation in the hydrodynamic radius, R_h with pH, as shown in Fig. 5. For PEG-DGE microgels, R_h decreased from pH 3–6 and increased again from pH 7–11. A minimum in size was also found for the BS3 crosslinked microgels, but shifted to pH 7. The collapse was in both cases fully reversible. Similarly to the temperature-dependent measurements of the hydrodynamic radius, the collapse was more pronounced for the loosely crosslinked samples.

Degradation of the elastin microgels is expected to be catalyzed by the enzyme elastase. Elastase is known to cleave peptidic bonds at the lysine units, i.e., in the hydrophilic segments. In order to evaluate the enzymatic degradation of the elastin microgels, the dispersed microgels were incubated with the enzyme at 37°C in a BPS buffered solution at 37°C and samples characterized by DLS for the decrease in hydrodynamic radius with time. At this temperature, the microgels are in the collapsed state and the enzymatic degradation is expected to occur as an erosion process from the surface. Figure 6 depicts the change in particle size within a period of 1 day for the least crosslinked elastin microgels. Initially, the hydrodynamic radius increased as the particles were further swollen when the first elastin bridges were split. Afterwards, the radius decreased nearly linearly to full degradation after about 16 h for the PEG-DGE-elastin microgel, while the BS3-elastin microgel clearly degraded in two steps, more quickly at the beginning and then with a significantly reduced degradation rate. Such an effect might be explained by a change in crosslinking density and swelling from the outside towards the core of the particles.

As an example of a water-soluble biopolymer that can be entrapped in and released from the elastin microgels we choose a dextran that has been used as a blood plasma expander. Loading of the microgels with the model drug dextran was achieved by addition of dextran to the inverse emulsion during microgel

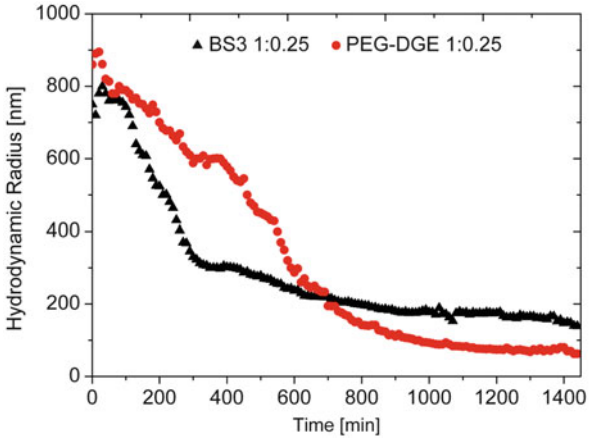

Fig. 6 Degradability of PEG-DGE (1:0.25) and BS3 (1:0.25) crosslinked microgels, as measured by the change in hydrodynamic radius (R_h) as a function of time using 5 mM elastase

Table 2 Loading of Texas Red-marked dextran to PEG-DGE and BS3 microgels

		PEG-DGE			BS3		
			R_h (PDI)			R_h (PDI)	
ES 12 / Linker (mol/mol)	Dextran loading of microgels (mg/wt%)[1]	Initial uptake of dextran (mg/wt%)[2]	20°C (nm)	40°C (nm)	Initial loading of microgels (mg/wt%)	20°C (nm)	40°C (nm)
4	3.75/15	2.41/64.2	890 (0.3)	510 (0.3)	2.75/73.3	765 (0.5)	450 (0.3)
2	3.75/15	2.89/77.2	750 (0.4)	470 (0.2)	3.01/80.3	456 (0.4)	320 (0.3)

[1]Loading is expressed both as milligrams and relative to the weight of elastin (wt%)
[2]Uptake expresses both as millograms and percentage relative to the loading (wt%)

preparation. The particles were isolated by centrifugation and washed according to the procedure for particles prepared without dextran. The loading of the particles by the Texas Red-labeled dextran was corrected for the dextran washed out during the washing procedure. The microgel particles were taken up in water for a defined time and the release of dextran was determined after centrifugation by the calibrated extinction of the decanted aqueous solution. Sedimented particles were redispersed in fresh buffer solution and extracted again. The release was analyzed as the cumulative ratio of the original loading. The procedure was performed at 20°C with the non-collapsed particles and at 40°, above the coacervation temperature.

Table 2 summarizes data on the initial loading and the hydrodynamic radii of the microgels prepared at 20°C and characterized for their hydrodynamic radius at temperatures below and above the volume change transition. Regarding the fact that the dextran did not participate in the crosslinking reaction but serves just as another component in the solvent, it appears unsurprising that the particle sizes came out similar to those prepared without dextran (see Table 1). Figure 7 depicts

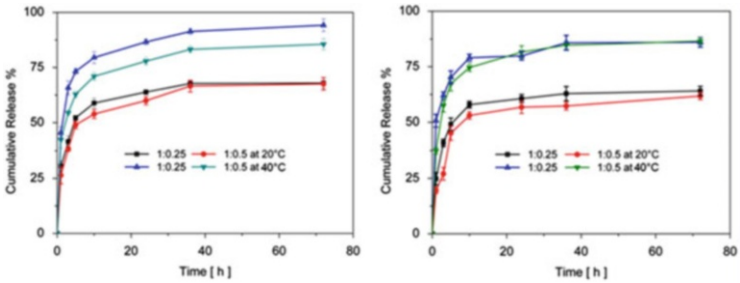

Fig. 7 Temperature-dependent release of dextran from PEG-DGE 1:0.25, 1:0.50 (*left*) and BS3 1:0.25, 1:0.50 (*right*) crosslinked microgels at 20 and 40°C

the cumulative release curves for the two different crosslinking densities and at the two temperatures. Release was slower for the more densely crosslinked BS3-elastin microgels than for the hydrophilic PEG-DGE crosslinked gels. With the exception of the release experiments with the PEG-DGE-elastin microgels above the coacervation temperature, the release rates did not depend significantly on the degree of crosslinking. For both types of microgels, the release rate is higher above than below the coacervation temperature. Also, because the diffusion coefficient increases with temperature we regard this as an indication that the dextran is squeezed out by the collapsed gel structure.

4 Conclusions

In summary, we have shown that rather well-defined thermo- and pH-responsive microgels with sizes in the submicron range can be prepared by an easy procedure with soluble elastin obtained by acidic hydrolysis of native elastin. The temperature- and pH-dependent collapse was most pronounced for low degrees of crosslinking and coincided rather well with the coacervation transition of free elastin. It can thus be concluded that the transition is related to the conformational transformation of the elastin peptide that causes the coacervation process. The fact that the biohybrid particles remained soluble and did not aggregate can be seen as evidence for an intramolecular collapse, whereby the elastin aggregates become stabilized against precipitation by a corona formed of water-soluble segments. As might be expected, this is more pronounced for the conetwork microgels with hydrophilic PEG segments; however, it was also observed when the elastin peptides were crosslinked by a hydrophobic diester segment. This can be explained by the rather broad molecular weight distribution of the elastin peptides, whereby only the longer peptides are expected to undergo coacervation while the shorter peptides remain fully solubilized. Regarding the temperature and pH response, the microgel particles resemble hydrophilic polyacrylamide microgels, which are also considered smart particles due to their volume change phase transition. However, the

hybridization with defined proteins or peptides offers additional and very specific tools for the design of properties. In our example, the microgels exhibited a dual stimulus-response such that the thermal transition was shifted to higher temperatures below and above the isoelectric point of the peptide.

Because soluble elastin peptides are highly biocompatible, do not trigger a thrombogenic response, and show low immunogenicity elastin is suitable as a component of stealth-type microgel particles [26]. To begin with this aspect, we have concentrated on microgel use as a potential drug carrier by demonstrating the cytocompatibility and the biodegradability of the microgel. Furthermore, we have performed a model study on the release properties with dextran as a water-soluble biomacromolecule. The results demonstrate the ability of the concept to significantly retard release. However, elastin peptides are also known to influence signaling and proliferation by binding to several cell receptors, the most well investigated being the elastin binding protein (EBP) [27, 28]. Within this aspect, elastin is an example of a bioactive compound with an activity that can be expected to be manipulated by the collapse of the microgel particles. Recombinant or synthetic ELPs will offer new possibilities to tailor the responsive properties and to introduce switchable receptor affinities, also with other specific peptide segments as ligands [13].

Acknowledgements F.T. thanks Marie Curie ITN project Hierarchy (contract: PITN-2007-215851) for the Ph.D. fellowship. The authors thank Mr. Arpit Bajpai for cell tests and Ms. Helin Li for support during microgel preparation.

References

1. Goncalves C, Pereira P, Gama M (2010) Materials 3:1420–1460
2. Singh S, Möller M, Pich A (2013) J Polym Sci Polym Chem 51:3044
3. Das M, Zhang H, Kumacheva E (2006) Ann Rev Mater Res 36:117
4. Balanceanu A, Demco DE, Möller M, Pich A (2011) Macromolecules 44:2161
5. Storm G, Belliot S, Daemen T, Lasic DD (1995) Adv Drug Deliv Rev 17:31
6. Matsumura Y, Maeda HA (1986) Cancer Res 46:6387
7. Partridge SM, Davis HF, Adair GS (1948) Biochem J 43:387
8. Urry DW, Starcher B, Partridge SM (1969) Nature 222:795
9. Volpin D, Urry DW, Cox BA, Gotte L (1976) Biochim Biophys Acta 439:253
10. Amiram M, Luginbuhl KM, Feinglos MN, Chilkoti A (2013) J Contr Release 172:144–151 doi:10.1016/j.jconrel.2013.07.021
11. Hassouneh W, Fischer K, MacEwan S, Branscheid R, Fu CL, Liu R, Schmidt M, Chilokoti A (2012) Biomacromolecules 13:1598
12. Patel D, Vandromme SE, Reid ME, Taite LJ (2012) Biomacromolecules 13:1420
13. Rodriguez-Cabello JC (2004) Smart elastin-like polymers. In: Hasirci N, Hasirci V (eds) Biomaterials: from molecules to engineered tissues. Advances in experimental medicine, vol 553. Kluwer Academic/Plenum, New York, p 45
14. Kumashiro KK, Ho JP, Niemczura WP, Keeley FW (2006) J Biol Chem 281:23757

15. Baldock C, Oberhauser AF, Ma L, Lammie D, Siegler V, Mithieux SM, Tu Y, Yuen J, Chow H, Suleman F, Malfois M, Rogers S, Guo L, Irving TC, Wess TJ, Weiss AS (2011) Proc Natl Acad Sci USA 108(11):4322
16. Conticello VP, Desai HC (2012) In: Langer R, Tirrell D (eds) Polymer science: a comprehensive reference, vol 9. Elsevier, Amsterdam, p 71
17. Maeda I, Fukumoto Y, Nose T, Shimohigashi Y, Nezu T, Terada Y, Kodama H, Kaibara K, Okamoto K (2011) J Pept Sci 17:735
18. Yeo GC, Keeley FW, Weiss AS (2011) Adv Colloid Interface Sci 167:94
19. Bochicchio B, Floquet N, Pepe A, Alix AJP, Tamburro AM (2004) Chem Eur J 10:3166
20. MacEvan SR, Chilkoti A (2012) Nano Lett 12:3322
21. Ferreon JC, Hilser VJ (2003) Protein Sci 12:447
22. Lin T, Quinn TP, Grandgenett D, Walsh MT (1989) Proteins 5:156
23. Greenfield N, Fasman GD (1969) Biochemistry 8:4108
24. Mattice WL, Lo JT, Mandelkern L (1972) Macromolecules 5:729
25. Vidakovic P, Rondelez F (1984) Macromolecules 17:418
26. Darnule T, Likhite V, Turino GM, Mandl I (1977) Connect Tissue Res 5:67
27. Privitera S, Prody CA, Callahan JW, Hinck A (1998) J Biol Chem 99:870
28. Daamen WF, Veerkamp JH, van Hest JCM, Kuppervelt TH (2007) Biomaterials 28:4378

Adv Polym Sci (2013) 262: 431–446
DOI: 10.1007/12_2013_256

Published online: 6 November 2013

Nanostructured Polymeric Ionic Liquids

Benjamin Kerscher, Fabian Schüler, Anna-Katharina Appel, Kristina Schadt, and Rolf Mülhaupt

Abstract Nanophase separation, self-assembly, and molecular nanostructure design of liquid polyelectrolytes afford new families of ionic liquids containing nanometer-scaled compartments. Key intermediates of nanostructured polymeric ionic liquids (nanoPILs) are PILs with micelle-like topologies, block copolymers and polymer electrolytes dissolved in ionic liquids (ILs), and nanoparticle dispersions. In contrast to micellar ILs, micelle-like nanoPILs consist of a nonionic hyperbranched polyether core with low glass transition temperature and covalently attached alkyl-substituted IL moieties in its periphery. Such hyperbranched nanoPILs are thermally stable dispersants, nanoreactors, and transporters that are useful in nanoparticle synthesis and polymer melt compounding. As new molecular carbon/polyelectrolyte composite materials, tree-like nanoPILs are grafted onto functionalized graphene. Here, we highlight recent progress made in nanoPIL science and engineering, illustrated by selected examples.

Keywords Dispersion · Hyperbranched polymer · Ionic liquids · Nanocomposite · Nanoparticles · Polylelectrolyte · Polymeric ionic liquids

Contents

B. Kerscher, F. Schüler, A.-K. Appel, K. Schadt, and R. Mülhaupt (✉)
Freiburg Materials Research Center, FMF, Institute for Macromolecular Chemistry, and Freiburg Center for Interactive Materials and Bioinspired Technologies, FIT, of the Albert-Ludwigs-University Freiburg, Stefan-Meier-Strasse 31, 79104 Freiburg, Germany
e-mail: rolfmuelhaupt@web.de

Abbreviations

[BMIm][PF6]	1-Butyl-3-methylimidazolium hexafluorophosphate
ATRP	Atom transfer polymerization
BMImTos	1-Butyl-3-methylimidazolium tosylate
cryo-TEM	Cryoscopic transmission electron microscopy
IL	Ionic liquid
Im	Imidazole
nanoPIL	Nanostructured polymeric ionic liquid
NBR	Poly(butadiene-*co*-acrylonitrile) rubber
PB-*b*-PEO	Poly(1,2-butadiene)-*block*-poly(ethylene oxide)
PEHO	Poly(3-ethyl-3-hydroxymethyloxetane)
PIB	Polyisobutylene
PIL	Polymeric ionic liquid
PP	Polypropylene
RAFT	Reversible addition-fragmentation chain transfer polymerization
SAN	Poly(styrene-*co*-acrylonitrile)
Tos	Tosylate

1 Introduction

As salts melting below 100°C, ionic liquids (ILs) are powerful solvents, combining negligible vapor pressure with low flammability, good electrochemical stability, and high ionic conductivity. Their applications range from organic reaction and separation media to sorbents, supports for catalysts, dispersants, sensor components, and battery electrolytes [1–9]. During the last decade, nanostructured ILs have attracted considerable attention in academia and industry. Structured ILs, containing nanometer-sized compartments, serve as reactors and templates in nanoparticle and nanopore syntheses. As pointed out by Canongia Lopes and Pádua, the self-assembly of ILs containing long-chain alkyl groups enables nanostructural IL self-organization [10]. Similarly, the dissolution of ILs in aqueous surfactant solutions [11] as well as the dissolution of various other surfactants in ILs [12, 13] can create micellar IL systems. According to Armstrong and coworkers [13], micelle formation in ILs markedly changes their solvation characteristics without requiring chemical modification of their molecular architectures. However, most micellar ILs are highly sensitive to shear forces and to changes in pH and temperature. Polymeric ionic liquids (PILs) combine IL-like properties with polymer-like facile processing, polymer self-assembly, and design of multifunctional macromolecular systems [14–17]. Dispersions, films, and moldings are prepared from nanoPILs without

encountering any of the leakage problems typical for all low molecular weight ILs. Today, four strategies lead to nanoPILs, mesoporous systems, and unconventional nanostructured polyelectrolyte hybrid materials:

1. Self-assembly of amphiphilic and liquid crystalline PILs
2. Nanophase separation of IL blends with amphiphilic block copolymers
3. In-situ formation of nanoparticle dispersions in (P)ILs
4. Design of molecular nanoPIL architectures resembling micelles

The latter strategy is of particular interest for the development of robust nanoPILs as polymer additives, which must sustain high shear forces and the elevated temperatures typical for polymer melt processing.

2 Nanostructured Linear PILs

A wide variety of linear PILs have been prepared by free radical polymerization of vinyl, (meth)acrylic, and styrenic monomers containing IL moieties [14, 16, 17]. In PILs, the IL moieties are incorporated either in the PIL backbone or in the PIL side chains. Selected members of the linear PIL family are displayed in Fig. 1. The subsequent anion exchange of the counter anions enables facile tuning of the PIL properties [18, 19]. Prominent representatives of PILs are polycations such as poly (1-vinyl-3-alkylimidazolium), and polyanions such as poly(styrene sulfonate), which contains IL moieties as counter cations. In addition to random copolymers, a variety of block copolymers and zwitterionic PILs have been prepared [17, 20–24]. Among them are film-forming PILs exhibiting very low glass transition temperatures (T_g) below −75°C, combined with high ion conductivity [21, 25–28].

In the first strategy, the formation of nanoPILs exploits nanophase separation through self-assembly of liquid crystalline PILs [14, 29–36] and of amphiphilic PIL and PIL block copolymers [23, 24, 37, 38]. For example, Kato and coworkers polymerized an ion-conductive mesogenic monomer containing an IL moiety, thus enabling the formation of self-standing liquid crystalline polymer films. Upon macroscopic orientation, layered nanostructures are formed. Such oriented films exhibit high ion conductivity of 10^{-2} S cm^{-1}, as measured at 150°C in the smectic A phase [29]. In a recent advance, Binder and coworkers reported on the synthesis of nanostructured thermally stable nanoPILs (see PIB-IL in Fig. 1). Using click chemistry, they attached hydrophobic polyisobutylene (PIB) to methylimidazolium, pyrrolidinium, and triethylammonium IL moieties, which govern nanostructure formation, rheology, and relaxation times at constant PIB chain length [38].

According to the second strategy, polymer electrolytes as well as nonionic block copolymers are dissolved in ILs in order to achieve nanostructure formation of polymer-based ionic systems by nanophase separation. A great variety of polymer electrolytes have been integrated into ILs with the aim of improving the ion transport properties of electrochemical devices such as lithium ion batteries, fuel

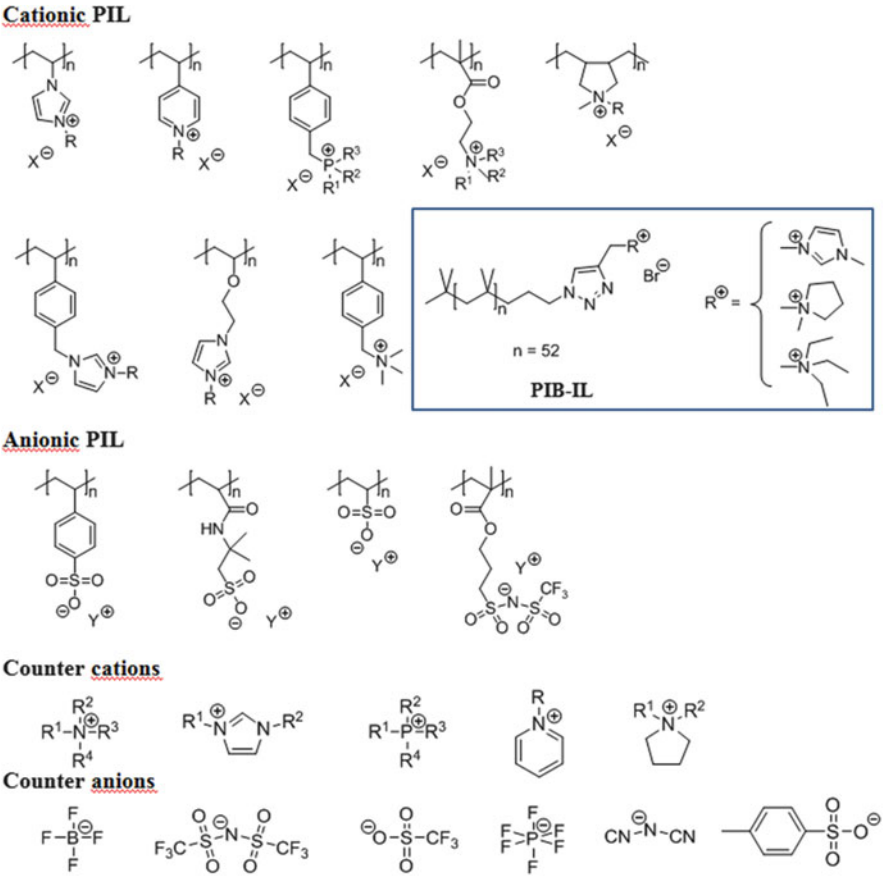

Fig. 1 Linear PILs

cells, and electroactive actuators [39]. Although (nano)phase separation is highly likely to occur, many of the resulting polyelectrolyte gels are rather ill-defined. Much better control of nanostructure formation is achieved when well-defined nanostructured block copolymers are blended together with ILs. For example, as reported by Park and coworkers, upon adding IL to polystyrene-*block*-polyethyleneoxide (PS-*b*-PEO) with lamellar nanostructure, the IL accumulates exclusively in the PEO nanophase. As a consequence, the lithium ion conductivity is markedly improved [40]. In an elegant approach, Lodge and coworkers exploited nanostructure formation of IL/block copolymer blends to render micellar polymer-based ILs smart and thermoresponsive. In their micellar shuttle system, 1-butyl-3-methylimidazolium hexafluorophosphate, [BMIm][PF6], is blended together with amphiphilic diblock copolymers such as poly(1,2-butadiene)-*block*-poly(ethylene oxide), abbreviated as PB-*b*-PEO. As verified by cryo-TEM and light scattering, the PB-*b*-PEO self-assembly in IL produced spherical, worm-like, and bilayered

vesicles. The morphology development was governed by the PEO block length [41]. As a function of the temperature, the micelles reversibly transfer between the two immiscible fluids, traveling in and out of the water and IL phases. This temperature-driven micelle partitioning creates versatile micelle shuttles and nanocarriers that are useful in "round-trip" delivery systems, biphase catalysis, and separation technology [42].

In the third strategy, heterophase polymerization reactions such as suspension polymerizations and micro- and mini-emulsion polymerizations produce stable dispersions of monodisperse PIL particles. Typically, their average diameters vary from nano- to micrometer dimensions [43–46]. Such processes also enable the preparation of gel-like PIL particles [47, 48] and of solvent-reversible poration in copolymer ionic liquids [49]. Moreover, in aqueous precipitation polymerization, highly ordered PIL nanoparticles with average diameter of 20–40 nm are obtained. Their tunable multilamellar and unilamellar vesicular inner structures resemble those of liposomes [50, 51]. NanoPILs, mesoporous PILs, and PIL nanoparticles are tailored for applications in biocatalysis and sensing [45–49, 52]. The incorporation of three-dimensionally ordered macropores and nanoparticles in nanoPILs is the key to a new generation of smart materials and functional films that are useful as tunable photonic crystals, anion-directed molecular gating systems, electrooptical switches, and functional surfaces with tunable wettability [53]. Most PILs are highly effective phase-transfer media and dispersing agents for nanoparticles such as carbon nanotubes (CNT) and metal nanoparticles, enabling their transport from aqueous into nonaqueous phases [54–56]. Novel PIL/CNT nanohybrid materials represent electroactive nanomaterials, known as "bucky plastics" [57, 58].

3 Nanostructured Hyperbranched PILs with Micelle-Like Topologies

Whereas numerous reports describe linear nanoPILs, much less is known regarding dendritic and hyperbranched nanoPILs with molecular architectures resembling micelles. Unlike micellar ILs, tree-like branched nanoPILs with core–shell and onion-like topologies are much less sensitive to high shear forces and changes in pH and temperature. For the first time, the groups of Aida and Percec succeeded in preparing dendritic polyelectrolytes that self-organized [59] and formed cylindrical nanoobjects [60]. In order to qualify for PIL applications, however, low viscosity and low glass transition temperatures are required. Moreover, in view of scale-up, the one-pot formation of hyperbranched PILs is highly advantageous with respect to dendrimer-based nanoPILs, produced in tedious multistep syntheses. As commercially available highly branched liquid polymers, polyethyleneimines, containing quarternary ammonium cations, are attractive intermediates for PIL formation. For example, Domb and coworkers derived amphiphilic nanoPILs from commercially available polyethyleneimine, which was crosslinked with dibromopentane,

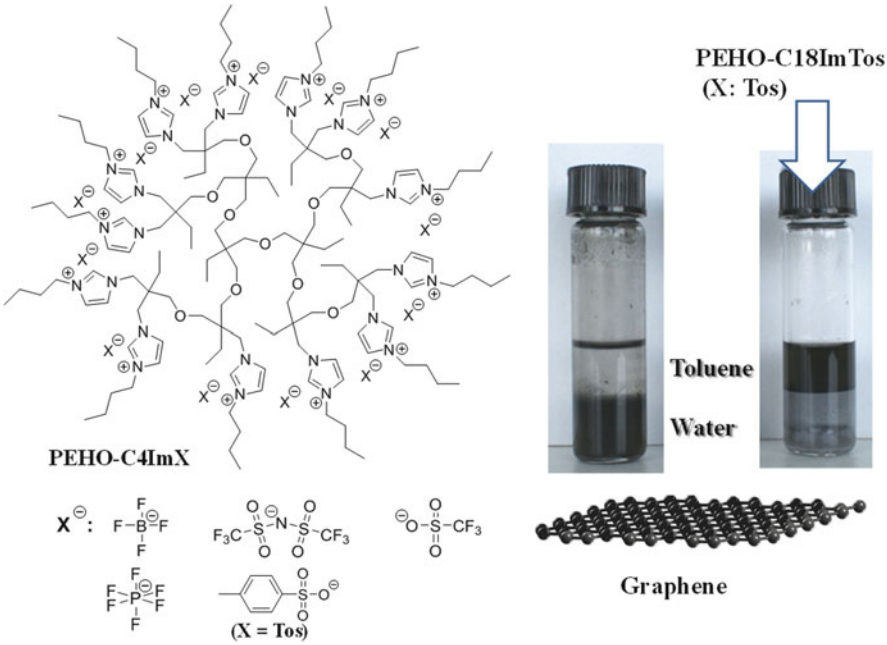

Fig. 2 Micelle-like hyperbranched nanoPIL (PEHO-C18ImTos) enables the transport of functionalized graphene nanosheets from the aqueous phase into toluene [68]

N-alkylated with long-chain alkyl halides, and rendered amphiphilic by subsequent quaternization with methyl iodide. They employed their hyperbranched nanoPIL amphiphiles as antimicrobial agents, embedded in restorative dental composites [61, 62]. Dispersed in NBR rubber, PILs derived from hyperbranched PEI enabled self-healing [63]. Following a similar ionene synthetic route, Fradet and coworkers obtained hyperbranched nanoPILs by poly(*N*-alkylation) of lutidine derivatives [64].

Mimicking micelles and vesicles, new generations of nanoPILs incorporate IL moieties in the periphery of nonionic hyperbranched polyether cores with low glass transition temperature. One of the first examples was reported by Mecking and coworkers, who used such hyperbranched PILs as catalyst supports. They employed anionic ring-opening polymerization of glycidol to prepare liquid polyglycidol polyols. In the subsequent step, the hyperbranched polyols were reacted with ω-acylbromides in 1,2-dimethylimidazole or pyridine, thus forming a shell of covalently attached imidazolium or pyridinium groups, respectively [65, 66]. Similar core–shell-type nanoPILs containing imidazolium endgroups, obtained by tosylation of polyglycidol and substitution of the tosylate groups by 1-methylimidazole, were tailored as solvents with lower critical solution temperature, thus enabling liquid–liquid and liquid–solid phase transition in organic separation media [67].

As illustrated in Fig. 2, another family of micelle-like nanoPILs with tunable polarities contains a nonionic polyoxetane core, an inner shell of covalently attached

imidazolium cations, and an outer shell of *n*-alkyl chains [68]. Here, ring-opening cationic polymerization of 3-ethyl-3-hydroxymethyloxetane yields polyoxetane polyols (PEHO) with number-average molar mass of 1,800–2,400 g/mol and degree of branching of 50%. In a polymer-analogous reaction, the tosylate endgroups alkylate 1-(*n*-alkyl)imidazoles to produce nanoPILs with onion-like topology. Whereas methylimidazolium-functionalized nanoPILs with tosylate counter anions (PEHO-C1ImTos) are water soluble, both increasing the *n*-alkyl chain length and exchanging the tosylate counter ions for 4-dodecylbenzenesulfonate render such nanoPILs organophilic. As evidenced by the absence of weight loss under nitrogen atmosphere up to 300°C, such nanoPILs are remarkably thermally stable, thus meeting the demands of polymer melt processing. Organophilic micelle-like nanoPILs containing a nonpolar outer *n*-octadecyl shell (PEHO-C18ImTos) are highly effective phase-transfer agents and transporters. Hence, they enable the transfer of water-soluble food colorants such as Brilliant Blue FCF (E133) from water into chloroform and even into polypropylene melts. Moreover, as illustrated in Fig. 2, functionalized graphene is transported from the aqueous phase into toluene. Stable nonaqueous graphene dispersions are obtained. The addition of polystyrene to nanoPIL-stabilized graphene dispersions affords melt-processable graphene/polystyrene nanocomposites exhibiting improved electrical conductivity [68]. Both the *n*-alkyl-substituted and the corresponding semifluorinated nanoPILs are highly effective as reactors and dispersing agents, thus enabling the preparation of transition metal nanoparticle dispersions in organic media [69].

Owing to their good thermal stability, nanoPILs containing polyoxetane cores and *N*-butylimidazolium shells (PEHO-C4ImTos) are useful additives and blend components for melt processing of thermoplastics. For example, PEHO-C4ImTos was blended with poly(styrene-*co*-acrylonitrile), SAN, containing 30 wt % acrylonitrile. After extrusion blending in a twin-screw mini-extruder at 210°C, the samples were injection molded at the same temperature. For comparison, the corresponding low molecular weight IL, 1-butyl-3-methylimidazolium tosylate (BMImTos), was also melt blended together with SAN using the identical processing conditions. The contents of nanoPIL and the corresponding IL were varied between 0 and 20 wt%. As is apparent from Fig. 3, the low molecular weight BMImTos is fully miscible with SAN and severely plasticizes the SAN matrix. In fact, with increasing BMImTos content, the SAN is rendered soft and flexible, as evidenced by the drastic decrease in glass transition temperature. This is paralleled by a drastic decay in strength and stiffness. In sharp contrast, PEHO-C4ImTos does not affect the SAN glass transition temperature, even at high content.

The close inspection of the SAN/PEHO-C4ImTos blend morphology by means of TEM revealed that PEHO-C4ImTos phase separated. Hence, uniformly dispersed nanodroplets are formed within the SAN matrix. The average nanodroplet diameter varied between 50 and 200 nm. Taking into account the high molecular weight of this nanoPIL, it is not surprising that no leaching problems were encountered. Upon matching the compatibility by increasing the *n*-alkyl chain length to *n*-octadecyl, PIL nanodroplets were formed in nonpolar polymers such as polypropylene (PP) [68]. With increasing PEHO-C18ImTos content, the average nanodroplet size

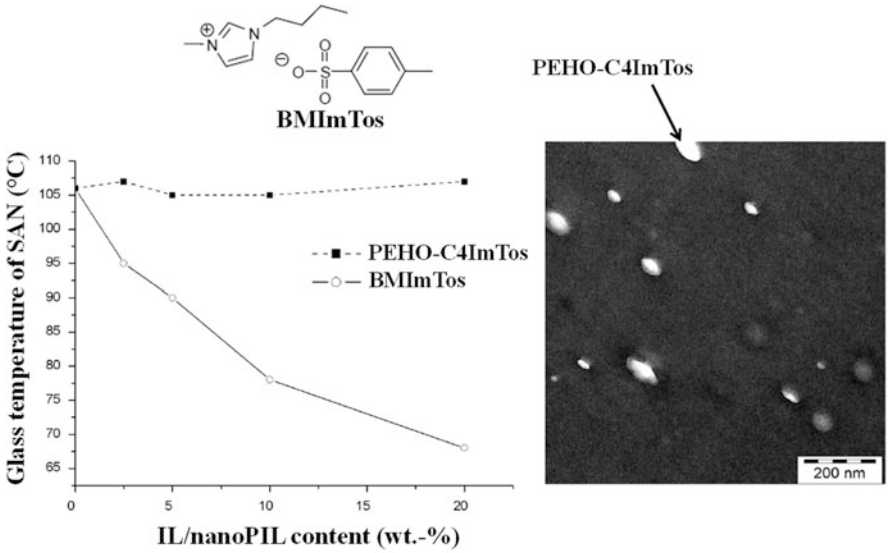

Fig. 3 Glass transition temperature of SAN as a function of the BMImTos and PEHO-C4ImTos content (*left*) and morphology of a SAN/PEHO-C4ImTos blend, as imaged by TEM (*right*)

in PP increased from 121 nm at 0.25 wt% to 163 nm at 2.0 wt%. Neither the shape nor the uniform distribution was affected. In contrast to blends with SAN, the more polar *n*-butyl-substituted nanoPIL afforded very poor dispersion of much larger droplets in nonpolar PP. Obviously, the facile polarity matching obtained by varying the *n*-alkyl length of the outer shell enables adjustments of the compatibility. As nanometer-sized compartments in polymers, PIL nanodroplets host a large variety of organic and inorganic (nano)materials. For example, compatibilized PEHO-C18ImTos enables the uniform dispersion of hydrophilic dye E133 in PP, whereas the corresponding low molecular weight IL is ineffective [68].

4 Graphene/PIL Hybrids

As a single carbon layer of the graphite lattice, graphene is a two-dimensional carbon macromolecule. It exhibits high electrical and thermal conductivity, ultrahigh stiffness and strength, and barrier resistance [70–72]. Specific interactions between imidazolium groups and the polycyclic aromatic carbon layers were proposed to account for improved adhesion of IL to graphene or CNTs, respectively [57, 73]. Hence, this is expected to improve dispersion of graphene in ILs and also in the presence of PILs [74, 75]. As reported above, the PIL addition enables the phase transfer and efficient dispersion of graphene [55, 68] and of CNTs [54]. Most likely, PIL assembles at the graphene interface. Blending graphene with PILs such

as poly(1-vinyl-3-butylimidazolium) bromide afforded polyelectrolyte membranes with enhanced ionic conductivity [76]. As electrode materials for supercapacitors, graphene in conjunction with poly(1-vinyl-3-ethylimidazolium) bis(trifluoromethylsulfonyl)amide accounted for substantial improvement in capacity [77]. As highly selective gas sensors, multilayer carbon composite films were obtained by reducing graphite oxide dissolved in ILs, followed by electrostatic layer-by-layer assembly [78]. In an elegant one-pot synthesis, fluorescent carbon nanoribbons, nanoparticles, and graphene were prepared by IL-mediated electrochemical exfoliation of graphite [79]. Novel IL/graphene lubricants exploit interfacial nanostructure formation, owing to thin film formation resulting from self-assembly of graphene. This contributes to a reduction in frictional forces, thus enhancing tribological performance [80].

Going well beyond the noncovalent graphene/PIL interactions and the assembly of PIL at the graphene interface, several successful approaches have been reported on the covalent attachment of IL and PIL to graphene. Yang and coworkers reported on the immobilization of 1-(3-aminopropyl)-3-methylimidazolium bromide on graphite oxide [81]. In an alternative approach, graphite oxide was amidated using 1-(3-aminopropyl)imidazole, followed by alkylation of the imidazole with 1-bromobutane [82]. Using 1,3-dipolar cycloaddition reactions, Quintana et al. decorated graphene sheets with ammonium chloride functions [83] and protonated polyamidoamine dendrons [84], both of which were linked to the graphene surface via pyrrolidine rings. In a mild, one-step electrochemical process, IL-functionalized graphene nanosheets were produced from graphite [85].

Several "grafting-from" and "grafting-to" strategies were introduced for covalent attachment of polymer chains to graphene, aiming at the formation of novel molecular carbon/polymer composites and graphene brushes. Progress was reviewed by Salavagione et al. [86]. In grafting-from processes, a variety of initiators and transfer agents were covalently attached to graphene. For example, graphite oxide was reacted with α-bromoisobutyryl bromide in order to prepare macro-initiators for grafting by means of atom transfer radical polymerization, ATRP [87, 88]. In the grafting-from process, by means of reversible addition fragmentation chain transfer polymerizations (RAFT), various dithioesters, trithiocarbonates, dithiocarbamates, and xanthogenates were covalently attached to functionalized graphene and graphite oxide and used as macrochain transfer agents [89–91]. For example, in a multistep process, the carboxylic acid groups of graphite oxide were transformed into dithiobenzoates [92]. In a recent advance, the self-initiated styrene homo- and copolymerization was initiated by organophilic stearylamine-modified graphite oxide. In this process, efficient graphene grafting was achieved without requiring either the addition or the incorporation of initiators, transfer agents, or polymerizable groups. According to an on-line electron paramagnetic resonance (EPR) monitoring of this reaction, both the addition of polymer radicals to graphene and hydrogen transfer from graphene play important roles [93]. Little is known with respect to grafting PILs onto graphene and CNTs. CNTs with partially quaternized, covalently attached poly(4-vinylpyridine) brushes represent an example of PIL-functionalized nanostructured carbon materials [94].

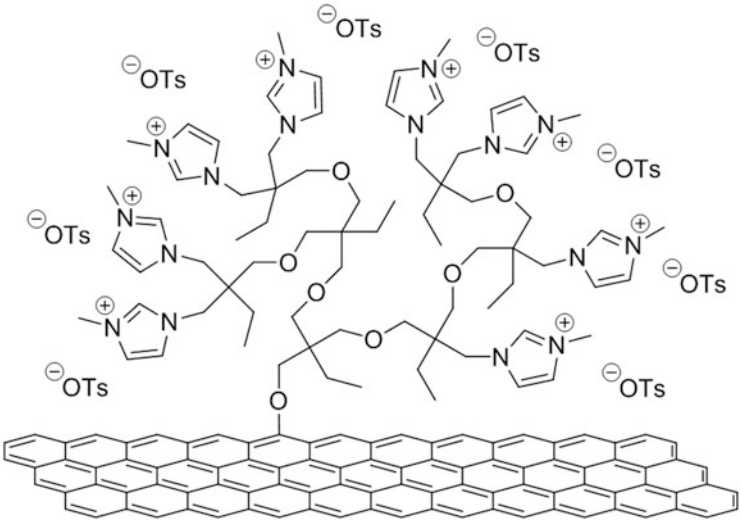

Fig. 4 Tree-like PIL grafted onto functionalized graphene [98]

In their grafting-from process, Pei and coworkers employed the surface-initiated ATRP of 2-(1-butylimidazolium-3-yl)ethyl methacrylate hexafluorophosphate for grafting PIL chains onto CNTs [95]. Such materials were reported to be useful as an antiwear and friction-reducing additive for IL lubricants. In a similar functionalization of graphite oxide, poly([2-(methacryloyloxy)ethyl]trimethylammonium tetrafluoroborate) brushes were obtained by graphene-initiated ATRP [96]. In grafting-to processes, the functional groups of graphene function as chain terminators in polymerization reactions. For example, in cationic ring-opening polymerization of 3-ethyl-3-hydroxymethyloxetane, hyperbranched polyoxetanes are grafted onto functionalized CNTs [97] and graphene [98, 99]. Following the reaction pathway described above for hyperbranched nanoPILs, the hydroxy endgroups are readily converted into tosylates, which alkylate 1-alkylmindazoles. As illustrated in Fig. 4, tree-like PILs are grafted onto graphene [98]. In principle, such covalent attachment of PILs to graphene greatly improves the graphene dispersibility in various solvents. Moreover, in contrast to nonmodified graphene, thin films were obtained. As a consequence, molecular graphene/PIL composites represent attractive intermediates for applications in electrochemical devices, catalysis, and even 3D printing of multifunctional carbon materials.

5 Conclusion

During recent years, a great variety of molecular PIL architectures have been tailored by incoporating IL moieties into the backbone and side chains of polymers and by varying the type of ion pairs. An important objective in PIL research is to

combine the properties of ILs such as high ion conductivity, electrochemical stability, and negligable vapor pressure with the prominent benefits of polymers regarding their facile processing and easy design of multifunctional materials. Today, films, coatings, dispersions, gels, solid electrolytes, and composite materials are made from PILs. The envisioned PIL applications range from advanced electrochemical devices such as batteries, fuel cells, and sensors to membranes for highly diversified applications in separation technology. Going well beyond the scope of traditional polyelectrolytes and polymer ionomers, this remarkable progress made in PIL research and development is opening up new horizons in polymer electrolyte science and engineering.

Inspite of these obvious PIL advantages, there exist several shortcomings, especially with repect to PIL appliactions in electrochemical devices. Above all, it is well recognized that the ion conductivities of high molecular weight PILs are much lower than those of the low molecular weight ILs. In fact, with increasing molecular weight, the decrease in ion mobility is frequently paralleled by increasing glass transition temperature [17]. Although the variation of linear PIL architectures has only limited potential to overcome this problem, controlled nanostructure formation offers unique unexplored opportunities. On the one hand, novel dendritic and hyperbranched nanometer-scaled PILs are being tailored to exhibit micelle-like structure and properties. On the other hand, nanophase separation is being exploited to produce novel polymer electrolyte nanomaterials from tailored amphiphilic PILs, PIL blends, PIL interpenetrating networks, and PIL nanoparticle dispersions. In the future, better understanding and control of PIL nanostructure formation will be the key issue for achieving success in commercial PIL applications.

References

1. Welton T (1999) Room-temperature ionic liquids. Solvents for synthesis and catalysis. Chem Rev 99:2071–2084
2. Hallett JP, Welton T (2011) Room-temperature ionic liquids: solvents for synthesis and catalysis. 2. Chem Rev 111:3508–3576
3. Dupont J, de Souza RF, Suarez PAZ (2002) Ionic liquid (molten salt) phase organometallic catalysis. Chem Rev 102:3667–3692
4. Pârvulescu VI, Hardacre C (2007) Catalysis in ionic liquids. Chem Rev 107:2615–2665
5. Wasserscheid P, Keim W (2000) Ionic liquids – new “solutions” for transition metal catalysis. Angew Chem Int Ed 39:3772–3789
6. Olivier-Bourbigou H, Magna L, Morvan D (2010) Ionic liquids and catalysis: recent progress from knowledge to applications. Appl Catal A 373:1–56
7. Wasserscheid P, Welton T (2007) Ionic liquids in synthesis, vol 2. Wiley-VCH, Weinheim
8. Wasserscheid P, Welton T (2003) Ionic liquids in synthesis. Wiley-VCH, Weinheim
9. Brazel CS, Rogers RD (2005) Ionic liquids in polymer systems solvents additives and novel applications. American Chemical Society, Washington, DC
10. Canongia Lopes JNA, Pádua AAH (2006) Nanostructural organization in ionic liquids. J Phys Chem B 110:3330–3335

11. Friberg SE, Yin Q, Pavel F, Mackay RA, Holbrey JD, Seddon KR, Aikens PA (2000) Solubilization of an ionic liquid, l-Butyl-3-methylimidazolium hexafluorophosphate, in a surfactant-water system. J Dispersion Sci Technol 21:185–197
12. Hoffmann MM, Heitz MP, Carr JB, Tubbs JD (2003) Surfactants in green solvent systems – current and future research directions. J Dispersion Sci Technol 24:155–171
13. Anderson JL, Pino V, Hagberg EC, Sheares VV, Armstrong DW (2003) Surfactant solvation effects and micelle formation in ionic liquids. Chem Commun 2003(19):2444–2445
14. Green O, Grubjesic S, Lee S, Firestone MA (2009) The design of polymeric ionic liquids for the preparation of functional materials. Polym Rev 49:339–360
15. Lu J, Yan F, Texter J (2009) Advanced applications of ionic liquids in polymer science. Prog Polym Sci 34:431–448
16. Yuan J, Antonietti M (2011) Poly(ionic liquid)s: polymers expanding classical property profiles. Polymer 52:1469–1482
17. Mecerreyes D (2011) Polymeric ionic liquids: broadening the properties and applications of polyelectrolytes. Prog Polym Sci 36:1629–1648
18. Marcilla R, Blazquez JA, Fernandez R, Grande H, Pomposo JA, Mecerreyes D (2005) Synthesis of novel polycations using the chemistry of ionic liquids. Macromol Chem Phys 206:299–304
19. Weber RL, Ye Y, Banik SM, Elabd YA, Hickner MA, Mahanthappa MK (2011) Thermal and ion transport properties of hydrophilic and hydrophobic polymerized styrenic imidazolium ionic liquids. J Polym Sci B Polym Phys 49:1287–1296
20. Yuan J, Mecerreyes D, Antonietti M (2013) Poly(ionic liquid)s: an update. Prog Polym Sci 38:1009–1036
21. Yoshizawa M, Hirao M, Ito-Akita K, Ohno H (2001) Ion conduction in zwitterionic-type molten salts and their polymers. J Mater Chem 11:1057–1062
22. Gu Y, Lodge TP (2011) Synthesis and gas separation performance of triblock copolymer ion gels with a polymerized ionic liquid mid-block. Macromolecules 44:1732–1736
23. Ye Y, Choi J-H, Winey KI, Elabd YA (2012) Polymerized ionic liquid block and random copolymers: effect of weak microphase separation on ion transport. Macromolecules 45:7027–7035
24. Wang Z, Lai H, Wu P (2012) Influence of PIL segment on solution properties of poly (N-isopropylacrylamide)-b-poly(ionic liquid) copolymer: micelles, thermal phase behavior and microdynamics. Soft Matter 8:11644–11653
25. Ohno H, Ito K (1998) Room-temperature molten salt polymers as a matrix for fast ion conduction. Chem Lett 27:751–752
26. Ohno H (2001) Molten salt type polymer electrolytes. Electrochim Acta 46:1407–1411
27. Ohno H, Yoshizawa M, Ogihara W (2004) Development of new class of ion conductive polymers based on ionic liquids. Electrochim Acta 50:255–261
28. Ohno H (2007) Design of ion conductive polymers based on ionic liquids. Macromol Symp 249–250:551–556
29. Hoshino K, Yoshio M, Mukai T, Kishimoto K, Ohno H, Kato T (2003) Nanostructured ion-conductive films: layered assembly of a side-chain liquid-crystalline polymer with an imidazolium ionic moiety. J Polym Sci A Polym Chem 41:3486–3492
30. Lu X, Xiao S, Chen X, Lu Q (2011) A photosensitive fluorinated ionic complex with tunable surface wetting properties: mesostructure and photosensitivity. Polym Chem 2:2528–2535
31. Binnemans K (2005) Ionic liquid crystals. Chem Rev 105:4148–4204
32. Haramoto Y, Kusakabe Y, Nanasawa M, Ujiie S, Mang S, Schwarzwalder C, Holmes AB (2000) Side chain type ionic liquid crystalline polymers having high preliminary communication molecular weight. Liq Cryst 27:1393–1397
33. Vuillaume PY, Galin J-C, Bazuin CG (2001) Ionomer and mesomorphic behavior in a tail-end, ionic mesogen-containing, comblike copolymer series. Macromolecules 34:859–867
34. Batra D, Hay DNT, Firestone MA (2007) Formation of a biomimetic, liquid-crystalline hydrogel by self-assembly and polymerization of an ionic liquid. Chem Mater 19:4423–4431

35. Batra D, Seifert S, Varela LM, Liu ACY, Firestone MA (2007) Solvent-mediated plasmon tuning in a gold-nanoparticle–poly(ionic liquid) composite. Adv Funct Mater 17:1279–1287
36. Lee S, Becht GA, Lee B, Burns CT, Firestone MA (2010) Electropolymerization of a bifunctional ionic liquid monomer yields an electroactive liquid-crystalline polymer. Adv Funct Mater 20:2063–2070
37. Li X, Ni X, Liang Z, Shen Z (2012) Preparation of main-chain imidazolium-functionalized amphiphilic block copolymers through combination of condensation polymerization and nitroxide-mediated free radical polymerization and their micelle study. J Polym Sci A Polym Chem 50:2037–2044
38. Zare P, Stojanovic A, Herbst F, Akbarzadeh J, Peterlik H, Binder WH (2012) Hierarchically nanostructured polyisobutylene-based ionic liquids. Macromolecules 45:2074–2084
39. Park MJ, Choi I, Hong J, Kim O (2013) Polymer electrolytes integrated with ionic liquids for future electrochemical devices. J Appl Polym Sci 129:2363–2376
40. Choi I, Ahn H, Park MJ (2011) Enhanced performance in lithium-polymer batteries using surface-functionalized Si nanoparticle anodes and self-assembled block copolymer electrolytes. Macromolecules 44:7327–7334
41. He Y, Li Z, Simone P, Lodge TP (2006) Self-assembly of block copolymer micelles in an ionic liquid. J Am Chem Soc 128:2745–2750
42. Bai Z, Lodge TP (2010) Pluronic micelle shuttle between water and an ionic liquid. Langmuir 26:8887–8892
43. Tokuda M, Minami H, Mizuta Y, Yamagami T (2012) Preparation of micron-sized monodisperse poly(ionic liquid) particles. Macromol Rapid Commun 33:1130–1134
44. Yuan J, Antonietti M (2011) Poly(ionic liquid) latexes prepared by dispersion polymerization of ionic liquid monomers. Macromolecules 44:744–750
45. Yan F, Texter J (2006) Surfactant ionic liquid-based microemulsions for polymerization. Chem Commun 2006(25):2696–2698
46. Zhao J, Yan F, Chen Z, Diao H, Chu F, Yu S, Lu J (2009) Microemulsion polymerization of cationic pyrroles bearing an imidazolum-ionic liquid moiety. J Polym Sci A Polym Chem 47:746–753
47. Muldoon MJ, Gordon CM (2004) Synthesis of gel-type polymer beads from ionic liquid monomers. J Polym Sci A Polym Chem 42:3865–3869
48. Marcilla R, Sanchez-Paniagua M, Lopez-Ruiz B, Lopez-Cabarcos E, Ochoteco E, Grande H, Mecerreyes D (2006) Synthesis and characterization of new polymeric ionic liquid microgels. J Polym Sci A Polym Chem 44:3958–3965
49. Yan F, Texter J (2007) Solvent-reversible poration in ionic liquid copolymers. Angew Chem Int Ed 46:2440–2443
50. Yuan J, Soll S, Drechsler M, Müller AHE, Antonietti M (2011) Self-assembly of poly(ionic liquid)s: polymerization, mesostructure formation, and directional alignment in one step. J Am Chem Soc 133:17556–17559
51. Koebe M, Drechsler M, Weber J, Yuan J (2012) Crosslinked poly(ionic liquid) nanoparticles: inner structure, size, and morphology. Macromol Rapid Commun 33:646–651
52. López MS-P, Mecerreyes D, López-Cabarcos E, López-Ruiz B (2006) Amperometric glucose biosensor based on polymerized ionic liquid microparticles. Biosens Bioelectron 21:2320–2328
53. Huang J, Tao C-a, An Q, Zhang W, Wu Y, Li X, Shen D, Li G (2010) 3D-ordered macroporous poly(ionic liquid) films as multifunctional materials. Chem Commun 46:967–969
54. Marcilla R, Curri ML, Cozzoli PD, Martínez MT, Loinaz I, Grande H, Pomposo JA, Mecerreyes D (2006) Nano-objects on a round trip from water to organics in a polymeric ionic liquid vehicle. Small 2:507–512
55. Kim T, Lee H, Kim J, Suh KS (2010) Synthesis of phase transferable graphene sheets using ionic liquid polymers. ACS Nano 4:1612–1618

56. X-D M, J-Q M, Li Z-C, Kou Y (2005) Rhodium nanoparticles stabilized by ionic copolymers in ionic liquids: long lifetime nanocluster catalysts for benzene hydrogenation. J Am Chem Soc 127:9694–9695
57. Fukushima T, Kosaka A, Yamamoto Y, Aimiya T, Notazawa S, Takigawa T, Inabe T, Aida T (2006) Dramatic effect of dispersed carbon nanotubes on the mechanical and electroconductive properties of polymers derived from ionic liquids. Small 2:554–560
58. Wu B, Hu D, Kuang Y, Liu B, Zhang X, Chen J (2009) Functionalization of carbon nanotubes by an ionic-liquid polymer: dispersion of Pt and PtRu nanoparticles on carbon nanotubes and their electrocatalytic oxidation of methanol. Angew Chem Int Ed 48:4751–4754
59. Tomioka N, Takasu D, Takahashi T, Aida T (1998) Electrostatic assembly of dendrimer electrolytes: negatively and positively charged dendrimer porphyrins. Angew Chem Int Ed 37:1531–1534
60. Imam MR, Peterca M, Edlund U, Balagurusamy VSK, Percec V (2009) Dendronized supramolecular polymers self-assembled from dendritic ionic liquids. J Polym Sci A Polym Chem 47:4165–4193
61. Beyth N, Yudovin-Farber I, Bahir R, Domb AJ, Weiss EI (2006) Antibacterial activity of dental composites containing quaternary ammonium polyethylenimine nanoparticles against *Streptococcus mutans*. Biomaterials 27:3995–4002
62. Yudovin-Farber I, Beyth N, Weiss EI, Domb AJ (2010) Antibacterial effect of composite resins containing quaternary ammonium polyethyleneimine nanoparticles. J Nanopart Res 12:591–603
63. Schüssele AC, Nübling F, Thomann Y, Carstensen O, Bauer G, Speck T, Mülhaupt R (2012) Self-healing rubbers based on NBR blends with hyperbranched polyethylenimines. Macromol Mater Eng 297:411–419
64. Monmoton S, Lefebvre H, Costa-Torro F, Fradet A (2008) Hyperbranched poly[bis(alkylene) pyridinium]s. Macromol Chem Phys 209:2382–2389
65. Schwab E, Mecking S (2005) Synthesis and properties of highly branched polycations with an aliphatic polyether scaffold. J Polym Sci A Polym Chem 43:4609–4617
66. Schwab E, Mecking S (2005) Recoverable catalysts noncovalently bound to a hyperbranched polyelectrolyte. Organometallics 24:3758–3763
67. Tamaki M, Taguchi T, Kitajyo Y, Takahashi K, Sakai R, Kakuchi T, Satoh T (2009) LCST-type liquid–liquid and liquid–solid phase transition behaviors of hyperbranched polyglycerol bearing imidazolium salt. J Polym Sci A Polym Chem 47:7032–7042
68. Schüler F, Kerscher B, Beckert F, Thomann R, Mülhaupt R (2013) Hyperbranched polymeric ionic liquids with onion-like topology as transporters and compartmentalized systems. Angew Chem Int Ed 52:455–458
69. Schadt K, Kerscher B, Thomann R, Mülhaupt R (2013) Structured semifluorinated polymer ionic liquids for metal nanoparticle preparation and dispersion in fluorous compartments. Macromolecules 46:4799–4804
70. Novoselov KS, Geim AK, Morozov SV, Jiang D, Zhang Y, Dubonos SV, Grigorieva IV, Firsov AA (2004) Electric field effect in atomically thin carbon films. Science 306:666–669
71. Lee C, Wei X, Kysar JW, Hone J (2008) Measurement of the elastic properties and intrinsic strength of monolayer graphene. Science 321:385–388
72. Castro Neto AH, Guinea F, Peres NMR, Novoselov KS, Geim AK (2009) The electronic properties of graphene. Rev Mod Phys 81:109–162
73. Georgakilas V, Otyepka M, Bourlinos AB, Chandra V, Kim N, Kemp KC, Hobza P, Zboril R, Kim KS (2012) Functionalization of graphene: covalent and non-covalent approaches, derivatives and applications. Chem Rev 112:6156–6214
74. Tung TT, Kim TY, Shim JP, Yang WS, Kim H, Suh KS (2011) Poly(ionic liquid)-stabilized graphene sheets and their hybrid with poly(3,4-ethylenedioxythiophene). Org Electron 12:2215–2224
75. Zhou X, Wu T, Ding K, Hu B, Hou M, Han B (2010) Dispersion of graphene sheets in ionic liquid [bmim][PF6] stabilized by an ionic liquid polymer. Chem Commun 46:386–388

76. Ye Y-S, Tseng C-Y, Shen W-C, Wang J-S, Chen K-J, Cheng M-Y, Rick J, Huang Y-J, Chang F-C, Hwang B-J (2011) A new graphene-modified protic ionic liquid-based composite membrane for solid polymer electrolytes. J Mater Chem 21:10448–10453
77. Kim TY, Lee HW, Stoller M, Dreyer DR, Bielawski CW, Ruoff RS, Suh KS (2011) High-performance supercapacitors based on poly(ionic liquid)-modified graphene electrodes. ACS Nano 5:436–442
78. Ji Q, Honma I, Paek S-M, Akada M, Hill JP, Vinu A, Ariga K (2010) Layer-by-layer films of graphene and ionic liquids for highly selective gas sensing. Angew Chem Int Ed 49:9737–9739
79. Lu J, Yang J-X, Wang J, Lim A, Wang S, Loh KP (2009) One-pot synthesis of fluorescent carbon nanoribbons, nanoparticles, and graphene by the exfoliation of graphite in ionic liquids. ACS Nano 3:2367–2375
80. Khare V, Pham M-Q, Kumari N, Yoon H-S, Kim C-S, Park J-IL, Ahn S-H (2013) Graphene-ionic liquid based hybrid nanomaterials as novel lubricant for low friction and wear. ACS Appl Mater Interfaces 5:4063–4075
81. Yang H, Shan C, Li F, Han D, Zhang Q, Niu L (2009) Covalent functionalization of polydisperse chemically-converted graphene sheets with amine-terminated ionic liquid. Chem Commun 2009(26):3880–3882
82. Karousis N, Economopoulos SP, Sarantopoulou E, Tagmatarchis N (2010) Porphyrin counter anion in imidazolium-modified graphene-oxide. Carbon 48:854–860
83. Quintana M, Spyrou K, Grzelczak M, Browne WR, Rudolf P, Prato M (2010) Functionalization of graphene via 1,3-dipolar cycloaddition. ACS Nano 4:3527–3533
84. Quintana M, Montellano A, del Rio Castillo AE, Tendeloo GV, Bittencourt C, Prato M (2011) Selective organic functionalization of graphene bulk or graphene edges. Chem Commun 47:9330–9332
85. Liu N, Luo F, Wu H, Liu Y, Zhang C, Chen J (2008) One-step ionic-liquid-assisted electrochemical synthesis of ionic-liquid-functionalized graphene sheets directly from graphite. Adv Funct Mater 18:1518–1525
86. Salavagione HJ, Martínez G, Ellis G (2011) Recent advances in the covalent modification of graphene with polymers. Macromol Rapid Commun 32:1771–1789
87. Fang M, Wang K, Lu H, Yang Y, Nutt S (2009) Covalent polymer functionalization of graphene nanosheets and mechanical properties of composites. J Mater Chem 19:7098–7105
88. Lee SH, Dreyer DR, An J, Velamakanni A, Piner RD, Park S, Zhu Y, Kim SO, Bielawski CW, Ruoff RS (2010) Polymer brushes via controlled, surface-initiated Atom Transfer Radical Polymerization (ATRP) from graphene oxide. Macromol Rapid Commun 31:281–288
89. Etmimi HM, Tonge MP, Sanderson RD (2011) Synthesis and characterization of polystyrene-graphite nanocomposites via surface RAFT-mediated miniemulsion polymerization. J Polym Sci A Polym Chem 49:1621–1632
90. Zhang B, Chen Y, Xu L, Zeng L, He Y, Kang E-T, Zhang J (2011) Growing poly (N-vinylcarbazole) from the surface of graphene oxide via RAFT polymerization. J Polym Sci A Polym Chem 49:2043–2050
91. Beckert F, Friedrich C, Thomann R, Mülhaupt R (2012) Sulfur-functionalized graphenes as macro-chain-transfer and RAFT agents for producing graphene polymer brushes and polystyrene nanocomposites. Macromolecules 45:7083–7090
92. Li Y, Li X, Dong C, Qi J, Han X (2010) A graphene oxide-based molecularly imprinted polymer platform for detecting endocrine disrupting chemicals. Carbon 48:3427–3433
93. Beckert F, Rostas AM, Thomann R, Weber S, Schleicher E, Friedrich C, Mülhaupt R (2013) Self-initiated free radical grafting of styrene homo- and copolymers onto functionalized graphene. Macromolecules 46:5488–5496
94. Katsigiannopoulos D, Grana E, Avgeropoulos A, Carrasco PM, Garcia I, Odriozola I, Diamanti E, Gournis D (2012) Nanohybrids based on polymeric ionic liquid prepared from functionalized MWCNTs by modification of anionically synthesized poly(4-vinylpyridine). J Polym Sci A Polym Chem 50:1181–1186

95. Pei X, Xia Y, Liu W, Yu B, Hao J (2008) Polyelectrolyte-grafted carbon nanotubes: synthesis, reversible phase-transition behavior, and tribological properties as lubricant additives. J Polym Sci A Polym Chem 46:7225–7237
96. Yang J, Yan X, Chen F, Fan P, Zhong M (2013) Graphite oxide platelets functionalized by poly(ionic liquid) brushes and their chemical reduction. J Nanopart Res 15:1383
97. Xu Y, Gao C, Kong H, Yan D, Jin YZ, Watts PCP (2004) Growing multihydroxyl hyperbranched polymers on the surfaces of carbon nanotubes by in situ ring-opening polymerization. Macromolecules 37:8846–8853
98. Kerscher B, Appel A-K, Thomann R, Mülhaupt R (2013) Treelike polymeric ionic liquids grafted onto graphene nanosheets. Macromolecules 46:4395–4402
99. Appel A-K, Thomann R, Mülhaupt R (2013) Hydroxyalkylation and polyether polyol grafting of graphene tailored for graphene/polyurethane nanocomposites. Macromol Rapid Commun. doi:10.1002/marc.201300363

Index